Neuroinflammation in frontotemporal dementia

A thesis submitted to University College London

for the degree of Doctor of Philosophy

Ione Olivia Clara Woollacott

Dementia Research Centre

Department of Neurodegenerative Disease

Queen Square Institute of Neurology

University College London

February 2021

Declaration

I, Ione Olivia Clara Woollacott, confirm that the work presented in this thesis is my own. Where information has been derived from other sources, I confirm that this has been indicated in the thesis.

My thesis was originally submitted for examination in October 2020. The viva took place in December 2020 and this version of my thesis, which incorporates minor corrections, was submitted in February 2021.

Ione Woollacott

Acknowledgements

During my PhD I was amazed by and eternally grateful for the commitment, bravery and selflessness of people with FTD, their carers and their relatives, who dedicated their time to participating in studies at UCL. Their willingness to allow me to perform lumbar punctures and multiple other assessments, sometimes repeatedly, year on year, has made a major contribution to my work and the work of others. They inspired me to keep going with my research and to furthering our knowledge about this disease. I hope that this research somehow brings them closer to improvements in care and successful treatments that several years ago seemed so far away.

I am grateful to the Medical Research Council, who provided my PhD funding for three years through a Clinical Research Training Fellowship. The clinical salary, funding for experiments and conferences, and research training were invaluable during a busy PhD incorporating both clinical and research roles at the National Hospital for Neurology and Neurosurgery and the UCL Queen Square Institute of Neurology.

My primary supervisor Jonathan Rohrer, and my secondary supervisors Tammaryn Lashley, Henrik Zetterberg and Amanda Heslegrave, have been excellent mentors throughout my PhD. I first met Jon while I was on an Oncology SHO night shift in UCLH A&E in 2012. I am so glad that he convinced me to pursue FTD research, opened my eyes to Cognitive Neurology, and encouraged me during my Academic Clinical Fellowship at UCL to develop a PhD proposal and apply for independent research funding. I am grateful that he has continued to support me both professionally and personally over the last 8 years. I am always inspired by his dedication to his patients, students, research studies and his family, his immense organisational skills, and his conceptualisation and leadership of GENFI. Tammaryn's pragmatism, sense of humour, kindness and love for neuropathology have helped me throughout my PhD and have

kept me going while I was writing this thesis during my return to clinical training and other life events. Her multi-tasking abilities at work and at home are an inspiration and she is an excellent role model for women in academia. Henrik's boundless enthusiasm, energy and expertise have been much appreciated, and I am very grateful for his advice on all things biomarker related. Amanda's patience, guidance and tuition while I learnt biomarker techniques, and her ability to turn ideas into action, have also been incredibly helpful for my research. Thank you all for your support.

I have worked with a wonderful team at the Dementia Research Centre (DRC), including all members of the Rohrer lab. In particular, Katrina Moore has provided great friendship, advice and encouragement both at UCL and beyond. I am also grateful to Carolin Heller, Martha Foiani, Elizabeth Gordon, Lucy Russell, Martina Bocchetta, Rachelle Shafei, Mica Clarke, Rhian Convery, Caroline Greaves and Mollie Neason for their help with my research and friendship. I have also worked alongside multiple Clinical Fellows while at the DRC, including Camilla Clark, Catherine Slattery, Chris Lane, Tom Parker, Ashvini Keshavan, Ross Paterson, Antoinette O'Connor, Sarah Keuss, Sarah Buchanan, Charlie Marshall, Alex Foulkes, Carolin Koriath, Dexter Penn and Harri Sivasathiaseelan. They have all been a pleasure to work with and have often helped me, amused me or inspired me during late nights or after long days or failed experiments.

Thank you so much to Jennifer Nicholas for her excellent statistical guidance and assistance. Thank you to my other DRC colleagues, including Hugh Pemberton for tea breaks and motivational chats, and Chris Hardy, Carole Sudre, Anne Parnell, Suzie Barker, Ayesha Khatun and Susie Henley for great support or invaluable advice. I would also like to thank all of the DRC consultants, but especially Nick Fox, Jonathan Schott and Jason Warren, for their clinical and research training and for taking the time to

discuss ideas. Thank you also to Simon Mead for his mentorship during my Academic Clinical Fellowship.

Multiple colleagues at the Queen Square Brain Bank provided excellent advice, training or assistance with my histological research. Thank you to Janice Holton, Christina Toomey, Sandrine Foti, Bridget Benson, Karen Davey, Robert Courtney, Catherine Strand, Linda Parsons and Lynn Haddon. I am also grateful to Carolin Heller, Martha Foiani, Jamie Toombs and Elena Veleva at the Leonard Wolfson Biomarker Laboratory, who helped me with finding CSF samples or reagents and taught me how to do biomarker immunoassays.

Over the last two years I have been finishing writing up my thesis during my Neurology registrar training and while being Senior Neurology Registrar at the Royal Free Hospital. This has not been easy, particularly over the last few months during the Covid pandemic. I would like to thank my all of my colleagues, but particularly Jonathan Kennedy, Gerard Davies, Tim Yates, Nadia Magdalinou, Anna Nagy and Katherine Stockton, for their understanding and friendship.

Finally, I would like to thank my friends and family, who have been an incredible source of support, as always. My fellow Quartelles Alice Baxter, Becky Mursell and Natalie Mensah and my friend Joanna Bourguignon have often cheered me up by providing musical, comic or cake-based relief and positive messages or phone calls. I am indebted and eternally grateful to my parents Sue and Nick Woollacott, who have always encouraged me to be curious, enjoy science and pursue my passion for neuroscience research. They have been endlessly supportive, always believing that I would achieve my aims, and provided a listening ear, a constant supply of food, hugs and practical advice, and several motivational speeches to keep me going. Thank you.

I would like to dedicate this thesis to my wonderful husband, Dominic Davenport. I absolutely could not have done this without his love and support. So many times over the last five years, throughout wedding planning, house moves, career moves, health issues, and of course the Covid pandemic, he has encouraged me and reminded me that this ‘Pretty Huge Degree’ was achievable. He was right, and I am eternally grateful. Thank you for everything.

Abstract

Frontotemporal dementia (FTD) is a clinically and pathologically diverse disease with few reliable biomarkers and no effective treatments. Increasing evidence suggests that chronic neuroinflammation and microglial dysfunction contribute to disease, particularly in genetic FTD due to progranulin (*GRN*) mutations. This thesis examines the clinical, histological and fluid biomarker evidence of immune dysregulation and neuroinflammation in FTD, with a focus on microglia.

Assessment of systemic autoimmune diseases in individuals with genetic FTD demonstrates that non-thyroid autoimmune diseases are more prevalent in *GRN* mutation carriers than controls. Exploration of the histopathological correlates of MRI white matter hyperintensities (WMH) in a patient with FTD due to a *GRN* mutation links severe WMH in the frontal lobes to extensive white matter demyelination and microglial dystrophy. Immunohistochemical assessment of microglia in frontal and temporal *post-mortem* brain tissue from individuals with different sporadic and genetic subtypes of frontotemporal lobar degeneration (FTLD), Alzheimer's disease (AD) and controls demonstrates regional differences in microglial burden, activation and dystrophy, which vary by microglial phenotype, pathological subtype and disease mechanism. Measurement of levels of glia-derived biomarkers (sTREM2, YKL-40 and chitotriosidase) in cerebrospinal fluid (CSF) of individuals with sporadic and genetic FTD and controls shows that levels are elevated in certain subgroups, particularly in those with *GRN* mutations, or likely underlying AD rather than FTLD. Investigation of these biomarkers in CSF of presymptomatic mutation carriers (PMC) and symptomatic individuals with genetic FTD reveals raised chitotriosidase levels in *GRN* and *MAPT* mutation carriers with FTD, with elevation several years before expected onset in *GRN* PMC.

In conclusion, this thesis provides multimodal evidence of dysregulated neuroinflammation in FTD and highlights the role of microglial dysfunction and senescence in the pathogenesis of FTLD, particularly in *GRN* mutation carriers. Further investigation of these processes may guide therapeutic and biomarker approaches for use in future clinical trials.

Impact statement

Novel insights arising from this thesis regarding the role of neuroinflammation in FTD, particularly microglial senescence and use of glia-derived biomarkers, have improved our understanding of what causes this devastating disease. I have disseminated my work through five first author publications, 14 oral presentations and 11 posters and also co-authored 18 additional publications during my PhD. In 2018 my work was awarded Winner of the UCL Faculty of Brain Sciences Three Minute Thesis Prize, and Runner Up in the UCL-wide Three Minute Thesis Prize and the International Society for Frontotemporal Dementias Early Career Researcher Prize.

As CSF biomarkers are useful for clinical trials, I presented my findings to international academics and pharmaceutical companies at annual GENFI Investigator meetings, highlighting the role of glia-derived biomarkers in genetic FTD. Encouragingly, there are now clinical trials for genetic FTD on the horizon, with collaboration between UCL and pharmaceutical companies. Inspired by my work on microglia in brain tissue, I helped to design and carry out a microglial PET study in FTD at UCL, which is ongoing. This may validate findings of regional microglial dysfunction identified within this thesis.

During my PhD I contributed to UCL FTD research studies (GENFI and LIFTD), performing multiple clinical assessments, venipunctures, lumbar punctures and skin biopsies. My work on systemic autoimmune diseases in genetic FTD modified study protocols, improving data collection across GENFI sites. I also strengthened external and internal collaborations for projects on lysosomal biomarkers at the University of Gothenburg, plasma white cell enzymes at the UCL Institute of Child Health and induced pluripotent stem cell models of FTD within the UCL Department of Neurodegenerative Disease.

To improve awareness of immune dysfunction in FTD within wider audiences, I communicated my work to scientists and the public via the Video Journal of Dementia, a Dementia Researcher podcast, the UCL Faculty of Brain Sciences website, the FTDtalk website, and the 2016 UCL Development and Alumni Relations Office Campaign Event. Presenting my CSF biomarker research to patients and relatives at UCL Rare Dementia Support Groups reduced fear about lumbar punctures and increased participation in UCL studies.

Raising awareness of FTD and other rare dementias is key to aiding earlier diagnosis and appropriate support. I enabled this through my involvement in public engagement events, including the London Science Museum Lates Event (2016), FTD Awareness Week (2017) and Pint of Science Festival (2018). As an FTD Working Group member for the European Reference Network for Rare Neurological Diseases I contributed to the development of policies for clinical management and research registries for FTD.

It is vital that research on FTD continues beyond this thesis, so during my PhD I mentored the next generation of researchers by co-supervising two Dementia MSc students on CSF biomarker and histological projects at UCL. In collaboration with MindTorch I organised a visit for sixth form students to the UCL Institute of Neurology, encouraging them to pursue scientific careers. With greater diversity comes ingenuity, perspective and passion, all of which are needed to continue the fight against FTD.

Table of contents

List of tables

List of figures

List of abbreviations

AAD	Age at death
AAO	Age at onset
Aβ	Amyloid beta
Aβ42	Amyloid beta 1-42
AD	Alzheimer's disease
aFTLD-U	Atypical frontotemporal lobar degeneration with ubiquitin positive inclusions
ALS	Amyotrophic lateral sclerosis
ANOVA	Analysis of variance
BBB	Blood-brain barrier
BIBD	Basophilic inclusion body disease
BSA	Bovine serum albumin
BvFTD	Behavioural variant frontotemporal dementia
CAA	Cerebral amyloid angiopathy
CBD	Corticobasal degeneration (pathology)
CBS	Corticobasal syndrome
CCNF	Cyclin F (gene)
CD68	Cluster of differentiation 68
CHCHD10	Coiled-coil-helix-coiled-coil-helix domain containing protein 10 (gene)
CHIT1	Chitinase 1 (gene)
CHMP2B	Charged multivesicular body protein 2B (gene)
CNS	Central nervous system
C9orf72	Chromosome 9 open reading frame 72 (gene)
C9orf72	Chromosome 9 open reading frame 72 (protein)

CSF	Cerebrospinal fluid
CSF1R	Colony stimulating factor 1 receptor (gene)
CV	Coefficient of variation
DAB	3,3'-diaminobenzidine
DCTN1	Dynactin-1 (gene)
DLB	Dementia with Lewy bodies
DNA	Deoxyribonucleic acid
DNs	Dystrophic neurites
DPRs	Dipeptide repeat proteins
DRC	Dementia Research Centre
ELISA	Enzyme-linked immunosorbent assay
EYO	Expected years from onset
FDG-PET	Fluorodeoxyglucose positron emission tomography
FET	FUS, Ewing's sarcoma and TATA binding protein associated factor 15
FFPE	Formalin fixed paraffin embedded
FG	Frontal grey matter
FLAIR	Fluid-attenuated inversion recovery
FTD	Frontotemporal dementia
FTLD	Frontotemporal lobar degeneration
FTD-MND	Frontotemporal dementia with motor neuron disease
FUS	Fused in sarcoma (gene)
FUS	Fused in sarcoma (protein)
FW	Frontal white matter
GCIs	Glial cytoplasmic inclusions
GENFI	Genetic Frontotemporal Dementia Initiative
GFAP	Glial fibrillary acidic protein

GRN	Progranulin (gene)
GWAS	Genome wide association studies
H&E	Haematoxylin & eosin
HD	Huntington's disease
HLA	Human leucocyte antigen (gene)
HLA-DR	Human leucocyte antigen-D related protein-R
H_20_2	Hydrogen peroxide
Iba1	Ionised calcium-binding adapter molecule 1
IL	Interleukin
IFN-γ	Interferon-gamma
iPSCs	Induced pluripotent stem cells
LFB	Luxol fast blue
LIFTD	Longitudinal Investigation of Frontotemporal Dementia
Ln	Natural log
LvPPA	Logopenic variant primary progressive aphasia
LWBL	Leonard Wolfson Biomarker Laboratory
MAPT	Microtubule-associated protein tau (gene)
MCP-1	Monocyte chemoattractant protein-1
MHC	Major histocompatibility complex
MND	Motor neuron disease
MRC	Medical Research Council
MRI	Magnetic Resonance Imaging
MSD	Meso Scale Discovery
NCIs	Neuronal cytoplasmic inclusions
NF-κβ	Nuclear factor-kappa beta
NfL	Neurofilament light chain
NFTs	Neurofibrillary tangles

NfvPPA	Non-fluent variant primary progressive aphasia
NHNN	National Hospital for Neurology and Neurosurgery
NIFID	Neuronal intermediate filament inclusion disease
NNIs	Neuronal nuclear inclusions
OPTN	Optineurin (gene)
P2RY12	Purinergic receptor P2Y12
PBR	Peripheral benzodiazepine receptor
PBS	Phosphate buffered saline
PET	Positron emission tomography
PMC	Presymptomatic mutation carriers
PPA	Primary progressive aphasia
PPA-NOS	Primary progressive aphasia – not otherwise specified
PSP	Progressive supranuclear palsy (pathology)
PSPS	Progressive supranuclear palsy syndrome
P-tau	Phosphorylated-tau-181
QSBB	Queen Square Brain Bank
RAN	Repeat associated non-ATG
RNA	Ribonucleic acid
Rpm	Revolutions per minute
SQSTM1	Sequestosome-1 (gene)
SPECT	Single photon emission computed tomography
SPM	Statistical Parametric Mapping
sTREM2	Soluble triggering receptor expressed on myeloid cells 2
SvPPA	Semantic variant primary progressive aphasia
TARDBP	Transactive response DNA binding protein (gene)
TBK1	TRAF family member-associated NF-κβ activator (TANK)-binding kinase 1 (gene)

TBS	Tris buffered saline
TBS-T	TBS-Tween
TDP-43	Transactive response DNA binding protein 43
TG	Temporal grey matter
TIA-1	T-cell restricted intracellular antigen-1 (gene)
TMEM106B	Transmembrane protein 106B (gene)
TMEM119	Transmembrane protein 119 (protein)
TNF-α	Tumour necrosis factor-alpha
T-tau	Total tau
TREM2	Triggering receptor expressed on myeloid cells 2 (gene)
TREM2	Triggering receptor expressed on myeloid cells 2 (protein)
TSPO	Translocator protein
TW	Temporal white matter
UBQLN2	Ubiquilin 2 (gene)
UCL	University College London
VCING	Vascular Cognitive Impairment Neuropathology Guidelines
VCP	Valosin containing protein (gene)
WMH	White matter hyperintensities
YKL-40	Chitinase-3-like protein 1
+/-	Heterozygous knockout
-/-	Homozygous knockout

1 Introduction

1.1 An overview of frontotemporal dementia (FTD)

Frontotemporal dementia (FTD) is a clinically, genetically and neuropathologically diverse neurodegenerative disorder leading to progressive frontal and temporal atrophy and changes in behaviour, language and motor function. Although it occurs less frequently than Alzheimer's disease (AD), FTD is the second most common cause of young-onset dementia, typically presenting in individuals aged between 45 to 65 years (Onyike and Diehl-Schmid, 2013). However, it can affect individuals from their 30s to their 90s and it may be under-diagnosed in older individuals due to misdiagnoses of AD, other types of dementia, or late-onset psychiatric disorders. The overall prevalence of FTD is 10-15 per 100,000 and the lifetime risk of developing FTD in the United Kingdom is 1 in 742 (Coyle-Gilchrist et al., 2016).

The majority of FTD has no known cause ('sporadic' FTD), but around 30-50% of cases are familial (Goldman et al., 2005; Rohrer et al., 2009a), with around 10-30% of FTD cases overall due to autosomal dominant mutations in one of several genes (Seelaar et al., 2011; Wood et al., 2013); this is known as genetic FTD. The most common genes involved are chromosome 9 open reading frame 72 (*C9orf72*) (DeJesus-Hernandez et al., 2011; Renton et al., 2011), progranulin (*GRN*) (Baker et al., 2006; Cruts et al., 2006) and microtubule-associated protein tau (*MAPT*) (Hutton et al., 1998; Spillantini et al., 1998). Although multiple clinical trials are on the horizon, there remains no current effective or disease modifying treatment for FTD.

This introductory chapter summarises the clinical, genetic and neuropathological aspects of FTD, the current state of fluid biomarkers of FTD and the evidence that implicates aberrant neuroinflammation, particularly microglial dysfunction, in disease pathogenesis.

1.1.1 Clinical syndromes

There are two main initial clinical presentations of FTD. Over 50% of individuals present with behavioural variant FTD (bvFTD), which leads to progressive behavioural change, inappropriate social conduct and executive dysfunction. The remainder present with primary progressive aphasia (PPA), which leads to progressive language decline and speech difficulties (Warren et al., 2013). Individuals with FTD can also develop 'overlap syndromes' of motor neuron disease (MND) (Devenney et al., 2015) or atypical parkinsonian disorders: either corticobasal syndrome (CBS) or progressive supranuclear palsy syndrome (PSPS) (Park and Chung, 2013).

BvFTD presents with progressive changes in personality and behaviour, a decline in social skills and impaired higher level thinking due to executive dysfunction. Early on, there is relative preservation of other cognitive areas such as episodic memory and visuospatial function (Warren et al., 2013). The current clinical diagnostic criteria for bvFTD (Rascovsky et al., 2011) are displayed in Table 1.1. Individuals must attain three of six clinical features: five behavioural (disinhibition, apathy or inertia, loss of sympathy or empathy, stereotyped or compulsive behaviors, or hyperorality) and one cognitive (predominant executive dysfunction on neuropsychological assessment). Individuals with PPA, CBS, PSPS or MND can also develop similar behavioural changes, but they must not be predominant initially. BvFTD is associated with frontal and temporal lobe atrophy on neuroimaging, which may be asymmetrical, and the pattern of atrophy can vary between individuals with similar clinical presentations (Rascovsky et al., 2011).

Behavioural and cognitive symptoms of bvFTD Diagnosis of possible bvFTD requires at least 3 of the following symptoms to be fulfilled:	**Examples of specific symptoms**
Early behavioural disinhibition ≥ 1 of:	
Socially inappropriate behaviour	Staring, inappropriate physical contact with strangers, verbal or physical aggression
Loss of manners or decorum	Lack of social etiquette, insensitive or rude comments, preference for crass jokes and slapstick humour, inappropriate choices of clothing or gifts
Impulsive, rash or careless actions	New gambling behaviour, driving or investing recklessly, overspending, gullibility to phishing/internet scams
Early apathy or inertia ≥ 1 of:	
Apathy	Reduced drive, stops previous hobbies, stops going out, reduced bathing or personal care
Inertia	Lack of persistence or completion of an activity, does not initiate activities or conversations
Early loss of sympathy or empathy ≥ 1 of:	
Diminished response to other people's needs and feelings	Selfish or hurtful comments or actions, inability to perceive when someone is upset, embarrassed, or in pain, reduced appreciation of sarcasm or sophisticated humor
Diminished social interest, interrelatedness, or personal warmth	Emotionally cold or detached, lack of rapport in conversation, loss of interest or affection in relationships with friends or family members, reduced interest in sex
Early perseverative, stereotyped or compulsive or ritualistic behavior ≥ 1 of:	
Simple repetitive movements	Repetitive rocking, tapping, clapping, or rubbing
Complex compulsive or ritualistic behaviours	Hoarding, strict grooming or walking routines, timekeeping and counting, checking or sorting items, cleaning or tidying, new obsessions or interests (usually spiritual, religious, artistic, or musical)
Stereotypy of speech	Habitual repetition of particular words, sentences or topics
Hyperorality and dietary changes ≥ 1 of:	
Altered food preferences	Sweet tooth (sweets, biscuits, ice cream), carbohydrates, or obsessive food fads
Binge eating, increased consumption of alcohol or cigarettes	Cramming food into mouth, overeating or messy eating, new addictions to alcohol or smoking
Oral exploration or consumption of inedible objects	Pica
Neuropsychological profile – all 3 of:	
Deficits in executive tasks	Vary as per neuropsychological assessment used
Relative sparing of episodic memory	
Relative sparing of visuospatial skills	
Other features of bvFTD (not in diagnostic criteria)	**Examples of specific symptoms**
Loss of insight	Lack of awareness of own condition or symptoms
Rigidity of thought	Inflexible towards new ideas or routines, stubbornness, becomes angry or irritable if contradicted
Irritability and aggression	Easily riled or annoyed, verbally aggressive or shouts at relatives
Altered sensitivity to pain	Heightened perception of a non-painful stimulus or reduced response to painful stimulus; hypochondriasis or overly focusing on mild physical complaints
Altered tolerance of temperature	Inappropriate clothing for the ambient temperature, such as wearing multiple coats or blankets
Psychotic features	Delusions (usually somatic or paranoid) and hallucinations (usually tactile or visual)

Table 1.1 Current diagnostic criteria for bvFTD and other commonly seen features

Table content is adapted from Rascovsky et al. (2011) and Warren et al. (2013) and published in (Woollacott and Rohrer, 2016). The term 'early' refers to within three years of initial symptom onset as per Rascovsky et al. (2011).

PPA presents with progressive language decline affecting at least one of object naming, word comprehension, speech production, or syntax (Gorno-Tempini et al., 2011). Other cognitive or behavioural deficits can develop but must not be the initial, predominant complaint. There are three variants of PPA: semantic variant PPA (svPPA), previously known as semantic dementia; nonfluent variant PPA (nfvPPA), previously known as progressive non-fluent aphasia; and logopenic variant PPA (lvPPA), previously known as logopenic aphasia (Gorno-Tempini et al., 2011). Distinct language features can be used to differentiate between these variants, summarised in Table 1.2.

	svPPA	**nfvPPA**	**lvPPA**
Proportion of PPA cases	20%	25%	30%
Heritability	Vast majority sporadic	Often sporadic, but some genetic (*GRN or MAPT > C9orf72* mutations)	Mostly sporadic, around 70% AD pathology
Neuroimaging phenotype	Asymmetrical anteroinferior temporal lobe atrophy (usually left temporal, but right temporal lobe variant exists)	Left posteroinferior frontal lobe and insular atrophy	Left posterior temporo-parietal atrophy
Behavioural and other cognitive features	Obsessionality, mental rigidity, time-keeping, narrowed interests; heightened sensitivity to pain/temperature/sound, food fads	May develop features of bvFTD, as well as orofacial apraxia and limb apraxia	Prominent AD-like features e.g. episodic memory problems, visuoperceptual problems, limb apraxia
Spontaneous speech (fluency; errors; grammar; prosody)	Fluent, garrulous and circumlocutory; semantic errors; intact grammar and prosody	Slow and hesitant, effortful +/- apraxic; phonetic errors; +/- agrammatic; aprosodic	Hesitant; not effortful or apraxic; frequent word-finding pauses and loss of train of sentence; intact grammar; intact prosody
Naming	Severe anomia with semantic paraphasias and errors	Moderate anomia with phonetic errors	Mild-moderate anomia with visual and verbal errors
Single word comprehension	Poor	Intact early on, but affected later on	Intact early on
Sentence comprehension	Initially preserved, later on becomes impaired as word comprehension is impaired	Impaired if grammatically complex	Impaired, especially if long
Single word repetition	Intact if word comprehended	Mild to moderately impaired if polysyllabic, otherwise intact	Relatively intact
Sentence repetition	Intact if words comprehended	Can be effortful; impaired if grammatically complex	Impaired
Reading	Surface dyslexia	Effortful phonological dyslexia +/- phonetic errors	Can have phonological dyslexia
Writing	Surface dysgraphia	Phonological dysgraphia	Phonological/mixed dysgraphia

Table 1.2 Clinical features of the PPA syndromes

Clinical features are adapted from tables in Gorno-Tempini et al., 2011; Rohrer et al., 2010, 2008; Seelaar et al., 2011; Woollacott and Rohrer, 2016.

SvPPA affects semantic memory, impairing object naming and single word comprehension. This leads to initially fluent but garrulous, circumlocutory speech, progressive anomia, and difficulty in reading and pronouncing irregularly spelled words (surface dyslexia). There are often behavioural changes as the disease evolves. SvPPA is associated with bilateral, asymmetrical (typically left more than right) anteroinferior temporal lobe atrophy (Rohrer et al., 2009b). NfvPPA presents with non-fluent, effortful speech, impaired single word repetition and sentence comprehension, sometimes with later behavioural changes. Some individuals have prominent speech apraxia, with phonemic (sound) or phonetic (articulation) speech errors (often associated with orofacial apraxia). Others have prominent agrammatism, which disrupts sentence structure and flow. NfvPPA is associated with left inferoposterior frontal and insular atrophy (Rohrer et al., 2009b). LvPPA presents with hesitant speech, word-finding pauses, anomia and impaired sentence repetition, although it also affects episodic memory and visuoperceptual function. It is associated with asymmetrical (left more than right) temporoparietal atrophy (Rohrer et al., 2013). In around 70% of cases lvPPA is due to AD pathology, so is often called an ‘atypical AD syndrome’, but it can also be due to FTD-associated pathology, so sits within the FTD spectrum (Lashley et al., 2015). Some individuals develop a language or speech disorder which does not fit criteria for any of these PPA variants, called ‘PPA-not otherwise specified’ (PPA-NOS) (Sajjadi et al., 2012).

Around 10-15% of individuals with FTD later develop MND; most had bvFTD initially, although some start with nfvPPA (Burrell et al., 2011). Individuals with FTD-MND usually develop the amyotrophic lateral sclerosis (ALS) variant of MND, but other phenotypes are occasionally seen. FTD-MND is often genetic, most commonly due to a *C9orf72* expansion (Mahoney et al., 2012). Whilst 10-20% of individuals initially presenting with MND later meet diagnostic criteria for FTD (typically bvFTD), at least 50% of MND cases

develop less severe behavioural (Strong et al., 2009) or language (Taylor et al., 2013) impairment. Although CBS and PSPS are encompassed within the FTD spectrum, they have their own set of diagnostic criteria (Armstrong et al., 2013; Höglinger et al., 2017; Litvan et al., 1996). Some individuals who also meet diagnostic criteria for bvFTD or PPA (typically nfvPPA) may initially present with or later develop CBS (asymmetrical limb apraxia and an 'alien limb', rigidity, myoclonus) or PSPS (vertical gaze palsy, early postural instability with falls, marked cognitive slowing). However, less obvious parkinsonism (bradykinesia, rigidity, tremor, postural instability) not fully consistent with CBS or PSPS is seen in around 20% of FTD cases early on, and a larger proportion develop parkinsonism by end-stage disease (Park and Chung, 2013). Rarely, individuals develop FTD, MND and parkinsonism (Mahoney et al., 2012).

1.1.2 Diagnosis

Diagnosis of FTD relies on a thorough clinical assessment, with a detailed history from the patient and, importantly, their friend or relative (due to impaired insight in many FTD cases), to establish whether they meet clinical diagnostic criteria for bvFTD (Table 1.1) or PPA (Table 1.2). A neurological examination should look for signs of parkinsonism, CBS, PSPS, and MND, or other signs, for example chorea, which may indicate presence of an alternative neurodegenerative disorder, such as Huntington's disease (HD). A clinical cognitive examination and detailed neuropsychological assessments help to clarify the pattern and severity of cognitive impairment, identify psychiatric disorders, and, if repeated, assess for decline over time (Warren et al., 2013). Neuroimaging using magnetic resonance imaging (MRI) is vital to rule out structural lesions (such as frontal lobe tumours, demyelination or leukodystrophies) that are FTD 'disease mimics', delineate the pattern of atrophy to confirm a frontal and/or temporal predominance, and exclude atrophy patterns more commonly seen in other neurodegenerative disorders such as AD (bilateral hippocampal atrophy or posterior cortical atrophy), or prominent cerebrovascular disease (Warren et al., 2013). Pronounced asymmetry of atrophy may

be helpful for confirmation of certain FTD syndromes such as svPPA, nfvPPA or lvPPA, and characteristic patterns of atrophy or other neuroimaging changes are seen in different genetic FTD subtypes (Cash et al., 2018; Fumagalli et al., 2018; Jiskoot et al., 2018; Panman et al., 2019; Rohrer et al., 2015). Serial MRIs with comparison of images over time can establish whether there is progressive atrophy if it remains unclear whether there is a neurodegenerative disorder, or where the initial MRI appears normal. Metabolic brain imaging with fluorodeoxyglucose positron emission tomography (FDG-PET), which detects cerebral glucose metabolism, or with single photon emission computed tomography (SPECT), which quantifies cerebral blood flow, can detect regional abnormalities if the MRI scan appears normal, demonstrating hypometabolism or hypoperfusion in frontal and temporal regions before atrophy is evident (Warren et al., 2013).

Individuals with suspected FTD may benefit from having a lumbar puncture for assessment of cerebrospinal fluid (CSF). This is used to exclude infective or neuroinflammatory mimics of FTD (through analysis of white cell count, protein and glucose levels) and to examine levels of proteins altered in AD or prion disease. Levels of amyloid beta 1-42 (Aβ42), total tau (T-tau), and phosphorylated-tau-181 (P-tau) in CSF help to differentiate AD from other types of dementia (including FTD) or those with subjective cognitive impairment. Some centres offer amyloid PET imaging, where a tracer detects fibrillar amyloid beta (Aβ) in the brain. This is a useful non-invasive way of detecting amyloid pathology and therefore diagnosing AD, although dual pathology (AD and other) can lead to FTD syndromes, and some cognitively normal individuals have positive amyloid PET scans.

1.1.3 Genetics

Despite detailed clinical, neuropsychological, neuroimaging and CSF assessments, the diagnosis of FTD can remain challenging in clinical practice. Currently, the only confirmed risk factors for FTD are mutations in certain genes, so identification of a causative gene mutation can substantially aid diagnosis. Between 30-50% of individuals report a history of FTD or another neurodegenerative disorder in at least one family member (Goldman et al., 2005; Rohrer et al., 2009a), and an autosomal dominant inheritance pattern is seen in 10-30% of individuals (Seelaar et al., 2011; Wood et al., 2013). BvFTD is much more heritable than nfvPPA, whereas svPPA and lvPPA are rarely genetic. Autosomal dominant mutations in three genes (*C9orf72, GRN* and *MAPT)* account for the majority of genetic FTD cases, but mutations in several other genes are more rarely associated with FTD. Very rarely there are dual mutations present, for example in *GRN* and *C9orf72* (Lashley et al., 2014). The various genetic FTD syndromes have different but often overlapping clinical presentations and disease trajectories; these are summarised below.

1.1.3.1 *MAPT* mutations

The first genetic cause of FTD was established in 1998, with identification of mutations in the *MAPT* gene on chromosome 17, which encodes the protein tau (Hutton et al., 1998; Spillantini et al., 1998). There are currently at least 67 known pathogenic mutations in *MAPT*, making up between 5-20% of FTD cases overall, 23% of genetic FTD cases, and 1-2% of sporadic cases (Moore et al., 2020; Pickering-Brown et al., 2008). *MAPT* mutations either affect the splicing of exon 10, leading to an imbalance in the tau isoforms in the brain (shifting it from equal proportions of 3 repeat [3R] and 4 repeat [4R] tau, to a predominance of either of these isoforms and subsequent aggregation of insoluble 3R tau, 4R tau or both), or occur as missense mutations in exons 9 to 13, affecting tau protein function in microtubule stabilisation (for example by hyperphosphorylation), or they affect both mechanisms, ultimately promoting tau aggregation (Hutton et al., 1998).

Individuals with *MAPT* mutations typically develop FTD at a younger age than those with *GRN* or *C9orf72* mutations, with a mean age at onset (AAO) of 49.5 years, but this varies widely, from 24-93 years (Moore et al., 2020). Penetrance is almost 100%, and mean disease duration is 9.3 years, but ranges from 0-45 years (Moore et al., 2020). The typical clinical picture is bvFTD, often with parkinsonism, typically with later language decline (usually semantic impairment) (Benussi et al., 2015; Pickering-Brown et al., 2008; Seelaar et al., 2011). MND is extremely rare, but there can be prominent episodic memory impairment and bilateral hippocampal atrophy, sometimes leading to a misdiagnosis of AD (Tolboom et al., 2010). There is generally poor correlation of clinical features with the specific mutation type (Benussi et al., 2015).

1.1.3.2 *GRN* mutations

Despite the discovery of *MAPT* mutations, many families clearly had familial FTD linked to chromosome 17, but without mutations in *MAPT* or tau pathology. Mutations in *GRN* on chromosome 17 were identified in 2006 (Baker et al., 2006; Cruts et al., 2006), and there are currently at least 130 known pathogenic *GRN* mutations. *GRN* mutations are the second most common genetic cause of FTD, making up 5-10% of FTD overall (Seelaar et al., 2011), 35% of genetic FTD (Moore et al., 2020) and 5% of 'sporadic' FTD.

GRN mutations include nonsense, frameshift, missense and splice mutations, with rarer partial and complete deletions, but all lead to a heterozygous (50%) loss-of-function of the protein progranulin, due to premature degradation of *GRN* messenger ribonucleic acid (mRNA) by nonsense-mediated decay (Baker et al., 2006). This also leads to deficiency in progranulin's cleavage products, the granulins (granulins A to G). Progranulin is a multi-functional transmembrane protein consisting of seven and a half repeats of cysteine-rich granulin motifs separated by linker regions (Baker et al., 2006). It is expressed on a variety of epithelial and haematopoietic cells, and by neurons and microglia, especially activated microglia (Baker et al., 2006). Progranulin is a growth

factor, with key roles in wound healing, angiogenesis and tumourigenesis (Townley et al., 2018), and regulates the formation and function of lysosomes, interacting with other lysosomal proteins including sortilin (Hu et al., 2010a) and prosaposin (Zhou et al., 2015). Progranulin has neurotrophic and neuroprotective properties and regulates synaptic function (Townley et al., 2018). It is also integral to the regulation of systemic and central inflammatory pathways and the function of microglia: it exerts anti-inflammatory effects through binding to tumour necrosis factor (TNF) receptors, antagonising the proinflammatory cytokine TNF-α (Jian et al., 2013; Tang et al., 2011), and inhibits proinflammatory signaling via TNF-α/nuclear factor-κβ (NF-κβ) pathways (Alquezar et al., 2016). Progranulin is a chemoattractant for microglia (Pickford et al., 2011), alters microglial endocytosis (Pickford et al., 2011) and phagocytosis (Lui et al., 2016) and downregulates microglial activation during aging (Lui et al., 2016). Granulins have opposing, proinflammatory effects, but also affect lysosomal function (Holler et al., 2017).

Mean AAO of symptoms in *GRN* mutation carriers is 61.3 years, but ranges from 25-90 years (Moore et al., 2020), and penetrance is age dependent. Mean disease duration is 7.1 years, but ranges from 0-27 years (Moore et al., 2020). The clinical picture is variable: the most common presentation is bvFTD and less commonly PPA (Benussi et al., 2015; Le Ber et al., 2008), typically nfvPPA or a distinct language phenotype (PPA-NOS) (Rohrer et al., 2010a). Due to asymmetrical striatal, parietal and temporal involvement, parkinsonism, CBS and visuoperceptual or episodic memory impairment are common and neuropsychiatric phenomena such as visual hallucinations are described (Le Ber et al., 2008). This can lead to a misdiagnosis of idiopathic Parkinson's disease, sporadic CBS, dementia with Lewy bodies (DLB) or AD. The clinical syndrome varies within the same family, and correlates poorly with mutation type.

1.1.3.3 *C9orf72* expansions

Many families without *MAPT* or *GRN* mutations clearly had familial FTD, MND, or both, but for years a genetic cause remained elusive. However, in 2011 a heterozygous hexanucleotide (GGGGCC) repeat expansion was identified in a non-coding region of the *C9orf72* gene on chromosome 9 (DeJesus-Hernandez et al., 2011; Renton et al., 2011). This mutation was later found to be the most common cause of genetic FTD, genetic MND and FTD-MND in Europe and North America, accounting for 25-42% of genetic FTD, 40% of genetic MND, 6% of sporadic FTD and 5% of sporadic MND (Majounie et al., 2012; Moore et al., 2020).

Normally there are 2-11 repeats on each *C9orf72* allele, but individuals with the heterozygous expansion possess 400-4400 repeats on one allele (Beck et al., 2013). Although the role of the C9orf72 protein remains unclear, several studies implicate C9orf72 in microglial and endolysosomal function and nucleocytoplasmic transport. There are several proposed disease mechanisms for the *C9orf72* expansion. These include: loss of function of the C9orf72 protein (due to abortive transcription of mRNA containing the expansion) leading to impaired autophagy and endolysosomal trafficking; toxicity through formation of RNA foci, which sequester and deplete RNA-binding proteins; or toxicity from production of dipeptide repeat proteins (DPRs) produced via repeat-associated non-ATG (RAN) translation of the expansion, which impair nucleocytoplasmic transport (Balendra and Isaacs, 2018).

AAO of symptoms in *C9orf72* expansion carriers is variable, with a mean of 58.2 years but range of 20-91 years (Moore et al., 2020). Mean disease duration is 6.4 years, but highly variable, ranging from 0-36 years, although typically shorter in FTD-MND (Moore et al., 2020). Penetrance is age-dependent and nearly 100% by 80 years (Majounie et al., 2012). The typical presentation is bvFTD (31%), MND (19%) or both (11%) (Mahoney

et al., 2012; Moore et al., 2020; Snowden et al., 2012). Parkinsonism, episodic memory impairment and psychiatric presentations (anxiety or psychosis with auditory or tactile hallucinations) are common (Downey et al., 2012; Mahoney et al., 2012; Snowden et al., 2012; Woollacott and Mead, 2014), so misdiagnoses of late-onset psychiatric disorders are sometimes made.

1.1.3.4 Rarer FTD associated mutations

There are several rarer mutations associated with FTD, which account for less than 5% of familial cases. Mutations in TRAF family member-associated NF-κβ activator (TANK)-binding kinase 1 (*TBK1*) are associated with FTD-MND, FTD or MND (Freischmidt et al., 2015; Gijselinck et al., 2015; Koriath et al., 2017; Le Ber et al., 2015; Pottier et al., 2015). Valosin containing protein (*VCP*) mutations cause FTD with a multisystem proteinopathy, inclusion body myopathy and Paget's disease of the bone (Watts et al., 2004). Charged multivesicular body protein 2B (*CHMP2B*) mutations cause FTD in Danish cohorts (Skibinski et al., 2005). FTD is also associated with p62/sequestosome-1 (*SQSTM1*) (Rubino et al., 2012), optineurin (*OPTN*) (Pottier et al., 2015), transactive response DNA binding protein (*TARDBP)* (Synofzik et al., 2014), ubiquilin 2 (*UBQLN2*) (Gellera et al., 2013), dynactin-1 (*DCTN1)* (Münch et al., 2005), and fused in sarcoma (*FUS*) (Vance et al., 2009) mutations, although these more commonly lead to MND. More recently, mutations in cyclin F (*CCNF*) (Williams et al., 2016), coiled-coil-helix-coiled-coil-helix domain-containing protein 10 (*CHCHD10*) (Bannwarth et al., 2014), and T-cell restricted intracellular antigen-1 (*TIA1*) (Mackenzie et al., 2017) have been identified associated with FTD or FTD-MND.

There are variants in several genes that may be associated with FTD or can modify its phenotype. Homozyogous mutations in triggering receptor expressed on myeloid cells 2 (*TREM2*), which is expressed by myeloid cells including microglia, are associated with polycystic lipomembranous osteodysplasia with sclerosing leucoencephalopathy (or

Nasu-Hakola disease), a rare disease leading to an early-onset FTD-like syndrome and bony cysts (Paloneva et al., 2000). Homozygous or compound heterozygous *TREM2* mutations are associated with an FTD syndrome without bony involvement (Guerreiro et al., 2013), but it is unclear whether heterozygous *TREM2* variants cause typical FTD. Protective variants in transmembrane protein 106B (*TMEM106B)*, a gene involved in lysosomal function, can delay AAO of FTD in *GRN* mutation carriers (Cruchaga et al., 2011; Finch et al., 2011) and delay AAO and prolong survival in *C9orf72* expansion carriers with FTD or MND (Gallagher et al., 2014; Van Blitterswijk et al., 2014). There are also likely to be more genetic mutations or variants yet undiscovered that cause or modify the risk of developing FTD, as many families with a clearly autosomal dominant inheritance pattern have no identified causative mutations.

1.1.4 Neuropathology

The terminology of FTD and its associated pathologies has evolved significantly since the first description of a patient with progressive language disturbance and left superior temporal gyrus atrophy by Arnold Pick in 1892 (Pick, 1892). Histopathological presence of argyrophilic globular neuronal cytoplasmic inclusions (later termed Pick bodies) was described not by Pick but by Alois Alzheimer in 1911 (Alzheimer, 1911), but the concept of FTD was named ‘Pick’s disease’ by a Dutch group in 1925 (Gans, 1925) and by a German group in 1926 (Onari and Spatz, 1926). By the 1950s it had become evident that true Pick’s pathology was present in only around 20% of clinical FTD cases (Escourolle, 1956) and subsequent studies confirmed that there were multiple other pathologies associated with atrophy of the frontal and/or temporal lobes in patients with the clinical syndrome of FTD (Brun, 1987; Mann et al., 1993). The term ‘frontotemporal lobar degeneration’ (FTLD) has since been designated to describe a heterogeneous group of neurodegenerative diseases characterised by selective frontal and temporal lobe atrophy in individuals who have non-AD neuropathology (Neary et al., 1998).

Macroscopically, the predominant feature of FTLD is atrophy of the frontal and anterior temporal cortices, with variable destruction of associated subcortical white matter, although individuals may have involvement of other cortical and subcortical regions, including the parietal cortices, mesial temporal lobes (hippocampi and amygdalae), hypothalamus, thalami, and basal ganglia (Neumann and Mackenzie, 2019). There is typically relative sparing of the cerebellum and occipital cortices, although some cases, particularly those with the *C9orf72* expansion, have cerebellar involvement (Mahoney et al., 2012). Macroscopic changes are often asymmetrical, most commonly in those with PPA syndromes. Microscopically, there is aggregation of misfolded proteins in neurons, glial cells (microglia and astrocytes), or both cell types. There is cortical neuronal loss and microvacuolation (spongiform change), particularly in layer II of the cortex but this can be transcortical, and white matter axonal loss and loss of myelin, often accompanied by gliosis (presence of many activated astrocytes and microglia) (Mackenzie and Neumann, 2016; Neumann and Mackenzie, 2019).

Current classifications of FTLD include five main pathological types, divided according to the type and location of the underlying protein aggregates (inclusions) (Table 1.3) (Lashley et al., 2015; Mackenzie and Neumann, 2016). Inclusions can occur as neuronal cytoplasmic inclusions (NCIs), neuronal nuclear inclusions (NNIs), glial cytoplasmic inclusions (GCIs) or dystrophic neurites (DNs). In around 50% of FTLD cases, individuals have ubiquitin-positive inclusions of transactive response DNA-binding protein 43 (TDP-43), termed FTLD-TDP, and in around 40% of cases, individuals have ubiquitin-negative inclusions of hyperphosphorylated tau, termed FTLD-tau (Rohrer et al., 2011). Rarely (5-10% of ubiquitin-positive cases), fused in sarcoma (FUS) proteins are present (FTLD-FUS) (Rohrer et al., 2011). Some classifications use FTLD-FET (FUS, Ewing's sarcoma and TATA-binding protein associated factor 15) instead of FTLD-FUS (Mackenzie and Neumann, 2016), but this is not always widely accepted. Infrequently, inclusions are

ubiquitin-positive but not otherwise determined (FTLD-ubiquitin-proteosome system [FTLD-UPS]), or no inclusions are present (FTLD-ni).

FTLD group	Subtype	Characteristics of subtype
FTLD-TDP	FTLD-TDPA (Type A)	Numerous NCIs and short DNs in layer II of neocortex, lentiform NIIs
	FTLD-TDPB (Type B)	Numerous compact or granular NCIs in all cortical layers, few NIIs, occasional wispy neurites and pre-inclusions; NCIs in lower motor neurons
	FTLD-TDPC (Type C)	Abundant long corkscrew DNs in all cortical layers, few/no NCIs in cortex
	FTLD-TDPD (Type D)	Numerous lentiform NIIs and short DNs, rare NCIs
	FTLD-TDPE (Type E)	Abundant grains, oligodendroglial inclusions, granulofilamentous neuronal inclusions
FTLD-tau	FTLD-Picks (Pick's disease)	3R tau, argyrophilic NCIs (Pick bodies), ramified astrocytes
	FTLD-PSP	4R tau, globose and flame-shaped NFTs/coiled bodies in white matter, tufted astrocytes in grey matter
	FTLD-CBD	4R tau, threads, coiled bodies, ramified astrocytes, astrocytic tau plaques
	FTLD-*MAPT*	3R and 4R tau, or predominant 3R or 4R tau (mutation dependent); neuronal and glial hyperphosphorylated tau
	FTLD-AGD	4R tau, tau-immunoreactive grains
	FTLD-GGT	4R tau, globular oligodendroglial and astrocytic tau inclusions
	PART	3R and 4R tau
FTLD-FUS	FTLD-NIFID	Heterogeneous shapes of NCIs, rare NIIs; alpha-internexin positive inclusions
	aFTLD-U	Bean-shaped NCIs, vermiform NIIs, no alpha-internexin positive inclusions; hippocampal sclerosis
	FTLD-BIBD	Basophilic NCIs, no alpha-internexin positive inclusions
FTLD-UPS	FTLD-UPS	Ubiquitin and p62 positive, TDP-43, tau, FUS-negative inclusions; usually due to *CHMP2B* mutations
FTLD-ni	FTLD-ni	No inclusions present

Table 1.3 Classification and subtypes of FTLD pathologies

AGD = argyrophilic grain disease; GGT = globular glial tauopathy; PART = primary age-related tauopathy; for other abbreviations see main text.

FTLD-TDP can be further subdivided into four main subtypes (FTLD-TDP type A to D) based on the type and location of TDP-43 inclusions (Table 1.3). A fifth subtype has been identified (FTLD-TDP type E) associated with rapid disease progression, but this is rare

(Lee et al., 2017). FTLD-tau is divided into seven subtypes based on the predominant tau isoform present in inclusions within neurons or glia (either 3R tau, 4R tau, or a mixture of both) and using other features, such as glial cell appearances and morphological differences in tau filaments (Table 1.3). The most common FTLD-tau subtypes are Pick's disease (FTLD-Picks), progressive supranuclear palsy (FTLD-PSP), corticobasal degeneration (FTLD-CBD) and FTLD due to *MAPT* mutations (FTLD-*MAPT*). FTLD-FUS can be further subdivided into neuronal intermediate filament inclusion disease (FTLD-NIFID), atypical FTLD-U (aFTLD-U) or basophilic inclusion body disease (FTLD-BIBD) (Table 1.3) (Lashley et al., 2015). Each of these pathological subtypes can initially affect different brain regions or sub-regions, which contributes to different regional patterns of neurodegeneration, grey matter atrophy and white matter damage across the spectrum of FTLD (Lashley et al., 2015).

It is often difficult to predict the underlying pathology (FTLD subtype) in individuals with sporadic FTD syndromes, as there is significant heterogeneity and lack of clinicopathological correlation (Figure 1.1). Although nfvPPA is more commonly associated with FTLD-tau, and FTD-MND is mostly due to FTLD-TDP, bvFTD is particularly heterogeneous pathologically (Figure 1.1) (Rohrer et al., 2011). Adding to this complexity, some individuals presenting with bvFTD, PPA or CBS instead have AD pathology (particularly those with lvPPA), or other neurodegenerative pathologies such as Lewy bodies, or mixed pathology (FTLD and AD, or concurrent vascular pathology). The exceptions are svPPA, which is almost always due to FTLD-TDPC, young onset bvFTD with caudate atrophy, which is rare and due to aFTLD-U, and PSPS, which is often a tauopathy (typically FTLD-PSP) (Rohrer et al., 2011) (Figure 1.1).

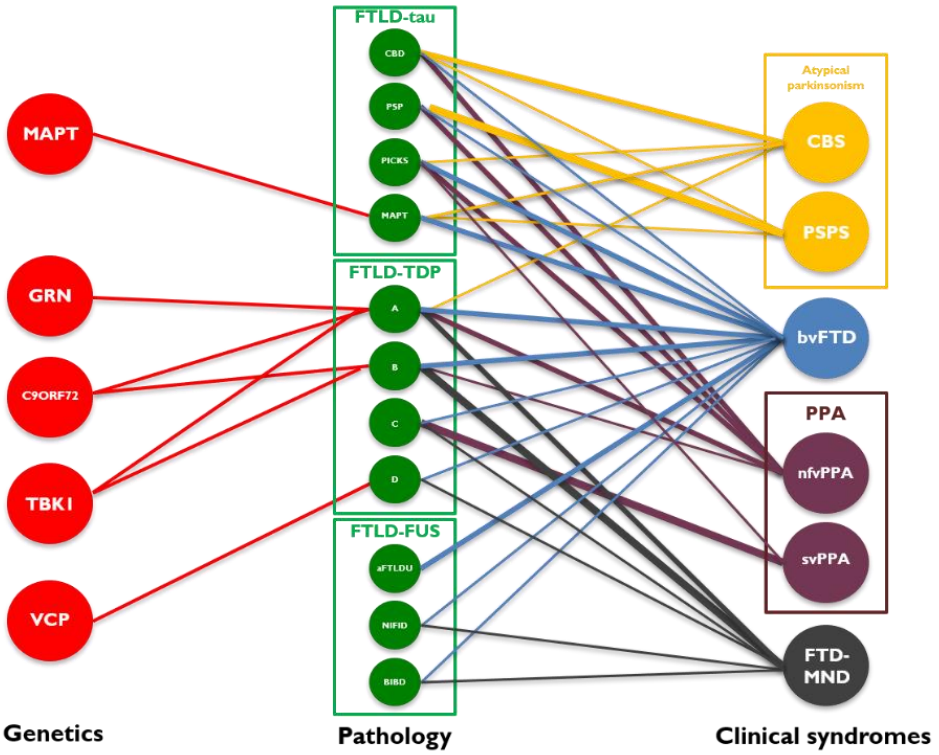

Figure 1.1 The clinical, genetic and pathological heterogeneity of FTLD

Figure adapted with permission from a figure produced by Dr J. Rohrer. LvPPA is not shown within the PPA box, but in 30% cases is due to FTLD and in 70% cases due to AD pathology. Rare mutations not shown.

In contrast to sporadic FTD, individuals with genetic FTD have good clinicopathological correlation (Figure 1.1). FTLD due to *GRN* mutations (FTLD-*GRN*) is almost universally FTLD-TDPA, and FTLD due to *C9orf72* expansions (FTLD-*C9orf72*) is either FTLD-TDPA or FTLD-TDPB, although FTLD-TDPB is more common and more often associated with MND (Lashley et al., 2015). FTLD-*C9orf72* cases also display ubiquitin-positive, p62/sequestesome-1-positive, TDP-43-negative inclusions, comprised of DPRs, predominantly in cerebral and cerebellar cortices, hippocampi, basal ganglia and thalami (Mahoney et al., 2012). FTLD due to *MAPT* mutations (FTLD-*MAPT*) is either neuronal and glial tau pathology with predominant 4R tau (if mutations affect the splicing of exon 10), or predominant neuronal inclusions comprised of 3R tau with Pick bodies or mixed 3R and 4R tau with AD-like neurofibrillary tangles (NFTs) of tau (if mutations affect exons 9, 11, 12 or 13) (Mackenzie and Neumann, 2016). *TBK1* mutations lead to FTLD-TDPA or FTLD-TDPB (Koriath et al., 2017), *VCP* mutations lead to FTLD-TDPD, and

CHMP2B mutations lead to FTLD-UPS (Lashley et al., 2015). It remains unclear why these mutations lead to these specific patterns or types of pathology and why these often affect different brain regions.

1.2 Biomarkers for FTD

1.2.1 Why biomarkers are needed

The clinical heterogeneity of FTD means that is often challenging to establish a firm, early diagnosis or advise accurately on prognosis in those already symptomatic with FTD. It is also difficult to predict accurately the timing of disease onset (and symptom onset) in individuals at risk of genetic FTD who carry a causative gene mutation but are yet to develop symptoms, called presymptomatic mutation carriers (PMC). The overlap between several bvFTD symptoms and psychiatric presentations, prominent early episodic memory deficits or parkinsonism in some individuals with FTD, and sometimes subtle atrophy patterns, can lead to an initial misdiagnosis of a psychiatric disorder or an alternative neurodegenerative disease. This can lead to unnecessary, ineffective, and sometimes harmful treatments, inaccurate prognostication and missed opportunities to identify a potentially inheritable disease, which is important for other family members.

The lack of clinicopathological correlation in most sporadic FTD syndromes makes selection of future disease-modifying treatments that will target specific pathologies or disease mechanisms incredibly challenging. Despite a wealth of studies on FTD and FTLD, much remains unknown about the cause of the disease. It is unclear how or whether the hallmark protein aggregations of FTLD lead to neuronal death, what other processes contribute to this, and how quickly this will progress over time in an individual. This has led to an intensive search for biomarkers of the disease process and underlying pathologies across clinical, neuropsychological, neuroimaging and biofluid fields.

A biomarker is “a characteristic that is measured as an indicator of normal biological processes, pathogenic processes or responses to an exposure or intervention” (National Institutes of Health and Food and Drug Administration Biomarker Working Group, 2016). Biomarkers can be used for different purposes, including diagnosis, prognosis, assessment of susceptibility or risk, prediction, monitoring, safety and measurement of pharmacodynamic or other responses (Califf, 2018). By studying a variety of biomarker modalities in individuals with FTD we can gain insights into how these correlate with specific clinical presentations, disease trajectories, underlying pathologies and disease mechanisms, and with each other.

If a biomarker changes well before symptom onset, this could be used to help predict disease proximity (how close an individual is to the beginning of the disease process, and when symptoms will first occur) in those at risk of FTD, which is vital for PMC. This would help to guide when it is best to intervene with disease modifying treatments in clinical trials, to minimise or prevent neurodegeneration. In symptomatic individuals, prognostic biomarkers that indicate disease intensity (how fast a disease will progress) or survival are vital for determining the disease trajectory, allowing better planning for the future. Biomarkers indicative of the underlying pathological subtype (for example FTLD-TDP versus FTLD-tau) would allow an earlier firm diagnosis of FTD *in vivo*, followed by better targeting of novel treatments designed to ameliorate specific pathologies. Biomarkers of other disease processes, such as immune, lysosomal, mitochondrial and synaptic dysfunction, which are all linked to neurodegenerative diseases in general, may aid understanding of what contributes to neuronal death in FTD, when these processes occur, and which pathways can be targeted to ameliorate this. Finally, biomarkers of treatment response are urgently needed for upcoming clinical trials, which are currently focused on individuals with genetic FTD and PMC, as current neuroimaging and neuropsychological measures are not always sensitive to subtle

changes over time, particularly in PMC who are many years away from their estimated onset.

1.2.2 CSF biomarkers for FTD

Due to the focus of this thesis on biomarkers detectable in CSF, this section will summarise findings from FTD studies on biomarkers of neurodegeneration or underlying pathology detectable in CSF. An overview of inflammatory biomarkers is presented later on.

CSF is a clear colourless fluid, which lies within the subarachnoid space of the brain and spinal cord between the arachnoid mater and the pia mater, supporting the brain in a 'cushion' of fluid. CSF is produced within the choroid plexus of the lateral, third and fourth ventricles of the brain, by a combination of passive filtration of plasma across the choroidal capillary endothelium and active secretion of water, ions and macromolecules across a single-layered epithelium (Johanson et al., 2008). Normally, approximately 500ml is produced in 24 hours and usually there is around 150ml of CSF surrounding the brain and spinal cord. CSF constantly passes through the ventricular system, following a pressure gradient between cerebral and spinal blood vessels and choroidal interstitial fluid (Johanson et al., 2008). CSF is reabsorbed through arachnoid villi into blood or diffuses along a series of perivascular channels within the glymphatic system, re-entering into blood vessels. Normally, CSF and blood are separated by the blood-brain barrier (BBB), a layer comprised of tight junctions between endothelial cells and astrocytes. This allows transport of small, lipid soluble molecules but prevents passage of larger or insoluble molecules. As well as physically protecting the brain, CSF aids nutrition (by transporting glucose) and removal of waste products and allows diffusion of molecules involved in the immune response between cells.

Biomarkers in CSF are particularly useful as they aid understanding of the biological processes contributing to neurodegeneration and levels can be assessed repeatedly over time using standardised quantification techniques, which is vital for clinical trials. Although obtaining blood samples for plasma or serum analysis is less invasive than obtaining CSF, biomarkers in CSF more closely reflect the intracerebral milieu. Brain derived proteins and metabolites are present in greatest concentration in CSF because of its proximity to the brain, and other factors such as the BBB, the peripheral immune system, proteases, or large plasma proteins (which bind smaller molecules) have less of an effect on biomarker levels in CSF than in blood.

In individuals with AD, there are several pathology-linked biomarkers detectable in CSF, including Aβ42, P-tau, and T-tau, which reflect Aβ deposition in plaques, hyperphosphorylated tau in NFTs, and neuronal injury, respectively. In combination, these can reliably differentiate AD from controls or other causes of dementia, but discussion of the sensitivity and specificity of these biomarkers in differentiating AD from FTD and other disorders is outside the scope of this thesis. Low Aβ42 and raised P-tau levels are particularly indicative of AD, as raised T-tau can be found in other dementia syndromes, including FTD (Olsson et al., 2016). The CSF T-tau/Aβ42 ratio is often used in clinical practice to differentiate individuals with AD from other diagnoses, with a raised ratio (often ≥1.0) in AD, but P-tau/Aβ42 and Aβ42/Aβ40 ratios may also be useful (Gossye et al., 2019). Aβ42, T-tau and P-tau levels are not generally useful for differentiating between clinical or pathological FTD subtypes (Ljubenkov et al., 2018). However, the CSF P-tau/T-tau ratio is lower in most clinical FTD syndromes than controls, particularly FTD-MND (Meeter et al., 2018), and FTLD-TDP cases have a lower P-tau/T-tau ratio than FTLD-tau cases (Abu-Rumeileh et al., 2018; Ljubenkov et al., 2018; Meeter et al., 2018). Surprisingly, CSF T-tau levels are not consistently higher in

FTLD-tau cases when compared with controls (Bian et al., 2008) or FTLD-TDP cases (Foiani et al., 2019).

Several studies have tried to detect biomarkers indicative of specific pathological inclusions, including TDP-43 and tau isoforms, in biofluids from patients with FTD, but results have not been promising. Most studies have lacked pathologically confirmed FTLD cases or combined clinical subtypes in groups. Quantification of TDP-43 isoforms in CSF has been difficult due to post-translational modifications of TDP-43, low concentrations in CSF, low antibody binding and contamination from TDP-43 in blood. Studies of tau isoforms in CSF have been very limited. CSF TDP-43 results have been highly variable: higher levels of full-length TDP-43 were detected in CSF of clinically diagnosed FTD or MND cases compared with controls (Steinacker et al., 2008), but lower full length and phosphorylated TDP-43 levels were detected in CSF of FTLD-TDP cases compared with controls, with similar levels in FTLD-TDP and FTLD-tau cases (Kuiperij et al., 2017). Although a recent study identified several novel tau species raised in CSF of FTLD-tau cases compared with controls, none reliably differentiated between individuals with likely FTLD-tau versus FTLD-TDP (Foiani et al., 2019).

Neurofilament light chain (NfL), which is a protein released by degenerating myelinated axons, is the most promising biomarker so far for monitoring and prognosis of FTD. CSF NfL levels are higher in FTD than controls, with less consistent findings of higher levels in FTD compared with AD cases (Abu-Rumeileh et al., 2018; De Jong et al., 2007; Landqvist Waldö et al., 2013; Pijnenburg et al., 2007; Skillbäck et al., 2014). However, CSF NfL levels are elevated in a variety of other disorders, including AD (Zetterberg et al., 2016), HD (Byrne et al., 2018b), MND (Tortelli et al., 2012), vascular dementia (Skillbäck et al., 2014) and multiple sclerosis (Teunissen et al., 2005), so are not specific for FTD. CSF NfL levels cannot reliably differentiate between clinical FTD syndromes,

except for FTD-MND, which is associated with very high levels (Abu-Rumeileh et al., 2018; Meeter et al., 2018a). CSF NfL levels may link to the underlying pathology, as higher levels were present in FTLD-TDP than FTLD-tau cases in one study (Abu-Rumeileh et al., 2018), although this may have been due to inclusion of many FTD-MND cases in the FTLD-TDP group, as others contradict this (Meeter et al., 2018). In sporadic FTD, CSF NfL levels are associated with disease severity (Skillbäck et al., 2014), intensity (Ljubenkov et al., 2018) and survival (Skillbäck et al., 2014), albeit not in svPPA (Ljubenkov et al., 2018; Meeter et al., 2019), and serum NfL levels correlate with disease intensity (Rohrer et al., 2016). Therefore, although CSF or serum NfL levels may be useful to monitor disease and predict trajectories in some individuals with confirmed FTD, their use in the differential diagnosis of FTD and predicting the underlying pathology in sporadic disease remains limited.

Studying biomarkers of neurodegeneration in genetic FTD cohorts (both patients and PMC) provides a unique opportunity to examine how these are altered in individuals with known pathology and many years before predicted onset of symptoms. CSF (Meeter et al., 2016a) and serum (van der Ende et al., 2019) NfL levels vary by mutation type and change presymptomatically in genetic FTD, and CSF NfL levels are useful measures of disease severity, progression and survival (Meeter et al., 2016a). CSF and serum NfL levels are higher in patients with *GRN* mutations than with *MAPT* or *C9orf72* mutations, suggesting greater axonal degeneration associated with *GRN* mutations (Meeter et al., 2016a; van der Ende et al., 2019). Although PMC of *GRN* mutations have similar CSF and serum NfL levels to non-carriers, levels rise sharply in PMC in the peri-symptomatic phase (converters), suggesting they can be used as a biomarker of immediate disease proximity (Meeter et al., 2016a; van der Ende et al., 2019). CSF NfL levels are also raised in patients and PMC with *CHMP2B* mutations compared with non-carriers, with higher levels in patients than PMC (Rostgaard et al., 2018). In conclusion, NfL is clearly a useful

biomarker for several purposes in genetic FTD, but levels may not rise early enough in PMC to enable early prediction of disease proximity, which limits use in clinical trials.

Levels of other CSF biomarkers are altered in specific genetic FTD subtypes, due to effects of the mutation itself. CSF (Meeter et al., 2016b) and plasma (Finch et al., 2009; Meeter et al., 2016b) progranulin levels are reduced to 25-40% of normal levels in patients with *GRN* mutations and *GRN* PMC, compared with non-carriers. Although low plasma levels are diagnostic of a pathogenic *GRN* mutation, there is poor correlation between CSF and plasma levels (Meeter et al., 2016b), so CSF levels may be more useful to assess the effects of treatments aimed at increasing progranulin levels in the brain. Although CSF T-tau levels are not raised in patients with *MAPT* mutations compared with controls (Rosso et al., 2003a), plasma tau levels are higher in patients with *MAPT* mutations (but not *GRN* or *C9orf72* mutations) (Foiani et al., 2018) than controls, but have not been examined in *MAPT* PMC. Levels of certain DPRs including poly(GP) are raised in CSF of patients with FTD or MND due to *C9orf72* expansions, and in *C9orf72* PMC, compared with non-carriers (Lehmer et al., 2017; Meeter et al., 2018b). Although one study found higher levels in patients than PMC (Meeter et al., 2018b), others have found similar levels (Lehmer et al., 2017). However, CSF progranulin and poly(GP) levels are altered for many years before symptom onset, remain fairly constant over time (Lehmer et al., 2017; Meeter et al., 2018b; Meeter et al., 2016b), and do not correlate with disease intensity or survival (Lehmer et al., 2017). They may be better for assessing response to therapeutic interventions, rather than for predicting disease proximity or trajectories.

Due to a lack of pathology-specific biomarkers and neurodegenerative biomarkers which change early enough in the presymptomatic period in sporadic and genetic FTD, research has focused on exploring biomarkers of contributory mechanisms to

neurodegeneration, particularly chronic neuroinflammation. Increasing evidence suggests that chronic neuroinflammation and glial cell dysfunction contribute to FTD, and this may be particularly relevant for genetic FTD due to *GRN* mutations, more so than the general neuroinflammatory dysregulation seen associated with multiple other neurodegenerative diseases, as progranulin regulates microglial function. Detailed exploration of different aspects of neuroinflammation and microglial dysfunction in FTD may therefore tackle the challenges outlined above and identify promising processes or biomarkers for further study. The next section summarises current evidence for the role of neuroinflammation in FTD, including inflammatory biomarkers.

1.3 Neuroinflammation in FTD

1.3.1 Neuroinflammation and neurodegeneration

Although chronic neuroinflammation is linked to a variety of neurodegenerative diseases, transient neuroinflammation is a normal physiological response within the central nervous system (CNS) to toxic, infectious, or other harmful insults. Neuroinflammation involves activation of the innate CNS immune system, which primarily involves microglia and astrocytes, and release of a cascade of proinflammatory factors such as cytokines, chemokines and complement molecules, which affect neurons, glial cells and the CNS microenvironment (Bright et al., 2019). This process is tightly controlled and usually self-limiting, as the CNS feeds back to the immune system to limit ongoing inflammation once the insult has been managed. However, excessive, uncontrolled, or chronic neuroinflammation can lead to progressive synaptic and neuronal loss due to persistent activation of glial cells and sustained release of proinflammatory molecules, which also impair synaptic and neuronal function. A proinflammatory milieu can also disrupt the BBB, allowing migration of peripheral immune cells such as T and B lymphocytes into the CNS. These may worsen neuronal and synaptic damage through the adaptive immune response, involving both cell-mediated and antibody-mediated cytotoxicity.

It remains unclear whether chronic neuroinflammation is a primary event that triggers neurodegenerative disease, or is secondary to evolving protein aggregation and neurodegeneration, or both. However, increasing evidence implicates chronic neuroinflammation and central and systemic immune dysfunction in FTD, and proposes that these processes are involved early on in its pathogenesis (Bright et al., 2019).

1.3.2 Genetic evidence of neuroinflammation in FTD

As progranulin directly regulates inflammatory pathways and microglial function, research in the FTD field has focused on establishing the link between *GRN* mutations, neuroinflammation and neurodegeneration. Several mouse models suggest that progranulin deficiency produces systemic and CNS immune dysregulation (particularly microglial dysfunction) and that this contributes to neuronal loss and FTD-like symptoms. Homozygous *GRN* knockout (-/-) mice have excessive numbers of activated microglia or astrocytes (Ahmed et al., 2010; Lui et al., 2016; Martens et al., 2012; Tanaka et al., 2013a, 2013b, 2014; Wils et al., 2012; Yin et al., 2009, 2010), excessive release of proinflammatory cytokines such as TNF-α (Minami et al., 2015), inflammatory arthritis (Tang et al., 2011), poor response to bacterial infection (Yin et al., 2010) and sepsis (Song et al., 2016), and exaggerated neuronal damage in response to traumatic brain injury (Minami et al., 2015). Progranulin deficient microglia produce excess proinflammatory cytokines and display heightened phagocytic responses, leading to excessive synaptic pruning, heightened neuronal loss, obsessive-compulsive-like behaviour (excessive grooming) and early death in mice (Lui et al., 2016). As this can be ameliorated by blocking activation of complement (Lui et al., 2016), innate immune pathways and microglial dysfunction seem to be key drivers of neurodegeneration in *GRN* models.

However, *GRN* -/- models do not closely capitulate the effects of heterozygous *GRN* mutations in humans with FTD, and heterozygous (+/-) *GRN* mice do not show

substantial neuroinflammation or reactive changes in microglia (microgliosis), although they do have similar behavioural deficits to *GRN* -/- mice (Filiano et al., 2013). Homozygous *GRN* mutations in humans cause a lysosomal storage disorder called neuronal ceroid lipofuscinosis, which leads to cognitive and visual impairment, epilepsy and ataxia (Smith et al., 2012), associated with microglial lipofuscin accumulation (Götzl et al., 2014; Ward et al., 2017). *GRN* cell and mouse models demonstrate that progranulin regulates microglial lysosomal function, which influences innate immune mechanisms (Evers et al., 2017; Götzl et al., 2014; Marschallinger et al., 2020; Nguyen et al., 2018; Tanaka et al., 2014; Wils et al., 2012). However, human heterozygous *GRN* mutation carriers with FTD do display evidence of systemic immune dysregulation, including an increased prevalence of systemic autoimmune diseases, raised serum TNF-α levels (Miller et al., 2013), and increased expression of immune genes linked to systemic autoimmune diseases in *post-mortem* brain tissue, particularly within microglia (Broce et al., 2018).

Mouse models of the *C9orf72* expansion also develop altered neuroinflammation and systemic autoimmunity: *C9orf72* -/- and C9orf72 deficient mice display microglial lysosomal dysfunction, excess peripheral T cell activation, elevated levels of proinflammatory cytokines (IL-17 and IL-23), splenomegaly, lymphadenopathy, immune-mediated kidney disease and thrombocytopaenia, and high titres of autoantibodies (Atanasio et al., 2016; Burberry et al., 2016, 2020; O'Rourke et al., 2016; Sullivan et al., 2016). Although different *C9orf72* mouse models display varying degrees of immune dysfunction, with less consistent findings than in *GRN* models, a recent study suggests there is an influence of the mouse gut microbiome on C9orf72-deficient microglia (Burberry et al., 2020). Environmental factors could therefore contribute to significant heterogeneity in immune dysfunction in *C9orf72* expansion carriers by modifying systemic and CNS inflammatory pathways.

Fewer studies of neuroinflammation have been carried out in *MAPT* models. *MAPT* P301S mice display marked microgliosis around tau aggregates (Bellucci et al., 2004), with microglial activation and synaptic loss preceding tangle formation (Yoshiyama et al., 2007). Several histological and microglial PET studies in human *MAPT* mutation carriers also suggest heightened microglial activation, particularly in the temporal lobes (Bellucci et al., 2011; Bevan-Jones et al., 2019; Lant et al., 2014; Miyoshi et al., 2010), including presymptomatically (Bevan-Jones et al., 2019; Miyoshi et al., 2010); these are discussed later on.

Other genes less commonly associated with FTD are also involved in neuroinflammation. *TBK1* activates NF-κβ-mediated pathways, controlling multiple genes including interferon-gamma (IFN-γ), but is also involved in autophagy by interacting with *OPTN* and *SQSTM1* (other FTD and MND linked genes) (Ahmad et al., 2016). *TBK1* mutant mice develop raised serum IL-6 and TNF-α levels and infiltration of immune cells into multiple tissues (Marchlik et al., 2010). Human *CHMP2B* mutation carriers with FTD and *CHMP2B* mice display excessive microgliosis, which precedes neuronal loss and is accompanied by increased expression of IL-1β and TNF-α in mouse brain tissue (Clayton et al., 2017). Individuals with homozygous *TREM2* mutations linked to FTD-like syndromes have reduced TREM2 cell surface expression and impaired microglial phagocytosis (Kleinberger et al., 2014).

Genome wide association studies (GWAS) implicate the adaptive immune system in the pathogenesis of FTD. GWAS in a mixed FTD cohort (Ferrari et al., 2014) and sporadic FTD cases (Ferrari et al., 2017) have identified associations of FTD with polymorphisms in loci within human leucocyte antigen (*HLA*) genes, which encode major histocompatibility complex (MHC) molecules involved in antigen presentation by macrophages and microglia. Another GWAS in FTLD-TDP cases without known gene

mutations identified risk variants in *HLA-DQA2* and in several genes linked to the *TBK1*-mediated immune pathway, implicating systemic immune dysfunction in FTLD-TDP pathogenesis (Pottier et al., 2019). Yet another GWAS in individuals with FTD identified polymorphisms in immune genes (predominantly in the *HLA* region) also linked to systemic autoimmune diseases, including rheumatoid arthritis, psoriasis, type 1 diabetes, coeliac disease and ulcerative colitis (Broce et al., 2018). Expression of immune genes (including *HLA*) was also increased in *post-mortem* brain tissue from a mixed FTLD cohort, and particularly enriched within microglia in cases with *GRN* mutations (Broce et al., 2018), further strengthening the link between systemic and CNS immune dysfunction in FTD, particularly in *GRN* mutation carriers.

1.3.3 Microglia in FTD

1.3.3.1 The role of microglia in neurodegeneration

"It is sufficient to find the microglial alterations to recognise the areas more deeply affected by the disease" (del Rio Hortega, 1932)

Nearly 100 years ago, the neuropathologist Pio del Rio Hortega established that understanding changes in microglia was vital for understanding neurodegenerative disease, and that abnormalities in microglia occurred wherever there was neurodegenerative pathology. Since then, histological studies of microglia in *post-mortem* brain tissue have provided useful information about how the number (or burden) of microglia, and the appearance of microglia (morphology, often used to assess activation state), are altered in individuals with a variety of neurodegenerative diseases.

As microglia are the primary innate immune cells of the CNS, it is important to understand their usual function, and hence how dysfunction may contribute to neurodegeneration.

Microglia arise from macrophage progenitors within the yolk sac during embryonic development. They undergo constant self-renewal, maintaining a steady population of microglia throughout life (Ajami et al., 2007), and exert their functions through diverse phenotypes and morphologies (Streit et al., 2014). During constitutive homeostatic activity in the brain, microglia appear 'ramified', with a small body and extensively branched, long processes (Boche et al., 2013; Torres-Platas et al., 2014). However, ramified cells are not resting; they constantly survey the environment, prune synapses and liaise with other glial cells (astrocytes and oligodendrocytes) to support and influence the function of neurons (Boche et al., 2013).

Following insults such as external pathogens, misfolded proteins or dying neurons, ramified microglia respond to proinflammatory molecules and become primed to react to further inflammatory triggers. Their morphology rapidly changes, with a retraction of processes and enlargement of the cell body, initially becoming 'bushy' and hypertrophic. With persistent stimulation they become activated, with a rounded, 'amoeboid' shape, displaying no or few unbranched processes (Boche et al., 2013; Torres-Platas et al., 2014). Activated microglia migrate towards the insult, proliferate, and produce further proinflammatory cytokines, chemokines and reactive oxygen species, and activate complement production, contributing to a state of neuroinflammation. Proinflammatory cytokines and chemokines can recruit additional microglia to encourage destruction and clearance of the insult. Activated microglia phagocytose pathogens, proteins, synapses and neurons, and can present antigens to other glial cells and to systemic immune cells (T or B lymphocytes and macrophages) which may infiltrate the CNS (Boche et al., 2013). This promotes further phagocytosis through an antibody-mediated, adaptive immune response. These functions are vital for the protection of, and maintenance of homeostasis within, the brain. However, persistent activation of microglia and the CNS immune pathways leads to a state of chronic neuroinflammation. This is thought to

compound protein aggregation, promote excessive phagocytosis and worsen neuronal and synaptic damage.

In individuals with pre-clinical AD pathology (without dementia), activated microglia mainly surround Aβ aggregates, with few activated microglia elsewhere, despite plentiful tau pathology (which precedes Aβ deposition) (Streit et al., 2018). In many *post-mortem* histological studies of humans with later stage AD, there does not seem to be the widespread microgliosis initially suggested by AD mouse models, particularly within the hippocampus (Navarro et al., 2018). This suggests that in humans with AD there is an early, protective and highly-localised inflammatory response by microglia trying to remove insoluble Aβ, rather than a generalised neuroinflammatory response to amyloid pathology. Microglial activation may be variably involved in different stages of AD, with microglia reacting differently to different pathologies (Gentleman, 2013).

There is now a concept of diseased, dysfunctional, senescent microglia contributing to aging and neurodegenerative disease. As microglia undergo repeated self-renewal and telomere shortening throughout the lifetime, they are vulnerable to replicative senescence, becoming dysfunctional and degenerative with age (Streit et al., 2014). Senescent cells are detected histologically as dystrophic microglia, which have abnormal morphology: thin, short and few distal branches (deramification), shortened, tortuous or beaded cell processes, fragmented cytoplasm, and spheroidal inclusions (rounded swellings) (Streit et al., 2004). Dystrophic microglia are seen in the healthy aging brain but are rare in younger brains (Bachstetter et al., 2015; Davies et al., 2017; Grabert et al., 2016; Lopes et al., 2008; Streit et al., 2004, 2009), supporting a notion of increasing microglial dysfunction with age. However, they are seen more commonly in individuals with neurodegenerative disease, especially AD (Bachstetter et al., 2015; Davies et al., 2017; El Hajj et al., 2019; Lopes et al., 2008; Navarro et al., 2018; Sanchez-Mejias et al.,

2016; Streit et al., 2009, 2014, 2018; Tischer et al., 2016) and DLB (Bachstetter et al., 2015), and in hippocampal sclerosis (Bachstetter et al., 2015). Dystrophic microglia are also present in mouse models of HD (Johnson et al., 2015; Simmons et al., 2007). This suggests that by the end stage of a variety of neurodegenerative diseases, many microglia are dysfunctional and senescent. It remains unclear when, and to what extent, microglial senescence occurs in relation to microglial activation and development of neuropathology, or how this contributes to neurodegeneration.

1.3.3.2 Microglial markers

To understand the role of various microglial phenotypes and morphologies in neurodegenerative disease, one must first appreciate the heterogeneous populations of microglia present within the human brain, and how different techniques can be used to detect these.

Previously, microglia were thought to exist in one of two polarised activation states in the human brain: an M1 pro-inflammatory 'classical activation' phenotype, induced by TNF-α or IFN-γ, promoting release of further proinflammatory molecules including TNF-α or IL-1β, or an M2 anti-inflammatory 'alternative activation' phenotype, induced by anti-inflammatory molecules such as IL-4, IL-10 or TGF-α, releasing healing and trophic molecules such as TGF-β or BDNF to promote wound healing and clearance of debris (Cherry et al., 2014). Early studies tried to detect these molecules in brain tissue. However, this classification is rather artificial; instead, microglia exist along a continuum of activation states and phenotypes (Hu et al., 2015; Walker and Lue, 2015). Specific phenotypes such as 'disease-associated microglia' or 'damage-associated microglia' have been identified in mouse models of neurodegenerative diseases, particularly AD (Keren-Shaul et al., 2017), but these differ significantly from human microglial phenotypes (Friedman et al., 2018). It is now clear that there are several distinct populations of microglia present at any one time within a brain region, and that a

microglial cell may adopt several different phenotypes and morphologies, with evolution between these (Bonham et al., 2019; Böttcher et al., 2018; Grabert et al., 2016). It may therefore be the development of a predominant microglial phenotype or activation state, failure of microglia to transition between phenotypes or states, or predilection of a certain phenotype for premature senescence, which over time leads to neuronal damage, lack of neuronal support and accelerated neurodegeneration. This could occur in a region-specific manner within the brain, which may underlie variations in regional vulnerability seen across neurodegenerative diseases.

Microglia can be detected in histological studies by performing immunohistochemistry on fixed sections of brain tissue. Other techniques include quantification of protein or mRNA expressed by microglia or RNA sequencing of microglial cells within frozen brain tissue. Immunohistochemistry uses antibodies to detect antigens (histochemical markers) expressed by microglial cells with differing functions (phenotypes) and in different activation states. Immunohistochemistry has the advantage of allowing detailed anatomical localisation and quantification of microglia and appreciation of the range of microglial phenotypes and morphologies *in situ* in different brain regions. Microglial burden can be assessed in each region through automated or visual manual cell counts of cells stained with different antibodies, or qualitative or quantitative measurements of area stained or staining intensity. Microglial morphology can be examined qualitatively (visual scoring of cell appearances) or quantitatively to appreciate different activation states and degrees of dystrophy. Many different microglial markers exist, but antibodies directed against the following three markers have been most commonly used in human brain tissue: cluster of differentiation 68 (CD68), human leucocyte antigen-D related protein-R (HLA-DR), and ionised calcium-binding adapter molecule 1 (Iba1) (Boche et al., 2013; Hopperton et al., 2018).

CD68 is an intracellular transmembrane bound glycoprotein expressed within the lysosomal, endosomal and plasma membranes of microglia and macrophages (da Silva and Gordon, 1999). Although CD68 is expressed on ramified microglia, it is commonly thought of as a marker of activated microglia as it is upregulated on microglia with phagocytic properties and more easily detects lysosomes within the centre of activated, amoeboid microglia than the sparse lysosomes within more ramified microglial cell processes (Boche et al., 2013). The CD68 antibody is widely used to detect phagocytic microglia in mouse models of neurodegenerative disease and in human brain tissue (Hopperton et al., 2018).

HLA-DR is an MHC class II molecule, which are glycoproteins expressed on the surface of cells with antigen-presenting function, and also include HLA-DP and HLA-DQ. These molecules enable cells to present processed extracellular antigens to T lymphocytes and other immune cells (Hendrickx et al., 2017). In the CNS, they are expressed by microglia, but not by oligodendrocytes or astrocytes (Streit et al., 2014). They are mainly expressed on the cell body and processes of activated microglia but are also expressed constitutively by ramified microglia (Gehrmann et al., 1993). Antibodies which detect these molecules have been used extensively in histological studies of microglia in AD (Hopperton et al., 2018), often using the anti-HLA-DR antibody (Gehrmann et al., 1993), or the CR3/43 antibody, which detects HLA-DP, HLA-DQ and HLA-DR (Graeber et al., 1994). This allows detection of microglia with antigen-presenting properties in activated and ramified states (Hendrickx et al., 2017; Lopes et al., 2008; Streit et al., 2004).

Iba1 is an intracellular calcium-binding protein constitutively expressed within the cytoplasm of ramified microglia (Ito et al., 1998; Sasaki et al., 2001). It is upregulated on activated microglia (Ito et al., 1998; Streit et al., 2009) but detects all microglial cells. Iba1 may play a role in actin-cross linking (Sasaki et al., 2001), and in microglial motility and

phagocytosis through membrane ruffling (Ohsawa et al., 2000). The Iba1 antibody allows comprehensive assessment of microglial morphology as it fully stains cell bodies and processes and is robust to variations in *post-mortem* delay, tissue fixation and processing protocols (Streit et al., 2009, 2014; Torres-Platas et al., 2014). Iba1 is therefore commonly used to differentiate between microglial morphologies, including ramified, hypertrophic, amoeboid or rod-shaped microglia (Bachstetter et al., 2015, 2017; Torres-Platas et al., 2014), and to identify microglial dystrophy (Bachstetter et al., 2015; Davies et al., 2017; Streit et al., 2009, 2014, 2018; Tischer et al., 2016).

All of these 'microglial markers' are also expressed by macrophages, so may detect perivascular macrophages in the CNS or infiltrating peripheral macrophages or monocytes within brain tissue, as well as microglia. More recently, markers have been identified which are more exclusively expressed by microglia, such as the purinergic receptor P2Y12 (P2RY12), the chemokine receptor CX3CR1, transmembrane protein 119 (TMEM119) and TREM2 (Butovsky et al., 2014; Sarlus and Heneka, 2017). However, most human and mouse histological studies have used CD68, HLA-DR, CR3/43 or Iba1 antibodies to detect microglia, and these remain invaluable for examination of different microglial phenotypes, activation states and morphologies.

Although many studies have examined only one microglial marker, there is no single marker that can reliably differentiate microglial phenotypes (Streit et al., 2014). One study therefore used antibodies against several markers, including CD68, HLA-DR and Iba1, to analyse microglia in AD cases and controls (Minett et al., 2016). This demonstrated that there were different patterns for each marker: there was an increase in CD68-positive microglia, but reduction in Iba1-positive microglia, in AD cases, suggestive of increased phagocytosis but reduced motility. Another study concluded that HLA-DR and CD68 were useful for assessing microglial activation and response to tissue damage in

AD cases, but Iba1 was more useful for detailed assessment of microglial morphology (Hendrickx et al., 2017). Using several of these antibodies sequentially in the same region, combined with morphological assessment of microglia, may therefore more comprehensively examine regional patterns of microglial burden, activation and dystrophy in individuals with neurodegenerative disease.

1.3.3.3 Microglia in FTD – histological studies

Most histological evidence for microglial involvement in FTD has arisen from mouse models of genetic FTD. *GRN* -/- or progranulin deficient mice display excessive numbers of activated microglia, including more amoeboid CD68-positive (Lui et al., 2016; Tanaka et al., 2013a, 2013b; Yin et al., 2009, 2010), or Iba1-positive (Ahmed et al., 2010; Lui et al., 2016; Martens et al., 2012; Wils et al., 2012) microglia. *C9orf72* -/- or C9orf72 deficient mouse models also display microglial activation and dysfunction, including more amoeboid CD68 or Iba1-positive microglia (Atanasio et al., 2016; Burberry et al., 2020; O'Rourke et al., 2016), with enlarged lysosomes (Schludi et al., 2017). Mouse models of the *MAPT* P301S mutation display marked microgliosis around tau aggregates (Bellucci et al., 2004), with activated HLA-DR-positive microglia and synaptic loss preceding tangle formation in the hippocampus (Yoshiyama et al., 2007). Mice with *CHMP2B* mutations have an early increase in Iba1-positive microglia in the hippocampus and thalamus, preceding neuronal loss and behavioural deficits (Clayton et al., 2017). Although mouse models of genetic FTD may not always accurately recapitulate processes in the human brain, these studies suggest that microglial and neuroinflammatory dysfunction contribute to synaptic and neuronal loss at an early stage of disease.

Although early histological studies of humans with FTLD noted extensive microgliosis and astrocytosis (Arnold et al., 2000; Cooper et al., 1996; Englund and Brun, 1987; Kersaitis et al., 2004; Mann, 1998; Martinac et al., 2001; Neary et al., 1998; Paulus et

al., 1993; Schofield et al., 2003) relatively few studies have examined patterns of microglia in FTLD cohorts. Only one study has examined microglial burden and activation across the spectrum of FTLD, compared with AD cases and controls (Lant et al., 2014). FTLD cases had more numerous and/or more activated CD68-positive microglia in frontal and temporal grey matter and white matter than controls. In FTLD cases, microglia were more numerous and/or more activated in white matter compared with grey matter, but in AD cases the reverse was present, suggesting microglial dysfunction may particularly affect white matter in FTLD.

Smaller histological studies have examined microglia in specific subtypes of sporadic FTLD, mainly FTLD-TDP (Bevan-Jones et al., 2020; Kim et al., 2018a, 2018b; Mao et al., 2019; Nilson et al., 2017; Ohm et al., 2018; Taipa et al., 2017). Microglial burden and/or activation varied across the spectrum of FTLD-TDP, both regionally and between grey and white matter, and regional patterns of microglial changes correlated with clinically affected areas and neuroimaging changes, sometimes preceding onset of neurodegenerative pathology. In addition, a proteomic study of frontal cortex tissue from patients with FTLD-TDP and either FTD, FTD-MND or MND found enrichment of microglial and RNA-binding protein modules in disease groups compared with controls, which correlated with TDP-43 burden (Umoh et al., 2017). An inflammatory module comprised of proteins expressed by microglia or astrocytes was also upregulated in those with FTD alone, compared with MND alone and controls (Umoh et al., 2017). This evidence links microglial and RNA-binding protein dysfunction to TDP-43 pathology and suggests this varies regionally according to the clinical phenotype within FTLD-TDP.

Few histological studies have explored microglia in humans with genetic FTLD, but these have shown that CD68, Iba1 or HLA-DR-positive microglia are increased, more activated or more dystrophic in FTLD-*GRN* (Chen-Plotkin et al., 2010; Kim et al., 2016; Lui et al.,

2016; Mao et al., 2019; Sakae et al., 2019b), FTLD-*MAPT* (Bellucci et al., 2011; Lant et al., 2014), FTLD-*C9orf72* (Sakae et al., 2019b) and FTLD due to *CHMP2B* mutations (Clayton et al., 2017). Patterns of CD68 or Iba1-positive microglia varied in the temporal lobe between FTLD-*MAPT* cases and FTLD-*GRN* or FTLD-*C9orf72* cases (Lant et al., 2014), and in the frontal lobe between FTLD-*GRN* and FTLD-*C9orf72* cases (Sakae et al., 2019b). A proteomic study of frontal cortex from MND patients with or without the *C9orf72* expansion identified enrichment of microglial and astrocytic modules in expansion carriers compared with non-carriers (Umoh et al., 2017). This links different FTD-associated mutations to regionally altered microglial burden, morphology and function.

These initial studies suggest that microglial activation or dysfunction may contribute to the pathogenesis of FTLD, and that this varies regionally and sub-regionally between different clinical, pathological and genetic FTLD subtypes. Early region-specific or microglial phenotype-specific variations in microglial dysfunction could contribute to regional vulnerabilities to onset of specific pathologies. Exploration of different microglial phenotypes across the full spectrum of sporadic and genetic FTLD may aid understanding of whether this contributes to the clinicopathological heterogeneity of FTLD.

1.3.3.4 Microglia in FTD – PET studies

Although histological studies provide useful information about microglia at the end stage of disease, techniques that can assess microglia *in vivo* are needed. Microglial PET brain imaging has been used in many AD mouse models and human AD cohorts, but few studies have used this technique in FTD. Most microglial PET tracers bind to translocator protein (TSPO), an 18kDa ubiquitous cholesterol transporter in the outer mitochondrial membrane of steroid-synthesising cells, including activated and ramified microglia. An early study using the TSPO radioligand ^{11}C-PK-11195 in five FTD cases and eight

controls showed increased binding in the left dorsolateral prefrontal cortex and medial temporal and subcortical regions in the FTD group (Cagnin et al., 2004). Binding matched areas of clinically relevant atrophy, but there was also binding in areas with minimal atrophy on MRI, suggesting an increased burden or activation of microglia before significant neuroanatomical changes had occurred. A recent study of 31 FTD cases (ten bvFTD, ten nfvPPA and 11 svPPA) and 15 controls who underwent PET imaging with ^{11}C-PK-11195 (to detect microglia) and a radioligand called ^{18}F-AV-1451 (which detects non-Aβ pathology) showed that there was increased ^{11}C-PK-11195 binding in frontotemporal regions of FTD cases versus controls, and a strong positive correlation between both radioligands across multiple cortical regions in all disease groups (Bevan-Jones et al., 2020). Notably, the distribution of ^{11}C-PK-11195 binding (rather than ^{18}F-AV-1451 binding) correlated more with the clinical phenotype. This suggests that the distribution of microglia correlates closely with neuropathology, but also with the clinical syndrome, and this may contribute significantly to the clinical diversity of FTLD.

As ^{11}C-PK-11195 has low sensitivity for TSPO and significant non-specific binding, novel PET tracers such as ^{11}C-PBR28 have been developed, which bind to peripheral benzodiazepine receptors (PBR) on activated and ramified microglia. A recent study found increased ^{11}C-PBR28 binding in frontal, lateral temporal, parietal and occipital cortices of four FTD cases compared with 22 controls, with binding regionally matching clinical phenotypes (bvFTD or nfvPPA) and structural and functional neuroimaging changes (Kim et al., 2019). A preliminary study of five genetic FTD cases (three *MAPT*, one *GRN* and one *C9orf72*) has also demonstrated increased ^{11}C-PBR28 binding in these cortical areas compared with controls, again matching clinically affected regions (Clarke et al., 2019).

Two studies have used microglial PET in PMC of FTD-associated mutations. ^{11}C-PK-11195 binding in a *MAPT 10+16* PMC was increased in the left anterior temporal region and both fusiform gyri, preceding significant ^{18}F-AV-1451 binding, grey matter atrophy and symptom onset (Bevan-Jones et al., 2019). Binding of ^{11}C-DAA1106 (another PBR ligand) was increased in several *MAPT N279K* PMC in multiple brain regions, although hippocampal atrophy and striatal dopaminergic dysfunction was already present (Miyoshi et al., 2010). These suggest that increased microglial burden, activation (or both) occur before significant neurodegeneration or symptoms are present in *MAPT* PMC, colocalising with pathology and eventual neuroimaging changes. However, current microglial PET tracers do not bind selectively to activated microglia, and ^{18}F-AV-1451 binds to both tau and TDP-43 inclusions and other non-Aβ pathology (Bevan-Jones et al., 2020), limiting appreciation of how microglial dysfunction is linked to regional development of specific pathologies in FTLD.

1.3.4 Inflammatory biomarkers for FTD

In further attempts to find biomarkers of neuroinflammation *in vivo*, several studies of FTD have examined levels of inflammatory biomarkers in biofluids (CSF, serum or plasma). Most have examined panels of proinflammatory cytokines or chemokines in mixed FTD cohorts, without comparing levels between clinical FTD syndromes or genetic or pathological subtypes. Unfortunately, inflammatory biomarker levels in blood are highly influenced by systemic immune or infective processes and often do not correlate well with CSF levels, so CSF levels may be more informative for neurodegenerative disease cohorts.

Previous CSF studies of inflammatory biomarkers in FTD have shown mixed results. CSF levels of the proinflammatory molecules IL-8 (Galimberti et al., 2006), IL-11 (Galimberti et al., 2008), IL-15 (Rentzos et al., 2006b), monocyte chemoattractant protein-1 (MCP-1) (Galimberti et al., 2006, 2009) and TNF-α (Sjögren et al., 2004) were

higher in patients with FTD compared with controls. However, levels of other proinflammatory cytokines including IL-6 were similar (Galimberti et al., 2008) and IL-12 were reduced (Rentzos et al., 2006a) in CSF of FTD patients versus controls, and levels of an anti-inflammatory cytokine (TGF-β) were increased in FTD cases (Sjögren et al., 2004). Few studies have analysed inflammatory biomarkers in specific FTLD subtypes, but CSF levels of Fas, eotaxin-3 and IL-17 and the neuropeptides ACTH and aguti-related peptide differentiated FTLD-TDP from FTLD-tau cases, with a sensitivity of 86% and specificity of 78% for FTLD-TDP (Hu et al., 2010b).

Although these studies suggest that there may be excess neuroinflammation in association with FTD, none of these inflammatory biomarkers is specific for FTD, as altered levels of inflammatory biomarkers in CSF are found in a variety of neurodegenerative diseases. In addition, some molecules released in the periphery (such as IL-6) can cross the BBB into the CNS, so CSF levels of these biomarkers may also be influenced by systemic inflammation. Differences in handling of samples, assays used, and types of patients included between studies have also made comparison across FTD cohorts difficult. A harmonised approach using standardised CSF collection procedures and assays in large, well-characterised FTD cohorts with known pathology (such as genetic FTD) is needed to explore this further.

Most inflammatory biomarker studies in genetic FTD have focused on individuals with FTD due to *GRN* mutations (Benussi et al., 2020; Bossù et al., 2011; Galimberti et al., 2015; Gibbons et al., 2015; Heller et al., 2020; Miller et al., 2013; Sudre et al., 2019). A study examining 27 cytokines and chemokines in CSF from ten FTD cases with *GRN* mutations, seven sporadic FTD cases and seven controls, revealed higher interferon-γ-inducible protein-10 (IP-10) and CCL5 levels, but reduced TNF-α and IL-15 levels, in *GRN* mutation carriers than in other groups (Galimberti et al., 2015). Oddly, MCP-1 levels

were higher in sporadic FTD cases (but not *GRN* mutation carriers) compared with controls. However, other studies have found raised serum TNF-α levels in sporadic FTD cases (with svPPA) compared with controls (Miller et al., 2013), and raised CSF or serum levels of TNF-α (Miller et al., 2013) and IL-6 (Bossù et al., 2011) in FTD cases with *GRN* mutations. Although results somewhat contradict each other, the general picture is one of excessive systemic and neuroinflammation in association with both sporadic and genetic FTLD-TDP. As serum IL-6 levels were higher in FTD cases with *GRN* mutations compared with *GRN* PMC (Bossù et al., 2011), there may also be progressive immune dysfunction over time.

More recently, studies have tried to focus on assessing more 'CNS specific' biomarkers of neuroinflammation in neurodegenerative disease cohorts, by examining glia-derived biomarkers (proteins arising from microglia or astrocytes) in CSF. Most have examined CSF levels of microglia-derived biomarkers, predominantly soluble triggering receptor expressed on myeloid cells 2 (sTREM2), YKL-40 (also known as chitinase-3-like protein 1, CHI3L1), and chitotriosidase (also known as CHIT1). TREM2 is an innate immune receptor expressed on the membrane of myeloid cells, including microglia and peripheral macrophages, and is upregulated on activated microglia (Schmid et al., 2002). TREM2 undergoes cleavage of its ectodomain to release a soluble fragment into the extracellular space, which is detectable in CSF and blood as sTREM2 (Kleinberger et al., 2014). sTREM2 is involved in promoting microglial proliferation, migration, activation, phagocytosis, survival, proinflammatory cytokine release and handling of lipids and apolipoproteins (Götzl et al., 2019; Zhong et al., 2017, 2019). YKL-40 is a proinflammatory molecule released predominantly by activated astrocytes (but also by microglia) into the CSF and by activated peripheral macrophages into blood, as well as by chondrocytes, fibroblasts and endothelial cells (Baldacci et al., 2017a). It stimulates production of proinflammatory cytokines and regulates microglial, astrocytic and

macrophage function, endothelial cell migration, and tumour angiogenesis. Chitotriosidase is a chitin-degrading enzyme expressed by microglia (but not by astrocytes) in CSF (Mishra et al., 2017), and by peripheral macrophages in blood (Hollak et al., 1994). It is part of the innate immune response to chitin (present in the cell walls of fungi and protozoa), but its release from activated microglia and macrophages is stimulated by multiple immune pathways, and in lysosomal storage disorders such as Gaucher's disease (Elmonem et al., 2016). Chitotriosidase induces a proinflammatory microglial phenotype, indirectly activates T helper cells and eosinophils, regulates antigen presentation, promotes cell migration, and enables fibrosis and tissue remodeling (Elmonem et al., 2016).

Although most studies have focused on assessing glia-derived biomarkers in AD cohorts, several studies have identified elevated CSF levels of sTREM2, YKL-40 and chitotriosidase in mixed FTD cohorts compared with controls (Abu-Rumeileh et al., 2019; Alcolea et al., 2014, 2017, 2018; Antonell et al., 2020; Baldacci et al., 2017b; Craig-Schapiro et al., 2010; Illán-Gala et al., 2018; Janelidze et al., 2016; Oeckl et al., 2019; Piccio et al., 2016; Steinacker et al., 2018; Teunissen et al., 2016; Vijverberg et al., 2017). Although some have found higher levels in FTD than AD, others have found similar or lower levels in FTD compared with AD. Few have compared glia-derived biomarker levels between clinical FTD syndromes or in specific FTLD subtypes, although YKL-40 levels were higher in FTLD-tau cases compared with controls (Abu-Rumeileh et al., 2019; Alcolea et al., 2017; Teunissen et al., 2016). Levels of glial fibrillary acidic protein (GFAP), which is released by activated astrocytes, are also raised in CSF, serum or plasma in sporadic FTD (Abu-Rumeileh et al., 2019; Benussi et al., 2020; Ishiki et al., 2016; Marelli et al., 2020; Oeckl et al., 2019).

Few studies have examined glia-derived biomarker levels in genetic FTD cohorts, and very few have analysed levels in PMC (Abu-Rumeileh et al., 2019; Antonell et al., 2020; Barschke et al., 2020; Benussi et al., 2020; Heller et al., 2020; Oeckl et al., 2019). Most have combined individuals with different mutations (*GRN, C9orf72* and *MAPT*) within groups, leading to non-significant differences in blood or CSF sTREM2, YKL-40 or chitotriosidase levels between patients and controls or between PMC and controls. However, two recent studies have identified raised plasma (Heller et al., 2020) and serum (Benussi et al., 2020) GFAP levels in patients with *GRN* mutations compared with controls and carriers of mutations in other genes. Importantly, GFAP levels were not raised in patients with *MAPT* mutations (Benussi et al., 2020; Heller et al., 2020) or *C9orf72* expansions (Heller et al., 2020) compared with controls, suggesting that pronounced astrocytic activation is due to progranulin haploinsufficiency itself rather than a general effect of neurodegeneration in genetic FTD.

Overall, past research suggests that neuroinflammatory biomarkers are detectable and elevated in CSF samples from individuals with sporadic and genetic FTD, but there have been few studies in this field, and minimal examination of biomarker levels in PMC. Recent studies suggest that glia-derived biomarkers may be particularly elevated in specific genetic FTD subtypes, such as *GRN* mutation carriers. Further work is needed to determine how glia-derived biomarkers are altered across the clinical, pathological and genetic spectrum of FTD, and to confirm whether and when levels change in PMC.

1.4 Thesis aims and objectives

Although previous research suggests that chronic neuroinflammation, and particularly microglial dysfunction, contributes to the pathogenesis of FTD, it remains unclear when and to what extent these processes contribute to different sporadic and genetic forms of the disease. Excessive microglial activation or senescence could be involved based on evidence from mouse models and similar studies in AD, but this has not been examined

in large, diverse FTLD cohorts. Inflammatory biomarkers in CSF, particularly glia-derived biomarkers, could be useful in future clinical trials for individuals with FTD or PMC, but these have not been examined in well-characterised sporadic FTD cohorts, compared across genetic FTD subtypes (*GRN, MAPT* and *C9orf72* mutation carriers), or assessed adequately in PMC.

To improve understanding of how neuroinflammation and microglial dysfunction is linked to FTD, this thesis therefore undertook a comprehensive research approach, employing several different modalities (clinical, histological and CSF biomarker) to analyse different aspects of systemic immune dysfunction and neuroinflammation in FTD, with a focus on microglia. Studies were carried out within large, well-phenotyped cohorts of individuals with clinically confirmed FTD or pathologically confirmed FTLD. Changes in microglia and glia-derived biomarker levels were, wherever possible, linked to specific pathologies or gene mutations. Differentiation of findings across clinical, genetic and pathological subtypes was performed, as this was crucial given the heterogeneity of this disease.

The **primary aims** of this thesis were as follows:

(i) To explore whether there is evidence of systemic and central immune dysfunction in individuals with FTD and determine how this varies across the spectrum of disease.

(ii) To examine whether changes indicative of microglial dysfunction vary across the spectrum of disease.

(iii) To examine whether inflammatory biomarkers in CSF of individuals with sporadic or genetic FTD enable differentiation of clinical syndromes or mutation types and link to existing biomarkers of neurodegeneration.

(iv) To establish whether levels of inflammatory biomarkers in CSF change presymptomatically and could therefore help guide prediction of disease proximity in individuals at risk of genetic FTD, for use in clinical trials.

The **key objectives** were as follows:

1. **In Chapter 3**, to examine clinical aspects of systemic immune dysregulation in genetic FTD, through study of the prevalence of systemic autoimmune diseases in individuals with FTD due to *GRN*, *C9orf72* or *MAPT* mutations compared with controls.
2. **In Chapter 4**, to analyse correlations between histological changes (in microglia and other pathology) in *post-mortem* brain tissue and neuroimaging changes observed in case of *GRN* mutation associated FTLD.
3. **In Chapters 5 and 6**, to examine in detail the changes in microglia in FTLD by analysing regional patterns of the burden, activation and dystrophy of different microglial phenotypes in *post-mortem* brain tissue of individuals with a wide range of different sporadic and genetic FTLD subtypes, compared with controls and AD cases.
4. **In Chapter 7**, to compare levels of glia-derived biomarkers in CSF from individuals with different clinical subtypes of sporadic FTD and controls, and to perform an exploratory analysis in individuals with genetic FTD. In addition, to explore if levels of these biomarkers differ between those with underlying FTLD versus AD pathology or correlate with levels of other CSF neurodegenerative biomarkers currently used in clinical practice.
5. **In Chapter 8**, to extend exploration of glia-derived biomarker levels in CSF to a larger genetic FTD cohort to confirm if these vary by genetic subtype (*GRN*, *C9orf72* or *MAPT* mutation carriers), and to examine levels in PMC to establish if, and when, levels change presymptomatically.

1.5 Publications relating to this chapter

Sections of this chapter relating to the overview of FTD were published as:

Woollacott IOC and Rohrer JD (2016) The clinical spectrum of sporadic and familial forms of frontotemporal dementia. *J Neurochem* 138 (Suppl. 1), 6-31

2 General methods

This chapter summarises the cohorts, techniques and statistical approaches used in this thesis and lists the work done by the author and the contributions by others.

2.1 Cohorts and ethical considerations

2.1.1 Cohort for histological studies

The histological studies in Chapters 5 and 6 examined FTLD and AD cases and controls provided by the Queen Square Brain Bank (QSBB) for Neurological Disorders, UCL Queen Square Institute of Neurology, London, UK, although 14 of the FTLD cases were provided by the Medical Research Council (MRC) London Neurodegenerative Diseases Brain Bank, Institute of Psychiatry, King's College London, UK. The FTLD case analysed in Chapter 4 was provided by the QSBB and was also included in the cohort in Chapters 5 and 6. Brain donation protocols were approved by a London Research Ethics Committee and ethical approval for these studies was provided by the NHS Health Research Authority. Tissue was stored for research purposes under a license from the Human Tissue Authority.

Sixty individuals were selected for analysis; demographics are summarised in Table 2.1 and details of all individual cases are listed in Appendix 1. Fifty cases with FTLD were selected to give a broad range of different underlying pathologies. Five healthy controls and five sporadic typical AD cases of a similar age at death (AAD) to FTLD cases were included as comparison groups. FTLD cases were selected from a list of patients seen through the Specialist Cognitive Disorders Clinic at the National Hospital for Neurology and Neurosurgery (NHNN), who had a clinical diagnosis of FTD (bvFTD or PPA) or an overlap syndrome (FTD-MND, PSPS or CBS), had donated their brain after death to the QSBB or the MRC London Neurodegenerative Diseases Brain Bank, and had a confirmed pathological diagnosis of FTLD (Cairns et al., 2007) made by

neuropathologists at these centres. All had undergone genetic testing for known FTD-associated mutations (Pottier et al., 2016) on a clinical or research basis, with appropriate consent in place. Due to the relative rarity of FTLD cases available in certain subgroups, at least five cases per subgroup were selected for analysis within most of the following FTLD subtypes:

- **FTLD-tau:** FTLD-CBD, FTLD-*MAPT*, FTLD-Picks and FTLD-PSP.
- **FTLD-TDP**: sporadic FTLD-TDPA, genetic FTLD-TDPA (due to *GRN* or *C9orf72* mutations, although one case had a *TBK1* mutation), sporadic FTLD-TDPB, genetic FTLD-TDPB (all had *C9orf72* expansions) and FTLD-TDPC (all sporadic). No FTLD-TDPD or FTLD-TDPE cases were available.
- **FTLD-FUS**: all cases available were sporadic cases with FUS pathology with an aFTLD-U subtype (denoted as FTLD-FUS for brevity).

For some FTLD subtypes (FTLD-FUS, sporadic FTLD-TDPB and genetic FTLD-TDPB) fewer than five cases were available due to the rarity of these pathologies. The final FTLD cohort contained: 31 sporadic and 19 genetic FTLD cases, of which 26 had FTLD-TDP (16 FTLD-TDPA [five sporadic, 11 genetic], five FTLD-TDPB [two sporadic, three genetic] and five FTLD-TDPC), 20 had FTLD-tau (five each of FTLD-CBD, FTLD-*MAPT,* FTLD-Picks and FTLD-PSP) and four had FTLD-FUS (all aFTLD-U). The 19 genetic cases included five with *GRN* mutations (FTLD-*GRN*; four C31fs and one Q130fs(388_391delCAGT); all FTLD-TDPA), five with +16 splice site mutations on the intron to exon 10 (10+16 mutations) in *MAPT* (FTLD-*MAPT*), eight with the *C9orf72* expansion (FTLD-*C9orf72*; five with FTLD-TDPA and three with FTLD-TDPB) and one with a *TBK1* A705fs mutation (FTLD-TDPA)**.**

Controls and AD cases were carefully selected so that the AAD of these groups was similar to the overall FTLD cohort, which tended to be much younger than most diseased or healthy control cases available from the QSBB. This is because age can affect microglial burden and function (Gefen et al., 2019), alter expression of CD68 and HLA-DR/DP/DQ (Tischer et al., 2016) and alter microglial morphology, increasing dystrophy (Streit et al., 2004). Controls were selected from a list of individuals with no cognitive symptoms, and no clinical or neuropathological diagnosis of dementia, who had donated their brain to QSBB, and had a similar AAD and *post-mortem* delay to the FTLD and AD cases. Many controls in QSBB had to be excluded as they were much older than the FTLD cases. Three of the five selected controls had evidence of mild pathological ageing (Braak and Braak stage 2 or below) but otherwise there was no abnormal pathology. Individuals with a clinical diagnosis of sporadic amnestic (typical) AD that had a similar AAD and *post-mortem* delay to FTLD and control groups were also recruited from the QSBB. All AD cases met pathological criteria for a definite diagnosis of AD (Hyman et al., 2012), with Braak and Braak stage >5, and had negative genetic testing for AD-associated mutations. Individuals within each FTLD subgroup were also chosen for a similar AAD to controls and each other wherever possible, but due to the rarity of certain FTLD subtypes it was difficult to match AAD and *post-mortem* delay closely across every FTLD subgroup. Due to small numbers of young controls and sporadic AD cases being available, and the variety of *post-mortem* delays in the FTLD group, it was difficult to match *post-mortem* delays closely between these groups.

Data were collected for all cases and controls regarding clinical diagnosis, sex, AAD, AAO and disease duration (for AD and FTLD cases), genetic mutation (for genetic FTLD cases), *post-mortem* delay (where available) and main and secondary neuropathological diagnoses. All available case notes and *post-mortem* clinical summaries were reviewed to confirm the clinical syndrome and demographic data. All available *post-mortem* reports

were reviewed to confirm the *post-mortem* delay, main neuropathological diagnosis and secondary pathology. Any cases with significant secondary neurodegenerative pathologies were excluded.

Neuro-pathological diagnosis	Number of cases	Genetic mutation (N)	Clinical diagnosis (N)	Sex (M/F)	Mean (range) age at symptom onset in years	Mean (range) age at death in years	Mean (range) disease duration in years	Mean (range) *post-mortem* delay in hours
Healthy controls	5	n/a	Control	1/4	n/a	67.4 (38-80)	n/a	45.7 (24.0-80.6)
AD	5	n/a	Amnestic AD	3/2	58.8 (49-65)	69.2 (62.0-73.0)	10.4 (5.0-17.0)	45.8 (31.1-76.7)
FTLD	50	Sporadic = 31 Genetic = 19: *GRN* = 5 *C9orf72* = 8 *MAPT* = 5 *TBK1* = 1	bvFTD = 23 nfvPPA = 8 FTD-MND = 8 svPPA = 5 PSPS = 5 CBS = 1	29/21	57.8 (37-66)	66.5 (51.3-84.0)	8.7 (2.1-18.7)	60.7 (10.8-157.6)
FTLD subgroups								
FTLD-tau	20	Sporadic = 15 Genetic = 5 (*MAPT*)	bvFTD = 10 nfvPPA = 4 PSPS = 5 CBS = 1	13/7	58.2 (37-71)	68.1 (52.4-84.0)	9.9 (5.5-16.4)	54.9 (24.0-103.3)
FTLD-CBD	5	All sporadic	nfvPPA = 3 PSPS =1 CBS = 1	2/3	60.2 (57-65)	69.0 (64.8-73.8)	8.8 (5.5-11.1)	68.9 (37.2-103.3)
FTLD-*MAPT*	5	Genetic = 5 (all *MAPT* 10+16)	bvFTD = 5	2/3	48.0 (37-58)	59.6 (52.4-68.4)	11.6 (8.1-16.4)	45.9 (24.0-64.0)
FTLD-Picks	5	All sporadic	bvFTD = 5	5/0	57.6 (52-64)	68.1 (63.5-75.6)	10.5 (5.5-15.6)	47.8 (24.0-94.7)
FTLD-PSP	5	All sporadic	PSP = 4 nfvPPA = 1	4/1	67.0 (62-71)	75.6 (68.0-84.0)	8.6 (6.0-13.0)	57.2 (25.5-86.4)
FTLD-TDP	26	Sporadic = 12 Genetic = 14 *C9orf72* = 8 *GRN* = 5 *TBK1* = 1	bvFTD = 9 nfvPPA = 4 FTD-MND = 8 svPPA = 5	12/14	59.4 (50-76)	67.2 (53.1-78.6)	7.8 (2.1-18.7)	68.8 * (10.8-157.6)
FTLD-TDPA	16	Sporadic = 5 Genetic = 11 *C9orf72* = 5 *GRN* = 5 *TBK1* = 1	bvFTD = 7 nfvPPA = 4 FTD-MND = 5	7/9	60.6 (50-76)	67.0 (53.1-78.6)	6.4 (2.1-10.3)	77.3 (29.3-157.6)
FTLD-TDPB	5	Sporadic = 2 Genetic = 3 (*C9orf72*)	bvFTD = 2 FTD-MND = 3	2/3	56.2 (50-63)	62.1 (56.2-67.2)	5.9 (4.2-8.1)	68.5 (10.8-96.0)
FTLD-TDPC	5	All sporadic	svPPA = 5	3/2	58.8 (52-64)	73.0 (65.4-78.6)	14.2 (10.3-18.7)	43.8 (19.0-83.7)
FTLD-FUS (All aFTLD-U)	4	All sporadic	bvFTD = 4	4/0	45.4 (40-51)	53.9 51.3-60.4	8.4 (5.5-11.3)	39.0 (12.0-72.0)
FTLD cases used for genetic group analysis (all included in groups above)	15	*GRN* = 5 (all FTLD-TDPA) *MAPT* = 5 (all FTLD-*MAPT*) *C9orf72* = 5 (all FTLD-TDPA)	bvFTD=4 nfvPPA=1 bvFTD = 5 FTD-MND = 3 nfvPPA = 2	2/3 2/3 1/4	58.0 (62-67) 48.0 (37-58) 60.8 (55-68)	64.6 (55.3-74.2) 59.6 (52.4-68.4) 68.6 (62.7-75.1)	6.6 (5.3-8.4) 11.6 (8.1-16.4) 7.8 (5.7-10.3)	83.1 (29.3-157.6) 45.9 (24.0-64.0) 78.7 (51.9-107.1)

*3 FTLD-TDP cases had no *post-mortem* delay data

Table 2.1 Summary of cases selected for histopathological studies

2.1.2 Cohorts for clinical and CSF biomarker studies

For clinical (Chapter 3) and CSF biomarker (Chapters 7 and 8) studies, participants were selected from four main FTD studies at UCL:

- The Genetic FTD Initiative (GENFI) – patients with genetic FTD, PMC and mutation negative controls.
- The Longitudinal Investigation of Frontotemporal Dementia (LIFTD) – patients with sporadic FTD and healthy controls.
- Previous longitudinal studies of FTD at the UCL Dementia Research Centre (DRC) – patients with sporadic or genetic FTD and healthy controls.
- A prospective DRC CSF collection study of individuals with suspected neurodegenerative diseases at the NHNN – patients with sporadic or genetic FTD and healthy controls.

All these studies were approved by the UCL/UCL Hospitals Joint Research Ethics Committee and the Health Research Authority. All participants were aged 18 years or over and gave informed written consent to participate.

GENFI is a prospective, longitudinal, multi-centre cohort study of individuals with symptomatic genetic FTD (patients) and presymptomatic individuals who are at risk of genetic FTD (both PMC and their mutation negative relatives) who are from families with mutations in *GRN*, *C9orf72* or *MAPT*. It is led by the author's primary supervisor, Dr Jonathan Rohrer, at UCL. The initial pilot phase ran from 2012-2015 (GENFI1) and since 2015 a five-year study (GENFI2) has been running. There were 25 participating sites and over 800 participants across Europe and Canada during the period that the studies for this thesis were performed. Participants are typically recruited from local clinical centres in each country. Patients with FTD meet consensus diagnostic criteria for either bvFTD (Rascovsky et al., 2011) or PPA (Gorno-Tempini et al., 2011), although some

have overlap syndromes of PSPS or CBS (Armstrong et al., 2013; Höglinger et al., 2017). A few patients have FTD-MND, and even fewer have MND only (Strong et al., 2009); these typically have *C9orf72* expansions. PMC carry mutations which predispose them to developing FTD but do not have symptoms meeting criteria for a diagnosis of FTD or related syndromes. Individuals who are relatives of patients or PMC but lack mutations in these genes are mutation negative controls. Study visits and assessments are carried out on participants annually using harmonised study protocols at each site, with assessments as described below. Data and biosamples are shared for studies across sites following application to the GENFI Data Committee.

LIFTD is a longitudinal observational cohort study run by the UCL DRC, which started in 2015, led by Dr Jonathan Rohrer and Professor Jason Warren. It recruits participants with a diagnosis of sporadic FTD and its associated disorders, including individuals that fulfil consensus diagnostic criteria for bvFTD (Rascovsky et al., 2011), PPA (Gorno-Tempini et al., 2011), CBS (Armstrong et al., 2013), PSPS (Höglinger et al., 2017; Litvan et al., 1996) or MND (Strong et al., 2009). It also recruits healthy controls (typically spouses or relatives of participants with FTD in LIFTD) with no cognitive symptoms, normal cognitive testing scores, normal neurological examinations and no neurological conditions. Prior to LIFTD and GENFI, other studies at the UCL DRC had also recruited individuals with genetic or sporadic FTD who met diagnostic criteria for bvFTD or PPA, and healthy controls.

All participants within GENFI and LIFTD have an annual study visit, which includes a clinical assessment consisting of a standardised history and neurological examination, including scales to measure changes in behaviour and cognitive function such as the Mini-Mental State Examination, revised Cambridge Behavioural Inventory, Frontotemporal Dementia Rating Scale and the Clinical Dementia Rating plus National

Alzheimer's Coordinating Centre FTLD (CDR plus NACC FTLD). Participants undergo venipuncture for collection of up to 60ml blood for genetics (DNA and RNA) and biomarker (serum and plasma) analysis. Participants may also have a lumbar puncture, enabling collection of up to 20ml CSF on each occasion. Participants also undergo standardised, detailed neuropsychological assessments including tests of executive function, working memory and attention, social cognition, naming and semantic knowledge, visuospatial skills and memory, and a standardised MRI brain protocol including volumetric T1, volumetric T2, resting state functional MRI, arterial spin labeling perfusion MRI and diffusion tensor imaging sequences on a 3 Tesla (3T) scanner. Participants have assessments at baseline and longitudinally, at one-year interval follow-ups, with MR image registration for sequential comparison. A significant proportion of participants have had several annual visits with longitudinal collection of blood and CSF samples, and longitudinal clinical, neuropsychological and neuroimaging assessments.

All new participant DNA samples from GENFI and LIFTD undergo sequencing for a panel of known neurodegenerative disease gene mutations and are also tested for the *C9orf72* expansion, within the Neurogenetics Laboratory at the UCL Queen Square Institute of Neurology. DNA, RNA, plasma, serum and CSF samples from GENFI participants are processed within the Leonard Wolfson Biomarker Laboratory (LWBL) and stored at the GENFI Biobank at the UCL Queen Square Institute of Neurology. Samples for LIFTD participants are processed and stored within the LWBL. Given that many participants within GENFI are presymptomatic and have chosen not to have genetic testing on a clinical basis, all research genetic test results for participants within GENFI are placed on a secure database by a named Genetic Guardian at each GENFI site (who is not involved in assessment of the participants). Research staff remain blinded to the genetic status of presymptomatic participants if they have not chosen to have a separate clinical genetic test.

The DRC CSF collection study for individuals with suspected neurodegenerative disease is a prospective longitudinal cohort study led by Professor Jonathan Schott at the UCL DRC since 2013. Participants recruited with suspected neurodegenerative disease (including FTD, AD or other disorders) have usually been seen for assessment of cognitive symptoms within the Specialist Cognitive Disorders Service at the NHNN and have been referred for a clinical, diagnostic lumbar puncture. Healthy control participants are also recruited (typically spouses or relatives of those with cognitive symptoms); these have no cognitive symptoms, normal cognitive testing scores, normal neurological examinations and no neurological conditions. Participants give informed, written consent to use of their clinical details and collection of extra blood (plasma and serum, up to 18.5ml), urine (25 to 100ml) and CSF (15ml) samples for research purposes during the diagnostic lumbar puncture or (for controls) consent to having a purely research focused blood, urine and CSF collection. Although most individuals have one lumbar puncture, several individuals have consented to having lumbar punctures on an annual basis for longitudinal research CSF examination.

2.2 Techniques

2.2.1 Histological techniques

2.2.1.1 Tissue processing and routine immunohistochemistry

The FTLD case in Chapter 4 and all FTLD and AD cases and controls in Chapters 5 and 6 underwent routine brain tissue processing and immunohistochemistry, and clinical neuropathological assessment, prior to further detailed research analyses within these studies. Brains donated to the QSBB are weighed and hemi-dissected and the right half of the brain is cut coronally and flash frozen at -80C. The left half of the brain is immersed for three weeks in formalin solution, examined macroscopically and then cut coronally into multiple 5mm thick slices. Small blocks of tissue are cut from these slices using a standardised protocol encompassing numerous cortical and subcortical regions, then

processed on a six-day cycle of graded alcohols and chloroform and embedded in paraffin wax, producing blocks of formalin fixed paraffin embedded (FFPE) tissue. Sections of FFPE tissue are cut from these blocks, typically at 8μm thickness using a rotary microtome (ThermoFisher), and undergo immunohistochemistry using antibodies used routinely in diagnostic practice at QSBB, as well as haematoxylin and eosin (H&E) staining to assess the degree of neuronal loss and spongiosis. Where clinically indicated, sections in selected cases are also stained with Luxol fast blue (LFB) and Perl stains to assess the degree of myelin loss and haemosiderin deposition.

For immunohistochemistry, FFPE sections are placed onto 30% alcohol solution, floated onto warm water, picked up onto frosted positively charged microslides (Solmedia), dried overnight at 37°C, then adhered at 60°C overnight in preparation for immunohistochemistry. Sections are de-paraffinised in three changes of xylene for two minutes each, then rehydrated in two changes of absolute alcohol (100%) for two minutes. Endogenous peroxidase activity is blocked by submerging sections in 0.3% hydrogen peroxide (H_2O_2) (BDH) in methanol for ten minutes (10ml H_2O_2 30% in 1000ml methanol). Antibodies are used to detect TDP-43 (Proteintech; dilution 1:800), Aβ (Dako; 1:100), tau (AT8 antibody, Thermo Scientific; 1:600), alpha-synuclein (BD Bioscience; 1:1000), phosphorylated neurofilaments for axons (SMI31 antibody, Sternberger Monoclonals; dilution 1:5000), p62 (BD Transduction; 1:200), activated astrocytes (GFAP antibody, Dako; 1:1000), and microglia (CD68 antibody, Dako; 1:100). Immunohistochemistry for all antibodies requires pre-treatment in citrate buffer (0.45g citric acid and 5.8g tri-sodium citrate in two litres deionised water at pH 6.0) for ten minutes at 120°C once maximum pressure is reached (>15kPa), with additional pre-treatment with formic acid for Aβ. Non-specific binding is blocked by incubating sections in 10% non-fat milk in Tris-buffered saline (TBS, pH 7.2) for 30 minutes at room temperature. Tissue sections are incubated in primary antibodies for 60 minutes at room

temperature, then washed in TBS-Tween (TBS-T, Thermo Scientific) and incubated in biotinylated anti-rabbit IgG (Dako; 1:200) or biotinylated anti-mouse IgG (Dako; 1:200) secondary antibodies for 30 minutes. Following further TBS-T washes, sections are incubated in Avidin–Biotin Complex (ABC Kit, Vectorstain Elite, Vector Laboratories Inc.) for 30 minutes, and colour is developed with 3,3'-diaminobenzidine (DAB, Sigma) as the chromogen by placing sections in a DAB/TBS-T/H_2O_2 solution (4ml of 5% DAB in 400ml TBS-T with 128µl of 30% H_2O_2) for three minutes. Sections are dehydrated through three grades of alcohol solution (70%, 90% and 100%) for two minutes each then cleared using two changes of xylene for two minutes and mounted onto slides using DePeX (BDH).

Detailed diagnostic histological assessments were carried out by neuropathologists at the QSBB on FFPE sections for all cases, examining for spongiosis, neuronal and axonal loss, astrogliosis, microgliosis and TDP-43, Aβ, tau, alpha-synuclein and p62 deposition. Where relevant, cases were also analysed for myelin loss and FUS protein deposition. The circle of Willis and cortical, subcortical and hippocampal regions and vessels were examined for vascular changes. Slides were viewed using a Nikon Eclipse Ni microscope.

2.2.1.2 Immunohistochemistry for microglial markers

Further immunohistochemistry was performed by the author for the studies in Chapters 4, 5 and 6 to detect microglia using antibodies against three microglial markers (CD68, CR3/43 and Iba1; Table 2.2). In Chapter 4, FFPE sections were cut from tissue blocks from five brain regions as detailed in Chapter 4.4.3. In Chapters 5 and 6, FFPE sections were cut from left anterior frontal lobe and left temporal lobe tissue blocks from all 60 cases.

In these studies, 8µm thick sections were cut by the author from tissue blocks using a rotary microtome (ThermoFisher). Sections were placed onto 30% alcohol solution,

floated onto warm water, picked up onto frosted positively charged microslides (Solmedia), dried overnight at 37°C, then adhered at 60°C overnight in preparation for immunohistochemistry. Positive controls consisting of sections of lymphoid tissue or appendix were included for each experiment, as these contain many macrophages, which are also detected using these antibodies. Sections were de-paraffinised in three changes of xylene for two minutes each, then rehydrated in two changes of absolute alcohol (100%) for two minutes. Endogenous peroxidase activity was blocked by immersing sections in a 0.3% H_2O_2 in methanol solution (10ml H_2O_2 30% (BDH) in 1000ml methanol) for ten minutes followed by washing in running water. Pre-treatment was undertaken for retrieval of antigens by pressure cooking sections in citrate buffer (0.45g citric acid and 5.8g tri-sodium citrate in two litres deionized water at pH 6.0) for ten minutes at 120°C once maximum pressure was reached (>15kPa), then washed in running water. Non-specific protein binding was blocked through incubation of sections in 10% non-fat milk in TBS (pH 7.2) for 30 minutes at room temperature.

The relevant primary antibody (Table 2.2) was applied, and sections were incubated for 60 minutes at room temperature, followed by three washes in TBS-T (Thermo Scientific) each for five minutes. Sections were then incubated in the relevant biotinylated secondary antibody (Table 2.2) for 30 minutes at room temperature before a further three five-minute washes in TBS-T. Sections were incubated in ABC solution (ABC Kit, Vectorstain Elite, Vector Laboratories Inc.) for 30 minutes at room temperature, followed by three five-minute washes in TBS-T. The antigen-antibody interaction was visualised using DAB (Sigma) as the chromogen by placing sections in a DAB/TBS-T/H_2O_2 solution (4ml of 5% DAB in 400ml TBS-T with 128µl of 30% H_2O_2 (BDH)) for three minutes. Sections were washed in cold water and counterstained (to better visualise grey and white matter) by submerging them in Mayer's Haematoxylin solution (1g haematoxylin, 50g aluminium potassium sulphate, 0.2g sodium iodate, 50g chloral hydrate (BDH) in 1

litre distilled water) for 20 seconds, then washed in warm water. Sections were dehydrated through three grades of alcohol solution (70%, 90% and 100%) for two minutes each then cleared using two changes of xylene for two minutes. Sections were mounted onto slides, coverslipped using DPX mounting medium (Thermo Scientific) and left to dry overnight. Slides were viewed using a Nikon Eclipse Ni microscope.

Primary antibody	Antigen	Source	Species	Dilution
CD68	CD68	Dako	Mouse monoclonal	1:100
Iba1	Iba1	Wako Chemicals	Rabbit polyclonal	1:1000
CR3/43	HLA-DR/DP/DQ	Dako	Mouse monoclonal	1:150
Secondary antibody	**Antigen**	**Source**	**Species**	**Dilution**
Biotinylated antibody	CD68-Ab complex	Dako	Polyclonal rabbit anti-mouse	1:200
Biotinylated antibody	Iba1-Ab complex	Dako	Polyclonal swine anti-rabbit	1:200
Biotinylated antibody	HLA-Ab complex	Dako	Polyclonal rabbit anti-mouse	1:200

Table 2.2 Antibodies used for immunohistochemistry to detect microglial markers

2.2.2 CSF biomarker techniques

2.2.2.1 CSF collection, processing and storage

CSF samples from participants in studies at UCL were collected via lumbar puncture at the Leonard Wolfson Experimental Neurology Centre or the NHNN Daycare unit. Lumbar punctures were performed using standardised protocols, without use of manometers, collecting up to 20ml of CSF into Sarstedt polypropylene tubes. CSF samples were transferred immediately at room temperature to the LWBL. CSF samples were immediately centrifuged at 1750 relative centrifugal force for five minutes at room temperature and the supernatant aliquoted into 1ml volumes within 1.5ml polypropylene storage tubes. Tubes were labelled at room temperature with nylon labels printed by a

Brady BMP53 printer with Ribbon appropriate for storage conditions of up to -100 degrees Celsius (-100°C). Unique identifiers for each aliquot (generated by Itemtracker software) were printed on the labels, which allowed accurate tracking of the date of sample collection, freezer location and participant anonymisation.

Tubes containing the aliquots of CSF were placed in a -80°C freezer within 60 minutes of sample arrival to the laboratory and stored at -80°C until needed for analysis. The tubes were allocated freezer storage positions using Itemtracker software, and the individual aliquots given specific positions on the rack with individually unique identifiers. Location information was stored in the LWBL and GENFI Biobank databases to allow later sample location and identification.

CSF samples from external GENFI sites were collected at these sites and processed using the same protocol as above, and stored as 1ml aliquots at -80°C. Requested aliquots were then couriered frozen to UCL and kept frozen at -80°C until being thawed on the day of experiments.

2.2.2.2 Routine analysis of biomarkers in CSF

CSF samples from lumbar punctures performed for the DRC prospective CSF study through the NHNN Daycare unit had been analysed for microscopy and cell count, protein and glucose levels for clinical diagnostic purposes. However, these parameters were not analysed for most of the other CSF samples used in Chapter 7 arising from the LIFTD or GENFI studies, or any of the CSF samples in Chapter 8 arising from the GENFI study, as this was not within the study protocol. For the study in Chapter 7, CSF samples had levels of T-tau, P-tau and Aβ42 measured using commercially available INNOTEST sandwich enzyme-linked immunosorbent assays (ELISAs) (Fujirebio Europe, Gent, Belgium). For the study in Chapter 8 these assays were not performed due to insufficient CSF volumes being available for most external GENFI participants.

2.2.2.3 Immunoassays for glia-derived biomarkers in CSF

The author performed immunoassays for the studies in Chapters 7 and 8 to measure levels of sTREM2, YKL-40 and chitotriosidase in CSF samples. All samples and reagents were thawed to room temperature on the day of experiments. In each experiment, CSF samples and standards were assayed in duplicate and measured on the same day by the author using the same reagents. Intra-assay coefficient of variation (CV) values for biomarker levels between samples were less than 10% for each experiment.

CSF sTREM2 levels were measured using an immunoassay protocol produced by Dr Amanda Heslegrave, adapted from one published previously (Kleinberger et al., 2014). Streptavidin-coated 96-well plates (Meso Scale Discovery (MSD), Rockville, MD, USA) were blocked overnight at 4°C in block buffer (0.5% bovine serum albumin (BSA) and 0.05% Tween 20 in phosphate-buffered saline [PBS]; pH 7.4). The plates were then incubated with the biotinylated polyclonal goat anti-human TREM2 capture antibody (0.25 µg/ml; BAF1828, R&D Systems, Minneapolis, MN, USA) diluted in block buffer, shaking for 1 hour at room temperature at 500 revolutions per minute (rpm). Plates were subsequently washed five times with wash buffer (0.05% Tween 20 in PBS) and incubated for 2 hours shaking at room temperature at 500 rpm with 50 µL per well of either the standard curve constructed from recombinant human TREM2 protein (11084-H08H-50, Sino Biological Inc., Beijing, China) diluted in assay buffer (0.25% BSA and 0.05% Tween 20 in PBS; pH 7.4) to produce concentrations ranging between 4000 pg/ml and 62.5 pg/ml, or CSF samples diluted 1 in 4 in assay buffer. Plates were again washed five times with wash buffer before incubation for 1 hour shaking at room temperature at 500 rpm with the detection antibody, monoclonal mouse anti-human TREM2 antibody (1 µg/ml; (B-3): sc373828, Santa Cruz Biotechnology, Texas, USA), diluted in block buffer. After five additional washing steps, plates were incubated with the secondary antibody (SULFO-TAG-labeled goat anti-mouse secondary antibody, R32AC-5, MSD) and

incubated shaking for 1 hour at 500 rpm in the dark. Lastly, plates were washed three times with wash buffer then twice in PBS alone. The electrochemical signal was developed by adding MSD Read buffer T 4x (R92TC-2, MSD) diluted 1 in 2, and the light emission measured using the MSD Sector Imager 6000. The concentration (level) of sTREM2 was calculated using a five-parameter logistic curve fitting method with the MSD Workbench software package.

CSF YKL-40 levels were measured using the commercially available Human YKL-40 Immunoassay Kit on the MSD (Rockville, MD, USA) platform. CSF samples were diluted 1 in 400 with dilution buffer, and the provided standard reconstituted 1 in 20 using dilution buffer and serially diluted 1 in 4 to produce concentrations ranging from 50,000 to 12.2 pg/mL. 150 µL blocking agent was added to each well and plates were sealed and incubated at room temperature shaking at 500 rpm for 1 hour. Plates were washed 3 times with 300 µL per well of PBS-T, then 50 µL of either diluted CSF sample, standard or blank (dilution buffer) was added to each well (pre-coated with capture antibody), and plates were sealed and incubated at room temperature, shaking at 500 rpm for 2 hours. Plates were washed 3 times with 300 µL of PBS-T and then 25 µL of detection antibody solution (diluted to 1 in 50) was added per well. Plates were sealed and incubated at room temperature shaking at 500 rpm for 2 hours. After a further 3 washes with PBS-T, 150 µL of Read Buffer T (diluted 1 in 2) was added to each well. The plate was immediately analysed on the SECTOR Imager, which determined the YKL-40 level using a 4-parameter logistic model with averaged replicates.

CSF chitotriosidase levels were measured using the commercially available CircuLex Human ELISA Kit (MBL International, Woburn, MA, USA). CSF samples were diluted 1 in 5 with dilution buffer and the provided standard was diluted to produce concentrations ranging from 3600 to 56.25 pg/mL. 100 µL of either diluted CSF sample, standard or

blank (dilution buffer) was added to each well, and plates were sealed and incubated at room temperature for 1 hour shaking at 300 rpm, then washed 4 times with 350 µL of wash buffer. 100 µL of HRP conjugated detection antibody was added and plates were sealed and incubated at room temperature for 1 hour shaking at 300 rpm, then washed 4 times with 350 µL of wash buffer. 100 µL of substrate agent was added to each well and plates were sealed, covered in foil, and incubated for 15 minutes at room temperature shaking at 300 rpm. Finally, 100 µL of stop solution was added to each well in the same order as the substrate agent, and plate absorbance was read immediately on a microplate reader at dual wavelengths of 450/540 nm. The chitotriosidase level in each sample was calculated using a four-parameter fitting method based on the standard curve, using values which were blank corrected and averaged over replicates.

2.3 Statistical methods

This section outlines the general approach for statistical analyses used across several studies in this thesis. More detailed descriptions of statistical methods are included in each chapter. Statistical analyses were mainly performed in STATA version 14 (Stata Corporation, College Station, TX, USA), or in IBM SPSS Statistics for Windows, version 24.0 (Armonk, NY, USA: IBM Corp.), with occasional use of Microsoft Office Excel for data collection. Graphs were mainly produced using STATA version 14 or GraphPad Prism version 7.00 for Windows (GraphPad Software, La Jolla, CA, USA) and occasionally using Microsoft Excel. The significance threshold was $P<0.05$ for all analyses.

2.3.1 Normality tests and handling of non-parametric data

Parametric tests and linear regression models that are used to compare variables between groups, or associations between variables, rely on data having a normal distribution (and other factors for linear regressions such as a linear relationship between variables). Two methods were used to test whether data were normally distributed:

Shapiro-Wilk tests of normality in STATA or SPSS, and visual assessment of Q-Q plots of residuals from multivariable linear regressions in STATA.

Normally distributed data were analysed with two tailed t-tests (if two groups) or one-way analysis of variance (ANOVA) with Bonferroni *post hoc* analyses (if more than two groups). Multivariable linear regressions were used to compare groups when adjustment for covariates was required or associations between variables were analysed.

Group comparisons of data that were not normally distributed (non-parametric), and did not need adjustment for covariates, were performed using non-parametric analyses: either Mann Whitney tests (for two groups) or Kruskal Wallis tests with Dunn's *post hoc* tests (for more than two groups). Wilcoxon signed rank tests were used for paired comparisons (intra-individual group comparisons). For non-parametric data requiring adjustment for covariates or association analyses, and therefore multivariable linear regressions, data were natural log (Ln) transformed and visual assessments of Q-Q plots of the residuals of Ln(values) were reassessed to ensure they met assumptions required for analysis, including normality and a linear distribution. The bootstrapping technique was considered but was deemed unnecessary due to satisfactory correction of variables through Ln transformation.

2.3.2 Covariates

Certain confounding variables such as age or sex may differ significantly between comparison groups, or, despite being similar between groups, may be significantly and independently associated with an outcome variable. If left uncorrected, this may falsely affect the result of associations being assessed. For example, microglial activation increases with age, so an increase in the level of a glia-derived biomarker in CSF could simply arise from increased release due to age itself in patients with genetic FTD versus their (generally younger) relatives who are PMC or non-carriers (controls). It is therefore

important to identify and adjust for these variables, either by matching groups based on these variables, or, if not possible (or if concern remains or evidence exists that there is a strong, independent association with the outcome variable), by using these variables as covariates in multivariable linear regressions.

In the histological studies in Chapters 5 and 6, FTLD and AD cases and controls, and FTLD subgroups, were matched for AAD as closely as possible. In the CSF biomarker studies in Chapters 7 and 8, age was used as a covariate in all multivariable linear regressions. Sex was also used as a covariate in biomarker analyses as glia-derived protein expression may differ by sex. Disease duration was often used as a covariate in biomarker analyses, as biological processes and glial function may change throughout the disease course. Other covariates were sometimes used, as specified in the statistical analysis sections of each chapter.

2.4 Statement of contributions

The author carried out all experiments and analyses in this thesis, and produced all text, figures and tables, with additional contributions from colleagues as stated below. The list of contributors (initials and names) follows this section.

Chapter 2 – General methods:

- **Cohorts:**
    - **Histological cohort:** Neurology consultants at the DRC (including NCF, CJM, JDR, MNR, JMS and JDW) liaised with JH, TR, TL, LH and LP at the QSBB to arrange for individuals to donate their brains to the QSBB. LP, CT and SS assisted the author with obtaining brain tissue for cases from King's College London. SB assisted with ethics applications for brain donation protocols at the QSBB.

- **Clinical and biomarker cohorts:** JDR is principal investigator for the GENFI study. JDR and JDW are principal investigators of the LIFTD study. JMS is principal investigator for the DRC prospective CSF study. MNR and NCF led previous longitudinal studies of FTD at UCL. KMM was the GENFI study coordinator and LR was the LIFTD study coordinator; both recruited participants into these studies at UCL, with assistance of the author, CC, CG, RSC, CJDH, JDR and JDW. RSC collated data from external GENFI sites with assistance from KMM, CH and JDR. AK and RP assisted with recruitment of participants into the DRC prospective CSF study. Clinical assessments were performed for LIFTD by CRM, CC and the author, and for GENFI predominantly by the author and latterly by RS. Neuropsychological testing was predominantly performed by LR and CJDH (LIFTD) and KMM (GENFI). Neuroimaging protocols were coordinated by DC, DT and JDR and image processing and analyses were performed by MB, EG, CHS and HP. Genetic testing was enabled through SM. LWBL and GENFI biobanks and databases were coordinated by CH and MF with input from JT, AH, HZ and JDR. SB assisted with ethics applications for all studies.

- **Techniques:**
  - **Histological techniques:** Routine brain tissue processing for clinical neuropathological assessments was carried out by technicians including RC, CS, KD and CET at the QSBB. Routine immunohistochemistry was performed by RC, CS and KD. Clinical neuropathological assessments were performed by JH and TR at the QSBB. All tissue sections analysed within Chapters 4, 5 and 6 were cut by the author. Immunohistochemistry in Chapters 4, 5 and 6 was performed by the author, with occasional

assistance from TL, CET, CS and RC. Stained slides were scanned and uploaded into digital databases by BB and CET.

- **CSF biomarker techniques:** The author performed all lumbar punctures to collect CSF samples from LIFTD and GENFI study participants at UCL for this thesis, with a few additional samples collected by RS. CSF from participants at other GENFI sites was collected by clinicians at those centres. The author and other Clinical Research Fellows at the DRC including AK and RP performed lumbar punctures to collect CSF samples from participants in the DRC prospective CSF study. All CSF samples were processed in the LWBL by CH, MF and JT and catalogued with supervision from AH and HZ. Routine clinical analysis of CSF samples was performed by technicians in the NHNN Neuroimmunology Laboratory, managed by MC. Assays for neurodegenerative biomarkers for Chapter 7 were performed by CH and MF within the LWBL. Immunoassays of glia-derived biomarkers for studies in Chapters 7 and 8 were performed by the author within the LWBL.
- **Statistical methods**:
  - All statistical analyses carried out in this thesis were performed by the author, with assistance from JN for statistical methods and STATA code.

Chapter 3 – Systemic autoimmune disease in genetic FTD:

The study was designed by the author and JDR. Participants were recruited from studies at UCL by individuals listed above. The author performed all case notes reviews and analyses and produced all figures and tables.

Chapter 4 – Histopathological correlates of white matter hyperintensities in *GRN* mutation associated FTD:

The study was designed by the author, JDR and TL with input from JH. NCF and MNR were involved in clinical care of the patient and BR coordinated the cadaveric MRI study, which had been led by SO and MJC. Genetic testing was done via SM. MB and CHS performed neuroimaging analyses. TR performed the original clinical neuropathological analysis. The author cut further brain tissue sections and performed immunohistochemistry for the study, assisted by TL, CS and RC. The author, JH and TL reviewed slides and JH and TL scored them for histopathological changes. TL assisted the author with production of immunohistochemistry figures and MB and CHS assisted with production of neuroimaging figures.

Chapter 5 – Microglial phenotypes across the spectrum of FTLD:

The study was designed by the author, JDR and TL. Participants were recruited and tissue processing and immunohistochemistry were performed as described above for Chapter 2. The macro for microglial analysis was developed by a collaborator, YL, at King's College London. Assistance with STATA code was provided by CA. Analysis of microglia was performed predominantly by the author, with assistance from CET. All tables and figures were produced by the author, with some assistance from TL for immunohistochemistry figures.

Chapter 6 – Microglial dystrophy across the spectrum of FTLD:

The study was designed by the author, with approval from TL and JDR. Participants were recruited and tissue processing and immunohistochemistry were performed by as described above for Chapter 2. Analysis of microglia was performed by the author. All tables and figures were produced by the author, with assistance from TL for immunohistochemistry figures.

Chapter 7 – CSF glia-derived biomarkers in sporadic and genetic FTD:

The study was designed by the author and JDR, with input from AH and HZ. Participants were recruited, CSF samples were collected and processed, and biomarker assays were performed as described above for Chapter 2. All analyses were performed, and all tables and figures were produced, by the author, with statistical assistance from JN.

Chapter 8 – CSF glia-derived biomarkers in presymptomatic and symptomatic genetic FTD:

The study was designed by the author and JDR, with input from AH and HZ. Participants were recruited, CSF samples were collected and processed, and biomarker immunoassays were performed as described above for Chapter 2. All analyses were performed, and all tables and figures were produced, by the author, with statistical assistance from JN.

List of contributors:

CA Cono Ariti

SB Suzie Barker

BB Bridget Benson

MB Martina Bocchetta

MJC M. Jorge Cardoso

DC Dave Cash

MC Miles Chapman

CC Camilla Clark

RSC Rhian Convery

RC Robert Courtney

KD Karen Davey

MF Martha Foiani

NCF Nick Fox

EG Elizabeth Gordon

CG Caroline Greaves

CJDH Chris Hardy

CH Carolin Heller

AH Amanda Heslegrave

LH Lynn Haddon

JH Janice Holton

AK Ashvini Keshavan

TL Tammaryn Lashley

YL Yau Lim

CRM Charles Marshall

SM Simon Mead

KMM Katrina Moore

CJM Catherine Mummery

JN Jennifer Nicholas

SO Sebastien Ourselin

LP Linda Parsons

RP Ross Paterson

HP Hugh Pemberton

TR Tamas Revesz

BR Basil Ridha

JDR Jonathan Rohrer

MNR Martin Rossor

LR Lucy Russell

JMS Jonathan Schott

SS Sashika Selvackadunco

RS Rachelle Shafei

CS Catherine Strand

CHS Carole Sudre

DT David Thomas

JT Jamie Toombs

CET Christina Toomey

CT Claire Troakes

JDW Jason Warren

HZ Henrik Zetterberg

3 Systemic autoimmune disease in genetic FTD

3.1 Chapter summary

Introduction: Initial studies have suggested heightened systemic autoimmunity in mouse models of genetic FTD and an increased prevalence of systemic autoimmune disease in individuals with *GRN* or *C9orf72* mutations. However, systemic autoimmune diseases have not been compared directly between *GRN* and *C9orf72* mutation carriers or explored in *MAPT* mutation carriers.

Methods: This study analysed the prevalence of systemic autoimmune disease in individuals with genetic FTD through retrospective notes review of individuals with FTD due to mutations in *GRN* (n=31), *MAPT* (n=40), or *C9orf72* (n=36) and in 24 cognitively normal controls. Total (all) autoimmune diseases were analysed, then sub-classified into 'thyroid' or 'non-thyroid' categories, and prevalence was compared between groups.

Results: The prevalence of total autoimmune disease (thyroid and non-thyroid diseases combined) was higher in the *GRN* group (35.5%) than the *MAPT* group (7.5%), although did not reach significance compared with controls (12.5%), and did not differ between *C9orf72* (22.2%) or *MAPT* groups and controls. The prevalence of thyroid disease did not differ significantly between groups. However, non-thyroid disease was significantly more prevalent in the *GRN* group (19.4%) compared with controls (0%), and in the *GRN* group compared with the *MAPT* group (2.5%) but did not differ significantly between other genetic groups and controls or between *GRN* and *C9orf72* (8.3%) groups.

Conclusions: The high prevalence of non-thyroid autoimmune disease in *GRN* mutation associated FTD is consistent with previous research and suggests that progranulin haploinsufficiency causes systemic immune dysregulation in *GRN* mutation carriers, as

observed in *GRN* mouse models. The similar prevalence of autoimmune disease in *C9orf72* or *MAPT* mutation carriers compared with controls suggests there is less of a link between these mutations and systemic autoimmunity.

3.2 Introduction

As discussed in Chapter 1, there is evidence of central and systemic immune dysfunction in models of genetic FTD. Mouse models of *GRN* mutations and *C9orf72* expansions display altered innate and adaptive immunity. This includes microglial dysfunction, excessive T cell activation, enlarged spleens and lymph nodes infiltrated by engorged macrophages, and elevated autoantibodies and proinflammatory cytokines. These models develop systemic autoimmune diseases, with *GRN* -/- mice developing inflammatory arthritis (Tang et al., 2011), and *C9orf72* -/- or deficient mice developing immune-mediated kidney disease (Atanasio et al., 2016) or thrombocytopaenia (Atanasio et al., 2016; Burberry et al., 2016, 2020). Humans with FTD due to these mutations may therefore also display altered systemic immune function, as well as chronic, excessive neuroinflammation.

Progranulin deficiency has been linked to systemic autoimmune disease in a rheumatological study, where high titres of anti-progranulin antibodies were present in serum samples of individuals with systemic vasculitides, rheumatoid arthritis and systemic lupus erythematosus compared with healthy controls (Thurner et al., 2013). Higher anti-progranulin antibody titres were associated with lower plasma progranulin levels and increased disease activity in individuals with vasculitides. This suggests that plasma progranulin deficiency, which is known to be present for many years in presymptomatic and symptomatic *GRN* mutation carriers (Finch et al., 2011; Meeter et al., 2016b), may be linked to certain systemic autoimmune diseases.

Several studies also implicate systemic immune dysfunction in sporadic FTD. GWAS have identified associations with polymorphisms in loci within *HLA* genes in FTD (Broce et al., 2018; Ferrari et al., 2014, 2017) and FTLD-TDP (Pottier et al., 2019), which encode MHC molecules involved in antigen presentation and the adaptive immune response. Polymorphisms in immune genes (predominantly in the *HLA* region) are jointly linked to FTD and systemic autoimmune diseases, including rheumatoid arthritis, type 1 diabetes, coeliac disease, ulcerative colitis and psoriasis (Broce et al., 2018). Individuals with sporadic FTD have higher titres of systemic antinuclear antibodies compared with controls (60% versus 13%) (Cavazzana et al., 2018). Although thyroid disease was historically associated with sporadic FTD (Rosso et al., 2003b), individuals with svPPA (which is almost universally sporadic) also have a higher prevalence of non-thyroid systemic autoimmune diseases, particularly rheumatological conditions, compared with controls (Miller et al., 2013).

Despite evidence of immune dysregulation in *GRN* mouse models, only one study has explored autoimmune disease in human *GRN* mutation carriers (Miller et al., 2013). This analysed the prevalence of autoimmune thyroid and non-thyroid systemic autoimmune diseases in 39 symptomatic or presymptomatic *GRN* mutation carriers (genetic FTLD-TDP), compared with 129 individuals with svPPA (sporadic FTLD-TDP), 158 individuals with AD, and 186 healthy controls. There was a higher prevalence of non-thyroid autoimmune diseases in genetic (13%) and sporadic (12%) FTLD-TDP cases compared with controls and AD (4% each), but the prevalence of thyroid disease did not differ significantly between groups. Notably, the overall (total) prevalence of systemic autoimmune disease (combining thyroid and non-thyroid) did not differ between groups, suggesting a specific link between *GRN* mutations (or perhaps FTLD-TDP) and non-thyroid autoimmune diseases. Interestingly, the non-thyroid diseases were grouped within clusters (inflammatory arthritides, gastrointestinal disorders and cutaneous

inflammatory disorders); the most common conditions included ankylosing spondylitis, rheumatoid arthritis, inflammatory bowel disease, coeliac disease, psoriasis and vitiligo.

Whether systemic autoimmune disease also occurs more commonly in *C9orf72* expansion carriers remains less clear. A study examined the prevalence of thyroid and non-thyroid autoimmune diseases in 66 individuals with FTD-MND (24 with the *C9orf72* expansion), and an additional 57 individuals with the *C9orf72* expansion (33 with bvFTD, 24 with FTD-MND), compared with 186 healthy controls, 158 AD and 107 PSPS cases (Miller et al., 2016). A group combining those with *C9orf72* expansions (bvFTD or FTD-MND) and individuals with FTD-MND (including FTD-MND cases *without* the *C9orf72* expansion) had a higher prevalence of non-thyroid autoimmune disease compared with healthy controls. The authors concluded that the *C9orf72* expansion was therefore associated with a higher prevalence of non-thyroid autoimmune disease. However, the prevalence in their bvFTD group with the *C9orf72* expansion was actually similar to the prevalence in an FTD-MND group *without* the *C9orf72* expansion. It is therefore more likely that it was FTLD-TDP itself (and MND particularly), rather than the *C9orf72* expansion, that was associated with an increased prevalence of autoimmunity. Another study of individuals with FTD or FTD-MND (either with or without *C9orf72* expansions) found a trend towards a *lower* prevalence of systemic autoimmune diseases in *C9orf72* expansion carriers than those without the expansion, particularly for gastrointestinal diseases (Katisko et al., 2018).

To establish whether there is a gene-specific link to systemic autoimmune disease in individuals with genetic FTD, or if this is actually linked to FTLD-TDP, one could directly compare the prevalence of systemic autoimmune diseases between individuals with FTD due to *GRN* mutations versus *C9orf72* expansions, as both have FTLD-TDP. However, this has not been done previously. It is also important to compare the prevalence of

autoimmune diseases between groups of individuals with definite FTLD-TDP (due to *GRN* mutations or *C9orf72* expansions) and definite FTLD-tau. Although one study included individuals with clinically presumed tauopathy (PSPS) as a comparison group for *C9orf72* expansion carriers (Miller et al., 2016), the underlying pathology in PSPS syndromes can be heterogeneous, even in those with detailed clinical phenotyping. A better comparison group would be individuals with FTD due to *MAPT* mutations, who have definite FTLD-tau. However, the prevalence of autoimmune disease has not been reported in *MAPT* mutation carriers previously.

3.3 Aims and hypotheses

This study aimed to improve upon the few previous studies of systemic autoimmune diseases in humans with genetic FTD (Katisko et al., 2018; Miller et al., 2013, 2016) by analysing prevalence of these diseases in a well-characterised cohort of individuals with genetic FTD due to either *GRN* mutations or *C9orf72* expansions, with comparison groups of individuals with genetic FTD due to *MAPT* mutations and healthy controls. In particular, it aimed to ascertain whether total, thyroid or non-thyroid systemic autoimmune diseases were more prevalent in a particular genetic group, if this differed between different causes of FTLD-TDP (*GRN* mutations versus *C9orf72* expansions) and whether individuals with FTLD-TDP (due to mutations in either *GRN* or *C9orf72*) had a higher prevalence of autoimmune disease than individuals with FTLD-tau (*MAPT* mutations).

The hypotheses were as follows:

1. Individuals with FTD due to *GRN* mutations or *C9orf72* expansions, but not *MAPT* mutations, will have a higher prevalence of systemic autoimmune disease (particularly non-thyroid diseases) compared with controls.

- This is due to a link between mutations in *GRN* or *C9orf72* and systemic autoimmunity, due to alterations in adaptive immune pathways as demonstrated in mouse models.

2. Individuals with FTD due to *GRN* mutations or *C9orf72* expansions will have a higher prevalence of non-thyroid autoimmune diseases compared with individuals with FTD due to *MAPT* mutations.
    - This is due to a stronger link between mutations in *GRN* or *C9orf72* and systemic autoimmunity than for *MAPT*, due to greater alterations in adaptive immune pathways. Alternatively, this is due to a stronger link between FTLD-TDP and systemic autoimmunity than for FTLD-tau.
3. Individuals with FTD due to *GRN* mutations will have a higher prevalence of non-thyroid autoimmune disease than individuals with *C9orf72* expansions.
    - This is due to a more significant effect of *GRN* mutations than the *C9orf72* expansion on systemic adaptive immune pathways, irrespective of the link between FTLD-TDP and autoimmunity.

3.4 Methods

3.4.1 Case selection and notes review

Data were obtained through retrospective review of clinical case report forms or medical notes for participants with FTD in previous or ongoing studies of individuals with FTD at UCL, including participants within LIFTD and GENFI (described in Chapter 2.1.2) who were enrolled at the time of this study. Case report forms for LIFTD and GENFI participants specifically included a question on whether there was a known diagnosis of autoimmune disease (yes or no). Available medical records of all individuals with FTD and a known mutation in *GRN* or *MAPT* or a *C9orf72* expansion in these studies and previous studies of FTD at UCL were analysed for recorded diagnoses of autoimmune disease. Healthy controls with available clinical data, who were participants in LIFTD,

were used as a comparison group; all these participants had had genetic testing and were negative for all known FTD-associated mutations. Presence or absence of a systemic autoimmune disease was recorded against a list of autoimmune diseases (Table 3.1) adapted from Miller et al. (2013). Other autoimmune diseases that were not present on this list were discussed by two researchers (the author and Dr. J. Rohrer) and, if identified and deemed relevant, were included. The autoimmune disease was sub-classified into either a thyroid disease (mainly 'hypothyroidism' or 'hyperthyroidism') or non-thyroid (any other) autoimmune disease, and the name of the disease was recorded. AAO of symptoms of FTD (or age at data collection for controls), clinical diagnosis and sex were also recorded. AAO of the autoimmune disease was often not available.

Cardiological	**Gastroenterological**	**Rheumatological**
Chronic rheumatic heart disease or rheumatic fever	Chronic lymphocytic colitis	Arthritides: rheumatoid arthritis, psoriatic arthritis, ankylosing spondylitis, reactive arthritis
Dermatological	Coeliac disease	Behcet's disease
Alopecia areata, totalis or universalis	Crohn's disease or ulcerative colitis	Eosinophilic granulomatosis with polyangiitis (Churg-Strauss)
Lichen sclerosus or localised scleroderma	Lupoid hepatitis	Granulomatosis with polyangiitis (Wegener's granulomatosis)
Pemphigus vulgaris or bullous pemphigoid	Pernicious anaemia	Polyarteritis nodosa, or other systemic vasculitis
Psoriasis, vitiligo or discoid lupus erythematosus	Primary biliary cirrhosis or primary sclerosis cholangitis	Polymyositis or dermatomyositis
Endocrinological	**Neurological**	Polymyalgia rheumatic Giant cell arteritis
Addison's disease	Acute or chronic inflammatory demyelinating polyneuropathy	Sarcoidosis
Hyperthyroidism – cause documented (if known)	Inclusion body myositis	Sjogren's syndrome
Hypothyroidism – cause documented	Myasthenia gravis	Systemic lupus erythematosus
Type 1 diabetes	Multiple sclerosis, neuromyelitis optica, other demyelinating diseases	Systemic sclerosis
Haematological	Sydenham's chorea (chorea minor)	
Autoimmune haemolytic anaemia	Transverse myelitis	
Immune thrombocytopaenic purpura		

Table 3.1 Autoimmune diseases analysed in case notes review

Records were identified for: 24 healthy controls, 36 individuals with a *GRN* mutation, 52 with a *MAPT* mutation and 40 with *C9orf72* expansions. However, limited clinical

information was available for four individuals with *GRN* mutations, 12 with *MAPT* mutations and four with *C9orf72* expansions, so these cases were excluded. The final cohort included: 24 healthy controls and 105 cases with genetic FTD: 31 with *GRN* mutations, 40 with *MAPT* mutations and 36 with a *C9orf72* expansion. Three individuals had dual gene mutations: two had *C9orf72/GRN* mutations and one had a *C9orf72/SQSTM1* mutation. One case in the *C9orf72* group was homozygous for the *C9orf72* expansion. Clinical data and demographics are shown in Table 3.2.

Group	N	Female (%)	Mean age at onset (FTD) or visit (controls) in years (range)	Diagnosis = N
GRN	31[a]	51.6	57.4 (45.0 - 67.0)	bvFTD = 16 PPA = 10 CBS = 2 FTD-MND = 3*
	29[b]	48.3	57.8 (45.0 - 67.0)	bvFTD = 16 PPA = 10 CBS = 2 FTD-MND = 1
MAPT	40	35.0	49.3 (33.0 - 70.0)	bvFTD = 36 CBS = 2 PSPS = 1 FTD-MND = 1
C9orf72	36[a]	44.4	55.5 (40.0 - 68.0)	bvFTD = 23 PPA = 3 FTD-MND = 10*
	33[b]	39.4	56.0 (40.0 - 68.0)	bvFTD = 23 PPA = 3 FTD-MND = 7
Healthy controls	24	54.2	68.5 (52.1 - 72.9)	n/a

Table 3.2 Demographics of genetic FTD groups and healthy controls

Data are shown for groups including[a] and excluding[b] individuals with dual gene mutations. The majority of PPA cases were nfvPPA although one *GRN* case had mixed semantic and non-fluent PPA features. *Two of the FTD-MND cases with *GRN* mutations had concurrent *C9orf72* expansions.

3.4.2 Statistical analysis

Analyses were performed using IBM SPSS Statistics for Windows, Version 24.0. AAO (or age at data collection visit for controls) was compared between groups using ANOVA with Bonferroni *post hoc* tests. The prevalence of any systemic autoimmune disease

('total autoimmune disease'), and sex (proportion of females) in each group, were compared between groups using Chi squared tests, or Fisher's exact tests (for cell counts ≤5). Similar sub-analyses were carried out for the prevalence of thyroid diseases and non-thyroid diseases. All analyses were then repeated across groups after excluding individuals with dual mutations (two with *GRN/C9orf72* mutations from both the *GRN* and *C9orf72* groups and one with *C9orf72/SQSTM1* mutations from the *C9orf72* group), to remove the potentially exacerbating effect of possessing a dual FTLD-TDP related mutation on autoimmune disease prevalence.

3.5 Results

Sex did not differ significantly between groups, but AAO of symptoms of FTD (or age at data collection for controls) significantly differed between all groups, except between *GRN* and *C9orf72* groups (Table 3.2 and 3.3). The *MAPT* group had a significantly younger AAO (49.3 years) than other genetic groups.

Group	***GRN***	***MAPT***	***C9orf72***	**Healthy controls**
GRN		8.4 (1.7, *P*<0.001)	2.2 (1.8, *P*>0.05)	-10.8 (1.9, *P*<0.001)
MAPT			-6.2 (1.7, *P*<0.001)	-19.2 (1.8, *P*<0.001)
C9orf72				-13.0 (1.9, *P*<0.001)
Healthy controls				

Table 3.3 Differences in AAO of FTD symptoms or age at data collection between groups

Values shown are mean differences in AAO in years (SEM, *P*) resulting from comparisons of rows versus columns, after excluding dual mutation carriers

Group	N	Total autoimmune disease N (%)	Thyroid disease N (%)	Non-thyroid disease N (%)
GRN	31[a]	11 (35.5%)	5 (16.1%)	6 (19.4%)
	29[b]	9 (31.0%)	5 (17.2%)	4 (13.8%)
MAPT	40	3 (7.5%)	2 (5.0%)	1 (2.5%)
C9orf72	36[a]	8 (22.2%)	5 (13.9%)	3 (8.3)
	33[b]	6 (18.2%)	5 (15.2%)	1 (3.0%)
Healthy controls	24	3 (12.5%)	3 (12.5%)	0 (0%)

Table 3.4 Prevalence of autoimmune disease across groups

Data are shown for analyses performed first including[a] and then excluding[b] individuals with dual gene mutations.

The prevalence of autoimmune disease within the cohort is summarised in Table 3.4 and displayed in Figure 3.1. Most cases of autoimmune disease across all genetic groups, and all cases in the control group, were thyroid disease (either hyperthyroidism or hypothyroidism). Non-thyroid autoimmune diseases within the *GRN* group included: coeliac disease (n=2; both had dual *GRN/C9orf72* mutations), sarcoidosis with nephritis (n=1), ankylosing spondylitis (n=1), recurrent polyarthritis and fever of unspecified cause (n=1) and persistent eosinophilia associated with pericardial effusion (n=1). The *C9orf72* group had two cases with coeliac disease (both had dual *GRN/C9orf72* mutations) and one other case had psoriasis. The *MAPT* group had one case with rheumatoid arthritis.

When analysis of autoimmune disease prevalence was performed on the cohort including the two dual *GRN/C9orf72* mutation carriers in both of the *GRN* and *C9orf72* groups, the prevalence of total autoimmune disease in the *GRN* group was high (35.5%), although this did not quite reach significance when compared with controls (12.5%; *P*=0.052). The prevalence of total autoimmune disease in the *C9orf72* and *MAPT* groups did not differ significantly from controls (*C9orf72* = 22.2%; *MAPT* = 7.5%). Notably, there

was a much higher prevalence of non-thyroid autoimmune disease in the *GRN* group (19.4%) compared with controls (0%; *P*=0.03) but not in the *C9orf72* (8.3%) or *MAPT* (2.5%) groups. The prevalence of thyroid disease was similar between the *GRN* group (16.1%) and controls (12.5%) and between the *C9orf72* (13.9%) and *MAPT* (5%) groups and controls. When directly comparing genetic groups, there was a much higher prevalence of total autoimmune disease in the *GRN* group compared with the *MAPT* group (35.5% vs. 7.5%; *P*=0.003). This was the case only for non-thyroid disease (19.4% vs. 2.5%; *P*=0.038) but not for thyroid disease (16.1% vs. 5%). There was no significant difference in the prevalence of total, non-thyroid or thyroid autoimmune diseases between the *GRN* and *C9orf72* groups, or between the *C9orf72* and *MAPT* groups.

When the two *GRN*/*C9orf72* cases were excluded from both the *GRN* and *C9orf72* groups and the single *C9orf72/SQSTM1* case was excluded from the *C9orf72* group, there remained a greater prevalence of total autoimmune disease in the *GRN* group compared with the *MAPT* group (31.0% vs. 7.5%; *P*=0.011). However, the prevalence of non-thyroid disease in each of these groups did not differ significantly (17.2% vs. 5%; *P*>0.05). In addition, the prevalence of total autoimmune disease in the *GRN* mutation group compared with controls did not differ significantly (31.0% vs. 12.5%; *P*>0.05) and this was also the case for non-thyroid disease (13.8% vs. 0%; *P*>0.05). The prevalence of total, thyroid and non-thyroid autoimmune disease remained similar between the *GRN* and *C9orf72* groups and the *C9orf72* and *MAPT* groups, and between the *C9orf72* or *MAPT* groups and controls.

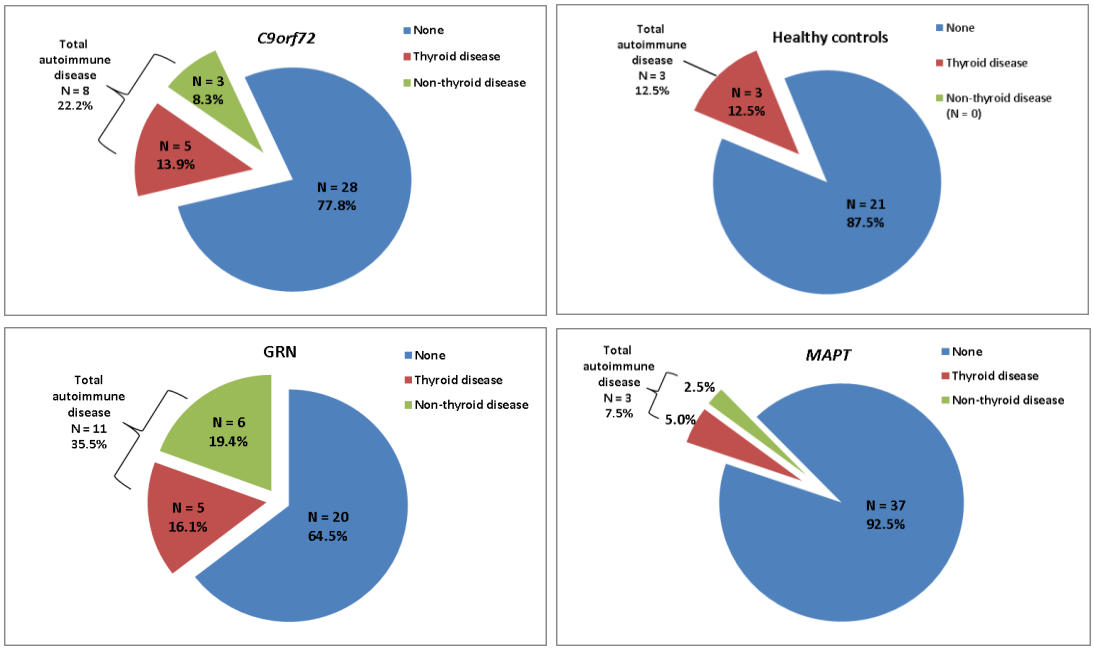

Figure 3.1 Prevalence of total, thyroid and non-thyroid autoimmune diseases within each group

N numbers and percentage of cases per group refer to analyses performed on groups including the three dual mutation carriers.

3.6 Discussion

This study confirms previous observations that there is a high prevalence of certain types of autoimmune disease in individuals with genetic FTD associated with *GRN* mutations (Miller et al., 2013). This group had a particularly high prevalence of non-thyroid autoimmune disease, differing from *MAPT* mutation carriers and controls. A higher prevalence of non-thyroid autoimmune disease in *GRN* mutation carriers compared with controls (Miller et al., 2013) and individuals with presumed tau pathology (PSPS) (Miller et al., 2016) has been described previously, but this is the first study to directly compare individuals with the three main genetic FTD subtypes and between those with definite FTLD-TDP and FTLD-tau pathology.

Diseases such as ankylosing spondylitis, non-specified polyarthritis, sarcoidosis and coeliac disease were present in the *GRN* group, consistent with clusters of inflammatory arthritides and gastrointestinal or cutaneous disorders described previously associated

with *GRN* mutations (Miller et al., 2013). Impairment of the proposed anti-inflammatory and other immune functions of progranulin, due to haploinsufficiency in *GRN* mutation carriers, could cause systemic immune dysregulation from an early age, impairing regulation of responses to self-antigens and leading to increased risk of various clusters of autoimmune disease, other than thyroid diseases, which are common in the general population. Why progranulin haploinsufficiency is linked to these particular clusters of autoimmune diseases remains unclear, although these findings are consistent with another study linking inflammatory arthritides and various rheumatological conditions to reduced plasma progranulin levels (Thurner et al., 2013), and with inflammatory arthritis seen in *GRN* -/- mice (Tang et al., 2011). This could be because tissues with a high content of macrophages and epithelial cells (such as the gut, blood vessels and skin) normally express high levels of progranulin and therefore are selectively impacted on by its haploinsufficiency.

Individuals with *MAPT* mutations had a similar prevalence of total, thyroid and non-thyroid autoimmune disease to controls, consistent with reports in individuals with presumed FTLD-tau (PSPS) (Miller et al., 2016). In fact, prevalence was seemingly reduced in the *MAPT* group: only three out of 40 individuals had an autoimmune disease, compared with three out of 24 controls, although this did not reach significance. This suggests that individuals with FTLD-tau may not have the same degree of systemic immune dysfunction as individuals with FTLD-TDP and may perhaps have impaired immunity. However, MAPT is preferentially expressed in the central and peripheral nervous system, whereas progranulin and C9orf72 expression have low tissue specificity and both are expressed systemically, so mutations in *GRN* and *C9orf72* may have more of a systemic effect than *MAPT* mutations. Although excessive neuroinflammation and microgliosis has been observed in several *MAPT* mouse models, dysregulated systemic

autoimmunity has not been demonstrated in these models or in humans with *MAPT* mutations, in contrast to several *GRN* and *C9orf72* mouse models.

There was no significant difference in the prevalence of total, thyroid or non-thyroid autoimmune disease between *GRN* and *C9orf72* groups. This similarity may be because both *GRN* and *C9orf72* mutation carriers have generalised immune dysfunction, as postulated by previous human studies (Miller et al., 2013, 2016) and mouse models. Alternatively, this could be due to a general link between FTLD-TDP and dysregulated autoimmunity. However, this study may have lacked the power to detect small differences in the prevalence of non-thyroid disease between *GRN* and *C9orf72* groups, due to the relatively small size of each group, so it is difficult to conclude what underlies this. These groups have not been directly compared in previous studies, but it is notable that the prevalence of non-thyroid disease in the *C9orf72* group did not differ significantly from controls (unlike the *GRN* group), suggesting perhaps that *GRN* mutations are more associated with autoimmunity than *C9orf72* expansions, irrespective of FTLD-TDP. Of note, the significantly higher prevalence of total autoimmune disease in *GRN* mutation carriers compared with *MAPT* mutation carriers persisted even after excluding cases with dual mutations (two of whom had concurrent *C9orf72* expansions) from the *GRN* group, suggesting that *GRN* mutations alone are still linked to high rates of systemic autoimmune disease.

Although a reasonably high proportion (22.2%) of the *C9orf72* group had an autoimmune disease, the prevalence of non-thyroid autoimmune disease in this group was not significantly different from healthy controls, in contrast to previous observations (Miller et al., 2016), but consistent with another study (Katisko et al., 2018). This may be due to the smaller group of *C9orf72* expansion carriers analysed in the present study, which could have reduced power to detect this difference. Alternatively, as most of this group

had bvFTD rather than FTD-MND, and MND seems to be associated with more extensive TDP-43 pathology and a stronger link to autoimmunity, this may explain the lower prevalence of autoimmune disease in the present study. Inclusion in a previous study of many individuals with FTD-MND, both with and without *C9orf72* expansions (Miller et al., 2016), may have augmented associations between the expansion and autoimmune disease, which were actually due to MND or FTLD-TDP instead.

In conclusion, this study confirms that only *GRN* mutations are associated with an increased prevalence of autoimmune disease, and specifically certain clusters of non-thyroid diseases, including inflammatory arthritides and gastrointestinal or cutaneous disorders. This could be due to persistent, lifelong progranulin haploinsufficiency affecting the function of peripheral adaptive immune pathways, particularly those involving self-antigen presentation by macrophages and other immune cells to T cells within the thymus. This may lead to impaired self-tolerance and heightened systemic autoimmunity.

3.7 Limitations and future work

This is the first study to directly compare the prevalence of systemic autoimmune disease across genetic FTD subtypes and with controls. However, the number of cases in each group (particularly controls) was not very large and diagnoses of autoimmune disease were based on retrospective data analysis with sometimes limited clinical case notes. Information available may have been affected or limited by the patient or relative not volunteering this information in the medical history, or clinicians not specifically asking about a diagnosis of autoimmune disease, particularly in historic cases where this was not a routine part of the clinical research assessment. This study highlighted the need for inclusion of dedicated questions in the clinical assessment sections of GENFI and LIFTD case report forms focusing not only on the presence of autoimmune disease (yes/no), but also the type (thyroid/non-thyroid), and name of the systemic autoimmune

disease, to enable better data collection going forward. Case report forms have now been amended accordingly.

Replication of this study in a larger cohort of individuals with genetic FTD and mutations in *GRN*, *C9orf72* and *MAPT*, as well as different forms of sporadic FTD due to FTLD-TDP (particularly svPPA) is required to clarify the link between mutations in *GRN* or *C9orf72*, versus FTLD-TDP alone, and systemic autoimmune disease. Analysis of longitudinal data on the incidence of autoimmune diseases from PMC within GENFI would allow appreciation of the onset of these diseases in those who are many years before predicted onset of symptoms of FTD. Most young PMC will lack florid FTLD-TDP pathology, but already possess a causative gene mutation implicated in FTD, and this could lead to systemic immune dysfunction. This may help to explore the relative contributions of the early downstream effects of specific gene mutations (*GRN* or *C9orf72* haploinsufficiency or protein dysfunction), versus presence of FTLD-TDP itself, to onset of autoimmune disease in genetic FTD. Analysis of mutation negative relatives within GENFI would also allow inclusion of a larger number of controls for comparison.

Examination of systemic levels of inflammatory biomarkers such as cytokines or chemokines, and titres of autoantibodies involved in systemic autoimmune disease, in blood samples from symptomatic and presymptomatic individuals compared with controls, may help to elucidate whether the clinical observations from this study correlate with quantifiable evidence of systemic immune dysregulation.

One individual in this study, who had bvFTD due to a *GRN* mutation, had developed an unusual autoimmune disease (persistent eosinophilia associated with pericardial effusion), and was noted to have significant white matter changes, known as white matter hyperintensities (WMH), on her MRI brain scans, similar to those seen in individuals with

CNS demyelinating diseases such as multiple sclerosis (Sarbu et al., 2016). These WMH have been described in several studies of *GRN* mutation carriers (Ameur et al., 2016; Caroppo et al., 2014; Kelley et al., 2009; Le Ber et al., 2008; Paternicò et al., 2016; Pietroboni et al., 2011; Sudre et al., 2017a, 2019) but their aetiology remained unknown. This led to a decision to examine the histopathological correlates of WMH in this individual, to explore whether dysfunction in neuroinflammatory mechanisms, such as microglia or astrocytes, or excessive demyelination, may have contributed to these, particularly given that systemic immune dysfunction was likely also present. Results of this study are presented within the next chapter.

3.8 Publications relating to this chapter

A manuscript of this study has been prepared and is awaiting review by authors before submission. The work within this chapter was published as abstract following presentation at the Alzheimer's Association International Conference in 2017:

Woollacott IOC et al. (2017) Increased prevalence of non-thyroid autoimmune disease in patients with familial frontotemporal dementia associated with progranulin mutations. *Alzheimer's and Dementia* 13:Issue 7S_Part_10, P517

4 Histopathological correlates of white matter hyperintensities in *GRN* mutation associated FTLD

4.1 Chapter summary

Introduction: White matter hyperintensities (WMH) are often seen on MRI brain scans of presymptomatic and symptomatic individuals with *GRN* mutations, but they differ in appearance from WMH due to vascular disease, and their histopathological correlates are unknown. As progranulin regulates microglial function, non-vascular, neuroinflammatory mechanisms could contribute to white matter damage in these individuals. This study investigated the histopathological changes underlying WMH in an individual with bvFTD who had confirmed FTLD due to a *GRN* mutation (FTLD-*GRN*).

Methods: *Post-mortem* tissue from specific brain regions was directly matched to the location of WMH seen on fluid-attenuated inversion recovery (FLAIR) images of a cadaveric MRI scan. Volumetric T1 images of *in vivo* and cadaveric MRI scans were compared to assess grey matter atrophy. Segmentation of WMH on cadaveric FLAIR MRI images enabled regional WMH quantification and selection of five brain regions for histological analysis corresponding to differing severities of WMH. Immunohistochemistry was used to assess histopathological changes in grey and white matter of: the right frontal pole (severe WMH), right anterior frontal lobe (moderate to severe), right temporal lobe (mild to moderate), right posterior frontal lobe (very mild), and right occipital lobe (none). The severity of vascular pathology, spongiosis, neuronal and axonal loss, demyelination, TDP-43 burden and astrogliosis, and the burden and morphology of CD68, CR3/43 and Iba1-positive microglia, were assessed in each region.

Results: *In vivo* and cadaveric MRI brain scans showed progressive, asymmetric frontotemporal and parietal atrophy (worse on the left), and bilateral, asymmetrical WMH

(also worse on the left) predominantly affecting frontal mid-zones. Regions with the most severe WMH displayed the most severe white matter and cortical pathology, including demyelination, but minimal vascular pathology and only mild axonal loss. There were many amoeboid CD68 and CR3/43-positive microglia, but few and very dystrophic Iba1-positive microglia, in regions with severe WMH, particularly in frontal white matter.

Conclusions: This study demonstrates that the extensive WMH seen on MRI in *GRN* mutation carriers are not due to vascular pathology. Whilst axonal degeneration induced by cortical pathology could contribute to white matter damage and development of WMH, individuals with *GRN* mutations could develop regionally selective white matter vulnerability and myelin loss due to chronic, regional microglial dysfunction and excessive microglial senescence.

4.2 Introduction

Observations in Chapter 3 and previous studies (Miller et al., 2013) suggest that there is heightened systemic autoimmunity in individuals with FTD due to *GRN* mutations. This has strengthened evidence from *GRN* mouse models showing dysregulated systemic and CNS immune pathways. If heightened autoimmunity is also present in the CNS of *GRN* mutation carriers, this may contribute to immune-mediated neuronal and axonal damage. Several studies have reported significant white matter neuroimaging abnormalities in individuals with FTD due to *GRN* mutations, particularly the presence of cerebral white matter hyperintensities (WMH) (Ameur et al., 2016; Caroppo et al., 2014; Kelley et al., 2009; Le Ber et al., 2008; Paternicò et al., 2016; Pietroboni et al., 2011; Sudre et al., 2017a, 2019). WMH are seen on MRI brain scans as hyperintense lesions on T2-weighted and FLAIR sequences, reflecting an abnormal tissue fat/water ratio within myelinated brain areas (Wardlaw et al., 2015). They are present in healthy aging, appearing as lesions within the periventricular and deep white matter (Haller et al., 2013; Murray et al., 2012), in small vessel cerebrovascular disease, where they are more

extensive (Wardlaw et al., 2015), and in vascular dementia (Snyder et al., 2015) and AD (Lee et al., 2016; McAleese et al., 2015, 2017; Ryan et al., 2015). However, WMH are also present in neuroinflammatory disorders such as multiple sclerosis and neuromyelitis optica (Sarbu et al., 2016).

The majority of *GRN* mutation carriers with WMH lack vascular risk factors (Ameur et al., 2016; Caroppo et al., 2014), and the location and appearance of WMH in these individuals is different from WMH due to small vessel disease. WMH in *GRN* mutation carriers are located predominantly in the frontal lobes, and to a lesser extent in the occipital and parietal lobes, within both periventricular and medial white matter regions (Sudre et al., 2017a, 2019). In fact, they seem more like the WMH in neuroinflammatory disorders, which are due to autoimmune-mediated demyelination, rather than vascular disease (Sarbu et al., 2016). Symptomatic individuals with FTD due to *GRN* mutations also have significant differences in WMH compared with individuals with FTD due to *MAPT* or *C9orf72* mutations, including a higher global load of WMH and more homogeneity in lesion appearance (Sudre et al., 2017a). WMH occur presymptomatically in *GRN* mutation carriers within parietal and occipital regions (Sudre et al., 2017a, 2019), accumulating over time in symptomatic individuals (Sudre et al., 2019). They may be directly associated with the disease process, as the burden of WMH correlates with frontal grey matter atrophy, impairments in executive function and plasma biomarkers of neuroinflammation (GFAP levels) and white matter damage (NfL levels) in *GRN* mutation carriers (Sudre et al., 2019).

There is extensive research into the histopathological correlates of WMH in healthy aging, where they are associated with enlarged perivascular spaces, vacuolation, demyelination, axonal loss, microgliosis and astrogliosis (Haller et al., 2013; Murray et al., 2012), and in small vessel cerebrovascular disease, where they are associated with

demyelination, axonal loss, gliosis and arteriosclerosis (Wardlaw et al., 2015). In vascular dementia, these changes are more extensive due to severe ischaemic damage (Snyder et al., 2015). In sporadic AD, WMH are multifactorial in aetiology, including due to small vessel sclerosis and ischaemia (Englund, 1998) and cortical neurodegenerative pathology leading to secondary axonal loss and demyelination (McAleese et al., 2015, 2017). In familial AD, the severity of WMH correlates with the burden of cerebral amyloid angiopathy (CAA) (Ryan et al., 2015). In multiple sclerosis, WMH are associated with reactive microgliosis, macrophage infiltration and demyelination but relatively preserved axons (Sarbu et al., 2016).

The underlying histopathological correlates of WMH in cases with confirmed *GRN* mutation associated FTLD (FTLD-*GRN*) have not been explored in detail, and it remains unclear whether there are underlying vascular changes. One small study examined *post-mortem* brain tissue from two FTLD-*GRN* cases, in brain regions broadly corresponding to areas of significant WMH on FLAIR imaging (frontal white matter) (Kelley et al., 2009). There was marked demyelination and significant astrogliosis and microglial activation in these regions. However, precise correlation with neuroimaging changes was not performed, control (unaffected) brain regions were not examined, and evidence of other contributory pathology, such as vascular disease, was not explored.

A hypothesis of a non-vascular, inflammatory aetiology of WMH in *GRN* mutation carriers is intriguing given the role of progranulin in various inflammatory pathways. To establish accurately the histopathological correlates of WMH in FTLD-*GRN* cases, there needs to be precise correlation of neuroimaging abnormalities with histopathological changes in corresponding brain regions. However, this was previously difficult to establish through use of *in vivo* MRI in individuals who subsequently had a *post-mortem* examination, as WMH evident on the last available MRI brain scan (often carried out several years before

death) may not match the localisation and severity of brain tissue abnormalities seen *post-mortem*. In contrast, cadaveric brain MRI enables scanning of the intact post-mortem brain *in situ* in individuals within 24 hours of death, limiting degradation of brain tissue (Tofts et al., 2008). It provides detailed, undistorted images of the brain, avoiding the changes that occur following brain removal and fixation and with *post-mortem* scanning. It therefore allows precise spatial and quantitative correlations of neuroimaging abnormalities with histopathological findings in brain tissue.

4.3 Aims and hypothesis

This study aimed to examine the histopathological changes underlying WMH in *post-mortem* brain tissue from an individual with *GRN* mutation associated FTD (with confirmed FTLD-*GRN*), who had extensive WMH on *in vivo* brain MRI, and who underwent detailed cadaveric brain MRI examination and *post-mortem* brain donation. Vascular changes would be extensively explored using consensus guidelines for vascular pathology (Skrobot et al., 2016), alongside detailed histological examination of neuronal and axonal degeneration, myelin loss, protein aggregation, and astrocytes and microglia. The severity of these histopathological changes would be correlated with the severity of WMH and degree of grey matter atrophy on MRI.

The hypothesis was that WMH seen on MRI in *GRN* mutation-associated FTD are not due to vascular pathology from ischaemia or cerebrovascular disease, but secondary to non-vascular processes such as immune-mediated demyelination due to altered glial function within white matter areas. WMH may or may not correlate regionally with the degree of white matter pathology, cortical pathology and grey matter atrophy, and may be associated with changes in microglia and astrocytes in grey or white matter.

4.4 Methods

4.4.1 Case report

A 60-year-old left-handed female developed progressive behavioural change, episodic memory impairment and speech disturbance. Initially she developed prominent apathy and flat affect, reduced social interaction, sweet tooth, laughing in inappropriate situations, and new obsessions. She subsequently developed reduced speech output, repetition of stereotypic phrases, and over the next four years eventual mutism. Two years after onset she had difficulty remembering recent events and conversations and got lost in familiar places. She then developed dyscalculia, made unwise financial investments and stopped all her hobbies. Her condition rapidly worsened four years after onset and she was admitted to a nursing home aged 65, with impaired spatial awareness, prosopagnosia, visual hallucinations, wandering and incontinence. She later developed an asymmetrical extrapyramidal syndrome with right limb dystonia. She died aged 68 with a final clinical diagnosis of bvFTD. She donated her brain to the QSBB for *post-mortem* analysis.

Her medical history included progressive right-sided facial hemiatrophy diagnosed 15 years prior to the onset of cognitive symptoms, with no cause identified. Two years after onset of cognitive symptoms she developed a persistent cough and peripheral eosinophilia, pericardial thickening and an anterior pericardial effusion. Bronchoscopy was normal and bronchial washings were negative for acid fast bacilli. Heaf test for tuberculosis was negative. The cause of these symptoms was not identified, but they were felt to be autoimmune in origin, and they improved on inhaled corticosteroids. There were no vascular risk factors. She was on a corticosteroid inhaler on first assessment but no other medications, was a non-smoker, and drank moderate amounts of alcohol. Her mother had developed an acute psychosis with delusions and odd behaviour aged 65, followed by progressive cognitive decline and admission to a mental health unit for

20 years, with an eventual diagnosis of dementia. There was no other family history of dementia or neurological or vascular disease.

Investigations included a volumetric 1.5T MRI brain performed 2.6 years before death. This showed bilateral but asymmetric frontal, temporal and parietal atrophy, worse on the left, and significant bilateral periventricular WMH, worst in the frontal lobes and on the left side. A SPECT scan showed left frontal hypoperfusion. Electroencephalogram was normal and CSF results, including oligoclonal bands, treponemal and viral screens and Whipple's polymerase chain reaction, were normal or negative (neurodegenerative markers were not assessed as these tests were not widely available at that time). A wide variety of blood tests were normal, except for a peripheral eosinophilia of 1.11 (range 0 to 0.4 x 10^9/L) and positive rheumatoid particle agglutination test (1/80 titre). DNA analysis identified a *GRN* Q130fs mutation but no other FTD-associated mutations and no mutations in colony stimulating factor 1 receptor (*CSF1R*).

4.4.2 Imaging techniques

The *in vivo* 1.5T MRI was performed on a GE Signa scanner and included volumetric T1 and T2-weighted but not FLAIR sequences. The patient and her husband had consented to her participation in a cadaveric MRI study, approved by the NHNN and Institute of Neurology Joint Research Ethics Committee. Within 24 hours after her death, she underwent a cadaveric brain MRI on a 1.5T GE Signa scanner, with the brain *in situ* in the skull, including volumetric T1 and FLAIR sequences, as described previously (Tofts et al., 2008). The *in vivo* and cadaveric volumetric T1 MRI sequences were compared using the Statistical Parametric Mapping (SPM) 12 Serial Longitudinal Registration tool (www.fil.ion.ucl.ac.uk/spm) to estimate the percentage of volumetric contraction for each voxel between the two scans, in order to assess the degree of brain atrophy over time. Although WMH were present on both the *in vivo* and cadaveric MRI, only the cadaveric MRI could be segmented for further imaging analysis, due to lack of *in vivo* FLAIR and

poor quality *in vivo* T2-weighted imaging. This precluded quantitative comparison of the interval change in WMH between scans.

Regional quantification of WMH was performed on the cadaveric FLAIR sequences, using methods described in previous studies (Sudre et al., 2015, 2017b, 2017a, 2018, 2019). WMH were first automatically segmented using an algorithm based on outlier modelling in a multivariate Gaussian mixture model (Sudre et al., 2015, 2017b). Localisation of WMH was then performed by aggregating cortical regions into four lobes (frontal, temporal, parietal or occipital) and discretising the white matter into four equidistant layers within each lobe, based on the relative distance between the ventricular surface and the cortical sheet (1st layer most periventricular, 4th layer most juxtacortical) (Sudre et al., 2018). Infratentorial regions were excluded from analysis and subcortical regions (basal ganglia or thalami) were segmented separately. WMH were apportioned into zones based on whether they were nearest to one of the four cortical lobes, and whether they were in each cortical layer.

This localisation and discretisation analysis produced two measures of WMH burden (severity) from the cadaveric MRI: lesion distribution (volume of lesion in a region divided by the total volume of lesion, i.e. the proportion of the lesion load present in that brain region) and the lesion frequency (volume of lesion in a region divided by the volume of this region, i.e. the proportion of the volume of a brain region taken up by the lesion) (Sudre et al., 2018). This enabled quantification and visual representation of WMH seen on the cadaveric MRI within each lobe and across different cortical layers and subcortical brain regions. This guided selection of brain regions for histopathological analysis, based on different severities of WMH in each region and layer.

4.4.3 Histological techniques

The patient's brain was donated *post-mortem* to the QSBB under protocols detailed in Chapter 2.1.2. However, in this case, both hemispheres had been fixed, using techniques as detailed in Chapter 2.2.1.1. Blocks of tissue from many brain regions were cut from 5mm fixed slices obtained from each hemisphere, processed, and used for tissue sectioning and diagnostic staining and immunohistochemistry, and clinical neuropathological analysis, as detailed in Chapter 2.2.1.1.

Five brain regions within the right hemisphere were selected for further histological analysis for this study, as the left hemisphere was severely atrophied and so provided inadequate tissue for detailed imaging correlation and histological examination. Selection of these five regions was based on visual inspection (Figure 4.1) and imaging analyses (Figure 4.4) of WMH in the cadaveric MRI FLAIR images. The five regions corresponded anatomically to areas with differing severities of WMH: the right frontal pole (severe WMH), right anterior frontal lobe (moderate to severe), right temporal lobe (mild to moderate), right posterior frontal lobe (very mild), and right occipital lobe (none). Blocks of tissue were cut from these regions based on their location in coronal, sagittal and axial views of the cadaveric MRI FLAIR images (Figure 4.1).

FFPE sections were cut from tissue blocks at 8μm (or 12 μm, for LFB stain) thickness, using a Thermo rotary microtome. Sections were placed onto 30% alcohol solution and floated onto warm water. Sections were mounted onto Plus Frost positively charged microslides (Solmedia) and left to dry at 37°C for several hours. Before staining or immunohistochemistry, slides were incubated overnight at 60°C. Sections from each of the five regions were stained with H&E, LFB and Perl stains to assess the degree of neuronal loss and spongiosis, myelin loss and haemosiderin deposition. Immunohistochemistry was performed on sections using antibodies to detect the

presence of TDP-43, Aβ, tau, alpha-synuclein, phosphorylated neurofilaments (axons) and activated astrocytes, using antibodies and techniques detailed in Chapter 2.2.1.1. To assess different microglial phenotypes and morphologies, immunohistochemistry was also performed on sequential sections from each region using antibodies to detect three different microglial markers (CD68, CR3/43 and Iba1), as detailed in Chapter 2.2.1.2.

Grey and white matter from each region were assessed for histopathological changes through microscopic examination and consensus opinion of two neuropathologists blinded to the severity of WMH. Sections were qualitatively assessed for the severity of neuronal loss and spongiosis and semi-quantitatively assessed for the severity of axonal loss, myelin loss, astrogliosis, the burden of TDP-43, and the burden of CD68, CR3/43 and Iba1-positive microglia.

Axonal and myelin loss were scored in white matter of each region, neuronal loss and spongiosis were scored in grey matter, and both grey and white matter were assessed for other histopathological changes, but these were only scored separately for microglial markers or if significant differences in other histological changes were present.

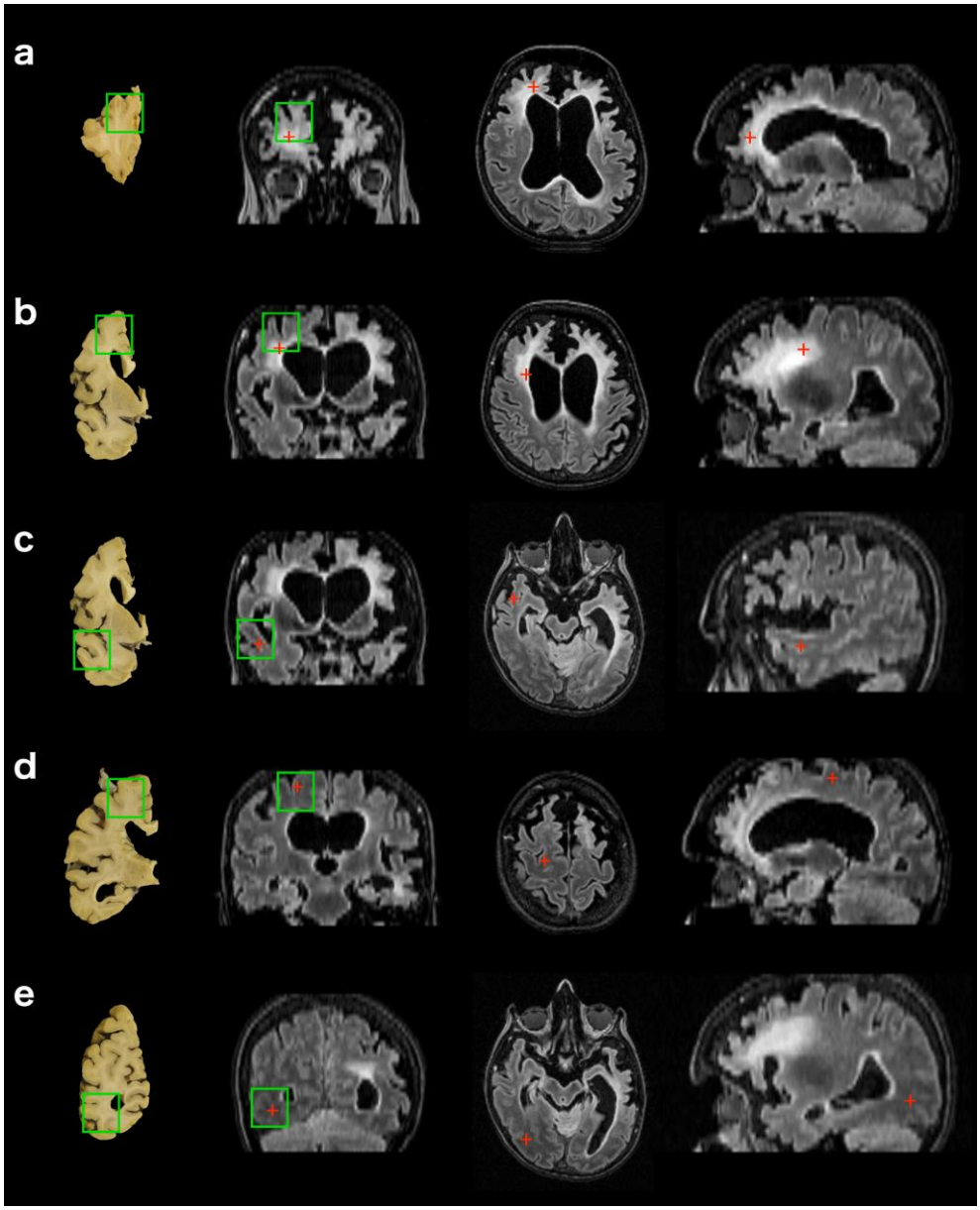

Figure 4.1 Comparison of brain tissue sections with cadaveric FLAIR MRI appearances to enable accurate tissue block selection

(**a**) right frontal pole, (**b**) right anterior frontal lobe, (**c**) right temporal lobe, (**d**) right posterior frontal lobe and (**e**) right occipital lobe. Images in the far left column show where tissue blocks (green boxes) were obtained from *post-mortem* brain tissue slices. Right three columns show, from left to right, cadaveric brain MRI images in the coronal, axial and sagittal planes. Green boxes indicate borders of the tissue block cut from this region, superimposed onto the corresponding tissue slice and MRI image. Red crosses represent the same anatomical point viewed across all three planes.

Semi-quantitative assessment used a multi-tier scoring system modified from a previous study (Ryan et al., 2015), where: ‘0' represents no axonal loss, no white matter pallor,

no TDP-43 present, no astrogliosis or no visible microglia; “+” or ‘1' represents a mild degree of axonal loss, white matter pallor, TDP-43 burden, astrogliosis or presence of few microglia; “++” or ‘2' represents a moderate degree of these changes or presence of moderate numbers of microglia; and “+++” or ‘3' represents a severe degree of these changes or presence of many microglia. In addition, qualitative descriptions of microglial morphology were recorded, for example whether microglia appeared amoeboid (round), suggestive of microglial activation, or ramified (with extended processes), or any other atypical morphological appearances, including microglial dystrophy: thin, short and few distal branches, shortened tortuous or beaded cell processes, fragmented cytoplasm, or spheroidal inclusions (Streit et al., 2004).

Vascular pathology was semi-quantitatively assessed in grey and white matter of the five regions of interest using a comprehensive scoring system based on the consensus recommendations of the Vascular Cognitive Impairment Neuropathology Guidelines (VCING) for staging of cerebrovascular pathology in cognitive impairment (Skrobot et al., 2016) (Table 4.1). Leptomeningeal vessels were examined for presence of atheroma in all five brain regions. Presence of atheroma in the circle of Willis and vascular changes in other cortical and subcortical areas had been examined during diagnostic *post-mortem* analysis. Although the VCING include scores for myelin loss, all regions were also scored for white matter pallor using a modified multi-tier scoring system (Ryan et al., 2015) to allow direct comparison between this score of myelin loss and scores for non-vascular histopathological changes.

Vascular changes scoring	Vessel wall pathology scoring
Myelin loss 0 = dense and homogeneous myelin staining 1 = mild diffuse or focal myelin pallor 2 = severe focal/diffuse myelin pallor with vacuolation or tigroid appearance of the white matter 3 = total focal/diffuse destruction of the myelin, or white matter infarcts	**Arteriolosclerosis/arteriosclerosis** 0 = normal 1 = mild thickening of the vessel media, mild fibrosis 2 = partial loss of smooth muscle cells in the media, moderate hyaline fibrosis 3 = complete loss of smooth muscle cells in the media, severe hyaline fibrosis, lumen stenosis
Perivascular space dilatation 0 = absent 1 = perivascular space < artery diameter in all sections 2 = perivascular space ≥ artery diameter in the minority of sections 3 = perivascular space ≥ artery diameter in the majority of sections	**Fibrinoid necrosis or microaneurysms** 0 = absent 1 = present
Perivascular haemosiderin leakage 0 = absent 1 = <3 haemosiderin granule deposits in the perivascular space 2 = 3-5 haemosiderin granule deposits in the perivascular space 3 = >5 haemosiderin granule deposits in the perivascular space	**Cerebral amyloid angiopathy (leptomeningeal, cortical and capillary)** 0 = absent 1= trace or occasional vessels affected 2 = one or a few vessels circumferentially affected 3 = widespread involvement of circumferentially affected vessels 4 = as 3, with secondary changes
Microinfarcts 0 = absent 1 = present	**Circle of Willis atherosclerosis** 0 = no atheroma 1 = atheroma present but no artery >50% occluded 2 = atheroma and one vessel ≥50% occluded 3 = atheroma and >1 vessel ≥50% occluded
Large infarcts 0 = absent 1 = present	
Lacunar infarcts 0 = absent 1 = solitary 2 = 2-4 3 = 5 or more	
Microhaemorrhage 0 = absent 1 = present	
Larger haemorrhage 0 = absent 1 = present	

Table 4.1 Parameters of vascular pathology analysed in brain regions of interest

Parameters were based on recommendations of the VCING for staging of cerebrovascular pathology in cognitive impairment (Skrobot et al., 2016).

4.5 Results

4.5.1 Imaging findings

The i*n vivo* MRI brain scan showed progressive, asymmetric (left worse than right) frontal, temporal and parietal atrophy (Figure 4.2). Between the *in vivo* and cadaveric MRI scans there had been volume loss, particularly affecting left posterior frontal and parietal and right frontal areas (Figure 4.2). WMH were present asymmetrically on both *in vivo* T2 (Figure 4.3) and cadaveric FLAIR (Figure 4.1 and Figure 4.3) images, predominantly affecting both frontal lobes, as confirmed by the localisation analysis of cadaveric FLAIR images (Figure 4.4). WMH were most severe in the left frontal pole and anterior frontal lobe (Figures 4.1, 4.3 and 4.4), matching areas of most significant cortical atrophy (Figure 4.2), although were also severe in the right frontal pole and anterior frontal lobe. WMH were present predominantly in the intermediate layers (layers two to three), or 'mid-zones', of the frontal lobes, rather than just immediately periventricularly or juxtacortically (Figure 4.4). WMH were also seen in the parietal lobes (more on the left than the right), and to a much lesser extent in the posterior frontal and temporal lobes, with minimal or no WMH in the occipital lobes (Figures 4.1, 4.3 and 4.4).

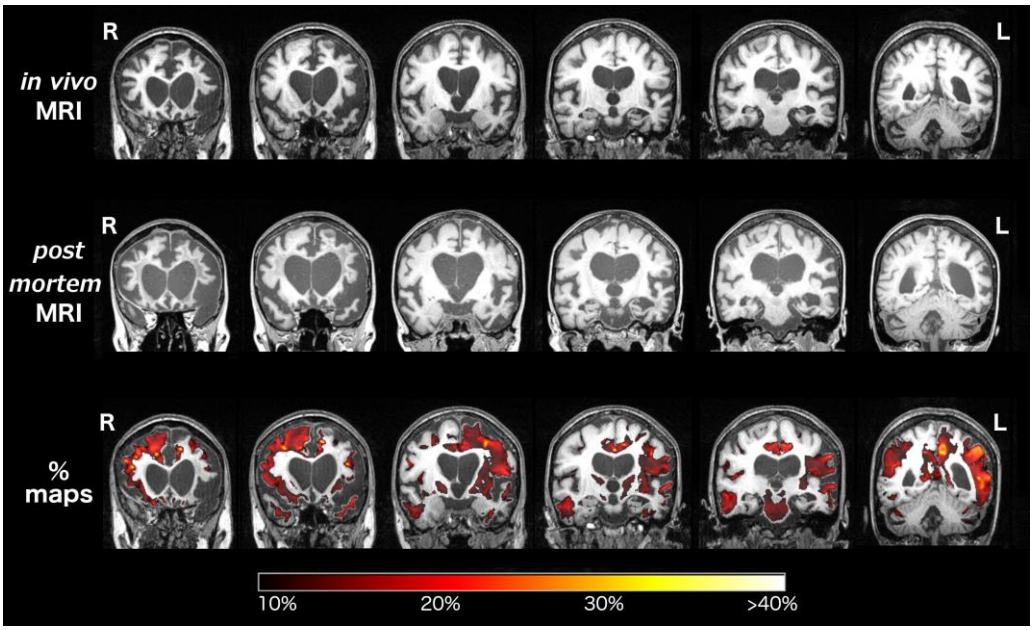

Figure 4.2 Coronal sections of *in vivo* and cadaveric T1-weighted MRI and changes in grey matter volume between scans

The top row shows the *in vivo* MRI and the middle row shows the cadaveric (*post-mortem*) MRI. The bottom row shows the longitudinal SPM overlay showing changes between these two scans (2.6 year interval), with 10% or greater volumetric contraction at the time of death from the *in vivo* scan shown on the corresponding colour bar scale. R = right; L = left.

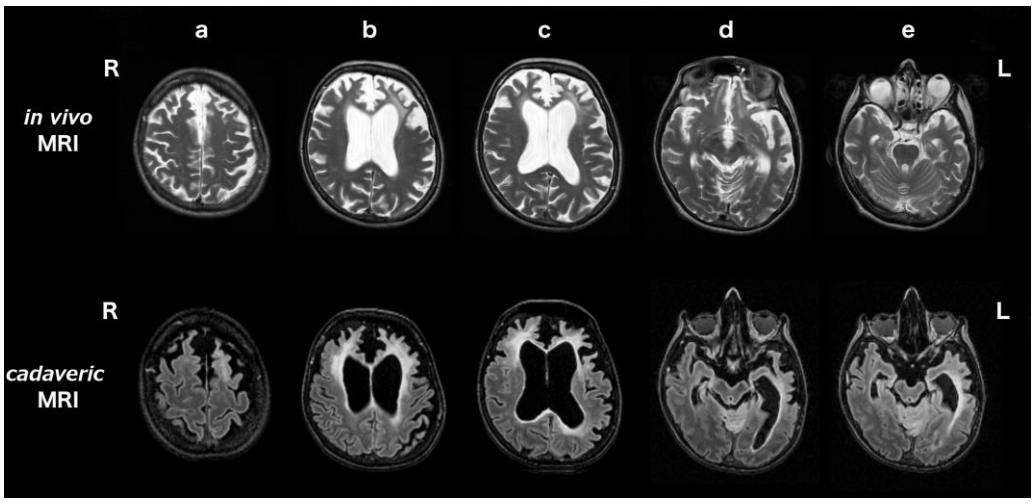

Figure 4.3 WMH are present on *in vivo* T2-weighted and cadaveric FLAIR MRI

The top row shows axial sections of the *in vivo* T2-weighted MRI and the bottom row shows axial sections of the cadaveric FLAIR MRI. This demonstrates the change in severity and distribution of WMH in the 2.6 year interval between scans, in the rostro-caudal direction from (**a**) to (**e**). (**a**) posterior frontal lobes, (**b**) anterior frontal lobes, (**c**) frontal poles, (**d**) occipital lobes and (**e**) temporal lobes. R = right; L= left.

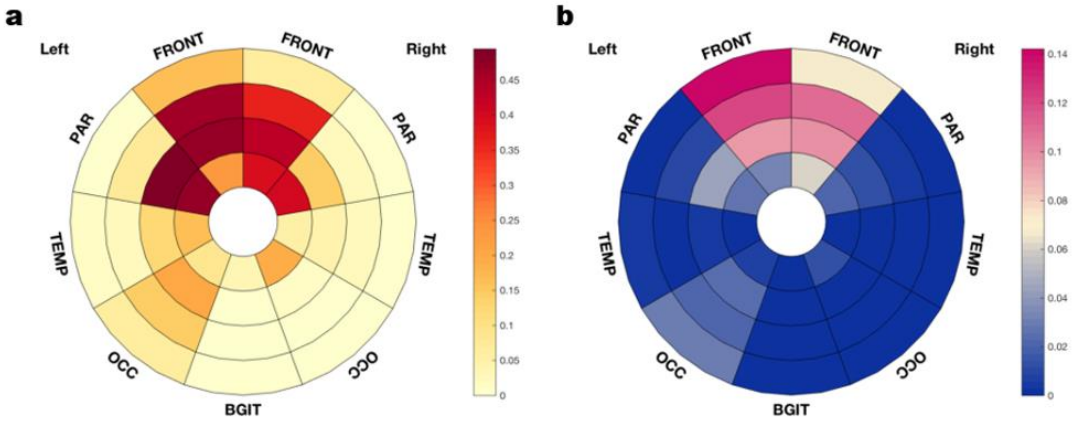

Figure 4.4 Bull's-eye schematic of WMH lesion frequency and lesion distribution within the cadaveric MRI in different brain regions

Lesion frequency (**a**) is the proportion of the volume of a region taken up by lesion. Lesion distribution (**b**) is the proportion of the lesion load present in that region. FRONT=frontal lobe; PAR=parietal; TEMP=temporal; OCC=occipital; BGIT=basal ganglia and thalami. Colour bars show the burden of WMH (highest = red).

4.5.2 Histopathological changes and correlation with imaging

Routine diagnostic neuropathological analysis had revealed severe neuronal loss and spongiosis, particularly in the anterior frontal, temporal and insular cortices and caudate, and severe myelin loss and gliosis in the frontal and temporal lobes. There was severe myelin loss in the external capsule, extreme capsule and anterior internal capsule but comparatively milder axonal loss in the frontal and temporal lobes. The cerebellum and occipital lobes had minimal pathology. TDP-43 inclusions were present in neuronal cytoplasm and occasional neuronal nuclei, and TDP-43 positive neuropil threads were seen, particularly in frontal lobe grey and white matter, consistent with FTLD-TDPA (Mackenzie et al., 2011), which was in keeping with the patient's *GRN* mutation (FTLD-*GRN*). There was no Aβ, tau or alpha-synuclein pathology. There was no atheroma in most leptomeningeal vessels in cortical and subcortical regions (very rare vessels had atheroma with less than 50% vessel occlusion), and no other vascular pathology. There was only mild (grade 1) atheroma in the circle of Willis.

Results of detailed regional histological analyses are summarised in Tables 4.2 and 4.3. Representative appearances in brain regions with the most severe WMH and least severe WMH are presented in Figures 4.5 and 4.6. Brain regions with the most severe WMH (frontal pole and anterior frontal lobe) displayed the most severe white matter pathology, including myelin pallor and astrogliosis (Table 4.2; Figure 4.5c and 4.5g) and severe TDP-43 burden, but no or minimal vascular pathology (Table 4.2) and relative preservation of axons (Figure 4.5e). Regions with very mild or absent WMH, such as the posterior frontal lobe or occipital lobe, generally had very mild or no histopathological changes in both grey and white matter (Figure 4.5b, d, f, h). Regions with the most severe WMH on MRI also displayed the most severe cortical (grey matter) pathology, including neuronal loss, spongiosis, astrogliosis and TDP-43 burden (Table 4.2). The severity of cortical pathology corresponded with the degree of white matter pathology in all regions analysed, with the exception of axonal loss in the frontal pole (Figure 4.5e), anterior frontal lobe and temporal lobe, where there was notably mild axonal loss despite more severe degrees of other grey and white matter pathology.

Except for myelin loss on LFB staining, there were minimal features of vascular pathology in all regions analysed (Table 4.2). There was very mild arteriolosclerosis present in occasional white matter vessels in all five brain regions of interest but no atheroma in leptomeningeal vessels.

	Right frontal pole	Right anterior frontal lobe	Right temporal lobe	Right posterior frontal lobe	Right occipital lobe
WMH severity	Severe	Moderate to severe	Mild to moderate	Very mild	None
Cortical spongiosis (None/mild/moderate/ full thickness)	Full thickness; U fibres preserved	Full thickness; U fibres preserved	Severe	Very mild	None
Cortical neuronal loss (No loss/mild/moderate/ severe)	Severe	Severe	Severe	Mild	No loss
White matter myelin pallor (0=none; 1=mild; 2=moderate; 3=severe)	3	3	3	0	0
White matter axonal loss (0=none; 1=mild; 2=moderate; 3=severe)	1	1	1	0	0
Astrogliosis (0=none; 1=mild; 2=moderate; 3=severe)	GM: 3 WM:3	GM:3 WM: 3	GM: 1 WM: 3	GM: 1 WM: 3	GM: 1 WM:1
TDP-43 (Type A) (0/+/++/+++)	++ Moderate cytoplasmic and nuclear inclusions plus threads	++/+++ Moderate cytoplasmic and nuclear inclusions plus threads	+ Sparse nuclear inclusions, a few threads	+ Sparse nuclear inclusions, a few threads	+ Only a few threads
Arteriosclerosis (0-3)	1	1	1	1	1
Fibrinoid necrosis (0/1)	0	0	0	0	0
Microaneurysms (0/1)	0	0	0	0	0
Perivascular space dilation (0-3)	1	2	2	1	0
Perivascular haemosiderin leakage (0-3)	0	1	0	0	0
Microinfarcts (0/1)	0	0	0	0	0
Large infarcts (0/1)	0	0	0	0	0
Lacunar infarcts (0-3)	0	0	0	0	0
Microhaemorrhage (0/1)	0	0	0	0	0
Larger haemorrhage (0/1)	0	0	0	0	0
Leptomeningeal CAA (0-4)	0	0	0	0	0
Cortical CAA (0-4)	0	0	0	0	0
Capillary CAA (0/1)	0	0	0	0	0

Table 4.2 Histopathological changes assessed across five brain regions with different severities of WMH on MRI

CAA = cerebral amyloid angiopathy, GM = grey matter, WM = white matter.

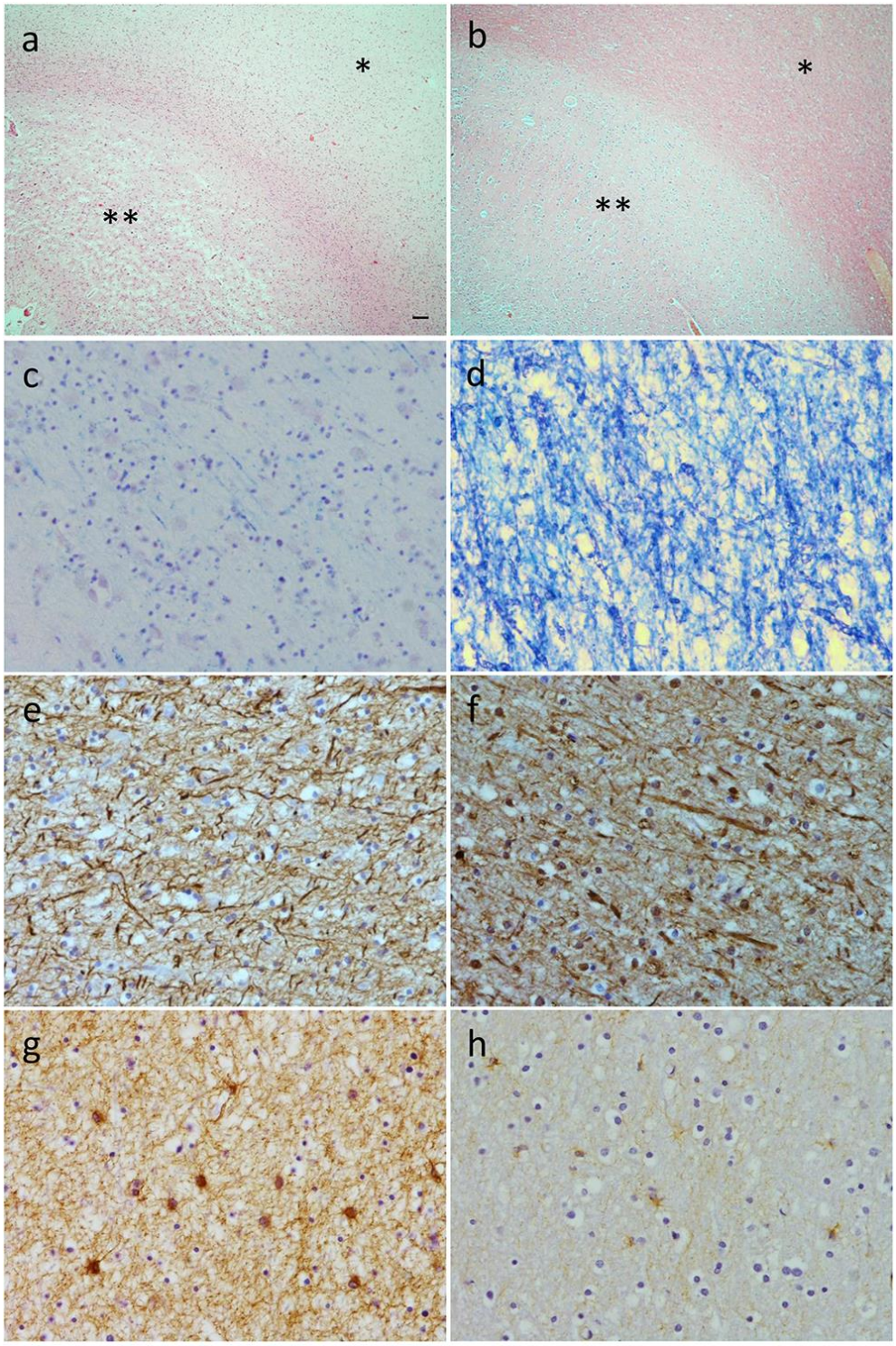

Figure 4.5 Histopathological changes in regions with severe WMH (frontal pole) and no WMH (occipital lobe)

Right frontal pole (**a, c, e**, and **g**); right occipital lobe (**b, d, f** and **h**). Hematoxylin and eosin staining reveals severe grey matter spongiosis (**) and pallor of the white matter (*) in the frontal pole (**a**). In the occipital lobe (**b**) there is intact cytoarchitecture of the grey matter (**) and white matter (*). LFB staining demonstrates extensive myelin pallor in the white matter of the frontal pole (**c**) but intact myelin in the occipital lobe (**d**). SMI31 immunohistochemistry demonstrates relative preservation of axons in the white matter of both frontal pole (**e**) and occipital lobe (**f**). Severe astrogliosis was present in frontal pole white matter (**g**) but only mild in occipital lobe white matter (**h**). Scale bar in (**a**) represents 100μm for (**a**) and (**b**), and 10μm for (**c**) to (**h**).

4.5.3 Patterns of microglia

Microglial burden and morphology differed between regions with severe WMH (frontal lobe), and those without WMH (occipital lobe) (Table 4.3; Figure 4.6). There was a higher burden of CD68, CR3/43 and Iba1-positive microglia in frontal and temporal grey matter than occipital grey matter (Table 4.3). There was also a higher burden of CD68 (Figure 4.6a) and CR3/43 (Figure 4.6c) positive microglia present in frontal than occipital white matter (Figure 4.6b, d), but similarly few Iba1-positive microglia in white matter of both regions (Figure 4.6e, f). Although there were generally more CD68 and CR3/43-positive microglia present in white matter than in grey matter of all regions, there were much fewer Iba1-positive microglia in frontal and temporal white matter than grey matter (Table 4.3). In contrast, in the occipital lobe, the burden of Iba1-positive microglia was similar in grey and white matter.

In terms of morphology, CD68 and CR3/43-positive microglia were generally amoeboid in appearance in frontal grey and white matter (Table 4.3; Figure 4.6a, c), but ramified in occipital grey and white matter (Table 4.2; Figure 4.6b, d). There was a mixture of amoeboid and ramified CD68 and CR3/43-positive microglia in regions with intermediate WMH severity (posterior frontal or temporal lobe; Table 4.3). Iba1-positive microglia were sometimes amoeboid in appearance in frontal grey matter (Table 4.3). However, in the frontal pole and anterior frontal white matter, where there were severe WMH, Iba1-positive microglia displayed punctate staining throughout microglial cell processes, and a fragmented appearance typical of severely dystrophic microglia (Figure 4.6e) (Streit et al., 2004). This contrasted with the ramified and much less dystrophic appearance of Iba1-positive microglia present in occipital white matter, where WMH were absent (Figure 4.6f). Dystrophic microglia were present but not as severely disrupted in frontal grey matter (despite a similar burden of TDP-43 and other pathology) or in grey matter of any other region analysed (Table 4.3). Microglia were less dystrophic in white matter

within the temporal lobe (moderate WMH) and posterior frontal lobe (mild WMH) compared with the frontal lobe.

	Brain region	Right frontal pole	Right anterior frontal	Right temporal	Right posterior frontal	Right occipital
Microglial marker	**WMH severity**	Severe	Moderate to severe	Mild to moderate	Very mild	None
CD68	**Grey matter**	+ Amoeboid	++ Amoeboid	+ Amoeboid & Ramified	+ Ramified	+ Ramified
	White matter	++ Amoeboid	+++ Amoeboid	+++ Amoeboid & Ramified	+++ Amoeboid & Ramified	++ Ramified
CR3/43	**Grey matter**	+ Amoeboid	+ Amoeboid	++ Amoeboid	++ Amoeboid & Ramified	+ Ramified
	White matter	++ Amoeboid	+++ Amoeboid	+++ Amoeboid & Ramified	+++ Ramified	++ Ramified
Iba1	**Grey matter**	+++ Amoeboid Few dystrophic	+++ Amoeboid Few dystrophic	++ Amoeboid & Ramified	++ Amoeboid	+ Ramified
	White matter	+ Severely dystrophic	+ Severely dystrophic	+ Moderately dystrophic	+ Ramified, few dystrophic	+ Ramified, very few dystrophic

Table 4.3 Microglial burden and morphology in five brain regions with different severities of WMH on MRI

'Amoeboid': majority of microglia were round. 'Ramified': majority of microglia had branched processes. 'Amoeboid and ramified': a mixture of both morphologies. 'Dystrophic': fragmented, beaded appearance. + few microglia, ++ moderate numbers of microglia, +++ many microglia.

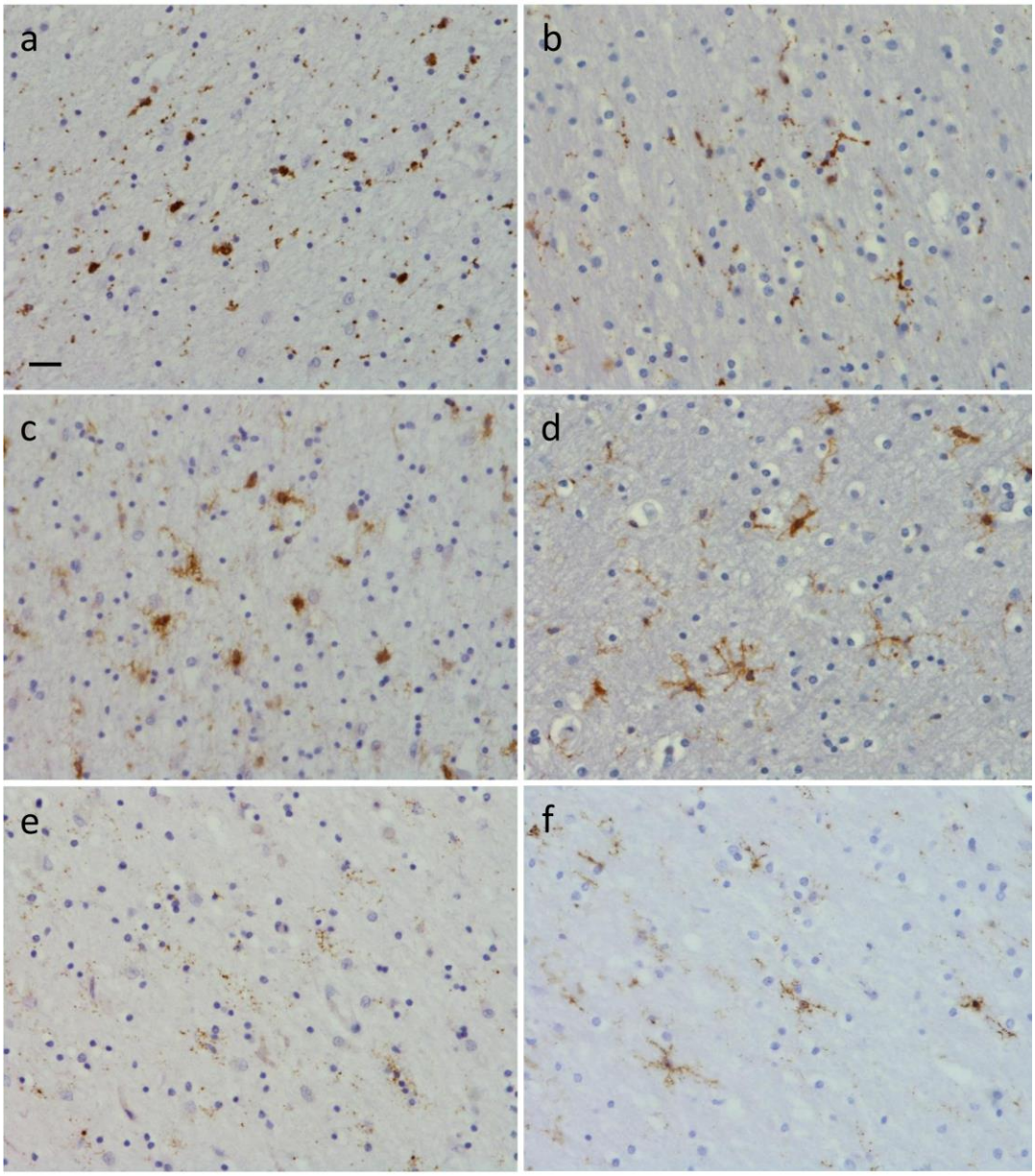

Figure 4.6 Microglia in white matter of right frontal pole (severe WMH) and right occipital lobe (no WMH)

Right frontal pole white matter (**a, c, e**) and right occipital white matter (**b, d, f**). Images show results of immunohistochemistry for CD68 (**a**) and (**b**), CR3/43 (**c**) and (**d**) and Iba1 (**e**) and (**f**) positive microglia. There were more amoeboid microglia in the frontal versus occipital white matter detected using CD68 (**a**) versus (**b**), and CR3/43 (**c**) versus (**d**). Iba1-positive microglia were severely dystrophic in frontal white matter (**e**) but less dystrophic and typically ramified in occipital white matter (**f**). Scale bar in (**a**) represents 20μm in all panels.

4.6 Discussion

Histopathological changes in white matter were observed in early studies of FTLD, including microgliosis, astrogliosis and demyelination (Englund and Brun, 1987) and several groups have observed significant WMH on MRI brain scans of *GRN* mutation carriers with FTD who lack vascular risk factors (Ameur et al., 2016; Caroppo et al., 2014; Kelley et al., 2009; Le Ber et al., 2008; Paternicò et al., 2016; Pietroboni et al., 2011; Sudre et al., 2017a, 2019). However, this is the first study to characterise the histopathological correlates of WMH in a case with confirmed FTLD-*GRN* in detail. Segmentation and localisation analyses of WMH present on cadaveric MRI FLAIR images, and careful selection of, and correlation with, multiple *post-mortem* brain tissue regions, enabled analysis of histopathological changes in grey and white matter in regions affected by varying severities of WMH on MRI. Histological assessment encompassed a wide range of morphological vascular changes using recent consensus guidelines (Skrobot et al., 2016) and other relevant histopathological changes examined in studies of WMH in other dementias and in two previous FTLD-*GRN* cases (Kelley et al., 2009). Due to the potential neuroinflammatory basis of white matter damage in individuals with *GRN* mutations, the burden and morphology of three different microglial phenotypes, and presence of activated astrocytes, were also analysed across multiple brain regions.

This approach has demonstrated that WMH in *GRN* mutation carriers with FTD occur predominantly in frontal lobe mid-zones and are associated with significant cortical pathology and white matter demyelination and astrogliosis, but only mild axonal loss and minimal vascular pathology. Although there are many amoeboid CD68 and CR3/43-positive microglia in grey and white matter regions where there are significant WMH, Iba1-positive microglia are severely dystrophic in white matter, particularly in the frontal lobe. This is suggestive of regional microglial dysfunction and associated white matter

vulnerability in *GRN* mutation carriers, which could be due to progranulin haploinsufficiency.

Prominent, asymmetrical WMH were present on both *in vivo* and cadaveric brain MRI. Imaging analysis revealed that WMH were most severe in the middle layers of the frontal lobes, as well as being present in periventricular regions. WMH were present to a lesser degree in the parietal and temporal lobes but were minimal or absent in the occipital lobes. This pattern of predominantly frontal WMH, both in periventricular and 'mid-zone' (midway between the lateral ventricles and cortex) regions of white matter, is a feature of WMH in symptomatic *GRN* mutation carriers in other studies (Ameur et al., 2016; Caroppo et al., 2014; Sudre et al., 2017a, 2019). WMH initially form in periventricular white matter regions of parietal and occipital lobes in presymptomatic *GRN* mutation carriers (Sudre et al., 2019), but over time they accumulate in frontal regions and extend out to mid-zones within subcortical white matter (Sudre et al., 2017a, 2019).

Quantitative assessment of regional WMH burden and atrophy on MRI determined that the severity of WMH correlated with the location and extent of cortical atrophy. This is consistent with correlations of grey and white matter neuroimaging changes in other studies of *GRN* mutation carriers, particularly within the frontal lobe (Ameur et al., 2016; Caroppo et al., 2014; Kelley et al., 2009; Sudre et al., 2017a, 2019). However, precise anatomical correlation of cadaveric MRI brain images with *post-mortem* tissue allowed additional clarification that regions with the most severe WMH also displayed the most severe cortical pathology. The severity of white matter pathology also corresponded with WMH severity, and the degree of cortical pathology, in most brain regions analysed. This could suggest that WMH in *GRN* mutation carriers are due to white matter pathology (axonal degeneration and demyelination) secondary to cortical neuronal loss, perhaps due to TDP-43 aggregates. In AD, cortical hyperphosphorylated tau burden is predictive

of the severity of WMH on MRI, independent of cortical Aβ pathology and small vessel disease in white matter, suggesting that cortical tau pathology contributes to white matter damage (McAleese et al., 2015). The degree of cortical pathology, demyelination, axonal loss and Wallerian degeneration in AD cases also correlates with the extent of white matter lesions, suggesting a link between grey matter pathology, white matter pathology and neuroimaging abnormalities (McAleese et al., 2015, 2017). In the present study, there was a significant cortical TDP-43 burden and neuronal loss in regions with severe WMH on MRI (such as the frontal lobe), which correlated with the severity of demyelination and white matter gliosis in the same region. However, surprisingly, there was not significant axonal loss in white matter regions with severe WMH. This suggests that myelin loss itself, rather than axonal degeneration due to cortical pathology, may have led to the appearance of WMH on MRI. This echoes findings in multiple sclerosis, where there is immune-mediated extensive demyelination but initially relative preservation of axons in white matter regions (Sarbu et al., 2016).

An alternative hypothesis from immune-mediated demyelination is that WMH in *GRN* mutation carriers are secondary to small vessel disease. However, through comprehensive assessment of multiple brain regions this study has demonstrated that there was minimal vascular pathology, despite presence of significant other grey and white matter pathology, in regions with severe WMH. This suggests that small vessel disease does not underlie WMH in *GRN* mutation carriers with FTD. Although mild arteriolosclerosis was present, and there was mild atheroma in rare leptomeningeal vessels in subcortical regions and the circle of Willis, mild pathological changes such as these are commonly seen incidentally in healthy aging and in dementia. In a study of the pathological correlates of WMH in a mixed cohort of cases (aged controls, AD, and individuals with significant vascular risk factors) mild arteriosclerosis was present in 56/57 cases and not significantly different between those with and without WMH (Shim

et al., 2015). A lack of correlation between markers of ischaemia and small vessel sclerosis and parietal white matter lesions was also observed in two studies of AD (McAleese et al., 2015, 2017). These findings underline the importance of not simply attributing cortical WMH on MRI as due to cerebrovascular disease when assessing patients presenting with cognitive impairment.

Many sporadic FTLD cases who have significant grey and white matter spongiosis at *post-mortem* do not display WMH on MRI. In addition, although white matter pathology is generally more extensive in individuals with FTLD-tau than FTLD-TDP (Irwin et al., 2018; McMillan et al., 2013), WMH are much less common on MRI scans of *MAPT* mutation carriers, who have FTLD-tau, than in *GRN* mutation carriers, who have FTLD-TDP (Sudre et al., 2017a). Mechanisms independent of FTLD itself may therefore be responsible for white matter damage in individuals with *GRN* mutations. WMH are more extensive in symptomatic individuals with FTD due to *GRN* mutations than *C9orf72* expansions (Sudre et al., 2017a), despite both being associated with FTLD-TDP, indicating that there are mutation-specific mechanisms affecting white matter vulnerability in genetic FTD, irrespective of FTLD-TDP. As discussed in Chapter 1, increasing evidence implicates *GRN* in regulation of neuroinflammation, particularly in microglial and lysosomal function. A study of two FTLD-*GRN cases* observed significant microgliosis and astrocytosis broadly corresponding to areas of WMH on MRI (Kelley et al., 2009), and the extent of WMH correlates with plasma GFAP levels in symptomatic *GRN* mutation carriers (Sudre et al., 2019). White matter lesions in *GRN* mutation carriers could therefore be due to chronic excessive neuroinflammation, and microglial or astrocytic dysfunction. WMH would be expected to be associated with regional differences in microglia or astrocytes, which this study therefore explored comprehensively.

The severity of WMH correlated with severity of astrogliosis in white matter, but this study also used antibodies to detect three different microglial markers (CD68, CR3/43 and Iba1) to explore, in detail, differences in the burden and morphology of microglia between brain regions with and without WMH. There were many amoeboid CD68-positive microglia in both grey and white matter of regions with severe WMH (frontal lobe) or moderate WMH (temporal lobe), but particularly in white matter. This is consistent with the large number of highly-activated, phagocytic CD68-positive microglia in *GRN* -/- mouse models (Lui et al., 2016; Tanaka et al., 2013b, 2013a; Yin et al., 2009, 2010) and in frontal grey matter (Lant et al., 2014; Sakae et al., 2019b) and subcortical white matter (Lant et al., 2014) of individuals with FTLD-*GRN*. This could cause white matter damage through excessive phagocytosis of myelin and demyelination. There were also many amoeboid CR3/43-positive microglia in grey and white matter regions with severe WMH, suggesting that microglia with an antigen-presenting phenotype were also active in these regions. This is consistent with observations of many activated HLA-DR-positive microglia in cortical regions in FTLD-*GRN* cases (Chen-Plotkin et al., 2010; Kim et al., 2016), although previous studies did not examine this phenotype in white matter. Activated antigen-presenting microglia could contribute to white matter damage through increased presentation of self-epitopes of myelin, leading to antibody-mediated demyelination, as seen in autoimmune diseases such as neuromyelitis optica. In the occipital lobe, where WMH were absent, CD68 and CR3/43-positive microglia were less numerous and more ramified, indicating a less active phenotype, consistent with minimal other pathology.

In frontal and temporal grey matter, Iba1-positive microglia were typically numerous and often amoeboid in appearance. This is consistent with a recent study showing numerous amoeboid Iba1-positive microglia in the middle frontal cortex of FTLD-*GRN* cases (Sakae et al., 2019b). However, despite a similar burden of other histopathological changes

between frontal and temporal white and grey matter, the present study found few Iba1-positive microglia in white matter, and much fewer in white matter than grey matter, particularly in frontal regions where WMH was most severe. This was because the morphology of Iba1-positive microglia was severely dystrophic in frontal white matter, with microglia displaying punctate, fragmented staining and severely disrupted cell structure (Streit et al., 2004). The extent of dystrophy in both grey and white matter correlated regionally with the presence and location of WMH, but dystrophy was particularly severe in white matter. This suggests that there may be region-specific microglial dystrophy in *GRN* mutation carriers, perhaps due to excessive microglial dysfunction or senescence secondary to progranulin haploinsufficiency. A reduction in Iba1-positive microglia has been observed in AD (Minett et al., 2016) and dystrophic microglia are present in AD cases (Bachstetter et al., 2015; Davies et al., 2017; Streit et al., 2009, 2018; Tischer et al., 2016), preceding the spread of tau pathology (Streit et al., 2009) and symptom onset (Streit et al., 2018). Selectively premature or excessive microglial senescence within regions such as frontal white matter in *GRN* mutation carriers could reduce axonal support, leading to selective white matter vulnerability and development of regional WMH, even prior to symptom onset (Sudre et al., 2019).

Interestingly, not all *GRN* mutation carriers with FTD display significant WMH: in a recent study 25.0% had none or a mild load, 37.5% had a medium load and 37.5% had a severe load (Sudre et al., 2019). There are therefore likely to be other factors affecting white matter vulnerability, which could affect microglial function on a background of a *GRN* mutation. Presence of a homozygous TT risk variant in the lysosomal gene *TMEM106B* was associated with accelerated accrual of WMH over time in individuals with FTD due to *GRN* mutations (Sudre et al., 2019). This is intriguing, as a polymorphism in this gene modifies cognitive reserve, grey matter volume, functional connectivity and AAO of symptoms in presymptomatic *GRN* mutation carriers (Cruchaga et al., 2011; Premi et

al., 2014, 2017). Microglial lysosomal function is also disrupted in *GRN* mutation carriers (Götzl et al., 2018) and influenced by *TMEM160B* (Klein et al., 2017). This suggests that combined microglial immune and lysosomal dysfunction may contribute to microglial dystrophy and white matter vulnerability and damage in *GRN* mutation carriers.

In conclusion, presence of significant MRI WMH in someone presenting with symptoms of FTD, a positive family history, and no obvious vascular risk factors, particularly within frontal white matter, could signal an underlying *GRN* mutation and should prompt consideration of genetic testing (Paternicò et al., 2016). As WMH in this case were not associated with vascular pathology, they could instead be due to axonal degeneration secondary to cortical pathology, or due to region-specific demyelination and white matter vulnerability, contributed to by progranulin haploinsufficiency and microglial immune and lysosomal dysfunction. From a clinical trials perspective, the burden of WMH could act as a useful biomarker for assessment of disease progression, or treatment response, in presymptomatic or symptomatic *GRN* mutation carriers. However, variability in the presence of WMH between individuals ((Sudre et al., 2019) may limit this to intra-individual monitoring.

4.7 Limitations and future work

As this study included only one case, exploration of the histopathological correlates of WMH across a larger cohort of FTLD-*GRN* cases is needed to confirm these findings. Collaboration across several brain banks would enable this, but this may be limited by the scarcity of centres using cadaveric MRI and the rarity of FTLD-*GRN* cases. Theories of microglial and lysosomal dysfunction due to *GRN* mutations require validation in mechanistic studies, for example using microglia derived from induced pluripotent stem cells (iPSCs). IPSCs can be produced from fibroblasts present within skin biopsies obtained from presymptomatic and symptomatic *GRN* mutation carriers. These could be obtained from individuals either with or without WMH, and with and without risk variants

in genetic modifiers such as *TMEM106B*. Quantitative assessments of microglial burden, activation and dystrophy across relevant brain regions in a larger number of FTLD-*GRN* cases, and in individuals with a range of different subtypes of sporadic and genetic FTLD, would also help to clarify whether the qualitative and semi-quantitative regional differences in microglia noted in this single case are recapitulated across the spectrum of FTLD. This was explored further in the studies in Chapters 5 and 6.

4.8 Publications relating to this chapter

Work presented in this chapter was published as:

Woollacott IOC et al. (2018) Pathological correlates of white matter hyperintensities in a case of progranulin mutation associated frontotemporal dementia. *Neurocase* 24:3, 166-174.

Findings and theories discussed within this chapter also contributed to neuroimaging studies of WMH in *GRN* mutation carriers at UCL, which were published as:

Sudre CH et al. (2017) White matter hyperintensities are seen only in *GRN* mutation carriers in the GENFI cohort. *Neuroimage Clin* 15:171-180.

Sudre CH et al. (2019) White matter hyperintensities in progranulin-associated frontotemporal dementia: A longitudinal GENFI study. *NeuroImage Clin* 24:102077.

5 Microglial phenotypes across the spectrum of FTLD

5.1 Chapter summary

Introduction: Increasing evidence implicates microglial dysfunction in the aetiology of neurodegenerative disease. Many histological studies have examined microglia in AD, but few have explored this across the spectrum of FTLD. This study examined regional patterns of the burden and activation state of different microglial phenotypes in *post-mortem* brain tissue from a large cohort of individuals with sporadic and genetic FTLD, individuals with AD, and healthy controls.

Methods: Immunohistochemistry was performed to detect markers present on phagocytic (CD68), antigen-presenting (CR3/43 (HLA-DR/DP/DQ)) and general (Iba1) microglia in left anterior frontal and temporal lobe FFPE sections obtained from 50 FTLD cases (31 sporadic and 19 genetic: 20 FTLD-tau, 26 FTLD-TDP, four FTLD-FUS), five sporadic AD cases and five controls. Microglia were assessed in four regions: frontal grey (FG), frontal white (FW), temporal grey (TG) and temporal white (TW) matter. Microglial burden (percentage area) and activation state (cell circularity and perimeter) were quantitatively assessed in each region for each marker. Microglia were compared in each region between FTLD, AD and controls, and between different pathological subtypes of FTLD overall (FTLD-tau, FTLD-TDP, FTLD-FUS), FTLD-tau (FTLD-Picks, FTLD-CBD, FTLD-PSP, FTLD-*MAPT*), FTLD-TDP (FTLD-TDPA, FTLD-TDPB, FTLD-TDPC), FTLD-TDPA (sporadic, and genetic: FTLD-*GRN* and FTLD-*C9orf72*), and genetic FTLD (FTLD-*GRN*, FTLD-*C9orf72,* FTLD-*MAPT*). Microglia were also compared between grey and white matter in each lobe for each subtype.

Results: The burden of phagocytic and antigen-presenting microglia was generally higher in FTLD and AD cases than controls, but these microglia were not more activated

in most regions compared with controls. Microglial burden was generally higher in white matter than in grey matter, but activation was greater in grey matter. Regional patterns of microglia differed according to pathological subtype: FTLD-tau and FTLD-TDP cases showed similar patterns of microglia, but only FTLD-tau cases had more Iba1-positive microglia than controls, and FTLD-FUS cases had few, poorly activated microglia in all regions. FTLD-Picks cases had many highly activated phagocytic microglia in all regions, particularly FW, but many poorly activated antigen-presenting microglia in white matter. FTLD-CBD cases had many poorly activated phagocytic microglia in the frontal lobe and TW, but a few highly activated antigen-presenting microglia, mainly in FG. FTLD-PSP cases had few microglia in all regions, whereas FTLD-*MAPT* cases had many activated phagocytic microglia in the temporal lobe, particularly in white matter. FTLD-TDPA and FTLD-TDPC cases had many, poorly activated phagocytic microglia in TW and the frontal lobe, respectively, whereas FTLD-TDPB cases had few microglia in all regions. Microglia also differed by underlying disease mechanism and mutation. Sporadic FTLD-TDPA cases had few poorly activated phagocytic and antigen-presenting microglia in most regions, whereas FTLD-*GRN* cases had many poorly activated phagocytic microglia in the temporal lobe (especially TW), but highly activated phagocytic microglia in FG, and many poorly activated antigen-presenting microglia in FW. FTLD-*C9orf72* cases had many poorly activated phagocytic and general (Iba1-positive) microglia in the frontal lobe but few antigen-presenting microglia in all regions.

Conclusions: Microglial burden and activation are altered in FTLD, but this varies regionally and according to the microglial phenotype, pathological subtype, disease mechanism and mutation. Although microglial burden is generally higher in white matter, activation is generally greater in grey matter. Region-specific microglial dysfunction, particularly in white matter, could contribute to regional vulnerabilities to neurodegeneration and to the clinicopathological heterogeneity of FTLD.

5.2 Introduction

As discussed in Chapters 1 and 4, there is increasing evidence of microglial dysfunction in the pathogenesis of FTLD. Chapter 3 demonstrated an increased tendency for systemic autoimmune disease in *GRN* mutation carriers, so central immune dysfunction may also be present. Although microglial PET imaging can detect gross patterns of microglia *in vivo* in individuals with sporadic or genetic FTD (Bevan-Jones et al., 2020; Cagnin et al., 2004; Clarke et al., 2019; Kim et al., 2019) and PMC (Bevan-Jones et al., 2019; Miyoshi et al., 2010), histological studies that use immunohistochemistry to detect microglial markers allow much more detailed examination of regional patterns of microglia. They also enable appreciation of the diversity of microglial activation states, phenotypes and other morphological changes in individuals with different pathological subtypes of FTLD and different disease mechanisms (sporadic versus genetic disease or different gene mutations).

Observations of excessive microglial activation and dysfunction in mouse models of FTD (reviewed in Chapter 1) suggest that different disease mechanisms (for example mutations in *GRN*, *C9orf72* or *MAPT*) and pathologies may differentially affect microglial function, but this has not been examined extensively in humans. Only one study has explored microglia across the spectrum of FTLD, performing a semi-quantitative combined assessment of the frequency and activation state of CD68-positive microglia in frontal and temporal grey and white matter (Lant et al., 2014). This found that there were more numerous and/or more activated microglia in FTLD than controls, particularly in frontal white matter. In subgroup analyses, FTLD-*MAPT* cases had more numerous and/or more activated microglia in the temporal lobe than a combined group of FTLD-PSP/CBD cases, suggesting microglia may also differ regionally across FTLD subtypes. Since then, several small studies have examined microglia in specific subtypes of FTLD, mainly in combined groups of FTLD-TDPA and FTLD-TDPB cases (Kim et al., 2018a,

2018b; Ohm et al., 2018; Taipa et al., 2017). FTLD-TDP cases had more numerous and/or more activated CD68 and Iba1-positive microglia in frontal white matter compared with AD cases and controls, and in frontal, temporal and entorhinal white matter compared with grey matter (Taipa et al., 2017). In small FTLD-TDP case series, there were more HLA-DR-positive microglia in white matter than in grey matter (Ohm et al., 2018), but also many microglia in grey matter regions with significant cortical atrophy on imaging (Kim et al., 2018b, 2018a). Sporadic FTLD-TDPA cases had numerous Iba1-positive microglia in the hippocampal CA1 region and subiculum, but not in CA3 (Mao et al., 2019). FTLD-TDPA and FTLD-TDPC cases had many CD68-positive microglia in frontal, temporal and parietal cortices, with the density of amoeboid microglia correlating with the density of TDP-43 pathology (Bevan-Jones et al., 2020). These studies suggest that microglia are altered in FTLD-TDP in a regionally selective manner, particularly in white matter, but whether microglia vary across FTLD-TDP subtypes, or between other FTLD subtypes, has not been explored in detail.

As regional pathology (Lashley et al., 2015; Mackenzie and Neumann, 2016; Rohrer et al., 2011) and grey and white matter neuroimaging abnormalities (Cash et al., 2018; Fumagalli et al., 2018; Jiskoot et al., 2018; Panman et al., 2019; Rohrer et al., 2015) vary across the spectrum of genetic FTLD, microglia may also differ regionally between genetic FTLD subtypes. However, very few studies have explored this. Only one study has compared microglia between the three main genetic subtypes of FTLD, showing that FTLD-*MAPT* cases had more numerous and/or more activated CD68-positive microglia in temporal white matter compared with FTLD-*GRN*, FTLD-*C9orf72* and sporadic FTLD cases (Lant et al., 2014). A more recent study of FTLD-*GRN* and FTLD-*C9orf72* cases and controls found that the burden and morphology of CD68 and Iba1-positive microglia varied regionally depending the mutation (Sakae et al., 2019b). FTLD-*C9orf72* cases had more CD68-positive microglia in the hippocampus than FTLD-*GRN* cases, but a

similar burden of both microglial phenotypes in other regions, whereas FTLD-*GRN* cases had more amoeboid Iba1-positive microglia in superficial cortical layers and deep white matter of the middle frontal cortex compared FTLD-*C9orf72* cases. Other small studies of FTLD-*GRN* cases have found many HLA-DR-positive microglia in frontal, temporal and parietal grey matter (Kim et al., 2016) or frontal grey and white matter (Chen-Plotkin et al., 2010), and many activated Iba1-positive microglia in the frontal cortex (Lui et al., 2016) or subiculum (Mao et al., 2019). In the FTLD-*GRN* case in Chapter 4, numerous, amoeboid CD68 and CR3/43-positive microglia were present in frontotemporal grey and white matter, but few Iba1-positive microglia were present in white matter, particularly in the frontal lobe. These studies suggest that microglial burden and activation vary regionally and between grey and white matter in genetic FTLD, that this depends on the mutation type, and that this may vary according to the microglial phenotype. Validation of these observations across a larger number of genetic FTLD cases and more detailed comparison of different microglial phenotypes between FTLD-*GRN*, FTLD-*C9orf72* and FTLD-*MAPT* cases and compared with controls is needed.

In contrast to FTLD, there have been many histological studies of microglia in humans with AD (Hopperton et al., 2018). As several early AD mouse models suggested there was widespread microglial activation, it was initially proposed that chronic excessive microglial activation directly results in neurodegeneration in AD. Many previous studies examining CD68, HLA-DR or Iba1-positive microglia in human AD cohorts have concluded that in sporadic AD the burden of microglia was increased, or microglia were more activated, or both, in regions with significant pathology, such as the hippocampus or frontal or temporal lobes (Felsky et al., 2019; Hopperton et al., 2018; Lant et al., 2014; Minett et al., 2016; Taipa et al., 2017). However, *in vitro* studies or mouse models of AD can create high-level microglial stimulation, which is artificial and in excess of what occurs *in vivo*, so may not mimic the sequential changes in microglia and pathology seen

in humans (Streit et al., 2014). In fact, heightened microglial activation has not been identified in all human AD histological studies. Few activated microglia were associated with early diffuse Aβ plaques (Hendrickx et al., 2017) and few Iba1-positive microglia surrounded established, neuritic plaques in the hippocampus (Navarro et al., 2018) in other AD cohorts. Excessive microglial dystrophy, representing senescence or premature failure of microglia, is also emerging as a potential contributor to AD and other neurodegenerative diseases (Bachstetter et al., 2015; Davies et al., 2017; El Hajj et al., 2019; Lopes et al., 2008; Navarro et al., 2018; Sanchez-Mejias et al., 2016; Streit et al., 2009, 2014, 2018; Tischer et al., 2016). There may also be different phases of microglial activation and senescence at different disease stages, which may variably contribute to neuronal protection or neurodegeneration (Gentleman, 2013).

Given that AD can overlap clinically and radiologically with FTD, it is useful to compare how microglia are altered in each disease. This may help to explore whether changes in microglia occur *in general* in regions involved in neurodegenerative disease or relate to specific underlying pathologies. Few studies have directly compared microglia in FTLD and AD, but these suggest that regional microglial patterns differ between these diseases. Microglial burden and activation differed in frontal white matter (FTLD greater than AD) and temporal grey matter (AD greater than FTLD) in one study (Lant et al., 2014) and in the dentate gyrus (AD greater than FTLD-TDP) in another (Taipa et al., 2017). Microglia also seem to be differentially affected in grey and white matter in each disease: FTLD cases had more numerous and/or more activated microglia in frontotemporal white matter than grey matter (Lant et al., 2014; Taipa et al., 2017), whereas in AD cases the opposite pattern was present (Lant et al., 2014). Although microglia have been compared between FTLD-TDP and AD cases (Taipa et al., 2017), FTLD-tau and AD cases have not been compared previously. As there may be different effects of various tau isoforms or strains on glial cells, and different contributions of

aberrant neuroinflammation and glial cell dysfunction to neurodegeneration in different tauopathies (Kahlson and Colodner, 2015; Leyns and Holtzman, 2017), this is worth exploring.

Despite useful evidence from prior studies of microglia in FTLD and AD, they have had several limitations. First, most have only examined one FTLD subtype, or have pooled different FTLD subtypes into one group for analysis. Different pathologies may be associated with differing regional patterns and degrees of microglial dysfunction, and this approach has precluded exploration of this. Second, most studies have focused on only one type of dementia and have not compared cases with different neurodegenerative diseases (such as FTLD and AD) to see if regional microglial patterns differ depending on the type of pathology. Third, most studies have used a single microglial marker (usually CD68), so the range of microglial phenotypes assessed and morphological assessments for examining activation state were rather limited. Finally, the two largest histological studies of microglia in FTLD (Lant et al., 2014; Taipa et al., 2017) used semi-quantitative visual rating scales rather than quantitative assessments to assess microglial burden and morphology (activation) and assessed these jointly to produce one 'microglial score'. Quantitative approaches have less of a tendency for rater bias, can capture more subtle information about microglial burden and morphology, and can assess these parameters separately. This is important, as an increase in the burden of microglia within a region may not necessarily be accompanied by an increase in cell activation.

5.3 Aims and hypotheses

To address these issues, there needed to be a comprehensive, quantitative assessment of microglial burden and activation across sporadic and genetic forms of FTLD, in clinically relevant brain regions, using a panel of antibodies that can detect markers indicative of different microglial phenotypes and morphologies. FTLD cases should be

compared with cognitively normal controls and with cases with another neurodegenerative disease affecting similar brain regions and producing clinically overlapping syndromes, such as sporadic amnestic AD. The full spectrum of pathological FTLD subtypes must be analysed and compared, and grey and white matter must be compared within each region.

This study therefore aimed to perform a detailed histological assessment of microglial burden and activation within *post-mortem* brain tissue in a large FTLD cohort, including cases with the main pathological subtypes of FTLD (FTLD-tau, FTLD-TDP and FTLD-FUS), who have either sporadic FTLD or the most common genetic forms of the disease (FTLD-*GRN*, FTLD-*C9orf72*, or FTLD-*MAPT*). Comparisons would be made with sporadic AD cases and cognitively normal controls and between different pathological and genetic FTLD subtypes. Microglia would be examined in frontal grey matter (FG), frontal white matter (FW), temporal grey matter (TG) and temporal white matter (TW). Microglia would also be compared between grey and white matter within each lobe (FG versus FW, and TG versus TW) for each group (FTLD, AD, controls) and FTLD subtype.

Three different antibodies would be used to detect microglial markers indicative of different microglial phenotypes and to optimise assessment of morphology (to determine activation state): CD68 (detects phagocytic microglia, with expression increased by activation), CR3/43 (detects HLA-DR/DP/DQ molecules on antigen-presenting microglia, with expression increased by activation) and Iba1 (detects microglia in general and allows excellent assessment of cell morphology) (Boche et al., 2013). Chapter 1.3.3.2 provides further information on each marker. The burden of each microglial phenotype would be quantitatively assessed in each region (FG, FW, TG, TW) by measurement of the percentage area of that region comprised of microglial cells stained by each antibody.

The degree of microglial activation would be assessed by quantitative measurement of aspects of the morphology of microglial cells stained using each antibody in that region. The key hypotheses of this study were that the burden and/or the activation of microglia would differ in some, or all, of the four brain regions analysed, in the following ways:

- Between FTLD cases and controls, and between AD cases and controls, due to the role of microglial dysfunction in neurodegenerative disease.
- Between FTLD and AD cases, due to different pathologies or disease mechanisms interacting with and impacting on microglia in different ways within the same brain regions.
- Between different FTLD subtypes, due to different pathologies or disease mechanisms interacting with and impacting on microglia in different ways in the same regions, namely:
    - Between FTLD-tau, FTLD-TDP, FTLD-FUS, and between each of these subtypes and AD.
    - Between different FTLD-tau subtypes: FTLD-CBD, FTLD-*MAPT*, FTLD-Picks and FTLD-PSP.
    - Between different FTLD-TDP subtypes: FTLD-TDPA, FTLD-TDPB and FTLD-TDPC.
    - Between cases with the same type of pathology but different disease mechanisms: sporadic FTLD-TDPA versus genetic FTLD-TDPA due to *GRN* mutations (FTLD-*GRN*) or *C9orf72* expansions (FTLD-*C9orf72*).
    - Between genetic FTLD subtypes, due to different gene mutations differentially influencing microglial function: FTLD-*GRN*, FTLD-*C9orf72* and FTLD-*MAPT*.

In addition, this study hypothesised that microglial burden and/or activation would differ between grey and white matter within the frontal and temporal lobes. This may vary by lobe (i.e. only be the case in frontal, or temporal, or both lobes), according to the underlying pathology or gene mutation. This could be due to pre-existing differences in microglial function between grey and white matter contributing to sub-regional variations in neuronal or glial vulnerability, and hence evolvement of sub-regional pathologies. Alternatively, there may be a secondary effect of differing burdens of neurodegenerative pathologies present in grey versus white matter in each subtype in each lobe, which differentially impacts upon microglia.

5.4 Methods

5.4.1 Case selection and demographics

Sixty cases were selected for analysis, including 50 FTLD cases, five sporadic amnestic AD cases, and five cognitively normal controls without neurodegenerative pathology. These were selected from the QSBB and the MRC London Neurodegenerative Diseases Brain Bank, Institute of Psychiatry, King's College London, as detailed in Chapter 2.1.1. Case demographics and pathological subtypes are summarised in Table 2.1 (Chapter 2) and individual cases are detailed in Appendix 1.

5.4.2 Tissue processing and immunohistochemistry

All 60 cases had undergone tissue processing, immunohistochemistry and clinical neuropathological assessment of a wide variety of brain regions at the QSBB as detailed in Chapter 2.2.1.1, to confirm the neuropathological findings. Further sections were cut by the author from left anterior frontal lobe and left temporal lobe FFPE tissue blocks from all cases. Immunohistochemistry was performed sequentially on these sections by the author, using one of three different antibodies each time, directed against the microglial markers CD68, CR3/43 or Iba1. Immunohistochemistry techniques and

antibodies were detailed in Chapter 2.2.1.2. Figure 5.1 shows microglia in grey and white matter tissue sections detected using each antibody.

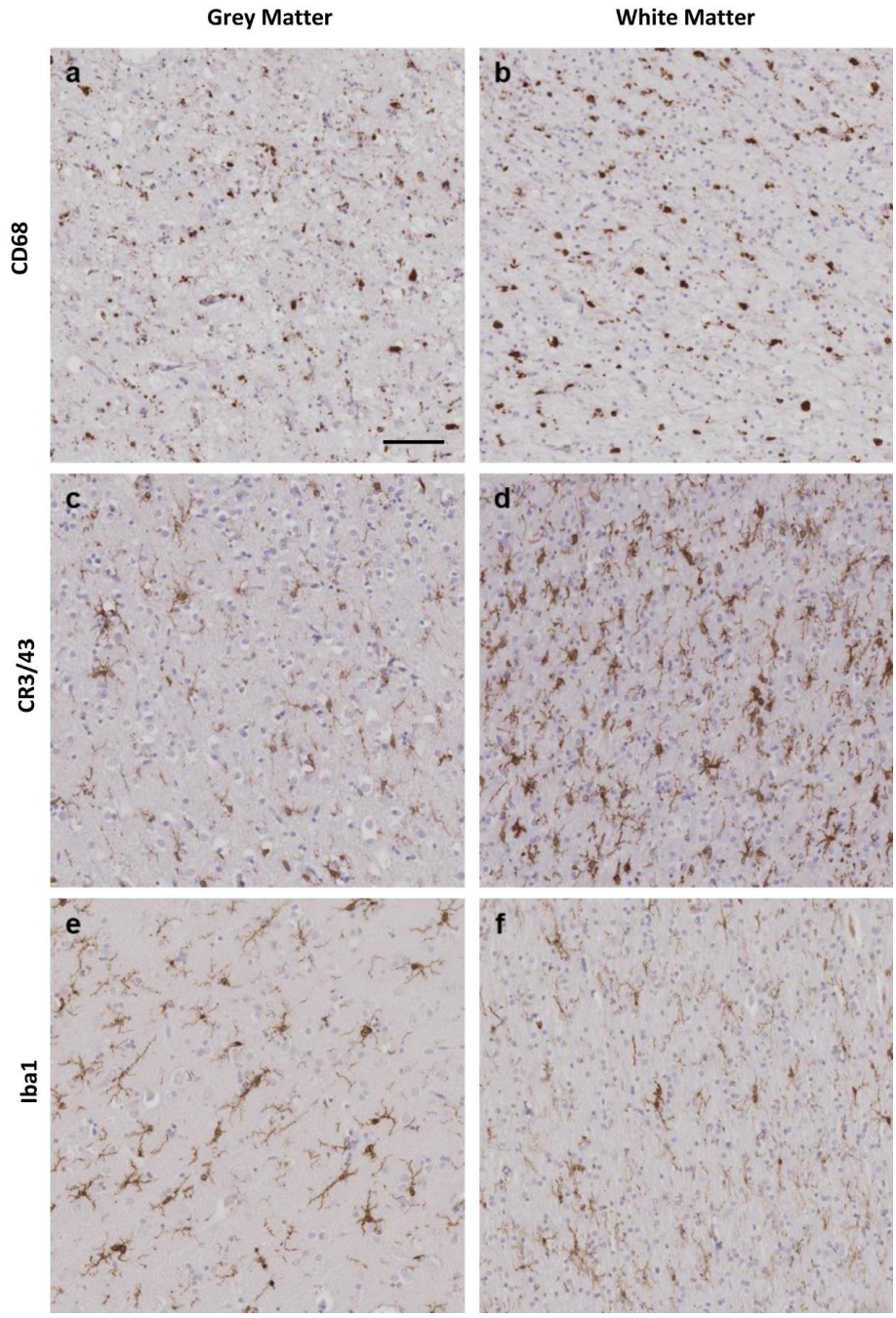

Figure 5.1 Immunohistochemical staining of microglia using different antibodies

Representative images of frontal grey matter (**a, c, e**) and subcortical white matter (**b, d, f**) of sections with CD68-positive microglia (**a, b**) CR3/43-positive microglia (**c, d**) and Iba1-positive microglia (**e, f**). Images were taken from the following cases (Appendix 1): **a** and **b** from case 25 (FTLD-Picks); **c** to **f** from case 55 (FTLD-TDPC). Scale bar represents 50µm in all images.

5.4.3 Analysis of microglia

5.4.3.1 Regions analysed

Anterior frontal and temporal lobe sections contained both cortical grey matter (all cortical layers were analysed) and subcortical white matter. Four regions were selected for analysis for all cases: FG, FW, TG and TW. This enabled analysis of differences in microglia in the same region (for example FG) across groups, and comparison of microglia in grey matter versus white matter within the frontal lobe (FG versus FW) and temporal lobe (TG versus TW) within each group.

5.4.3.2 Scanning, area selection and identification of microglia

The sequential sections stained for each of the three microglial markers were digitally scanned using a Leica SCN400F scanner (Leica Microsystems) at 40x magnification and high resolution digital images were stored on a digital hub (http://slidepath.ion.ucl.ac.uk/dih/login.php). Images were loaded into Aperio ImageScope software (version 12.3.0.5056) and identical areas of interest for analysis were identified within each of the four regions (FG, FW, TG and TW) within each section for each case across all markers. This was to ensure that results were not influenced by intraregional variations in microglia.

A macro using Aperio ImageScope, ImageJ and Python programming software developed by a collaborator (Yau Lim at King's College London) was used to identify microglia in each of the four regions of interest for each marker, and to analyse the microglial percentage area, and morphological parameters indicating microglial shape and size (circularity and perimeter), for each case. First, the image of the extracted area of interest from a region (generated in Aperio ImageScope) was loaded into ImageJ. The macro allowed an area within the cortical grey matter or subcortical white matter to be manually selected within the image, generating its coordinates (Figure 5.2a). The same

area was selected each time to ensure consistency. A Python script used these coordinates to randomly generate pairs of coordinates for ten different squares (each 1000 x 1000 pixels in size, equivalent to 500 x 500 μm) within the selected area in order to give an unbiased measurement of microglia present across this area (Figure 5.2a). Prior to this, Bland-Altman plots with linear regression analyses had been used to ascertain whether analysis of five or ten random squares led to best reproducibility of results for microglial percentage area and circularity, using five test cases from the cohort (Appendix 2). Bland-Altman plots are typically used to evaluate the level of agreement between two similar techniques, identifying any systemic difference between measurements. This approach had confirmed that analysis of ten random squares was best. Ten random squares were therefore generated for all cases in each region and microglia within each square were analysed further.

ImageJ was used to identify DAB staining for each marker (CD68, Iba1 and CR3/43) in each square, employing a pre-set colour threshold, with a hue of zero to 30 (for DAB detection), a saturation of 60 to 80 (adjusted according to background staining level), and a mean thresholding method for brightness. These settings were used to ensure consistent selection of only DAB stained cells rather than weaker, non-specific staining. Brown DAB staining was highlighted as red within the macro (Figure 5.2b). A pre-set diameter of ten pixels for cell selection (equivalent to five μm) was then used to exclude selection of any stained matter that was smaller than this, to minimise inclusion of parts of microglia that were predominantly on a different plane (Figure 5.2c). This diameter was necessarily small to ensure that the cell bodies and processes of CD68-positive cells, which were typically very small, were not excluded from analysis.

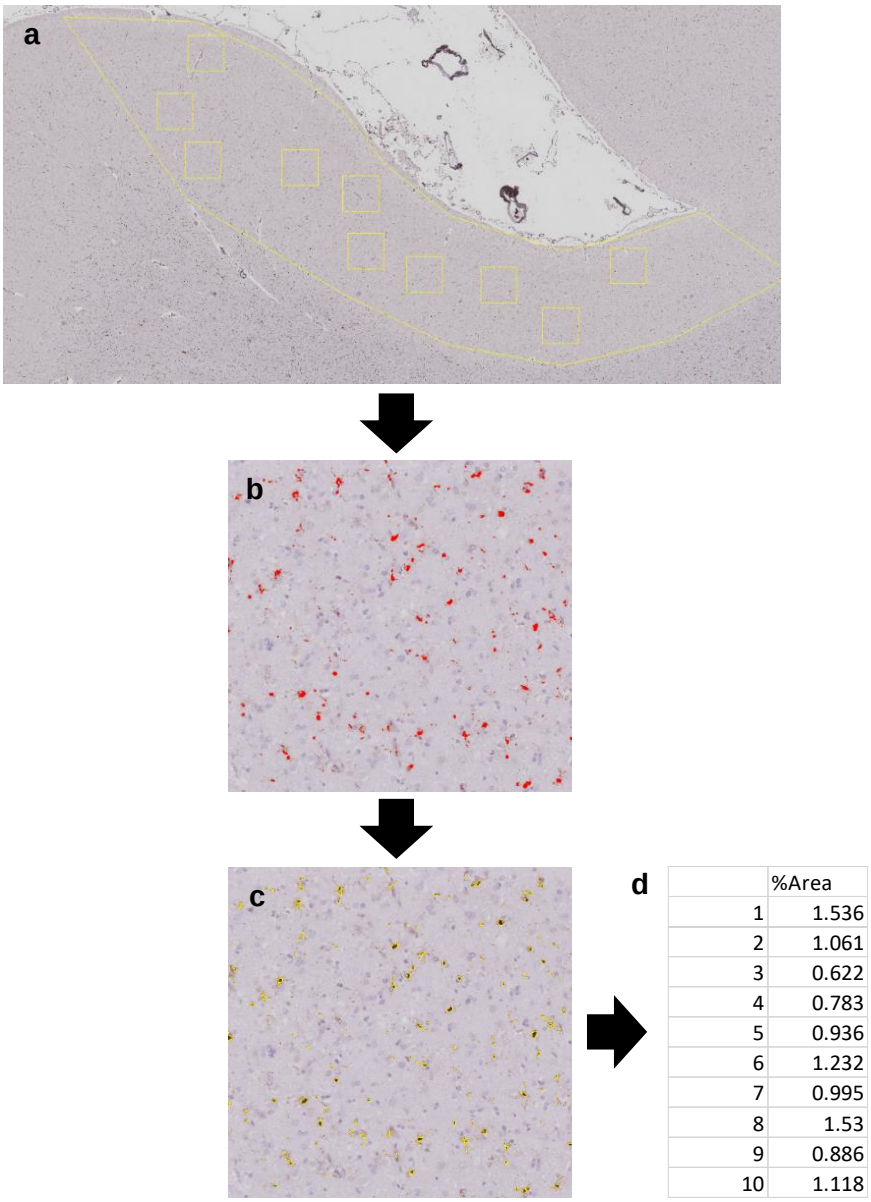

	%Area
1	1.536
2	1.061
3	0.622
4	0.783
5	0.936
6	1.232
7	0.995
8	1.53
9	0.886
10	1.118

Figure 5.2 Process of analysis of microglial burden and morphology (activation)

The macro used ImageJ and Python to enable selection of an area of interest in each region and to generate ten random squares for analysis within this area, each of size 1000x1000 pixels (500µm^2) (**a**). ImageJ and colour thresholding was used to identify all cells stained with DAB in a square, which were then highlighted in red (**b**), and to select only cells above a pre-set diameter of ten pixels (five µm), which were outlined in yellow (**c**) for further analysis. The macro calculated mean percentage area stained values for each of the ten squares, generating this in an Excel output (**d**), as well as circularity and perimeter values for individual cells present within each square (not shown).

5.4.3.3 Microglial percentage area

The macro used the ImageJ measure function to determine the percentage area (areal fraction) of each of the ten squares in a region stained with DAB for each marker. This produced a percentage area value for each of the ten squares, with a higher value representing a higher burden of that microglial phenotype (CD68-positive, CR3/43-positive or Iba1-positive cells) present. Percentage area values were generated by the macro for each of the ten squares in each region within a Microsoft Excel spreadsheet for that region, for each case (Figure 5.2d). These values were then imported from Microsoft Excel into STATA version 14 and averaged across all ten squares to give a mean percentage area value for each region (FG, FW, TG or TW) for each case.

5.4.3.4 Microglial circularity and perimeter

The macro also used ImageJ to assess microglial morphology, quantifying the circularity (how round a cell is) and perimeter (cell size) of every DAB stained cell (above the pre-set diameter of ten pixels) detected within each of the ten squares. This allowed assessment of the degree of microglial activation: microglial circularity and perimeter have been shown to correlate strongly with the degree of activation as measured by expression of the proinflammatory cytokine IL-1β (Fernández-Arjona et al., 2019).

For the circularity assessment, the shape of each cell was measured using the Hull and Circle function in ImageJ. A circularity value of between zero and one was calculated and assigned to that cell, to represent how round the cell was, with zero representing an imperfect shape and one representing a perfect circle. Cells that were less circular in shape were assigned lower circularity values, closer to zero, indicating more ramified morphology and less activation (Figure 5.3a). Those that were more circular in shape were assigned a higher circularity value, closer to one, indicating more amoeboid morphology and greater activation (Figure 5.3b) (Fernández-Arjona et al., 2017, 2019; Torres-Platas et al., 2014). For the perimeter assessment, the outline of each cell above

the pre-set diameter was quantified using the Hull and Circle function in ImageJ and each cell was assigned a perimeter value representing its size (including all ramified processes) in µm. Cells with larger perimeters were more ramified and less activated (Figure 5.3a) whereas those with smaller perimeters were less ramified (more amoeboid) and more activated (Figure 5.3b) (Fernández-Arjona et al., 2017, 2019).

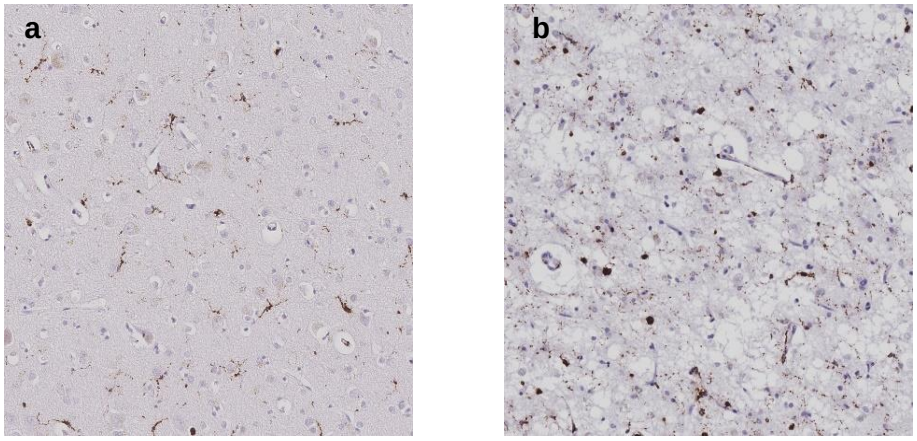

Figure 5.3 CD68-positive microglia with different circularity and perimeter values

(**a**) One of ten squares selected from FG of a control (case 1, Appendix 1), showing CD68-positive microglia with a mean cell circularity value of 0.342 and mean perimeter value of 61.7 µm, indicating non-amoeboid, highly ramified microglia. (**b**) One of ten squares selected from FG of an FTLD-Picks case (case 21, Appendix 1), showing CD68-positive microglia with a mean circularity value of 0.606 and a mean perimeter value of 46.3 µm, indicating highly amoeboid, poorly ramified microglia.

The macro calculated individual circularity and perimeter values for every stained cell (above the pre-set diameter) detected in each square. These were generated within a separate text file (containing values for all cells present) for each of the ten squares for each region. Circularity and perimeter values were imported from text files into STATA version 14 and averaged across individual cell values to give a mean circularity value and mean perimeter value per square. These were then averaged across the ten squares in each region to give mean circularity and perimeter values for that region (FG, FW, TG or TW) for each case. This was performed separately for each of the three markers (CD68, CR3/43 and Iba1).

5.4.4 Statistical analysis

STATA version 14 was used to import Excel and text file outputs of microglial parameters (percentage area, circularity and perimeter) generated by the macro and was also used to analyse data. The significance threshold was $P<0.05$ and confidence interval 95% for all statistical tests. Microglial parameters were compared between groups using a hierarchical, multi-level approach as detailed in Figure 5.4. This was performed to allow appreciation of how microglia differed between overall disease groups (FTLD, AD and controls) and between the various pathological and genetic subtypes of FTLD.

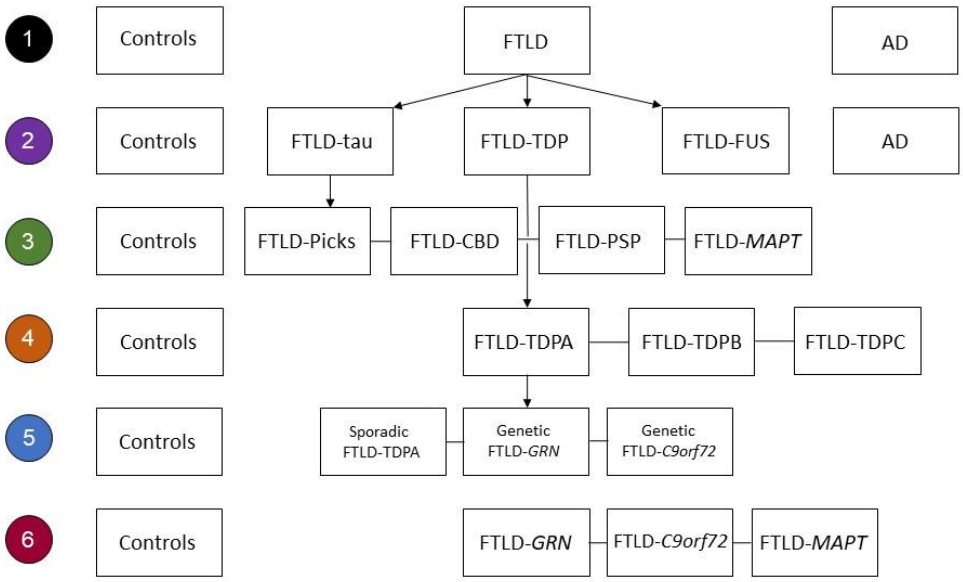

Figure 5.4 Approach to group comparisons of demographics and microglia

Demographics and microglial parameters were compared between groups using six levels of comparison (numbers in circles denote level). **1**: controls and different neurodegenerative diseases; **2**: controls, main FTLD subtypes (all FTLD-FUS had aFTLD-U) and AD; **3:** controls and FTLD-tau subtypes; **4**: controls and FTLD-TDP subtypes; **5**: controls and either sporadic or genetic FTLD-TDPA (genetic had either *GRN* mutations, FTLD-*GRN*, or *C9orf72* expansions, FTLD-*C9orf72*); **6**: controls and genetic FTLD subtypes (the FTLD-*C9orf72* group included only FTLD-TDPA cases to ensure comparison of mutation rather than pathological subtype).

Demographics including AAD, AAO, disease duration and *post-mortem* delay were compared between groups using non-parametric tests, given the small group sizes. Rank

sum tests (for two groups) or Kruskal Wallis tests (for more than two groups) were used followed by Dunn's *post hoc* test for multiple comparisons. Sex was compared between groups using Fisher's exact tests.

Mean and median group values for each microglial parameter were calculated for every region (FG, FW, TG, TW) using values from all cases within each group. Given the small sample size of many groups, non-parametric Kruskal Wallis tests with Dunn's *post hoc* tests for multiple comparisons were used to compare median values of each microglial parameter (percentage area, circularity and perimeter) for each marker (CD68, CR3/43 and Iba1) within each of the four regions (FG, FW, TG and TW) between each group. Non-parametric Wilcoxon signed rank tests for paired comparisons were used to perform grey versus white matter comparisons of microglial parameters within the frontal lobe (FG versus FW) and temporal lobe (TG versus TW) for each group, for each marker.

Graphs of comparisons of microglial parameters between groups and between grey and white matter within each group were produced in GraphPad Prism version 7. Heat maps of *P* values for all comparisons of microglial parameters between groups and between grey and white matter within each group (Appendix 3) were produced in Microsoft Excel.

5.5 Results

5.5.1 Demographics

Demographics of cases in each group were summarised in Table 2.1 in Chapter 2 and are presented for individual cases in Appendix 1. Comparisons of AAO, AAD, disease duration and *post-mortem* delay between groups are displayed in Figure 5.5.

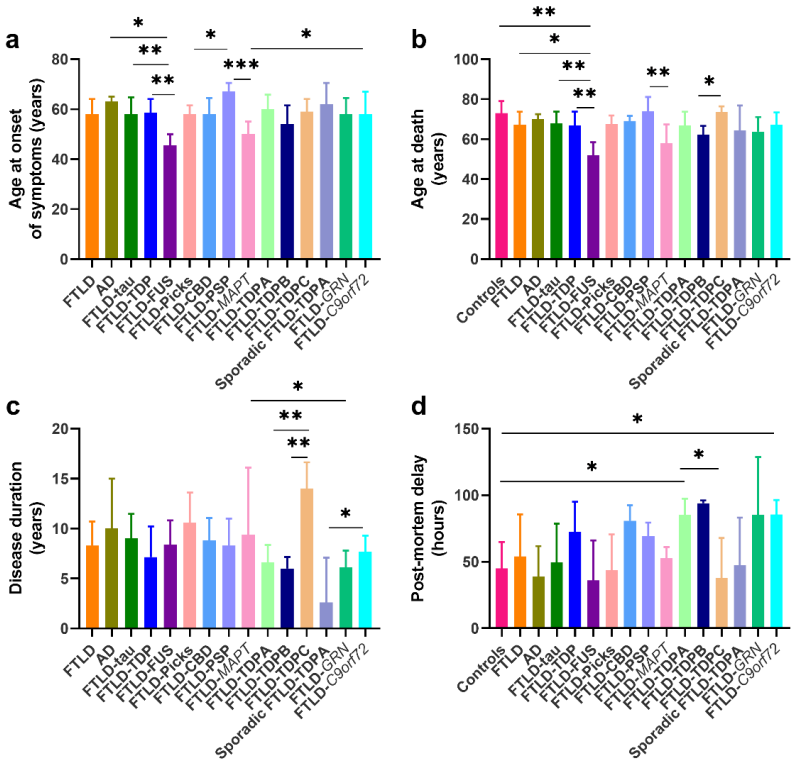

Figure 5.5 Comparison of demographics between groups

Graphs show comparisons of age at onset (**a**), age at death (**b**), disease duration (**c**) and *post-mortem* delay (**d**) across groups. Bars show medians and error bars represent interquartile ranges. **P*<0.05; ***P* <0.01; ****P* ≤0.001; *****P* ≤0.0001.

Sex did not differ significantly between any group (*P*>0.05). Other demographics were similar between groups, with a few exceptions (Figure 5.5). FTLD-FUS cases had an earlier AAO than FTLD-TDP (*P*=0.004), FTLD-tau (*P*=0.006) and AD (*P*=0.022) cases. AAO differed across FTLD-tau subtypes (*P*=0.005): FTLD-PSP cases had a later AAO than FTLD-Picks (*P*=0.034) and FTLD-*MAPT* (*P*=0.0004) cases. AAO did not differ across FTLD-TDP subtypes or between sporadic and genetic FTLD-TDPA cases. However, FTLD-*MAPT* cases had an earlier AAO than FTLD-*C9orf72* cases (*P*=0.025). AAD was matched as much as possible, but FTLD-FUS cases had a younger AAD compared with controls (*P*=0.006), FTLD-TDP (*P*=0.008), FTLD-tau (*P*=0.004) and AD (*P*=0.012) cases. FTLD-*MAPT* cases had a younger AAD than FTLD-PSP cases (*P*=0.004) and FTLD-TDPC cases had an older AAD than FTLD-TDPB cases (*P*=0.022). FTLD-TDPC cases had a longer disease duration than FTLD-TDPA (*P*=0.002) and

FTLD-TDPB (*P*=0.004) cases. FTLD-TDPA cases with *C9orf72* expansions had a longer disease duration than sporadic FTLD-TDPA cases (*P*=0.04). FTLD-*MAPT* cases had a longer disease duration than FTLD-*GRN* cases (*P*=0.011). *Post-mortem* delay was similar across groups, except that FTLD-TDPA cases had a longer delay than FTLD-TDPC cases (*P*=0.033) and controls (*P*=0.046), and FTLD-*C9orf72* cases had a longer delay than controls (*P*=0.039).

5.5.2 Microglial burden

Detailed results of all group comparisons of microglial burden are presented sequentially in subsequent sections, for each level of group comparison performed, following the order in Figure 5.4. The heat maps in Appendix 3 contain *P* values for every comparison between groups and between grey and white matter within each group, so *P* values are not presented again in the text. Graphs show results from each level of group comparison, also corresponding to levels in Figure 5.4.

5.5.2.1 Neurodegenerative disease comparisons

FTLD cases had more CD68-positive microglia in FG, FW and TW compared with controls (Figure 5.6a). AD cases had a higher burden in FG compared with controls and FTLD cases, but the burden in TG did not differ significantly from controls. The burden of CR3/43-positive and Iba1-positive microglia was highly variable across cases within each group and comparisons between groups did not reach significance in any region (Figure 5.6b, c).

Grey versus white matter comparisons revealed that the burden of CD68 and CR3/43-positive microglia was generally higher in white matter than grey matter for all groups (Figure 5.6d, e). For the frontal lobe, values were significantly higher in white matter for FTLD cases and controls, but not for AD cases. For the temporal lobe, values were significantly higher in white matter for all three groups, particularly for FTLD but less so

for AD and controls. For Iba1-positive microglia the only significant difference was a higher burden of microglia in TW compared with TG in FTLD cases (Figure 5.6f).

5.5.2.2 Main FTLD subtypes

FTLD-tau and FTLD-TDP cases had a higher burden of CD68-positive microglia in FG and FW compared with controls, but there was a similar burden between these subtypes in all regions (Figure 5.6g). FTLD-TDP cases also had a higher burden in TW compared with controls and FTLD-FUS cases. In contrast, the burden of CD68-positive microglia in FTLD-FUS cases was low, similar to controls in all regions. AD cases had a higher burden of CD68-positive microglia in FG compared with controls and in FG and TG compared with FTLD-FUS cases. AD and FTLD-tau cases had a similar burden of this phenotype in all regions (Figure 5.6g). There were no significant differences in the burden of CR3/43-positive microglia between any group (Figure 5.6h). FTLD-tau cases had a particularly high burden of Iba1-positive microglia in white matter, with more cells in both FW and TW compared with FTLD-TDP and AD cases, but only in TW compared with controls (Figure 5.6i). However, FTLD-TDP and FTLD-FUS cases had a similar burden of Iba1-positive microglia to controls in all regions.

Grey versus white matter comparisons showed a significant difference in the burden of CD68 and CR3/43-positive microglia between grey and white matter in frontal and temporal regions of FTLD-tau and FTLD-TDP cases, with a much higher burden in white matter (Figure 5.6j,k). Iba1-positive microglia only differed in the temporal lobe of FTLD-tau cases, with a higher burden in white matter (Figure 5.6l).

5.5.2.3 FTLD-tau subtypes

FTLD-Picks cases had a higher burden of all microglial phenotypes compared with controls in the frontal and temporal lobes, except for Iba1-positive microglia in FW, where the burden was surprisingly low (Figure 5.6m-o). FTLD-CBD cases had a higher burden

of CD68-positive microglia in the frontal lobe and TW compared with controls, but a similar burden of CR3/43 and Iba1-positive microglia to controls in all regions, except for TW, where the burden of Iba1-positive microglia was higher than controls (Figure 5.6o). FTLD-PSP and FTLD-*MAPT* cases had a modest burden of Iba1 and CR3/43-positive microglia and a low burden of CD68-positive microglia, similar to controls in most regions (Figure 5.6m-o), although in TW FTLD-*MAPT* cases had a higher burden of CD68-positive microglia compared with controls (Figure 5.6m).

Comparing cases with underlying tau pathology, FTLD-Picks and FTLD-CBD cases had similar burdens of each microglial phenotype in each region. However, FTLD-Picks cases had a higher burden of CD68-positive microglia in TW and TG, and CR3/43-positive microglia in all regions, compared with FTLD-PSP cases (Figure 5.6m,n). FTLD-Picks cases also had a higher burden of CD68-positive microglia in FW and Iba1-positive microglia in TG compared with FTLD-*MAPT* cases, (Figure 5.6m,o). FTLD-CBD cases had a higher burden of CD68-positive microglia in the frontal lobe compared with FTLD-*MAPT* cases and in TW compared with FTLD-PSP cases (Figure 5.6m) but a similar burden of CR3/43 and Iba1-positive microglia to other FTLD-tau subtypes (Figure 5.6n,o).

Grey versus white matter comparisons showed that in most FTLD-tau groups microglial burden was higher in white matter than grey matter, although this varied regionally by FTLD-tau subtype and microglial phenotype (Figure 5.6p-r).

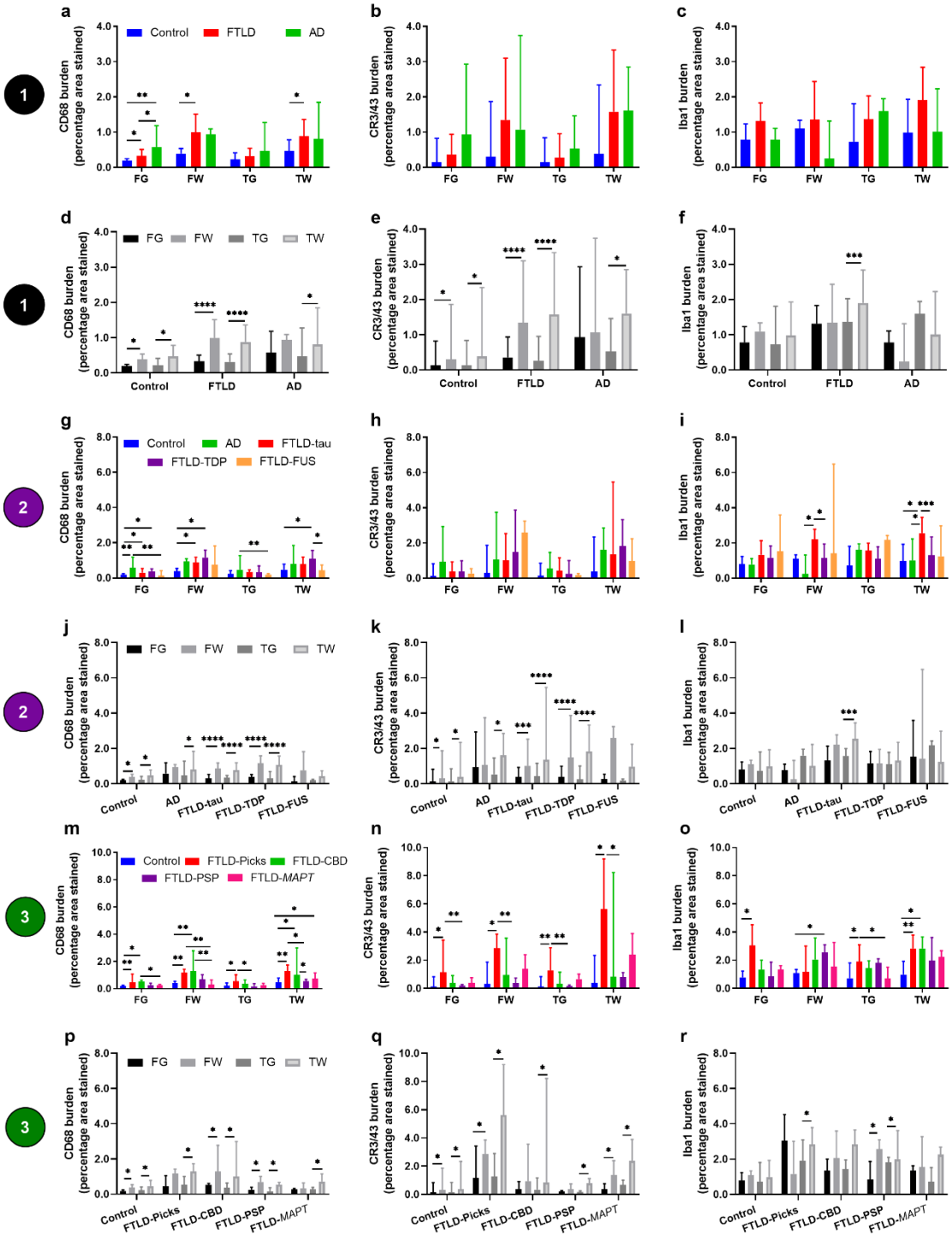

Figure 5.6 Microglial burden compared between groups in each region and between grey and white matter in each lobe for each group (levels 1-3)

Comparisons of the burden of CD68-positive (**a, d, g, j, m, p**), CR3/43-positive (**b, e, h, k, n, q**), and Iba1-positive (**c, f, i, l, o, r**) microglia for each group comparison level shown within Figure 5.4 (numbers in coloured circles on left represent level of comparison). The top row of graphs in each numbered level shows comparisons of microglia in each region between groups. The bottom row of graphs in each numbered level shows comparisons of microglia between grey and white matter within each lobe for each group. Graphs show median microglial burden (percentage area values) in each brain region: frontal grey (FG), frontal white (FW), temporal grey (TG) and temporal white (TW) matter. See legend in first graph on each row for bar colours. Error bars represent interquartile range. *P<0.05; **P<0.01; ***P≤0.001; ****P≤0.0001.

5.5.2.4 FTLD-TDP subtypes

FTLD-TDPA and FTLD-TDPC cases generally had a high burden of CD68-positive microglia, particularly in white matter, with a significant difference from controls in TW for FTLD-TDPA cases and in FG and FW for FTLD-TDPC cases (Figure 5.7a). The burden of CR3/43-positive microglia varied considerably across FTLD-TDPA and FTLD-TDPC cases, particularly in white matter, and overall, there was no significant difference from controls (Figure 5.7b). In contrast, FTLD-TDPB cases had a similar burden of CD68 and CR3/43-positive microglia to controls in all regions (Figure 5.7a,b).

When comparing FTLD-TDP subtypes, the burden of CD68 and CR3/43-positive microglia did not differ between FTLD-TDPA and FTLD-TDPC subtypes in any region but there was a lower burden of burden of CD68 and CR3/43-positive microglia in TG of FTLD-TDPB compared with FTLD-TDPA cases (Figure 5.7a,b). The burden of Iba1-positive microglia was similar between FTLD-TDP subtypes and when compared with controls, except for FTLD-TDPC cases, which had a higher burden in FG compared with controls (Figure 5.7c).

Grey versus white matter comparisons revealed that FTLD-TDPA and FTLD-TDPC cases had a higher burden of CD68 and CR3/43-positive microglia in white than grey matter, particularly in the frontal lobe (Figure 5.7d,e). FTLD-TDPA cases also had a higher burden of these phenotypes in TW than TG. In contrast, FTLD-TDPB cases had similar burdens of these microglial phenotypes in grey and white matter. The burden of Iba1-positive microglia was similar in grey and white matter within each lobe for all FTLD-TDP subtypes (Figure 5.7f).

5.5.2.5 Sporadic and genetic FTLD-TDPA subtypes

Sporadic FTLD-TDPA cases had a similar burden of CD68-positive microglia to controls and FTLD-*C9orf72* cases in all regions, but a lower burden of CD68-positive microglia in the temporal lobe compared with FTLD-*GRN* cases (Figure 5.7g). FTLD-*GRN* cases had a notably high burden of CD68-positive microglia in the temporal lobe and FW, differing significantly from controls in TW (Figure 5.7g). The burden of CD68-positive microglia did not differ significantly between FTLD-*C9orf72* cases and controls in any region. Although many FTLD-TDPA cases, particularly sporadic and FTLD-*GRN* cases, had a high burden of CR3/43-positive microglia, particularly in FW, this varied considerably within each group and overall did not differ significantly from controls (Figure 5.7h). The burden of Iba1-positive microglia was only elevated in the frontal lobe of FTLD-*C9orf72* cases, differing from FTLD-*GRN* cases in FG and FW and from controls and sporadic cases in FW (Figure 5.7i).

Grey versus white matter comparisons revealed that all FTLD-TDPA subtypes had a higher burden of CD68 and CR3/43-positive microglia in white matter than grey matter (Figure 5.7j,k). In contrast, the burden of Iba1-positive microglia was similar between white and grey matter for all groups, except for FTLD-*C9orf72* cases, which had a higher burden in FW than FG (Figure 5.7l).

5.5.2.6 Genetic FTLD subtypes

FTLD-*GRN* cases had a high burden of CD68-positive microglia in most regions, differing significantly from controls in the temporal lobe, especially in TW, but in FW this did not reach significance, and in FG there was a notably similar burden to controls (Figure 5.7m). In this analysis, FTLD-*C9orf72* cases also had a high burden of CD68-positive microglia, particularly in white matter, differing from controls in all regions except TG (Figure 5.7m). In contrast, FTLD-*MAPT* cases only had a higher burden of this phenotype compared with controls in TW, with a lower burden compared with FTLD-*C9orf72* cases

in FW. The burden of CR3/43-positive microglia was highly variable across cases in each group but was higher in FW of FTLD-*GRN* cases compared with controls (Figure 5.7n). Again, there was a particularly high burden of Iba1-positive microglia in the frontal lobe of FTLD-*C9orf72* cases, differing significantly from controls in FG. However, there was a low burden of this phenotype in all regions in FTLD-*GRN* cases, particularly in FW.

Comparisons between genetic groups revealed that FTLD-*C9orf72* cases had a higher burden of CD68-positive microglia in FW than FTLD-*MAPT* cases (Figure 5.7m), and FTLD-*GRN* cases had a lower burden of Iba1-positive microglia throughout the frontal lobe than FTLD-*C9orf72* cases, particularly in FW (Figure 5.7o).

Grey versus white matter comparisons revealed that burdens of CD68 and CR3/43-positive microglia were generally higher in white matter than grey matter in all genetic FTLD subtypes (Figure 5.7p-q). However, there was no significant difference in the burden of Iba1-positive microglia, apart from a higher burden in FW than FG in FTLD-*C9orf72* cases (Figure 5.7r).

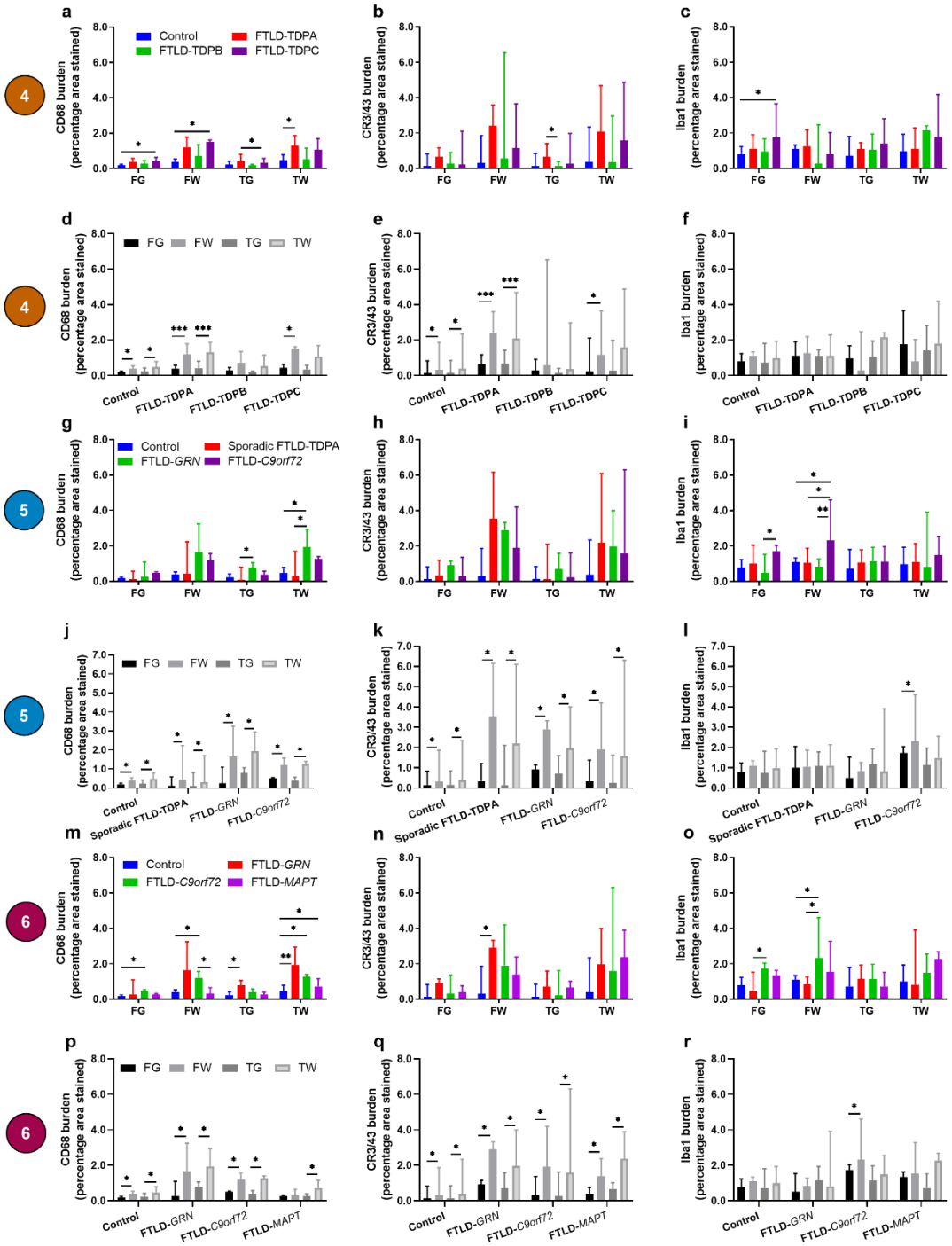

Figure 5.7 Microglial burden compared between groups in each region and between grey and white matter in each lobe for each group (levels 4-6)

Comparisons of the burden of CD68-positive (**a, d, g, j, m, p**), CR3/43-positive (**b, e, h, k, n, q**), and Iba1-positive (**c, f, i, l, o, r**) microglia for each group comparison level shown within Figure 5.4 (numbers in coloured circles on left represent level of comparison). The top row of graphs in each numbered level shows comparisons of microglia in each region between groups. The bottom row of graphs in each numbered level shows comparisons of microglia between grey and white matter within each lobe for each group. Graphs show median microglial burden (percentage area values) in each brain region: frontal grey (FG), frontal white (FW), temporal grey (TG) and temporal white (TW) matter. See legend in first graph on each row for bar colours. Error bars represent interquartile range. **P*<0.05; ***P*<0.01; ****P*≤0.001; *****P*≤0.0001.

5.5.3 Microglial circularity

Detailed results of all group comparisons of microglial circularity are presented sequentially in subsequent sections, for each level of group comparison performed, following the order in Figure 5.4. The heat maps in Appendix 3 contain *P* values for every comparison between groups and between grey and white matter within each group, so *P* values are not presented again in the text. Graphs show results from each level of group comparison, also corresponding to levels in Figure 5.4.

5.5.3.1 Neurodegenerative disease comparisons

Circularity of CD68, CR3/43 and Iba1-positive microglia was similar between all groups, apart from FTLD cases having more circular CD68-positive microglia in TG than AD cases (Figure 5.8a-c).

Grey versus white matter comparisons revealed that only FTLD cases had much more circular CD68 and CR3/43-positive microglia in frontotemporal grey matter compared with white matter (Figure 5.8d,e). There were no differences between grey and white matter for Iba1-positive microglia in any disease group (Figure 5.8f).

5.5.3.2 Main FTLD subtypes

Circularity of CD68, CR3/43 and Iba1-positive microglia did not differ between the main FTLD subtypes and controls in any region (Figure 5.8g-i) but all three FTLD subtypes had more circular CD68-positive microglia in TG compared with AD cases (Figure 5.8g) and FTLD-tau cases had more circular CR3/43-positive microglia in FW compared with FTLD-TDP cases (Figure 5.8h).

Grey versus white matter comparisons revealed that FTLD-tau and FTLD-TDP cases had more circular CD68 and CR3/43-positive microglia in grey matter than white matter

(Figure 5.8j,k). Circularity of Iba1-positive microglia was similar in grey and white matter for all main FTLD subtypes (Figure 5.8l).

5.5.3.3 FTLD-tau subtypes

FTLD-Picks cases had more circular CD68-positive microglia in the frontal lobe compared with controls and all other FTLD-tau subtypes (Figure 5.8m). Circularity of CD68-positive microglia in FTLD-CBD cases did not differ from controls but was lower in FW compared with FTLD-Picks cases and in FW and TW compared with FTLD-*MAPT* cases (Figure 5.8m). FTLD-*MAPT* cases had more circular CD68-positive microglia in TG than controls, in FW and TW compared with FTLD-CBD cases and in FG and TW compared with FTLD-PSP cases (Figure 5.8m). Despite a high burden of CR3/43-positive microglia in FTLD-Picks cases in most regions, circularity of this phenotype did not differ significantly from other groups, apart from being lower than FTLD-CBD cases in FG (Figure 5.8n). FTLD-CBD cases had very circular CR3/43-positive microglia in FG, differing significantly from all other FTLD-tau groups (Figure 5.8n). Circularity of Iba1-positive microglia did not differ between groups, apart from more circular microglia in FW of FTLD-Picks cases and controls compared with FTLD-PSP cases (Figure 5.8o).

Grey versus white matter comparisons revealed that FTLD-Picks cases had similarly high circularity values for CD68 and CR3/43-positive microglia in both areas in both lobes, and FTLD-PSP cases had similarly low values in grey and white matter (Figure 5.8p,q). In contrast, FTLD-CBD cases had more circular microglia of both phenotypes in grey matter of both lobes and FTLD-*MAPT* cases had more circular CD68-positive microglia in TG than TW. Circularity of Iba1-positive microglia was similar between areas except for more circular microglia in TW than TG in FTLD-Picks cases (Figure 5.8r).

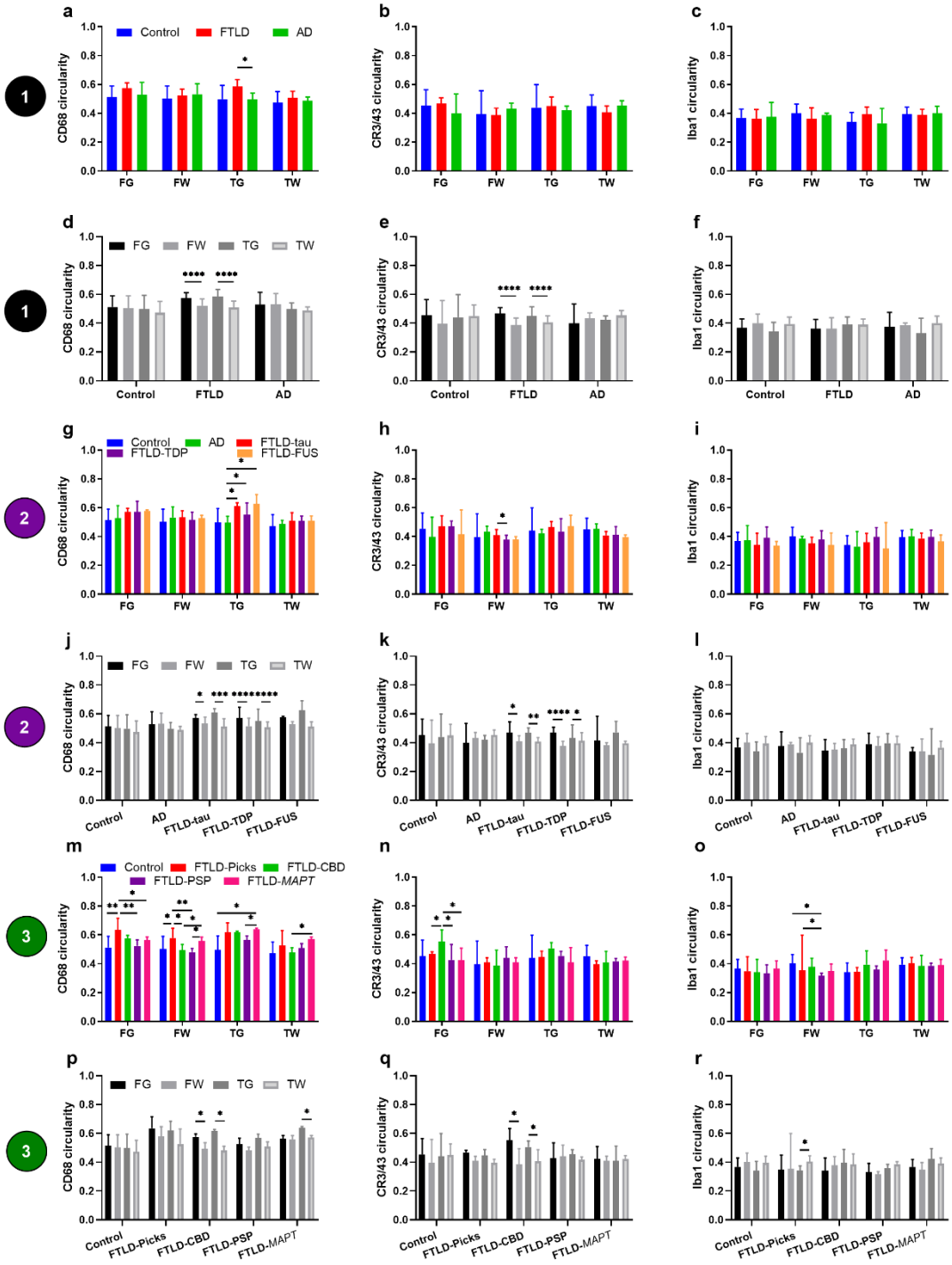

Figure 5.8 Microglial circularity compared between groups in each region and between grey and white matter in each lobe for each group (levels 1-3)

Comparisons of the circularity of CD68-positive (**a, d, g, j, m, p**), CR3/43-positive (**b, e, h, k, n, q**), and Iba1-positive (**c, f, i, l, o, r**) microglia for each group comparison level shown within Figure 5.4 (numbers in coloured circles on left represent level of comparison). The top row of graphs in each numbered level shows comparisons of microglia in each region between groups. The bottom row of graphs in each numbered level shows comparisons of microglia between grey and white matter within each lobe for each group. Graphs show median circularity values in each brain region: frontal grey (FG), frontal white (FW), temporal grey (TG) and temporal white (TW) matter. See legend in first graph on each row for bar colours. Error bars represent interquartile range. **P*<0.05; ***P*<0.01; ****P*≤0.001; *****P*≤0.0001.

5.5.3.4 FTLD-TDP subtypes

There were no significant differences in the circularity of CD68 or CR3/43-positive microglia between any FTLD-TDP subtype and controls (Figure 5.9a,b). However, FTLD-TDPA cases had more circular Iba1-positive microglia in TG than controls, in TW than FTLD-TDPB cases and in FG compared with FTLD-TDPC cases (Figure 5.9c).

Grey versus white matter comparisons revealed that FTLD-TDPA cases had more circular CD68 and CR3/43-positive microglia in grey matter than white matter of both lobes (Figure 5.9d,e), and circularity of CD68-positive microglia in FTLD-TDPC cases was also higher in grey matter of both lobes (Figure 5.9d), but in FTLD-TDPB cases circularity values did not differ significantly between grey and white matter. Circularity of Iba1-positive microglia was similar in grey and white matter for each FTLD-TDP subtype (Figure 5.9f).

5.5.3.5 Sporadic and genetic FTLD-TDPA subtypes

FTLD-*GRN* cases had higher circularity values for CD68 and Iba1-positive microglia in FG compared with controls (Figure 5.9g,i). Sporadic FTLD-TDPA and FTLD-*C9orf72* cases had similar circularity values to other groups for all microglial phenotypes in all regions.

Grey versus white matter comparisons revealed that circularity values for CD68-positive microglia were generally higher in grey matter than white matter (Figure 5.9j). CR3/43-positive microglia were more circular in TG than TW of FTLD-*C9orf72* cases (Figure 5.9k). Circularity of Iba1-positive microglia was similar between grey and white matter in all groups (Figure 5.9l).

5.5.3.6 Genetic FTLD subtypes

FTLD-*GRN* cases had more circular CD68-positive microglia than controls in FG and FTLD-*MAPT* cases had more circular CD68-positive microglia than controls in TG (Figure 5.9m). However, circularity of this phenotype did not differ between genetic FTLD subtypes in any region. Circularity of CR3/43-positive microglia did not differ between genetic FTLD subtypes or from controls (Figure 5.9n). Despite a low burden of Iba1-positive microglia in all regions in FTLD-*GRN* cases, circularity was higher in FG and TG compared with controls, and in FG compared with FTLD-*MAPT* cases (Figure 5.9o).

Grey versus white matter comparisons revealed that circularity of CD68-positive microglia was generally higher in grey matter than white matter, but this varied regionally according to the mutation: FTLD-*GRN* and FTLD-*C9orf72* cases had more circular CD68-positive microglia in grey matter of both lobes, whereas FTLD-*MAPT* cases only had more circular CD68-positive microglia in TG compared with TW (Figure 5.9p). FTLD-*C9orf72* cases also had more circular CR3/43-positive microglia in FG compared with FW (Figure 5.9q). Circularity of Iba1-positive microglia did not differ significantly between grey and white matter in any group (Figure 5.9r).

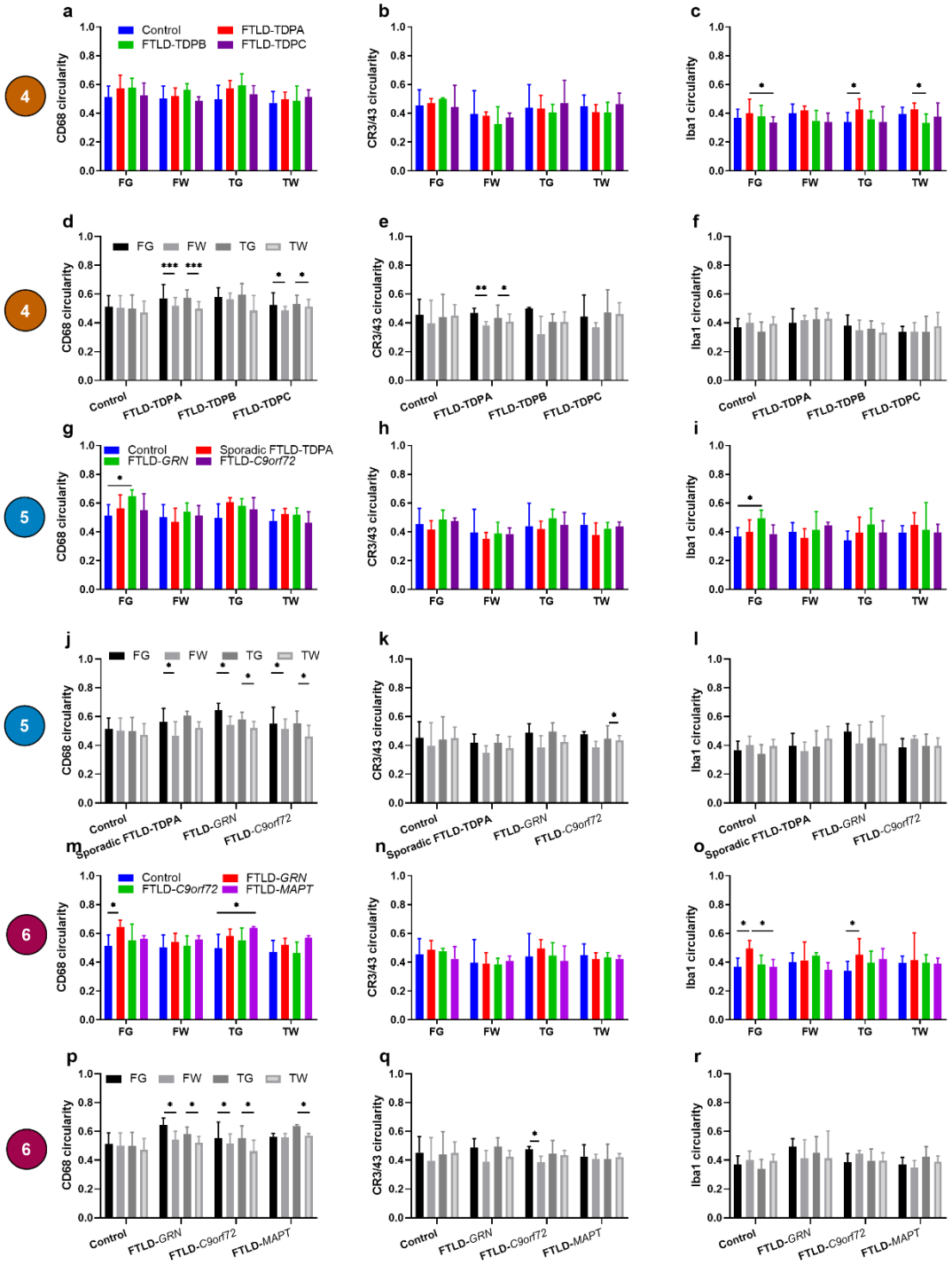

Figure 5.9 Microglial circularity compared between groups in each region and between grey and white matter in each lobe for each group (levels 4-6)

Comparisons of the circularity of CD68-positive (**a, d, g, j, m, p**), CR3/43-positive (**b, e, h, k, n, q**), and Iba1-positive (**c, f, i, l, o, r**) microglia for each group comparison level shown within Figure 5.4 (numbers in coloured circles on left represent level of comparison). The top row of graphs in each numbered level shows comparisons of microglia in each region between groups. The bottom row of graphs in each numbered level shows comparisons of microglia between grey and white matter within each lobe for each group. Graphs show median circularity values in each brain region: frontal grey (FG), frontal white (FW), temporal grey (TG) and temporal white (TW) matter. See legend in first graph on each row for bar colours. Error bars represent interquartile range. * $P<0.05$; ** $P<0.01$; *** $P\leq0.001$; **** $P\leq0.0001$.

5.5.4 Microglial perimeter

Detailed results of all group comparisons of microglial perimeter are presented sequentially in subsequent sections, for each level of group comparison performed, following the order in Figure 5.4. The heat maps in Appendix 3 contain *P* values for every comparison between groups and between grey and white matter within each group, so *P* values are not presented again in the text. Graphs show results from each level of group comparison, also corresponding to levels in Figure 5.4.

5.5.4.1 Neurodegenerative disease comparisons

FTLD cases had smaller perimeter CD68 and CR3/43-positive microglia in FG and TG compared with AD cases, consistent with the higher circularity values in TG, but perimeter did not differ significantly from controls (Figure 5.10a,b). Iba1-positive microglia had a larger perimeter in FTLD cases in FW and TW compared with controls (Figure 5.10c).

Grey versus white matter comparisons revealed that FTLD cases had smaller perimeter CD68 and CR3/43-positive microglia in grey matter compared with white matter in both lobes (Figure 5.10d,e), consistent with higher circularity here. In contrast, AD cases had smaller perimeter CD68-positive microglia in TW than TG. Controls had smaller perimeter CR3/43-positive microglia in FG than FW. The perimeter of Iba-1 positive microglia was similar in grey and white matter in all groups, except for controls, where it was smaller in TW than TG (Figure 5.10f).

5.5.4.2 Main FTLD subtypes

All three FTLD subtypes had smaller perimeter CD68-positive microglia in TG compared with AD cases, and perimeter was smaller in FG of FTLD-tau and FTLD-TDP (but not FTLD-FUS) cases compared with AD cases (Figure 5.10g). FTLD-tau cases had smaller perimeter CR3/43-positive microglia in FW compared with FTLD-TDP cases, and in FG

compared with AD cases, whereas FTLD-FUS cases had smaller perimeter CR3/43-positive microglia in TG compared with AD cases (Figure 5.10h). Although circularity of Iba1-positive microglia had been similar across groups, there were larger perimeter Iba1-positive microglia in FW and TW of FTLD-tau cases compared with controls (Figure 5.10h,i).

Grey versus white matter comparisons revealed that FTLD-TDP cases had smaller perimeter CD68 and CR3/43-positive microglia in grey matter compared with white matter (Figure 5.10j,k), consistent with higher circularity here. FTLD-tau cases also had smaller perimeter CR3/43-positive microglia in grey matter (Figure 5.10k), but no significant differences for CD68-positive microglia. The perimeter of Iba1-positive microglia did not differ significantly between grey and white matter in any FTLD subtype (Figure 5.10l).

5.5.4.3 FTLD-tau subtypes

FTLD-Picks cases had smaller perimeter CD68-positive microglia in FG compared with FTLD-PSP and FTLD-*MAPT* cases (Figure 5.10m). FTLD-CBD cases had much smaller perimeter CR3/43-positive microglia in FG compared with FTLD-Picks and FTLD-*MAPT* cases, whereas FTLD-PSP cases had smaller perimeter CR3/43-positive microglia in TW than FTLD-*MAPT* cases (Figure 5.10n). The perimeter of Iba1-positive microglia was similar across groups, except for FTLD-*MAPT* and FTLD-PSP cases, which had a larger perimeter in FW than controls (Figure 5.10o).

Grey versus white matter comparisons revealed that FTLD-CBD cases had smaller perimeter CD68 and CR3/43-positive microglia in FG than FW and smaller perimeter CD68-positive microglia in TG than TW (Figure 5.10p,q). In contrast, FTLD-Picks cases had smaller perimeter Iba1-positive microglia in TW than TG (Figure 5.10r). Perimeter

did not differ significantly between grey and white matter in FTLD-PSP or FTLD-*MAPT* cases.

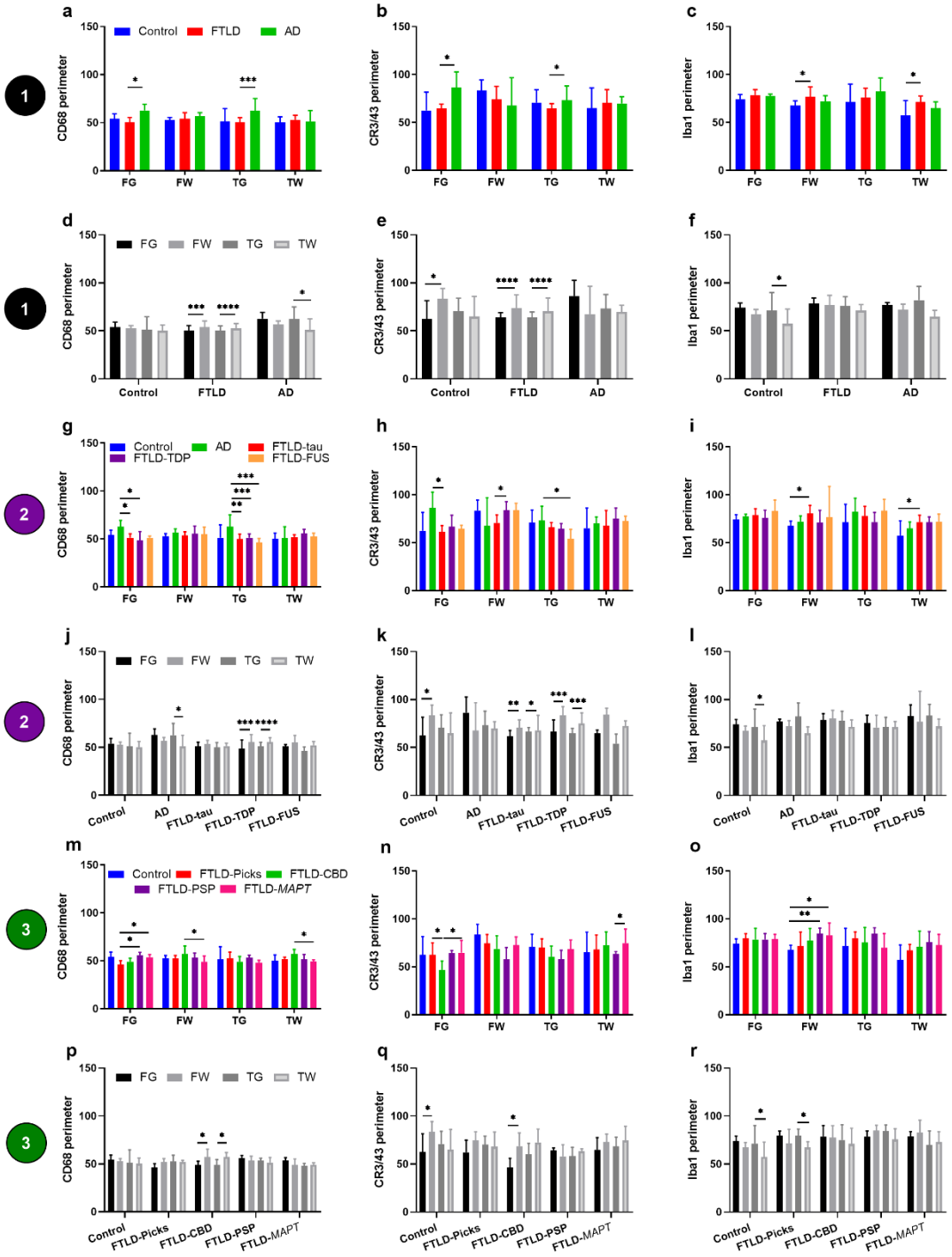

Figure 5.10 Microglial perimeter compared between groups in each region and between grey and white matter in each lobe for each group (levels 1-3)

Comparisons of the perimeter of CD68-positive (**a, d, g, j, m, p**), CR3/43-positive (**b, e, h, k, n, q**), and Iba1-positive (**c, f, i, l, o, r**) microglia for each group comparison level shown within Figure 5.4 (numbers in coloured circles on left represent level of comparison). The top row of graphs in each numbered level shows comparisons of microglia in each region between groups. The bottom row of graphs in each numbered level shows comparisons of microglia between grey and white matter within each lobe for each group. Graphs show median perimeter values in each brain region: frontal grey (FG), frontal white (FW), temporal grey (TG) and temporal white (TW) matter. See legend in first graph on each row for bar colours. Error bars represent interquartile range. *P<0.05; **P<0.01; ***P≤0.001; ****P≤0.0001.

5.5.4.4 FTLD-TDP subtypes

Like circularity, the perimeter of CD68 and CR3/43-positive microglia did not differ between FTLD-TDP subtypes and controls in any region (Figure 5.11a,b). The perimeter of Iba1-positive microglia was smaller in FG of FTLD-TDPA cases compared with FTLD-TDPC cases but similar in other regions compared with other groups, whereas FTLD-TDPB cases had larger perimeter Iba1-positive microglia than controls in TW (Figure 5.11c).

Grey versus white matter comparisons revealed smaller perimeter CD68 and CR3/43-positive microglia in grey matter than white matter of both lobes in FTLD-TDPA cases (Figure 5.11d,e), matching circularity results. In FTLD-TDPC cases, CR3/43-positive microglia were of smaller perimeter in FG than FW (Figure 5.11e). The perimeter of Iba1-positive microglia was similar in grey and white matter of each FTLD-TDP subtype (Figure 5.11f).

5.5.4.5 Sporadic and genetic FTLD-TDPA subtypes

The perimeter of CD68-positive microglia was smaller in TW of sporadic FTLD-TDPA cases than FTLD-*GRN* cases (Figure 5.11g), despite no difference in circularity between these groups. The perimeter of CR3/43-positive and Iba1-positive microglia did not differ significantly between groups (Figure 5.11h,i).

Grey versus white matter comparisons showed that perimeter was often smaller in grey matter than white matter. There were smaller perimeter CD68 and CR3/43-positive microglia in FG than FW of sporadic FTLD-TDPA and FTLD-*GRN* cases (Figure 5.11j,k), and smaller perimeter CD68-positive microglia in TG than TW of FTLD-*GRN* and FTLD-*C9orf72* cases (Figure 5.11j). The perimeter of Iba1-positive microglia was smaller in TW than TG in sporadic FTLD-TDPA cases (Figure 5.11l).

5.5.4.6 Genetic FTLD subtypes

Unlike circularity, perimeter did not significantly differ between genetic groups or between any group and controls for any microglial phenotype, apart from larger perimeter Iba1-positive microglia in FW of FTLD-*MAPT* cases compared with controls (Figure 5.11m-o).

Grey versus white matter comparisons generally revealed smaller perimeter microglia in grey matter than white matter, matching circularity results, but this varied regionally according to mutation. FTLD-*GRN* cases had smaller perimeter CD68 and CR3/43-positive microglia in grey matter of both lobes, whereas FTLD-*C9orf72* cases had smaller perimeter of CD68-positive microglia only in TG compared with TW (Figure 5.11p,q). In FTLD-*MAPT* cases the perimeter of CD68-positive microglia did not differ significantly, in contrast to the higher circularity seen in TG compared with TW. The perimeter of Iba-1 positive microglia was similar in grey and white matter for all groups (Figure 5.11r).

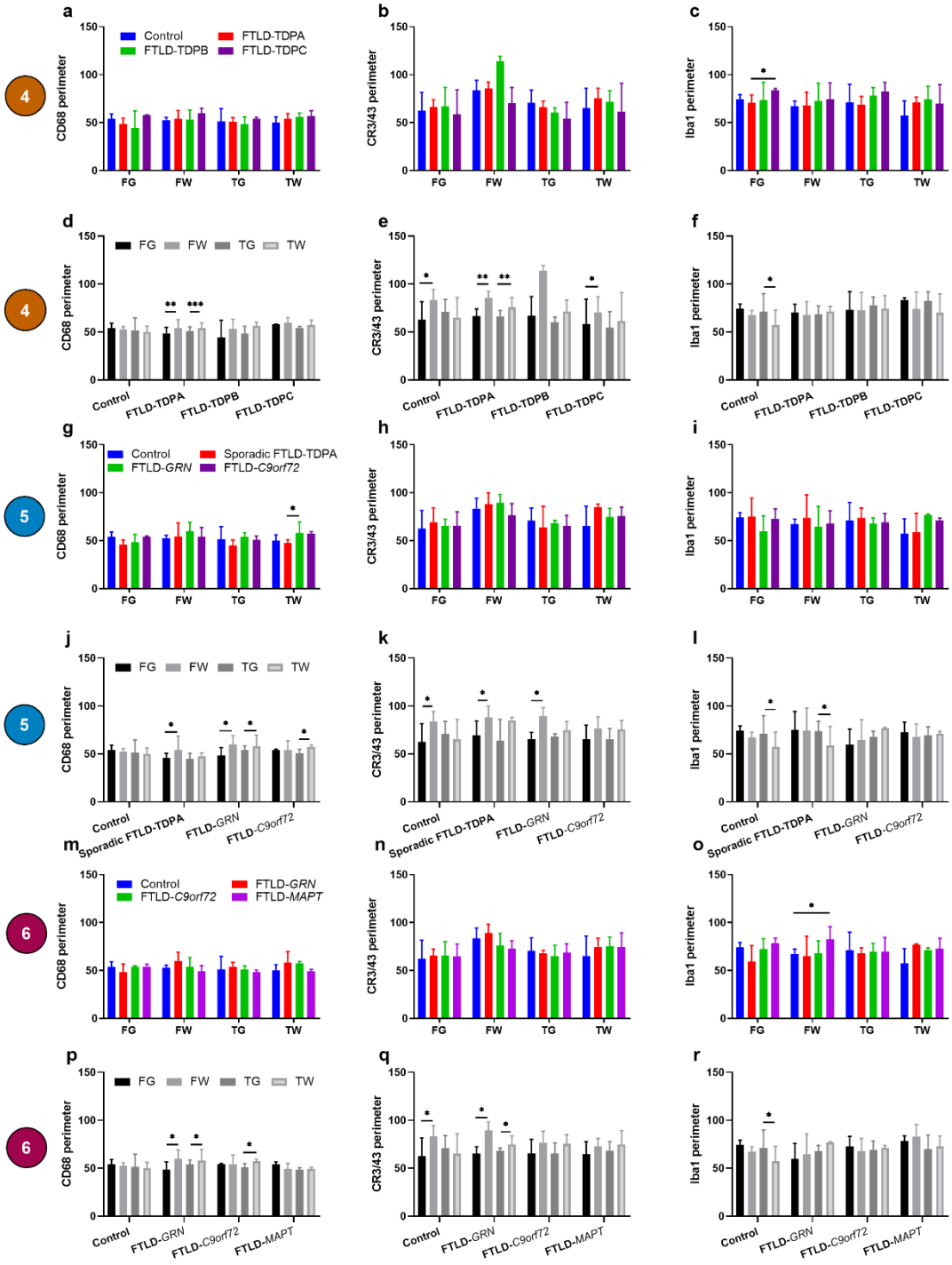

Figure 5.11 Microglial perimeter compared between groups in each region and between grey and white matter in each lobe for each group (levels 4-6)

Comparisons of the perimeter of CD68-positive (**a, d, g, j, m, p**), CR3/43-positive (**b, e, h, k, n, q**), and Iba1-positive (**c, f, i, l, o, r**) microglia for each group comparison level shown within Figure 5.4 (numbers in coloured circles on left represent level of comparison). The top row of graphs in each numbered level shows comparisons of microglia in each region between groups. The bottom row of graphs in each numbered level shows comparisons of microglia between grey and white matter within each lobe for each group. Graphs show median perimeter values in each brain region: frontal grey (FG), frontal white (FW), temporal grey (TG) and temporal white (TW) matter. See legend in first graph on each row for bar colours. Error bars represent interquartile range. *P<0.05; **P<0.01; ***P≤0.001; ****P≤0.0001.

5.6 Discussion

This study performed a comprehensive, quantitative assessment of the burden and activation state of three different microglial phenotypes (phagocytic, antigen-presenting and general microglia) in frontotemporal grey and white matter in *post-mortem* brain tissue from a large and diverse cohort of individuals with sporadic and genetic FTLD, sporadic AD and controls. This approach has demonstrated that microglia differ between individuals with a neurodegenerative disease (FTLD or AD) and controls, and between clinically overlapping neurodegenerative diseases (FTLD and AD). Regional patterns of microglial burden and activation differ across the spectrum of neuropathology within FTLD, not only between the main FTLD subtypes (FTLD-tau, FTLD-TDP and FTLD-FUS), but also between different pathological subtypes of FTLD-tau and FTLD-TDP, between individuals with the same pathology due to different disease mechanisms (sporadic and genetic FTLD-TDPA), and between individuals with genetic FTLD due to different mutations (FTLD-*GRN*, FTLD-*C9orf72* and FTLD-*MAPT*). Importantly, microglial burden and activation also vary according to the microglial phenotype and between grey and white matter; there were generally more phagocytic and antigen-presenting microglia present in white matter than grey matter, but these were in a less activated state.

5.6.1 Changes in microglia: a summary

Table 5.1 summarises the significant regional changes in microglial burden, and activation (combining circularity and perimeter), in each group compared with controls, for each microglial phenotype (phagocytic, antigen-presenting and general microglia). Results for all group comparisons are discussed further sequentially, following the order in Figure 5.4, for each level of group comparison performed.

Microglial phenotype	Phagocytic microglia (CD68-positive)		Antigen-presenting microglia (CR3/43-positive)		General microglia (Iba1-positive)	
Parameter	**Burden**	**Activation**	**Burden**	**Activation**	**Burden**	**Activation**
Neurodegenerative disease groups and controls						
Controls	↔	↔	↔	↔	↔	↔
FTLD	↑ Fronto-temporal except TG	↔	↔	↔	↔	↔
AD	↑ FG	↔	↔	↔	↔	↔
Main FTLD subtypes						
FTLD-tau	↑ Frontal	↔	↔	↔	↑ Fronto-temporal WM esp. TW	↓ Fronto-temporal WM
FTLD-TDP	↑ Frontal + TW	↔	↔	↔	↔	↔
FTLD-FUS	↔	↔	↔	↔	↔	↔
FTLD-tau subtypes						
FTLD-Picks	↑ Fronto-temporal esp. FW	↑ Frontal esp. FW	↑ Fronto-temporal WM	↔	↑ Fronto-temporal except FW	↔
FTLD-CBD	↑ Frontal + TW	↔	↔	↑ FG	↑ TW	↔
FTLD-PSP	↔	↔	↔	↔	↔	↓ FW
FTLD-*MAPT*	↑ TW	↑ TG (+TW)	↔	↔	↔	↔
FTLD-TDP subtypes						
FTLD-TDPA	↑ TW	↔	↔	↔	↔	↑ TG
FTLD-TDPB	↔	↔	↔	↔	↔	↓ TW
FTLD-TDPC	↑ Frontal	↔	↔	↔	↑ FG	↔
FTLD-TDPA subtypes						
Sporadic FTLD-TDPA	↔	↔	↔	↓ FG	↔	↔
FTLD-*GRN*	↑ Temporal esp. WM	↑ FG	↑ FW	↔	↓ Fronto-temporal esp. FW	↑ FG + TG
FTLD-*C9orf72*	↑ Frontal esp. WM	↔	↔	↔	↑ Frontal esp. WM	↔
Genetic FTLD subtypes						
FTLD-*GRN*	↑ Temporal esp. WM	↑ FG	↑ FW	↔	↓ Fronto-temporal esp. FW	↑ FG + TG
FTLD-*C9orf72*	↑ Frontal esp. WM	↔	↔	↔	↑ Frontal esp. WM	↔
FTLD-*MAPT*	↑ TW	↑ TG (+TW)	↔	↔	↔	↔

Table 5.1 Summary of changes in microglial burden and activation in each group.

Significant regional changes in microglial parameters in each group compared with controls. ↑ = increased; ↓ = decreased; ↔ = no significant difference; + = and; esp. = especially. Other abbreviations: see main text.

5.6.2 Neurodegenerative disease groups

Controls had a low burden of all microglial phenotypes, and a particularly low burden of phagocytic microglia, in all regions. This was unsurprising given the young AAD of the control group (to match to the FTLD group) and has been shown in previous studies of microglia in controls, particularly using Iba1 (Torres-Platas et al., 2014).

FTLD cases had a high burden of phagocytic microglia in frontotemporal grey and white matter, with significant differences from controls in all regions except TG. This is consistent with previous studies of this microglial phenotype in FTLD (Lant et al., 2014) and FTLD-TDP (Taipa et al., 2017). However, use of three different microglial markers in the present study has enabled appreciation that, overall, FTLD is associated with a higher burden of phagocytic microglia in these regions, without a concurrent increase in antigen-presenting microglia, or microglia in general. This was demonstrated by the fact that there was no significant difference in the burden of CR3/43-positive or Iba1-positive microglia between the FTLD group and controls in any region. However, the burden of various microglial phenotypes (including antigen-presenting microglia) did differ significantly between certain FTLD subtypes and controls (as discussed later). Initially, a high burden of phagocytic microglia within a brain region could represent a protective response of cells clearing soluble tau or TDP-43 oligomers, prior to the development of protein aggregates. However, over time, persistent phagocytosis could contribute to neuronal and axonal damage and neurodegeneration in FTLD.

AD cases had many phagocytic microglia in most regions, with a higher burden than controls in FG, but a similar burden of other microglial phenotypes to controls in all regions. Other studies of AD cases have also found more phagocytic (CD68-positive) microglia in FG (Lant et al., 2014), and the middle frontal cortex (Minett et al., 2016) compared with controls, as well as in areas affected early on in AD, including the

subiculum, entorhinal cortex and CA1 hippocampal region (Taipa et al., 2017). However, there were many activated antigen-presenting (HLA-DR-positive) microglia in various cortical regions (Hendrickx et al., 2017; Minett et al., 2016; Ohm et al., 2018) and more Iba1-positive microglia in the frontal cortex (Nilson et al., 2017) of AD cases, which was not found here. However, fewer Iba1-positive microglia in the middle frontal cortex (Minett et al., 2016), or similar numbers of Iba1-positive microglia in inferior temporal and anterior cingulate cortical grey matter (Davies et al., 2017) have also been observed in AD cases compared with controls. Disparities in regional microglial phenotypes between studies may be due to clinical heterogeneity of AD cohorts or techniques used to quantify microglia. Alternatively, this supports emerging hypotheses that distinct microglial phenotypes exist within the same brain region, and that the relative functions of different populations of microglia contribute to regional vulnerabilities to chronic neuroinflammation and neurodegeneration in AD (Ayata et al., 2018; Bonham et al., 2019; Böttcher et al., 2018; Friedman et al., 2018; Grabert et al., 2016; Keren-Shaul et al., 2017). In pre-clinical AD, many phagocytic microglia appear in the mesial temporal lobe after tau pathology but become activated only after amyloid deposition (Streit et al., 2018). This study shows that by the end stage of disease there is also a high burden of phagocytic microglia in cortical regions outside the mesial temporal lobe in AD cases, perhaps reflecting the anatomical spread of AD pathology (Felsky et al., 2019).

FTLD cases had a similar burden of all microglial phenotypes to AD cases in all regions, except in FG, where FTLD cases had a lower burden of phagocytic microglia. This was unexpected; previous studies have found more phagocytic microglia in FW of FTLD (Lant et al., 2014) and FTLD-TDP (Taipa et al., 2017) cases compared with AD cases, but more phagocytic microglia in TG of AD compared with FTLD cases (Lant et al., 2014). This would fit more with a predilection for most FTLD pathologies for the frontal lobe, particularly white matter. However, there was a suggestion of more microglia in general

in FG of FTLD cases compared with AD cases (although this did not reach significance), and later analyses demonstrated that microglial burden does vary according to FTLD subtype. This variability may have led to non-significance when comparing the large, heterogeneous FTLD group with the much smaller group of AD cases.

Microglial activation was also compared between FTLD, AD and control groups. In controls, all microglial phenotypes had low circularity and high perimeter values in all regions, suggestive of limited microglial activation in both grey and white matter. This is consistent with presence of mainly ramified microglia in these regions in other studies examining controls (Lant et al., 2014; Taipa et al., 2017; Torres-Platas et al., 2014). Despite a higher *burden* of phagocytic microglia in FTLD and AD groups compared with controls in several regions, this phenotype was *not* more activated in any region in either group compared with controls, and other microglial phenotypes were similarly poorly activated. This contradicts other studies showing more activated phagocytic microglia in frontotemporal grey and white matter of FTLD cases (Lant et al., 2014), and in frontal (Lant et al., 2014) and temporal (Lant et al., 2014; Taipa et al., 2017) grey matter and TW (Lant et al., 2014) of AD cases compared with controls. However, the quantitative techniques used in the present study enabled more comprehensive characterisation of microglial burden and activation state (circularity and perimeter) than the visual rating and semi-quantitative scoring systems used in these studies. It was also possible to differentiate microglial burden from activation, whereas previously these were assessed jointly.

When comparing microglial activation between FTLD and AD cases, FTLD cases displayed more activated phagocytic and antigen-presenting microglia in frontotemporal grey matter than AD cases. This suggests that FTLD pathology is associated with greater activation in cortical regions than AD pathology. In contrast, others have found greater

activation of phagocytic microglia in FW of FTLD or FTLD-TDP cases compared with AD cases (Lant et al., 2014; Taipa et al., 2017), implicating excessive white matter microglial activation in FTLD. Differences in clinical and pathological subtypes within FTLD cohorts and analysis techniques may underlie contrasting results between studies. Analysis of other affected regions such as the hippocampus and replication within a larger AD cohort could explore this in more detail.

Comparisons of microglial burden and activation within grey versus white matter within each lobe revealed distinct differences according to disease group and microglial phenotype. Controls had a higher burden of phagocytic and antigen-presenting microglia in frontotemporal white matter compared with grey matter. This was unsurprising, as these phenotypes are more numerous in white matter in controls in other studies (Hendrickx et al., 2017; Mittelbronn et al., 2001; Taipa et al., 2017). In contrast, the burden of microglia overall (Iba1-positive) was similar in grey and white matter, as shown previously (Hendrickx et al., 2017). However, all microglial phenotypes were similarly activated in grey and white matter. This suggests that in the healthy brain, microglia with phagocytic and antigen-presenting functions have a predilection for white matter, but activation of these microglia does not usually differ significantly between grey and white matter.

In FTLD cases, the burden of all phenotypes was also generally higher in white matter than grey matter, but activation of phagocytic and antigen-presenting microglia was greater in grey matter than white matter, whereas general microglia were similarly activated in both areas. These results support recent studies showing more phagocytic microglia in FW than FG in FTLD cases (Lant et al., 2014) and in frontal, temporal and entorhinal white matter than grey matter in FTLD-TDP cases (Taipa et al., 2017), although in these studies microglia were also more activated in white matter. It seems

that there is a microglial 'white matter signal' in FTLD, with an influx of microglial phenotypes with key immune functions into white matter, but with reduced activation in white matter by the end stage of disease. This could be due to greater activation in grey matter (where there is more extensive cortical pathology), or due to more extensive dysfunction and failed activation in white matter. Neuroimaging studies of sporadic and genetic FTD demonstrate early, widespread loss of white matter integrity, preceding grey matter atrophy, which varies by clinical and genetic phenotype (Mahoney et al., 2014; Sudre et al., 2017a), occurs presymptomatically (Jiskoot et al., 2018; Sudre et al., 2019) and progresses over time (Elahi et al., 2017; Sudre et al., 2019). There could be an initial influx of phagocytic and antigen-presenting microglia into white matter at early stages of disease, with activated microglia initiating or exacerbating white matter damage through direct phagocytosis of myelin or axons, recruitment of other immune cells and release of proinflammatory cytokines. However, gradual dysfunction and senescence of these microglia in white matter could over time also lead to impaired phagocytosis and debris clearance and reduced neuronal, axonal and immune support, despite increased microglial presence. This may result in excessive demyelination and white matter vulnerability in FTLD, as suggested in Chapter 4.

In AD cases, microglia differed between grey and white matter only in the temporal lobe: phagocytic and overall microglia were more numerous, and phagocytic microglia were more activated, in TW compared with TG. Although this makes sense given the high burden of pathology in temporal regions in most AD cases, another study showed more numerous and/or more activated phagocytic microglia in frontotemporal grey matter than white matter of AD cases, often clustered around Aβ plaques (Lant et al., 2014). However, other AD studies have found similar numbers of activated CD68 and Iba1-positive microglia in grey and white matter (Taipa et al., 2017) or more numerous activated antigen-presenting (HLA-DR-positive) microglia in temporoparietal white

matter than grey matter (Ohm et al., 2018). AD cases also have significant white matter pathology and early neuroimaging white matter abnormalities, particularly in the parietal and temporal lobes (McAleese et al., 2015, 2017), including presymptomatically (Lee et al., 2016). The increased activation of phagocytic microglia in TW of AD cases could therefore be due to a high regional burden of white matter AD pathology.

In conclusion, there are changes in microglial burden and activation in FTLD and AD, which vary regionally. Microglia seem to play a role in both diseases but may contribute to regional vulnerability to the type of pathology, particularly in white matter. Significant variability in microglia was noted across pathological subtypes within the FTLD group and subsequent analyses explored this in detail.

5.6.3 Main FTLD subtypes

The pattern of phagocytic microglia in FTLD-tau and FTLD-TDP cases echoed those in the overall FTLD group; both subtypes had a higher burden of phagocytic microglia throughout the frontal lobe compared with controls. FTLD-TDP cases also had a higher burden of phagocytic microglia in TW than controls, and a similar pattern was seen in FTLD-tau cases, although this did not reach significance. However, phagocytic microglia were not more activated in any region in either FTLD-tau or FTLD-TDP groups compared with controls. Overall, FTLD-tau and FTLD-TDP groups had a similar burden and activation state of phagocytic microglia in all regions, perhaps in general response to excess tau or TDP-43 oligomers, then subsequently protein aggregates and dying neurons and axons. However, by the end stage of disease, there again appears to be impaired microglial activation and potentially reduced phagocytosis. In a mouse model of ALS and TDP-43, phagocytic (CD68-positive) microglia were initially protectively clearing TDP-43, rather than destructive, before microglial senescence rendered them ineffective (Spiller et al., 2018). This may be the case in FTLD-TDP, and perhaps in FTLD-tau as well.

Other studies of FTLD-tau and FTLD-TDP have also shown more phagocytic microglia in frontal grey and white matter of FTLD-tau cases (Lant et al., 2014) and in frontal (Lant et al., 2014; Taipa et al., 2017) and temporal (Lant et al., 2014) grey and white matter of FTLD-TDP cases compared with controls. Again, there were similar patterns of phagocytic microglia in FTLD-TDP and FTLD-tau (Lant et al., 2014). However, microglia were also more activated in both disease groups in these regions compared with controls, which was not the case here, although the semi-quantitative techniques used in previous studies likely prevented differentiation between microglial burden and activation. More nuanced patterns of microglial morphology were detected in the present study.

Surprisingly, FTLD-FUS cases had a relatively low burden of phagocytic microglia in frontal and temporal lobes, with a lower burden of this phenotype in TW compared with FTLD-TDP cases. Activation of all microglial phenotypes was similar to controls and other FTLD subtypes in most regions, except for in TG, where phagocytic microglia were more activated than in AD cases. All FTLD-FUS cases had aFTLD-U, so this specific pathology may not be associated with a significant influx or activation of phagocytic microglia. However, aFTLD-U cases tend to have more severe pathology in the hippocampus and subcortical grey and brainstem nuclei, with less cortical and subcortical white matter involvement (Rohrer et al., 2011). The frontal and temporal regions chosen for analysis may have had less severe pathology in FTLD-FUS than FTLD-tau or FTLD-TDP cases, and this may have led to low microglial burden and activation here. Microglial phenotypes have not been explored in FTLD-FUS previously, but ALS mouse models expressing wild-type FUS display a proinflammatory microglial phenotype and excessive release of proinflammatory cytokines (Ajmone-Cat et al.,

2019). Different mechanisms may be involved in FTLD-FUS or they may be altered by the end stage of disease.

Other microglial phenotypes differed according to the FTLD subtype. Although the burden of antigen-presenting microglia was similar between groups, this phenotype was highly activated in the frontal lobe of FTLD-tau cases, where there is a high burden of tau pathology (McMillan et al., 2013). These microglia were more activated in FW of FTLD-tau compared with FTLD-TDP cases and in FG of FTLD-tau compared with AD cases. Others have found many activated antigen-presenting (HLA-DR-positive) microglia in white matter of FTLD-Picks cases (Hollister et al., 1997; Schofield et al., 2003) and in several regions in FTLD-PSP and FTLD-CBD cases (Ishizawa and Dickson, 2001), suggesting this phenotype is particularly prominent in tauopathies. Transfection of tau leads to increased microglial activation, phagocytosis and migration, which contributes to tau spreading, and is reduced by depletion of microglia in tau models (Kahlson and Colodner, 2015; Vogels et al., 2019). Activated antigen-presenting microglia could have a direct role in interacting with tau and propagating pathology in FTLD-tau cases, particularly within the frontal lobe.

In FTLD-TDP cases, the burden and activation state of antigen-presenting microglia was overall similar to controls. However, certain FTLD-TDPA cases (sporadic FTLD-TDPA or FTLD-*GRN* cases) had a high burden of antigen-presenting microglia in white matter. Later analyses revealed that antigen-presenting microglia varied not only according to FTLD-TDP subtype but also by disease mechanism (sporadic versus genetic) and mutation type. Percentage area values were highly variable across cases within the overall FTLD-TDP group, which likely led to non-significance at an overall group level. This emphasises the importance of analysing pathological subtypes separately in a disease as heterogenous as FTLD.

FTLD-TDP cases had a similar burden and activation state of microglia overall (Iba1-positive) to controls, but FTLD-tau cases had a much higher burden of this phenotype in white matter, differing significantly in TW compared with controls and in FW and TW compared with both FTLD-TDP and AD cases. However, these microglia were less activated in frontotemporal white matter of FTLD-tau cases compared with controls. Profuse microgliosis in white matter has been described in FTLD-tau previously, including in FTLD-Picks (Cooper et al., 1996; Hollister et al., 1997; Paulus et al., 1993; Schofield et al., 2003), FTLD-CBD and FTLD-PSP (Fernández-Botrán et al., 2011; Ishizawa and Dickson, 2001; Sakae et al., 2019a) and FTLD-*MAPT* (Bellucci et al., 2011; Lant et al., 2014) cases. FTLD-tau is associated with significant glial tau pathology in white matter (Komori, 1999; Lant et al., 2014), and prominent axonal degeneration (Kneynsberg et al., 2017; McMillan et al., 2013). FTLD-tau cases have extensive white matter neuroimaging abnormalities (McMillan et al., 2013), which occur presymptomatically (Jiskoot et al., 2018). This suggests that there is early loss of white matter integrity associated with FTLD-tau, which may coincide with an increased microglial and tau burden.

Microglial burden mostly did not differ significantly between AD cases and either FTLD-tau or FTLD-TDP cases. In FG, there was a suggestion of a higher burden of phagocytic microglia in AD compared with FTLD-TDP cases, although this did not reach significance However, there was a much higher burden of microglia overall (Iba1-positive) in frontotemporal white matter of FTLD-tau cases than AD cases. This is unsurprising given the very high burden of this phenotype in white matter in FTLD-tau cases, and it suggests that subcortical white matter tau pathology in FTLD-tau is associated with greater microglial influx than tau pathology in AD. However, all three FTLD subtypes had greater activation of phagocytic microglia in TG compared with AD cases, and FTLD-tau and

FTLD-TDP cases had greater activation of phagocytic microglia in FG than AD cases. This suggests there is greater microglial response associated with FTLD-tau or FTLD-TDP than to AD pathology in frontotemporal grey matter, although this may have been due to the more substantial pathological involvement of these areas in FTLD than AD cases. Others have found more activated phagocytic microglia in FW of FTLD-TDP compared with AD cases (Taipa et al., 2017) but did not explore this in FTLD-tau cases. Interestingly, AD cases had a higher burden of phagocytic microglia than FTLD-FUS cases in frontotemporal grey matter, consistent with the low burden of phagocytic microglia (and microglia in general) observed in FTLD-FUS cases in these regions.

Grey versus white matter comparisons of microglia in the main FTLD subtypes echoed findings in FTLD overall, with a higher burden of phagocytic and antigen-presenting microglia in frontotemporal white matter than grey matter in FTLD-tau and FTLD-TDP. FTLD-FUS cases showed a similar pattern, although this did not reach significance. Phagocytic and antigen-presenting microglia were more activated in grey matter than white matter in FTLD-tau and FTLD-TDP but did not differ between areas in FTLD-FUS cases. This could be due to greater microglial activation in response to cortical tau and TDP-43 pathology. However, given that there is extensive white matter pathology in both FTLD-tau and FTLD-TDP (Irwin et al., 2018), there may be selectively impaired microglial function in white matter, which could also contribute to white matter damage.

There have been few previous comparisons of microglia between grey and white matter in FTLD-tau and FTLD-TDP, and none in FTLD-FUS. In other studies, both FTLD-tau (Lant et al., 2014) and FTLD-TDP (Lant et al., 2014; Taipa et al., 2017) cases had more phagocytic microglia in frontotemporal white matter compared with grey matter, but microglia were also more activated in white matter. A smaller study of FTLD-TDP cases found a higher burden of antigen-presenting microglia in white matter than grey matter,

but microglia were more activated in white matter (Ohm et al., 2018). Differences between studies may have been due to inclusion of different pathological subtypes within FTLD-tau or FTLD-TDP groups, or differences in analysis techniques.

In conclusion, FTLD-tau and FTLD-TDP cases, but not FTLD-FUS cases, have a high burden of phagocytic microglia in frontotemporal grey matter and white matter. FTLD-tau cases have a particularly high burden of microglia overall in white matter, more so than AD cases, but these are poorly activated by the end stage of disease. Although the burden of phagocytic and antigen-presenting microglia is higher in white matter than grey matter, these phenotypes are more activated in grey matter, suggesting that microglial dysfunction as well as activation occurs in regions with extensive TDP-43 and tau pathology. There was notable regional variability in microglia across different FTLD-tau and FTLD-TDP subtypes and subsequent analyses explored this further.

5.6.4 FTLD-tau subtypes

Microglia were compared between FTLD-tau subtypes and between each subtype and controls; such detailed comparisons have not been reported previously. This demonstrated that microglial burden and activation vary regionally according to FTLD-tau subtype, and that microglia are particularly abundant and activated in frontotemporal regions of FTLD-Picks cases, especially in white matter.

FTLD-Picks cases had a much higher burden of all microglial phenotypes in all regions compared with controls, particularly the frontal lobe, except for Iba1-positive microglia in FW, where the burden was low (similar to controls). There was a particularly high burden of phagocytic microglia throughout FW and the temporal lobe of FTLD-Picks cases, differing from FTLD-*MAPT* cases in FW and FTLD-PSP cases in the temporal lobe. However, FTLD-Picks and FTLD-CBD cases had a similarly high burden of phagocytic microglia all regions. FTLD-Picks cases also had highly activated phagocytic microglia throughout the frontal lobe, with more amoeboid morphology compared with controls and

FTLD-PSP cases in FG and FW, FTLD-*MAPT* cases in FG, and FTLD-CBD cases in FW. FTLD-Picks cases also had a particularly high burden of antigen-presenting microglia in frontotemporal white matter, differing significantly from controls and FTLD-PSP cases here. However, activation of this phenotype was similar to other groups in all regions.

A high burden of activated phagocytic microglia in the frontal lobe of FTLD-Picks cases, particularly in white matter, and the presence of numerous antigen-presenting microglia in frontotemporal white matter, is consistent with regional pathology and grey and white matter imaging patterns found in this subtype (Irwin et al., 2016; Kneynsberg et al., 2017; Rohrer et al., 2011). In particular, FTLD-Picks cases display extensive white matter axonal degeneration and demyelination, and early white matter changes on neuroimaging (Irwin et al., 2016; Kneynsberg et al., 2017). Intense white matter microgliosis may be due to high regional burdens of tau pathology: FTLD-Picks is associated with a high burden of tau pathology within axons in frontal subcortical and limbic white matter (Irwin et al., 2016; Kneynsberg et al., 2017; Komori, 1999; Mimuro et al., 2010; Zhukareva et al., 2002), which may upregulate phagocytic and antigen-presenting microglia. In addition, glial tau inclusions were present in temporal white matter of a preclinical FTLD-Picks case before significant neurodegeneration was evident, suggesting early glial involvement (Mimuro et al., 2010).

Extensive microglial (Bevan-Jones et al., 2020; Cooper et al., 1996; Hollister et al., 1997; Schofield et al., 2003) and astrocytic (Irwin et al., 2016; Kersaitis et al., 2004; Schofield et al., 2003) activation have been described in other histological studies of FTLD-Picks cases. A recent study found many, highly amoeboid phagocytic microglia in frontal, temporal and parietal cortices of three FTLD-Picks cases, the density of which correlated regionally with the density of tau pathology (Bevan-Jones et al., 2020). Others have

observed numerous activated antigen-presenting (HLA-DR-positive) microglia in FW at early stages of FTLD-Picks (Schofield et al., 2003) and upregulated HLA-DR expression in FTLD cases with Pick bodies (Hollister et al., 1997), so altered antigen-presentation may play a particular role in disease.

As microglia in FTLD-Picks cases differed from most other FTLD-tau subtypes, this could suggest that microglia are more involved in the pathogenesis of FTLD-Picks than other tauopathies. However, this finding may simply have been due to the choice of brain regions examined and differing clinical presentations and regional burdens of tau pathology of cases within each group. Most FTLD-Picks cases had bvFTD, whereas other FTLD-tau subtypes had a range of clinical diagnoses. Only one previous study has compared microglia between different FTLD-tau subtypes, but this combined FTLD-CBD and FTLD-PSP into one group (FTLD-CBD/PSP) and only analysed phagocytic microglia (Lant et al., 2014). Phagocytic microglia were more numerous and/or more activated in FTLD-*MAPT* cases compared with FTLD-CBD/PSP cases in the temporal lobe, although there were no differences between other FTLD-tau subtypes.

Although FTLD-CBD cases generally had a moderate microglial burden, there was a particularly high burden of phagocytic microglia in the frontal lobe and TW. This differed from controls in both regions, in the frontal lobe from FTLD-*MAPT* cases and in TW from FTLD-PSP cases. However, phagocytic microglia in FTLD-CBD cases were similarly activated to controls in all regions and were less activated in frontotemporal white matter compared with FTLD-*MAPT* cases. As FTLD-CBD pathology often targets frontotemporal grey and white matter (Rohrer et al., 2011), and most cases here had nfvPPA, patterns of phagocytic microglia may again be reflecting regional burdens or effects of tau pathology. In other studies, CBD more often affects cortical grey and subcortical white matter than PSP (Ishizawa and Dickson, 2001; Ling and Macerollo,

2018), and FTLD-CBD cases have less extensive pathology in the temporal lobe than FTLD-*MAPT*, particularly in TW (Pickering-Brown et al., 2002; Rohrer et al., 2011). In a study of antigen-presenting (HLA-DR-positive) microglia in CBD and PSP cases, microglial burden correlated regionally with tau pathology: CBD cases had a lower microglial burden in infratentorial grey and white matter than PSP cases, but there was a similar burden in supratentorial regions (Ishizawa and Dickson, 2001). This may explain regional differences in microglia between FTLD-tau subtypes.

A microglial PET study of CBD cases identified increased microglial activation in the frontal lobe and subcortical structures (Gerhard et al., 2004). However, the limited activation of phagocytic microglia in most regions in FTLD-CBD cases here suggests there may be dysfunction of this phenotype in areas of particularly high tau burden, such as white matter, by the end stage of disease, and CBD is indeed associated with significant glial pathology, including astrocytic tau inclusions in white matter (Kneynsberg et al., 2017; Komori, 1999). Interestingly, in contrast to phagocytic microglia, the burden of antigen-presenting and overall (Iba1-positive) microglia did not differ significantly between FTLD-CBD cases and controls or other FTLD-tau subtypes. However, antigen-presenting microglia were more activated in FG of FTLD-CBD cases compared with all other FTLD-tau subtypes (even FTLD-Picks cases). Numerous, activated antigen-presenting (HLA-DR positive) microglia were present in superior frontal and temporal grey and white matter regions of CBD cases in another study (Ishizawa and Dickson, 2001). Highly activated antigen-presenting microglia in FG could be a feature of FTLD-CBD, although this requires confirmation in a larger cohort, with differing clinical presentations.

FTLD-PSP cases had a low burden of all microglial phenotypes, similar to controls, and particularly few antigen-presenting microglia. Microglial burden was lower in FTLD-PSP

than FTLD-Picks cases in frontal grey and white matter (antigen-presenting microglia) and temporal grey and white matter (phagocytic and antigen-presenting microglia), and lower than FTLD-CBD cases in TW (phagocytic microglia). Activation did not differ significantly between FTLD-PSP cases and controls or from other FTLD-tau subtypes in all regions, except in FW, where Iba1-positive microglia were less activated than controls and FTLD-Picks cases. This low level of microgliosis was initially surprising given the extensive neuronal and glial tau pathology and white matter involvement historically seen in PSP (Kneynsberg et al., 2017; Komori, 1999; Sakae et al., 2019a). Numerous activated antigen-presenting (HLA-DR positive) microglia were present in cortical and subcortical brain regions in other studies of PSP (Fernández-Botrán et al., 2011; Ishizawa and Dickson, 2001). However, most cases in the present study had the PSP-Richardson syndrome variant of PSPS rather than bvFTD or PPA, and hence were likely to have more significant tau pathology in deeper subcortical structures and less in frontotemporal grey and subcortical white matter regions. Supporting this hypothesis, other studies of PSPS cases with this variant show that microgliosis is most pronounced in subcortical and infratentorial structures, correlating with tau burden (Fernández-Botrán et al., 2011; Ishizawa and Dickson, 2001), and that activation detected using microglial PET is upregulated in subcortical but not cortical regions (Passamonti et al., 2018).

Surprisingly, FTLD-*MAPT* cases only had a modest microglial burden in most regions, except for TW, where there was a much higher burden of phagocytic microglia compared with controls. FTLD-*MAPT* cases had a lower burden of this phenotype throughout the frontal lobe compared with FTLD-CBD cases and in FW compared with FTLD-Picks cases. However, phagocytic microglia were more activated throughout the temporal lobe of FTLD-*MAPT* cases compared with controls and FTLD-PSP cases, in FW and TW compared with FTLD-CBD cases, and in FW compared with FTLD-PSP cases. Another study identified significant temporal lobe microgliosis in FTLD-*MAPT* cases, with more numerous, activated phagocytic microglia in TW (but not FW) compared with FTLD-

PSP/CBD cases, and proposed that this was due to a high regional burden of tau pathology (Lant et al., 2014).

MAPT 10+16 mutation carriers display significant neuronal and glial tau inclusions in frontotemporal grey and white matter (Lant et al., 2014; Pickering-Brown et al., 2002; Rohrer et al., 2011) and several *MAPT* mutation models support a link between microglial activation and tau pathology. Many activated phagocytic microglia were present in hippocampal and cortical regions of a *MAPT* P301S mutation carrier, clustered around tau-positive neurons (Bellucci et al., 2011). In *MAPT* P301S mice, numerous proinflammatory microglia surrounded tau-positive neurons (Bellucci et al., 2004; Nilson et al., 2017), directly stimulating microglia to phagocytose them through production of reactive oxygen species (Brelstaff et al., 2018). Microglial activation preceded tau aggregation in one *MAPT* P301S mouse model (Yoshiyama et al., 2007) but followed aggregation in another (van Olst et al., 2020). Suppression of neuroinflammation ameliorated tau pathology and improved survival in P301S mice, suggesting microglial activation may directly contribute to tau pathology and neurodegeneration (Yoshiyama et al., 2007), although whether this is the case in *MAPT* 10+16 mutation carriers remains unclear.

In a microglial PET study of a presymptomatic *MAPT* 10+16 mutation carrier, increased binding in the temporal lobe preceded significant tau PET ligand binding, grey matter atrophy and symptom onset (Bevan-Jones et al., 2019). Another study of three presymptomatic *MAPT* N279K mutation carriers showed increased binding in frontal, occipital or posterior cingulate cortices, although not in the temporal cortex (Miyoshi et al., 2010). This suggests that regionally selective microglial activation occurs several years before other neuroimaging changes and symptom onset in *MAPT* mutation carriers, preceding tau pathology, and this may vary regionally according to the specific *MAPT* mutation. The present study confirms this remains the case by the end stage of

disease in the temporal lobe of *MAPT* 10+16 mutation carriers, but whether this occurs in other *MAPT* mutation carriers, or in other regions, was not explored.

Grey versus white matter comparisons of microglial burden in each FTLD-tau subtype generally showed a higher burden in white matter than in grey matter, and greater activation in grey matter, consistent with findings in FTLD and FTLD-tau overall. However, burden varied regionally and according to microglial phenotype for each subtype: FTLD-Picks cases had a higher burden of all microglial phenotypes in TW than TG, and of antigen-presenting microglia in FW than FG, but a similarly high burden of phagocytic microglia in FW and FG. FTLD-CBD and FTLD-PSP cases had a higher burden of phagocytic microglia in FW than FG and of phagocytic and antigen-presenting microglia in TW than TG. FTLD-*MAPT* cases had a higher burden of phagocytic microglia in TW than TG and of antigen-presenting microglia in FW and TW compared with FG and TG.

This white matter 'microglial signal' in all FTLD-tau subtypes is unsurprising, as extensive white matter microgliosis has been demonstrated in histological studies of FTLD-tau previously (Bellucci et al., 2011; Cooper et al., 1996; Hollister et al., 1997; Ishizawa and Dickson, 2001; Lant et al., 2014; Paulus et al., 1993; Schofield et al., 2003). FTLD-Picks and FTLD-*MAPT* are particularly associated with a high burden of tau pathology in white matter (Lant et al., 2014; Pickering-Brown et al., 2002; Zhukareva et al., 2002) and early white matter tract degeneration on neuroimaging (Chen et al., 2019; Irwin et al., 2016; Jiskoot et al., 2018). FTLD-CBD and FTLD-PSP cases also have significant white matter pathology (Kneynsberg et al., 2017; Komori, 1999). It is possible that the regional distribution of changes for specific microglial phenotypes correlates with regional patterns of different tau pathologies in white matter, but this was not specifically explored.

Microglial activation also varied between grey and white matter, differing regionally by FTLD-tau subtype. In contrast to other subtypes, FTLD-Picks cases had greater activation of general microglia in TW than in TG and similarly high activation of other phenotypes in grey and white matter, perhaps due to significant tau pathology in both areas (Irwin et al., 2016). FTLD-CBD cases had greater activation of phagocytic and antigen-presenting microglia in grey matter (FG and TG) and FTLD-*MAPT* cases had more activated phagocytic microglia in TG than TW. This suggests that microglia are more activated in the presence of cortical grey matter tau pathology, despite more microglia being present in white matter. In FTLD-PSP cases, activation was similarly low in frontotemporal grey and white matter, perhaps due to a relatively low burden of tau pathology in both areas. A previous study comparing microglia between grey and white matter in FTLD-tau found more activated phagocytic microglia in frontotemporal grey matter compared with white matter in FTLD-Picks cases, but in white matter of FTLD-*MAPT* and FTLD-PSP/CBD cases (Lant et al., 2014). However, their FTLD-tau cohort differed significantly from the current cohort, FTLD-CBD and FTLD-PSP cases were combined, and semi-quantitative techniques could not separate scores for microglial burden and activation.

In conclusion, regional patterns of microglial burden and activation vary according to FTLD-tau subtype, and different microglial phenotypes seem involved in each subtype. Microglial burden is typically higher in white matter, but activation generally greater in grey matter. FTLD-Picks cases have numerous phagocytic and antigen-presenting microglia in frontotemporal regions, and particularly significant activation of phagocytic microglia in white matter. FTLD-CBD cases have intermediate levels of microgliosis but significant activation of phagocytic and antigen-presenting microglia in the frontal lobe, particularly in grey matter. FTLD-PSP cases have fewer and less activated microglia. FTLD-*MAPT* cases have a modest burden of microglia in most regions, but numerous

activated phagocytic microglia in the temporal lobe, particularly in white matter. These different microglial patterns may be due to, or contribute to, regional differences in tau pathology, especially different tau strains or cell-specific tau burdens.

5.6.5 FTLD-TDP subtypes

Microglia were next compared between FTLD-TDP subtypes and controls, which has not been performed previously. This demonstrated that regional patterns of microglial burden and activation also differ according to FTLD-TDP subtype.

FTLD-TDPA cases had a particularly high burden of phagocytic microglia in the temporal lobe and in white matter. A larger study found more phagocytic microglia in frontotemporal grey and white matter of FTLD-TDP cases (19 FTLD-TPDA, 18 FTLD-TDPB and seven FTLD-TDPC) overall compared with controls, but each FTLD-TDP subtype was not compared individually with controls (Lant et al., 2014). A more recent study found numerous phagocytic microglia in frontal, temporal and entorhinal grey and white matter regions of FTLD-TDP cases, with the topographic distribution of microglia matching pathological changes, although cases only differed significantly from controls in FW (Taipa et al., 2017). Although most of their FTLD-TDP group had FTLD-TDPA, several FTLD-TDPB and FTLD-TDPC cases were also included, which may have affected results.

Many individuals with FTLD-TDPA (particularly FTLD-*GRN*) have significant frontotemporal grey and white matter pathology (Mackenzie, 2007; Rohrer et al., 2011), and out of 16 FTLD-TDPA cases included in the present study, 11 had mutations in genes linked to aberrant microglial phagocytosis (five *GRN*, five *C9orf72* and one *TBK1*). It is therefore unsurprising that there was a high burden of phagocytic microglia in this group. Many FTLD-TDPA cases also had a high burden of antigen-presenting microglia, particularly in FW and TG, but this was rather variable and overall did not differ

significantly from controls. The burden of all microglia (Iba1-positive cells) did not differ significantly between FTLD-TDPA cases and controls in any region, and Iba1 staining was notably very low in many cases, particularly in the frontal lobe.

Although FTLD-TPDA cases had more activated microglia overall (Iba1-positive cells) in TG compared with controls, activation of phagocytic and antigen-presenting microglia did not significantly differ from controls in any region, again suggesting these phenotypes are poorly activated by the end stage of disease. In contrast, a recent study found many amoeboid phagocytic microglia in frontal, temporal and parietal regions of three FTLD-TDPA cases, with the density of microglia correlating with the density of TDP-43 pathology (Bevan-Jones et al., 2020). Other small studies have shown many, activated antigen-presenting (HLA-DR positive) microglia in grey and white matter of sporadic FTLD-TDP cases (Kim et al., 2018b, 2018a; Ohm et al., 2018) and in grey matter of FTLD-TDPA cases with *GRN* mutations (Kim et al., 2016), as described in Chapter 4. However, sporadic FTLD-TDPA and FTLD-TDPB cases were often included in the same group, precluding assessment of whether different FTLD-TDP subtypes were associated with differential activation of microglia. Subsequent analyses in this study revealed that regional activation patterns within FTLD-TDPA subtypes differed according to underlying disease mechanism and gene mutation, which was undetectable at the group level.

FTLD-TDPB cases had a low but variable microglial burden of all microglial phenotypes, with similar burdens and activation states to controls in all regions, except for less activated Iba1-positive microglia in TW. Another study found a similar burden of phagocytic microglia between FTLD-TDPB cases and other FTLD-TDP subtypes in frontotemporal regions, but did not directly compare FTLD-TDPB cases with controls (Lant et al., 2014). Other studies have found many activated antigen-presenting microglia in small FTLD-TDP cohorts containing a few FTLD-TPDB cases (Kim et al., 2018a; Ohm et al., 2018) but these also included FTLD-TDPA cases, which may have contributed to

this. Different mechanisms may affect microglia in sporadic versus genetic FTLD-TDPB, particularly as most genetic FTLD-TDPB cases have *C9orf72* expansions and *C9orf72* mouse models show extensive microglial activation or dysfunction, as discussed in Chapter 1. However, small group sizes meant it was not possible to compare microglia between sporadic and genetic FTLD-TDPB cases in this study.

FTLD-TDPC cases had a much higher burden of phagocytic microglia throughout the frontal lobe, and a higher burden of microglia overall in FG, compared with controls. Although several FTLD-TDPC cases had many phagocytic and antigen-presenting microglia in the temporal lobe, this varied considerably between cases, and the overall burden did not differ from controls in this region. This was unexpected, given all cases had svPPA and hence severe temporal lobe pathology. However, there is also significant frontal TDP-43 pathology by the end stage of disease in svPPA cases (Acosta-Cabronero et al., 2011; Lam et al., 2014; Landin-Romero et al., 2016; Rohrer et al., 2011). Another study found similar burdens of activated phagocytic microglia in frontotemporal grey and white matter of FTLD-TDPC cases compared with other FTLD-TDP subtypes (Lant et al., 2014). However, FTLD-TDPC cases were not directly compared with controls. A more recent study found many amoeboid phagocytic microglia in cortical regions of three FTLD-TDPC cases, with the density of microglia correlating with the density of TDP-43 pathology, although results in frontal regions were not specifically reported (Bevan-Jones et al., 2020). In contrast, in the present study, all microglial phenotypes were similarly poorly activated in all regions in FTLD-TDPC cases and controls, suggesting microglial dysfunction by the end stage of disease.

Comparison of microglia between FTLD-TDP subtypes showed that although FTLD-TDPA cases had prominent temporal microgliosis and FTLD-TDPC cases had prominent frontal microgliosis when compared with controls, both groups had a similar burden of

each microglial phenotype in each region. However, FTLD-TPDA cases had more activated microglia overall (Iba1-positive cells) compared with FTLD-TDPC cases in FG. Although FTLD-TDPC cases typically have more pronounced temporal lobe pathology than FTLD-TDPA cases (Rohrer et al., 2011), and both subtypes have significant frontal pathology by the end stage of disease (Landin-Romero et al., 2016; Rohrer et al., 2011), FTLD-TDPA has been associated with more glial pathology than FTLD-TDPC (Geser et al., 2009), so perhaps this is unsurprising. FTLD-TDPA cases had a higher burden of phagocytic and antigen-presenting microglia in TG than FTLD-TDPB cases and more activated microglia overall (Iba1-positive) in TW. This could have been due to less extensive temporal lobe pathology in FTLD-TDPB cases, as all had clinical syndromes associated with predominant frontal or motor cortex pathology (bvFTD and FTD-MND). Alternatively, different TDP-43 strains may exert differential effects on microglial proliferation and function in each region. Only one study has compared microglia between all FTLD-TDP subtypes, and this found no differences in the burden or activation state of phagocytic microglia in frontal or temporal lobes between groups (Lant et al., 2014). However, different techniques were used, and other microglial phenotypes were not examined.

Grey versus white matter comparisons confirmed that FTLD-TDPA and FTLD-TDPC cases had a higher burden of phagocytic and antigen-presenting microglia in FW than FG, and FTLD-TDPA cases also had a higher burden of these phenotypes in TW than TG. FTLD-TDPC cases echoed these findings when comparing TW and TG, but this did not reach significance. In contrast, FTLD-TDPB cases had a similar burden of these phenotypes in frontotemporal grey and white matter. The burden of microglia in general (Iba1-positive) was similar between grey and white matter in all FTLD-TDP subtypes. Phagocytic and antigen-presenting microglia were more activated in frontotemporal grey matter of FTLD-TDPA and FTLD-TDPC cases, but similarly activated in grey and white

matter in FTLD-TDPB cases. This dissociation between microglial burden and activation was identified in FTLD-TDP in general and in FTLD overall. However, it seems that FTLD-TDPA and FTLD-TDPC, but not FTLD-TDPB, are associated with a profuse influx of phagocytic and antigen-presenting microglia into white matter, which are poorly activated by the end stage of disease.

Another study also found more phagocytic microglia in white matter than grey matter in FTLD-TDPA and FTLD-TDPC (but not FTLD-TDPB) cases, but in contrast to the present results, activation was also greater in white matter (Lant et al., 2014). A smaller, combined cohort of FTLD-TDPA and FTLD-TDPB cases had more antigen-presenting microglia in white matter than grey matter, also with greater activation in white matter (Ohm et al., 2018). Despite extensive cortical TDP-43 pathology in FTLD-TDP cases, TDP-43 deposition also occurs in many subcortical white matter regions, and FW pathology has been shown to be highest in FTLD-TDPA, then FTLD-TDPB, then FTLD-TDPC (Geser et al., 2009). FTLD-TDPA cases have significant neuroimaging abnormalities in FW tracts, including the superior and inferior longitudinal fasciculi and corpus callosum (Rohrer et al., 2011) and svPPA cases (with FTLD-TDPC) have early neuroimaging changes in frontotemporal white matter pathways including the uncinate and inferior longitudinal fasciculi and fornix (Acosta-Cabronero et al., 2011; Elahi et al., 2017; Lam et al., 2014). As FTLD-TDPA and FTLD-TDPC target white matter early on in disease, regionally impaired microglial activation could contribute to the development of white matter pathology in these subtypes.

In conclusion, microglial burden and activation vary regionally according to FTLD-TDP subtype and differ between grey and white matter. A recent microglial PET study using ^{11}C-PK-11195 showed that binding correlates regionally with binding of a radioligand (^{18}F-AV-1451) which localises to TDP-43 (and tau) pathology (Bevan-Jones et al., 2020).

Longitudinal microglial PET studies which also use radioligands against specific TDP-43 strains (once developed) could explore how microglia correlate with the development of regional TDP-43 pathology and disease progression.

5.6.6 Sporadic and genetic FTLD-TDPA subtypes

Microglia were next compared between FTLD-TDPA cases with different disease mechanisms: sporadic FTLD-TDPA cases, and genetic FTLD-TDPA cases with different underlying mutations (FTLD-*GRN* and FTLD-*C9orf72*). Each group was also compared with controls. This established that different causes of the same pathology were associated with different microglial patterns in each region.

Several sporadic FTLD-TDPA cases had a very high burden of antigen-presenting microglia in white matter, especially in FW, although this did not reach significance when compared with controls overall. This could be due to a high burden of pathology in frontal regions in these cases (Rohrer et al., 2011). However, the burden of phagocytic microglia and overall microglia was similar to controls in all regions, so it seems an antigen-presenting phenotype is prominent in white matter of some cases with sporadic disease. Microglial activation in sporadic FTLD-TDPA cases was similar to other groups in most other regions, except for antigen-presenting microglia. Surprisingly, this phenotype was less activated in FG of sporadic cases compared with FTLD-*GRN* cases, and perhaps less activated in FW compared with controls (although this did not reach significance). This is interesting given the high burden of this phenotype in some sporadic cases; this suggests these microglia may be dysfunctional in areas of TDP-43 abundance.

Although the cause of sporadic FTLD-TDPA remains unknown, upregulated or dysfunctional antigen presentation by microglia could predispose an individual to TDP-43 aggregation. A proportion of FTLD-TDP cases with no known pathogenic mutations have variants in *TBK1*-related immune pathway genes that affect autophagy or cytokine

signaling, or variants in *HLA-DQA2,* which is involved in antigen presentation (Pottier et al., 2019). Additionally, a proportion of FTLD-TDPA patients without *GRN* mutations have a risk variant in *GRN* (Pottier et al., 2019; Rademakers et al., 2008) leading to reduced progranulin expression in brain, plasma and CSF, albeit to a less severe extent than *GRN* mutation carriers (Rademakers et al., 2008). These variants could potentially influence the phenotype or function of microglia, and the regulation of innate and adaptive immune pathways in certain individuals, leading to sporadic FTLD-TDPA. The mechanistic effects of these genetic variants on microglial function, particularly antigen presentation, need to be explored further.

FTLD-*GRN* cases had a higher burden of phagocytic microglia in TW, and greater activation in FG, compared with controls. This may be due to significant TDP-43 pathology in frontotemporal regions associated with *GRN* mutations (Mackenzie, 2007; Rohrer et al., 2011) and this also echoes the many phagocytic microglia observed in *GRN* -/- mice as discussed in Chapter 1. Interestingly, FTLD-*GRN* cases also had a higher burden of phagocytic microglia than sporadic FTLD-TDPA cases throughout the temporal lobe. This could be due to differing clinical presentations: all FTLD-*GRN* cases had frontotemporal involvement (four bvFTD and one nfvPPA) whereas most sporadic cases had predominantly frontal involvement (two FTD-MND, one nfvPPA and one bvFTD). Alternatively, given that the burden and activation of antigen-presenting microglia was similar between FTLD-*GRN* cases and controls in all regions, *GRN* mutations could predispose an individual to regionally selective upregulation of phagocytic microglia in the temporal lobe, which could explain the extensive, asymmetrical temporoparietal pathology seen in *GRN* mutation carriers (Rohrer et al., 2011). Consistent with this, regional variation in microglia has been seen in another study comparing FTLD-TDPA subtypes: FTLD-*GRN* cases had more Iba1-positive microglia in

the subiculum but fewer Iba1-positive microglia in the hippocampal CA1 region compared with sporadic FTLD-TDPA cases (Mao et al., 2019).

FTLD-*C9orf72* cases had a much higher burden of microglia overall (Iba1-positive) in the frontal lobe of compared with controls, sporadic FTLD-TDPA and FTLD-*GRN* cases, but a similar burden of phagocytic microglia. This suggests that the *C9orf72* expansion is associated with an increased influx of microglia overall, particularly into white matter. Others have shown many phagocytic microglia in white matter (corticospinal tracts) of *C9orf72* expansion cases with ALS (Cooper-Knock et al., 2012), but Iba1-positive microglia and FTD cases were not examined. Surprisingly, microglial activation in FTLD-*C9orf72* cases did not significantly differ from controls or sporadic FTLD-TDPA cases in any region, in contrast to the highly activated microglia seen in *C9orf72* mouse models discussed in Chapter 1. However, most mouse models were homozygous knockouts, so may not recapitulate the more subtle disease processes occurring in heterozygous *C9orf72* expansion carriers.

All FTLD-TDPA subtypes had a higher burden of phagocytic and antigen-presenting microglia in frontotemporal white matter than in grey matter, consistent with the pattern seen in FTLD and FTLD-TDP overall. In contrast, the burden of Iba1-positive microglia was similar (and very low) in white and grey matter of FTLD-*GRN* and sporadic FTLD-TDPA cases, whereas FTLD-*C9orf72* cases had a higher burden of Iba1-positive microglia in FW than FG. On visual inspection, Iba1 staining was minimal in white matter of many FTLD-*GRN* and sporadic FTLD-TDPA cases, due to extensive dystrophy (particularly in FW) leading to apparently low percentage area values. There was generally greater activation of microglia in grey than white matter, but this was regionally variable depending on the disease mechanism: phagocytic microglia were more activated in FG than FW in all FTLD-TDPA subtypes, but only genetic FTLD-TDPA

subtypes also had more activated phagocytic microglia in TG than TW, and only FTLD-*C9orf72* cases had more activated antigen-presenting microglia in TG than TW. The greater activation of microglia in grey matter could be due to greater microglial response to cortical TDP-43 pathology, or reduced activation in white matter due to increased microglial dysfunction.

Overall, these results suggest that sporadic FTLD-TDPA is associated with an abundance of poorly activated antigen-presenting microglia in white matter, particularly in the frontal lobe, whereas genetic FTLD-TDPA due to *GRN* mutations is associated with an abundance of phagocytic microglia in the temporal lobe, especially TW, but these are only well activated in FG. Genetic FTLD-TDPA due to *C9orf72* expansions is associated with a relatively high burden of Iba1-positive microglia, particularly in the frontal lobe, but not other phenotypes. Although *GRN* mutations and *C9orf72* expansions are clearly linked to microglial dysfunction based on evidence from mouse models, mechanisms in sporadic FTLD-TDPA remain unclear. However, regional and phenotypic variability in microglial dysfunction could contribute to the clinicopathological heterogeneity of FTLD-TDPA.

5.6.7 Genetic FTLD subtypes

Few other studies have examined microglia in humans with genetic FTLD, and this study performed a more comprehensive assessment than those previously, revealing distinct regional patterns of microglia according to the underlying mutation.

Again, FTLD-*GRN* cases had abundant phagocytic microglia in the temporal lobe, especially in TW. There were also abundant antigen-presenting microglia in FW, but a low burden of Iba1-positive microglia in the frontal lobe, particularly in FW. This time, FTLD-*C9orf72* cases had abundant phagocytic and Iba1-positive microglia within the frontal lobe, but few antigen-presenting microglia (similar to controls). FTLD-*MAPT* cases

generally had a low microglial burden, except in TW, where there were abundant phagocytic microglia compared with controls.

Despite these patterns, the burden of each microglial phenotype was similar between all genetic groups in each region, except for phagocytic microglia, which were more abundant in FW of FTLD-*C9orf72* than FTLD-*MAPT* cases, and Iba1-positive microglia, which were significantly reduced in the frontal lobe of FTLD-*GRN* compared with FTLD-*C9orf72* cases. Microglial activation was similar between each group and when compared with controls in most regions, apart from phagocytic microglia, which were more activated in FG of FTLD-*GRN* cases and TG of FTLD-*MAPT* cases compared with controls, and Iba1-positive microglia, which were more activated in frontotemporal grey matter of FTLD-*GRN* cases compared with controls and in FG of FTLD-*GRN* than FTLD-*MAPT* cases. All genetic groups generally had a higher burden of microglia in white matter than grey matter, and greater activation of microglia in grey matter.

The numerous phagocytic and antigen-presenting microglia in frontotemporal regions of FTLD-*GRN* cases, particularly in white matter, fits with the presence of abundant TDP-43 aggregates and other pathology in these regions in *GRN* mutation carriers (Mackenzie, 2007; Rohrer et al., 2011; Woollacott et al., 2018). Although other brain regions were not analysed, this microgliosis appears to be regionally selective, as few phagocytic and antigen-presenting microglia were found in unaffected occipital regions in the FTLD-*GRN* case in Chapter 4 (Woollacott et al., 2018). As discussed in Chapter 1, *GRN* -/- mice have abundant activated phagocytic microglia in cortical areas, but these have aberrant properties, including excessive phagocytosis and heightened complement-mediated synaptic pruning (Lui et al., 2016). The many activated phagocytic microglia in FG of FTLD-*GRN* cases could represent a persistently overactive response to TDP-43 inclusions in this region, with failed activation elsewhere.

No previous studies have compared antigen-presenting microglia across genetic FTLD groups, but this phenotype seems particularly altered in *GRN* mutation carriers in FW. This may be due to the combined role of progranulin in lysosomal and immune pathways, which are involved in antigen processing and presentation. Smaller studies have identified many antigen-presenting microglia in frontotemporal grey matter (Kim et al., 2016) and white matter (Chen-Plotkin et al., 2010) of FTLD-*GRN* cases, and these were numerous in these regions in the FTLD-*GRN* case in Chapter 4 (Woollacott et al., 2018). As in Chapter 4 the distribution of antigen-presenting microglia correlated with severity of TDP-43 pathology, neuronal loss and regional atrophy patterns and presence of white matter pathology and WMH, this suggests that the regional burden of antigen-presenting microglia is linked to regional burdens of pathology in both grey and white matter. Despite limited activation of antigen-presenting microglia in most FTLD-*GRN* cases within the present study, there were numerous amoeboid antigen-presenting microglia in frontotemporal lobes of the case in Chapter 4, so this may vary between individuals. If initially highly activated, antigen-presenting microglia could excessively present TDP-43 and other cellular antigens to other microglia and other immune cells. Increased microglial presentation of internalised TDP-43 propagates TDP-43 spread in ALS models (Spiller et al., 2018) and directly activates, and recruits, microglia to affected regions, worsening neuroinflammation (Zhao et al., 2015). Dysfunctional presentation and targeting of self-antigens (such as myelin) by many antigen-presenting microglia in white matter could also contribute to the prominent demyelination seen in humans with *GRN* mutations (Chapter 4) and *GRN* -/- mouse models (Tanaka et al., 2014). Systemically altered antigen presentation by macrophages in *GRN* mutation carriers could also underlie the increased prevalence of systemic autoimmune diseases in this group demonstrated in Chapter 3 and previously (Miller et al., 2013).

Surprisingly, the burden of microglia overall (Iba1-positive) was low in all regions in FTLD-*GRN* cases, and lower than FTLD-*C9orf72* cases in the frontal lobe. In contrast, another study found fewer amoeboid Iba1-positive microglia in superficial layers of the middle frontal cortex in FTLD-*C9orf72* cases compared with FTLD-*GRN* cases (Sakae et al., 2019b). However, on visual inspection of Iba1 stained sections of FTLD-*GRN* cases in the present study, there was minimal staining of Iba1-positive microglia and severely disrupted morphology, particularly in FW, suggestive of extensive microglial dystrophy (Streit et al., 2004). Microglial dystrophy has been observed in another study of FTLD-*GRN* cases (Sakae et al., 2019b), and was prominent in FW in the case in Chapter 4 (Woollacott et al., 2018). This could represent impaired activation of microglia, or premature microglial senescence, and may explain the poor activation of phagocytic and antigen-presenting phenotypes in most regions by the end stage of disease. In contrast, FTLD-*GRN* cases appeared to have greater activation of Iba1-positive microglia in frontotemporal grey matter compared with controls. However, morphology of this phenotype may have been altered due to extensive dystrophy, leading to loss of cell processes and punctate staining, and more circular or less ramified cells. This may have produced higher circularity and lower perimeter values in quantitative analyses of activation of Iba1-positive microglia in cases with severe dystrophy, when in fact these cells were not truly more activated. Microglial dystrophy was explored further in a subsequent study (Chapter 6).

FTLD-*GRN* cases had a higher burden of phagocytic and antigen-presenting microglia in frontotemporal white matter than in grey matter, but these were poorly activated. In aged *GRN* -/- mice, many phagocytic microglia colocalise with impaired myelination in cortical and thalamic areas (Tanaka et al., 2014), and in Chapter 4, severe dystrophy of Iba1-positive microglia in white matter correlated with marked demyelination and WMH (Woollacott et al., 2018). *GRN* mutations may therefore particularly affect white matter

integrity due to focal dysfunction of microglia, perhaps underlying the significant frontal MRI WMH seen in presymptomatic and symptomatic *GRN* mutation carriers, as discussed in Chapter 4. However, as not all *GRN* mutation carriers display WMH (Sudre et al., 2019), white matter vulnerability may be modified by genetic or other factors which affect microglial function, such as variants in *TREM2* or *TMEM106B*, which may contribute to the heterogeneity of disease.

FTLD-*C9orf72* cases had many phagocytic microglia in frontal regions, particularly in FW, where the burden was higher than both FTLD-*MAPT* cases and controls. However, unlike in FTLD-*GRN* cases, the burden of antigen-presenting microglia was not increased in FTLD-*C9orf72* cases. There were also many microglia in general (Iba1-positive) in the frontal lobe of FTLD-*C9orf72* cases, particularly in FW, consistent with significant frontal pathology associated with the *C9orf72* expansion (Mahoney et al., 2012; Snowden et al., 2012) and the clinical syndromes of the five cases analysed (three FTD-MND, two nfvPPA). Compared with sporadic ALS cases, individuals with ALS due to *C9orf72* expansions have increased microglial (Umoh et al., 2017) and immune pathway (O'Rourke et al., 2016) genes in the frontal cortex. Many phagocytic microglia are also present in corticospinal tracts of ALS cases with *C9orf72* expansions (Cooper-Knock et al., 2012), implicating microglial dysfunction in frontal grey and white matter in *C9orf72* expansion carriers, irrespective of clinical phenotype.

Although mouse models of the *C9orf72* expansion display numerous activated phagocytic microglia (Atanasio et al., 2016; Burberry et al., 2016, 2020; O'Rourke et al., 2016; Schludi et al., 2017; Sudria-Lopez et al., 2016; Sullivan et al., 2016), in this study, all microglial phenotypes were similarly activated in FTLD-*C9orf72* cases and controls in all regions. This suggests that impaired microglial activation is present by the end stage of disease in humans with FTLD-*C9orf72*, although earlier excessive activation or

heightened activation in other regions cannot be ruled out given the nature of this study. Regional microglial dysfunction in *C9orf72* expansion carriers could be modified by environmental, genetic or epigenetic factors, leading to regional differences in vulnerability to onset of pathology. A recent study showed that microglial activation in the spinal cord of *C9orf72* -/- mice was modified by the mouse gut microbiome (Burberry et al., 2020). This suggests that environmental factors substantially modulate microglial function in the presence of the expansion, and this could also be the case in FTLD-*C9orf72* cases, perhaps contributing to the heterogeneity in clinical syndromes observed in families with similar expansions (Woollacott and Mead, 2014).

Although FTLD-*C9orf72* cases had a higher burden of phagocytic and antigen-presenting microglia in frontotemporal white matter than in grey matter, this difference was less pronounced than seen in FTLD-*GRN* cases. The burden of Iba1-positive microglia in FTLD-*C9orf72* cases was also higher in FW than FG, due to apparently less severe dystrophy. However, FTLD-*C9orf72* cases had greater microglial activation in grey matter than white matter, as seen in FTLD-*GRN* cases. Although early white matter abnormalities are present in neuroimaging studies of *C9orf72* expansion carriers, these predominantly affect thalamic and posterior white matter tracts (Jiskoot et al., 2018; Mahoney et al., 2014; Panman et al., 2019; Papma et al., 2017), and only *GRN* mutation carriers have prominent frontal WMH on MRI (Sudre et al., 2017a). *C9orf72* expansion carriers may therefore have less microglial dysfunction in FW than *GRN* mutation carriers, but more dysfunction in other regions that were not analysed in this study.

FTLD-*MAPT* cases only had moderate microgliosis, primarily in the temporal lobe. In TW the burden of phagocytic microglia was significantly higher than in controls, perhaps due to extensive tau pathology in this region, as described in other studies of *MAPT* 10+16 carriers (Lant et al., 2014; Pickering-Brown et al., 2002; Rohrer et al., 2011) . Phagocytic

microglia were more activated in TG of FTLD-*MAPT* cases compared with controls, consistent with a microglial PET study of a presymptomatic *MAPT* 10+16 mutation carrier, which showed early temporal microglial activation (Bevan-Jones et al., 2019), although another histological study showed greater activation of phagocytic microglia in TW of FTLD-*MAPT* cases (Lant et al., 2014). Antigen-presenting microglia did not differ significantly between FTLD-*MAPT* cases and controls, suggesting that phagocytic microglia are selectively altered in the temporal lobe of *MAPT* 10+16 mutation carriers. FTLD-*MAPT* cases had more microglia in white matter than grey matter, but activation of phagocytic microglia was higher in grey matter within the temporal lobe. White matter neuroimaging changes occur presymptomatically within the temporal lobes of *MAPT* mutation carriers, increasing as they approach expected symptom onset and tracking with disease progression (Chen et al., 2019; Jiskoot et al., 2018), suggesting early white matter involvement and pathology. Evidence for heightened microglial activation associated with tau pathology in *MAPT* P301S mutation models was discussed in Section 5.6.3, but it remains unclear whether other *MAPT* mutations would lead to similar mechanisms. A microglial PET study of three presymptomatic *MAPT N279K* mutation carriers found increased binding in frontal, occipital or posterior cingulate cortices, and not in the temporal cortex (Miyoshi et al., 2010), suggesting regional microglial activation patterns may well vary according to *MAPT* mutation subtype.

When comparing microglia across genetic groups, FTLD-*C9orf72* cases had a higher burden of phagocytic microglia in FW compared with FTLD-*MAPT* cases, perhaps due to more frontal pathology. There was a higher burden of microglia overall (Iba1-positive) in the frontal lobe (particularly in FW) of FTLD-*C9orf72* cases compared with FTLD-*GRN* cases, likely due to less severe frontal microglial dystrophy. Another study found fewer activated phagocytic microglia in TW of FTLD-*C9orf72* and FTLD-*GRN* cases than in FTLD-*MAPT* cases, but no differences within FW (Lant et al., 2014). However, their

FTLD-*C9orf72* group also contained FTLD-TDPB cases (which have few phagocytic microglia, as identified in this study) and Iba1-positive microglia were not examined. Another recent study found similar densities of phagocytic and general (Iba1-positive) microglia in FTLD-*GRN* and FTLD-*C9orf72* cases in middle frontal, superior temporal, inferior parietal and motor cortices (Sakae et al., 2019b). However, FTLD-*GRN* cases had fewer CD68-positive microglia in the hippocampus and more amoeboid Iba1-positive microglia in superficial layers of the middle frontal cortex and deep white matter compared with FTLD-*C9orf72* cases. This suggests that microglia vary regionally and sub-regionally across genetic FTLD subtypes and this varies by microglial phenotype. This seems to be linked to the mutation itself, rather than differences in pathology, as both groups had FTLD-TDPA (Sakae et al., 2019b). This is supported by results in the present study, which also extends this to FTLD-*MAPT* cases.

In conclusion, there are distinct patterns of microglial burden and activation in genetic FTLD subtypes, which differ regionally and by microglial phenotype, and differ between grey and white matter. These patterns may underlie different regional vulnerabilities to pathology and differences in grey and white matter pathology, neuroimaging changes and clinical presentations between *GRN*, *C9orf72* and *MAPT* mutation carriers. Observations of severe dystrophy of Iba1-positive microglia in certain regions, particularly in FW of FTLD-*GRN* cases, prompted a more comprehensive study of patterns of microglial dystrophy in FTLD, presented in Chapter 6.

5.7 Limitations and future work

This study has several advantages compared with previous studies of microglia in FTLD. First, the cohort encompassed a wide variety of FTLD subtypes, with extensive clinical, neuropathological and genetic phenotyping, which aided reliable correlation of changes in microglia with pathological and genetic subtype. Second, it compared FTLD and FTLD-subtypes with AD cases to determine associations of microglia with differing

pathologies affecting similar regions and performed detailed subgroup analyses of FTLD-tau and FTLD-TDP subtypes, which few studies have done previously. This allowed more detailed insights into microglial involvement across the spectrum of FTLD than those available previously. Third, it performed separate analyses of grey and white matter, demonstrating that microglial activation in white matter is surprisingly limited in FTLD, despite many microglia being present in these regions. This hints at possible microglial dysfunction in white matter, extending previous observations of significant white matter pathology and early white matter neuroimaging changes in FTLD. Fourth, it compared different microglial phenotypes across all three main genetic FTLD subtypes, which no studies have described previously, revealing distinct regional patterns of different microglial phenotypes according to the underlying mutation. Fifth, three different markers (CD68, CR3/43 and Iba1) were used to examine different microglial phenotypes (phagocytic microglia, antigen-presenting microglia and general microglia), combined with quantitative assessments of percentage area stained, and a separate quantitative assessment of two aspects of microglial morphology (cell shape and size, through circularity and perimeter). This allowed appreciation of both the microglial burden, and degree of microglial activation, for each microglial phenotype.

Such a comprehensive phenotypic analysis has not been performed in previous studies of microglia in FTLD. This approach has enabled appreciation that distinct phenotypes of microglia are altered in each region, and that this varies according to FTLD subtype: some subtypes displayed many phagocytic microglia, others many antigen-presenting microglia, others both, and others neither. Abnormal, disrupted morphology of Iba1-positive microglia observed in certain FTLD subtypes also suggested that microglial dystrophy is present in FTLD and that this may also vary across the spectrum of pathology. This led to a further study of microglial dystrophy within this cohort, presented in Chapter 6. Previously, microglial activation in FTLD was assessed by visual inspection

and semi-quantitative scoring of cell frequency and morphology, or by qualitative assessment of morphology alone. These scoring systems often combined assessment of cell frequency with morphological signs of activation to generate one score (Lant et al., 2014; Taipa et al., 2017), precluding appreciation of how burden and activation state differed separately within a region. This study has shown that these parameters are differentially altered in each region, so should be assessed separately.

There were several potential limitations. The small sizes of some subgroups (particularly controls and AD cases) and small number of brain regions analysed may have limited appreciation of the full extent of microglial changes in FTLD. However, small group sizes (particularly for rarer pathologies such as FTLD-FUS or sporadic FTLD-TDPB) are inherent to human histological studies of a disease as diverse and rare as FTLD. More controls and AD cases would have been useful to increase power, but these were very difficult to find given the need for a similar AAD to the FTLD cohort, who were much younger than most controls and AD cases in the QSBB. Hence, a practical approach was taken to allow analysis of a wide selection of cases with different pathologies, balanced with a reasonable number of cases in each subgroup to allow comparisons. Analysis of a larger cohort and more cortical and subcortical regions, including typically involved regions (hippocampus or basal ganglia) and less involved regions (cerebellum) in FTLD would have been useful, but this was outside the time and manpower constraints of this study.

The composition of cases with various clinical syndromes differed between pathological and genetic subtypes, so differences in regional microglial patterns could purely be due to regional differences in the burden of pathology (rather than the type of pathology or disease mechanism) influencing microglia. Ideally, all cases in each subtype would have had the same clinical diagnosis and pathologically affected regions, to allow analysis of

whether microglia are altered in association with pathological subtype alone. For example, all FTLD-PSP or FTLD-CBD cases ideally should have had bvFTD, allowing regional comparisons with FTLD-Picks or FTLD-*MAPT* cases (which more typically have this syndrome). However, such cases are rare, and were not available in the QSBB.

Given the small group sizes in the FTLD-TDPA subtype and genetic FTLD analyses, and the potential implications of these initial findings regarding effects of disease mechanisms on different phenotypes of microglia, replication should be carried out in a larger cohort. Ideally the effects of different types of mutations and different sub-pathologies (such as dipeptide repeat proteins versus TDP-43 in FTLD-*C9orf72* cases) on microglial burden and activation should be assessed. It would also be useful to examine a wider range of brain regions in genetic FTLD cases, to understand how microglia vary alongside regional pathology burdens and clinical phenotypes (for example PPA subtypes versus bvFTD versus FTD-MND) across these notoriously diverse genetic entities.

All three markers (CD68, HLA-DR/DP/DQ [detected using CR3/43] and Iba1) are expressed mainly by microglia, but also to a certain extent by peripheral macrophages (Boche et al., 2013; Hopperton et al., 2018). It is possible that this led to detection of some perivascular or infiltrating macrophages (which had breached the BBB) within sections, rather than just microglia. The macro used for analysis was unable to remove such cells from calculations, but on visually inspecting sections, perivascular cells were scarce and unlikely to have impacted substantially on results. Additional use of more specific microglial markers, such as P2RY12 (which detects predominantly ramified microglia) (Butovsky et al., 2014) may have been useful, but was not possible during the timescale of this study.

The CD68 marker is more readily expressed by lysosomes near the nuclei of microglia than by ramified cell processes (Boche et al., 2013), so CD68-positive microglia all tended to look rather small and circular in both activated and ramified states. It is possible that this led the software to find similar circularity and perimeter values for most CD68-positive cells in each group and hence failed to detect differences in activation state for phagocytic microglia. Against this, there were no significant group differences in the activation state of microglia detected using CR3/43 and Iba1 between FTLD and AD groups, and these markers adequately detect cell processes. There is also good correlation between microglial scores for CD68 and Iba1-positive microglia in other studies (Taipa et al., 2017). In addition, the software was able to detect significant differences in the activation state of CD68-positive microglia between FTLD and AD cases and between various FTLD subtypes.

The question remains as to whether different markers expressed by microglia truly indicate the predominant function of those cells present within a region, particularly as one cell is likely to express a variety of markers at one time, which may change rapidly over time. It is difficult to prove through histological assessments alone that a morphological appearance represents a particular activation state, function or dysfunction of that cell, how that relates to nearby pathology, or when this played a role in disease (if at all). Future correlation of these findings with regional microglial PET imaging changes in presymptomatic and symptomatic individuals with different clinical phenotypes or gene mutations could aid differentiation of pathology based on regional microglial patterns *in vivo*.

5.8 Publications relating to this chapter

The work presented in this chapter, combined with the work in Chapter 6, has been published as:

Woollacott IOC et al. (2020) Microglial burden, activation and dystrophy patterns in frontotemporal lobar degeneration. *Journal of Neuroinflammation.*17:234

6 Microglial dystrophy across the spectrum of FTLD

6.1 Chapter summary

Introduction: Increasing evidence implicates premature microglial dysfunction and senescence in the aetiology of neurodegenerative disease. Many studies of AD have identified morphological changes suggestive of microglial senescence (microglial dystrophy) and cells with other unusual morphologies such as rod-shaped or hypertrophic microglia, but no studies have explored these across the spectrum of FTLD. This study examined regional patterns of microglial dystrophy and rod-shaped and hypertrophic microglia in *post-mortem* brain tissue from a large cohort of individuals with sporadic and genetic FTLD, sporadic AD and cognitively normal controls.

Methods: Immunohistochemistry was performed to detect Iba1, expressed by microglia, in left anterior frontal and temporal lobe FFPE sections obtained from 50 FTLD cases (31 sporadic and 19 genetic: 20 FTLD-tau, 26 FTLD-TDP, four FTLD-FUS (all aFTLD-U), five sporadic AD cases and five controls. Morphology of Iba1-positive microglia was visually assessed in four regions in each case: frontal grey (FG), frontal white (FW), temporal grey (TG) and temporal white (TW) matter. Dystrophy severity was rated in each region using semi-quantitative scores, ranging from 1 (no/minimal) to 5 (very severe). Presence of rod-shaped and hypertrophic microglia was qualitatively assessed in each region in each case. Dystrophy scores were compared in each region between FTLD, AD and controls, and between different pathological subtypes of FTLD, including main subtypes (FTLD-tau, FTLD-TDP, FTLD-FUS), and FTLD-tau (FTLD-Picks, FTLD-CBD, FTLD-PSP, FTLD-*MAPT*), FTLD-TDP (FTLD-TDPA, FTLD-TDPB, FTLD-TDPC), FTLD-TDPA (sporadic and genetic [FTLD-*GRN* and FTLD-*C9orf72*]) and genetic (FTLD-*GRN*, FTLD-*C9orf72,* FTLD-*MAPT*) subtypes. Dystrophy scores were also compared between grey and white matter within each lobe for each subtype.

Results: Microglial dystrophy was more severe in FTLD and AD compared with controls, but similar in FTLD and AD, in all regions. FTLD-TDP cases had more severe dystrophy than FTLD-tau cases in all regions except in TW. Dystrophy varied regionally by subtype: FTLD-TDPA, FTLD-TDPC and FTLD-Picks cases had more severe dystrophy than controls in all regions, whereas dystrophy in FTLD-TDPB and FTLD-CBD cases only differed from controls in FW and dystrophy in FTLD-PSP cases differed from controls only in FG. Sporadic FTLD-TDPA, FTLD-*GRN* and FTLD-*C9orf72* cases had much more severe dystrophy than controls in all regions, but dystrophy in FTLD-*MAPT* cases only differed from controls in FG and TW. There was a suggestion of more severe dystrophy in FW of FTLD-*GRN* cases compared with FTLD-*C9orf72* cases, although this did not reach significance. Dystrophy was more severe in frontotemporal white matter than grey matter in FTLD overall and in FTLD-tau, FTLD-TDP and FTLD-Picks cases. In FTLD-CBD, FTLD-TDPA and FTLD-*GRN* cases, dystrophy was more severe in FW than FG, whereas in AD and FTLD-PSP cases, dystrophy was more severe in TW than TG. Rod shaped microglia were present in FTLD and AD, but most prominent in FTLD-CBD and FTLD-*MAPT* cases and in FTLD-TDPA or FTLD-TDPB cases with *C9orf72* expansions. Hypertrophic microglia were prominent in FTLD-Picks and FTLD-TPDC cases.

Conclusions: Microglial dystrophy is present in FTLD, but its severity varies regionally according to pathological subtype and disease mechanism. Dystrophy is more severe in white than grey matter, but this also varies regionally, and is particularly severe in FW of FTLD-*GRN* cases. Rod-shaped and hypertrophic microglia are present in FTLD, but this varies by pathological subtype. Region-specific differences in the severity of microglial senescence could contribute to regional patterns of grey and white matter pathology, and to the clinicopathological heterogeneity of FTLD.

6.2 Introduction

As discussed in Chapter 5, microglial activation was not as florid as expected by the end stage of disease in AD cases or in most FTLD subtypes. Chronic microglial activation may therefore not be the only contributor to neurodegeneration over time, as a build-up of protein inclusions in the aging human brain may contribute to, or be due to, premature microglial failure, or senescence of microglial cells. In certain individuals this may lead to neurodegenerative disease (Streit et al., 2004). Several groups have therefore shifted their focus away from studying microglial activation and towards detecting premature or heightened microglial senescence in neurodegenerative disease cohorts.

In the AD field a hypothesis has arisen that after initial microglial activation and attempts to clear amyloid fibrils or early aggregates of insoluble Aβ, and due to repeated mitotic self-renewal and increasing exposure to free radicals, iron molecules and the toxic effects of Aβ, microglia may become exhausted and disintegrate. These dysfunctional, senescent microglia are thought to fail to support neurons that are degenerating in the context of ensuing tau pathology, and under-perform their usual roles including phagocytosis (Streit et al., 2014, 2018). Chronic microglial dysfunction therefore likely contributes significantly to neuronal loss in AD through lack of neuronal support, rather than just due to sustained cytotoxic damage to neurons within a proinflammatory milieu (Gentleman, 2013). As dystrophic microglia, which are the morphological correlate of senescent cells (Streit et al., 2004), cluster around Aβ aggregates in individuals with pre-clinical AD pathology (Streit et al., 2018), microglial dysfunction, senescence and failed attempts to clear inclusions start well before symptom onset.

Dystrophic microglia display thin, short and few distal branches, shortened tortuous or beaded cell processes, fragmented cytoplasm, and spheroidal inclusions (Streit et al., 2004). With increasing dystrophy there is increasing disintegration of cell integrity and

structure, or ‘cytorrhexis’, which likely impacts significantly on microglial motility and function (Tischer et al., 2016). Extremely dystrophic microglia are visualised as sparse but diffuse punctate Iba1 staining (due to generalised distribution of microglial debris). These are present in individuals with advanced AD pathology, for example due to Down’s syndrome (Streit et al., 2009). Although dystrophic microglia are present in hippocampal and cortical regions of aged controls, they are more prominent in individuals with AD (Bachstetter et al., 2015; Davies et al., 2017; El Hajj et al., 2019; Lopes et al., 2008; Navarro et al., 2018; Sanchez-Mejias et al., 2016; Streit et al., 2009, 2014, 2018; Tischer et al., 2016). They are also present in DLB cases (Bachstetter et al., 2015), models of MND (Fendrick et al., 2007) and HD (Ma et al., 2003; Simmons et al., 2007) and aged individuals with hippocampal sclerosis (Bachstetter et al., 2015).

Other unusual morphological changes, such rod-shaped microglia, which are cells with an elongated, thin, narrow cell body with few processes, have been noted in the hippocampus of individuals with AD, DLB, or hippocampal sclerosis (Bachstetter et al., 2015) and in frontal, temporal and parietal cortices of individuals with AD (Bachstetter et al., 2017). They are also present in the hippocampus (Bachstetter et al., 2015, 2017) and frontal, temporal and parietal cortices (Bachstetter et al., 2017) of individuals without dementia, increasing with age. The relevance of rod-shaped microglia is not understood, but they may represent cells in an intermediate state between ramified and amoeboid morphology responding to axonal transport deficits (Au and Ma, 2017) . As they are seen in rodent models of traumatic brain injury and humans with chronic viral and post-viral encephalitides (Au and Ma, 2017), development of rod-shaped morphology may be a protective response by microglia, promoting neuronal survival in response to chronic neuronal injury, although the mechanisms behind this remain unclear. Hypertrophic microglia, which are hyper-ramified and have short, thickened, bushy processes, are also increased in AD cases compared with controls (Bachstetter et al., 2015). Although

these may be primed microglia with an increased tendency for activation (Bachstetter et al., 2015), their role in the healthy brain and in neurodegenerative disease remains unclear.

Microglial dystrophy and rod-shaped microglia have only been examined in three small studies of FTLD, all of which have focused on genetic FTLD (Mao et al., 2019; Sakae et al., 2019b; Woollacott et al., 2018). In Chapter 4 (Woollacott et al., 2018), the FTLD-*GRN* case had profoundly dystrophic Iba1-positive microglia in FW, more severe than in FG, which correlated regionally with the severity of WMH on MRI. A subsequent semi-quantitative study by another group, which examined microglia in several FTLD-*GRN* and FTLD-*C9orf72* cases, demonstrated that both genetic subtypes had more dystrophic Iba1-positive microglia than controls in the middle frontal cortex, but that FTLD-*GRN* cases had more Iba1 and CD68-positive rod-shaped microglia than FTLD-*C9orf72* cases and controls in this region (Sakae et al., 2019b). Another study found that FTLD-TDPA cases with *GRN* mutations had more rod-shaped Iba1-positive microglia in the CA1 hippocampal region compared with sporadic FTLD-TDPA cases, but dystrophy was not evaluated (Mao et al., 2019).

These few studies suggest that microglial dystrophy and rod-shaped microglia are present in individuals with FTLD, particularly in *GRN* mutation carriers, but that this varies regionally between cases with the same pathology but different disease mechanisms, and between grey and white matter. It was noted by the author during analysis for the study in Chapter 5 that Iba1 staining was rather variable across FTLD subtypes and in fact was markedly reduced, almost down to control levels, in some cases, particularly in FTLD-*GRN* and FTLD-Picks cases. On visual inspection of these cases, microglial cell structure was often severely disrupted, with scanty, punctate staining, suggestive of extensive dystrophy, but this seemed to vary regionally and seemed worse in white

matter. In some cases, multiple rod-shaped microglia were observed, and in others these were not visible. This led to a hypothesis that extensive microglial dysfunction and senescence could explain the lack of microglial activation in some FTLD cases by the end stage of disease, particularly in white matter.

Microglial dystrophy and rod-shaped and hypertrophic microglia clearly occur in aged individuals and in a range of neurodegenerative diseases, but it remains unclear if microglial senescence or adoption of these unusual morphologies relates to development of pathology in FTLD, and how this contributes to neurodegeneration. Premature microglial senescence could contribute to neurodegeneration through impaired neuronal support or clearance of protein aggregates. This may occur many years prior to symptom onset, as seen in pre-clinical AD (Streit et al., 2018), and vary regionally, potentially contributing to the clinicopathological heterogeneity of FTLD.

Comparison of the severity and regional distribution of microglial dystrophy and rod-shaped and hypertrophic microglia between individuals with different neurodegenerative pathologies such as AD and various FTLD subtypes may further understanding of whether different disease processes have a similar effect on microglial senescence or morphology. This may indicate whether therapies aimed at preserving microglial integrity or clearing senescent cells (Bussian et al., 2018) could be useful for individuals with different FTLD subtypes, and in PMC of FTD-associated mutations.

6.3 Aims and hypotheses

This study aimed to perform a histological assessment of microglial dystrophy within *post-mortem* brain tissue in a large FTLD cohort, including all the main pathological subtypes (FTLD-tau, FTLD-TDP and FTLD-FUS) and both sporadic and the most common genetic (FTLD-*GRN*, FTLD-*C9orf72*, FTLD-*MAPT*) forms of the disease. Comparison groups would be sporadic amnestic AD cases and cognitively normal

controls. In addition, an exploratory, qualitative assessment would be performed to identify rod-shaped and hypertrophic microglia in each group.

A similar approach to the study in Chapter 5 would be employed, analysing microglia in grey and white matter of four clinically relevant brain regions (FG, FW, TG and TW) within the same cohort. Microglial dystrophy would be compared between FTLD cases, sporadic AD cases and controls, and between different FTLD subtypes. Given the differences in microglial burden and activation between grey and white matter identified in Chapter 5, microglial dystrophy would also be compared between grey and white matter within each lobe for each group.

As Iba1 detects all microglia and allows most reliable assessment of cell morphology and dystrophy (Streit et al., 2009) the severity of dystrophy in each region and the presence of rod-shaped and hypertrophic microglia would be assessed through morphological characterisation of Iba1-positive microglia only, a technique used in Chapter 4 (Woollacott et al., 2018) and in multiple other studies (Bachstetter et al., 2015, 2017; Davies et al., 2017; Mao et al., 2019; Sakae et al., 2019b; Streit et al., 2004, 2009; Tischer et al., 2016). The severity of dystrophy would be rated using a semi-quantitative scoring system, due to the complexity of performing a quantitative assessment of the full range of morphological changes seen in dystrophic cells (El Hajj et al., 2019). The presence of any rod-shaped and hypertrophic microglia would be qualitatively assessed and recorded for each case in each region.

The key hypotheses of this study were that the severity of microglial dystrophy would differ in some, or all, of the four brain regions analysed, in the following ways:

- Between FTLD and controls, and between AD and controls, due to excessive microglial senescence in individuals with neurodegenerative diseases.

- Between FTLD and AD, due to different pathologies or disease mechanisms being associated with differing degrees of microglial senescence within the same brain regions.
- Between different FTLD subtypes, and between each subtype and controls, due to different pathologies or disease mechanisms being associated with differing degrees of microglial senescence in the same regions, namely:
    - Between FTLD-tau, FTLD-TDP and FTLD-FUS, and between each of these subtypes and AD.
    - Between different FTLD-tau subtypes: FTLD-CBD, FTLD-*MAPT*, FTLD-Picks and FTLD-PSP.
    - Between different FTLD-TDP subtypes: FTLD-TDPA, FTLD-TDPB and FTLD-TDPC.
    - Between individuals with the same pathology but different disease mechanisms: sporadic FTLD-TDPA, and genetic FTLD-TDPA due to *GRN* mutations (FTLD-*GRN*) or a *C9orf72* expansion (FTLD-*C9orf72*).
    - Between genetic FTLD subtypes: FTLD-*GRN*, FTLD-*C9orf72* and FTLD-*MAPT*.

In addition, this study hypothesised that microglial dystrophy would be more severe in white matter than grey matter (as activation had been less in white matter in Chapter 5), but that this may also vary regionally according to the underlying pathology or disease mechanism. This could be due to differing burdens of neurodegenerative pathology present in white versus grey matter impacting on microglial function and senescence, or pre-existing differences in the function or senescence of microglia present in white versus grey matter contributing to development of neuronal or glial vulnerability and subsequent regional variations in pathology and neurodegeneration.

Finally, this study hypothesised that rod-shaped and hypertrophic microglia would be more commonly seen in FTLD and AD cases than controls, but that their presence may vary across FTLD subtypes, due to a potential link between alterations in microglial morphology and different causes of neuronal or axonal dysfunction.

6.4 Methods

6.4.1 Case selection and demographics

Sixty cases were selected for analysis, including 50 FTLD cases, five sporadic AD cases and five cognitively normal controls of a similar AAD to the other groups. These were selected from the QSBB and the MRC London Neurodegenerative Diseases Brain Bank, Institute of Psychiatry, King's College London, as detailed in Chapter 2.1.2. Case demographics and histological subtypes are summarised in Table 2.1 (Chapter 2) and individual cases are detailed in Appendix 1.

6.4.2 Tissue processing and immunohistochemistry

All 60 cases had undergone tissue processing and clinical neuropathological assessment of a wide variety of brain regions at the QSBB using immunohistochemistry as detailed in Chapter 2.2.1.1. For the study in Chapter 5, further FFPE sections had been cut from left anterior frontal lobe and left temporal lobe blocks for all cases, and immunohistochemistry had been performed using techniques detailed in Chapter 2.2.1.2 to detect CD68, CR3/43 and Iba1-positive microglia. However, only Iba1-positive microglia were assessed for this study.

6.4.3 Analysis of microglia

6.4.3.1 Regions analysed

Anterior frontal and temporal lobe sections contained both cortical grey matter (all cortical layers were analysed) and subcortical white matter. Four regions were selected for analysis for all cases: FG, FW, TG and TW. This enabled comparisons of microglial

dystrophy in the same region (for example FG) across groups, and comparison of microglial dystrophy in grey matter versus white matter within the frontal lobe (FG versus FW) and temporal lobe (TG versus TW) within each group.

6.4.3.2 Scanning, area selection and identification of microglia

Slides were scanned, areas of interest were selected within each region and Iba1-positive microglia were identified in ten randomly selected squares within each region for each case, as detailed in Chapter 5.4.3.2.

6.4.3.3 Microglial dystrophy scoring

All cases were examined for the morphology of microglial cells using Iba1 stained sections. Microglial dystrophy was assessed by visually inspecting Iba1-positive microglia in each of the ten squares that had been randomly generated in each region. Dystrophy was determined as the presence of cells with loss of fine branches (deramification), or thin, shortened, beaded, tortuous or fragmented processes or cytoplasm, or all of these changes (Streit et al., 2004). The severity of dystrophy was assessed using a semi-quantitative, ordinal scoring system to score the typical morphology of visualised microglial cells observed across the ten squares in that region. This was adapted from the semi-quantitative scoring system used to assess the burden and morphology (activation) of CD68 or Iba1-positive microglia in other histological studies of FTLD cases (Lant et al., 2014; Taipa et al., 2017).

Dystrophy scores were allocated as follows:

- 1 = no dystrophy: microglia were of normal morphology (ramified or amoeboid) and not dystrophic.
- 2 = mild dystrophy: some dystrophic microglia seen, but at least half present were of non-dystrophic morphology.

- 3 = moderate dystrophy: most microglia had dystrophic morphology, but some were of non-dystrophic, normal morphology.
- 4 = severe dystrophy: all microglia had dystrophic morphology, but some cell bodies or processes were still visible.
- 5 = very severe dystrophy: all microglia were severely dystrophic, with few or no intact cell bodies or processes, or only generalised punctate staining was present.

Each case was assigned an overall 'dystrophy score' for each region (FG, FW, TG and TW), which was used in group analyses. Examples of sections containing microglia with each dystrophy score are shown in Figure 6.1a-e.

6.4.3.4 Rod-shaped and hypertrophic microglia

Presence of any rod-shaped microglia (Figure 6.1f) or hypertrophic microglia (Figure 6.1g) was noted qualitatively in each region for each case. The frequency of cells with these morphologies was not quantified given the exploratory nature of this part of the study; if at least one cell with this morphology was visible in at least one of the ten squares, this was recorded as being present, but if many were present this was also noted.

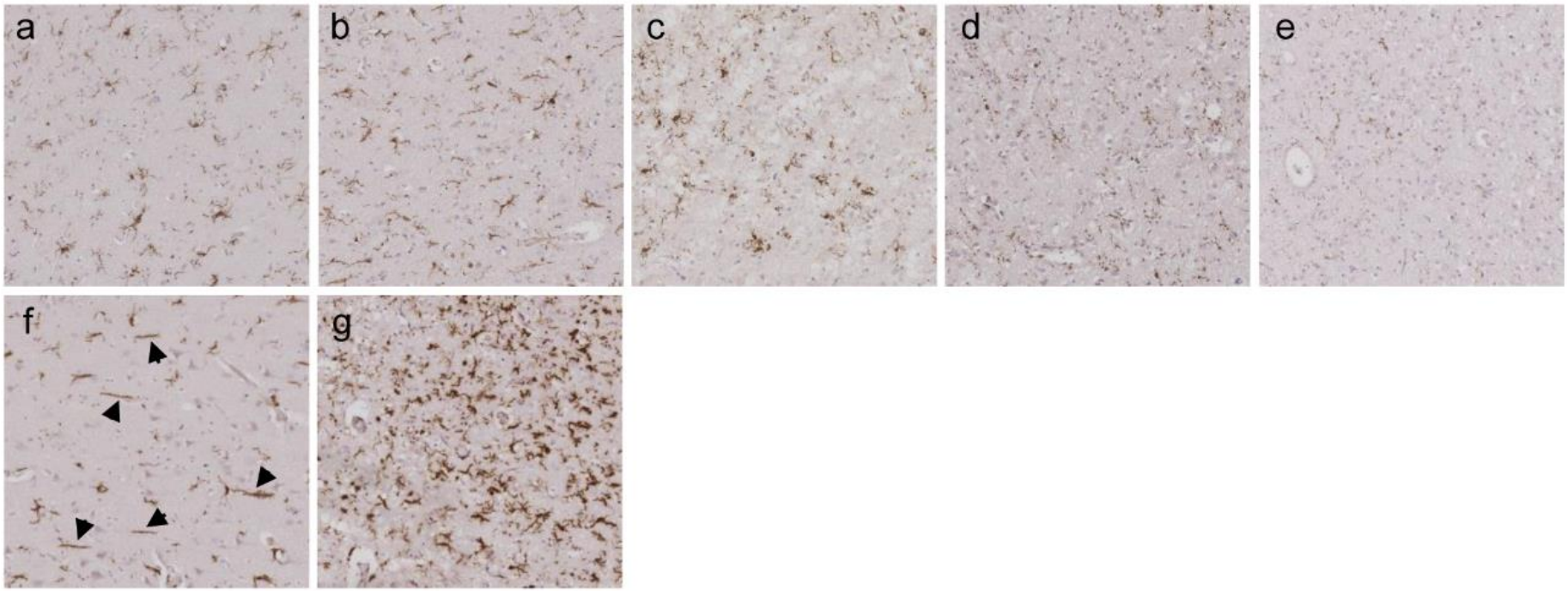

Figure 6.1 Scoring of the severity of microglial dystrophy and examples of rod-shaped and hypertrophic microglia

Iba1 immunohistochemical staining showing representative images of the semi-quantitative analysis of microglial dystrophy and the different microglial morphologies. Grey matter sections from a healthy control (**a**, case 2, Appendix 1) and four different FTLD cases (**b** case 44; **c** case 22; **d** case 42; **e** case 37), show appearances of dystrophic microglia, graded in severity, from **a** (1 = no dystrophy), **b** (2 = mild dystrophy), **c** (3 = moderate), **d** (4 = severe), **e** (5 = very severe). **f** Several rod-shaped microglia in FG of an FTLD-TDPB case with the *C9orf72* expansion (case 48; black arrows point to these cells). **g** Multiple hypertrophic microglia throughout FG of an FTLD-Picks case (case 25; most cells present have a bushy appearance with short, thick processes).

6.4.3.5 Statistical analysis

Microsoft Excel was used for inputting dystrophy scores, which were exported to STATA version 14 for analysis. The significance threshold was $P<0.05$ and confidence interval 95% for all statistical tests. Groups were compared using a hierarchical, multi-level approach as detailed in Figure 6.2. This echoed the approach in Chapter 5 and allowed appreciation of how dystrophy severity differed between overall disease groups (controls, FTLD and AD) and between the various subtypes of FTLD.

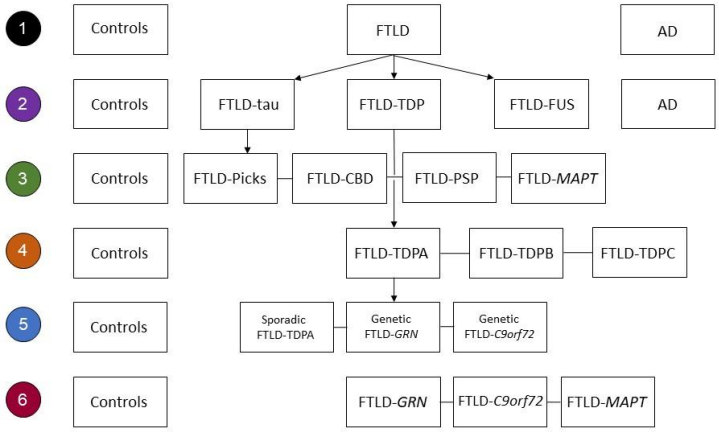

Figure 6.2 Approach to group comparisons of microglial dystrophy scores

Microglial dystrophy scores were compared between groups using six levels of comparison (numbers in circles denote level). **1**: controls and neurodegenerative disease groups; **2**: controls, main FTLD subtypes and AD; **3**: controls and FTLD-tau subtypes; **4**: controls and FTLD-TDP subtypes; **5**: controls and FTLD-TDPA subtypes; **6**: controls and genetic FTLD subtypes. The FTLD-*C9orf72* groups included only FTLD-TDPA cases, in order to compare mutations rather than different pathological subtypes. All FTLD-FUS cases had aFTLD-U.

Given that dystrophy scores were generated using an ordinal scoring system with five categories (1 to 5), this required tests for a non-parametric distribution, so Kruskal-Wallis tests with Dunn's tests for *post hoc* comparisons were used to compare median dystrophy scores between groups for each of the four regions. Dystrophy scores were also compared between grey and white matter areas within the frontal lobe (FG versus FW) and temporal lobe (TG versus TW) for each of the groups using Wilcoxon signed

rank tests for paired comparisons. Heat maps of *P* values for all comparisons were produced in Microsoft Excel**.**

6.5 Results

6.5.1 Demographics

Group demographics were summarised in Table 2.1 (Chapter 2) and demographics of individual cases are in Appendix 1. Results of group demographic comparisons were presented in Chapter 5.5.1.

6.5.2 Microglial dystrophy

Results are presented sequentially, following the order in Figure 6.2 for each level of group comparison performed. Presence of rod-shaped and hypertrophic microglia is described qualitatively for groups within each level. Comparisons of dystrophy scores between groups and between grey and white matter within each lobe for each group are shown in Figure 6.3. For *P* values for all comparisons of dystrophy scores between groups, and between grey and white matter within each group, see heat maps in Figure 6.4 (frontal lobe) and Figure 6.5 (temporal lobe); these are not repeated in the text.

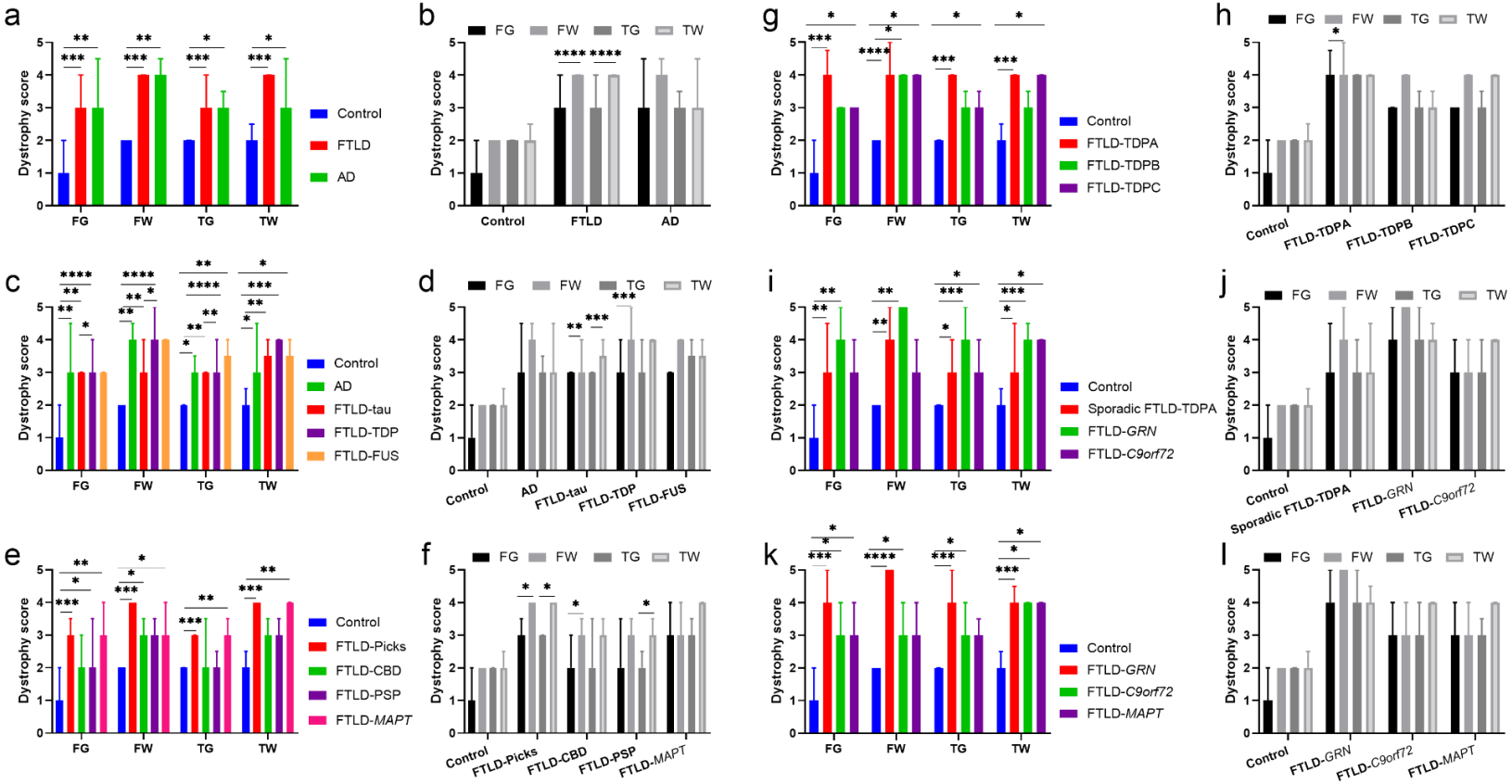

Figure 6.3 Comparisons of dystrophy scores across groups and between grey and white matter

Graphs show comparison of dystrophy scores in each region between groups (**a, c, e, g, i, k**) and between grey and white matter within each lobe for each group (**b, d, f, h, j, l**) for control, FTLD and AD groups (**a, b**), main FTLD subtypes (**c, d**), and subtypes of FTLD-tau (**e, f**), FTLD-TDP (**g, h**), sporadic and genetic FTLD-TDPA (**i, j**) and genetic FTLD (**k, l**). Bars show median dystrophy scores and error bars show interquartile range. FG = frontal grey; FW = frontal white; TG = temporal grey; TW = temporal white matter. *P<0.05; **P<0.01; ***P≤0.001; ****P≤0.0001.

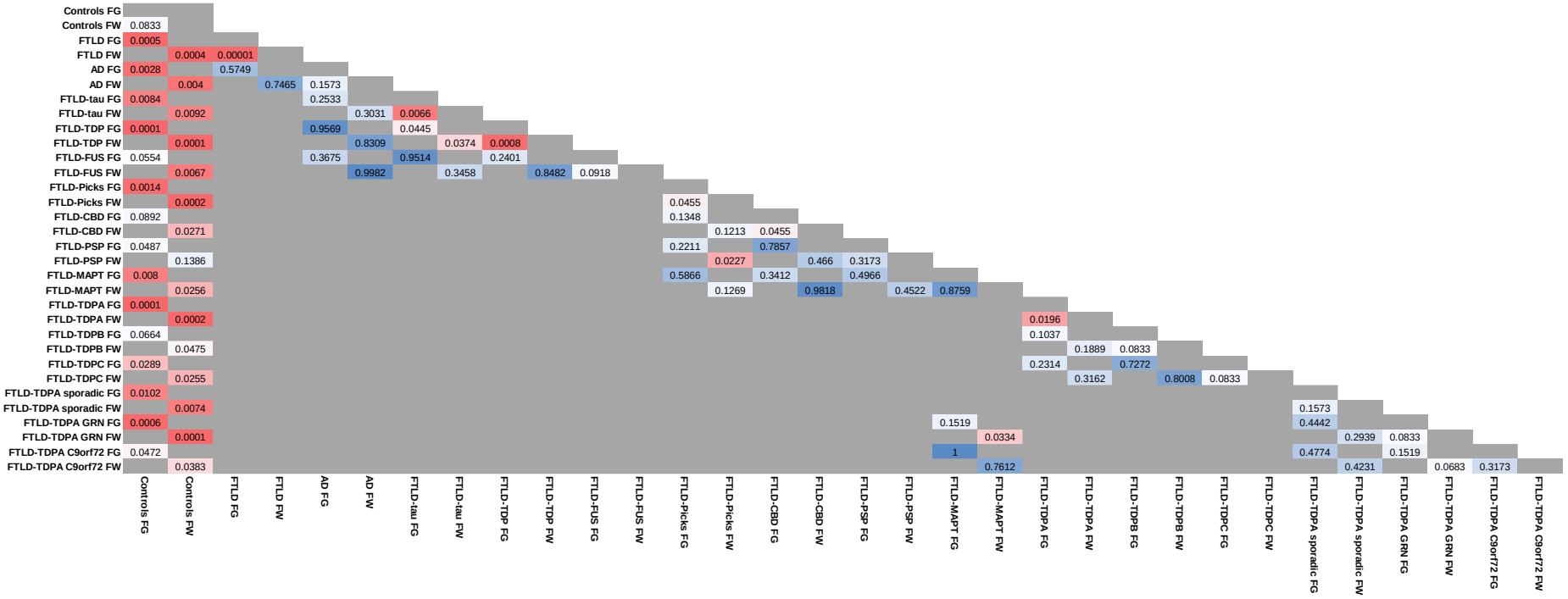

Figure 6.4 Heat map of *P* values for comparisons of microglial dystrophy scores in the frontal lobe

P values are presented in each box and represent results of comparisons between groups listed on vertical versus horizontal axes (between groups in FG and FW and between FG and FW within each group). The colour of each box represents the degree of statistical significance in the difference between groups, with red indicating a highly significant difference, blue a non-significant difference and white borderline (trend) or moderately significant difference, with gradations in between. FG = frontal grey matter; FW = frontal white matter

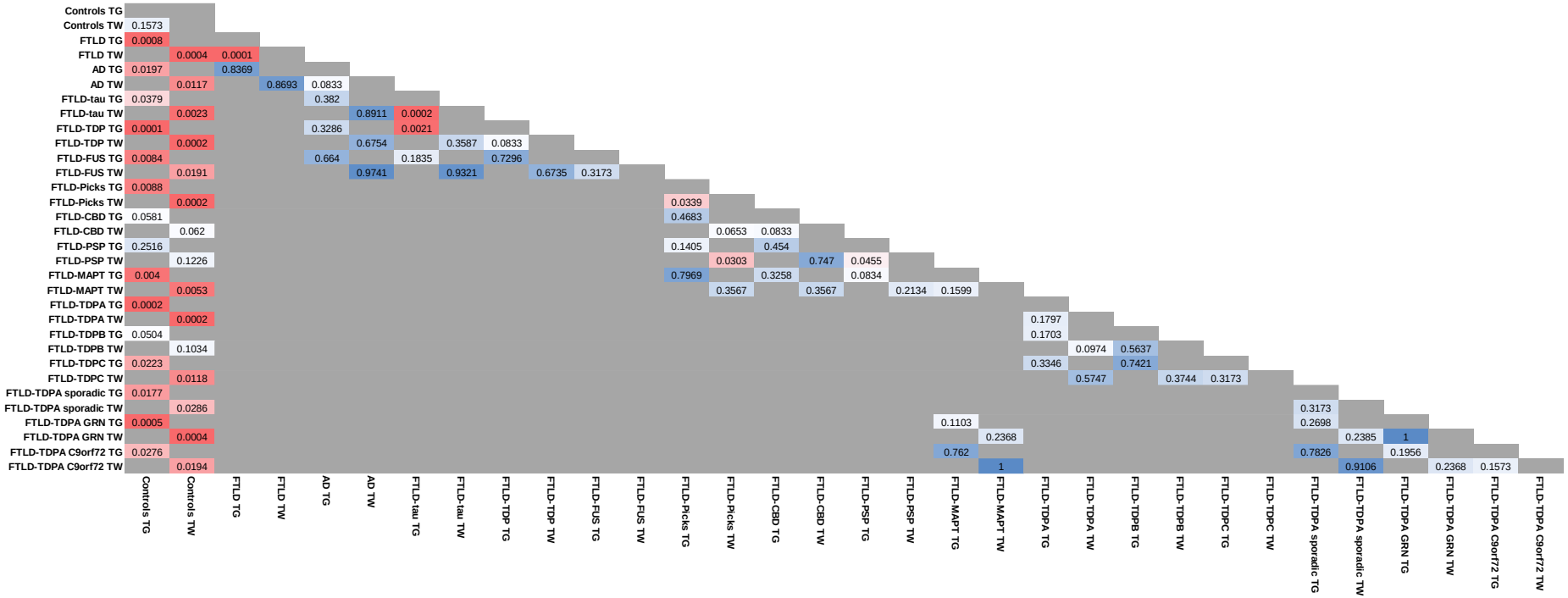

Figure 6.5 Heat map of *P* values for comparisons of microglial dystrophy scores in the temporal lobe

P values are presented in each box and represent results of comparisons between groups listed on vertical versus horizontal axes (between groups in TG and TW and between TG and TW within each group). The colour of each box represents the degree of statistical significance in the difference between groups, with red indicating a highly significant difference, blue a non-significant difference and white borderline (trend) or moderately significant difference, with gradations in between. TG = temporal grey matter; TW = temporal white matter

6.5.2.1 Neurodegenerative disease groups

Dystrophy scores differed significantly between controls, AD cases and FTLD cases in all regions (Figure 6.3a). Controls had no or mild dystrophy in most regions, with most cells appearing intact and ramified. AD cases had more severe dystrophy than controls in all regions, with moderate dystrophy in FG, TG and TW, and severe dystrophy in FW. FTLD cases had more severe dystrophy than controls in all regions, with moderate dystrophy in grey matter and severe dystrophy in white matter. However, within the FTLD group, dystrophy scores were variable across subtypes. There was no significant difference in the severity of dystrophy between FTLD and AD cases in any region.

Grey versus white matter comparisons revealed that controls had similarly minimal dystrophy in grey and white matter within each lobe, and AD cases had similarly severe dystrophy in FG and FW, with a suggestion of more severe dystrophy in TW than TG, although this did not reach significance (Figure 6.3b). In contrast, FTLD cases had much more severe dystrophy in white matter than grey matter, particularly in the frontal lobe but also in the temporal lobe, although this varied across the different FTLD subtypes.

Rod-shaped and hypertrophic microglia were infrequent in controls: three had a single rod-shaped cell present in one of the ten squares analysed in FG or TG. Rod-shaped microglia were more common in AD cases: three out of five AD cases had several rod-shaped microglia in grey matter, mainly in TG (but also in FG), but the other two cases had such severe dystrophy that normal cell structures were barely visible. Rod-shaped microglia were present in FTLD cases, but this varied by FTLD subtype. Hypertrophic microglia were not seen in controls or AD cases, and in FTLD cases their presence varied by subtype.

6.5.2.2 Main FTLD subtypes

FTLD-tau, FTLD-TDP and FTLD-FUS cases had more severe dystrophy than controls in most regions but dystrophy did not differ significantly between any of these FTLD subtypes and AD cases (Figure 6.3c). FTLD-TDP cases had more severe dystrophy than FTLD-tau cases in the frontal lobe and in TG, but not in TW, where dystrophy was particularly severe in many FTLD-tau cases.

Grey versus white matter comparisons revealed that dystrophy was more severe in white matter than grey matter for FTLD-tau and FTLD-TDP cases, but this varied regionally according to subtype (Figure 6.3d). FTLD-tau cases had much more severe dystrophy in TW than TG but only slightly more severe dystrophy in FW than FG. FTLD-TDP cases had much more severe dystrophy in FW than FG, whereas dystrophy in TW did not differ significantly from TG. In contrast, FTLD-FUS cases had similar dystrophy scores in grey and white matter.

Rod-shaped and hypertrophic microglia were present in FTLD-tau and FTLD-TDP cases but varied according to the specific subtype. Two of the four FTLD-FUS cases had several rod-shaped microglia in FG. Two other FTLD-FUS cases had no rod-shaped microglia but had several hypertrophic microglia, particularly in frontotemporal white matter.

6.5.2.3 FTLD-tau subtypes

Dystrophy was more severe in most FTLD-tau subtypes compared with controls, but this varied regionally by pathological subtype (Figure 6.3e). FTLD-Picks cases had more severe dystrophy than controls in all regions, with moderate to severe dystrophy in grey matter and severe dystrophy in white matter. FTLD-CBD cases differed from controls only in FW, with mild to moderate dystrophy in grey matter but moderate to severe dystrophy in white matter. FTLD-PSP cases had slightly more severe dystrophy than

controls in FG, but scores were otherwise similar to controls, with only mild to moderate dystrophy in all regions. Dystrophy was rather variable across FTLD-*MAPT* cases, but overall dystrophy was more severe than controls in all regions. Despite these subtype specific patterns, there were no significant differences in dystrophy in any region between the four FTLD-tau subtypes, except for in TW, where FTLD-Picks cases had more severe dystrophy than FTLD-PSP cases.

Grey versus white matter comparisons revealed that dystrophy was generally more severe in white than grey matter but again this varied regionally according to pathological subtype (Figure 6.3f). FTLD-Picks cases had more severe dystrophy in frontotemporal white than grey matter, whereas FTLD-CBD cases had more severe dystrophy only in FW than FG and FTLD-PSP cases only in TW than TG. FTLD-*MAPT* cases had similar dystrophy scores in grey and white matter of both lobes.

Rod-shaped microglia were notably scarce in FTLD-Picks cases (present in TG of two cases only) and FTLD-PSP cases (in TG of one case). In contrast, all FTLD-CBD cases and four out of five FTLD-*MAPT* cases had multiple rod-shaped microglia in FG and TG, and all FTLD-*MAPT* cases had multiple rod-shaped microglia in FW or TW. Most FTLD-Picks cases had numerous hypertrophic microglia in FG and TG, but these were typically not visible in FW or TW, where there was more severe dystrophy. Hypertrophic cells were infrequent or absent in other FTLD-tau subtypes.

6.5.2.4 FTLD-TDP subtypes

Dystrophy was more severe in most FTLD-TDP subtypes compared with controls in most regions, but this varied by pathological subtype (Figure 6.3g). FTLD-TDPA cases had more severe dystrophy than controls in all regions, but dystrophy was particularly severe in FTLD-*GRN* cases and in the FTLD-TDPA case with a *TBK1* mutation, which had severe or very severe scores in all regions. Dystrophy in FTLD-TDPB cases differed from

controls only in FW and was more variable between cases. The sporadic FTLD-TDPB cases had moderate to severe dystrophy in all regions, worse in white matter. Of the three genetic FTLD-TDPB cases with *C9orf72* expansions, one (with bvFTD) had mild dystrophy in three out of four regions but moderate dystrophy in TW, and the other two (bvFTD or FTD-MND) had moderate dystrophy in three regions but severe dystrophy in the remaining region (FW for bvFTD and TG for FTD-MND). FTLD-TDPC cases had more homogeneous dystrophy scores, with moderate to severe dystrophy, differing from controls in all regions. Although many FTLD-TDPA and FTLD-TDPC cases appeared to have more severe dystrophy in most regions than FTLD-TDPB cases, this was variable within each group and did not reach significance at a group level in any region.

Grey versus white matter comparisons showed that dystrophy was generally more severe in FW than FG, but similar in TW and TG, in all FTLD-TDP subtypes (Figure 6.3h). This difference was most noticeable for FTLD-TDPA cases, who typically had severe or very severe dystrophy in FW.

The presence of rod-shaped microglia varied according to pathological subtype: several FTLD-TDPA cases had rod-shaped microglia, mainly those with *C9orf72* expansions or sporadic cases. Occasional rod-shaped microglia were present in grey matter of sporadic FTLD-TDPB cases, but they were frequent in grey matter of all FTLD-TDPB cases with *C9orf72* expansions. One FTLD-TDPC case had rod-shaped microglia in FG, but these were infrequent. All FTLD-TDPC cases had many hypertrophic microglia in frontotemporal grey and white matter (particularly white matter), whereas these were not seen frequently in FTLD-TDPA or FTLD-TDPB cases.

6.5.2.5 Sporadic and genetic FTLD-TDPA subtypes

Dystrophy was more severe in sporadic FTLD-TDPA and FTLD-*GRN* cases than controls in all regions, whereas FTLD-*C9orf72* cases had more severe dystrophy than

controls only in the temporal lobe (Figure 6.3i). There was a suggestion of more severe dystrophy in FW of FTLD-*GRN* cases compared with FTLD-*C9orf72* cases, although this did not reach significance, and dystrophy scores were otherwise similar between FTLD-TDPA subtypes. However, dystrophy in sporadic cases was rather variable: three out of five cases (two FTD-MND and one nfvPPA) had moderate dystrophy in most regions but the other two cases (bvFTD) had severe or very severe dystrophy in all regions. In contrast, FTLD-*GRN* cases were more homogeneous, displaying severe or very severe dystrophy in all regions.

Grey versus white matter comparisons revealed that all FTLD-TDPA subtypes had similarly severe dystrophy scores in grey and white matter, except for perhaps more severe dystrophy in FW than FG of FTLD-*GRN* cases, although this did not reach significance (Figure 6.3j).

Occasional rod-shaped microglia were seen in FG of three out of five sporadic FTLD-TDPA cases, but these were frequent in grey matter of FTLD-*C9orf72* cases, particularly in FG. Rod-shaped microglia were not visible in any FTLD-*GRN* cases as extensive dystrophy disrupted cell structure. Hypertrophic microglia were not observed in any group.

6.5.2.6 Genetic FTLD subtypes

Dystrophy in FTLD-*GRN* cases differed significantly from controls in all regions, especially in white matter (Figure 6.3k; Figure 6.6). Although in this analysis FTLD-*C9orf72* cases had more severe dystrophy than controls in all regions (rather than just the temporal lobe), dystrophy appeared less consistently severe on an individual case basis than for FTLD-*GRN* cases (Figure 6.6). Dystrophy was also rather variable across FTLD-*C9orf72* cases: out of three with FTD-MND, one had mild dystrophy in FG and TG but moderate dystrophy in FW and TW, the second had severe dystrophy throughout the

frontal lobe but moderate dystrophy in the temporal lobe, and the third had moderate dystrophy in FG but severe dystrophy in all other regions. The remaining two FTLD-*C9orf72* cases had nfvPPA; one had severe dystrophy in all regions except FW (moderate) and the other had mild dystrophy in FG, moderate in FW and TG and severe in TW. FTLD-*MAPT* cases had much more severe dystrophy in TW and more severe dystrophy in FG than controls (Figure 6.3k), although dystrophy was rather variable across cases. One FTLD-*MAPT* case had severe dystrophy in all regions, but others had either mild to moderate dystrophy or moderate to severe dystrophy in all regions.

When comparing dystrophy across genetic subtypes, there was a suggestion of more severe dystrophy in FW of FTLD-*GRN* cases compared with FTLD-*C9orf72* cases, although this was not significant (Figure 6.6). Although most FTLD-*MAPT* cases appeared to have less severe dystrophy than most FTLD-*GRN* or FTLD-*C9orf72* cases, at the group level this did not reach significance in any region.

Grey versus white matter comparisons revealed that dystrophy was similarly severe in grey and white matter in all genetic subtypes (Figure 6.3l; Figure 6.6). Although there was a suggestion of more severe dystrophy in FW than FG of FTLD-*GRN* cases, this did not reach significance.

Frequent rod-shaped microglia were present in grey matter (FG and TG) of *C9orf72* expansion carriers with FTLD-TDPA. Although not included in the FTLD-*C9orf72* group for the semi-quantitative dystrophy analysis, all three FTLD-TDPB cases with *C9orf72* expansions also had numerous rod-shaped microglia in grey matter. All five FTLD-*MAPT* cases had several rod-shaped microglia in white matter, and in four cases, these were also seen in grey matter. Rod-shaped microglia were not visible in any FTLD-*GRN* cases. Hypertrophic microglia were not observed in any genetic FTLD cases.

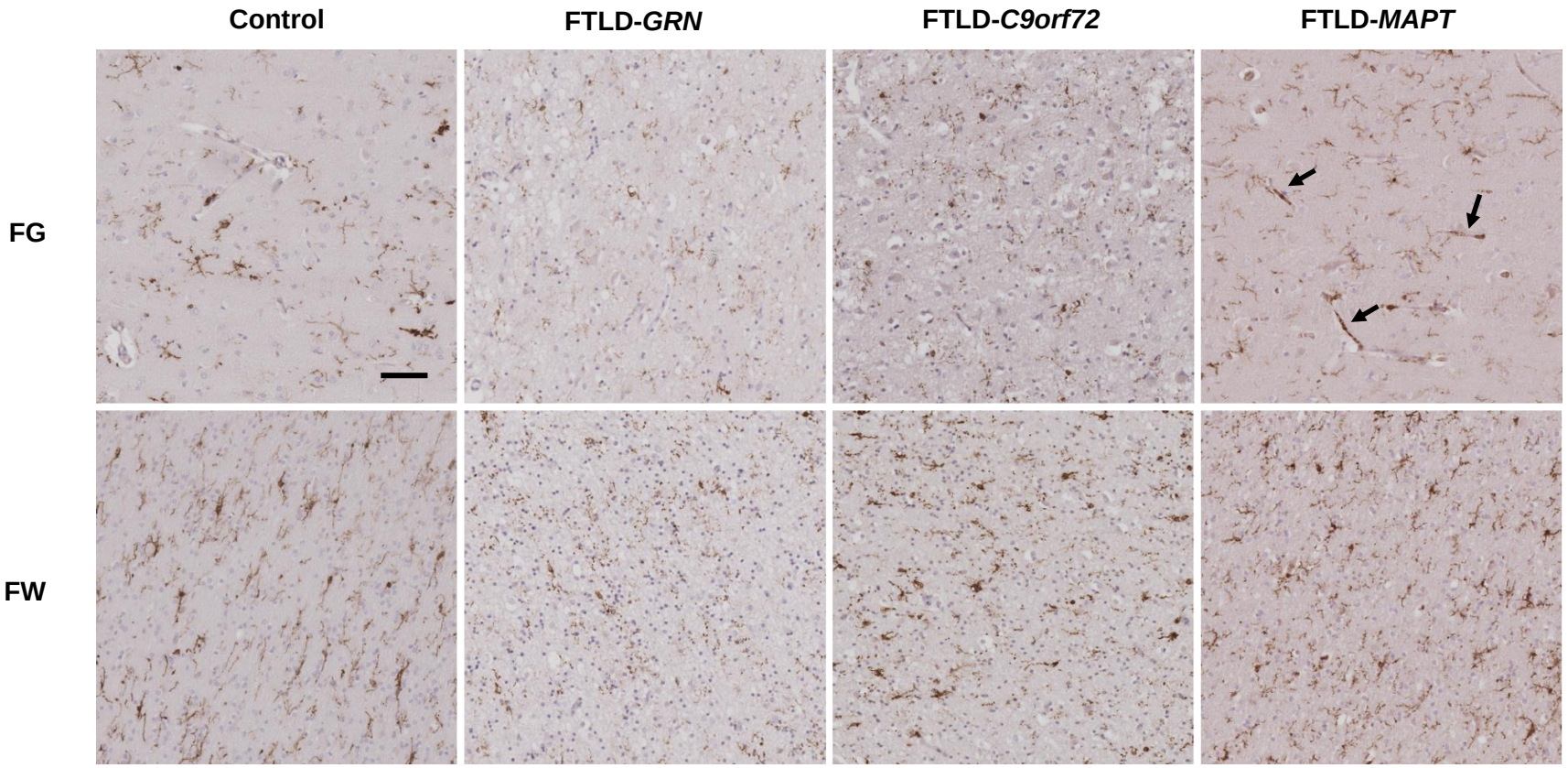

Figure 6.6 The severity of microglial dystrophy differed between controls and genetic FTLD subtypes

Iba1-positive microglia with varying severities of dystrophy are visible in frontal grey matter (FG) and frontal white matter (FW) of controls and different genetic FTLD subtypes. In the FTLD-*GRN* case, there is particularly sparse, generalised punctate Iba1 staining, especially in FW, consistent with severe cellular disruption due to extensive dystrophy. Images were taken from the following cases (Appendix 1): control (case 4), FTLD-*GRN* (case 40, FTLD-TDPA), FTLD-*C9orf72* (case 42, FTLD-TDPA) and FTLD-*MAPT* (case 16). Several rod-shaped microglia can also be seen in FG of the FTLD-*MAPT* case (black arrows). Scale bar represents 50µm in all images.

6.6 Discussion

This study is the first reported comprehensive assessment of microglial dystrophy and other microglial morphologies (rod-shaped and hypertrophic microglia) across the full spectrum of FTLD, in comparison with AD cases and controls. Dystrophy is more severe in FTLD and AD cases compared with controls, but similarly severe in FTLD overall and AD, and generally more severe in white than grey matter. However, the severity of dystrophy in FTLD and presence of rod-shaped and hypertrophic microglia varies regionally according to the underlying pathology, disease mechanism and gene mutation. Results are discussed sequentially, following the order in Figure 6.2**,** for each level of group comparison.

6.6.1 Neurodegenerative disease groups

Microglia in controls typically had ramified morphology and no or mild dystrophy in all regions, with continuous Iba1 staining along processes, as described previously (Davies et al., 2017; Streit et al., 2004). This ramified morphology is consistent with the low level of activation identified in controls in Chapter 5. Microglial dystrophy is present up to a mild degree in healthy individuals in their 60s (Bachstetter et al., 2015; Davies et al., 2017; Streit et al., 2004) but increases with age. As the control group was relatively young (to match the FTLD group), the presence of minimal dystrophy is unsurprising. Age is thought to accelerate microglial senescence by leading to telomere shortening and cell disintegration (Streit et al., 2004). This impairs functions essential for microglia to support neurons, through changes in microglial morphology, motility, migration, intercellular communication, phagocytosis and proteostasis (Gentleman, 2013; Streit et al., 2009, 2014). In certain individuals with pre-existing genetic or environmental risk factors for protein aggregation or immune dysfunction, premature or excessive microglial senescence may occur earlier on during the aging process, perhaps initiating or compounding protein aggregation and neurodegeneration. This could initially occur in certain regions which are more sensitive to microglial dysfunction (Ayata et al., 2018;

Bonham et al., 2019; Böttcher et al., 2018; Friedman et al., 2018; Grabert et al., 2016; Keren-Shaul et al., 2017), perhaps underlying regional specificity for onset of certain neurodegenerative pathologies.

FTLD and AD cases had more severe dystrophy than controls in all regions but, as predicted, the severity of dystrophy in FTLD varied regionally according to underlying pathology and disease mechanism. As demonstrated by later analyses, some FTLD subtypes (particularly FTLD-PSP) displayed only mild dystrophy in most regions, and others (such as FTLD-*GRN* and FTLD-Picks) displayed severe or very severe dystrophy in most regions. Few studies have examined dystrophy in FTLD, and these focused on genetic cases (Sakae et al., 2019b; Woollacott et al., 2018), so this is the first study to explore dystrophy across the full spectrum of disease. Several histological studies have described more severe dystrophy in AD than controls (Bachstetter et al., 2015; Davies et al., 2017; El Hajj et al., 2019; Lopes et al., 2008; Navarro et al., 2018; Sanchez-Mejias et al., 2016; Streit et al., 2009, 2014, 2018; Tischer et al., 2016) but these mostly analysed microglia in hippocampal regions. The present study extends this observation to frontotemporal regions, suggesting that by the end stage of AD, dystrophy has spread to other regions.

Microglial dystrophy has not been compared previously between FTLD and AD, but as dystrophy was similarly severe in all regions in both groups, this suggests that there is a common mechanism of excessive microglial senescence in FTLD and AD, despite different pathologies. However, the variability in scores across cases within the large FTLD group may have led to a non-significant difference between FTLD and AD overall. Whether certain FTLD subtypes were associated with more severe microglial dystrophy compared with AD pathology was explored in later analyses.

The more significant dystrophy in frontotemporal white matter than grey matter of FTLD cases could be due to significant white matter pathology associated with FTLD. Alternatively, more pronounced microglial senescence in white matter could have itself contributed to pathology, leading to white matter vulnerability in FTLD. Significant dystrophy in white matter may explain the high burden of minimally activated phagocytic and antigen-presenting microglia present within white matter of FTLD cases identified in Chapter 5, as these were poorly functioning. In addition, more severe dystrophy in white matter likely underlies the similar burden of Iba1-positive microglia in frontal grey and white matter in most FTLD cases in Chapter 5, whereas other microglial phenotypes had a higher burden in white matter than grey matter. This is because extensive dystrophy severely disrupts the structure of Iba1-positive microglia, leading to very limited, patchy Iba1 staining and therefore low percentage area values in white matter. Using CD68 and CR3/43 (or other markers) to detect microglia, rather than Iba1, may therefore be a more reliable way to assess microglial burden in future histological studies where cases have significant dystrophy. The more severe dystrophy seen in TW than TG of AD cases could be related to a high burden of AD pathology in TW, as seen in histological and imaging studies (Lee et al., 2016; McAleese et al., 2015, 2017).

AD cases had more severe dystrophy in all regions than controls. Although *post-mortem* studies generally examine individuals at the end stage of AD, numerous dystrophic microglia are also present in individuals with pre-clinical AD in the context of neurofibrillary tau pathology (Streit et al., 2018). Dystrophic microglia colocalise with tau deposition and precede the spread of tau pathology in established AD (Streit et al., 2009). They appear early on related to phosphorylated tau aggregates in *MAPT* P301S models (van Olst et al., 2020), and microglial senescence is induced very early on by intraneuronal soluble phospho-tau in tau models (Sanchez-Mejias et al., 2016). This links tau, rather than Aβ, to widespread microglial dysfunction, senescence and dystrophy, and suggests microglial senescence may be an early contributor to neurodegeneration.

Aging microglia develop lipofuscin-like lysosomal inclusions arising from myelin fragmentation and accumulate lipid droplets (El Hajj et al., 2019; Marschallinger et al., 2020). In mouse models of AD, aged microglia display reduced phagocytosis of Aβ and reduced motility and migration towards sites of injury (Spittau, 2017). This suggests that microglial lipid mishandling during aging may contribute to senescence, which directly impacts on microglial function, and this may be exacerbated in neurodegenerative disease cohorts. When senescent microglia are cleared pharmacologically, this reduces development of tau pathology (Bussian et al., 2018; Musi et al., 2018) and cortical atrophy (Musi et al., 2018), further strengthening a link between microglial failure, tau and neurodegeneration. Targeting lipid handling, lysosomal function or senescent microglia could therefore be useful therapeutic avenues in AD and other tauopathies.

Rod-shaped microglia were infrequent in controls, which was unsurprising, as although rod-shaped microglia are present in cognitively normal controls in other studies, they increase with age (Bachstetter et al., 2017). Rod-shaped microglia in aged controls are thought to indicate attempts at protective remodeling of neuronal and synaptic circuitry following chronic, low-level neuronal injury that occurs with aging, to modify and protect surviving neurons via contact-dependent trophic support or mitochondrial transfer (Bachstetter et al., 2017). Genetic or environmental factors could modify microglial adoption of rod-shaped morphology in certain regions, which may impact on protection of neuronal function and regional vulnerability or resilience to neurodegenerative disease in aging individuals.

Rod-shaped microglia were frequent in AD cases and have been observed in other studies of AD in the hippocampus (Bachstetter et al., 2015) and parietal cortex (Bachstetter et al., 2017), co-located with Aβ and tau pathology (Bachstetter et al., 2017). In the present study, rod-shaped microglia were frequently present in grey matter, particularly TG (but also FG), of AD cases, perhaps as AD pathology is commonly seen

in TG. However, rod-shaped microglia were not present in all AD cases, consistent with other studies (Bachstetter et al., 2015). Their presence may be region-specific in different individuals (Bachstetter et al., 2017), perhaps contributing further to the heterogeneity of pathology and clinical presentations in individuals with similar burdens of AD pathology.

Rod-shaped microglia were variably present in FTLD cases, typically in grey matter, with certain subtypes such as FTLD-TDPA or FTLD-TDPB cases with *C9orf72* expansions, FTLD-CBD cases and FTLD-*MAPT* cases displaying many rod-shaped microglia, and others few or none. Only two studies have examined rod-shaped microglia in FTLD (Mao et al., 2019; Sakae et al., 2019b). Both found many rod-shaped microglia in FTLD-TDPA cases with *GRN* mutations, more so than sporadic FTLD-TDPA cases (Mao et al., 2019) or cases with *C9orf72* expansions (Sakae et al., 2019b), but other FTLD subtypes were not explored, and the link between rod-shaped microglia and specific pathologies remains unclear. Certain FTLD subtypes (mainly FTLD-Picks and FTLD-TDPC) had very hypertrophic microglia in frontotemporal grey matter, suggestive of primed, activated microglia, but these were not present in other subtypes or in AD cases. The role of hypertrophic versus amoeboid microglia remains unclear, but variability in microglial morphology across the spectrum of FTLD may be due to different pathologies or gene mutations being associated with differing degrees of microglial activation, as discussed in Chapter 5.

6.6.2 Main FTLD subtypes

FTLD-tau, FTLD-TDP and FTLD-FUS cases had more severe dystrophy than controls in most regions, and dystrophy was similar severe between AD cases and each FTLD subtype in each region. This suggests that tau, TDP-43 and FUS pathology are associated with similar degrees of microglial dysfunction as AD pathology in these regions. However, the severity of microglial dystrophy differed in frontal regions and TG between FTLD-TDP and FTLD-tau cases, and (in later analyses) between various FTLD-

tau and FTLD-TDP subtypes, particularly in white matter, which was not detectable at the group level, so there still seems to be pathology-related differences in microglial senescence. Dystrophy in FTLD-FUS cases appeared homogeneous, which was unsurprising given that this group had more homogeneous pathology (aFTLD-U) and clinical syndromes (bvFTD) than the diverse FTLD-TDP and FTLD-tau groups.

The more extensive dystrophy in the frontal lobe and TG of FTLD-TDP compared with FTLD-tau cases likely arose from the FTLD-TDPA cases, especially genetic cases with FTLD-*GRN* or FTLD-*C9orf72*, which had severe dystrophy. This suggests that TDP-43 pathology is particularly associated with microglial senescence in frontal regions. However, dystrophy did not significantly differ between FTLD-TDP and FTLD-tau cases in TW, most likely as certain FTLD-tau subtypes (particularly FTLD-Picks or FTLD-*MAPT*) had extensive dystrophy in this region. This may relate to a high tau burden in TW, especially in FTLD-*MAPT* cases with 10+16 mutations (Lant et al., 2014; Pickering-Brown et al., 2002), and an association of tau with significant microglial dysfunction and senescence (Bussian et al., 2018; Musi et al., 2018; Sanchez-Mejias et al., 2016; Streit et al., 2009, 2018; van Olst et al., 2020).

Dystrophy was more severe in white than grey matter in FTLD-tau and FTLD-TDP, as seen in FTLD overall. This supports findings of poor activation of all microglial phenotypes in white matter in FTLD-tau and FTLD-TDP cases in Chapter 5, and hypotheses of greater microglial dysfunction in white matter. In contrast, dystrophy was similarly severe in grey and white matter in FTLD-FUS cases, perhaps due to less severe white matter pathology (Rohrer et al., 2011).

Rod-shaped microglia were variably present according to FTLD-tau or FTLD-TDP subtype; they were prominent in FTLD-CBD and FTLD-*MAPT* cases and in FTLD-TDPA or FTLD-TPDB cases with *C9orf72* expansions. They were also present in FG of two of

the four FTLD-FUS cases, where pathology is often severe (Rohrer et al., 2011). Hypertrophic microglia were seen in grey and white matter of the other two FTLD-FUS cases (which lacked rod-shaped microglia) suggesting that unknown factors differentially influence microglia even in individuals with the same pathology and clinical presentation. Hypertrophic microglia were prominent in FTLD-Picks and FTLD-TDPC cases but not present in other FTLD-tau or FTLD-TDP subtypes. It remains unclear what determines development and maintenance of microglia with rod-shaped or hypertrophic morphology and how these are linked to pathology, neuronal remodeling or neurodegeneration.

6.6.3 FTLD-tau subtypes

Dystrophy was more severe in most FTLD-tau subtypes compared with controls in most regions and was generally more severe in white than grey matter. However, this varied regionally according to FTLD-tau subtype, matching regional pathology patterns described in other histological studies of tauopathies (Irwin et al., 2016; Ishizawa and Dickson, 2001; Komori, 1999; Pickering-Brown et al., 2002; Rohrer et al., 2011; Schofield et al., 2003; Zhukareva et al., 2002). Surprisingly, there was no significant difference in dystrophy scores between the four FTLD-tau subtypes in each region, except for in TW, where FTLD-Picks cases had more severe dystrophy than FTLD-PSP cases. However, there was large variability in dystrophy scores within certain subtypes such as FTLD-*MAPT* cases, which may have limited power to detect subtle differences when compared with other subtypes, given the small number of cases in each group.

FTLD-Picks cases had much more severe dystrophy than controls in all regions, particularly in FW. This is consistent with florid frontotemporal grey and white matter pathology and common bvFTD presentations in FTLD-Picks cases (Irwin et al., 2016; Mimuro et al., 2010; Zhukareva et al., 2002). Profound selective microglial dysfunction or senescence may underlie particular white matter vulnerability to pathology in FTLD-Picks cases (Kneynsberg et al., 2017; Zhukareva et al., 2002). In Chapter 5, a particularly

high burden of phagocytic and antigen-presenting microglia was noted in FW of FTLD-Picks cases, with florid activation of phagocytic microglia but limited activation of antigen-presenting microglia in FW and TW. However, the severe dystrophy observed here suggests that microglia (and perhaps antigen-presenting cells in particular) are very dysfunctional. The very severe dystrophy in FW also explains the apparently low burden of Iba1-positive microglia in this region in Chapter 5.

FTLD-CBD cases had less pronounced dystrophy, but dystrophy was severe in FW, differing significantly from controls in this region. This pattern is consistent with significant pathology in FW in CBD studies (Ishizawa and Dickson, 2001; Komori, 1999). In Chapter 5, phagocytic microglia were not more activated (despite a higher burden) than controls in the frontal lobe, and antigen-presenting microglia were poorly activated in FW. It is possible that FTLD-CBD is associated with premature failure of phagocytic or antigen-presenting microglia in frontal regions, particularly in white matter, leading to frequent frontal pathology and presentations with nfvPPA or bvFTD (Lashley et al., 2015).

FTLD-PSP cases had mild to moderate dystrophy in most regions, differing significantly from controls only in FG. This may have been due to less regional tau pathology, as most cases had the PSP-Richardson syndrome variant of PSPS and hence greater subcortical pathology. Alternatively, cortical microglial dysfunction may not play a major role in development of FTLD-PSP, as suggested by other histological (Fernández-Botrán et al., 2011; Ishizawa and Dickson, 2001) and microglial PET (Passamonti et al., 2018) studies. It would be useful to study microglial dystrophy in other subcortical and deep white matter regions in FTLD-PSP cases, to see if the extent of dystrophy correlates with pathology here.

Dystrophy in the FTLD-*MAPT* group was more variable across cases than for other FTLD-tau subtypes. However, overall, FTLD-*MAPT* cases had more severe dystrophy

than controls in all regions, particularly in TW. Dystrophy has not been explored in *MAPT* 10+16 mutation carriers previously, but dystrophy may be particularly severe in TW as tau burden is high here (Lant et al., 2014; Pickering-Brown et al., 2002), and tau is closely linked to microglial senescence, as discussed above. It remains unclear why dystrophy was so variable between cases; there may be environmental or genetic factors which impact on the transition from heightened microglial activation, which occurs presymptomatically in *MAPT* 10+16 mutation carriers (Bevan-Jones et al., 2019), to microglial dysfunction and senescence.

All FTLD-tau subtypes except FTLD-*MAPT* cases had more severe dystrophy in white matter than grey matter. However, this varied regionally according to subtype: in FTLD-Picks cases, dystrophy was more severe in both FW and TW, in FTLD-CBD cases only in FW, and in FTLD-PSP cases only in TW, and in FTLD-MAPT cases, scores were similarly severe in grey and white matter. Microglial senescence in white matter may vary regionally due to differential effects of the various tau isoforms (including the extent of glial involvement) in each region. Alternatively, pre-existing regional vulnerability in microglia and differential senescence rates could contribute to regional development of specific tau pathologies in certain cell types. This could be explored in cell models, including microglia derived from iPSCs obtained from individuals with each FTLD-tau subtype and different *MAPT* mutations.

Other morphologies such as rod-shaped or hypertrophic microglia also varied between FTLD-tau subtypes. Rod-shaped microglia were scarce in FTLD-Picks and FTLD-PSP cases, but all FTLD-CBD and most FTLD-*MAPT* cases had several rod-shaped microglia in grey matter, with additional rod-shaped microglia in white matter of all FTLD-*MAPT* cases. This suggests that certain tauopathies are associated with persistent attempts at neuronal repair in highly affected areas. This has not been explored in FTLD-tau previously, although other studies have found that presence of rod-shaped microglia

varies between individuals with FTLD-TDPA due to different disease mechanisms (Mao et al., 2019; Sakae et al., 2019b). Most FTLD-Picks cases had numerous hypertrophic microglia in grey matter, but these were not present in other FTLD-tau subtypes. This suggests that FTLD-Picks pathology is associated with heightened activation of certain microglial phenotypes, as supported by analyses of phagocytic microglia in Chapter 5.

6.6.4 FTLD-TDP subtypes

Microglial dystrophy was present in all FTLD-TDP subtypes but was particularly severe in the frontal lobe of FTLD-TDPA and FTLD-TDPC cases and in the temporal lobe of FTLD-TDPC cases. FTLD-TDPA and FTLD-TDPC cases had more severe dystrophy than controls in all regions, whereas FTLD-TDPB cases only differed from controls in FW. Although several FTLD-TDPA and FTLD-TDPC cases appeared to have much more severe dystrophy than FTLD-TDPB cases, overall dystrophy did not significantly differ between FTLD-TDP subtypes in any region. This may have been due to significant intragroup variability in dystrophy scores, particularly within the large and diverse FTLD-TDPA group, and inclusion of both sporadic and genetic cases within FTLD-TDPA and FTLD-TDPB groups. This emphasises the importance of analysing cases with different disease mechanisms separately in histological studies wherever possible.

FTLD-TDPA was associated with particularly severe dystrophy in all regions, but this varied according to the disease mechanism, as explored later. The single *TBK1* mutation case (which was not included in group analyses) had extensive dystrophy in all regions, perhaps due to the combined role of this gene in immune and lysosomal pathways (Ahmad et al., 2016). In contrast, dystrophy in FTLD-TDPB cases only differed from controls in FW, perhaps due to significant frontal pathology (three had FTD-MND and two bvFTD). Although dystrophy was not compared semi-quantitatively between FTLD-TDPB subtypes due to small numbers, the two sporadic cases, both of whom had FTD-MND, had moderate to severe dystrophy in all regions, worse in white matter. This was

unsurprising given that MND is associated with significant microglial dysfunction in both grey and white matter (Brettschneider et al., 2012). However, surprisingly, dystrophy severity varied considerably in each region across the three genetic FTLD-TDPB cases with the *C9orf72* expansion. Microglial dystrophy has not been explored previously in sporadic or genetic FTLD-TDPB, but regional variations in dystrophy could be due to different clinical syndromes and regional pathology burdens, or may be affected by genetic or other factors influencing regional effects of the *C9orf72* expansion on microglial function (Burberry et al., 2020).

FTLD-TDPC cases had more severe dystrophy than controls in all regions. Unsurprisingly, this was less variable across cases than in FTLD-TDPA or FTLD-TDPB, given the similar clinical presentations (all svPPA) and pathology patterns within this group. Dystrophy was particularly severe in the temporal lobe; early microglial senescence here could underlie an initial predilection for FTLD-TDPC pathology in this region (Rohrer et al., 2011), or could have developed due to a high burden of focal TDP-43 pathology. Dysfunction of the many antigen-presenting microglia present in these cases (which were poorly activated in Chapter 5) could lead to altered presentation of self-antigens in the CNS and altered TDP-43 clearance. If dysfunction of systemic macrophages presenting self-antigens to T cells in the thymus also occurs early on, this could be linked to the increased prevalence of systemic autoimmune disease seen in svPPA (Miller et al., 2013) due to reduced development of immune tolerance.

Dystrophy was more severe in white than grey matter for all FTLD-TDP subtypes, but only within the frontal lobe. Extensive dystrophy in FW of the five FTLD-*GRN* cases, one *TBK1* case, and most sporadic FTLD-TDPA cases likely contributed to this pattern for the FTLD-TDPA group. This may underlie the many poorly activated phagocytic and antigen-presenting microglia in FW of FTLD-TDPA cases in Chapter 5. Pathology is particularly severe in FW of FTLD-TDPA cases, more so than in other FTLD-TDP

subtypes (Geser et al., 2009), and this could be due to, or contribute to, greater microglial senescence. Both sporadic (Rohrer et al., 2011) and genetic (Jiskoot et al., 2018; Sudre et al., 2017a, 2019; Woollacott et al., 2018) FTLD-TDPA cases have significant neuroimaging abnormalities in FW, including presymptomatic *GRN* mutation carriers (Jiskoot et al., 2018; Sudre et al., 2019). These results support the hypothesis in Chapter 4 that early white matter changes in the frontal lobes of *GRN* mutation carriers may be due to early, regionally selective microglial senescence, and extends this to other causes of FTLD-TDPA.

Rod-shaped microglia were present in grey matter of FTLD-TDP cases, but this varied according to subtype and disease mechanism. They were numerous in grey matter of FTLD-TDPA and FTLD-TDPB cases with *C9orf72* expansions, occasionally present in FG of sporadic FTLD-TDPA cases and FG or TG of some sporadic FTLD-TDPB cases, but rare in FTLD-TDPC cases. They were not seen in any FTLD-TDPA cases with *GRN* or *TBK1* mutations, although extensive dystrophy likely precluded their detection. Other studies of FTLD-TDPA have shown rod-shaped microglia in the hippocampi of sporadic cases and genetic cases with *GRN* mutations (Mao et al., 2019) and in cortical areas of cases with *GRN* or *C9orf72* mutations (Sakae et al., 2019b), but rod-shaped microglia have not been examined previously in FTLD-TDPB or FTLD-TDPC cases. The relevance of variations in presence of these cells across the spectrum of FTLD-TDP remains unclear, although their prominence in *C9orf72* expansion carriers is intriguing. All FTLD-TDPC cases had several hypertrophic microglia in grey and white matter, which were not prominent in FTLD-TDPA or FTLD-TDPB cases. Why hypertrophic cells would be particularly upregulated in association with FTLD-TDPC remains unclear.

6.6.5 Sporadic and genetic FTLD-TDPA subtypes

Most FTLD-*GRN* cases and several sporadic FTLD-TDPA cases had very severe or severe dystrophy in all regions, particularly in FW, with severe cytorrhexis similar to

Down's syndrome cases (Streit et al., 2009). Several FTLD-TDPA cases had such faint Iba1 staining that new sections were re-stained several times in different experiments in case immunohistochemistry had failed (despite positive controls staining well). However, the same staining pattern appeared, confirming that severe cellular disruption was present. Extensive dystrophy could explain findings in Chapter 5 of many poorly activated antigen-presenting microglia in sporadic FTLD-TDPA cases, and many poorly activated phagocytic microglia in FTLD-*GRN* cases, especially in FW. It may also explain the relatively high burden of Iba1-positive microglia in the frontal lobe of FTLD-*C9orf72* cases, as dystrophy was less severe here, only differing from controls in the temporal lobe.

Dystrophy was variable in each region across cases within the sporadic FTLD-TDPA group, perhaps due to differences in the location of pathology or other factors (such as unknown genetic variants) differentially influencing microglial senescence in apparently sporadic disease. Variability was also seen in the FTLD-*C9orf72* group, perhaps due to modification of the effects of the *C9orf72* expansion on microglia by other environmental or genetic factors. In contrast, in the FTLD-*GRN* group, dystrophy was much more homogeneous, suggestive of extensive microglial senescence in frontotemporal regions associated with this mutation, particularly in white matter, as hypothesised in Chapter 4. Dystrophy did not differ significantly between genetic and sporadic FTLD-TDPA subtypes, although as many had maximally severe dystrophy scores, this was unsurprising. Although several FTLD-*GRN* cases appeared to have more severe dystrophy in FW compared with FTLD-*C9orf72* cases, at the group level, scores did not differ significantly.

Despite more severe dystrophy in FW than FG of FTLD-TDPA cases overall, this was not seen in the FTLD-TDPA subtype analysis. Although several FTLD-*GRN* cases appeared to have more severe dystrophy in FW than FG, this did not reach significance

at the group level. Small group sizes and more variability in scores across cases may have reduced power to detect more subtle differences between areas in each group, although as dystrophy in FW of most FTLD-*GRN* cases was particularly severe, perhaps *GRN* mutations are associated with a regional predilection for microglial senescence and pathology in FW. This could explain the prominence of frontal WMH on MRI in symptomatic *GRN* mutation carriers, which is not seen in symptomatic *C9orf72* expansion carriers (Sudre et al., 2017a).

Occasional rod-shaped microglia were seen in FG of most sporadic FTLD-TDPA cases, but these were numerous in grey matter of most FTLD-*C9orf72* cases and not seen in any FTLD-*GRN* cases. Although dystrophy has not been previously been explored in sporadic FTLD-TDPA, rod-shaped microglia do vary within hippocampal sub-regions between sporadic FTLD-TDPA and FTLD-*GRN* cases, with the former having frequent rod-shaped microglia in the subiculum and few in CA1, and the latter, the opposite pattern (Mao et al., 2019). This suggests that different disease mechanisms affect microglial morphology at the sub-regional level within the same pathological subtype. Others have found more rod-shaped microglia in the middle frontal cortex of FTLD-*GRN* cases compared with controls and FTLD-*C9orf72* cases (Sakae et al., 2019b), but FTLD-*GRN* cases had extensive dystrophy in the present study, which may have precluded their detection. Hypertrophic microglia were not present in any FTLD-TDPA subtype; this may have been due to extensive dystrophy precluding identification, or, given that hypertrophic cells were still seen in FTLD-TDPC cases (who also had severe dystrophy), there may be a true lack of hypertrophic microglia in individuals who develop FTLD-TDPA, although reasons for this remain clear.

6.6.6 Genetic FTLD subtypes

This study extends the very few previous studies of microglial dystrophy in genetic FTLD, which have focused on FTLD-*GRN* (Sakae et al., 2019b; Woollacott et al., 2018) or

FTLD-*C9orf72* (Sakae et al., 2019b) cases, and describes dystrophy and rod-shaped microglia in FTLD-*MAPT* cases for the first time.

FTLD-*GRN* cases had much more severe dystrophy than controls in all regions, particularly in FW, where there was typically punctate, diffuse Iba1 staining consistent with total loss of cell integrity (Streit et al., 2009). In the single FTLD-*GRN* case in Chapter 4, dystrophy severity varied regionally and was worst in FW, correlating with the severity of histopathological changes in grey and white matter (TDP-43 burden, neuronal loss and demyelination) and neuroimaging changes in grey and white matter (cortical atrophy and WMH) (Woollacott et al., 2018). Inclusion of further cases in this study has allowed confirmation that extensive dystrophy in FW is a typical pattern in *GRN* mutation carriers. Another study found more severe dystrophy in middle frontal cortical grey matter of FTLD-*GRN* cases compared with controls, but dystrophy was similar between FTLD-*GRN* and FTLD-*C9orf72* cases, although subcortical white matter was not examined (Sakae et al., 2019b). In the present study, there was particularly severe dystrophy in FW of FTLD-*GRN* cases, with a suggestion of slightly less severe dystrophy in FW of FTLD-*C9orf72* cases. This highlights FW as a region that is particularly vulnerable to microglial senescence in *GRN* mutation carriers, and this is likely to be due to the mutation itself (rather than differences in pathology) as both groups had FTLD-TDPA.

Recently, lipid droplet accumulating microglia have been implicated in the pathogenesis of FTLD due to *GRN* mutations. Although these were previously identified in aging (Marschallinger et al., 2020) and AD (El Hajj et al., 2019; Srinivasan et al., 2020), microglia in *GRN* -/- mice display severe accumulation of lipids, significant defects in phagocytosis, and excessive proinflammatory cytokines (Marschallinger et al., 2020). There is also microglial lipofuscin accumulation (Tanaka et al., 2014) and foam cell formation in progranulin deficient macrophages (Nguyen et al., 2018) and accumulation of triacylglycerides in fibroblast and lysosomal lipidomes in humans and mice with *GRN*

mutations (Evers et al., 2017). Impaired lipid handling likely contributes to the significant lysosomal dysfunction observed in progranulin deficient microglia (Evers et al., 2017; Tanaka et al., 2014; Ward et al., 2017; Wils et al., 2012). Profound microglial dystrophy in FTLD-*GRN* cases could therefore arise from regionally altered microglial lipid metabolism contributing to, or exacerbated by, microglial lysosomal failure. Ameliorating these processes and reducing premature microglial senescence should be key therapeutic targets for study in *GRN* cell and mouse models, particularly in microglia derived from iPSCs obtained from human *GRN* mutation carriers.

Although dystrophy in FTLD-*C9orf72* cases was overall more severe than controls in all regions, dystrophy was rather variable between cases. Another study has found that FTLD-*C9orf72* cases had more severe dystrophy than controls in the middle frontal cortex, but dystrophy was not explored in subcortical white matter or other regions (Sakae et al., 2019b). Interestingly, individuals with MND due to *C9orf72* expansions have microglial dysfunction in the frontal cortex, even in clinically unaffected regions (Cooper-Knock et al., 2012; O'Rourke et al., 2016; Umoh et al., 2017), suggesting this occurs before significant neurodegeneration. Multiple mouse models indicate that *C9orf72* expansions cause microglial dysfunction through altered immune pathways, or lysosomal or autophagy mechanisms (Amick and Ferguson, 2017; Rostalski et al., 2019). However, microglial senescence may be modified by variants in genes that affect microglial lysosomal pathways in the presence of a *C9orf72* expansion, such as *TMEM106B* (Busch et al., 2016). A recent study showed that microglia in the spinal cord of a *C9orf72* mutant mouse model of ALS were modified by the mouse gut microbiome, with two identical mouse models at different institutions displaying completely different degrees of microglial activation, immune dysfunction and motor phenotypes due to different gut bacteria, which was modifiable by antibiotic therapy (Burberry et al., 2020). This suggests that environmental factors substantially modulate microglial dysfunction in the presence of a *C9orf72* expansion. Microglial senescence could therefore vary

regionally and between different *C9orf72* expansion carriers, so that certain individuals initially develop either frontotemporal cortex, or motor cortex, or spinal cord pathology.

Dystrophy in FTLD-*MAPT* cases was more severe than controls in FG and TW but was also rather variable across cases. As discussed in Section 6.6.3, areas of most severe dystrophy in FTLD-*MAPT* cases were matched to areas known to have a high tau burden, such as TW (Lant et al., 2014; Pickering-Brown et al., 2002). Despite seemingly less extensive dystrophy in many FTLD-*MAPT* cases, dystrophy scores did not differ significantly in any region from FTLD-*GRN* or FTLD-*C9orf72* cases. This may have been due to the variability of dystrophy across cases, combined with small group sizes, limiting power. Multiple studies link microglial dysfunction and senescence to tau pathology, including in *MAPT* models (Bussian et al., 2018; van Olst et al., 2020), and clearance of senescent cells prevents this (Bussian et al., 2018), so anti-senescence therapies may also be a promising approach for further exploration in *MAPT* 10+16 mouse or cell models.

Dystrophy was similarly severe in white and grey matter in most genetic groups (contrary to other group analyses). This may have been due to small group sizes and subtle differences in (predominantly severe) dystrophy scores between areas in these cases. Dystrophy has not been compared between grey and white matter in genetic FTLD previously, except in Chapter 4, where dystrophy was also more severe in FW than FG in a FTLD-*GRN* case (Woollacott et al., 2018). Only *GRN* mutation carriers display significant WMH in frontal regions (Sudre et al., 2017a), and although *C9orf72* expansion and *MAPT* mutation carriers display early white matter neuroimaging abnormalities, including WMH, this is typically in deep subcortical (*C9orf72*) or more posterior (*C9orf72*) or temporal (*MAPT*) regions (Jiskoot et al., 2018; Papma et al., 2017; Sudre et al., 2017a). Histological studies of microglia in brain regions typically affected by each of these mutations, such as the thalami, parietal lobes, cerebellum or hippocampi, may be

useful to explore whether regional patterns of microglial dystrophy in grey and white matter match regional neuroimaging and pathological changes across genetic FTLD subtypes.

Rod-shaped microglia were frequently present in frontotemporal grey matter of FTLD-*C9orf72* cases with either FTLD-TDPA or FTLD-TPDB, in white matter of all FTLD-*MAPT* cases, and in grey matter of nearly all FTLD-*MAPT* cases. They were not seen in any FTLD-*GRN* cases, but extensive cell disruption likely precluded identification. Others have found many rod-shaped microglia in the hippocampal CA1 region of FTLD-*GRN* cases but few in the subiculum (Mao et al., 2019), or more rod-shaped microglia in the middle frontal cortex of FTLD-*GRN* cases compared with FTLD-*C9orf72* cases and controls (Sakae et al., 2019b). Rod-shaped microglia have not been described in FTLD-*MAPT* cases previously but seem to be prominent in both grey and white matter. Whether specific mutations are linked to increased formation of rod-shaped microglia, and how this links to regional neurodegeneration patterns in genetic FTLD, remain unclear. Hypertrophic microglia were not observed in any genetic group, supporting quantitative findings of limited microglial activation in most genetic FTLD cases in Chapter 5, although these may have been difficult to identify in many genetic cases due to the degree of dystrophy.

In conclusion, microglial dystrophy is present in genetic FTLD, but varies regionally, and is particularly extensive in FTLD-*GRN* cases, perhaps due to the combined role of progranulin in immune pathways, lysosomal function and microglial lipid handling. Dystrophy is more variable within FTLD-*C9orf72* and FTLD-*MAPT* groups and this could be linked to phenotypic variability. Dystrophy is particularly severe in FW of FTLD-*GRN* cases, more so than FTLD-*C9orf72* cases, indicating a region-specific, mutation-specific effect of progranulin deficiency on microglial function. Variations in regional dystrophy patterns and presence of rod-shaped microglia across genetic FTLD subtypes suggest

that there may be regionally selective microglial dysfunction or senescence associated with different mutations. In addition to the regional alterations in microglial burden and activation observed in Chapter 5, this may contribute to differences in grey and white matter pathology, neuroimaging abnormalities and clinical presentations between *GRN*, *C9orf72* and *MAPT* mutation carriers.

6.7 Limitations and future work

This study has several advantages compared with previous studies of dystrophy in FTLD. First, dystrophy has not previously been examined across such a wide range of FTLD subtypes, in such clinically relevant regions, in both grey and white matter, or in FTLD versus AD. Rod-shaped microglia have also barely been explored in FTLD. The findings of this study support the concept that microglial senescence is present in both FTLD and AD and excessive compared with controls. Second, comparison of FTLD subtypes at a pathological, disease mechanism and mutation-specific level has enabled understanding that dystrophy varies regionally in FTLD and that this may be linked to pathological subtype or due to mutation-specific effects on microglial function. Third, it has demonstrated that rod-shaped microglia are more prominent in certain subgroups such as *C9orf72* or *MAPT* mutation carriers, and hypertrophic microglia are prominent in FTLD-Picks or FTLD-TDPC cases. Although the role of cells with these morphologies remains unclear, future studies may explore how these phenotypes are involved in neuronal remodeling and axonal transport. Finally, concurrent examination in Chapter 5 of other microglial parameters within the same cohort and brain regions has enabled appreciation of how regional changes in microglial burden and activation state could be linked to changes in microglial dystrophy. Extensive dystrophy may explain why limited microglial activation was present in many FTLD subtypes in Chapter 5, supporting increasing evidence that microglial senescence, rather than chronic activation, contributes to neurodegenerative disease.

There are some limitations, most of which were discussed in Chapter 5. Replication is needed in a larger cohort, across a wider selection of regions, with concurrent correlation with other pathological changes, to aid understanding of whether dystrophy is associated with regional pathology patterns. Analysis of dystrophy in unaffected 'control' regions such as the cerebellum (mostly spared in FTLD, except in FTLD-*C9orf72* cases) would increase confidence that changes in microglia are specific to clinically and pathologically affected regions, but this was not possible to do within the timeframe available.

As substantial dystrophy was present in many FTLD and AD cases, this raises the question of how reliable quantitative assessments of the burden of Iba1-positive microglia are in histological studies of individuals with neurodegenerative disease. Reduced Iba1 staining when dystrophy was severe likely under-represented the burden of Iba1-positive microglia in certain regions in some groups in Chapter 5, and this is likely to be the case in other studies. In addition, dystrophic Iba1-positive microglia were also not morphological normal and cell boundaries were often highly disrupted, which would have affected cell circularity and perimeter measurements and led to the appearance of over- or under-activated morphology. However, in Chapter 5 two other microglia markers (CD68 and CR3/43) were also used in the same cohort to assess microglial burden and activation. These bind to the cell cytoplasm and membrane of microglia (respectively) and are less affected by dystrophy (Tischer et al., 2016), so will have allowed a more reliable assessment of burden and activation in the same regions. These factors emphasise the importance of using a variety of microglial markers when analysing microglia in *post-mortem* brain tissue and appreciation of the advantages and disadvantages of different markers and quantitative analysis techniques.

Semi-quantitative scoring systems, as used here to assess dystrophy, are potentially subject to rater bias, and as visual assessment was performed across ten randomly selected squares in a region, this only captured a general sense of severity in a region,

whereas dystrophy may vary intra-regionally. However, these systems have been used in many other histological studies assessing morphological changes in microglia to determine regional activation states, including in FTLD (Lant et al., 2014; Taipa et al., 2017). Given the technical complexity of quantitatively assessing all dystrophic changes (El Hajj et al., 2019), and the fact that this study was carried as an extension study after the author had noted disrupted staining and abnormal morphology of Iba1-positive microglia in certain FTLD subtypes during the analysis for Chapter 5, this approach was felt to be a satisfactory and pragmatic way to carry out an initial, exploratory study of dystrophy within the timeframe available.

Although morphological changes in microglia suggestive of dystrophy are thought to represent cellular senescence or dysfunction of microglia (Streit et al., 2004), this remains unconfirmed, and cannot be substantiated by a histological study of this nature. Comparison of mechanisms of phagocytosis, antigen presentation and other key microglial supportive and immune functions through use of models of cellular senescence in FTLD, corroborated by evidence of dystrophy in brain tissue, would be useful to investigate this further.

Future studies should explore mechanisms of microglial and lysosomal dysfunction and senescence in FTD, and the impact of genetic variants and environment on these processes. Use of neuronal and glial cell models of the different FTLD pathologies, especially iPSCs derived from fibroblasts within skin biopsies obtained from PMC and symptomatic individuals at different stages of sporadic and genetic FTLD, could explore how and when microglial dysfunction or senescence relate to onset of different neuronal and glial pathological inclusions and lead to neurodegeneration over time.

6.8 Publications relating to this chapter

The work presented in this chapter, combined with the study in Chapter 5, has been published as:

Woollacott IOC et al. (2020) Microglial burden, activation and dystrophy patterns in frontotemporal lobar degeneration. *Journal of Neuroinflammation.*17:234.

7 CSF glia-derived biomarkers in sporadic and genetic FTD

7.1 Chapter summary

Introduction: Chronic glial dysfunction may contribute to the pathogenesis of FTD. Levels of glia-derived biomarkers including sTREM2, YKL-40 and chitotriosidase are increased in CSF in AD cohorts but have not been explored in detail across the clinical or genetic spectrum of FTD.

Methods: Immunoassays were used to measure levels of glia-derived (sTREM2, YKL-40 and chitotriosidase) and neurodegenerative (T-tau, P-tau and Aβ42) biomarkers in CSF of 18 healthy controls (17 for sTREM2) and 64 individuals with clinical diagnoses of FTD (bvFTD, n=20; PPA, n=44: nfvPPA, n=16, svPPA, n=11, lvPPA, n =14, PPA-NOS, n=3). 10/64 individuals had genetic FTD, with mutations in *GRN* (n=3), *MAPT* (n=4), or *C9orf72* (n=3). 15/64 individuals had a CSF neurodegenerative biomarker profile consistent with AD pathology. Multivariable linear regressions were used to examine associations of glia-derived biomarkers with age, disease duration and neurodegenerative biomarkers, and between YKL-40 and chitotriosidase levels. Glia-derived biomarker levels were compared between individuals with FTD and controls, across different clinical and genetic subtypes of FTD, and between individuals with clinical FTD syndromes due to likely AD versus non-AD (FTLD) pathology (based on CSF neurodegenerative biomarkers).

Results: sTREM2 and YKL-40, but not chitotriosidase, levels were positively associated with age, and sTREM2 levels were negatively associated with disease duration. YKL-40 and chitotriosidase, but not sTREM2, levels were higher in FTD compared with controls, but only in lvPPA (both) and nfvPPA (YKL-40). *GRN* mutation carriers had highly elevated levels of all glia-derived biomarkers compared with controls and *C9orf72* expansion carriers, and YKL-40 levels were higher in *MAPT* mutation carriers than

controls. Individuals with likely underlying AD pathology had elevated levels of all glia-derived biomarkers compared with controls and individuals with likely FTLD pathology. Glia-derived biomarker levels were variably associated with T-tau, P-tau and Aβ42 levels, and YKL-40 and chitotriosidase levels were positively associated with each other, but this varied depending on the clinical syndrome and underlying pathology.

Conclusions: CSF YKL-40 and chitotriosidase levels are increased in individuals with sporadic FTD syndromes, but this is primarily in individuals with underlying AD pathology. However, sTREM2, YKL-40 and chitotriosidase levels are highly elevated in FTD due to *GRN* mutations, and YKL-40 is increased in FTD due to *MAPT* mutations, perhaps due to mutation-specific effects on glial function. As levels of glia-derived biomarkers correlate with T-tau in those with likely FTLD, they may reflect the glial contribution or response to neurodegeneration.

7.2 Introduction

Throughout this thesis there has been growing evidence that aberrant neuroinflammation, and particularly microglial dysfunction, contributes to FTD. Although glial cells such as microglia and astrocytes may be helpful in the initial response to ensuing protein aggregation, over time they may become dysfunctional and harmful. This may be through chronic activation and release of proinflammatory cytokines and other toxic molecules, or accelerated senescence, with premature failure of key functions such as lysosomal pathways, leading to altered phagocytic capabilities and impaired neuronal and axonal support.

Although histological studies are important for understanding disease pathogenesis in FTLD, there is a need for biomarkers of processes such as aberrant neuroinflammation that can be detected *in vivo* in individuals with sporadic and genetic FTD. Inflammatory biomarkers, particularly glia-derived proteins, are detectable in blood or CSF from

individuals with other neurodegenerative diseases such as AD or HD. These biomarkers could vary across the clinical, genetic and pathological spectrum of FTD, and hence may be useful not only for aiding diagnosis, pathological phenotyping or prediction of disease trajectories in clinical practice, but also for assessing disease proximity, intensity or treatment response in future clinical trials.

Although glia-derived biomarkers such as sTREM2 were initially studied in CSF of individuals with neuroinflammatory conditions like multiple sclerosis (Öhrfelt et al., 2016; Piccio et al., 2008), they have become of great interest in neurodegenerative disorders. Three glia-derived biomarkers have been most extensively explored: sTREM2, YKL-40 and chitotriosidase, although most studies have focused on AD cohorts. Non-stratified AD cohorts initially produced conflicting results, but recent studies show that, when compared with controls, AD cases have raised levels of sTREM2 (Gispert et al., 2016; Henjum et al., 2016; Heslegrave et al., 2016; Liu et al., 2018; Piccio et al., 2016; Suárez-Calvet et al., 2019, 2016b, 2016a; Suárez-Calvet et al., 2018), YKL40 (Baldacci et al., 2017b; Kester et al., 2015; Llorens et al., 2017; Morenas-Rodríguez et al., 2019; Nordengen et al., 2019; Sutphen et al., 2018; Zhang et al., 2018) and chitotriosidase (Abu-Rumeileh et al., 2019; Mattsson et al., 2011; Rosén et al., 2014; Steinacker et al., 2018; Watabe-Rudolph et al., 2012). However, levels change according to disease stage, with raised levels in presymptomatic genetic AD, mild cognitive impairment and the early stages of sporadic AD, but limited elevation in established disease (Liu et al., 2018; Nordengen et al., 2019; Suárez-Calvet et al., 2016b, 2016a, 2019). Levels of these biomarkers could be useful in tracking disease course in AD, or for determining proximity to disease onset in presymptomatic genetic AD cases. This may also be the case for FTD.

Levels of glia-derived biomarkers in AD cohorts generally correlate with CSF levels of neurodegenerative biomarkers used in clinical practice, mostly T-tau, a biomarker of

neuronal injury, and P-tau, a biomarker of hyperphosphorylated tau pathology, but not with Aβ42, a biomarker of Aβ pathology (Abu-Rumeileh et al., 2019; Alcolea et al., 2014; Antonell et al., 2014; Craig-Schapiro et al., 2010; Gispert et al., 2016a; Heslegrave et al., 2016; Olsson et al., 2013; Suárez-Calvet et al., 2016b, 2019; Sutphen et al., 2018; Zhang et al., 2018). The correlation with T-tau suggests that glia-derived biomarkers in CSF may be useful as indicators of the glial response to neuronal injury, irrespective of amyloid pathology, and hence worth exploring in FTD.

Several studies have examined how CSF levels of these glia-derived biomarkers are altered in FTD compared with controls or AD cases (Abu-Rumeileh et al., 2019; Alcolea et al., 2014, 2018; Antonell et al., 2020; Baldacci et al., 2017b; Craig-Schapiro et al., 2010; del Campo et al., 2018; Illán-Gala et al., 2018; Janelidze et al., 2016; Kleinberger et al., 2014; Oeckl et al., 2019; Piccio et al., 2016; Steinacker et al., 2018; Teunissen et al., 2016; Vijverberg et al., 2017). However, most of these have included small numbers of individuals with FTD, with undefined clinical subtypes, and lack of CSF biomarker or pathological confirmation, and have found widely differing results. It remains unclear whether sTREM2, YKL-40 and chitotriosidase levels are altered in FTD in general, or whether they differ between the various clinical subtypes of FTD.

No studies have compared sTREM2 levels across groups of individuals with genetic FTD due to *GRN, C9orf72* and *MAPT* mutations, and few studies have examined YKL-40 or chitotriosidase levels in genetic FTD cohorts (Abu-Rumeileh et al., 2019; Antonell et al., 2020; Barschke et al., 2020; Oeckl et al., 2019), with most of these failing to compare genetic subgroups. In addition, individuals may develop clinical syndromes consistent with FTD (bvFTD or PPA) due to underlying AD, rather than FTLD, pathology. It is unclear whether glia-derived biomarker levels differ between individuals with similar clinical FTD syndromes but contrasting pathologies. Few studies have explored how glia-derived biomarkers are associated with neurodegenerative biomarkers (T-tau, P-tau and

Aβ42) in FTD (Abu-Rumeileh et al., 2019; Craig-Schapiro et al., 2010; Teunissen et al., 2016), despite these being used in clinical practice to investigate individuals with dementia syndromes, including those with typical or atypical FTD.

7.3 Aims and hypotheses

Given the heterogeneous clinical, genetic, and pathological nature of FTD syndromes, this study aimed to carry out a comprehensive study of sTREM2, YKL-40 and chitotriosidase levels in CSF from individuals with clinical diagnoses of sporadic FTD and in healthy controls. It also aimed to perform an exploratory study of these biomarkers in CSF from a small number of individuals with genetic FTD due to mutations in *GRN, C9orf72* or *MAPT*, and to compare levels between individuals with clinical FTD syndromes due to underlying AD versus FTLD pathology.

The overarching hypothesis was that there is glial dysfunction in FTD, and that abnormal levels of these biomarkers will be detectable in CSF from individuals with FTD. Specific hypotheses were that levels of glia-derived biomarkers in CSF will differ:

1. Between individuals with dementia (clinically consistent with FTD) and healthy controls, due to increased glial dysfunction in FTD.
2. Between individuals with different clinical FTD syndromes, due to varying pathologies being associated with differing degrees of glial dysfunction.
3. Between individuals with different subtypes of genetic FTD (due to *GRN*, *C9orf72* or *MAPT* mutations) and controls, and between genetic FTD subtypes, due to differing degrees of glial dysfunction associated with each mutation type.
4. Between individuals with clinical FTD syndromes due to FTLD versus AD pathology, due to each pathology being associated with different degrees of glial dysfunction.

In addition, this study hypothesised that levels of glia-derived biomarkers would be associated with levels of CSF neurodegenerative biomarkers (T-tau, P-tau and Aβ42) currently used in clinical practice, due to a link between glial dysfunction and neurodegeneration. Associations in individuals with FTD and likely underlying FTLD may predominantly be with T-tau, as this is a biomarker of neuronal injury even in the absence of AD pathology. Associations in individuals with FTD clinically, but likely underlying AD pathology, are more likely to be with P-tau and T-tau, and perhaps Aβ42, due to hyperphosphorylated tau and amyloid pathology associated with neuronal injury. Levels of glia-derived biomarkers may also correlate with each other, as they may arise from similar neuroinflammatory processes.

7.4 Methods

7.4.1 Participants

The cohort for the sTREM2 study consisted of 64 consecutively recruited individuals with dementia, who met consensus diagnostic criteria for an FTD syndrome, either bvFTD (Rascovsky et al., 2011) or PPA (Gorno-Tempini et al., 2011), and 17 cognitively normal controls. The cohort for the YKL-40 and chitotriosidase study consisted of the same 64 individuals with dementia, but 18 cognitively normal controls (as an extra control was recruited after the sTREM2 study). Individuals with dementia and controls were recruited from previous longitudinal studies of FTD at UCL, GENFI, LIFTD and the prospective DRC CSF cohort study at UCL, as described in Chapter 2.1.2.

From the 64 individuals with dementia, there were five clinical subgroups: 20 had bvFTD, 16 nfvPPA, 11 svPPA, 14 lvPPA and three had PPA-NOS (Table 7.1). All participants with dementia were genetically screened for known FTD causative mutations, including the *C9orf72* expansion. Ten of these individuals had genetic FTD, producing three genetic subgroups, due to mutations in *GRN* (n=3), *MAPT* (n=4) or *C9orf72* (n=3). All genetic cases had a clinical syndrome of bvFTD except two individuals with *GRN*

mutations who had nfvPPA. Demographics are displayed in Table 7.1. Disease duration was calculated as the time, in years, between AAO of symptoms and date of CSF collection.

	Control	Dementia (FTD)	bvFTD	nfvPPA	svPPA	lvPPA	PPA-NOS
Number of participants	17[a] 18[b]	64	20	16	11	14	3
Male sex N (% group)	6 (54.5)[a] 7 (38.9)[b]	45 (70.3)	19 (95.0)	9 (56.2)	7 (63.6)	7 (50.0)	3 (100.0)
Age at CSF (years) Mean (SD)	63.7 (6.4)[a] 64.3 (6.6)[b]	64.6 (6.5)	63.4 (7.1)	66.9 (5.9)	60.8 (6.0)	66.5 (6.0)	64.6 (5.4)
Age at onset (years) Mean (SD)	n/a	59.5 (6.9)	56.1 (6.7)	62.7 (6.1)	56.1 (5.3)	63.0 (6.7)	61.3 (4.1)
Disease duration at CSF (years) Mean (SD) Median (IQR)	n/a	5.1 (3.8) 4.2 (2.7-6.3)	7.4 (5.6) 6.3 (3.4-8.8)	4.2 (1.9) 4.2 (2.8-5.1)	4.7 (2.1) 4.6 (3.4-6.3)	3.5 (2.0) 3.1 (1.9-4.8)	3.2 (1.3) 2.7 (2.3-4.7)
CSF sTREM2 (ng/ml) Mean (SD)	6.8 (1.6)	7.4 (3.2)	6.3 (3.7)	7.8 (2.2)	7.4 (2.4)	8.2 (4.1)	8.7 (1.9)
CSF YKL-40 (ng/ml) Mean (SD)	108.4 (29.9)	133.7 (52.7)	118.5 (49.6)	148.8 (56.6)	119.6 (29.5)	146.6 (64.3)	146.3 (45.0)
CSF chitotriosidase (pg/ml) Mean (SD)	1761.6 (1097.8)	3974.5 (4357.9)	3729.6 (3761.9)	4155.8 (5788.9)	2652.2 (1609.1)	5329.9 (5038.9)	3142.3 (3868.2)
Ln(chitotriosidase) Mean (SD)*	7.3 (0.6)	7.8 (0.9)	7.8 (0.9)	7.8 (0.9)	7.7 (0.6)	8.1 (1.1)	7.5 (1.3)
CSF Aβ42 (pg/ml) Mean (SD)	1032.2 (214.3)[a] 1028.5 (208.6)[b]	758.1 (280.7)	828.3 (171.7)	842.5 (298.0)	894.0 (247.4)	444.6 (148.3)	804.3 (434.2)
CSF T-tau (pg/ml) Mean (SD)	332.6 (82.4)[a] 338.8 (82.1)[b]	531.4 (404.5)	351.9 (135.5)	490.6 (247.8)	395.5 (200.3)	968.8 (617.0)	403.3 (208.5)
CSF P-tau (pg/ml) Mean (SD)	52.7 (10.6)[a] 53.1 (10.4)[b]	57.0 (30.6)	45.7 (17.0)	50.6 (18.1)	44.9 (19.8)	91.7 (41.6)	49.0 (14.4)
CSF T-tau/Aβ42 ratio Median (IQR)	0.3 (0.2-0.5)[a] 0.3 (0.2-0.5)[b]	0.5 (0.3-1.0)	0.4 (0.3-0.5)	0.6 (0.3-0.9)	0.4 (0.3-0.5)	2.0 (1.1-3.2)	0.4 (0.2-1.2)

Table 7.1 Demographics and CSF biomarker levels in dementia and control groups

Data are shown for both control groups, one used in the sTREM2 study[a] (n=17) and one used in the YKL-40 and chitotriosidase study[b] (n=18). IQR = interquartile range; SD = standard deviation. *Ln(chitotriosidase) values were used for analysis.

7.4.2 CSF collection, processing and biomarkers assays

CSF collection and processing were performed as detailed in Chapter 2.2.2.1. All CSF samples had levels of neurodegenerative (T-tau, P-tau and Aβ42) and glia-derived (sTREM2, YKL-40 and chitotriosidase) biomarkers assayed as detailed in Chapters 2.2.2.2 and 2.2.2.3.

7.4.3 CSF biomarker classification

To examine whether glia-derived biomarker levels differed according to the underlying pathology in FTD, rather than just by clinical syndrome (given that individuals with certain FTD syndromes such as lvPPA often have AD rather than FTLD pathology), individuals' CSF neurodegenerative biomarker profiles of T-tau and Aβ42 (Table 7.1) were used to calculate the T-tau/Aβ42 ratio for each participant. This ratio was used to classify all individuals with dementia into two 'pathological' subgroups (Table 7.2): an AD biomarker positive dementia group (ratio ≥1, indicating likely AD pathology), and an AD biomarker negative dementia group (ratio <1, indicating likely FTLD). The conservative cut-off of CSF T-tau/Aβ42 ratio ≥1 was based on a previous study (Paterson et al., 2016). The cognitively normal controls formed a comparison group; all had a ratio of <1.

In all analyses, the AD biomarker positive dementia group consisted of 15 individuals with dementia. As expected, the majority of these had lvPPA (n=11); other diagnoses were nfvPPA (n=2), svPPA (n=1) and PPA-NOS (n=1). The AD biomarker negative dementia group contained the remaining 49 individuals with dementia. No significant difference in age at CSF was seen between the two pathological subgroups and controls (Table 7.2), but median disease duration was shorter in the AD biomarker positive group than the AD biomarker negative group (2.9 versus 4.6 years: P=0.037). There were significantly more males in the AD biomarker negative group (73.4%) compared with controls (54.5% for sTREM2, 38.9% for YKL-40/chitotriosidase) and the

AD biomarker positive (60.0%) group (*P*=0.019 for sTREM2, *P*=0.032 for YKL-40/chitotriosidase).

	Control	AD biomarker negative dementia (CSF T-tau/Aβ42 <1.0)	AD biomarker positive dementia (CSF T-tau/Aβ42 ≥1.0)
Number of participants	17[a] 18[b]	49[+]	15
Male sex, N (% group)	6 (54.5)[a] 7 (38.9)[b]	36 (73.4)	9 (60.0)
Age at CSF (years), Mean (SD)	63.7 (6.4)[a] 64.3 (6.6)[b]	64.1 (6.7)	65.9 (6.0)
Age at onset (years), Mean (SD)	n/a	58.6 (6.8)	62.4 (6.7)
Disease duration at CSF (years) Mean (SD); Median (IQR)	n/a	5.6 (4.1); 4.6 (3.1-6.6)	3.5 (2.1); 2.9 (1.7-5.1)
CSF sTREM2 (ng/ml), Mean (SD)	6.8 (1.6)	6.9 (3.0)	9.0 (3.6)
CSF YKL-40 (ng/ml), Mean (SD)	108.4 (29.9)	124.7 (44.7)	163.2 (66.5)
CSF chitotriosidase (pg/ml), Mean (SD)	1761.6 (1097.8)	3336.0 (4120.5)	5975.1 (4615.5)
Ln(chitotriosidase), Mean (SD)*	7.3 (0.6)	7.8 (0.9)	8.4 (0.8)
CSF Aβ42 (pg/ml), Mean (SD)	1032.2 (214.3)[a] 1028.5 (208.6)[b]	833.9 (265.4)	510.5 (165.7)
CSF T-tau (pg/ml), Mean (SD)	332.6 (82.4)[a] 338.8 (82.1)[b]	373.5 (173.0)	1047.2 (511.3)
CSF P-tau (pg/ml), Mean (SD)	52.7 (10.6)[a] 53.1 (10.4)[b]	44.8 (15.3)	97.0 (34.3)
CSF T-tau/Aβ42 ratio, median (IQR)	0.3 (0.2-0.5)[a] 0.3 (0.2-0.5)[b]	0.4 (0.3-0.7)	1.6 (1.2-3.2)

Table 7.2 Demographics and CSF biomarker levels of control group and dementia groups defined by CSF neurodegenerative biomarker profile.

Data are shown for both control groups, one used in the sTREM2 study[a] (n=17) and one used in the YKL-40 and chitotriosidase study[b] (n=18). IQR = interquartile range; SD = standard deviation. *Ln(chitotriosidase) values were used for analysis. [+]For the chitotriosidase analysis n=47 as two individuals were excluded due to undetectable levels.

7.4.4 Statistical analysis

For sTREM2 and YKL-40, levels were detectable in CSF of all individuals, so analyses were performed on 64 individuals with dementia and 17 (sTREM2) and 18 (YKL-40) controls. However, for chitotriosidase, three individuals (one control, one sporadic bvFTD

and one sporadic nfvPPA) had persistently undetectable levels of chitotriosidase in CSF, despite performing assays again using the same dilution of CSF, and also using more concentrated samples (neat CSF). Approximately 6% of the population possess a homozygous 24 base pair duplication in exon 10 of the *CHIT1* gene, which leads to a complete enzymatic deficiency of chitotriosidase (Boot et al., 1998) and undetectable levels of chitotriosidase in CSF (Abu-Rumeileh et al., 2019). These three individuals were likely to be carriers of this mutation (although confirmation from DNA analysis was not possible) and their levels would unacceptably bias group comparisons if included, or assigned the lower limit of detection, as others have done (Abu-Rumeileh et al., 2019). These three individuals were therefore excluded from the chitotriosidase analysis, leaving 17 (out of 18) controls and 62 (out of 64) individuals with dementia in the analysis. Two of these individuals were in the AD biomarker negative dementia group, therefore 47 rather than 49 individuals were included in the pathological subgroup analysis of chitotriosidase levels.

The following analysis approach was used to compare demographics and biomarker levels between groups and subgroups, and to analyse relationships between glia-derived and neurodegenerative biomarkers, and between glia-derived biomarkers, within groups and subgroups:

1. **Dementia** (all FTD syndromes combined) versus **controls**
2. **Clinical subgroups**, comparing bvFTD, nfvPPA, svPPA, lvPPA, and PPA-NOS and controls
3. **Genetic subgroups**, comparing those with FTD due to *GRN* mutations, *MAPT* mutations, or *C9orf72* expansions and controls
4. **Pathological subgroups**, comparing AD biomarker positive and AD biomarker negative dementia groups, and each group with controls.

All analyses were carried out using STATA version 14, with a significance threshold of $P<0.05$. Shapiro Wilk tests of raw values and Q-Q plots of residuals from multivariable linear regressions were used to test assumptions of normality. The following demographics were compared between all groups and subgroups: age at CSF (using one-way ANOVA), disease duration at CSF (Kruskal Wallis tests with Dunn's test for *post hoc* comparisons, as the distribution was non-parametric) and sex (Chi squared tests).

Assessment of residuals in multivariable linear regression analyses of sTREM2 and YKL-40 levels across groups and subgroups revealed these were normally (parametrically) distributed and met the assumptions required for parametric linear regression analysis. Assessment for chitotriosidase levels revealed these were not parametrically distributed, so chitotriosidase values were natural log (Ln) transformed to produce Ln(chitotriosidase) values, the residuals of which then met assumptions required, so Ln(chitotriosidase) levels were used in all multivariable linear regressions.

First, multivariable linear regressions were used to assess associations of glia-derived biomarker levels with demographic parameters that may influence biomarker levels in group comparisons: age and disease duration at CSF. Associations with age were also analysed adjusted for sex in the control group and both sex and disease duration in the dementia group and clinical and pathological subgroups. Associations with disease duration were also analysed adjusted for age and sex for the dementia group and clinical and pathological subgroups. Interactions between group and age or disease duration were also analysed, to examine whether these associations differed by disease group (none were significant). These analyses were not performed in individual genetic subgroups due to small group size. Glia-derived biomarker levels were also compared between males and females within the whole cohort, within control and dementia groups, and within subgroups (except genetic subgroups), using Mann-Whitney U tests, as raw

values (rather than the residuals examined for regression analyses) were not normally distributed.

Multivariable linear regression analyses were then used to compare levels of glia-derived biomarkers between dementia and controls groups and between clinical, genetic and pathological subgroups, using the numbered analysis approach above. Based on the demographic regression analyses, group comparisons were adjusted for age and sex (for the control group and genetic subgroups) and for age, sex and disease duration (dementia group and clinical and pathological subgroups).

Multivariable linear regressions were also used to investigate the association between levels of each glia-derived biomarker and each neurodegenerative biomarker (T-tau, P-tau and Aβ42) within each group and subgroup (except for genetic groups due to small group size). Due to a non-linear relationship between T-tau levels and both YKL-40 and Ln(chitotriosidase) levels, T-tau values were Ln transformed and regressions performed for YKL-40 and Ln(chitotriosidase) using Ln(T-tau). Associations between YKL-40 and chitotriosidase levels in each group were examined using multivariable linear regressions of Ln(chitotriosidase) and Ln(YKL-40) levels, due a to non-linear relationship between raw YKL-40 values and Ln(chitotriosidase). Associations between sTREM2 levels and YKL-40 or chitotriosidase levels were not analysed as biomarker assays had been carried out on slightly different cohorts.

7.5 Results

7.5.1 Associations between glia-derived biomarkers and demographic parameters

7.5.1.1 Age

sTREM2 was positively associated with age at CSF within the whole cohort (β=0.165, *P*=0.001) and in the dementia group (β=0.189, *P*<0.001) (Figure 7.1a), but not in controls (β=0.061, *P*=0.591). The association with age was generally similar in the majority of clinical subgroups (bvFTD β=0.271, nfvPPA β=0.184, svPPA β=0.217, lvPPA β=0.219, PPA-NOS β=0.003) (Figure 7.1b), but this only reached significance for bvFTD (*P*=0.017). However, after adjusting for sex and disease duration there was no significant difference between the coefficients for age by clinical subgroup (*P*=0.964) suggesting all subgroups had a similarly positive association. sTREM2 was positively associated with age in the AD biomarker positive (β=0.282, *P*=0.043) and negative (β=0.185, *P*=0.006) dementia groups.

YKL-40 was positively associated with age within the whole cohort (β=1.99, *P*=0.018) and in the dementia group (β=1.86, *P*=0.043) but this did not reach significance in controls (β=2.47, *P*=0.169) (Figure 7.1c). Although most of the clinical subgroups apart from nfvPPA and PPA-NOS (Figure 7.1d) and both pathological subgroups appeared to have a positive slope for the association between YKL-40 and age, none reached significance. Chitotriosidase was not significantly associated with age in either the whole cohort (β=0.007, *P*=0.661) or the dementia (β=0.004, *P*=0.904) or control (β=0.008, *P*=0.628) groups (Figure 7.1e), or in any of the clinical (Figure 7.1f) or pathological subgroups.

7.5.1.2 Disease duration

sTREM2 was negatively associated with disease duration in the dementia group (β= -0.235, *P*=0.025) (Figure 7.2a). In the clinical subgroup analysis, sTREM2 was negatively associated with disease duration in bvFTD (β= -0.324, *P*=0.014), but no significant association was seen in other clinical subgroups (Figure 7.2b). Despite considerable heterogeneity in the slopes, there was no significant difference between the coefficients for disease duration by clinical subgroup (*P*=0.275). There was a significant difference in the coefficients for disease duration between the two pathological subgroups (*P*=0.027), with a negative association between sTREM2 and disease duration in the AD biomarker negative dementia group (β= -0.253, *P*=0.018) but a positive association in the biomarker positive group, although this was itself not significant (β=0.604, *P*=0.106). This resulted in the difference in sTREM2 levels between these two groups increasing as disease duration increased (Figure 7.2c).

There were no significant associations between either YKL-40 (Figure 7.2d) or chitotriosidase (Figure 7.2g) and disease duration in the dementia group (YKL-40: β= -1.874, *P*=0.292; Ln(chitotriosidase): β= -0.016, *P*=0.631) or within any of the clinical or pathological subgroups (Figure 7.2e, h, f, i).

7.5.1.3 Sex

sTREM2 levels did not differ by sex within the whole cohort (median: males = 7.08 versus females = 6.85 ng/ml; *P*=0.992), or in controls, dementia, or any of the clinical or pathological subgroups, apart from in the svPPA group, where males had higher sTREM2 levels than females (median = 9.51 versus 4.98 ng/ml; *P*=0.023). YKL-40 and chitotriosidase levels did not differ significantly by sex in the whole cohort or in any group.

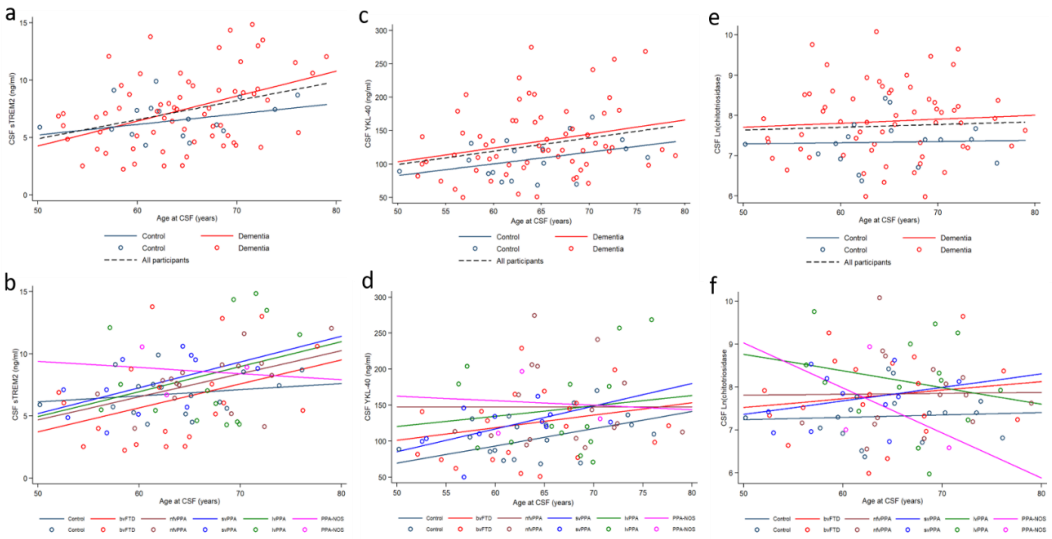

Figure 7.1 Relationships between glia-derived biomarkers and age

Graphs show CSF sTREM2 (**a, b**) YKL-40 (**c, d**) and Ln(chitotriosidase) (**e, f**) levels versus age at CSF in controls and dementia groups (**a, c, e**) and clinical subgroups (**b, d, f**). Lines in (**a, c, e**) are group regression lines adjusted for sex (all participants and controls) and sex and disease duration (dementia group). Lines in (**b, d, f**) are group regression lines for clinical subgroups adjusted for sex and disease duration. See main text for β and *P* values.

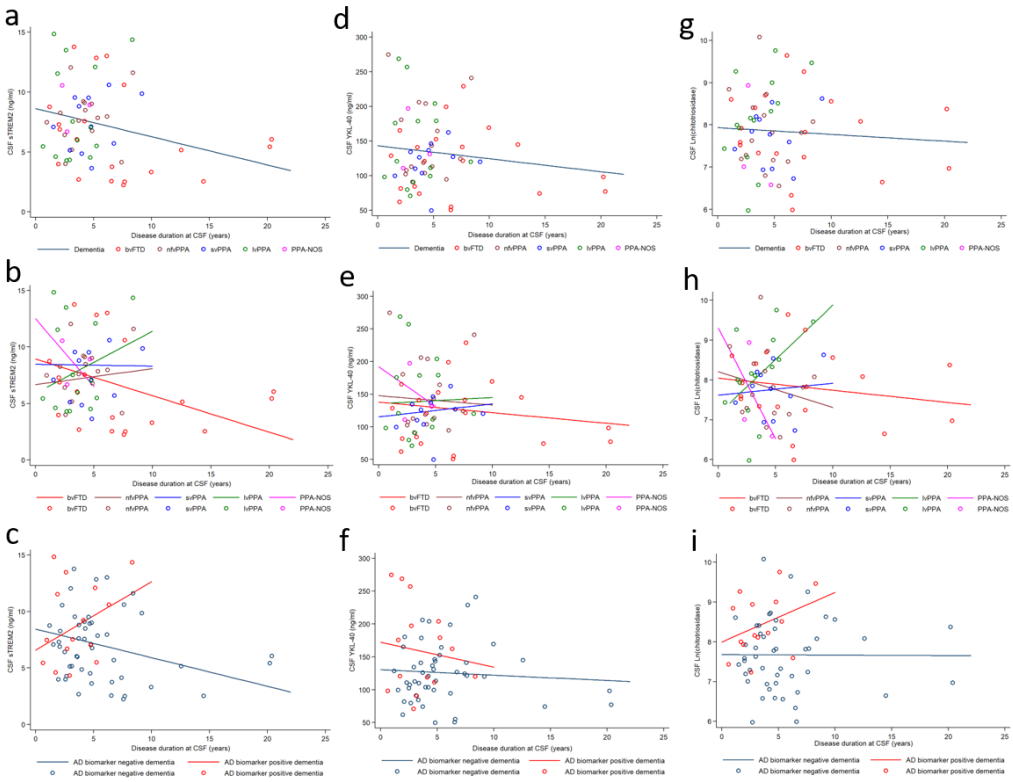

Figure 7.2 Relationships between glia-derived biomarkers and disease duration

Graphs show CSF sTREM2 (**a** - **c**) YKL-40 (**d** - **f**) and Ln(chitotriosidase) (**g** - **i**) levels versus disease duration in the overall dementia group (**a, d, g**), clinical subgroups (**b, e, h**) and pathological subgroups (**c, f, i**). Lines are group regression lines adjusted for age and sex. See main text for β and *P* values.

7.5.2 Group comparisons of glia-derived biomarkers

Glia-derived biomarker levels for each group and subgroup are summarised in Table 7.1 and Table 7.2 and comparisons are illustrated in Figure 7.3. Detailed results of regression analyses comparing levels between all groups and subgroups (including all β and *P* values) are listed in Table 7.3 and so are not repeated in the text.

7.5.2.1 Dementia group versus controls

sTREM2 levels did not significantly differ between the dementia and control groups (Figure 7.3a), but both YKL-40 (Figure 7.3e) and chitotriosidase (Figure 7.3i) levels were significantly higher in the dementia group.

7.5.2.2 Clinical subgroups

sTREM2 levels did not differ between individual clinical subgroups and controls or between any of the clinical subgroups (Figure 7.3b), but YKL-40 levels were raised in individuals with nfvPPA and lvPPA compared with controls (Figure 7.3f). Although individuals with PPA-NOS also had high YKL-40 levels, this did not reach significance compared with controls. No significant differences were seen between YKL-40 levels in bvFTD or svPPA compared with controls, and there were no significant differences between clinical subgroups. Although relatively high chitotriosidase levels were present in all clinical subgroups, this only reached statistical significance in lvPPA when compared with controls, and there were no significant differences between clinical subgroups (Figure 7.3j).

7.5.2.3 Genetic subgroups

The *GRN* group had high levels of all glia-derived biomarkers (Figure 7.3c, g, k). sTREM2 levels were higher in the *GRN* group compared with controls and also compared with *MAPT* and *C9orf72* groups (Figure 7.3c). However, sTREM2 levels were similar in *MAPT* and *C9orf72* groups compared with controls, and between these genetic groups. The *GRN* group had higher levels of YKL-40 compared with controls and the

C9orf72 group, although levels did not differ significantly from the *MAPT* group (Figure 7.3g). The *GRN* group also had much higher levels of chitotriosidase compared with controls, *MAPT* and *C9orf72* groups (Figure 7.3k). The *MAPT* group had higher YKL-40 levels than controls, but levels did not differ significantly from *GRN* or *C9orf72* groups. Chitotriosidase levels in the *MAPT* group were similar to controls and the *C9orf72* group.

7.5.2.4 Pathological subgroups

The AD biomarker positive dementia group had high levels of all glia-derived biomarkers (Figure 7.3d, h, l). There were significantly higher sTREM2 levels in this group compared with the AD biomarker negative group (Figure 7.3d), although when compared with controls, levels did not differ significantly. Differences in sTREM2 levels between the two pathological subgroups was affected by disease duration, with differences becoming more obvious as disease duration increased (Figure 7.2c). There was no difference in sTREM2 levels between the AD biomarker negative group and controls.

YKL-40 and chitotriosidase levels were higher in the AD biomarker positive group compared with controls and also compared with the AD biomarker negative group (Figure 7.3h, l). Although YKL-40 and chitotriosidase levels in the AD biomarker negative group were also generally high, these did not differ significantly when compared with controls (Figure 7.3l).

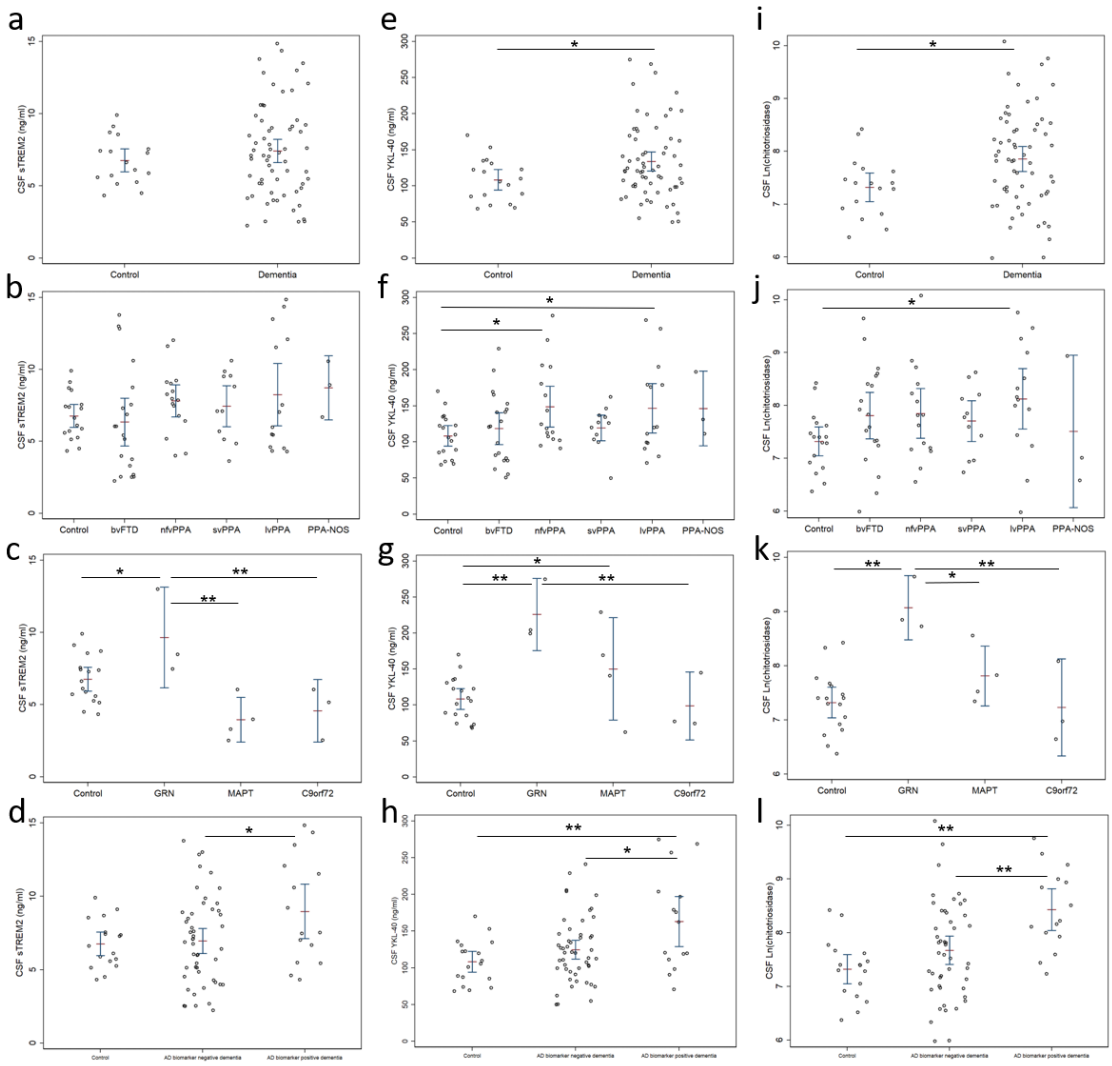

Figure 7.3 Comparison of glia-derived biomarkers between groups

Graphs show how CSF sTREM2 (**a** - **d**), YKL-40 (**e** - **h**) and Ln(chitotriosidase) (**i** - **l**) levels differ between controls and dementia groups (**a, e, i**), clinical subgroups (**b, f, j**), genetic subgroups (**c, g, k**), and pathological subgroups (**d, h, l**). Horizontal bars show mean biomarker levels and 95% confidence intervals for each group. **P*<0.05, ***P*<0.01.

Table 7.3 Detailed comparisons of glia-derived biomarker levels between groups

Mean differences and 95% confidence intervals are β values arising from multivariable linear regressions, adjusted for age and sex (disease groups versus controls), or age, sex and disease duration (between disease groups, except for between genetic subgroups, which were adjusted for age and sex only). The dementia group includes all individuals with FTD (bvFTD and PPA). *Significant at *P*<0.05. ⁺ Difference in sTREM2 levels between pathological subgroups changes with varying disease duration; results of regression analysis comparing these subgroups overall is presented, rather than a specific value for mean difference. SEM: standard error of the mean.

Groups compared	sTREM2 Mean (SEM) difference 95% confidence interval (ng/ml)	*P*	YKL-40 Mean (SEM) difference 95% confidence interval (ng/ml)	*P*	Ln(chitotriosidase) Mean (SEM) difference 95% confidence interval	*P*
Dementia vs. Control	0.638 (0.806) -0.966, 2.244	0.431	31.0 (12.9) 5.23, 56.8	**0.019***	0.522 (0.247) 0.031, 1.01	**0.038***
Clinical subgroups						
bvFTD vs. Control	-0.349 (1.04) -2.41, 1.71	0.736	20.7 (16.9) -12.9, 54.4	0.225	0.414 (0.322) -0.228, 1.06	0.202
nfvPPA vs. Control	0.544 (1.01) -1.47, 2.56	0.592	33.8 (16.5) 5.92, 71.8	**0.021***	0.506 (0.317) -0.126, 1.14	0.115
svPPA vs. Control	1.14 (1.13) -1.11, 3.39	0.314	20.9 (18.7) 16.3, 58.1	0.267	0.362 (0.353) -0.342, 1.07	0.309
lvPPA vs. Control	1.04 (1.04) -1.02, 3.11	0.319	36.3 (17.0) 2.40, 70.2	**0.036***	0.788 (0.321) 0.148, 1.43	**0.017***
PPA-NOS vs. Control	1.84 (1.84) -1.82, 5.50	0.320	47.4 (30.5) -13.2, 108.1	0.124	0.107 (0.571) -1.03, 1.24	0.852
nfvPPA vs. bvFTD	0.305 (1.15) -2.01, 2.62	0.792	12.5 (19.9) -27.3, 52.4	0.531	0.064 (0.386) -0.709, 0.837	0.869
svPPA vs. bvFTD	1.34 (1.19) -1.04, 3.73	0.264	-4.35 (20.6) -45.5, 36.8	0.833	-0.066 (0.388) -0.845, 0.712	0.399
lvPPA vs. bvFTD	0.723 (1.22) -1.73, 3.18	0.557	8.84 (21.1) -33.5, 51.2	0.677	0.339 (0.399) -0.461, 1.14	0.399

PPA-NOS vs. bvFTD	1.23 (1.93) -2.63, 5.09	0.526	21.7 (33.3) -44.9, 88.3	0.517	-0.355 (0.624) -1.61, 0.897	0.571
svPPA vs. nfvPPA	1.04 (1.25) -1.46, 3.54	0.409	-16.9 (21.5) -60.0, 26.2	0.436	-0.130 (0.411) -0.954, 0.693	0.752
lvPPA vs. nfvPPA	0.417 (1.10) -1.79, 2.62	0.706	-3.70 (19.0) -41.8, 34.4	0.846	0.276 (0.360) -0.447, 0.999	0.448
PPA-NOS vs. nfvPPA	0.922 (1.94) -2.96, 4.81	0.636	9.14 (33.5) -57.9, 76.2	0.786	-0.419 (0.631) -1.68, 0.847	0.509
lvPPA vs. svPPA	-0.621 (1.28) -3.19, 1.96	0.631	13.2 (22.2) -31.3, 57.7	0.458 0.555	0.406 (0.415) -0.426, 1.24	0.332
PPA-NOS vs. svPPA	-0.116 (2.02) -4.15, 3.92	0.954	26.0 (34.8) -43.7, 95.7	0.458	-0.289 (0.649) -1.59, 1.01	0.658
PPA-NOS vs. lvPPA	0.505 (1.97) -3.34, 4.45	0.798	12.8 (33.9) -55.2, 80.9	0.707	-0.695 (0.634) -1.96, 0.577	0.278
Genetic subgroups						
Groups compared	**sTREM2 Mean (SEM) difference 95% confidence interval (ng/ml)**	***P***	**YKL-40 Mean (SEM) difference 95% confidence interval (ng/ml)**	***P***	**Ln(chitotriosidase) Mean (SEM) difference 95% confidence interval**	***P***
GRN vs. Control	2.75 (1.16) 0.331, 5.16	**0.028***	111.9 (24.4) 61.5, 162.5	**<0.001***	1.69 (0.366) 0.930, 2.45	**<0.001***
MAPT vs. Control	-2.23 (1.144) -4.61, 0.149	0.065	51.3 (24.2) 1.10, 101.5	**0.046***	0.622 (0.366) -0.138, 1.38	0.104
C9orf72 vs. Control	-1.89 (1.27) -4.53, 0.735	0.149	-9.17 (26.6) -64.3, 45.9	0.733	-0.073 (0.399) -0.903, 0.758	0.857
GRN vs. *MAPT*	4.98 (1.48) 1.89, 8.06	**0.003***	60.7 (31.4) -4.47, 125.8	0.066	1.06 (0.471) 0.088, 2.05	**0.034***
. *GRN* vs. *C9orf72*	4.64 (1.54) 1.45, 7.84	**0.006***	121.2 (32.6) 53.5, 188.8	**0.001***	1.76 (0.489) 0.747, 2.78	**0.002***

C9orf72 vs. *MAPT*	0.334 (1.41) -2.59, 3.26	0.815	60.5 (29.8) -1.36, 122.3	0.055	0.695 (0.448) -0.236, 1.63	0.136
Pathological subgroups						
Groups compared	**sTREM2 Mean (SEM) difference 95% confidence interval (ng/ml)**	***P***	**YKL-40 Mean (SEM) difference 95% confidence interval (ng/ml)**	***P***	**Ln(chitotriosidase) Mean (SEM) difference 95% confidence interval**	***P***
AD biomarker positive dementia vs. Controls	1.92 (0.996) -0.062, 3.91	0.057	55.5 (16.1) 23.5, 87.4	**0.001***	1.09 (0.296) 0.495, 1.67	**<0.001***
AD biomarker negative dementia vs. Controls	0.183 (0.817) -1.45, 1.81	0.823	22.4 (13.1) -3.6, 48.4	0.091	0.318 (0.243) -0.166, 0.802	0.194
AD biomarker positive dementia vs. AD biomarker negative dementia	$F_{(2,58)}=3.77^{+}$	**0.029**$^{*+}$	30.7 (15.2) 0.308, 61.0	**0.048***	0.783 (0.277) 0.227, 1.34	**0.007***

7.5.3 Associations between glia-derived and neurodegenerative biomarkers

Associations between levels of glia-derived biomarkers and neurodegenerative biomarkers (T-tau, P-tau and Aβ42) differed according to clinical syndrome and likely underlying pathology (AD or FTLD).

7.5.3.1 T-tau

sTREM2 was positively associated with T-tau in the dementia (β=0.003, *P*<0.001) and control (β=0.01, *P*=0.033) groups (Figure 7.4a). This association was significant in lvPPA (β=0.005, *P*<0.001) but not in other clinical subgroups (Figure 7.4b). There was a positive association with T-tau in AD biomarker positive (β=0.005, *P*=0.002) and negative (β=0.004, *P*=0.049) dementia groups (Figure 7.4c).

YKL-40 was positively associated with T-tau in the dementia group (β=42.9, *P*<0.001) but not in controls (β=43.9, *P*=0.181) (Figure 7.4d). Most clinical subgroups showed positive slopes for the association between YKL-40 and T-tau (Figure 7.4e), but this only reached significance in bvFTD (β=109.3, *P*<0.001) and nfvPPA (β=69.9, *P*=0.009). Although both pathological subgroups also seemed to have positive slopes (Figure 7.4f), associations were only significant in the AD biomarker negative group (β=62.1, *P*<0.001) and not in the biomarker positive group (β=31.1, *P*=0.49).

Chitotriosidase was positively associated with T-tau in the dementia group (β=0.668, *P*<0.001) but not in controls (β= -0.704, *P*=0.328) (Figure 7.4g). This association was significant in bvFTD (β=1.31, *P*=0.003) and lvPPA (β=0.937, *P*=0.015) but not in other clinical subgroups (Figure 7.4h). Although there were positive slopes for the association between chitotriosidase and T-tau in the AD biomarker negative (β=0.631, *P*=0.051) and biomarker positive (β=0.348, *P*=0.498) groups, neither reached significance (Figure 7.4i).

7.5.3.2 P-tau

sTREM2 was positively associated with P-tau in the dementia group (β=0.038, *P*=0.002) but not in controls (β=0.009, *P*=0.825) (Figure 7.5a). This association was significant in lvPPA (β=0.075, *P*<0.001) but not in other clinical subgroups (Figure 7.5b), and in the AD biomarker positive dementia group (β=0.069, *P*=0.004) but not in the biomarker negative group (β=0.028, *P*=0.284) (Figure 7.5c).

YKL-40 was positively associated with P-tau in the dementia group (β=0.722, *P*<0.001) but not in controls (β=0.676, *P*=0.35) (Figure 7.5d). Most clinical groups showed positive slopes (Figure 7.5e), but associations only reached significance in bvFTD (β=1.75, *P*=0.005) and lvPPA (β=1.02, *P*=0.020). Although both pathological subgroups also had positive slopes (Figure 7.5f), associations were only significant in the AD biomarker negative group (β=1.06, *P*=0.010) and not in the biomarker positive group (β=0.689, *P*=0.236).

Chitotriosidase was positively associated with P-tau in the dementia group (β=0.009, *P*=0.028) but not in controls (β=0.016, *P*=0.274) (Figure 7.5g). This reached significance in lvPPA (β=0.014, *P*=0.043) but not in other clinical subgroups (Figure 7.5h). There were no significant associations in either pathological subgroup: AD biomarker positive (β=0.003, *P*=0.693); AD biomarker negative (β= -0.001, *P*=0.931) (Figure 7.5i).

7.5.3.3 Aβ42

sTREM2 was positively associated with Aβ42 in the dementia group (β=0.003, *P*=0.033), but not in controls (β=-0.0001, *P*=0.958) (Figure 7.6a). This association reached significance in lvPPA (β=0.015, *P*=0.005) but not in other clinical subgroups (Figure 7.6b), and in the AD biomarker negative group (β=0.005, *P*=0.002), but not in the biomarker positive group (β=0.009, *P*=0.083) (Figure 7.6c).

YKL-40 was not significantly associated with Aβ42 in dementia (β= -0.003, *P*=0.907) or control (β=0.011, *P*=0.765) groups (Figure 7.6d), or in most clinical subgroups, except in lvPPA, where there was a significant positive association (β=0.274, *P*=0.025) (Figure 7.6e). There was a positive association in the AD biomarker positive group (β=0.226, *P*=0.041) but not in the biomarker negative group (β=0.002, *P*=0.928) (Figure 7.6f).

Chitotriosidase was negatively associated with Aβ42 in the dementia group (β= -0.0009, *P*=0.044) but not in controls (β= -0.0002, *P*=0.827) (Figure 7.6g). Although most clinical subgroups (except lvPPA) had negative slopes (Figure 7.6h), no associations reached significance. There were no significant associations in either pathological subgroup: AD biomarker positive (β=0.0001, *P*=0.936); AD biomarker negative (β= -0.0004, *P*=0.434) (Figure 7.6i).

7.5.4 Associations between YKL-40 and chitotriosidase

YKL-40 levels were positively associated with chitotriosidase levels within the whole cohort (β=1.008, *P*<0.001), and in the dementia group (β=1.094, *P*<0.001) but not in controls (β=-0.203, *P*=0.774) (Figure 7.7a). There were positive associations in most clinical subgroups (Figure 7.7b), but this reached significance only in bvFTD (β=1.369, *P*=0.007) and nfvPPA (β=1.388, *P*=0.045). Levels were positively associated in the AD biomarker negative dementia group (β=1.226, *P*=0.001) but this did not reach significance in the biomarker positive group (β=0.275, *P*=0.604) (Figure 7.7c).

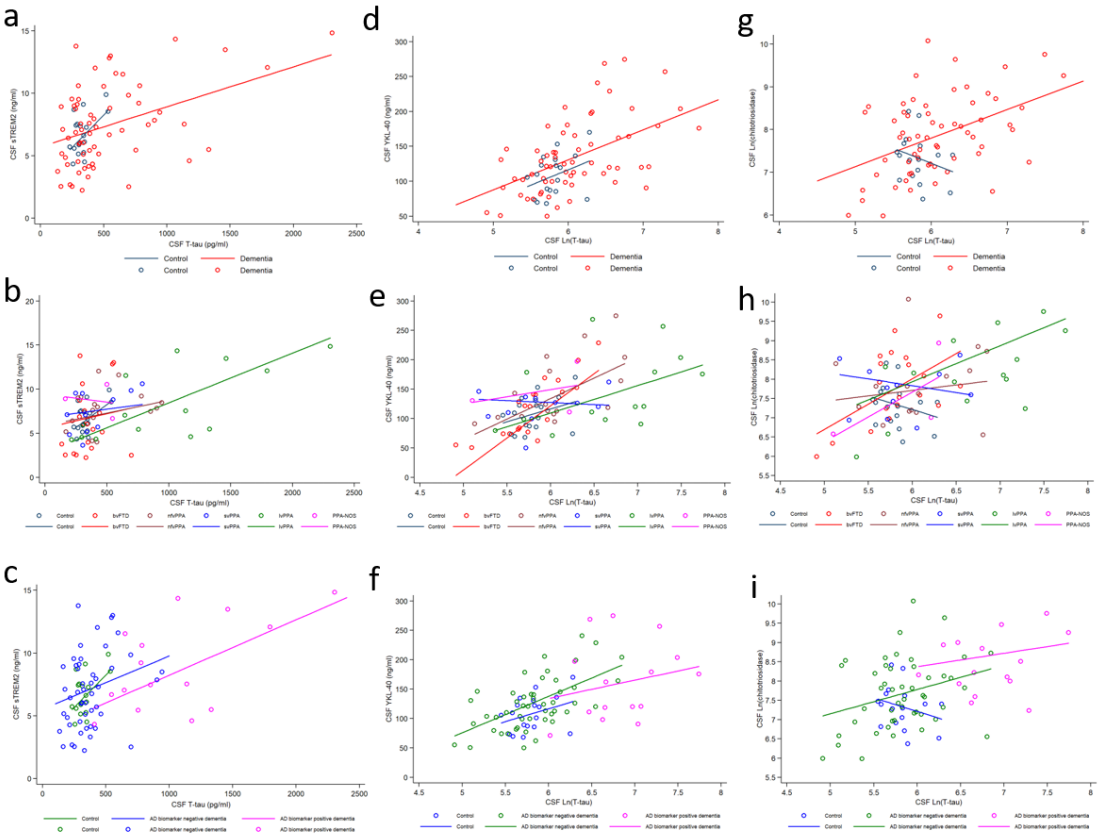

Figure 7.4 Relationships between glia-derived biomarkers and T-tau in CSF

Graphs show associations between CSF sTREM2 and T-tau levels (**a** - **c**), and between CSF YKL-40 and Ln(T-tau) (**d** - **f**) and Ln(chitotriosidase) and Ln(T-tau) (**g** - **i**) levels. Associations are shown for control and dementia groups (**a, d, g**), clinical subgroups (**b, e, h**), and pathological subgroups (**c, f, i**). Lines are group regression lines adjusted for age and sex (controls) and age, sex and disease duration (other groups). See main text for β and *P* values.

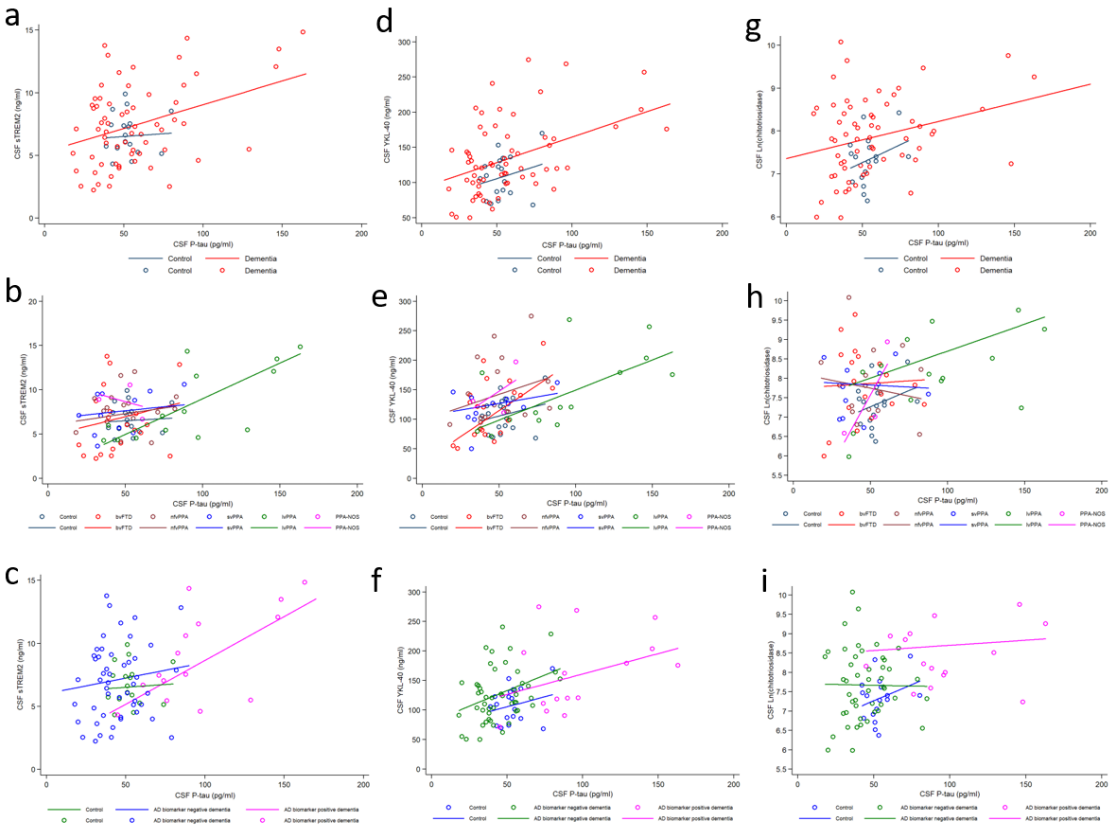

Figure 7.5 Relationships between glia-derived biomarkers and P-tau in CSF

Graphs show associations between CSF P-tau levels and sTREM2 (**a** - **c**), YKL-40 (**d** - **f**) and Ln(chitotriosidase) (**g** - **i**) levels. Associations are shown for control and dementia groups (**a, d, g**), clinical subgroups (**b, e, h**), and pathological subgroups (**c, f, i**) . Lines are group regression lines adjusted for age and sex (controls) and age, sex and disease duration (other groups). See main text for β and *P* values.

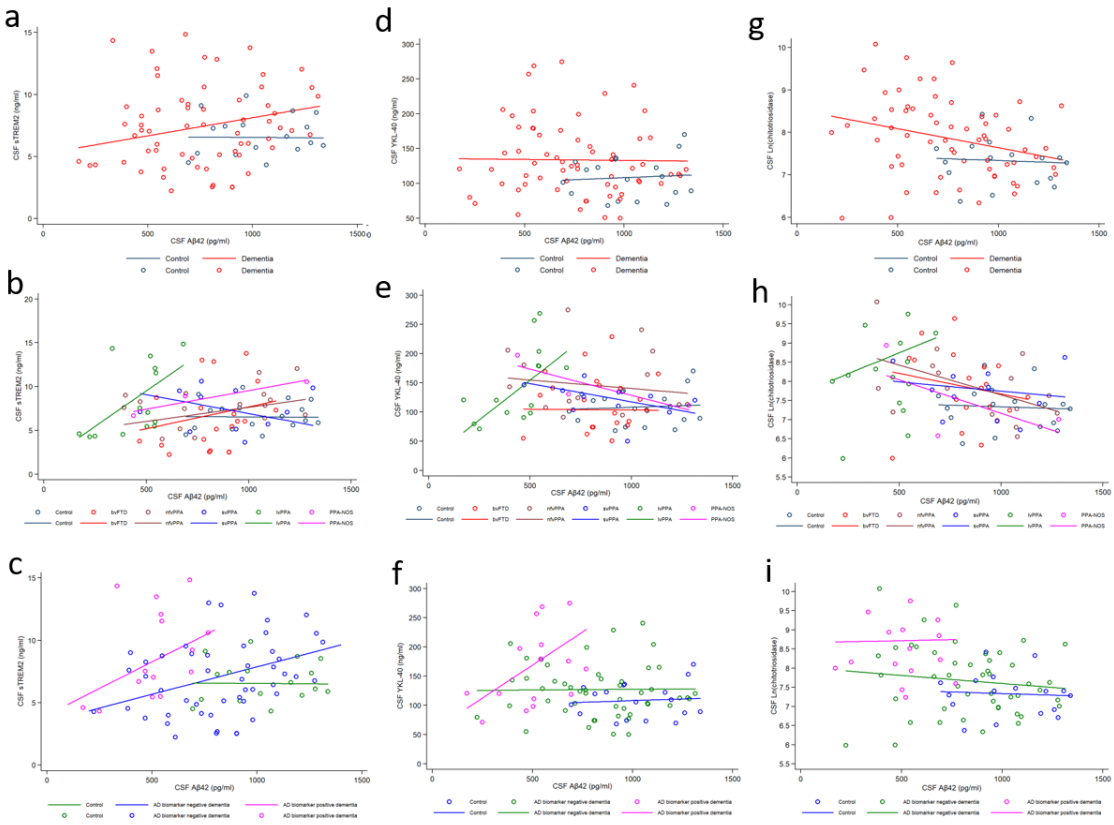

Figure 7.7 Relationships between glia-derived biomarkers and Aβ42 in CSF

Graphs show associations between CSF Aβ42 levels and sTREM2 (**a** - **c**), YKL-40 (**d** - **f**) and Ln(chitotriosidase) (**g** - **i**) levels. Associations are shown for control and dementia groups (**a, d, g**), clinical subgroups (**b, e, h**), and pathological subgroups (**c, f, i**) . Lines are group regression lines adjusted for age and sex (controls) and age, sex and disease duration (other groups). See main text for β and *P* values.

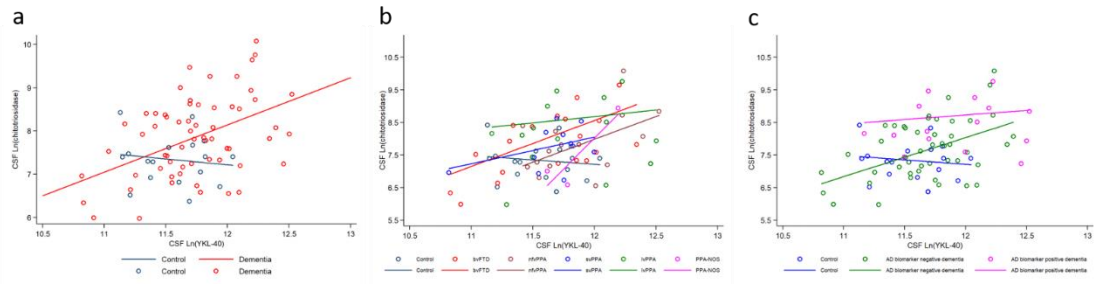

Figure 7.6 Relationships between YKL-40 and chitotriosidase levels in CSF

Graphs show CSF Ln(YKL-40) versus Ln(chitotriosidase) levels for control and dementia groups (**a**), clinical subgroups (**b**) and pathological subgroups (**c**). Lines in (**a**) are group regression lines adjusted for age and sex (controls) and age, sex and disease duration (dementia group). Lines in (**b**) and (**c**) are group regression lines adjusted for age and sex (controls) and age, sex and disease duration (other subgroups). See main text for β and *P* values.

7.6 Discussion

This study examined levels of three glia-derived biomarkers, sTREM2, YKL-40 and chitotriosidase, in the CSF of individuals with dementia clinically consistent with FTD and cognitively normal controls. It assessed how glia-derived biomarker levels were associated with age, disease duration and sex, and compared levels between individuals with dementia and controls, across clinical and genetic subtypes of FTD, and between two different pathological subgroups (individuals with a clinical FTD syndrome but CSF neurodegenerative biomarkers consistent with either AD or FTLD). It also assessed relationships between levels of glia-derived and neurodegenerative (T-tau, P-tau and Aβ42) biomarkers in CSF, and between YKL-40 and chitotriosidase levels. The main findings were as follows:

1) Both sTREM2 and YKL-40 levels, but not chitotriosidase levels, were positively associated with age in individuals with dementia, but only sTREM2 levels were negatively associated with disease duration. Only sTREM2 differed by sex, with higher levels in males than females with svPPA.
2) YKL-40 and chitotriosidase levels, but not sTREM2 levels, were raised in individuals with dementia compared with controls.
3) Levels were not consistently raised across all clinical subtypes of FTD: YKL-40 levels were only significantly raised in lvPPA and nfvPPA, and chitotriosidase levels in lvPPA, but neither were raised in bvFTD, svPPA or PPA-NOS.
4) Levels varied according to underlying pathology: individuals with a clinical FTD syndrome but likely AD pathology not only had higher levels of all glia-derived biomarkers compared with controls, but also higher levels than individuals with likely FTLD. Those with likely FTLD had similar sTREM2 levels, but a suggestion of higher YKL-40 and chitotriosidase levels, compared with controls.

5) All glia-derived biomarkers were markedly raised in individuals with FTD due to *GRN* mutations, and YKL-40 levels were raised in FTD due to *MAPT* mutations, but none were raised in FTD due to *C9orf72* expansions.
6) Glia-derived biomarkers were often positively associated with T-tau, P-tau and Aβ42 levels, but this varied according to clinical diagnosis and likely underlying pathology.
7) YKL-40 and chitotriosidase levels were positively associated in the dementia group overall, and in those with likely FTLD, including bvFTD and nfvPPA.

The positive association of both sTREM2 and YKL-40 levels with age in the dementia group is consistent with previous studies in AD cohorts (Gispert et al., 2016a; Henjum et al., 2016; Janelidze et al., 2016; Piccio et al., 2016; Suárez-Calvet et al., 2016b; Sutphen et al., 2018; Wennström et al., 2015) and FTD cohorts (Alcolea et al., 2017; del Campo et al., 2018; Teunissen et al., 2016). However, these biomarkers were not significantly associated with age in controls, contrary to previous positive associations (Abu-Rumeileh et al., 2019; Henjum et al., 2016; Oeckl et al., 2019; Suárez-Calvet et al., 2016b). There is increased microglial activity with aging, which leads to increased microglial TREM2 expression in brain tissue of healthy individuals (Forabosco et al., 2013), and this may also be the case for YKL-40. However, this effect may be exacerbated in those with neurodegeneration, as activated microglia augment release of sTREM2 as a protective response (Zhong et al., 2019). Chitotriosidase levels were not associated with age, consistent with most other studies of AD and FTD (Abu-Rumeileh et al., 2019; Mattsson et al., 2011; Oeckl et al., 2019; Rosén et al., 2014), suggesting that high levels represent excessive microglial activation or dysfunction related to neurodegeneration, rather than due to age itself.

CSF sTREM2 levels were negatively associated with disease duration in the dementia group, particularly in bvFTD, where the widest range of disease durations was present. However, YKL-40 and chitotriosidase were not significantly associated with disease duration, consistent with another study of YKL-40 in FTD (Alcolea et al., 2017). In the early stages of FTD, sTREM2 levels may rise due to increased release from microglia as a protective response to incipient neurodegeneration, as seen in the early phase of sporadic AD (Ewers et al., 2019; Falcon et al., 2019; Gispert et al., 2016b; Suárez‐Calvet et al., 2018). This may occur many years prior to onset of symptoms, as observed in PMC within longitudinal studies of autosomal dominantly inherited AD (Suárez-Calvet et al., 2016a). Later on in AD, levels decrease, perhaps as microglial TREM2 expression or cleavage of sTREM2 is overwhelmed in the context of widespread dysfunction and senescence of microglia (Nugent et al., 2020; Streit et al., 2018). An alternative explanation is that sTREM2 levels may just be lower in individuals with FTD who have less aggressive disease and hence longer disease durations, and hence could be a biomarker of rate of neuronal injury and disease intensity, like NfL levels are in FTD (Meeter et al., 2016a; Rohrer et al., 2016). However, the lack of longitudinal data precludes exploration of whether levels of sTREM2 rise then fall over the disease course in FTD, and whether YKL-40 or chitotriosidase levels change at different stages of disease from sTREM2 in FTD, as seen in AD (Bos et al., 2019; Nordengen et al., 2019).

Glia-derived biomarker levels did not differ by sex within dementia or control groups, but sTREM2 levels were higher in males with svPPA than females. Most studies of AD or FTD have not found an effect of sex on these biomarkers, although one study found significantly higher sTREM2 levels in males than females with AD (Piccio et al., 2016). It remains unclear whether sex affects these biomarkers, and why this would occur only in svPPA cases, so all analyses were adjusted for sex to account for this uncertainty.

sTREM2 levels in the dementia group were similar to controls, but other studies have found significantly higher (Piccio et al., 2016) or lower (Kleinberger et al., 2014) sTREM2 levels in FTD. However, these studies included few FTD cases, without clearly defined clinical subtypes, and without CSF biomarker confirmation. The large dementia group here included individuals with different clinical FTD syndromes, sporadic and genetic disease mechanisms, and likely AD or FTLD pathology. Significant variability in sTREM2 levels within this diverse group may have led to a non-significant difference compared with controls. Large intragroup variability has been noted in studies of sTREM2 levels in AD, which has limited the utility of sTREM2 to differentiate between AD and controls, despite generally higher levels in AD. sTREM2 levels are also raised in neuroinflammatory (Öhrfelt et al., 2016; Piccio et al., 2008) and other neurodegenerative (Byrne et al., 2018a; Heslegrave et al., 2016) diseases, limiting diagnostic specificity for FTD. Significant variability in sTREM2 levels across the spectrum of FTD supports the histological evidence of microglial heterogeneity across FTLD subtypes identified in Chapters 5 and 6. It may therefore be more useful to monitor sTREM2 levels over time in specific subtypes of FTLD, such as *GRN* mutation carriers, who have more homogenous pathology and, as demonstrated in Chapters 4 to 6, extensive microglial dysfunction.

YKL-40 and chitotriosidase levels were significantly raised in the dementia group versus controls. This is consistent with other studies of FTD (Abu-Rumeileh et al., 2019; Alcolea et al., 2014, 2017; Antonell et al., 2020; Baldacci et al., 2017b; del Campo et al., 2018; Illán-Gala et al., 2018; Janelidze et al., 2016; Oeckl et al., 2019; Steinacker et al., 2018; Teunissen et al., 2016; Vijverberg et al., 2017). However, these cohorts often lacked biomarker or pathological confirmation, so may have also included cases with underlying AD pathology (rather than, or in addition to, FTLD), which would have significantly raised YKL-40 and chitotriosidase levels. Against this, recent studies confirm that pathologically

or genetically confirmed FTD cases have raised CSF YKL-40 (Abu-Rumeileh et al., 2019; Alcolea et al., 2017; Antonell et al., 2020; del Campo et al., 2018; Oeckl et al., 2019; Teunissen et al., 2016) and chitotriosidase (Abu-Rumeileh et al., 2019) levels. As CSF YKL-40 or chitotriosidase levels are increased in a variety of neuroinflammatory and neurodegenerative conditions, including HD (Rodrigues et al., 2016), they likely represent general glial involvement in disease.

sTREM2 levels were not raised in any clinical subgroup, but YKL-40 and chitotriosidase levels were significantly raised in certain clinical subtypes: YKL-40 levels were raised in lvPPA and nfvPPA, and chitotriosidase levels were raised in lvPPA. The PPA-NOS subgroup had high YKL-40 levels, and other clinical subgroups appeared to have high chitotriosidase levels, but these did not reach significance when compared with controls, perhaps due to small sample sizes. There were no significant differences in YKL-40 or chitotriosidase levels between clinical subgroups, although this may have also been limited by group size. No other studies have compared sTREM2 levels between clinical FTD subtypes, and few studies have compared YKL-40 (Abu-Rumeileh et al., 2019; Alcolea et al., 2017; Antonell et al., 2020) or chitotriosidase (Abu-Rumeileh et al., 2019; Steinacker et al., 2018) levels. One study found raised YKL-40 levels in bvFTD, nfvPPA, svPPA and CBS (but not PSPS) compared with controls but no significant differences between subtypes, although individuals with lvPPA were not delineated from an accompanying typical AD group (Alcolea et al., 2017). Another found no difference in YKL-40 levels between bvFTD, nfvPPA and svPPA, and no difference between each subtype and controls (Antonell et al., 2020). Chitotriosidase levels did not differ between bvFTD and PPA or between PPA subtypes in another study (Steinacker et al., 2018), but most PPA subgroups were smaller than here.

However, FTD-MND cases have much higher YKL-40 levels than bvFTD or CBS cases, and higher chitotriosidase levels than CBS or PSPS cases (Abu-Rumeileh et al., 2019). This is likely because MND is associated with highly elevated levels of YKL-40 (Andrés-Benito et al., 2018; Illán-Gala et al., 2018; Oeckl et al., 2019; Sanfilippo et al., 2017; Thompson et al., 2018) and chitotriosidase (Mishra et al., 2017; Oeckl et al., 2019; Steinacker et al., 2018; Thompson et al., 2018; Varghese et al., 2013), as well as sTREM2 (Cooper-Knock et al., 2017). Individuals with clinical diagnoses of MND have higher chitotriosidase levels compared with clinically diagnosed FTD cases (Steinacker et al., 2018), and individuals with pathologically confirmed FTD-MND due to FTLD-TDP have higher chitotriosidase and YKL-40 levels compared with those with FTD alone due to FTLD-TDP (Abu-Rumeileh et al., 2019). This is thought to be due to enhanced activation of certain phenotypes of microglia and astrocytes in the spinal cord in MND (Abu-Rumeileh et al., 2019). The present study therefore deliberately excluded individuals with concurrent MND to avoid confounding results in the FTD group.

The particularly high YKL-40 and chitotriosidase levels in lvPPA and YKL-40 levels in nfvPPA may have been due to more pronounced glial activation in individuals with underlying AD pathology or *GRN* mutations within these groups. The majority (78%) of the lvPPA subgroup had a CSF neurodegenerative biomarker profile consistent with AD (rather than FTLD), and the nfvPPA subgroup contained two individuals with AD-like CSF biomarkers and two individuals with *GRN* mutations. In contrast, most individuals with bvFTD or svPPA had a non-AD CSF biomarker profile and a smaller percentage with (bvFTD) or no (svPPA) *GRN* mutations. The effect of AD pathology was explored further by stratifying the dementia group by CSF neurodegenerative biomarker profile (rather than by clinical diagnoses) into two groups: AD biomarker positive (likely AD group) and AD biomarker negative (likely FTLD group). This confirmed that there were higher levels of YKL-40 and chitotriosidase in the AD group compared with controls, and

higher levels than the FTLD group. sTREM2 levels were also higher in the AD group compared with the FTLD group, although levels did not differ significantly from controls. This suggests that individuals with AD pathology have more significant glial activation or dysfunction than those with FTLD in general, although, as identified in Chapter 5 and 6, this may vary according to FTLD subtype and disease mechanism. This could be due to the presence of soluble phosphorylated tau oligomers in AD cases, which colocalise with microglia, astrocytes and proinflammatory cytokines (Nilson et al., 2017) and are highly toxic to microglia (Sanchez-Mejias et al., 2016). This results in pronounced microglial activation, lysosomal dysfunction and eventual senescence (Musi et al., 2018; Navarro et al., 2018; Sanchez-Mejias et al., 2016; van Olst et al., 2020), which could alter release of glia-derived proteins. In contrast, other studies have shown similarly raised YKL-40 (Abu-Rumeileh et al., 2019; Antonell et al., 2020) and chitotriosidase (Abu-Rumeileh et al., 2019) levels in AD and FTD, although their FTD groups contained many individuals with genetic FTD, including *GRN* mutation carriers, which, as shown here, have highly raised levels of both biomarkers.

Although glia-derived biomarker levels did not differ significantly between the FTLD group and controls overall, many FTLD cases had high levels of YKL-40 and chitotriosidase. There was significant variability in levels across FTLD cases, particularly for chitotriosidase, supporting the histological evidence of microglial heterogeneity according to FTLD subtype identified in Chapters 5 and 6. Other studies have explored this further by stratifying groups of pathologically confirmed FTLD cases, with conflicting results. Both FTLD-tau and FTLD-TDP cases had higher YKL-40 levels than individuals with subjective memory impairment or controls (Alcolea et al., 2017, 2018; Teunissen et al., 2016). However, although one study found higher YKL-40 levels in FTLD-tau than in FTLD-TDP or AD (Alcolea et al., 2018), others have found similar levels in FTLD-TDP and FTLD-tau (Abu-Rumeileh et al., 2019) or only higher YKL-40 levels in FTLD-TDP

(but not FTLD-tau) compared with controls (Alcolea et al., 2017; del Campo et al., 2018). Only one study has examined chitotriosidase levels in FTLD subtypes, demonstrating higher levels in FTLD-TDP than FTLD-tau (Abu-Rumeileh et al., 2019). Differences in the number of genetic FTD cases in FTLD subgroups or inclusion of individuals with co-pathology are likely to have contributed to these disparities between studies. Most FTLD-TDP cohorts included individuals with concurrent MND, or *GRN* mutation carriers, who have highly elevated levels of both biomarkers. Most FTLD-tau cohorts included *MAPT* mutation carriers, who (as shown here) have significantly raised YKL-40 levels. This variability in levels according to pathology or disease mechanism has implications for use of these biomarkers in research studies and clinical trials for a disease as pathologically diverse as FTLD.

Although it was not possible to divide the dementia group into FTLD subtypes due to a lack of cases with pathological confirmation, inclusion of a small number of patients with genetic FTD enabled an exploratory analysis of glia-derived biomarker levels in individuals with known pathology (FTLD-TDP: *GRN* or *C9orf72* mutations, or FTLD-tau: *MAPT* mutations), and also differing disease mechanisms despite similar pathology (*GRN* and *C9orf72* mutations). This showed that all glia-derived biomarkers were markedly raised in the *GRN* group, and YKL-40 levels were raised in the *MAPT* group, compared with controls, but none were raised in the *C9orf72* group. Levels also differed between genetic subtypes: the *GRN* group had higher levels of sTREM2 and chitotriosidase than *MAPT* and *C9orf72* groups, and higher YKL-40 levels than the *C9orf72* group. Few studies have examined glia-derived biomarkers in genetic FTD (Abu-Rumeileh et al., 2019; Antonell et al., 2020; Barschke et al., 2020; Oeckl et al., 2019). One study measured CSF chitotriosidase and YKL-40 levels in symptomatic *GRN, MAPT* and *C9orf72* mutation carriers, but levels were not compared between individual genetic subtypes or between each subtype and controls (Abu-Rumeileh et al.,

2019). Another study found similar YKL-40 levels in genetic FTD overall to controls, but this did not separate genetic subtypes either (Antonell et al., 2020). Another mixed genetic FTD cohort had similar YKL-40 and chitotriosidase levels to controls, but genetic subtypes were again not compared (Oeckl et al., 2019). This cohort also contained a significant proportion of *C9orf72* expansions carriers (15/23), who (as shown here) have similar levels of both biomarkers to controls. A more recent study found that CSF chitotriosidase levels in FTD cases with *C9orf72* expansions were similar to controls, but lower than in MND cases with *C9orf72* expansions (Barschke et al., 2020).

The markedly raised levels of all glia-derived biomarkers in the *GRN* mutation group are consistent with multiple studies showing elevated levels of other inflammatory biomarkers in CSF or blood of *GRN* mutation carriers (Benussi et al., 2020; Bossù et al., 2011; Galimberti et al., 2015; Gibbons et al., 2015; Heller et al., 2020; Miller et al., 2013) and the significant microglial dysfunction and activation in *GRN* -/- mouse models (Lui et al., 2016; Martens et al., 2012; Tanaka et al., 2013a, 2013b, 2014; Wils et al., 2012; Yin et al., 2009, 2010). This supports the increased burden of phagocytic microglia in FTLD-*GRN* cases in Chapter 5, and severe microglial dystrophy in Chapter 6, suggestive of extensive senescence. Both progranulin and TREM2 are expressed by microglia, but they regulate microglial function and immune pathways in opposite ways (Götzl et al., 2019). *GRN* -/- mice have upregulated TREM2 gene expression and excessive synaptic pruning, mediated by aberrantly activated microglia (Lui et al., 2016). As sTREM2 enhances microglial activation, proliferation, migration, survival and phagocytosis (Zhong et al., 2017, 2019), raised CSF sTREM2 levels in *GRN* mutation carriers may initially be due to augmented release as a protective mechanism, as seen in AD. However, if sTREM2 levels remain chronically raised this could exacerbate neuronal damage through a persistently heightened microglial response and excessive phagocytosis.

GRN mutation carriers also display significant microglial lysosomal dysfunction (Götzl et al., 2014; Ward et al., 2017), due to the role of progranulin in lysosomal homeostasis, which could alter delivery of glia-derived proteins to the cell membrane or release into CSF. In the lysosomal storage disorder Gaucher's disease, where macrophage lysosomes are overwhelmed by accumulation of the sphingolipid glucocerebroside (Jian et al., 2018), both plasma (Hollak et al., 1994) and CSF (Zigdon et al., 2015) chitotriosidase levels are highly elevated. Given that *GRN* mouse models show lipid accumulation in microglia (Evers et al., 2017; Marschallinger et al., 2020; Nguyen et al., 2018), elevated CSF chitotriosidase levels in *GRN* mutation carriers may represent chronic microglial dysfunction due to lipid mishandling. Serum YKL-40 levels are also raised (and serum progranulin levels reduced) in Gaucher's disease, and recombinant progranulin reduces serum YKL-40 levels in *GRN* -/- mice and fibroblasts from patients with Gaucher's disease (Jian et al., 2018). This strengthens the link between progranulin haploinsufficiency, lipid mishandling, lysosomal dysfunction, glial dysfunction, and augmented release of glia-derived biomarkers in *GRN* mutation carriers with FTD.

Another marker of activated astrocytes, GFAP, is highly elevated in the plasma of symptomatic *GRN* mutation carriers, but not in *MAPT* or *C9orf72* mutation carriers (Heller et al., 2020). This suggests there is a mutation-specific effect of progranulin haploinsufficiency on glia, supported by the particularly severe dystrophy in FTLD-*GRN* cases in Chapter 6. This may explain the higher levels of sTREM2, YKL-40 and chitotriosidase in the *GRN* group compared with the *C9orf72* group, and the similar levels of all glia-derived biomarkers in the *C9orf72* group to controls, as observed elsewhere for chitotriosidase (Barschke et al., 2020). The extensive glial and immune dysfunction observed in *C9orf72* -/- mouse models is not present in heterozygous mice (Burberry et al., 2016, 2020; O'Rourke et al., 2016; Sudria-Lopez et al., 2016), so may not be present in human heterozygous expansion carriers. There is also marked variability in the degree

of immune dysfunction and microglial activation in *C9orf72* mouse models, modified by the mouse gut microbiome (Burberry et al., 2020). This may also be present in humans *C9orf72* expansion carriers, so environmental factors could modify glial dysfunction. This may contribute to significant variability in neuroinflammatory mechanisms, glia-derived biomarker levels and clinical phenotypes within groups of individuals with the same mutation.

CSF YKL-40 levels were also raised in the *MAPT* group compared with controls, consistent with elevated YKL-40 levels in FTLD-tau groups in other studies (Abu-Rumeileh et al., 2019; Alcolea et al., 2017; Teunissen et al., 2016). Activated or dysfunctional microglia and astrocytes colocalise with tau oligomers or aggregates in *MAPT* P301S mutation mouse models (Bellucci et al., 2004; Brelstaff et al., 2018; Nilson et al., 2017; van Olst et al., 2020) and patients with *MAPT* P301S mutations (Bellucci et al., 2011). There is pronounced microglial activation in the temporal lobes in histological studies of symptomatic *MAPT* 10+16 mutation carriers, as demonstrated in Chapter 5 and previously (Lant et al., 2014), and in microglial PET studies (Bevan-Jones et al., 2019). This suggests that tau pathology in *MAPT* mutation carriers promotes YKL-40 release through microglial (and perhaps astrocytic) activation or dysfunction. sTREM2 levels in the *MAPT* group were similar to controls, but lower than in the *GRN* group. Chitotriosidase levels were slightly raised in the *MAPT* group (but did not reach significance) compared with controls, although lower than in the *GRN* group. There could be less lysosomal dysfunction or lipid mishandling in *MAPT* than *GRN* mutation carriers, but replication in a larger cohort is needed to clarify these preliminary findings.

In order to explore further how glial activation or dysfunction link to neurodegeneration, this study examined relationships between levels of glia-derived biomarkers and neurodegenerative biomarkers that are used in clinical practice and which reflect

neuronal injury (T-tau), hyperphosphorylated tau (P-tau) and amyloid pathology (Aβ42). Overall, levels of all glia-derived biomarkers were positively associated with T-tau and P-tau levels in the dementia group, but this only reached significance in certain clinical or pathological subgroups. Unsurprisingly, sTREM2 levels were positively associated with T-tau and P-tau in those with underlying AD pathology (lvPPA and AD groups) but also with T-tau in the FTLD group. This is consistent with associations between sTREM2 and T-tau and/or P-tau levels in amnestic AD (Gispert et al., 2016b; Heslegrave et al., 2016; Suárez-Calvet et al., 2016b, 2019), suggesting sTREM2 rises in the context of neuronal injury, but particularly due to hyperphosphorylated tau pathology. However, the association with T-tau (but not P-tau) levels in those with likely FTLD indicates that sTREM2 levels also rise in the context of neuronal injury without concurrent AD pathology. There was a small but significant positive association between sTREM2 and Aβ42 levels in the dementia and lvPPA groups, perhaps as sTREM2 is released to bind to accumulating Aβ42 oligomers, as seen in mouse models of AD (Zhong et al., 2019). Surprisingly, there was also a positive association between sTREM2 and Aβ42 in the FTLD group, but not in the AD group. It is unclear why, although there is altered clearance of some amyloid species in the context of FTLD pathology (Illán-Gala et al., 2019).

As expected, YKL-40 levels were associated with T-tau and P-tau in the dementia group, and in bvFTD (both markers), nfvPPA (T-tau only) and lvPPA (P-tau only), as well as in the FTLD group (both markers), but surprisingly not in the AD group. Chitotriosidase levels were associated with T-tau and P-tau in the dementia group and in lvPPA (both markers) and bvFTD (T-tau only). However, associations did not reach significance in either the FTLD or AD group. YKL-40 levels were not significantly associated with Aβ42 in dementia overall but were positively associated in lvPPA and AD groups. There was a negative association between chitotriosidase and Aβ42 in the dementia group, but this

did not reach significance in any subgroups. These variations in associations across groups may be explained by differing underlying pathologies (FTLD subtypes or AD) in individuals within each group being associated with varying degrees of glial dysfunction, neurodegeneration and tau or amyloid pathology. Small sample sizes may have also limited power to detect significant associations in some subgroups.

Positive associations between YKL-40 or chitotriosidase and T-tau or P-tau in CSF have been identified in many studies of typical AD (Abu-Rumeileh et al., 2019; Alcolea et al., 2014; Antonell et al., 2014; Craig-Schapiro et al., 2010; Olsson et al., 2013; Sutphen et al., 2018; Zhang et al., 2018), linking neuronal injury and hyperphosphorylated tau pathology to glial dysfunction. Consistent with this, there was a strong association between levels of both YKL-40 and chitotriosidase and P-tau in the lvPPA subgroup, where most individuals had AD-like biomarkers. However, associations did not reach significance in the AD group overall, perhaps due to high levels of all biomarkers or small group size. Studies of pathologically or genetically confirmed FTLD have found strong associations between YKL-40 (Abu-Rumeileh et al., 2019; Craig-Schapiro et al., 2010; Teunissen et al., 2016) or chitotriosidase (Abu-Rumeileh et al., 2019) and T-tau, but no associations with P-tau. Similar results in the 'FTLD group' here support hypotheses that release of YKL-40 or chitotriosidase by glial cells is linked to neuronal injury in the absence of AD pathology. In a study of individuals with HD, CSF YKL-40 levels were also associated with T-tau (Rodrigues et al., 2016), extending this relationship to other neurodegenerative diseases.

This study also analysed associations between YKL-40 and chitotriosidase levels. There was a strong positive association between levels of both biomarkers in the dementia group overall, and in most clinical subgroups, although this reached significance only in bvFTD and nfvPPA. Levels of YKL-40 and chitotriosidase were also highly associated in

the FTLD group, but this did not reach significance in the AD group, either due to high levels of both biomarkers in most individuals, or smaller group size. These results are consistent with other studies identifying positive correlations between YKL-40 and chitotriosidase in AD (Abu-Rumeileh et al., 2019; Mattsson et al., 2011), FTD (Abu-Rumeileh et al., 2019) and a mixed genetic MND and FTD cohort (Oeckl et al., 2019). Astrocytic and microglial activation or dysfunction therefore appear to arise in tandem in FTLD.

In conclusion, CSF YKL-40 and chitotriosidase (but not sTREM2) levels were raised in individuals with dementia clinically consistent with FTD, suggesting extensive astrocytic and microglial activation or dysfunction in the context of neurodegeneration. However, due to significant variability across cases, levels of these biomarkers are likely not going to be useful for differentiating between individuals with FTD and healthy controls, or for delineating clinical subtypes of FTD. Levels of all three glia-derived biomarkers were higher in genetic FTD due to *GRN* mutations (albeit within a small preliminary cohort) and YKL-40 was higher in genetic FTD due to *MAPT* mutations, so these may be useful to explore further in individuals with presymptomatic or symptomatic genetic FTD. Levels of all three biomarkers were predominantly higher in individuals with a clinical syndrome consistent with FTD but due to underlying AD, rather than FTLD, pathology, perhaps due hyperphosphorylated tau pathology promoting more glial dysfunction than TDP-43 or tau pathology. As levels of all three biomarkers were consistently associated with a measure of neuronal injury (T-tau) in those with likely FTLD, and as YKL-40 and chitotriosidase levels were highly correlated, these biomarkers may represent the response (or contribution) of dysfunctional astrocytes and microglia to burgeoning pathology or neurodegeneration in FTLD.

7.7 Limitations and future work

Limitations of this study include the small size of certain subgroups, particularly genetic subgroups, which may have sometimes limited power to detect significant differences in biomarker levels. However, this is inherent to a rare disease such as FTD, which has multiple phenotypes, and is difficult to avoid when analysing biomarker levels across a broad spectrum of disease, while confining CSF collection and biomarker analysis to one site in order to minimise inter-centre variation.

The dementia group contained both individuals with a clinical diagnosis of an FTD syndrome likely due to FTLD (bvFTD, svPPA and nfvPPA) and those more commonly associated with AD pathology (lvPPA). The use of clinical diagnosis rather than pathological confirmation as an inclusion criterion meant a combination of different pathologies and mutations in the dementia group is likely to have affected YKL-40 and chitotriosidase levels in this group overall. However, it was possible to dissect out differences in biomarker levels between broad pathological (FTLD versus AD) and genetic (*GRN*, *C9orf72* and *MAPT*) entities through stratification of the FTD group by CSF biomarker profile and through a preliminary analysis by mutation type. A stringent cut-off of T-tau/Aβ42 ratio ≥1.0 as 'likely AD' was used to minimise misclassification of individuals with concurrent or primary AD pathology into the FTLD group, as employed previously (Paterson et al., 2016). In addition, all individuals with FTD were phenotyped in detail, meeting strict diagnostic criteria for bvFTD (Rascovsky et al., 2011) or PPA (Gorno-Tempini et al., 2011).

Future studies should analyse CSF sTREM2, YKL-40 and chitotriosidase levels within larger cohorts of individuals with sporadic FTD, ideally in pathologically confirmed cases. Exploration of relationships between baseline and longitudinal measurements of glia-derived biomarkers, and other biomarkers of disease intensity (such as serum or CSF

NfL levels or frontal lobe atrophy rate) would also enable determination of whether glia-derived biomarkers in CSF can be used as biomarkers of disease intensity in sporadic FTD. Inclusion of a larger number of genetic FTD cases with mutations in *GRN, C9orf72* and *MAPT* would be helpful to link glial processes to known pathology and disease mechanisms and would enable confirmation of preliminary observations of higher biomarker levels in symptomatic *GRN* and *MAPT* mutation carriers. Assessment of levels in PMC could establish if, and when, levels change prior to expected symptom onset. This could help to determine whether these biomarkers might be used to predict disease proximity in genetic FTD, maximising the chance of intervening with treatments in clinical trials before significant neurodegeneration occurs. The study in Chapter 8 explored this further.

7.8 Publications relating to this chapter

The work presented in this chapter was published sequentially as two separate papers, but figures and tables within both publications were significantly adapted for use in this chapter to present results of all three biomarker analyses concurrently:

Woollacott IOC et al. (2018) Cerebrospinal fluid soluble TREM2 levels in frontotemporal dementia differ by genetic and pathological subgroup. *Alzheimers Res Ther.* 10:79

Woollacott IOC et al. (2020) Cerebrospinal Fluid YKL-40 and Chitotriosidase Levels in Frontotemporal Dementia Vary by Clinical, Genetic and Pathological Subtype. *Dement Geriatr Cogn Disord,* 49:56-76.

8 CSF glia-derived biomarkers in symptomatic and presymptomatic genetic FTD

8.1 Chapter summary

Introduction: Chronic glial dysfunction may contribute to the pathogenesis of genetic FTD due to *GRN, C9orf72* or *MAPT* mutations. Preliminary examination of levels of three glia-derived biomarkers (sTREM2, YKL-40 and chitotriosidase) in CSF within a small genetic FTD cohort identified that patients with *GRN* mutations have raised levels of all biomarkers and patients with *MAPT* mutations have raised YKL-40 levels. This study assessed levels of these biomarkers in CSF of a larger genetic FTD cohort and in PMC of *GRN, C9orf72* or *MAPT* mutations to determine whether levels vary according to mutation type and whether, and when, levels change presymptomatically.

Methods: Immunoassays were used to measure levels of sTREM2, YKL-40 and chitotriosidase in CSF of 183 individuals: 36 patients with genetic FTD (13 *GRN*, 15 *C9orf72* and 8 *MAPT*), 83 PMC (36 *GRN*, 32 *C9orf72* and 15 *MAPT*) and 64 mutation negative controls. Associations of biomarker levels with age and disease duration were analysed, and levels were compared between patients, PMC and controls overall, and separately for each genetic subtype (*GRN, C9orf72* and *MAPT*). Levels were also compared between patients and early PMC (age at CSF >10 years from expected symptom onset [EYO]) and late PMC (<10 EYO) for each genetic subtype. Associations of biomarker levels with EYO were analysed in all mutation carriers versus controls, for each genetic subtype, to explore whether and when presymptomatic changes in levels occurred.

Results: CSF sTREM2 and YKL-40 (but not chitotriosidase) levels were positively associated with age in all groups. sTREM2 levels were negatively associated with

disease duration in *MAPT* patients. Chitotriosidase levels were higher in patients compared with PMC and controls overall, but only in *GRN* and *MAPT* (and not *C9orf72*) mutation carriers. Chitotriosidase levels were also higher in *GRN* and *MAPT* patients than respective late PMC. sTREM2 and YKL-40 levels were similar across groups once adjusted for age and sex. In *GRN* mutation carriers, chitotriosidase levels were significantly raised from six EYO compared with controls, whereas YKL-40 levels were significantly raised from between one and zero EYO. *MAPT* mutation carriers appeared to have high chitotriosidase levels from three EYO onwards, although levels did not differ significantly from controls at any timepoint.

Conclusions: CSF chitotriosidase levels are raised in *GRN* mutation carriers, differing from controls from six years before expected onset. YKL-40 levels in *GRN* mutation carriers differ from controls from between one to zero years before expected onset, but do not seem significantly raised in symptomatic individuals. CSF chitotriosidase levels are raised in patients with FTD due to *MAPT* mutations and may rise presymptomatically. CSF sTREM2 levels are not raised in presymptomatic or symptomatic genetic FTD. CSF chitotriosidase and YKL-40 may be promising biomarkers of disease proximity in *GRN* or *MAPT* mutation carriers, reflecting different phases of glial activation or dysfunction.

8.2 Introduction

Genetic FTD provides a unique opportunity to examine the pathogenesis and evolution of FTLD over time, including how chronic neuroinflammation and glial dysfunction contribute to disease in individuals with known pathology. Studying biomarkers in blood or CSF from PMC and patients with different mutations (*GRN, C9orf72* or *MAPT*) allows appreciation of how and when biomarkers of these processes are altered, and how this may be linked to the underlying mutation or pathology. As discussed in Chapter 1.3.4, raised levels of inflammatory biomarkers such as proinflammatory cytokines have been found in CSF or blood in genetic FTD cohorts, but few studies have examined glia-

derived biomarkers. Levels of astrocyte-derived GFAP are raised in CSF, serum or plasma in sporadic FTD (Abu-Rumeileh et al., 2019; Benussi et al., 2020; Ishiki et al., 2016; Marelli et al., 2020; Oeckl et al., 2019), but few have examined GFAP levels in genetic FTD (Benussi et al., 2020; Heller et al., 2020; Oeckl et al., 2019). Plasma (Heller et al., 2020) or serum (Benussi et al., 2020) GFAP levels are elevated in *GRN* mutation carriers with FTD, with levels rising just prior to expected onset in *GRN* PMC who are converting to the symptomatic phase (Heller et al., 2020). This suggests that glial dysfunction is detectable presymptomatically in *GRN* mutation carriers and this could be indicative of immediate disease proximity. Although another study found similar CSF GFAP levels in a mixed group of PMC of FTD-associated mutations compared with controls, levels were not explored in separate genetic groups (Oeckl et al., 2019).

It would, however, be more useful to identify glia-derived biomarkers that change much earlier on in the presymptomatic phase of genetic FTD (rather than just prior to conversion), given that glial dysfunction may occur well before symptom onset, and this could be targeted with future therapies. In PMC within longitudinal dominantly inherited AD cohorts there are raised CSF sTREM2 levels five years before expected onset compared with controls, suggesting sTREM2 could be useful as a biomarker of disease proximity in presymptomatic AD (Suárez-Calvet et al., 2016a). However, studies of sTREM2 and other glia-derived biomarkers (YKL-40 and chitotriosidase) are lacking in genetic FTD. No studies (other than in Chapter 7) have examined sTREM2 levels in genetic FTD, and only a few have examined YKL-40 or chitotriosidase levels, but this was in mixed genetic FTD cohorts (Abu-Rumeileh et al., 2019; Antonell et al., 2020; Oeckl et al., 2019), leading to variable results, or only in *C9orf72* expansion carriers (Barschke et al., 2020). In addition, no studies (other than Chapter 7) have compared levels between different genetic FTD subtypes. Only two studies have examined microglia-derived biomarkers in CSF of PMC with FTD-associated mutations, finding

similar YKL-40 or chitotriosidase levels to controls, most likely as PMC groups contained different mutation types, without comparison between these (Antonell et al., 2020; Oeckl et al., 2019).

Given the mounting evidence from Chapters 4 to 7 and other studies that microglial activation and dysfunction contribute to genetic FTD, and given insufficient examination of glia-derived biomarkers in genetic FTD and PMC so far, exploration of sTREM2, YKL-40 and chitotriosidase levels in CSF was needed within a large genetic FTD cohort and in PMC who are at varying proximities to expected symptom onset. Levels should be compared between patients and PMC with different mutation types (*GRN, C9orf72* and *MAPT*), as well as with mutation negative controls. This could establish whether levels of glia-derived biomarkers vary according to the genetic subtype (providing insights into disease pathogenesis) and determine whether and when levels change presymptomatically (useful for predicting disease proximity to benefit clinical practice and clinical trials).

8.3 Aims and hypotheses

This study aimed to carry out a comprehensive assessment of sTREM2, YKL-40 and chitotriosidase levels in the CSF of patients with genetic FTD due to mutations in *GRN, C9orf72* or *MAPT*, and in PMC of these mutations, compared with mutation negative controls (called controls for brevity). The overarching hypothesis was that there is glial dysfunction in genetic FTD, and that this occurs some time before onset of symptoms, so levels of glia-derived biomarkers will be raised in CSF of symptomatic mutation carriers, as well as at some point in PMC, compared with controls.

Specific hypotheses were that levels of sTREM2, YKL-40 and chitotriosidase in CSF will differ between:

1. Patients with genetic FTD and controls, due to increased glial dysfunction due to *GRN, C9orf72* or *MAPT* mutations, or associated with neurodegeneration itself.
2. Patients with mutations in different genes (*GRN, C9orf72* or *MAPT*), due to their different roles in glial function, with *GRN* mutation carriers particularly likely to have raised levels.
3. Patients and PMC within each mutation group, due to more extensive glial dysfunction in symptomatic than presymptomatic individuals.
4. PMC and controls, due to glial dysfunction arising several years before onset of symptoms in mutation carriers.

In addition, this study hypothesised that if levels of these biomarkers are raised presymptomatically, this may differ:

1. Between different genetic subtypes of PMC (*GRN, C9orf72* or *MAPT*), due to their different roles in glial function, with *GRN* PMC particularly likely to have raised levels presymptomatically.
2. Between PMC who are close to predicted symptom onset ('late PMC') and PMC who are many years away from onset ('early PMC'), due to increasing glial dysfunction throughout the disease process.
3. Between mutation carriers and controls at a certain timepoint in the presymptomatic phase; this timepoint may vary according to the genetic subtype.

8.4 Methods

8.4.1 Participants

The cohort consisted of 183 participants (Table 8.1). There were 119 mutation carriers (49 *GRN*, 47 *C9orf72* and 23 *MAPT*) and 64 mutation negative controls (controls). Of the 119 mutation carriers, 36 were symptomatic patients with FTD at the time of CSF collection, due to mutations in either *GRN* (n=13)*, C9orf72* (n=15), or *MAPT* (n=8) and

83 were PMC who had mutations in *GRN* (n=36), *C9orf72* (n=32) or *MAPT* (n=15). The 64 controls were relatives of patients or PMC (27 from *GRN* families, 25 from *C9orf72* and 12 from *MAPT*) who lacked mutations in these genes.

34 out 36 patients were recruited from multiple sites participating in GENFI (UCL and 13 external sites), and two patients were recruited from the prospective CSF study at the UCL DRC (one *GRN* and one *MAPT* mutation carrier), as detailed in Chapter 2.1.2. All patients met consensus diagnostic criteria for a definite FTD syndrome; most had either bvFTD or PPA, but one had CBS (*GRN*), one PSPS (*C9orf72*), and one FTD-MND (*C9orf72*). Patients with MND alone were excluded to ensure a focus on how glia-derived biomarkers are altered in genetic FTD. *GRN* mutations in patients included (n): IVS7-1G>A (three), T272fs (two), C31fs (two), and one each of: S78fs, S82fs, C253X, C482X, del*GRN*(Tubingen) and A350fs. *MAPT* mutations in patients included: R406W (four), 10+16 (two), Q351R (one) and P301L (one). All patients with *C9orf72* expansions were heterozygous carriers. All participants from GENFI underwent clinical and neuropsychological assessments, neuroimaging, and genetic testing on a research basis as detailed in Chapter 2.1.2.

PMC and controls were recruited from multiple sites participating in GENFI (UCL and 13 external sites) as detailed in Chapter 2.1.2. All underwent clinical and neuropsychological assessments, neuroimaging, and genetic testing on a research basis as detailed in Chapter 2.1.2. All were screened for symptoms of FTD or an overlap syndrome (MND, CBS and PSPS) and were either asymptomatic or reported very mild symptoms not meeting any diagnostic criteria. All had normal neurological examinations. Due to the sensitive nature of research-based genetic testing results in PMC, numbers of participants with each specific gene mutation are not presented.

Data were collected on all participants regarding: sex, age at CSF collection, mutation type, mean family AAO (calculated as an average of the AAO of symptoms of all known affected family members) and GENFI study site. For patients, data were also collected on clinical diagnosis, AAO and disease duration. Disease duration was calculated as the time, in years, between AAO and date of CSF collection. Each participant's age at CSF collection and the mean AAO in their family was used to estimate the number of expected years from symptom onset (EYO) that each participant was at the time of CSF collection. Every participant was also assigned a 'family number', pertaining to which family within GENFI they were a member of (or a unique family, for the two patients from the DRC CSF study), which was used as a covariate in analyses of how biomarker levels varied with EYO, as discussed later.

PMC in each genetic subgroup (*GRN, C9orf72* or *MAPT*) were also divided into 'early' PMC (age at CSF >10 EYO) and 'late' PMC (age <10 EYO) subgroups. These subgroups were later compared to establish whether biomarker levels differed between mutation carriers at different stages of the disease continuum. Of the 83 PMC, 45 were early PMC and 38 were late PMC. Cohort demographics, including for each genetic subgroup, are summarised further in Table 8.1.

Group	N	Sex (% M)	Clinical diagnosis N	Age at CSF in years	AAO in years	Mean family AAO in years	EYO	Disease duration in years
Mutation negative controls	64	45.3	n/a	46.0 (13.0)	n/a	58.2 (6.4)	-12.5 (12.4)	n/a
All PMC	83	43.4	n/a	45.8 (11.6)	n/a	57.4 (6.1)	-11.7 (10.4)	n/a
All *GRN* PMC	36	50.0	n/a	47.8 (12.7)	n/a	58.4 (3.6)	-10.6 (11.5)	n/a
Early *GRN* PMC	16	37.5	n/a	36.4 (8.6)	n/a	57.5 (3.7)	-21.1 (8.1)	n/a
Late *GRN* PMC	20	60.0	n/a	56.8 (6.5)	n/a	59.0 (3.4)	-2.2 (5.1)	n/a
All *C9orf72* PMC	32	37.5	n/a	44.9 (11.2)	n/a	59.2 (6.8)	-14.3 (9.2)	n/a
Early *C9orf72* PMC	22	40.9	n/a	40.4 (9.8)	n/a	59.5 (6.9)	-19.2 (6.1)	n/a
Late *C9orf72* PMC	10	30.0	n/a	54.8 (6.6)	n/a	58.6 (6.6)	-3.8 (4.9)	n/a
All *MAPT* PMC	15	40.0	n/a	42.9 (9.7)	n/a	51.5 (5.9)	-8.6 (9.1)	n/a
Early *MAPT* PMC	7	42.9	n/a	36.5 (6.8)	n/a	52.8 (5.7)	-16.3 (4.3)	n/a
Late *MAPT* PMC	8	37.5	n/a	48.5 (8.9)	n/a	50.4 (6.2)	-1.9 (6.3)	n/a
All patients	36	58.3	bvFTD = 28 nfvPPA = 4 svPPA = 1 CBS = 1 PSPS = 1 FTD-MND = 1	62.9 (7.7)	57.3 (7.9)	58.7 (6.8)	+4.2 (7.4)	5.6 (4.6)
GRN patients	13	46.1	bvFTD = 7 nfvPPA = 4 svPPA = 1 CBS = 1	64.0 (6.8)	59.8 (6.8)	59.1 (4.9)	+4.9 (8.2)	4.2 (3.1)
C9orf72 patients	15	73.3	bvFTD = 13 PSPS = 1 FTD-MND = 1	64.1 (9.2)	56.5 (9.9)	59.4 (9.2)	+4.6 (8.2)	7.6 (5.6)
MAPT patients	8	50.0	bvFTD = 8	59.2 (5.1)	54.8 (3.4)	56.8 (4.3)	+2.4 (4.5)	4.3 (3.3)

Table 8.1 Demographics of all participants

Values for demographics are mean (standard deviation), except for sex (percentage of sample male, % M) and N = number of participants. AAO = age at onset of symptoms; EYO = number of expected years from onset of symptoms, based on mean family AAO and age at CSF (negative = prior to expected onset, positive = after expected onset); n/a = not applicable; PMC = presymptomatic mutation carriers.

8.4.2 CSF collection, processing and biomarker immunoassays

CSF collection, processing and storage were performed as detailed in Chapter 2.2.2.1, with identical, standardised protocols across GENFI sites. Immunoassays were used to measure levels of sTREM2, YKL-40 and chitotriosidase as detailed in Chapter 2.2.2.3, with experiments for each assay carried out by the author on all samples on the same day. CVs were less than 10% for each assay.

8.4.3 Statistical analysis

8.4.3.1 Power calculations

Prospective power calculations for this study were performed at the beginning of the PhD research period, to allow time to recruit enough participants from GENFI who would have at least one lumbar puncture during this time. This was imperative as there are much fewer patients than at-risk individuals (PMC or controls) recruited into GENFI, so patient groups may have been underpowered if they were too small. During the planning phase of this study (which preceded completion of the study in Chapter 7) limited information was available regarding typical levels of each glia-derived biomarker in sporadic or genetic FTD. Power calculations were therefore based mainly on a preliminary study of mean levels of YKL-40, measured by another researcher (Dr R. Paterson) in CSF samples from ten symptomatic sporadic FTD patients and ten controls (FTD: mean [SD] = 202075 [75512] pg/mL versus controls: 98500 (55957) pg/mL; P=0.003). At a standard statistical significance level of 5%, power calculations confirmed that this study would have greater than 95% power to detect a difference in YKL-40 levels of this magnitude between 50 controls and 30 patients with genetic FTD, and also between controls and specific genetic FTD subtypes (aiming for n=10 in each subgroup). There would be greater than 90% power to detect this size of difference between two different genetic FTD subtypes. There would be 80% power to detect a difference of 45400 pg/mL or greater in the comparison of YKL-40 levels between 50 controls and 30 PMC.

The distribution of sTREM2 and chitotriosidase levels in genetic FTD was not known at the time of power calculations for this study, so these were performed based on standardised effect sizes (Cohen's D values). In general, with a standard statistical significance level of 5%, this study would have 80% power to detect an effect size of Cohen's D=0.66 or greater for the comparison of sTREM2 or chitotriosidase levels between 50 controls and 30 patients with genetic FTD, or 50 controls and 30 PMC. There would be 80% power to detect an effect size of Cohen's D=1.0 or greater for the comparison of biomarker levels between 50 controls and specific genetic FTD subtypes (n=10 each group) and an effect size of Cohen's D=1.3 between two genetic FTD subtypes.

The final number of participants in this study (patients = 36, PMC = 83, controls = 64) was therefore more than sufficient for at least 80% power to detect differences in YKL-40, sTREM2 and chitotriosidase levels between each group, including genetic subgroups. *Post hoc* power analyses were deemed by the GENFI study statistician as not being beneficial statistically, so these were not calculated retrospectively.

8.4.3.2 Statistical approach and tests

All analyses were carried out using STATA version 14, with a significance threshold of $P<0.05$. Shapiro Wilk tests of raw values and visual assessments of skew and kurtosis using Q-Q plots of residuals from multivariable linear regressions were used to test assumptions of normality. Assessment of residuals in multivariable linear regression analyses of raw sTREM2, YKL-40 and chitotriosidase levels across groups and subgroups revealed these were not normally distributed and so did not meet the assumptions required for parametric linear regression analysis. Biomarker levels were therefore Ln transformed, the residuals of which, on reassessment, met assumptions required. Ln(sTREM2), Ln(YKL-40) and Ln(chitotriosidase) levels were therefore used in all multivariable linear regressions.

For sTREM2 and YKL-40, levels were detectable in CSF of all participants. However, for chitotriosidase, five participants had persistently undetectable levels of chitotriosidase in CSF, despite repeating the assay using neat CSF samples for these individuals instead of 1 in 5 dilution: three patients (two C*9orf72,* one *MAPT*) and two controls (one from a *C9orf72* family, one from a *MAPT* family). Approximately 6% of the population possesses a homozygous 24 base pair duplication in exon 10 of the *CHIT1* gene, which leads to a complete enzymatic deficiency of chitotriosidase (Boot et al., 1998) and undetectable levels of chitotriosidase in CSF (Abu-Rumeileh et al., 2019). These five individuals (2.7% cohort) were likely to be carriers of this mutation, given their undetectable, rather than low in-range, levels. Confirmation from DNA analysis was not possible during this study, but it was felt that their chitotriosidase levels would unacceptably bias group comparisons if included or assigned the lower limit of detection, as others have done (Abu-Rumeileh et al., 2019). These participants were therefore excluded from the chitotriosidase analysis, leaving 178 (out of 183) participants in this analysis but 183 in the sTREM2 and YKL-40 analyses.

The following hierarchical approach was used to compare demographics and biomarker levels between groups:

1. **Overall group analysis:** patients (all mutations combined), PMC (all mutations combined) and controls.
2. **Genetic subtype analysis:** patient subgroups (*GRN, C9orf72* and *MAPT*), PMC subgroups (*GRN, C9orf72* and *MAPT*) and controls.
3. **Early and late PMC analysis:** early and late PMC subgroups, patient subgroups, and controls. Patient subgroups and early and late PMC subgroups were separated by genetic subtype (i.e. *GRN* patients, *C9orf72* patients, *MAPT* patients; early *GRN* PMC, late *GRN* PMC, early *C9orf72* PMC, late *C9orf72* PMC, early *MAPT* PMC, late *MAPT* PMC).

The following demographics were compared between all groups: age at CSF and EYO (using one-way ANOVA with Bonferroni *post hoc* tests for multiple comparisons) and sex (Chi squared tests). AAO was compared between patient groups using one-way ANOVA with Bonferroni *post hoc* tests. Disease duration was compared between patient groups using Kruskal Wallis tests with Dunn's test for *post hoc* comparisons, as the distribution was non-parametric.

Multivariable linear regressions were used to assess associations of glia-derived biomarker levels with demographic parameters that may independently influence glial function: age and disease duration at CSF. Associations with age were examined within the overall group and genetic subtype analyses, adjusted for sex in all groups. Associations with disease duration were examined in patient groups within the genetic subtype analysis, adjusted for age and sex.

Multivariable linear regression analyses were then used to compare levels of each glia-derived biomarker between groups and subgroups using the hierarchical approach above. These were adjusted for age and sex, given the strong associations with age for sTREM2 and YKL-40, and given that glia-derived biomarker levels may vary according to sex, as per previous studies of neurodegenerative diseases.

Linear mixed effects regression models were then used to examine how biomarker levels varied at different timepoints along the presymptomatic to symptomatic continuum in all mutation carriers (patients and PMC combined) and controls (non-carriers), first overall, and then for each genetic subtype (*GRN, C9orf72* or *MAPT*), to establish:

1. Whether mean levels of each biomarker differed between mutation carriers and controls and whether this varied according to the genetic subtype.

2. At what EYO timepoint any significant difference in levels between mutation carriers and controls occurred for each genetic subtype.

In each linear mixed effects regression model, the outcome variable was Ln(biomarker level), and the predictor variables of interest were mutation carrier status (carrier/control), EYO, EYO^2, interaction between mutation carrier status and EYO, and interaction between mutation carrier status and EYO^2. These analyses were adjusted for age and sex. A random intercept for family number was also included to allow values of the biomarker to be correlated between members of the same family rather than assuming independence. This is because mutation carriers and non-carriers (controls) from the same family are genetically more homogeneous, and this could independently influence both glial function and EYO (which is based on mean family AAO, also influenced by family membership).

8.5 Results

8.5.1 Demographic comparisons

Demographics for each group are shown in Table 8.1 and results of group demographic comparisons (mean differences and *P* values) are shown in Table 8.2 (except for sex, as all comparisons were non-significant, and AAO and disease duration, as these only applied to patient groups).

Sex did not differ significantly between patient, PMC and control groups (χ^2 = 2.37, *P*=0.306), patient and PMC genetic subtypes (χ^2 = 5.87, *P*=0.438), or early and late PMC genetic subgroups (χ^2 = 8.04; *P*=0.53). As shown in Table 8.1, AAO and disease duration were similar between patient groups (AAO: *C9orf72* vs. *GRN*: *P*=0.788; *MAPT* vs. *GRN*: *P*=0.501; *MAPT* vs. *C9orf72*: *P*=1.00; disease duration: *C9orf72* vs. *GRN*: *P*=0.077; *MAPT* vs. *GRN*: *P*=0.958; *MAPT* vs. *C9orf72*: *P*=0.139).

Age at CSF and EYO differed significantly across various groups and subgroups, as shown in Tables 8.1 and 8.2, but were similar between patient genetic subtypes and between PMC genetic subtypes. Early *GRN* and *C9orf72* PMC had a higher value for EYO compared with late PMC (as expected, as these subgroups were defined based on EYO), although this did not reach significance for *MAPT* late PMC versus early PMC after Bonferroni correction.

Table 8.2 Comparisons of demographics and CSF glia-derived biomarker levels between groups

Demographic values are inter-group mean differences (95% confidence intervals); *P* values from ANOVA which remained significant (*P*<0.05) after Bonferroni correction are highlighted in bold. Biomarker levels are inter-group mean differences (95% confidence intervals) from regressions adjusted for age and sex, with significant *P* values (*P*<0.05) highlighted in **bold**. EYO=expected years from symptom onset; PMC=presymptomatic mutation carrier.

Groups compared	Age at CSF In years	*P*	EYO at CSF	*P*	Ln(chitotriosidase) (pg/ml)	*P*	Ln(YKL-40) (pg/ml)	*P*	Ln(sTREM2) (pg/ml)	*P*
Overall group analysis										
Patients vs. controls	16.9 (11.1, 22.7)	**<0.0001**	16.7 (11.3, 21.1)	**<0.0001**	0.720 (0.272, 1.17)	**0.002**	0.093 (-0.077, 0.263)	0.280	-0.104 (-0.358, 0.149)	0.418
Patients vs. PMC	17.2 (11.7, 22.8)	**<0.0001**	15.9 (10.8, 21.1)	**<0.0001**	0.748 (0 .316, 1.18)	**0.001**	0.094 (-0.071, 0.260)	0.261	-0.147 (-0.394, 0.099)	0.240
PMC vs. controls	-0.268 (-4.99, 4.36)	1.00	0.791 (-3.49, 5.07)	1.00	-0.027 (-0.335, 0.280)	0.860	-0.001 (-0.121, 0.119)	0.982	0.043 (-0.135, 0 .221)	0.635
Genetic subtype analysis										
GRN patients vs. controls	18.0 (7.18, 28.8)	**<0.0001**	17.4 (7.40, 27.4)	**<0.0001**	0.839 (0.239, 1.44)	**0.006**	0.103 (-0.132, 0.339)	0.387	-0.187 (-0.539, 0.165)	0.295
C9orf72 patients vs. controls	18.0 (7.81, 28.2)	**<0.0001**	17.1 (7.7, 26.5)	**<0.0001**	0.328 (-0.272, 0.929)	0.283	0.030 (-0.196, 0.257)	0.793	0.012 (-0.325, 0.350)	0.942
MAPT patients vs. controls	13.2 (-0.16, 26.5)	0.056	14.9 (2.54, 27.2)	**0.006**	1.17 (0.425, 1.92)	**0.002**	0.161 (-0.117, 0.439)	0.255	-0.150 (-0.565, 0.265)	0.476

Groups compared	Age at CSF In years	*P*	EYO at CSF	*P*	Ln(chitotriosidase) (pg/ml)	*P*	Ln(YKL-40) (pg/ml)	*P*	Ln(sTREM2) (pg/ml)	*P*
GRN patients vs. *GRN* PMC	16.3 (4.77, 27.8)	**<0.0001**	15.5 (4.89, 26.1)	**<0.0001**	0.829 (0.206, 1.45)	**0.009**	0.141 (-0.106, 0.389)	0.262	-0.264 (-0.632, 0.103)	0.157
C9orf72 patients vs. *C9orf72* PMC	19.2 (8.07, 30.3)	**<0.0001**	18.9 (8.73, 29.3)	**<0.0001**	0.489 (-0.158, 1.13)	0.138	0.035 (-0.212, 0.283)	0.778	-0.055 (-0.423, 0.314)	0.771
MAPT patients vs. *MAPT* PMC	16.3 (0.72, 31.8)	**0.031**	10.9 (-3.40, 25.3)	0.415	1.01 (0.149, 1.87)	**0.022**	0.068 (-0.257, 0.395)	0.679	-0.058 (-0.544, 0.428)	0.815
GRN PMC vs. controls	1.72 (-5.78, 9.14)	1.00	1.87 (-4.96, 8.71)	1.00	0.011 (-0.372, 0.394)	0.954	-0.037 (-0.189, 0.115)	0.628	0.077 (-0.148, 0.303)	0.498
C9orf72 PMC vs. controls	-1.17 (-8.88, 6.52)	1.00	-1.87 (-8.98, 5.23)	1.00	-0.160 (-0.558, 0.237)	0.427	-0.005 (-0.162, 0.152)	0.948	0.067 (-0.167, 0.301)	0.573
MAPT PMC vs. controls	-3.119479 (-13.3, 7.09)	1.00	3.88 (-5.53, 13.3)	1.00	0.164 (-0.362, 0.689)	0.540	0.092 (-0.115, 0.301)	0.382	-0.092 (-0.403, 0.218)	0.558
C9orf72 vs. *GRN* patients	0.021 (-13.5, 13.5)	1.00	-0.269 (-12.7, 12.2)	1.00	-0.512 (-1.23, 0.207)	0.162	-0.073 (-0.349, 0.202)	0.599	0.199 (-0.211, 0.611)	0.339
MAPT vs. *GRN* patients	-4.83 (-20.8, 11.1)	1.00	-2.54 (-17.3, 12.2)	1.00	0.333 (-0.525, 1.19)	0.444	0.057 (-0.268, 0.383)	0.729	0.037 (-0.449, 0.523)	0.880
MAPT vs. *C9orf72* patients	-4.85 (-20.4, 10.7)	1.00	-2.27 (-16.6, 12.1)	1.00	0.845 (-0.013, 1.70)	0.053	0.132 (-0.188, 0.449)	0.419	-0.162 (-0.637, 0.312)	0.500
C9orf72 vs. *GRN* PMC	-2.90 (-11.5, 5.74)	1.00	-3.75 (-11.7, 4.23)	1.00	-0.171 (-0.618, 0.274)	0.448	0.032 (-0.146, 0.210)	0.721	-0.011 (-0.274, 0.253)	0.937

Groups compared	Age at CSF In years	*P*	EYO at CSF	*P*	Ln(chitotriosidase) (pg/ml)	*P*	Ln(YKL-40) (pg/ml)	*P*	Ln(sTREM2) (pg/ml)	*P*
MAPT vs. *GRN* PMC	-4.84 (-15.8, 6.09)	1.00	2.00 (-8.08, 12.1)	1.00	0.152 (-0.412, 0.717)	0.595	0.129 (-0.095, 0.355)	0.255	-0.169 (-0.503, 0.164)	0.316
MAPT vs.*C9orf72* PMC	-1.94 (-13.1, 9.19)	1.00	5.76 (-4.51, 16.0)	1.00	0.324 (-0.247, 0.895)	0.264	0.097 (-0.129, 0.324)	0.396	-0.159 (-0.497, 0.178)	0.353
Early and late PMC analysis										
GRN patients vs. late PMC	7.22 (0.093, 14.3)	**0.047**	7.14 (-3.64, 17.9)	1.00	0.880 (0.223, 1.55)	**0.009**	0.152 (-0.113, 0.417)	0.260	-0.273 (-0.665, 0.119)	0.172
GRN patients vs. early PMC	27.6 (20.1, 35.1)	**<0.0001**	25.9 (14.7, 37.3)	1.00	0.603 (-0.185, 1.39)	0.133	0.088 (-0.223, 0.398)	0.578	-0.257 (-0.722, 0.207)	0.276
Late vs. early *GRN* PMC	20.4 (13.7, 27.1)	**<0.0001**	18.9 (8.70, 28.9)	**<0.0001**	-0.281 (-0.965, 0.401)	0.417	-0.064 (-0.337, 0.209)	0.644	0.015 (-0.388, 0.418)	0.941
Late *GRN* PMC vs. controls	10.8 (5.66, 15.9)	**<0.0001**	10.2 (2.49, 18.0)	**0.001**	-0.124 (-0.624, 0.376)	0.625	-0.069 (-0.269, 0.132)	0.500	0.084 (-0.209, 0.377)	0.572
Early *GRN* PMC vs. controls	-9.59 (-15.2, -4.01)	**0.001**	-8.60 (-17.1, -0.14)	**0.041**	0.158 (-0.372, 0.688)	0.557	-0.004 (-0.215, 0.205)	0.966	0.069 (-0.245, 0.383)	0.665
C9orf72 patients vs. late PMC	9.29 (1.12, 17.5)	**0.026**	8.43 (-3.93, 20.8)	1.00	0.621 (-0.167, 1.41)	0.122	0.061 (-0.244, 0.367)	0.693	-0.071 (-0.528, 0.384)	0.757
C9orf72 patients vs. early PMC	23.7 (17.1, 30.4)	**<0.0001**	23.8 (13.7, 33.9)	**<0.0001**	0.311 (-0.413, 1.03)	0.398	-0.009 (-0.288, 0.270)	0.949	-0.048 (-0.465, 0.369)	0.820

Groups compared	Age at CSF In years	*P*	EYO at CSF	*P*	Ln(chitotriosidase) (pg/ml)	*P*	Ln(YKL-40) (pg/ml)	*P*	Ln(sTREM2) (pg/ml)	*P*
Late vs early *C9orf72* PMC	14.4 (6.79, 22.1)	**<0.0001**	15.4 (3.84, 26.9)	**0.001**	-0.309 (-1.04, 0.418)	0.402	-0.070 (-0.359, 0.218)	0.632	0.023 (-0.407, 0.455)	0.914
Late *C9orf72* PMC vs. controls	8.74 (1.93, 15.5)	**0.012**	8.69 (-1.59, 18.9)	0.254	-0.370 (-1.01, 0.269)	0.255	-0.052 (-0.304, 0.200)	0.685	0.083 (-0.294, 0.460)	0.664
Early *C9orf72* PMC vs. controls	-5.68 (-10.6, -0.74)	**0.025**	-6.68 (-14.2, 0.796)	0.156	-0.060 (-0.521, 0.400)	0.797	0.018 (-0.164, 0.201)	0.844	0.059 (-0.213, 0.332)	0.667
MAPT patients vs. late PMC	10.7 (0.67, 20.7)	**0.037**	4.25 (-10.9, 19.4)	1.00	1.08 (0.116, 2.04)	**0.028**	0.136 (-0.233, 0.504)	0.469	0.011 (-0.539, 0.562)	0.968
MAPT patients vs. early PMC	22.7 (12.4, 33.1)	**<0.0001**	18.6 (2.98, 34.3)	**0.005**	0.778 (-0.255, 1.81)	0.139	-0.048 (-0.444, 0.348)	0.811	-0.138 (-0.732, 0.454)	0.644
Late vs. early *MAPT* PMC	12.1 (1.69, 22.4)	**0.023**	14.4 (-1.26, 30.1)	0.120	-0.300 (-1.26, 0.663)	0.539	-0.184 (-0.566, 0.198)	0.344	-0.150 (-0.721, 0.421)	0.604
Late *MAPT* PMC vs. controls	2.50 (-5.0, 10.0)	0.511	10.6 (-0.746, 21.9)	0.102	0.035 (-0.655, 0.725)	0.921	0.010 (-0.263, 0.283)	0.941	-0.162 (-0.570, 0.246)	0.434
Early *MAPT* PMC vs. controls	-9.55 (-17.5, -1.58)	**0.019**	-3.79 (-15.8, 8.25)	1.00	0.335 (-0.406, 1.08)	0.373	0.194 (-0.100, 0.488)	0.195	-0.012 (-0.452, 0.428)	0.957
Early *C9orf72* PMC vs. early *GRN* PMC	3.91 (-2.66, 10.5)	0.242	1.91 (-8.02, 11.8)	1.00	-0.218 (-0.823, 0.386)	0.477	0.022 (-0.217, 0.263)	0.852	-0.009 (-0.368, 0.349)	0.959
Early *MAPT* PMC vs early *GRN* PMC	0.048 (-9.02, 9.12)	0.992	4.80 (-8.91, 18.5)	1.00	0.177 (-0.653, 1.01)	0.674	0.198 (-0.131, 0.528)	0.236	-0.081 (-0.574, 0.412)	0.746

Groups compared	Age at CSF In years	*P*	EYO at CSF	*P*	Ln(chitotriosidase) (pg/ml)	*P*	Ln(YKL-40) (pg/ml)	*P*	Ln(sTREM2) (pg/ml)	*P*
Early *MAPT* PMC vs early *C9orf72* PMC	-3.86 (-12.5, 4.82)	0.381	2.89 (-10.2, 16.0)	1.00	0.396 (-0.402, 1.19)	0.329	0.175 (-0.140, 0.492)	0.274	-0.071 (-0.544, 0.401)	0.765
Late *C9orf72* PMC vs late *GRN* PMC	-2.04 (-9.79, 5.71)	0.603	-1.56 (-13.3, 10.2)	1.00	-0.246 (-0.962, 0.469)	0.498	0.017 (-0.270, 0.303)	0.909	-0.001 (-0.425, 0.423)	0.996
Late *MAPT* PMC vs late *GRN* PMC	-8.28 (-16.6, 0.09)	0.053	0.35 (-12.3, 13.0)	1.00	0.159 (-0.619, 0.937)	0.688	0.079 (-0.233, 0.390)	0.617	-0.246 (-0.708, 0.215)	0.293
Late *MAPT* PMC vs late *C9orf72* PMC	-6.23 (-15.7, 3.26)	0.197	1.91 (-12.4, 16.3)	1.00	0.405 (-0.468, 1.28)	0.361	0.062 (-0.284, 0.409)	0.723	-0.245 (-0.764, 0.272)	0.351

8.5.2 Associations between glia-derived biomarkers and demographic parameters

8.5.2.1 Age at CSF

sTREM2 was positively associated with age in controls (β=0.015, *P*=0.005) and PMC (β=0.02, *P*<0.0001) (Figure 8.1a). There was a positive association in *GRN* PMC (*P*=0.008) and *C9orf72* PMC (*P*=0.001), but not for *MAPT* PMC (*P*=0.689) (Figure 8.1b). Despite a similarly positive slope for the association with age in the overall patient group (Figure 8.1a) this did not reach significance (β=0.019, *P*=0.111), nor in any genetic subgroup (Figure 8.1b). YKL-40 was positively associated with age in controls (β=0.024, *P*<0.0001*)*, PMC (β=0.023, *P*<0.0001) and patients (β=0.035, *P*<0.0001) (Figure 8.1c*).* There was a positive association with age in *GRN* PMC (*P*<0.0001) and *GRN* patients (*P*=0.022) and *C9orf72* PMC (*P*<0.0001) and *C9orf72* patients (*P*<0.0001), but this was not significant for *MAPT* PMC (*P*=0.968) or *MAPT* patients (*P*=0.774) (Figure 8.1d). Chitotriosidase was not significantly associated with age in any group (Figure 8.1e): controls (β=0.013, *P*=0.172), PMC (β=0.011, *P*=0.226), patients (β=0.034, *P*=0.137), or any genetic subtype (Figure 8.1f).

8.5.2.2 Disease duration

None of the biomarkers were significantly associated with disease duration in the overall patient group (sTREM2: β= -0.023, *P*=0.441; YKL-40: β= -0.003, *P*=0.849; chitotriosidase: β= -0.059, *P*=0.194), or in any genetic subgroup (Figure 8.2a-c), except for sTREM2, where there was a moderate negative association with disease duration in the *MAPT* patient group (β= -0.183, *P*=0.04) (Figure 8.2a).

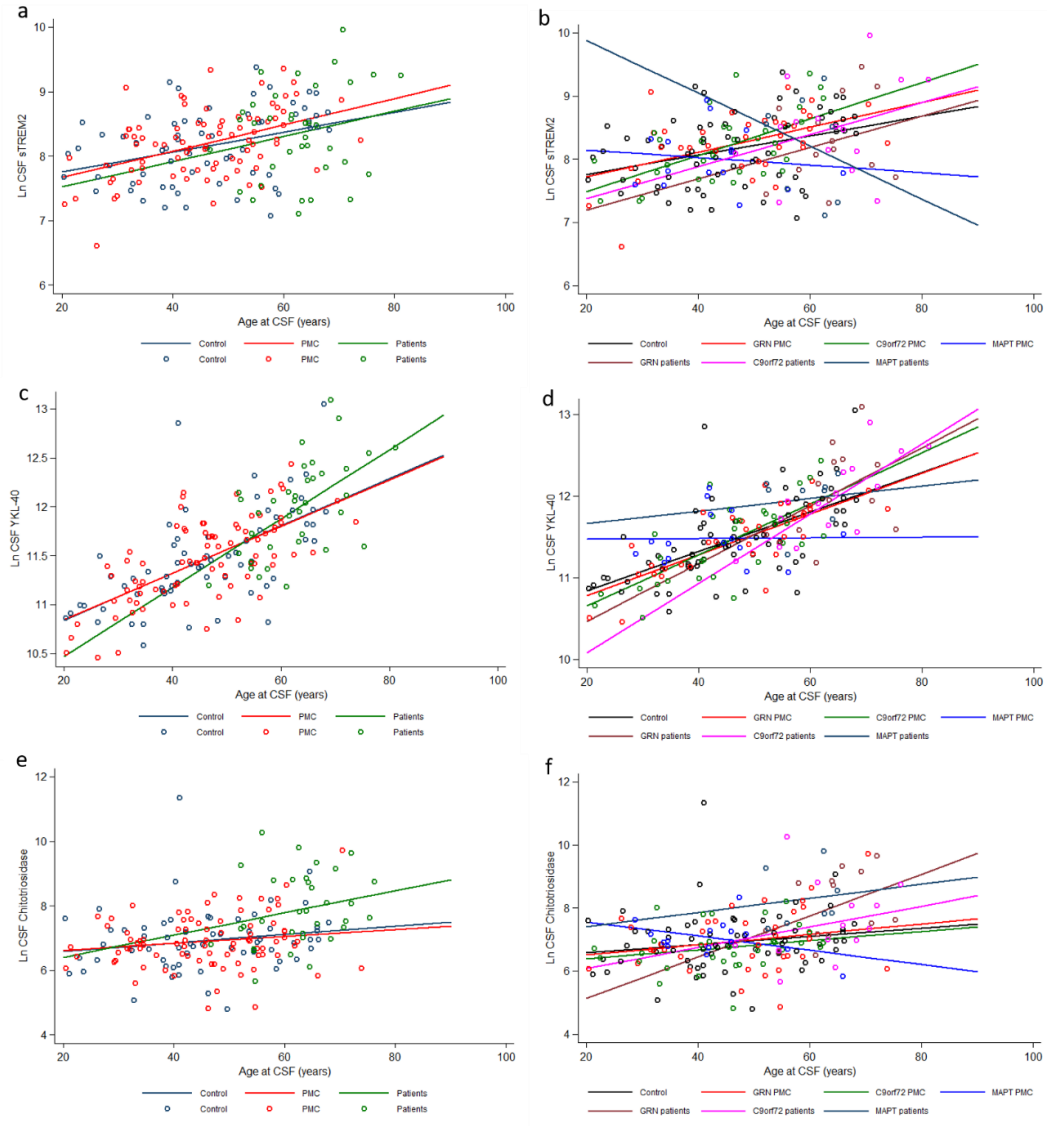

Figure 8.1 Associations between glia-derived biomarkers and age at CSF

Association between CSF levels of sTREM2 (**a, b**), YKL-40 (**c, d**) and chitotriosidase (**e, f**) and age at CSF in overall groups (**a, c, e**) and genetic subgroups (**b, d, f**). Associations were significant for sTREM2 and YKL-40 but not chitotriosidase; for relevant β and *P* values see main text.

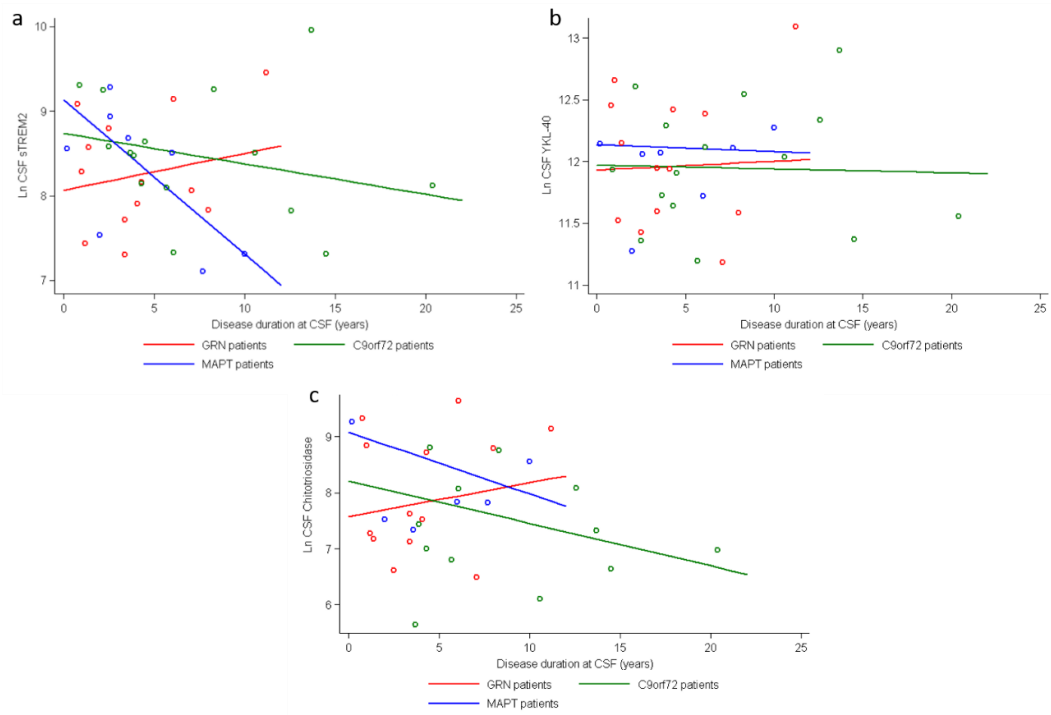

Figure 8.2 Associations between glia-derived biomarkers and disease duration

Associations between CSF levels of sTREM2 (**a**), YKL-40 (**b**) and chitotriosidase (**c**) and disease duration at CSF in each patient genetic group. Associations were not significant except for a negative association of sTREM2 with disease duration in *MAPT* patients (**a**): β= -0.183, *P*=0.04.

8.5.3 Group comparisons of glia-derived biomarkers

Glia-derived biomarker levels for each group are summarised as raw values in Table 8.3 and presented in Figures 8.3 and 8.4. Results of all group comparisons from linear regressions adjusted for age and sex are shown in Table 8.2 (mean differences and *P* values), so values are not repeated in the text.

8.5.3.1 Overall group analysis

Raw sTREM2 levels were similar across all groups (Table 8.3; Figure 8.3a) and this remained the case in adjusted regressions (Table 8.2). Although raw YKL-40 levels appeared higher in patients compared with controls and PMC (Table 8.3; Figure 8.3b), in adjusted regressions these comparisons became non-significant (Table 8.2) due to controlling for age, which differed significantly between patient and PMC groups and controls. Raw chitotriosidase levels were higher in patients than controls and PMC

(Table 8.3). This remained significant in adjusted regressions (Table 8.2; Figure 8.3c), demonstrating that raised levels in patients were not due to older age.

8.5.3.2 Genetic subtype analysis

Raw sTREM2 levels appeared higher in *C9orf72* patients than controls (Table 8.3, Figure 8.3d), but in adjusted regressions this lost significance due to controlling for age. Raw YKL-40 levels appeared higher in *GRN, C9orf72* and *MAPT* patients compared with controls and respective PMC groups (Table 8.3, Figure 8.3e). However, in adjusted regressions all comparisons became non-significant due to controlling for age (Table 8.2). Raw chitotriosidase levels also appeared higher in *GRN, C9orf72* and *MAPT* patients compared with controls and respective PMC groups (Table 8.3; Figure 8.3f). However, in adjusted regressions, results for *GRN* and *MAPT* patients remained significant, with higher chitotriosidase levels in both groups compared with controls and PMC, whereas for *C9orf72* patients this lost significance (Table 8.2; Figure 8.3f). Levels of all biomarkers were similar across patient genetic subtypes and across PMC genetic subtypes in unadjusted and adjusted analyses.

8.5.3.3 Early and late PMC analysis

Raw sTREM2 levels appeared higher in *C9orf72* patients than early PMC (Table 8.3, Figure 8.4a) but this lost significance in adjusted regressions due to controlling for age (Table 8.2). Raw YKL-40 levels appeared higher in *GRN* patients than early and late *GRN* PMC, higher in late *GRN* PMC than early *GRN* PMC, and higher in early *GRN* PMC than controls (Table 8.3, Figure 8.4b). Raw YKL-40 levels also appeared higher in *C9orf72* patients than early *C9orf72* PMC, and in *MAPT* patients than early *MAPT* PMC (Table 8.3; Figure 8.4b). However, all comparisons became non-significant in adjusted regressions due to controlling for age (Table 8.2). Raw chitotriosidase levels appeared higher in *GRN, C9orf72* and *MAPT* patients than both early and late PMC (Table 8.3). However, in adjusted regressions, this only remained significant for *GRN* and *MAPT* patients compared with late PMC (Table 8.2; Figure 8.4c).

Group	N *	CSF chitotriosidase (pg/ml)	CSF YKL-40 (pg/ml)	CSF sTREM2 (pg/ml)
Controls	64	2634.5 (10597.1)	109815.0 (72228.8)	4059.1 (2285.2)
All PMC	83	1447.9 (1986.2)	103195.9 (43552.3)	4136.0 (2215.3)
All *GRN* PMC	36	1821.4 (2831.1)	104114.5 (40462.8)	4332.1 (1914.2)
Early *GRN* PMC	16	1190.2 (782.9)	78321.7 (27842.9)	3623.6 (1890.2)
Late *GRN* PMC	20	2326.5 (3698.2)	125834.7 (36840.4)	4898.9 (1779.9)
All *C9orf72* PMC	32	1082.2 (845.3)	102977.3 (51028.4)	4274.1 (2657.1)
Early *C9orf72* PMC	22	1182.6 (992.5)	93245.2 (44496.1)	3840.7 (2283.1)
Late *C9orf72* PMC	10	861.3 (289.7)	124387.9 (60069.5)	5227.612 3269.112
All *MAPT* PMC	15	1332.1 (897.9)	101518.8 (35031.4)	3370.74 (1783.24)
Early *MAPT* PMC	7	1241.1 (393.3)	91991.6 (21824.8)	3027.4 (885.6)
Late *MAPT* PMC	8	1411.8 (1210.1)	109855.0 (43312.1)	3671.2 (2338.1)
All patients	36	4926.8 (6111.4)	180135.4 (92185.2)	5482.9 (4174.8)
GRN patients	13	4992.9 (4744.9)	193673.3 (115339.8)	4933.6 (3489.1)
C9orf72 patients	15	4275.8 (7555.1)	177448.1 (92765.9)	6285.6 (5146.9)
MAPT patients	8	6012.7 (6140.4)	163175.0 (42299.8)	4870.2 (3305.2)

Table 8.3 Glia-derived biomarker levels in each group

Biomarker levels are presented as raw, unadjusted mean (standard deviation) values. Controls are all mutation negative participants. * Values for chitotriosidase were calculated from 178 participants, as five participants were excluded from the chitotriosidase analysis due to undetectable levels.

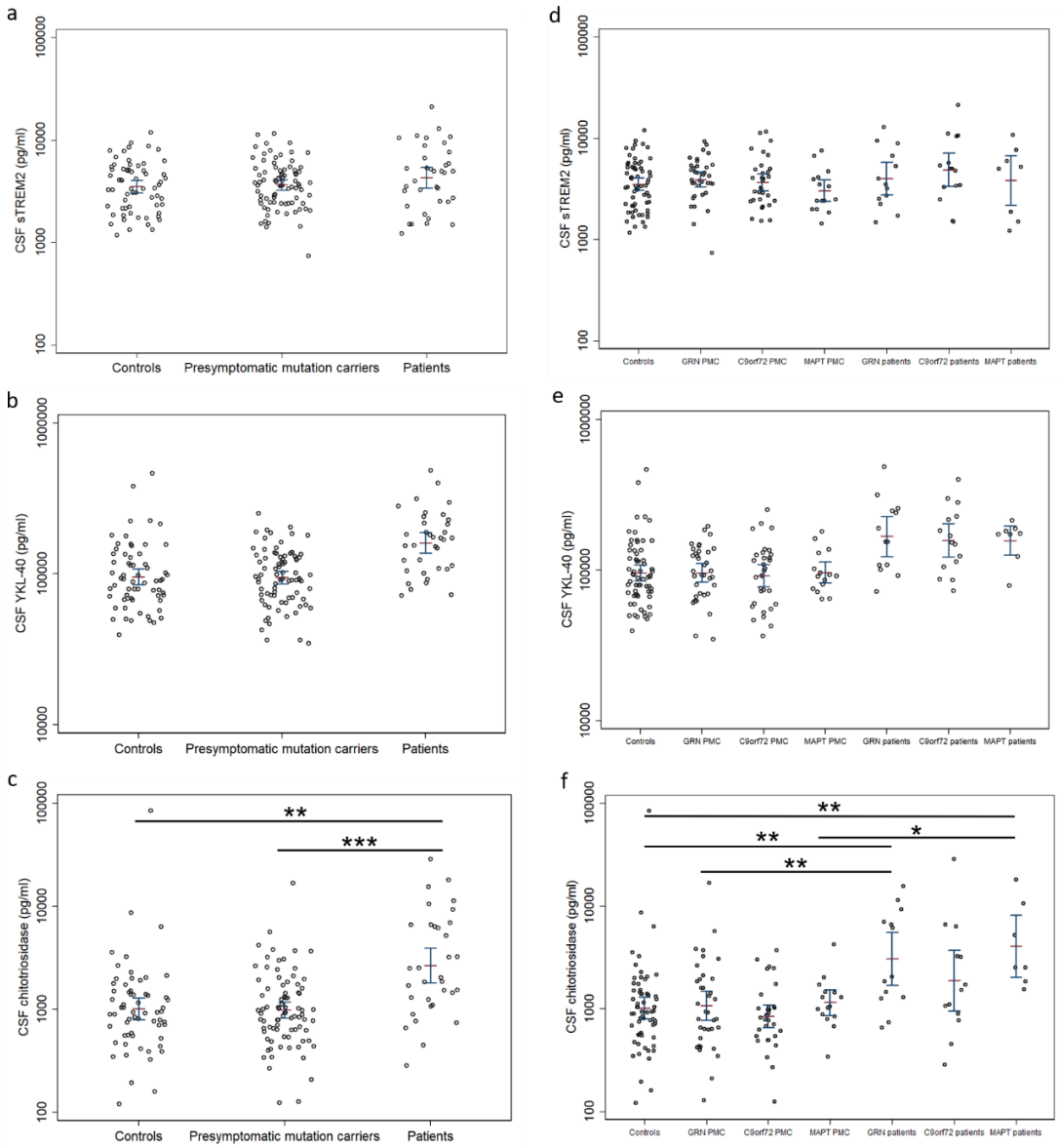

Figure 8.3 Glia-derived biomarker levels in overall groups and genetic subtypes

Graphs show CSF sTREM2 (**a, d**), YKL-40 (**b, e**) and chitotriosidase (**c, f**) levels in controls, PMC and patients (**a-c**), and controls and genetic PMC and patient subgroups (**d-f**). Y axes show raw biomarker values on a logarithmic scale due to outliers. Bars show means and 95% confidence intervals. After adjusting Ln transformed biomarker values for age and sex in regression analyses, only chitotriosidase comparisons remained significant (**c, f**): **P*<0.05; ***P*≤0.01, ****P*≤0.001.

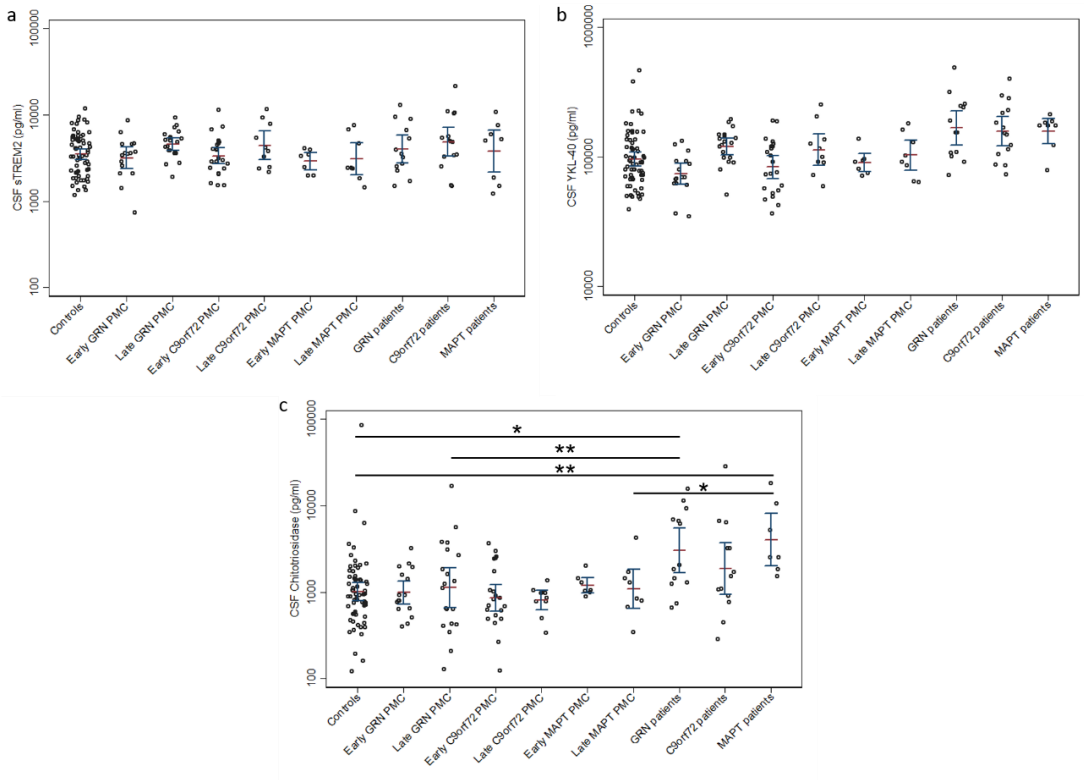

Figure 8.4 Glia-derived biomarker levels in controls, early and late PMC and patients

Graphs show CSF sTREM2 (**a**), YKL-40 (**b**) and chitotriosidase (**c**) levels in controls, PMC subgroups (split into early and late PMC) and patient subgroups. Early PMC were >10 years from expected onset of symptoms at time of CSF collection and late PMC were ≤10 years. Y axes show raw biomarker values on a logarithmic scale due to outliers. Bars show means and 95% confidence intervals. After adjusting Ln transformed biomarker values for age and sex in regression analyses, only chitotriosidase comparisons remained significant (**c**): *P<0.05; **P≤0.01.

8.5.4 Analysis of glia-derived biomarkers versus expected years from onset

There were no significant differences in biomarker levels between the combined group of all mutation carriers (all patients and PMC combined) and controls (non-carriers) at any EYO timepoint (sTREM2: P=0.694; YKL-40: P=0.239; chitotriosidase P=0.305). When examining individual genetic subtypes, sTREM2 levels did not differ significantly between any group at any EYO timepoint (Figure 8.5a). However, *GRN* mutation carriers had a significant difference in YKL-40 (P=0.017) and chitotriosidase (P=0.036) levels, but not sTREM2 levels (P=0.925), compared with controls. The association with EYO was significantly steeper for YKL-40 (P=0.005) (Figure 8.5b) and chitotriosidase (P=0.027) (Figure 8.5c) in *GRN* carriers, compared with controls, meaning that differences in biomarker levels between these groups grew larger as mutation carriers

approached the expected age of symptom onset. Levels continued to diverge between *GRN* mutation carriers and controls in the symptomatic phase. YKL-40 levels were raised presymptomatically in *GRN* mutation carriers, with significant differences from controls at between one (P=0.063) and zero (P=0.049) EYO i.e. immediately prior to predicted conversion, and levels continued to diverge in the symptomatic phase (Figure 8.5b). Chitotriosidase levels were also raised presymptomatically in *GRN* mutation carriers, but much earlier on, with significant differences from controls at six EYO (P=0.048), and levels continued to diverge in the symptomatic phase (Figure 8.5c).

Chitotriosidase levels in *MAPT* mutation carriers also appeared to differ from controls in the presymptomatic phase (Figure 8.5c), although group comparisons did not reach the level of significance seen in *GRN* mutation carriers. The *P* value for the mean difference in chitotriosidase levels between *MAPT* mutation carriers and controls was lowest at the actual predicted AAO (EYO=0; P=0.058), but there was a suggestion of differing levels from three EYO (P=0.065) onwards. For *C9orf72* mutation carriers, levels of YKL-40 and chitotriosidase did not differ significantly from controls at any EYO and were not raised significantly in either the presymptomatic or symptomatic phase (Figure 8.5b, c).

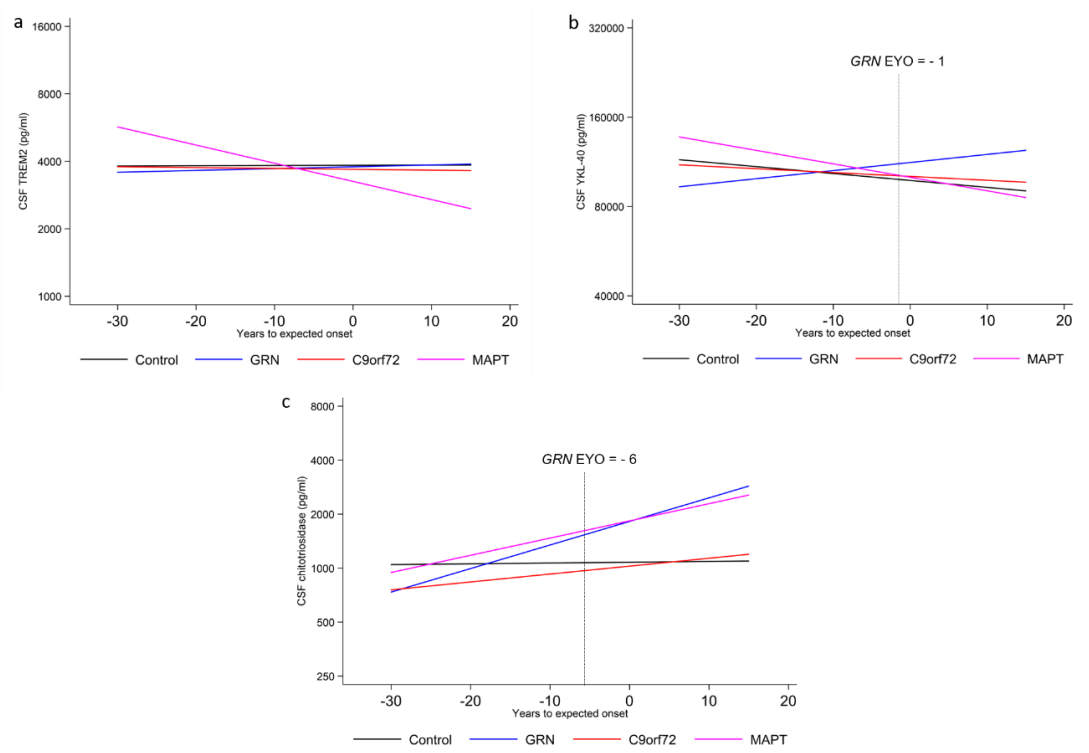

Figure 8.5 Glia-derived biomarkers are raised presymptomatically depending on mutation type and EYO

Graphs show how CSF levels of sTREM2 (**a**), YKL-40 (**b**) and chitotriosidase (**c**) vary with expected years from onset (EYO) in mutation carriers versus controls (non-carriers) during the presymptomatic and symptomatic phases for each mutation group. Regression lines rather than individual participant data points are shown to avoid revealing the genetic status of PMC who are at specific EYO. (**a**) sTREM2 levels are similar between all mutation carrier groups and controls and do not change with EYO. (**b**) YKL-40 levels differ significantly between *GRN* mutation carriers and controls from between one and zero years before expected onset (*P*=0.063 at EYO= -1 and *P*=0.049 at EYO=0). (**c**) Chitotriosidase levels differ significantly between *GRN* mutation carriers and controls from six years before onset (*P*=0.048 at EYO= -6). In *MAPT* mutation carriers there is a borderline difference in chitotriosidase levels compared with controls from three EYO (*P*=0.065 at EYO= -3), which is even more obvious at expected onset (*P*=0.058 at EYO=0).

8.6 Discussion

This study examined levels of three glia-derived biomarkers, sTREM2, YKL-40 and chitotriosidase, in the CSF of patients with genetic FTD, and in PMC with mutations in *GRN, C9orf72* and *MAPT*, compared with mutation negative controls. CSF sTREM2 and YKL-40 (but not chitotriosidase) levels were strongly positively associated with age, but only sTREM2 was associated with disease duration, with a negative association in *MAPT* patients. Chitotriosidase levels were raised in patients with genetic FTD compared with PMC and controls, but this was specifically in those with *GRN* and *MAPT* mutations, rather than *C9orf72* expansions, although levels were similar between genetic subtypes.

Although sTREM2 and YKL-40 levels initially appeared raised in certain patient groups, once adjusted for age, levels were similar across all groups. Levels of all biomarkers were similar between PMC and controls overall and for each genetic PMC subtype compared with controls. However, chitotriosidase levels were higher in *GRN* and *MAPT* patients than in respective late PMC. In *GRN* mutation carriers, chitotriosidase and YKL-40 levels were raised presymptomatically, with significantly higher levels than controls from six EYO (chitotriosidase) and between one and zero EYO (YKL-40). In *MAPT* mutation carriers there was a non-significant trend towards raised chitotriosidase levels from three EYO compared with controls.

The positive association of sTREM2 and YKL-40 levels with age replicates findings in Chapter 7 and is consistent with previous studies in sporadic FTD, AD (Alcolea et al., 2017; del Campo et al., 2018; Teunissen et al., 2016) and HD (Byrne et al., 2018a). Microglial activity increases with aging, which may augment release of sTREM2 by microglia as a protective response to neuronal loss in aging individuals (Zhong et al., 2019), and this may also be the case for YKL-40. Chitotriosidase levels were not associated with age in any group, consistent with Chapter 7 and other studies of AD and FTD (Abu-Rumeileh et al., 2019; Mattsson et al., 2011; Oeckl et al., 2019; Rosén et al., 2014). This suggests that the high CSF chitotriosidase levels in patients with *GRN* or *MAPT* mutations represent excessive microglial activation or dysfunction related to the underlying mutation itself, or neurodegeneration, rather than aging. It also emphasises the importance of adjusting analyses of fluid biomarker levels for age when comparing groups of individuals with large age ranges (such as PMC), particularly when age independently affects the biological function of interest. Age adjustment was crucial for this study, where although raw YKL-40 and sTREM2 levels initially appeared significantly raised in certain groups, all comparisons lost significance when adjusted for age.

None of the biomarkers was associated with disease duration, apart from sTREM2 in the *MAPT* patient group, where there was a moderate negative association. There was a negative association of sTREM2 with disease duration in the mixed FTD cohort in Chapter 7, but analysis in the small *MAPT* group had not been possible. The negative association here suggests that sTREM2 levels could reduce over time in *MAPT* mutation carriers, or could be a marker of disease intensity, like NfL levels (Meeter et al., 2016a; Rohrer et al., 2016). However, a lack of longitudinal CSF samples precluded exploration of how biomarker levels change over the disease course. Later analyses of cross-sectional biomarker levels versus EYO examined how levels in PMC differed from controls at various proximities to expected onset, but not over time. The lack of association for YKL-40 and chitotriosidase with disease duration is consistent with Chapter 7 and another study of YKL-40 in sporadic FTD (Alcolea et al., 2017), but longitudinal samples were not analysed in either of these studies. CSF chitotriosidase levels correlate negatively with disease duration in MND, and are higher in fast compared with slow progressors, so may indicate disease intensity in MND (Steinacker et al., 2018). This should be explored in larger FTD cohorts.

CSF chitotriosidase levels were significantly raised in patients with genetic FTD overall compared with controls and PMC, but this was only in those with *GRN* or *MAPT* mutations, and not in those with *C9orf72* expansions. This is consistent with raised chitotriosidase levels in the *GRN* patient group in Chapter 7, although levels in the rather small *MAPT* group had not reached significance. However, unlike in Chapter 7, chitotriosidase levels did not differ significantly between patients with each genetic subtype (previously *GRN* patients had had higher levels of sTREM2, YKL-40 and chitotriosidase than *MAPT* and *C9orf72* patients). Greater variability in chitotriosidase levels across individuals within the larger patient groups here may have reduced power to detect small differences between genetic subtypes, despite apparently sufficient

sample sizes from power calculations. Significant differences between genetic FTD subtypes in Chapter 7 may have instead arisen due to inclusion of only three patients with *GRN* mutations, all of whom happened to have markedly high levels, emphasising the benefits of replication in this larger cohort.

CSF YKL-40 levels also initially seemed higher in genetic FTD overall and specifically in *GRN* and *MAPT* mutation carriers compared with controls, but these comparisons became non-significant once adjusted for age. This contrasts with results in Chapter 7, where there were higher YKL-40 levels in *GRN* and *MAPT* patients than controls, and in *GRN* patients compared with *C9orf72* patients. Inclusion of a few patients with extremely high YKL-40 levels in Chapter 7 may have again affected results. Given that later EYO analyses in the present study demonstrated that *GRN* mutation carriers overall (patients and PMC combined) had a significant difference in both YKL-40 and chitotriosidase levels compared with controls, it is odd that YKL-40 levels were similar between the *GRN* patient group and controls. However, the rather variable ages and YKL-40 levels in these groups, particularly in controls, may have precluded detection of small differences, despite adjustment for age. In Chapter 7, YKL-40 levels were also higher in *MAPT* patients than controls. Other studies have found significantly raised YKL-40 levels in FTLD-tau cases compared with controls (Abu-Rumeileh et al., 2019; Alcolea et al., 2017; Teunissen et al., 2016), and although these also included *MAPT* mutation carriers, none analysed levels in this group specifically. The small size of the *MAPT* patient group (n=8) and variability in YKL-40 levels in the present study may have limited power, so replication in a larger cohort is needed.

Surprisingly, sTREM2 levels were not significantly raised in any genetic FTD group, unlike the study in Chapter 7, where levels were significantly higher in patients with *GRN* mutations compared with controls and other genetic groups. However, substantial

variability in sTREM2 levels within patient or PMC groups in the present study may have led to a non-significant difference compared with controls. Large intragroup variability in sTREM2 levels was noted in the mixed FTD cohort in Chapter 7, where levels were overall similar to controls. Alternatively, the high sTREM2 levels in the *GRN* patient group in Chapter 7 may have been spuriously raised, given that only three *GRN* mutation carriers were analysed, and sTREM2 levels may instead be inappropriately normal due to impaired release in individuals with genetic FTD.

There have been few other studies of glia-derived biomarkers in genetic FTD. A recent study presented raw chitotriosidase and YKL-40 values for patients with FTD due to *GRN* (n=12)*, C9orf72* (n=19) and *MAPT* (n=4) mutations, which were of a similar magnitude to observations here (apart from much lower chitotriosidase levels in their *MAPT* group) (Abu-Rumeileh et al., 2019). However, levels were not compared between genetic groups. Other studies have found raised CSF YKL-40 (Antonell et al., 2020; Oeckl et al., 2019), but similar chitotriosidase (Oeckl et al., 2019), levels in genetic FTD versus controls, but cohorts included a smaller number of FTD cases (n=16; n=23), combined genetic subtypes in one group, and did not compare levels for each subtype separately with controls. One cohort contained mostly patients with *C9orf72* expansions (15/23) (Oeckl et al., 2019), who, as shown here, have similar levels of glia-derived biomarkers to controls. The present results demonstrate that glia-derived biomarkers are altered only in certain genetic FTD subtypes, predominantly in *GRN* mutation carriers. This has been shown in studies of other fluid biomarkers in genetic FTD, where levels of plasma (Heller et al., 2020) or serum (Benussi et al., 2020) GFAP and CSF NfL (Meeter et al., 2016a) were selectively elevated in *GRN* mutation carriers. Patients with different mutations should therefore not be combined in genetic FTD cohorts for fluid biomarker analyses as there are clearly different mechanisms which may affect biomarker levels.

The raised chitotriosidase levels in patients with *GRN* mutations are consistent with multiple studies showing raised levels of other inflammatory biomarkers in CSF or blood in *GRN* mutation carriers and significant microglial dysfunction and activation in *GRN* mutation mouse models, as discussed in Chapters 1 and 7. *GRN* mutation models also display lipid accumulating microglia with extensive lysosomal dysfunction (Evers et al., 2017; Marschallinger et al., 2020; Nguyen et al., 2018), and microglial lysosomal dysfunction is seen in human *GRN* mutation carriers (Götzl et al., 2014; Ward et al., 2017). CSF chitotriosidase levels are highly elevated in the lysosomal storage disorder Gaucher's disease (Zigdon et al., 2015), so raised chitotriosidase levels in *GRN* mutation carriers may represent chronic lysosomal failure of microglia due to progranulin insufficiency and lipid mishandling. Raised CSF chitotriosidase levels in patients with *MAPT* mutations is consistent with pronounced microglial activation or dysfunction in the temporal lobes of *MAPT* 10+16 mutation carriers in histological and PET studies, and in mouse models of *MAPT* P301S mutations, as discussed in Chapters 1 and 7.

Chitotriosidase and YKL-40 may initially be released from glial cells as neurodegeneration develops, as a generalised protective response (like sTREM2 in AD). In *GRN* mutation carriers, dysfunctional, degenerating (senescent) microglia (as shown in Chapter 6) may lead to a sustained increase in release of these proteins. This is likely to occur presymptomatically, given that *GRN* PMC already display MRI WMH, which are associated with raised plasma GFAP and NfL levels (Sudre et al., 2019). In addition, microglial PET studies show elevated microglial activation in symptomatic individuals with genetic FTD (Clarke et al., 2019) and in PMC, albeit only *MAPT* PMC have been examined so far (Bevan-Jones et al., 2019; Miyoshi et al., 2010). As discussed in Chapter 1, chitotriosidase activates proinflammatory microglial phenotypes and YKL-40 also encourages a proinflammatory environment. Over time in *GRN* PMC, chronic activation of the innate immune response followed by premature microglial senescence

could therefore contribute to neuronal or synaptic damage, but this could be reversible if detected early enough. Plasma chitotriosidase levels are already used for diagnosis and monitoring treatment response in Gaucher's disease (Drugan et al., 2017), so CSF chitotriosidase levels should be explored as a potential biomarker of treatment response for clinical trials for genetic FTD.

The lack of raised sTREM2 levels in each group, particularly in patients with *GRN* mutations, was unexpected. However, although progranulin and TREM2 are both expressed by microglia, they regulate microglial function and immune pathways in opposite ways. Homozygous loss of TREM2 locks microglia in a homeostatic state (Götzl et al., 2019; Mazaheri et al., 2017), whereas homozygous loss of progranulin locks microglia in a proinflammatory state, promoting phagocytosis and cytokine release (Götzl et al., 2019). CSF levels of progranulin and sTREM2 rise in tandem in presymptomatic AD (Suárez-Calvet et al., 2018), suggesting that these proteins are linked and are part of the microglial response to ensuing neurodegeneration. Progranulin haploinsufficiency in *GRN* mutation carriers could somehow alter TREM2 expression and impair sTREM2 release, compounded by microglial lysosomal dysfunction and senescence. If sTREM2 levels fail to rise appropriately in *GRN* PMC, this may alter the homeostatic mechanisms mediated by sTREM2 from a young age. As sTREM2 normally promotes microglial activation, proliferation, migration, and survival (Zhong et al., 2019), normal sTREM2 levels in carriers of FTD-associated mutations may reflect an inadequate microglial response and this could in turn compound dysfunction of already degenerating microglia. A recent study used an anti-TREM2 antibody as an agonist to improve TREM2 activation in an AD model with the R47H variant in *TREM2* (which usually impairs TREM2 function) (Wang et al., 2020). This led to increased microglial proliferation, a less inflammatory microglial response and less AD pathology. A similar approach targeting TREM2 could be explored in *GRN* mutation models of FTD.

In the *C9orf72* patient group, levels of all glia-derived biomarkers were highly variable and did not differ significantly from controls. This was surprising given that several mouse models of *C9orf72* expansions demonstrate excessive microglial activation (Burberry et al., 2016, 2020; O'Rourke et al., 2016; Sudria-Lopez et al., 2016). However, levels of these biomarkers were also not elevated in *C9orf72* patients in the study in Chapter 7, albeit in a smaller group, and another study found similar CSF chitotriosidase levels in FTD cases with *C9orf72* expansions and controls (Barschke et al., 2020). A recent study found that immune dysfunction and microglial activation in the spinal cord of a *C9orf72* mouse model of ALS vary widely according to the mouse gut microbiome (Burberry et al., 2020). Variants in *TMEM106B* also modify effects of the *C9orf72* expansion by impacting lysosomal function (Busch et al., 2016). These mechanisms may underlie the variability in histological changes in microglia across FTLD-*C9orf72* cases in Chapters 5 and 6 and the variability in glia-derived biomarker levels in *C9orf72* expansion carriers seen here.

Biomarker levels may also vary according to the location of pathology: CSF chitotriosidase levels in MND cases with *C9orf72* expansions are higher than in FTD due to *C9orf72* expansions (Barschke et al., 2020), and both sporadic and genetic MND are associated with highly elevated levels of chitotriosidase (Mishra et al., 2017; Oeckl et al., 2019; Steinacker et al., 2018; Thompson et al., 2018; Varghese et al., 2013), sTREM2 (Cooper-Knock et al., 2017), and YKL-40 (Abu-Rumeileh et al., 2019; Andrés-Benito et al., 2018; Illán-Gala et al., 2018; Oeckl et al., 2019; Sanfilippo et al., 2017; Thompson et al., 2018). The present study deliberately excluded individuals with only MND, allowing demonstration that glia-derived biomarkers are not significantly raised in *C9orf72* expansion carriers with FTD.

This study also analysed glia-derived biomarkers in *GRN*, *C9orf72* and *MAPT* PMC, comparing levels between genetic subtypes, which no studies have done previously. Levels of all biomarkers were similar between PMC overall (all mutations combined) compared with controls, but also similar between controls and each PMC genetic subgroup, and between genetic PMC subgroups, most likely due to highly variable ages and EYO across PMC leading to significant variability in biomarker levels. As predicted, patients had higher levels of chitotriosidase than PMC overall, but this was specifically in *GRN* and *MAPT* mutation carriers.

Further analysis of biomarker levels in early and late PMC within each genetic subtype found that chitotriosidase levels were higher in *GRN* and *MAPT* patients than in late PMC (less than 10 EYO), but not compared with early PMC (more than 10 EYO). This was surprising, but participants in the early PMC subgroups had particularly variable ages, EYO and biomarker levels, which may have reduced power when compared with the smaller, more homogeneous patient groups. Other studies have found similar YKL-40 (Antonell et al., 2020; Oeckl et al., 2019) and chitotriosidase (Oeckl et al., 2019) levels in PMC overall compared with controls, and higher YKL-40 (but not chitotriosidase) levels in patients than PMC (Antonell et al., 2020; Oeckl et al., 2019), concluding that levels do not change until the symptomatic phase. However, these studies combined PMC genetic subgroups, did not separate early and late PMC, and did not analyse how levels changed with EYO.

A previous study using the GENFI cohort reported that *GRN*, *C9orf72* and *MAPT* mutation carriers displayed presymptomatic changes in neuroimaging and neuropsychological parameters from between 25 and 5 years, and around 5 years (respectively), before expected onset (Rohrer et al., 2015). These changes varied regionally and chronologically according to the genetic subtype. However, so far fluid

biomarker studies in GENFI have indicated that changes occur predominantly in individuals who are going through conversion to the symptomatic phase ('converters'), rather than earlier on. CSF NfL (Meeter et al., 2016a) and plasma GFAP (Heller et al., 2020) levels rise dramatically in *GRN* converters, and CSF neuronal pentraxin-2 levels fall in *GRN* or *MAPT* converters (van der Ende et al., 2020). Serum NfL levels rise sharply in converters with different mutations, but also rise gradually in *C9orf72* PMC over time (van der Ende et al., 2019). However, levels of these fluid biomarkers did not differ significantly between PMC groups overall and controls (similar to results here). Fluid biomarkers may vary at different timepoints, which may differ according to the underlying mutation, so group-level analyses of PMC will not detect this.

This study therefore analysed associations of glia-derived biomarker levels with EYO in each genetic subtype (*GRN*, *C9orf72* and *MAPT*), combining PMC and patients (i.e. all mutation carriers) in each group and analysing how levels change over EYO for each genetic subtype compared with non-carriers (controls). This approach revealed that CSF chitotriosidase and YKL-40 levels are raised presymptomatically in *GRN* mutation carriers, with significantly higher levels compared with controls from six years before expected onset for chitotriosidase, and between one and zero years before onset for YKL-40. Levels of both biomarkers differed increasingly between carriers and controls towards expected onset and into the symptomatic phase. Presymptomatic *MAPT* mutation carriers appeared to have be high chitotriosidase levels from three EYO, with more obviously diverging levels between symptomatic *MAPT* carriers and controls, although this did not reach significance compared with controls at any EYO timepoint. In contrast, sTREM2 levels did not differ significantly at any EYO timepoint between any mutation group and controls.

As CSF chitotriosidase levels are raised several years prior to expected onset in *GRN* PMC, they could be useful as a biomarker of disease proximity. If validated in further cross-sectional and longitudinal studies, this could be very useful for clinical trials. A similar approach in another GENFI study, which correlated age (instead of EYO) with serum NfL levels in PMC, showed that NfL levels differed between PMC and controls from age 48 onwards, i.e. several years prior to expected onset, although gene-specific differences were not analysed (van der Ende et al., 2019). Here, CSF YKL-40 levels were altered much closer to onset, suggesting a different phase of glial activation or dysfunction, and perhaps a sudden rise in astrocytic involvement during a decompensation phase immediately prior to conversion. Although YKL-40 levels may not predict an early enough prodromal phase to guide optimal therapeutic intervention, they could be useful for monitoring treatment response or predicting impending conversion. In a recent study of young individuals premanifest for HD, CSF and plasma NfL, CSF mutant huntingtin and CSF YKL-40 levels were all higher in PMC than controls, but although CSF NfL levels were abnormal in some individuals from 24 years before onset, NfL levels accelerated much closer to onset (Scahill et al., 2020). This suggests that different temporal changes in fluid biomarkers reflect progressive involvement of microglia, astrocytes and neuronal injury along the disease trajectory, and so may be useful for different purposes and at different timepoints in clinical trials.

In conclusion, CSF chitotriosidase levels are raised several years before expected symptom onset in *GRN* mutation carriers (and possibly in *MAPT* mutation carriers) and CSF YKL-40 levels are raised just before symptom onset in *GRN* mutation carriers. Levels of chitotriosidase remain markedly elevated in symptomatic *GRN* mutation carriers compared with controls. This is suggestive of extensive early microglial (and later astrocytic) activation or dysfunction contributing to disease in genetic FTD, with variable involvement according to the underlying mutation.

8.7 Limitations and future work

Although this study recruited large groups of PMC, controls and patients overall, the small size of some of the patient subgroups, particularly the *MAPT* group, may have limited power to detect significant differences between groups. However, this is inherent to a rare disease like genetic FTD, and compounded in longitudinal cohort studies like GENFI, where individuals often avoid having invasive lumbar punctures. The power calculations had demonstrated at least 80% power to detect reasonable effect sizes between groups, but these were based on generalised effect sizes for sTREM2 and chitotriosidase, as in the planning phase typical levels of these biomarkers in genetic FTD cohorts were not available. Smaller effect sizes may therefore have been difficult to detect. Significant differences in age between PMC, control and patient groups were adjusted for in all analyses, but due to the strong associations of YKL-40 and sTREM2 levels with age, this may have also tempered detection of subtle differences in biomarker levels between groups.

Symptom onset in patients was retrospectively assessed from caregiver or patient reports within a clinical setting, which may be influenced by multiple factors, and can be difficult to define accurately in an insidious disease like FTD. However, no better parameter exists for determining AAO in already symptomatic individuals. EYO was calculated based on age at CSF and values for mean family AAO, but AAO varies markedly even within families, and across specific mutation types, particularly for *MAPT* mutation carriers (Moore et al., 2020). However, individual AAO is significantly correlated with both parental AAO and mean family AAO in families of *GRN, C9orf72* and *MAPT* mutation carriers (Moore et al., 2020), so mean family AAO was a reasonable way of calculating predicted AAO and therefore EYO at the time of CSF collection.

Mutations in *CHIT1* should ideally have been analysed in the cohort, as these affect CSF chitotriosidase levels (Abu-Rumeileh et al., 2019). Although five individuals with undetectable levels were excluded due to likely homozygosity, there may have been heterozygous carriers with low-normal chitotriosidase levels in certain groups, which may have biased results. However, analysis of DNA samples for *CHIT1* mutations was not possible at the time of this study. This may be carried out in future, with agreement from participating GENFI sites, prior to extension of this study in a larger cohort.

Relationships of glia-derived biomarker levels with other cross sectional or longitudinal disease biomarkers such as serum or CSF NfL levels, neuroimaging changes (regional volumes or atrophy rates), and changes in neuropsychological scores, were not analysed in this study, due to time constraints. Longitudinal measurements of glia-derived biomarker levels were also not performed, predominantly due to a lack of serial CSF samples available from external sites, particularly in patients. These analyses would be helpful to determine how stable glia-derived biomarker levels are over time, and whether they can be used for prediction of disease proximity, intensity and progression. This may provide validation for their use in clinical trials.

8.8 Publications relating to this chapter

Analysis of these biomarkers in further GENFI CSF samples is underway and a manuscript will be prepared incorporating these results.

However, work arising from this chapter was delivered by the author in an oral platform presentation at the 11th International Conference on Frontotemporal Dementias in Sydney, Australia, in November 2018, and was awarded Runner Up in the 2018 International Society for Frontotemporal Dementias Early Career Researcher Prize.

9 General conclusions and future directions

The overarching aim of this thesis was to investigate different aspects of neuroinflammation in FTD, in order to understand more about the pathogenesis of disease and to identify processes and promising biomarkers for future study. Through a series of clinical, histological and CSF biomarker studies, this thesis has produced multimodal evidence that implicates systemic immune dysfunction, altered neuroinflammation and microglial dysfunction in FTD, particularly in *GRN* mutation carriers. This chapter summarises the findings of this thesis, the implications for our understanding of FTD and areas for future work.

9.1 Summary of findings

9.1.1 Previous evidence of neuroinflammation in FTD

Although multiple previous studies have indicated a link between chronic neuroinflammation or immune dysfunction and FTD, until now, a detailed review and critical appraisal of all the existing evidence was lacking. Chapter 1 therefore presented a comprehensive review of our current understanding of FTD, the challenges of this clinicopathologically heterogeneous disease, the current position on CSF biomarkers, and evidence from studies of neuroinflammation in FTD, in order to identify gaps in knowledge and areas for future work. Through this, several areas of imminent need for research were identified, and these were addressed as the main aims of this thesis:

(i) To explore whether there is evidence of systemic and central immune dysfunction in individuals with FTD and determine how this varies across the spectrum of disease.

(ii) To examine whether changes indicative of microglial dysfunction vary across the spectrum of disease.

(iii) To examine whether inflammatory biomarkers in CSF of individuals with sporadic or genetic FTD enable differentiation of clinical syndromes or mutation subtypes and link to existing biomarkers of neurodegeneration.

(iv) To establish whether levels of inflammatory biomarkers in CSF change presymptomatically and could therefore help guide prediction of disease proximity in individuals at risk of genetic FTD, for use in clinical trials.

Detailed discussion of the studies in this thesis carried out to address each of these aims was presented within the 'Discussion' and 'Limitations and future work' sections in each chapter. The following sections therefore summarise the findings of each chapter in order to demonstrate achievement of these aims and to discuss the general contributions of this thesis towards understanding the role of neuroinflammation in FTD.

9.1.2 Heightened systemic autoimmunity in *GRN* mutation associated FTD

The study in Chapter 3 analysed the prevalence of systemic autoimmune diseases in a genetic FTD cohort with either *GRN*, *C9orf72* or *MAPT* mutations, compared with cognitively normal controls. This was inspired by *GRN* or *C9orf72* -/- or deficient mouse models showing florid systemic autoimmune diseases, links to variants in immune genes such as *HLA* identified in GWAS of FTD cohorts, and presence of anti-progranulin antibodies in individuals with systemic autoimmune diseases such as vasculitis. This study found an increased prevalence of non-thyroid systemic autoimmune diseases, including coeliac disease, sarcoidosis, ankylosing spondylitis, recurrent polyarthritis, and persistent eosinophilia with pericarditis, in individuals with FTD due to *GRN* mutations, but not in those with *C9orf72* expansions or *MAPT* mutations. *C9orf72* or *MAPT* mutation carriers had a similar prevalence of autoimmune diseases to controls, suggesting less of a link between these genes and systemic autoimmunity.

Although this was a retrospective clinical study without fluid biomarker correlation, it achieved the first half of aim (i), demonstrating that there is clinical evidence of systemic immune dysfunction in individuals with FTD, and that this varies across the genetic spectrum of disease, being present predominantly in *GRN* mutation carriers. Given that a detrimental impact of systemic infections or chronic systemic inflammation on cognitive function is well recognised, for example delirium in cognitively normal individuals with sepsis, accelerated cognitive decline in patients with dementia who develop infections, and altered cognitive function in patients with systemic rheumatological conditions, heightened systemic autoimmunity and a chronic, proinflammatory systemic environment could contribute to neuronal damage in *GRN* mutation carriers.

The results of this study directly contributed to optimising data collection and protocols for ongoing longitudinal studies of FTD (GENFI and LIFTD), which will allow exploration of this in greater detail and on a larger scale in future. Prior to this study, the name of an autoimmune disease was not often not recorded on case report forms during UCL LIFTD assessments, and the subtype of autoimmune disease (thyroid/non-thyroid) and name of the disease were not consistently being recorded during clinical assessments at external (non-UCL) GENFI sites. However, as certain clusters of non-thyroid diseases were specifically increased in those with *GRN* mutations, a more detailed approach was deemed needed. A requirement for the subtype and name of autoimmune disease has now been included as standard within GENFI clinical case report forms for all sites, and LIFTD clinical case report forms at UCL. This should substantially improve the capability for replication of this study across multiple countries going forward. Analysis of the presence or development of autoimmune disease in PMC over time is planned and this will help to establish the chronological relationship between onset of systemic autoimmune disease and neurological disease in the various mutation groups. These findings have also highlighted the need for similar studies in sporadic FTD, given

autoimmune mechanisms may also contribute to disease in sporadic FTLD-TDP cases with svPPA (Miller et al., 2013), and this will be carried out in LIFTD participants in due course.

9.1.3 Microglia vary regionally across the spectrum of FTLD

Following exploration of systemic immune dysfunction in genetic FTD, this thesis then carried out a series of histological studies to examine whether changes indicative of central immune dysfunction, and in particular microglia, varied across the spectrum of disease in sporadic and genetic FTLD. This achieved the second half of aim (i) and the entirety of aim (ii).

The study in Chapter 4 used a histological and neuroimaging approach to explore the histopathological correlates of MRI WMH in five brain regions in a case of FTLD-*GRN*. This demonstrated that WMH were not due to vascular disease (as had been assumed previously) and were instead associated with profound white matter demyelination and region-specific alterations in microglia and astrocytes. Phagocytic and antigen-presenting microglia were highly activated in white matter, but microglia were also severely dystrophic here, particularly in the frontal lobe, where WMH in *GRN* mutation carriers are typically seen (Sudre et al., 2017a, 2019). The severity of histopathological changes varied regionally and between grey and white matter, correlating with the severity of grey and white matter neuroimaging changes. This study was, for the first time, able to directly link regionally variable microglial involvement and demyelination to changes in other biomarkers of disease studied in *GRN* mutation carriers (grey matter atrophy and WMH), leading to the conclusion that microglial dysfunction may contribute to region-specific grey and white matter damage and disease pathogenesis in genetic FTD. It also highlighted the presence of frontal WMH in individuals with a neurodegenerative, FTD-like disease as a signature of an underlying *GRN* mutation, confirming that there is a different imaging pattern and underlying histopathological

changes from cerebrovascular small vessel disease. This is important for clinicians assessing patients in cognitive disorders clinics, who may have otherwise assumed a primarily vascular aetiology.

Regional changes in microglia were explored further in Chapter 5 through a histological study of the burden and activation state of three different microglial phenotypes (phagocytic, antigen-presenting and general microglia) in frontotemporal grey and white matter of sporadic and genetic FTLD cases, with comparison groups of AD cases and controls. This study used immunohistochemistry and antibodies to detect three microglial markers (CD68, CR3/43 and Iba1) in *post-mortem* brain tissue. Quantitative assessment of microglia, performed for the first time in a large FTLD cohort, showed that there was typically an increased burden of phagocytic and antigen-presenting microglia in FTLD cases compared with controls, but often without an increase in microglial activation, particularly in white matter. In depth comparison of microglia across FTLD subtypes also demonstrated that the burden and activation of different microglial phenotypes varied regionally and between grey and white matter, differing across the pathological and genetic spectrum of FTLD. This strengthened hypotheses arising from the few previous studies of microglia in FTLD that region-specific microglial dysfunction or senescence may contribute to neurodegeneration, as activation was not necessarily increased in areas of high microglial burden. It also highlighted a potential role for variable involvement of specific microglial phenotypes (for example either phagocytic or antigen-presenting microglia), and failed activation of certain phenotypes in specific regions, in determining the clinicopathological heterogeneity of FTLD.

9.1.4 Microglial senescence may contribute to FTLD

The surprisingly minimal activation of microglia in many FTLD cases in Chapter 5, and observations of disrupted cell morphology suggestive of severely dystrophic microglia in Chapters 4 and 5, led to an extension study in Chapter 6, which examined histological

patterns of microglial dystrophy and microglia with other unusual morphologies (rod-shaped and hypertrophic microglia) in frontotemporal grey and white matter within the same cohort. This demonstrated that, as hypothesised in Chapters 4 and 5, microglial dystrophy varied regionally across the pathological and genetic spectrum of FTLD, and was particularly severe in white matter, but was also present in AD cases. Certain groups such as FTLD-*GRN* cases had extremely severe dystrophy in most regions, particularly in white matter. In addition, rod-shaped microglia were prominent in certain FTLD subtypes such as FTLD-*MAPT*, FTLD-CBD and FTLD-TDPA or FTLD-TDPB cases with *C9orf72* expansions, whereas hypertrophic microglia were prominent in others, mainly FTLD-Picks and FTLD-TDPC cases. As dystrophic microglia are thought to be the morphological correlate of senescent, degenerating microglia, this work suggests that microglial senescence and morphology varies across the spectrum of FTLD, and that certain pathological or genetic subtypes are associated with particularly severe microglial pathology. This may be due to disease mechanisms such as lysosomal dysfunction or lipid mishandling contributing to excessive microglial senescence. Given that these mechanisms are particularly linked to *GRN* mutations in various mouse and cell models of FTD, they could be a promising therapeutic target for further exploration.

Although these findings link histological changes in microglia to the pathogenesis and clinicopathological heterogeneity of FTLD, it remains difficult to prove through assessments of microglia in *post-mortem* tissue that the morphological appearance of a microglial cell represents a particular activation state, function or dysfunction (or senescence) of that cell, how that relates to nearby pathology, or when this played a role in disease (if at all). In addition, it remains unclear whether a subtle proteinopathy arises first in individuals who later develop FTLD, which then leads to microglial dysfunction and senescence due to immunological exhaustion from attempts at protein clearance in that region, or if pre-existing regional variations in microglial function and senescence

predispose a region to protein mishandling and neuronal vulnerability, or both. However, a study of microglial gene expression in mice suggests that epigenetic mechanisms alter microglial clearance activity differentially across brain regions, and this leads to regional vulnerabilities to neuronal dysfunction (Ayata et al., 2018). Although this is yet to be corroborated in human tissue, certain individuals may have pre-existing regional alterations in microglial function or survival. This could predispose them to dysfunctional clearance of accumulating proteins, excessive clearance of healthy or mildly diseased neurons in specific brain regions, and onset of neurodegenerative disease. Region-specific changes in microglial gene expression are also associated with differential responses to aging, the main risk factor for neurodegenerative disease (Grabert et al., 2016).

9.1.5 CSF glia-derived biomarker levels vary across the spectrum of FTD

Given the advent of various disease modifying treatments for genetic FTD in clinical trials, there is a pressing need to be able to repeatedly detect changes in disease processes and assess response to treatments *in vivo* over time, and this includes neuroinflammatory processes. Although microglial PET studies can assess the degree of neuroinflammation to a certain extent in individuals with FTD and in PMC, these are costly and not well validated, and due to the nature of current tracers may not be safe to replicate over many years. The review of current CSF biomarkers for FTD in Chapter 1, and the heterogeneity of microglia in FTLD in Chapters 5 and 6, highlighted a need for better fluid biomarkers of neuroinflammation, and specifically glial cell activation or dysfunction, for FTD, despite the potential usefulness of certain neurodegenerative biomarkers, such as CSF or serum NfL levels.

Although several studies had examined various inflammatory biomarkers such as cytokine levels in blood or CSF within FTD cohorts, CSF levels of glia-derived proteins such as sTREM2, YKL-40 and chitotriosidase may be more useful as these are directly

derived from microglia (and YKL-40 also from astrocytes) in the CNS. However, previous studies had not enabled adequate exploration of whether glia-derived biomarker levels differ across clinical FTD syndromes or genetic FTD subtypes, or linked them to levels of existing biomarkers of neurodegeneration used in clinical practice, such as T-tau, P-tau or Aβ42. Very few studies had examined levels in PMC to see if they change presymptomatically, and those that did had failed to compare levels between groups of individuals with different gene mutations. These gaps in research generated aims (iii) and (iv) of this thesis, which were achieved in Chapters 7 and 8.

The study in Chapter 7 examined levels of sTREM2, YKL-40 and chitotriosidase in CSF of a well-phenotyped cohort of individuals with sporadic FTD and a small number of individuals with genetic FTD, compared with cognitively normal controls, which no studies had done in combination previously. This demonstrated that levels of YKL-40 and chitotriosidase, but not sTREM2, were elevated in CSF in individuals with a clinical diagnosis of FTD. However, levels were not consistently raised across all clinical subtypes of FTD: YKL-40 was only significantly raised in lvPPA and nfvPPA, and chitotriosidase was raised in lvPPA, but neither were raised in bvFTD, svPPA or PPA-NOS. High levels in lvPPA or nfvPPA cases were likely due to a greater predominance of underlying AD pathology. In line with this, levels of all three biomarkers were higher in those with a clinical FTD syndrome but an AD-like CSF biomarker profile than in those with non-AD-like CSF, perhaps due to more extensive glial dysfunction from AD than FTLD pathology. Although pathologically confirmed FTLD cases were not available to clarify whether these biomarkers could differentiate between FTLD subtypes, analysis in a few individuals with genetic FTD illustrated that sTREM2, YKL-40 and chitotriosidase levels were highly elevated in *GRN* mutation carriers, and YKL-40 was increased in *MAPT* mutation carriers, but none of the biomarkers was elevated in *C9orf72* expansion carriers.

These results suggest that glia-derived biomarkers do not help in differentiating between clinical FTD syndromes in those with sporadic disease but may be useful in differentiating between genetic FTD subtypes. Although this study confirmed levels were higher in those with underlying likely AD than FTLD, this is not of great clinical utility, as this can already be reliably detected through analysis of CSF neurodegenerative biomarker profiles such as the T-tau/Aβ42 ratio, which are now established investigations for dementia in most specialist centres. However, this study again implicated *GRN* (and *MAPT*) mutations in glial dysfunction, and as levels of glia-derived biomarkers correlated with T-tau even in those with likely underlying FTLD, they do seem to reflect the glial contribution or response to neurodegeneration. This could be useful to monitor over time, particularly in individuals at risk of ensuing neurodegeneration, such as PMC of FTD-associated mutations, as has been demonstrated in presymptomatic AD cohorts (Suárez-Calvet et al., 2016a).

9.1.6 CSF glia-derived biomarkers are raised presymptomatically in *GRN* mutation carriers

To explore glia-derived biomarkers in genetic FTD in more detail, the study in Chapter 8 analysed sTREM2, YKL-40 and chitotriosidase levels in a much larger cohort of patients with *GRN*, *C9orf72* or *MAPT* mutations, compared with non-carriers (controls). It also analysed levels in PMC of these mutations, comparing levels across genetic subtypes, and correlated levels of each biomarker with time in years from expected onset of symptoms (EYO) in mutation carriers with each genetic subtype compared with controls, which had not been done previously. This helped to determine whether and when biomarker levels changed in the presymptomatic phase.

This study confirmed that CSF chitotriosidase levels were markedly raised in patients with FTD due to *GRN* mutations, and this was also present presymptomatically, with higher chitotriosidase levels from six years before expected onset when compared with

controls. In contrast, YKL-40 levels in *GRN* mutation carriers differed from controls from between one to zero years before expected onset but were not significantly raised in patients with *GRN* mutations, perhaps due to greater variability in levels in the smaller patient group when compared with controls. CSF chitotriosidase levels were also raised in patients with FTD due to *MAPT* mutations, but it was less clear whether these changed presymptomatically. Although levels in *MAPT* mutation carriers appeared high from three years before expected onset, this did not reach significance when compared with controls at any timepoint. Interestingly, CSF sTREM2 levels were not raised in any PMC or patient group, in contrast to the study in Chapter 7, and again none of the biomarkers was raised in *C9orf72* expansion carriers.

Although this study was cross-sectional and lacked correlation of glia-derived biomarkers with other biomarkers of neurodegeneration, it is the largest and most comprehensive study of glia-derived biomarkers in genetic FTD to date, and the only study in the literature to assess levels in separate PMC groups or correlate levels with EYO. The findings suggest that CSF chitotriosidase and YKL-40 levels may be useful as biomarkers of disease proximity in presymptomatic *GRN* or *MAPT* mutation carriers, but not in *C9orf72* expansion carriers, and may reflect different chronological phases of glial activation or dysfunction, which could be amenable to therapeutic intervention. It is therefore crucial to explore these biomarkers in other FTD cohorts with harmonised protocols, like the FTD Prevention Initiative, which brings together multiple genetic FTD cohorts from across Europe, North America, South America and Australasia. If they are to be used in clinical trials, these biomarkers need to be well validated and assessed longitudinally. The extent of variability within and between individuals, and relationships with other measures likely to be used alongside biofluid assessments in clinical trials (such as neuroimaging or neuropsychological changes), must also be confirmed on a large scale.

9.2 Future work

Specific areas for future work were discussed within each chapter, so this section focuses on key avenues for research that may improve our understanding of the role of systemic immune dysfunction and chronic neuroinflammation in FTD.

The mechanisms behind systemic immune dysfunction in *GRN* mutation carriers remain unclear, but given that progranulin regulates TNF-α and NF-κβ mediated pathways and macrophage and microglial function both systemically and in the CNS, these pathways could be a combined therapeutic target for individuals with *GRN* mutations. Examining peripheral macrophages, T and B lymphocytes and microglia in *GRN* mutation carriers, for example using peripheral blood mononuclear cells, or iPSCs derived from fibroblasts obtained from skin biopsies, would improve appreciation of how these are altered. Analysis of multi-site clinical data from GENFI would allow examination of the prevalence of specific autoimmune diseases in a large number of symptomatic *GRN, C9orf72* and *MAPT* mutation carriers, and their onset and relationship to onset of neurological disease in PMC. Analysis of future LIFTD data would allow assessment of autoimmune diseases across a variety of sporadic FTD subtypes and inclusion of more controls. Correlation of clinical data with biofluid levels of systemic and CSF inflammatory markers would enable confirmation of these clinical observations and quantitative comparison between individuals with, and without, autoimmune disease.

Although a large cohort of FTLD cases was used for the studies in Chapters 5 and 6, future histological studies of microglia in FTLD should ideally aim to replicate findings in a larger cohort to increase numbers in each FTLD subtype, and should include more AD cases and controls for comparison. This may be challenging given the rarity of FTLD cases within brain banks, but collaboration between centres may enable this. Correlation of histological changes in microglia with regional burdens of neuropathology across a

variety of different brain regions (including ‘control’ or less affected brain regions) would also be valuable. This would explore hypotheses arising from this thesis that regional changes in microglial burden, activation and dystrophy reflect or contribute to the regional extent and subtype of pathology, which is known to extend beyond the frontotemporal regions already examined. Quantitative examination of microglial dystrophy would also be useful, given only semi-quantitative dystrophy scoring was possible for this thesis, and much more information about microglial burden and activation was captured through quantitative analyses in Chapter 5.

A recent study of FTD cases with histological correlation used the microglial PET tracer ^{11}C-PK-11195 to demonstrate that binding correlated regionally with binding of another tracer (^{18}F-AV-1451) that localises to non-Aβ (including tau or TDP-43) pathology (Bevan-Jones et al., 2020). A longitudinal microglial PET study in FTD has been set up at UCL, which the author contributed to through protocol design, recruiting participants, and accompanying participants to PET scans. This study is ongoing, but it will be useful to explore regional patterns of microglia *in vivo* and compare them with the histological findings in this thesis. The relationship between microglia and regional burdens of different pathologies could in future be explored *in vivo*, particularly if better PET tracers were developed that could detect more specific pathological aggregates. However, this approach is currently limited by the non-specificity of available PET radioligands for specific FTLD pathologies. Correlation of histological patterns of microglia and neuropathology with microglial PET binding patterns *in vivo* could also be examined in individuals who later donate their brains for *post-mortem* analysis.

The mechanisms behind microglial dysfunction in FTLD remain unclear, but this thesis has discussed how impaired lipid handling and lysosomal dysfunction in microglia could play a role in *GRN* mutation carriers, by contributing to excessive microglial senescence.

This theory is based on several mouse models linking progranulin deficiency to dysfunction of these processes, the extent of microglial dystrophy in FTLD-*GRN* cases demonstrated in Chapters 4 and 6, and the markedly elevated chitotriosidase levels in CSF of *GRN* mutation carriers in Chapters 7 and 8 (which are also increased in the lysosomal storage disorder Gaucher's disease). However, mouse or cell models of mutations in a variety of other genes known to cause FTD (*C9orf72*, *MAPT, SQSTM1, VCP*, *TBK1,* or *CHMP2B*) also develop abnormalities in microglia or lysosomes, or autoimmune diseases, and these pathways could be valuable universal therapeutic targets for genetic or sporadic FTD. Future disease models should study the effects of different protein inclusions (tau and TDP-43 isoforms) and gene mutations on microglia, to aid understanding of the timeline, extent and mechanisms of microglial activation and senescence and lysosomal dysfunction across the spectrum of FTLD. This may also explore whether immunomodulatory, anti-senescence or lysosome-modulating therapies could be candidates for future clinical trials for FTD.

Microglial and lysosomal function and senescence are highly complex and likely also influenced by polygenic variants in immune system genes linked to FTD, such as *HLA* (Broce et al., 2018; Ferrari et al., 2014, 2017; Pottier et al., 2019) or *TREM2* (Guerreiro et al., 2013; Kleinberger et al., 2017) and in lysosomal genes linked to variability in FTLD-*GRN* and FTLD-*C9orf72*, such as *TMEM106B*, *SORT1* and *PSAP* (Busch et al., 2013, 2016; F. Hu et al., 2010; Nicholson et al., 2016; Pottier et al., 2018; Premi et al., 2017). Variants in several immune pathway or lysosomal genes are also linked to variability in sporadic FTD (Pottier et al., 2019). Other external or environmental factors may also play a role in determining the fate of microglia in an aging individual that subsequently develops FTLD. This complexity continues to provide a therapeutic challenge for both sporadic and genetic FTD, and it is likely to be several years before treatments targeting immune or lysosomal pathways show consistent promise in animal or cell models, let

alone in human clinical trials. Future studies should ideally analyse participants for variants in these genes, as well as causative FTD-associated mutations, and expand strategies to include exploration of novel parameters such as the gut microbiome, which may exert modifiable influences on CNS immune pathways (Burberry et al., 2020).

Although the findings in Chapter 7 and 8 regarding glia-derived biomarkers across the spectrum of FTD have been illuminating, future CSF biomarker studies should focus on analysing sTREM2, YKL-40 and chitotriosidase levels within larger cohorts of individuals with pathologically confirmed sporadic FTD and in more individuals with symptomatic and presymptomatic genetic FTD, to validate these findings. There should ideally be longitudinal measurements in CSF, including in individuals who convert from a presymptomatic to symptomatic phase during the study. This would elucidate how chitotriosidase and YKL-40 levels differ at various timepoints along the disease continuum in *GRN* or *MAPT* mutation carriers, including whether levels change over time, and how stable levels are in the presymptomatic and symptomatic phase. Comparison of glia-derived biomarkers with other promising fluid biomarkers such CSF and serum or plasma NfL and GFAP levels, and with changes in other biomarker modalities such as neuroimaging changes and neuropsychological scores, would also improve understanding of when, and how, chronic neuroinflammation and glial dysfunction link to neurodegeneration and functional decline.

Ultimately, the aim is to reach a point where we understand the sequential changes in neuroinflammatory and other pathways which contribute to neurodegeneration in FTD, so we can develop effective novel treatments or repurpose existing therapies to target these early enough. The work within this thesis has contributed to this process and this will hopefully bring us a step closer to helping future generations of people who are already living with, or who are at risk of developing, this devastating disease.

10 References

Abu-Rumeileh, S., Mometto, N., Bartoletti-Stella, A., Polischi, B., Oppi, F., Poda, R., Stanzani-Maserati, M., Cortelli, P., Liguori, R., Capellari, S., Parchi, P., 2018. Cerebrospinal fluid biomarkers in patients with frontotemporal dementia spectrum: A single-center study. J. Alzheimer's Dis. 66, 551–563. https://doi.org/10.3233/JAD-180409

Abu-Rumeileh, S., Steinacker, P., Polischi, B., Mammana, A., Bartoletti-Stella, A., Oeckl, P., Baiardi, S., Zenesini, C., Huss, A., Cortelli, P., Capellari, S., Otto, M., Parchi, P., 2019. CSF biomarkers of neuroinflammation in distinct forms and subtypes of neurodegenerative dementia. Alzheimer's Res. Ther. 12, 1–15. https://doi.org/10.1186/s13195-019-0562-4

Acosta-Cabronero, J., Patterson, K., Fryer, T.D., Hodges, J.R., Pengas, G., Williams, G.B., Nestor, P.J., 2011. Atrophy, hypometabolism and white matter abnormalities in semantic dementia tell a coherent story. Brain 134, 2025–2035. https://doi.org/10.1093/brain/awr119

Ahmad, L., Zhang, S.Y., Casanova, J.L., Sancho-Shimizu, V., 2016. Human TBK1: A Gatekeeper of Neuroinflammation. Trends Mol. Med. https://doi.org/10.1016/j.molmed.2016.04.006

Ahmed, Z., Sheng, H., Xu, Y.F., Lin, W.L., Innes, A.E., Gass, J., Yu, X., Hou, H., Chiba, S., Yamanouchi, K., Leissring, M., Petrucelli, L., Nishihara, M., Hutton, M.L., McGowan, E., Dickson, D.W., Lewis, J., 2010. Accelerated lipofuscinosis and ubiquitination in granulin knockout mice suggest a role for progranulin in successful aging. Am. J. Pathol. 177, 311–324. https://doi.org/10.2353/ajpath.2010.090915

Ajami, B., Bennett, J.L., Krieger, C., Tetzlaff, W., Rossi, F.M.V., 2007. Local self-renewal can sustain CNS microglia maintenance and function throughout adult life. Nat. Neurosci. 10, 1538–1543. https://doi.org/10.1038/nn2014

Ajmone-Cat, M.A., Onori, A., Toselli, C., Stronati, E., Morlando, M., Bozzoni, I., Monni,

E., Kokaia, Z., Lupo, G., Minghetti, L., Biagioni, S., Cacci, E., 2019. Increased FUS levels in astrocytes leads to astrocyte and microglia activation and neuronal death. Sci. Rep. 9, 4572. https://doi.org/10.1038/s41598-019-41040-4

Alcolea, D., Carmona-Iragui, M., Suárez-Calvet, M., Sánchez-Saudinós, M.B., Sala, I., Antón-Aguirre, S., Blesa, R., Clarimón, J., Fortea, J., Lleó, A., 2014. Relationship between β-Secretase, Inflammation and Core Cerebrospinal Fluid Biomarkers for Alzheimer's Disease. J. Alzheimer's Dis. 42, 157–167. https://doi.org/10.3233/JAD-140240

Alcolea, D., Irwin, D.J., Illán-Gala, I., Muñoz, L., Clarimón, J., McMillan, C.T., Fortea, J., Blesa, R., Lee, E.B., Trojanowski, J.Q., Grossman, M., Lleo, A., 2018. Elevated YKL-40 and low sAPPβ:YKL-40 ratio in antemortem cerebrospinal fluid of patients with pathologically confirmed FTLD. J. Neurol. Neurosurg. Psychiatry 90, 180–186. https://doi.org/10.1136/jnnp-2018-318993

Alcolea, D., Vilaplana, E., Suárez-Calvet, M., Illán-Gala, I., Blesa, R., Clarimón, J., Lladó, A., Sánchez-Valle, R., Molinuevo, J.L., García-Ribas, G., Compta, Y., Martí, M.J., Piñol-Ripoll, G., Amer-Ferrer, G., Noguera, A., García-Martín, A., Fortea, J., Lleó, A., 2017. CSF sAPPβ, YKL-40, and neurofilament light in frontotemporal lobar degeneration. Neurology 89, 178–188. https://doi.org/10.1212/WNL.0000000000004088

Alquezar, C., de la Encarnacion, A., Moreno, F., Lopez de Munain, A., Martin-Requero, A., 2016. Progranulin deficiency induces overactivation of WNT5A expression via TNF-a/NF-KB pathway in peripheral cells from frontotemporal dementia-linked granulin mutation carriers. J. Psychiatry Neurosci. 41, 225–239. https://doi.org/10.1503/jpn.150131

Alzheimer, A., 1911. Uber eigenartige Krankheitsfalle des spateren Alters. Zeitschrift fur die gesamte Neurol. und Psychiatr. 4, 356–385.

Ameur, F., Colliot, O., Caroppo, P., Stroer, S., Dormont, D., Brice, A., Azuar, C., Dubois,

B., Le Ber, I., Bertrand, A., 2016. White matter lesions in FTLD: distinct phenotypes characterize GRN and C9ORF72 mutations. Neurol. Genet. 2, e47–e47. https://doi.org/10.1212/NXG.0000000000000047

Amick, J., Ferguson, S.M., 2017. C9orf72: At the intersection of lysosome cell biology and neurodegenerative disease. Traffic. https://doi.org/10.1111/tra.12477

Andrés-Benito, P., Domínguez, R., Colomina, M.J., Llorens, F., Povedano, M., Ferrer, I., 2018. YKL40 in sporadic amyotrophic lateral sclerosis: Cerebrospinal fluid levels as a prognosis marker of disease progression. Aging (Albany. NY). 10, 2367–2382. https://doi.org/10.18632/aging.101551

Antonell, A., Mansilla, A., Rami, L., Lladó, A., Iranzo, A., Olives, J., Balasa, M., Sánchez-Valle, R., Molinuevo, J.L., 2014. Cerebrospinal fluid level of YKL-40 protein in preclinical and prodromal Alzheimer's disease. J. Alzheimer's Dis. 42, 901–908. https://doi.org/10.3233/JAD-140624

Antonell, A., Tort-Merino, A., Ríos, J., Balasa, M., Borrego-Écija, S., Auge, J.M., Muñoz-García, C., Bosch, B., Falgàs, N., Rami, L., Ramos-Campoy, O., Blennow, K., Zetterberg, H., Molinuevo, J.L., Lladó, A., Sánchez-Valle, R., 2020. Synaptic, axonal damage and inflammatory cerebrospinal fluid biomarkers in neurodegenerative dementias. Alzheimer's Dement. 16, 262–272. https://doi.org/10.1016/j.jalz.2019.09.001

Armstrong, M.J., Litvan, I., Lang, A.E., Bak, T.H., Bhatia, K.P., Borroni, B., Boxer, A.L., Dickson, D.W., Grossman, M., Hallett, M., Josephs, K.A., Kertesz, A., Lee, S.E., Miller, B.L., Reich, S.G., Riley, D.E., Tolosa, E., Tröster, A.I., Vidailhet, M., Weiner, W.J., 2013. Criteria for the diagnosis of corticobasal degeneration. Neurology 80, 496–503. https://doi.org/10.1212/WNL.0b013e31827f0fd1

Arnold, S.E., Han, L.-Y., Clark, C.M., Grossman, M., Trojanowski, J.Q., 2000. Quantitative neurohistological features of frontotemporal degeneration. Neurobiol. Aging 21, 913–919. https://doi.org/10.1016/S0197-4580(00)00173-1

Atanasio, A., Decman, V., White, D., Ramos, M., Ikiz, B., Lee, H.-C., Siao, C.-J., Brydges, S., LaRosa, E., Bai, Y., Fury, W., Burfeind, P., Zamfirova, R., Warshaw, G., Orengo, J., Oyejide, A., Fralish, M., Auerbach, W., Poueymirou, W., Freudenberg, J., Gong, G., Zambrowicz, B., Valenzuela, D., Yancopoulos, G., Murphy, A., Thurston, G., Lai, K.-M.V., 2016. C9orf72 ablation causes immune dysregulation characterized by leukocyte expansion, autoantibody production, and glomerulonephropathy in mice. Sci. Rep. 6, 23204. https://doi.org/10.1038/srep23204

Au, N.P.B., Ma, C.H.E., 2017. Recent advances in the study of bipolar/rod-shaped microglia and their roles in neurodegeneration. Front. Aging Neurosci. 9, 1–16. https://doi.org/10.3389/fnagi.2017.00128

Ayata, P., Badimon, A., Strasburger, H.J., Duff, M.K., Montgomery, S.E., Loh, Y.-H.E., Ebert, A., Pimenova, A.A., Ramirez, B.R., Chan, A.T., Sullivan, J.M., Purushothaman, I., Scarpa, J.R., Goate, A.M., Busslinger, M., Shen, L., Losic, B., Schaefer, A., 2018. Epigenetic regulation of brain region-specific microglia clearance activity. Nat. Neurosci. 21, 1049–1060. https://doi.org/10.1038/s41593-018-0192-3

Bachstetter, A.D., Ighodaro, E.T., Hassoun, Y., Aldeiri, D., Neltner, J.H., Patel, E., Abner, E.L., Nelson, P.T., 2017. Rod-shaped microglia morphology is associated with aging in 2 human autopsy series. Neurobiol. Aging 52, 98–105. https://doi.org/10.1016/j.neurobiolaging.2016.12.028

Bachstetter, A.D., Van Eldik, L.J., Schmitt, F.A., Neltner, J.H., Ighodaro, E.T., Webster, S.J., Patel, E., Abner, E.L., Kryscio, R.J., Nelson, P.T., 2015. Disease-related microglia heterogeneity in the hippocampus of Alzheimer's disease, dementia with Lewy bodies, and hippocampal sclerosis of aging. Acta Neuropathol. Commun. 3, 32. https://doi.org/10.1186/s40478-015-0209-z

Baker, M., Mackenzie, I.R., Pickering-Brown, S.M., Gass, J., Rademakers, R., Lindholm,

C., Snowden, J., Adamson, J., Sadovnick, A.D., Rollinson, S., Cannon, A., Dwosh, E., Neary, D., Melquist, S., Richardson, A., Dickson, D., Berger, Z., Eriksen, J., Robinson, T., Zehr, C., Dickey, C.A., Crook, R., McGowan, E., Mann, D., Boeve, B., Feldman, H., Hutton, M., 2006. Mutations in progranulin cause tau-negative frontotemporal dementia linked to chromosome 17. Nature 442, 916–919. https://doi.org/10.1038/nature05016

Baldacci, F., Lista, S., Cavedo, E., Bonuccelli, U., Hampel, H., 2017a. Diagnostic function of the neuroinflammatory biomarker YKL-40 in Alzheimer's disease and other neurodegenerative diseases. Expert Rev. Proteomics 14, 285–299. https://doi.org/10.1080/14789450.2017.1304217

Baldacci, F., Toschi, N., Lista, S., Zetterberg, H., Blennow, K., Kilimann, I., Teipel, S., Cavedo, E., dos Santos, A.M., Epelbaum, S., Lamari, F., Dubois, B., Floris, R., Garaci, F., Bonuccelli, U., Hampel, H., 2017b. Two-level diagnostic classification using cerebrospinal fluid YKL-40 in Alzheimer's disease. Alzheimer's Dement. 13, 993–1003. https://doi.org/10.1016/j.jalz.2017.01.021

Balendra, R., Isaacs, A.M., 2018. C9orf72 -mediated ALS and FTD: multiple pathways to disease. Nat. Rev. Neurol. 14, 544–558. https://doi.org/10.1038/s41582-018-0047-2.C9orf72

Bannwarth, S., Ait-El-Mkadem, S., Chaussenot, A., Genin, E.C., Lacas-Gervais, S., Fragaki, K., Berg-Alonso, L., Kageyama, Y., Serre, V., Moore, D.G., Verschueren, A., Rouzier, C., Le Ber, I., Augé, G., Cochaud, C., Lespinasse, F., N'guyen, K., De Septenville, A., Brice, A., Yu-Wai-Man, P., Sesaki, H., Pouget, J., Paquis-Flucklinger, V., 2014. A mitochondrial origin for frontotemporal dementia and amyotrophic lateral sclerosis through CHCHD10 involvement. Brain 137, 2329–2345. https://doi.org/10.1093/brain/awu138

Barschke, P., Oeckl, P., Steinacker, P., Al Shweiki, M.H.D.R., Weishaupt, J.H., Landwehrmeyer, G.B., Anderl-Straub, S., Weydt, P., Diehl-Schmid, J., Danek, A.,

Kornhuber, J., Schroeter, M.L., Prudlo, J., Jahn, H., Fassbender, K., Lauer, M., Van Der Ende, E.L., Van Swieten, J.C., Volk, A.E., Ludolph, A.C., Otto, M., 2020. Different CSF protein profiles in amyotrophic lateral sclerosis and frontotemporal dementia with C9orf72 hexanucleotide repeat expansion. J. Neurol. Neurosurg. Psychiatry 91, 503–511. https://doi.org/10.1136/jnnp-2019-322476

Beck, J., Poulter, M., Hensman, D., Rohrer, J.D., Mahoney, C.J., Adamson, G., Campbell, T., Uphill, J., Borg, A., Fratta, P., Orrell, R.W., Malaspina, A., Rowe, J., Brown, J., Hodges, J., Sidle, K., Polke, J.M., Houlden, H., Schott, J.M., Fox, N.C., Rossor, M.N., Tabrizi, S.J., Isaacs, A.M., Hardy, J., Warren, J.D., Collinge, J., Mead, S., 2013. Large C9orf72 Hexanucleotide Repeat Expansions Are Seen in Multiple Neurodegenerative Syndromes and Are More Frequent Than Expected in the UK Population. Am. J. Hum. Genet. 92, 345–353. https://doi.org/10.1016/j.ajhg.2013.01.011

Bellucci, A., Bugiani, O., Ghetti, B., Spillantini, M.G., 2011. Presence of reactive microglia and neuroinflammatory mediators in a case of frontotemporal dementia with P301S mutation. Neurodegener. Dis. 8, 221–229. https://doi.org/10.1159/000322228

Bellucci, A., Westwood, A.J., Ingram, E., Casamenti, F., Goedert, M., Spillantini, M.G., 2004. Induction of inflammatory mediators and microglial activation in mice transgenic for mutant human P301S tau protein. Am. J. Pathol. 165, 1643–1652. https://doi.org/10.1016/S0002-9440(10)63421-9

Benussi, A., Ashton, N.J., Karikari, T.K., Gazzina, S., Premi, E., Benussi, L., Ghidoni, R., Rodriguez, J.L., Emeršič, A., Binetti, G., Fostinelli, S., Giunta, M., Gasparotti, R., Zetterberg, H., Blennow, K., Borroni, B., 2020. Serum Glial Fibrillary Acidic Protein (GFAP) Is a Marker of Disease Severity in Frontotemporal Lobar Degeneration. J. Alzheimer's Dis. 77, 1129–1141. https://doi.org/10.3233/jad-200608

Benussi, A., Padovani, A., Borroni, B., 2015. Phenotypic heterogeneity of monogenic

frontotemporal dementia. Front. Aging Neurosci. 7, 171. https://doi.org/10.3389/fnagi.2015.00171

Bevan-Jones, W.R., Cope, T.E., Jones, P.S., Kaalund, S.S., Passamonti, L., Allinson, K., Green, O., Hong, Y.T., Fryer, T.D., Arnold, R., Coles, J.P., Aigbirhio, F.I., Larner, A.J., Patterson, K., O'Brien, J.T., Rowe, J.B., 2020. Neuroinflammation and protein aggregation co-localize across the frontotemporal dementia spectrum. Brain 143, 1010–1026. https://doi.org/10.1093/brain/awaa033

Bevan-Jones, W.R., Cope, T.E., Jones, P.S., Passamonti, L., Hong, Y.T., Fryer, T., Arnold, R., Coles, J.P., Aigbirhio, F.I., O'Brien, J.T., Rowe, J.B., 2019. In vivo evidence for pre-symptomatic neuroinflammation in a MAPT mutation carrier. Ann. Clin. Transl. Neurol. 6, 373–378. https://doi.org/10.1002/acn3.683

Bian, H., Van Swieten, J.C., Leight, S., Massimo, L., Wood, E., Forman, M., Moore, P., De Koning, I., Clark, C.M., Rosso, S., Trojanowski, J., Lee, V.M.Y., Grossman, M., 2008. CSF biomarkers in frontotemporal lobar degeneration with known pathology. Neurology 70, 1827–1835. https://doi.org/10.1212/01.wnl.0000311445.21321.fc

Boche, D., Perry, V.H., Nicoll, J.A.R., 2013. Review: activation patterns of microglia and their identification in the human brain. Neuropathol. Appl. Neurobiol. 39, 3–18. https://doi.org/10.1111/nan.12011

Bonham, L.W., Sirkis, D.W., Yokoyama, J.S., 2019. The Transcriptional Landscape of Microglial Genes in Aging and Neurodegenerative Disease. Front. Immunol. 10, 1170. https://doi.org/10.3389/fimmu.2019.01170

Boot, R.G., Renkema, G.H., Verhoek, M., Strijland, A., Bliek, J., de Meulemeester, T.M.A.M.O., Mannens, M.M.A.M., Aerts, J.M.F.G., 1998. The Human Chitotriosidase Gene. J. Biol. Chem. 273, 25680–25685. https://doi.org/10.1074/jbc.273.40.25680

Bos, I., Vos, S., Verhey, F., Scheltens, P., Teunissen, C., Engelborghs, S., Sleegers, K., Frisoni, G., Blin, O., Richardson, J.C., Bordet, R., Tsolaki, M., Popp, J., Peyratout,

G., Martinez-Lage, P., Tainta, M., Lleó, A., Johannsen, P., Freund-Levi, Y., Frölich, L., Vandenberghe, R., Westwood, S., Dobricic, V., Barkhof, F., Legido-Quigley, C., Bertram, L., Lovestone, S., Streffer, J., Andreasson, U., Blennow, K., Zetterberg, H., Visser, P.J., 2019. Cerebrospinal fluid biomarkers of neurodegeneration, synaptic integrity, and astroglial activation across the clinical Alzheimer's disease spectrum. Alzheimer's Dement. 15, 644–654. https://doi.org/10.1016/j.jalz.2019.01.004

Bossù, P., Salani, F., Alberici, A., Archetti, S., Bellelli, G., Galimberti, D., Scarpini, E., Spalletta, G., Caltagirone, C., Padovani, A., Borroni, B., 2011. Loss of function mutations in the progranulin gene are related to pro-inflammatory cytokine dysregulation in frontotemporal lobar degeneration patients. J. Neuroinflammation 8, 65. https://doi.org/10.1186/1742-2094-8-65

Böttcher, C., Schlickeiser, S., Sneeboer, M.A.M., Kunkel, D., Knop, A., Paza, E., Fidzinski, P., Kraus, L., Snijders, G.J.L., Kahn, R.S., Schulz, A.R., Mei, H.E., Hol, E.M., Siegmund, B., Glauben, R., Spruth, E.J., de Witte, L.D., Priller, J., 2018. Human microglia regional heterogeneity and phenotypes determined by multiplexed single-cell mass cytometry. Nat. Neurosci. 22, 78–90. https://doi.org/10.1038/s41593-018-0290-2

Brelstaff, J., Tolkovsky, A.M., Ghetti, B., Goedert, M., Spillantini, M.G., 2018. Living Neurons with Tau Filaments Aberrantly Expose Phosphatidylserine and Are Phagocytosed by Microglia. Cell Rep. 24, 1939-1948.e4. https://doi.org/10.1016/j.celrep.2018.07.072

Brettschneider, J., Libon, D.J., Toledo, J.B., Xie, S.X., McCluskey, L., Elman, L., Geser, F., Lee, V.M.Y., Grossman, M., Trojanowski, J.Q., 2012. Microglial activation and TDP-43 pathology correlate with executive dysfunction in amyotrophic lateral sclerosis. Acta Neuropathol. 123, 395–407. https://doi.org/10.1007/s00401-011-0932-x

Bright, F., Werry, E.L., Dobson-Stone, C., Piguet, O., Ittner, L.M., Halliday, G.M., Hodges, J.R., Kiernan, M.C., Loy, C.T., Kassiou, M., Kril, J.J., 2019. Neuroinflammation in frontotemporal dementia. Nat. Rev. Neurol. 15, 540–555. https://doi.org/10.1038/s41582-019-0231-z

Broce, I., Karch, C.M., Wen, N., Fan, C.C., Wang, Y., Hong Tan, C., Kouri, N., Ross, O.A., Höglinger, G.U., Muller, U., Hardy, J., Momeni, P., et al., 2018. Immune-related genetic enrichment in frontotemporal dementia: An analysis of genome-wide association studies. PLoS Med. 15, 1–20. https://doi.org/10.1371/journal.pmed.1002487

Brun, A., 1987. Frontal lobe degeneration of non-Alzheimer type. I. Neuropathol. Arch. Gerontol. Geriatr. 6, 193–208.

Burberry, A., Suzuki, N., Wang, J.Y., Moccia, R., Mordes, D.A., Stewart, M.H., Suzuki-Uematsu, S., Ghosh, S., Singh, A., Merkle, F.T., Koszka, K., Li, Q.Z., Zon, L., Rossi, D.J., Trowbridge, J.J., Notarangelo, L.D., Eggan, K., 2016. Loss-of-function mutations in the C9ORF72 mouse ortholog cause fatal autoimmune disease. Sci Transl Med 8, 347ra93. https://doi.org/10.1126/scitranslmed.aaf6038

Burberry, A., Wells, M.F., Limone, F., Couto, A., Smith, K.S., Keaney, J., Gillet, G., van Gastel, N., Wang, J.Y., Pietilainen, O., Qian, M., Eggan, P., Cantrell, C., Mok, J., Kadiu, I., Scadden, D.T., Eggan, K., 2020. C9orf72 suppresses systemic and neural inflammation induced by gut bacteria. Nature 582, 89–94. https://doi.org/10.1038/s41586-020-2288-7

Burrell, J.R., Kiernan, M.C., Vucic, S., Hodges, J.R., 2011. Motor Neuron dysfunction in frontotemporal dementia. Brain 134, 2582–2594. https://doi.org/10.1093/brain/awr195

Busch, J.I., Martinez-Lage, M., Ashbridge, E., Grossman, M., Van Deerlin, V.M., Hu, F., Lee, V.M., Trojanowski, J.Q., Chen-Plotkin, A.S., 2013. Expression of TMEM106B, the frontotemporal lobar degeneration-associated protein, in normal and diseased

human brain. Acta Neuropathol. Commun. 1, 1–8. https://doi.org/10.1186/2051-5960-1-36

Busch, J.I., Unger, T.L., Jain, N., Skrinak, T.R., Charan, R.A., Chen-Plotkin, A.S., 2016. Increased expression of the frontotemporal dementia risk factor TMEM106B causes C9orf72-dependent alterations in lysosomes. Hum. Mol. Genet. 25, 2681–2697.

Bussian, T.J., Aziz, A., Meyer, C.F., Swenson, B.L., van Deursen, J.M., Baker, D.J., 2018. Clearance of senescent glial cells prevents tau-dependent pathology and cognitive decline. Nature 562, 578–582. https://doi.org/10.1038/s41586-018-0543-y

Butovsky, O., Jedrychowski, M.P., Moore, C.S., Cialic, R., Lanser, A.J., Gabriely, G., Koeglsperger, T., Dake, B., Wu, P.M., Doykan, C.E., Fanek, Z., Liu, L., Chen, Z., Rothstein, J.D., Ransohoff, R.M., Gygi, S.P., Antel, J.P., Weiner, H.L., 2014. Identification of a unique TGF-β-dependent molecular and functional signature in microglia. Nat. Neurosci. 17, 131–143. https://doi.org/10.1038/nn.3599

Byrne, L.M., Rodrigues, F.B., Johnson, E.B., De Vita, E., Blennow, K., Scahill, R., Zetterberg, H., Heslegrave, A., Wild, E.J., 2018a. Cerebrospinal fluid neurogranin and TREM2 in Huntington's disease. Sci. Rep. 8, 1–7. https://doi.org/10.1038/s41598-018-21788-x

Byrne, L.M., Rodrigues, F.B., Johnson, E.B., Wijeratne, P.A., De Vita, E., Alexander, D.C., Palermo, G., Czech, C., Schobel, S., Scahill, R.I., Heslegrave, A., Zetterberg, H., Wild, E.J., 2018b. Evaluation of mutant huntingtin and neurofilament proteins as potential markers in Huntington's disease. Sci. Transl. Med. 10. https://doi.org/10.1126/scitranslmed.aat7108

Cagnin, A., Rossor, M., Sampson, E.L., MacKinnon, T., Banati, R.B., 2004. In vivo detection of microglial activation in frontotemporal dementia. Ann. Neurol. 56, 894–897. https://doi.org/10.1002/ana.20332

Cairns, N.J., Bigio, E.H., Mackenzie, I.R.A., Neumann, M., Lee, V.M.Y., Hatanpaa, K.J.,

White, C.L., Schneider, J.A., Grinberg, L.T., Halliday, G., Duyckaerts, C., Lowe, J.S., Holm, I.E., Tolnay, M., Okamoto, K., Yokoo, H., Murayama, S., Woulfe, J., Munoz, D.G., Dickson, D.W., Ince, P.G., Trojanowski, J.Q., Mann, D.M.A., 2007. Neuropathologic diagnostic and nosologic criteria for frontotemporal lobar degeneration: Consensus of the Consortium for Frontotemporal Lobar Degeneration. Acta Neuropathol. 114, 5–22. https://doi.org/10.1007/s00401-007-0237-2

Califf, R.M., 2018. Biomarker definitions and their applications. Exp. Biol. Med. 243, 213–221. https://doi.org/10.1177/1535370217750088

Caroppo, P., Le Ber, I., Camuzat, A., Clot, F., Naccache, L., Lamari, F., De Septenville, A., Bertrand, A., Belliard, S., Hannequin, D., Colliot, O., Brice, A., 2014. Extensive White Matter Involvement in Patients With Frontotemporal Lobar Degeneration. JAMA Neurol. 71, 1562. https://doi.org/10.1001/jamaneurol.2014.1316

Cash, D.M., Bocchetta, M., Thomas, D.L., Dick, K.M., van Swieten, J.C., Borroni, B., Galimberti, D., Masellis, M., Tartaglia, M.C., Rowe, J.B., Graff, C., Tagliavini, F., Frisoni, G.B., Laforce, R., Finger, E., de Mendonça, A., Sorbi, S., Rossor, M.N., Ourselin, S., Rohrer, J.D., 2018. Patterns of gray matter atrophy in genetic frontotemporal dementia: results from the GENFI study. Neurobiol. Aging 62, 191–196. https://doi.org/10.1016/j.neurobiolaging.2017.10.008

Cavazzana, I., Alberici, A., Bonomi, E., Ottaviani, R., Kumar, R., Archetti, S., Manes, M., Cosseddu, M., Buratti, E., Padovani, A., Tincani, A., Franceschini, F., Borroni, B., 2018. Antinuclear antibodies in Frontotemporal Dementia: the tip's of autoimmunity iceberg? J. Neuroimmunol. 325, 61–63. https://doi.org/10.1016/j.jneuroim.2018.10.006

Chen-Plotkin, A.S., Xiao, J., Geser, F., Martinez-Lage, M., Grossman, M., Unger, T., Wood, E.M., Van Deerlin, V.M., Trojanowski, J.Q., Lee, V.M.Y., 2010. Brain progranulin expression in GRN-associated frontotemporal lobar degeneration. Acta

Neuropathol. 119, 111–122. https://doi.org/10.1007/s00401-009-0576-2

Chen, Q., Boeve, B.F., Schwarz, C.G., Reid, R., Tosakulwong, N., Lesnick, T.G., Bove, J., Brannelly, P., Brushaber, D., Coppola, G., Dheel, C., Kantarci, K., et al., 2019. Tracking white matter degeneration in asymptomatic and symptomatic MAPT mutation carriers. Neurobiol. Aging 83, 54–62. https://doi.org/10.1016/j.neurobiolaging.2019.08.011

Cherry, J.D., Olschowka, J.A., O'Banion, M., 2014. Neuroinflammation and M2 microglia: the good, the bad, and the inflamed. J. Neuroinflammation 11, 98. https://doi.org/10.1186/1742-2094-11-98

Clarke, M., Woollacott, I., Shafei, R., Moore, K., Greaves, C., Russell, L., Neason, M., Bocchetta, M., Cash, D., Rohrer, J., 2019. [11C]PBR28 inflammatory PET imaging in frontotemporal dementia. J. Cereb. Blood Flow Metab. 39, 609–637. https://doi.org/10.1177/0271678X19850989

Clayton, E.L., Mancuso, R., Tolstrup Nielsen, T., Mizielinska, S., Holmes, H., Powell, N., Norona, F., Overgaard Larsen, J., Milioto, C., Wilson, K.M., Lythgoe, M.F., Ourselin, S., Nielsen, J.E., Johannsen, P., Holm, I., Collinge, J., Oliver, P.L., Gomez-Nicola, D., Isaacs, A.M., Gade, A., Englund, E., Fisher, E., Brown, J., Stockholm, J., Roos, P., Gydesen, S., Lindquist, S., Thusgaard, T., 2017. Early microgliosis precedes neuronal loss and behavioural impairment in mice with a frontotemporal dementia-causing CHMP2B mutation. Hum. Mol. Genet. 26, 873–887. https://doi.org/10.1093/hmg/ddx003

Cooper-Knock, J., Green, C., Altschuler, G., Wei, W., Bury, J.J., Heath, P.R., Wyles, M., Gelsthorpe, C., Highley, J.R., Lorente-Pons, A., Beck, T., Doyle, K., Otero, K., Traynor, B., Kirby, J., Shaw, P.J., Hide, W., 2017. A data-driven approach links microglia to pathology and prognosis in amyotrophic lateral sclerosis. Acta Neuropathol. Commun. 5, 23. https://doi.org/10.1186/s40478-017-0424-x

Cooper-Knock, J., Hewitt, C., Highley, J.R., Brockington, A., Milano, A., Man, S.,

Martindale, J., Hartley, J., Walsh, T., Gelsthorpe, C., Baxter, L., Forster, G., Fox, M., Bury, J., Mok, K., McDermott, C.J., Traynor, B.J., Kirby, J., Wharton, S.B., Ince, P.G., Hardy, J., Shaw, P.J., 2012. Clinico-pathological features in amyotrophic lateral sclerosis with expansions in C9ORF72. Brain 135, 751–764. https://doi.org/10.1093/brain/awr365

Cooper, P.N., Siddons, C.A., Mann, D.M.A., 1996. Patterns of glial cell activity in fronto-temporal dementia (lobar atrophy). Neuropathol. Appl. Neurobiol. 22, 17–22.

Coyle-Gilchrist, I.T.S., Dick, K.M., Patterson, K., Patricia Vázquez Rodríquez, Fm., Wehmann, E., Alicia Wilcox, Mp., Claire Lansdall, Mc.J., Dawson, K.E., Julie Wiggins, R., Mead, S., Brayne, C., James Rowe, Fm.B., 2016. Prevalence, characteristics, and survival of frontotemporal lobar degeneration syndromes. Neurology 86, 1736–1743. https://doi.org/10.77/100,000

Craig-Schapiro, R., Perrin, R.J., Roe, C.M., Xiong, C., Carter, D., Cairns, N.J., Mintun, M.A., Peskind, E.R., Li, G., Galasko, D.R., Clark, C.M., Quinn, J.F., D'Angelo, G., Malone, J.P., Townsend, R.R., Morris, J.C., Fagan, A.M., Holtzman, D.M., 2010. YKL-40: A novel prognostic fluid biomarker for preclinical Alzheimer's disease. Biol. Psychiatry 68, 903–912. https://doi.org/10.1016/j.biopsych.2010.08.025

Cruchaga, C., Graff, C., Chiang, H.H., Wang, J., Hinrichs, A.L., Spiegel, N., Bertelsen, S., Mayo, K., Norton, J.B., Morris, J.C., Goate, A., 2011. Association of TMEM106B gene polymorphism with age at onset in granulin mutation carriers and plasma granulin protein levels. Arch. Neurol. 68, 581–586. https://doi.org/10.1001/archneurol.2010.350

Cruts, M., Gijselinck, I., Van Der Zee, J., Engelborghs, S., Wils, H., Pirici, D., Rademakers, R., Vandenberghe, R., Dermaut, B., Martin, J.J., Van Duijn, C., Peeters, K., Sciot, R., Santens, P., De Pooter, T., Mattheijssens, M., Van Den Broeck, M., Cuijt, I., Vennekens, K., De Deyn, P.P., Kumar-Singh, S., Van Broeckhoven, C., 2006. Null mutations in progranulin cause ubiquitin-positive

frontotemporal dementia linked to chromosome 17q21. Nature 442, 920–924. https://doi.org/10.1038/nature05017

da Silva, R.P., Gordon, S., 1999. Phagocytosis stimulates alternative glycosylation of macrosialin (mouse CD68), a macrophage-specific endosomal protein. Biochem. J. 338, 687–694. https://doi.org/10.1042/BJ3380687

Davies, D.S., Ma, J., Jegathees, T., Goldsbury, C., 2017. Microglia show altered morphology and reduced arborization in human brain during aging and Alzheimer's disease. Brain Pathol. 27, 795–808. https://doi.org/10.1111/bpa.12456

De Jong, D., Jansen, R.W.M.M., Pijnenburg, Y.A.L., Van Geel, W.J.A., Borm, G.F., Kremer, H.P.H., Verbeek, M.M., 2007. CSF neurofilament proteins in the differential diagnosis of dementia. J. Neurol. Neurosurg. Psychiatry 78, 936–938. https://doi.org/10.1136/jnnp.2006.107326

DeJesus-Hernandez, M., Mackenzie, I.R., Boeve, B.F., Boxer, A.L., Baker, M., Rutherford, N.J., Nicholson, A.M., Finch, N.C.A., Flynn, H., Adamson, J., Kouri, N., Wojtas, A., Sengdy, P., Hsiung, G.Y.R., Karydas, A., Seeley, W.W., Josephs, K.A., Coppola, G., Geschwind, D.H., Wszolek, Z.K., Feldman, H., Knopman, D.S., Petersen, R.C., Miller, B.L., Dickson, D.W., Boylan, K.B., Graff-Radford, N.R., Rademakers, R., 2011. Expanded GGGGCC Hexanucleotide Repeat in Noncoding Region of C9ORF72 Causes Chromosome 9p-Linked FTD and ALS. Neuron 72, 245–256. https://doi.org/10.1016/j.neuron.2011.09.011

del Campo, M., Galimberti, D., Elias, N., Boonkamp, L., Pijnenburg, Y.A., van Swieten, J.C., Watts, K., Paciotti, S., Beccari, T., Hu, W., Teunissen, C.E., 2018. Novel CSF biomarkers to discriminate FTLD and its pathological subtypes. Ann. Clin. Transl. Neurol. 5, 1163–1175. https://doi.org/10.1002/acn3.629

del Rio Hortega, P., 1932. Microglia. In: Cytology and Cellular Pathology of the Nervous System. Hoeber, New York.

Devenney, E., Vucic, S., Hodges, J.R., Kiernan, M.C., 2015. Motor neuron disease-

frontotemporal dementia: a clinical continuum. Expert Rev. Neurother. 15, 509–522. https://doi.org/10.1586/14737175.2015.1034108

Downey, L.E., Mahoney, C.J., Rossor, M.N., Crutch, S.J., Warren, J.D., 2012. Impaired self-other differentiation in frontotemporal dementia due to the C9ORF72 expansion. Alzheimer's Res. Ther. 4, 42. https://doi.org/10.1186/alzrt145

Drugan, C., Drugan, T.C., Grigorescu-Sido, P., Naşcu, I., 2017. Modelling long-term evolution of chitotriosidase in non-neuronopathic Gaucher disease. Scand. J. Clin. Lab. Invest. 77, 275–282. https://doi.org/10.1080/00365513.2017.1303191

El Hajj, H., Savage, J.C., Bisht, K., Parent, M., Vallières, L., Rivest, S., Tremblay, M.-È., 2019. Ultrastructural evidence of microglial heterogeneity in Alzheimer's disease amyloid pathology. J. Neuroinflammation 16, 87. https://doi.org/10.1186/s12974-019-1473-9

Elahi, F.M., Marx, G., Cobigo, Y., Staffaroni, A.M., Kornak, J., Tosun, D., Boxer, A.L., Kramer, J.H., Miller, B.L., Rosen, H.J., 2017. Longitudinal white matter change in frontotemporal dementia subtypes and sporadic late onset Alzheimer's disease. NeuroImage Clin. 16, 595–603. https://doi.org/10.1016/j.nicl.2017.09.007

Elmonem, M.A., van den Heuvel, L.P., Levtchenko, E.N., 2016. Immunomodulatory Effects of Chitotriosidase Enzyme. Enzyme Res. 2016, 2682680. https://doi.org/10.1155/2016/2682680

Englund, E., 1998. Neuropathology of White Matter Changes in Alzheimer's Disease. Dement Geriatr Cogn Disord 9, 6–12.

Englund, E., Brun, A., 1987. Frontal lobe degeneration of non-Alzheimer type. IV. White matter changes. Arch Gerontol Geriatr 6, 235–243.

Escourolle, R., 1956. La maladie de Pick. Etude D'ensemble et Syntèse Anatomo-Clinique. Thesis, Foult. Ed. Paris.

Evers, B.M., Rodriguez-Navas, C., Tesla, R.J., Prange-Kiel, J., Wasser, C.R., Yoo, K.S., McDonald, J., Cenik, B., Ravenscroft, T.A., Plattner, F., Rademakers, R., Yu, G.,

White, C.L., Herz, J., 2017. Lipidomic and Transcriptomic Basis of Lysosomal Dysfunction in Progranulin Deficiency. Cell Rep. 20, 2565–2574. https://doi.org/10.1016/j.celrep.2017.08.056

Ewers, M., Franzmeier, N., Suárez-Calvet, M., Morenas-Rodriguez, E., Caballero, M.A.A., Kleinberger, G., Piccio, L., Cruchaga, C., Deming, Y., Dichgans, M., Trojanowski, J.Q., Shaw, L.M., Weiner, M.W., Haass, C., 2019. Increased soluble TREM2 in cerebrospinal fluid is associated with reduced cognitive and clinical decline in Alzheimer's disease. Sci. Transl. Med. 11. https://doi.org/10.1126/scitranslmed.aav6221

Falcon, C., Monté-Rubio, G.C., Grau-Rivera, O., Suárez-Calvet, M., Sánchez-Valle, R., Rami, L., Bosch, B., Haass, C., Gispert, J.D., Molinuevo, J.L., 2019. CSF glial biomarkers YKL40 and sTREM2 are associated with longitudinal volume and diffusivity changes in cognitively unimpaired individuals. NeuroImage Clin. 23, 101801. https://doi.org/10.1016/j.nicl.2019.101801

Felsky, D., Roostaei, T., Nho, K., Risacher, S.L., Bradshaw, E.M., Petyuk, V., Schneider, J.A., Saykin, A., Bennett, D.A., De Jager, P.L., 2019. Neuropathological correlates and genetic architecture of microglial activation in elderly human brain. Nat. Commun. 10, 1–12. https://doi.org/10.1038/s41467-018-08279-3

Fendrick, S.E., Xue, Q.-S., Streit, W.J., 2007. Formation of multinucleated giant cells and microglial degeneration in rats expressing a mutant Cu/Zn superoxide dismutase gene. J. Neuroinflammation 4. https://doi.org/10.1186/1742-2094-4-9

Fernández-Arjona, M. del M., Grondona, J.M., Fernández-Llebrez, P., López-Ávalos, M.D., 2019. Microglial Morphometric Parameters Correlate With the Expression Level of IL-1β, and Allow Identifying Different Activated Morphotypes. Front. Cell. Neurosci. 13, 1–15. https://doi.org/10.3389/fncel.2019.00472

Fernández-Arjona, M. del M., Grondona, J.M., Granados-Durán, P., Fernández-Llebrez, P., López-Ávalos, M.D., 2017. Microglia Morphological Categorization in a Rat

Model of Neuroinflammation by Hierarchical Cluster and Principal Components Analysis. Front. Cell. Neurosci. 11, 1–22. https://doi.org/10.3389/fncel.2017.00235

Fernández-Botrán, R., Ahmed, Z., Crespo, F.A., Gatenbee, C., Gonzalez, J., Dickson, D.W., Litvan, I., 2011. Cytokine expression and microglial activation in progressive supranuclear palsy. Park. Relat. Disord. 17, 683–688. https://doi.org/10.1016/j.parkreldis.2011.06.007

Ferrari, R., Hernandez, D.G., Nalls, M.A., Rohrer, J.D., Ramasamy, A., Kwok, J.B.J., Dobson-Stone, C., Brooks William S., B.S., Schofield, P.R., Halliday, G.M., Hodges, J.R., Momeni, P., et al., 2014. Frontotemporal dementia and its subtypes: A genome-wide association study. Lancet Neurol. 13, 686–699. https://doi.org/10.1016/S1474-4422(14)70065-1

Ferrari, R., Wang, Y., Vandrovcova, J., Guelfi, S., Witeolar, A., Karch, C.M., Schork, A.J., Fan, C.C., Brewer, J.B., Momeni, Parastoo, Schellenberg, G.D., Momeni, P., et al., 2017. Genetic architecture of sporadic frontotemporal dementia and overlap with Alzheimer's and Parkinson's diseases. J. Neurol. Neurosurg. Psychiatry 88, 152–164. https://doi.org/10.1136/jnnp-2016-314411

Filiano, A.J., Martens, L.H., Young, A.H., Warmus, B.A., Zhou, P., Diaz-Ramirez, G., Jiao, J., Zhang, Z., Huang, E.J., Gao, F.B., Farese, R. V., Roberson, E.D., 2013. Dissociation of frontotemporal dementia-related deficits and neuroinflammation in progranulin haploinsufficient mice. J. Neurosci. 33, 5361. https://doi.org/10.1523/JNEUROSCI.6103-11.2013

Finch, N., Baker, M., Crook, R., Swanson, K., Kuntz, K., Surtees, R., Bisceglio, G., Rovelet-Lecrux, A., Boeve, B., Petersen, R.C., Dickson, D.W., Younkin, S.G., Deramecourt, V., Crook, J., Graff-Radford, N.R., Rademakers, R., 2009. Plasma progranulin levels predict progranulin mutation status in frontotemporal dementia patients and asymptomatic family members. Brain 132, 583–91. https://doi.org/10.1093/brain/awn352

Finch, N., Carrasquillo, M.M., Baker, M., Rutherford, N.J., Coppola, G., Dejesus-Hernandez, M., Crook, R., Hunter, T., Ghidoni, R., Benussi, L., Crook, J., Finger, E., Hantanpaa, K.J., Karydas, A.M., Sengdy, P., Gonzalez, J., Seeley, W.W., Johnson, N., Beach, T.G., Mesulam, M., Forloni, G., Kertesz, A., Knopman, D.S., Uitti, R., White, C.L., Caselli, R., Lippa, C., Bigio, E.H., Wszolek, Z.K., Binetti, G., MacKenzie, I.R., Miller, B.L., Boeve, B.F., Younkin, S.G., Dickson, D.W., Petersen, R.C., Graff-Radford, N.R., Geschwind, D.H., Rademakers, R., 2011. TMEM106B regulates progranulin levels and the penetrance of FTLD in GRN mutation carriers. Neurology 76, 467–474. https://doi.org/10.1212/WNL.0b013e31820a0e3b

Foiani, M.S., Cicognola, C., Ermann, N., Woollacott, I.O.C., Heller, C., Heslegrave, A.J., Keshavan, A., Paterson, R.W., Ye, K., Kornhuber, J., Fox, N.C., Schott, J.M., Warren, J.D., Lewczuk, P., Zetterberg, H., Blennow, K., Höglund, K., Rohrer, J.D., 2019. Searching for novel cerebrospinal fluid biomarkers of tau pathology in frontotemporal dementia: An elusive quest. J. Neurol. Neurosurg. Psychiatry 90, 740–746. https://doi.org/10.1136/jnnp-2018-319266

Foiani, M.S., Woollacott, I.O.C., Heller, C., Bocchetta, M., Heslegrave, A., Dick, K.M., Russell, L.L., Marshall, C.R., Mead, S., Schott, J.M., Fox, N.C., Warren, J.D., Zetterberg, H., Rohrer, J.D., 2018. Plasma tau is increased in frontotemporal dementia. J. Neurol. Neurosurg. Psychiatry 89, 804–807. https://doi.org/10.1136/jnnp-2017-317260

Forabosco, P., Ramasamy, A., Trabzuni, D., Walker, R., Smith, C., Bras, J., Levine, A.P., Hardy, J., Pocock, J.M., Guerreiro, R., Weale, M.E., Ryten, M., 2013. Insights into TREM2 biology by network analysis of human brain gene expression data. Neurobiol. Aging 34, 2699–2714. https://doi.org/10.1016/j.neurobiolaging.2013.05.001

Freischmidt, A., Wieland, T., Richter, B., Ruf, W., Schaeffer, V., Müller, K., Marroquin, N., Nordin, F., Hübers, A., Weydt, P., Pinto, S., Press, R., Millecamps, S., Molko,

N., Bernard, E., Desnuelle, C., Soriani, M.H., Dorst, J., Graf, E., Nordström, U., Feiler, M.S., Putz, S., Boeckers, T.M., Meyer, T., Winkler, A.S., Winkelman, J., De Carvalho, M., Thal, D.R., Otto, M., Brännström, T., Volk, A.E., Kursula, P., Danzer, K.M., Lichtner, P., Dikic, I., Meitinger, T., Ludolph, A.C., Strom, T.M., Andersen, P.M., Weishaupt, J.H., 2015. Haploinsufficiency of TBK1 causes familial ALS and fronto-temporal dementia. Nat. Neurosci. 18, 631–636. https://doi.org/10.1038/nn.4000

Friedman, B.A., Srinivasan, K., Ayalon, G., Meilandt, W.J., Lin, H., Huntley, M.A., Cao, Y., Lee, S.-H., Haddick, P.C.G., Ngu, H., Modrusan, Z., Larson, J.L., Kaminker, J.S., van der Brug, M.P., Hansen, D. V, 2018. Diverse Brain Myeloid Expression Profiles Reveal Distinct Microglial Activation States and Aspects of Alzheimer's Disease Not Evident in Mouse Models. Cell Rep. 22, 832–847. https://doi.org/10.1016/j.celrep.2017.12.066

Fumagalli, G.G., Basilico, P., Arighi, A., Bocchetta, M., Dick, K.M., Cash, D.M., Harding, S., Mercurio, M., Fenoglio, C., Pietroboni, A.M., Ghezzi, L., Van Swieten, J., Borroni, B., De Mendonça, A., Masellis, M., Tartaglia, M.C., Rowe, J.B., Graff, C., Tagliavini, F., Frisoni, G.B., Laforce, R., Finger, E., Sorbi, S., Scarpini, E., Rohrer, J.D., Galimberti, D., Genetic FTD Initiative (GENFI), 2018. Distinct patterns of brain atrophy in Genetic Frontotemporal Dementia Initiative (GENFI) cohort revealed by visual rating scales. Alzheimer's Res. Ther. 10, 46. https://doi.org/10.1186/s13195-018-0376-9

Galimberti, D., Bonsi, R., Fenoglio, C., Serpente, M., Cioffi, S.M.G., Fumagalli, G., Arighi, A., Ghezzi, L., Arcaro, M., Mercurio, M., Rotondo, E., Scarpini, E., 2015. Inflammatory molecules in Frontotemporal Dementia: Cerebrospinal fluid signature of progranulin mutation carriers. Brain. Behav. Immun. 49, 182–187. https://doi.org/10.1016/j.bbi.2015.05.006

Galimberti, D., Schoonenboom, N., Scheltens, P., Fenoglio, C., Venturelli, E.,

Pijnenburg, Y.A.L., Bresolin, N., Scarpini, E., 2006. Intrathecal chemokine levels in Alzheimer disease and frontotemporal lobar degeneration. Neurology 66, 146–147. https://doi.org/10.1212/01.wnl.0000191324.08289.9d

Galimberti, D., Venturelli, E., Fenoglio, C., Guidi, I., Villa, C., Bergamaschini, L., Cortini, F., Scalabrini, D., Baron, P., Vergani, C., Bresolin, N., Scarpini, E., 2008. Intrathecal levels of IL-6, IL-11 and LIF in Alzheimer's disease and frontotemporal lobar degeneration. J. Neurol. 255, 539–544. https://doi.org/10.1007/s00415-008-0737-6

Galimberti, D., Venturelli, E., Villa, C., Fenoglio, C., Clerici, F., Marcone, A., Benussi, L., Cortini, F., Scalabrini, D., Perini, L., Restelli, I., Binetti, G., Cappa, S., Mariani, C., Bresolin, N., Scarpini, E., 2009. MCP-1 A-2518G polymorphism: Effect on susceptibility for frontotemporal lobar degeneration and on cerebrospinal fluid MCP-1 levels. J. Alzheimer's Dis. 17, 125–133. https://doi.org/10.3233/JAD-2009-1019

Gallagher, M.D., Suh, E., Grossman, M., Elman, L., McCluskey, L., Van Swieten, J.C., Al-Sarraj, S., Neumann, M., Gelpi, E., Ghetti, B., Rohrer, J.D., Chen-Plotkin, A.S., et al., 2014. TMEM106B is a genetic modifier of frontotemporal lobar degeneration with C9orf72 hexanucleotide repeat expansions. Acta Neuropathol. 127, 407–418. https://doi.org/10.1007/s00401-013-1239-x

Gans, A., 1925. De Ziekten van Pick en van Alzheimer. Ned. Tijdschr. Geneeskd. 68, 1953.

Gefen, T., Kim, G., Bolbolan, K., Geoly, A., Ohm, D., Oboudiyat, C., Shahidehpour, R., Rademaker, A., Weintraub, S., Bigio, E.H., Mesulam, M.-M., Rogalski, E., Geula, C., 2019. Activated Microglia in Cortical White Matter Across Cognitive Aging Trajectories. Front. Aging Neurosci. 11, 94. https://doi.org/10.3389/fnagi.2019.00094

Gehrmann, J., Banati, R.B., Kreutzberg, G.W., 1993. Microglia in the immune surveillance of the brain: Human microglia constitutively express HLA-DR molecules. J. Neuroimmunol. 48, 189–198. https://doi.org/10.1016/0165-

5728(93)90191-Z

Gellera, C., Tiloca, C., Del Bo, R., Corrado, L., Pensato, V., Agostini, J., Cereda, C., Ratti, A., Castellotti, B., Corti, S., Bagarotti, A., Cagnin, A., Milani, P., Gabelli, C., Riboldi, G., Mazzini, L., Sorarù, G., D'Alfonso, S., Taroni, F., Comi, G. Pietro, Ticozzi, N., Silani, V., 2013. Ubiquilin 2 mutations in Italian patients with amyotrophic lateral sclerosis and frontotemporal dementia. J. Neurol. Neurosurg. Psychiatry 84, 183–187. https://doi.org/10.1136/jnnp-2012-303433

Gentleman, S.M., 2013. Review: Microglia in protein aggregation disorders: Friend or foe? Neuropathol. Appl. Neurobiol. 39, 45–50. https://doi.org/10.1111/nan.12017

Gerhard, A., Watts, J., Trender-Gerhard, I., Turkheimer, F., Banati, R.B., Bhatia, K., Brooks, D.J., 2004. In vivo imaging of microglial activation with [11C](R)-PK11195 PET in corticobasal degeneration. Mov. Disord. 19, 1221–1226. https://doi.org/10.1002/mds.20162

Geser, F., Martinez-Lage, M., Robinson, J., Uryu, K., Neumann, M., Brandmeir, N.J., Xie, S.X., Kwong, L.K., Elman, L., McCluskey, L., Clark, C.M., Malunda, J., Miller, B.L., Zimmerman, E.A., Qian, J., Van Deerlin, V., Grossman, M., Lee, V.M.Y., Trojanowski, J.Q., 2009. Clinical and pathological continuum of multisystem TDP-43 proteinopathies. Arch. Neurol. 66, 180–189. https://doi.org/10.1001/archneurol.2008.558

Gibbons, L., Rollinson, S., Thompson, J.C., Robinson, A., Davidson, Y.S., Richardson, A., Neary, D., Pickering-Brown, S.M., Snowden, J.S., Mann, D.M.A., 2015. Plasma levels of progranulin and interleukin-6 in frontotemporal lobar degeneration. Neurobiol. Aging 36, 1603.e1-e4. https://doi.org/10.1016/j.neurobiolaging.2014.10.023

Gijselinck, I., Van Mossevelde, S., Van Der Zee, J., Sieben, A., Philtjens, S., Heeman, B., Engelborghs, S., Vandenbulcke, M., De Baets, G., Bäumer, V., Cuijt, I., Van Den Broeck, M., Peeters, K., Mattheijssens, M., Rousseau, F., Vandenberghe, R., De

Jonghe, P., Cras, P., De Deyn, P.P., Martin, J.J., Cruts, M., Van Broeckhoven, C., 2015. Loss of TBK1 is a frequent cause of frontotemporal dementia in a Belgian cohort. Neurology 85, 2116–2125. https://doi.org/10.1212/WNL.0000000000002220

Gispert, J.D., Monté, G.C., Falcon, C., Tucholka, A., Rojas, S., Sánchez-Valle, R., Antonell, A., Lladó, A., Rami, L., Molinuevo, J.L., 2016a. CSF YKL-40 and pTau181 are related to different cerebral morphometric patterns in early AD. Neurobiol. Aging 38, 47–55. https://doi.org/10.1016/j.neurobiolaging.2015.10.022

Gispert, J.D., Suárez-Calvet, M., Monté, G.C., Tucholka, A., Falcon, C., Rojas, S., Rami, L., Sánchez-Valle, R., Lladó, A., Kleinberger, G., Haass, C., Molinuevo, J.L., 2016b. Cerebrospinal fluid sTREM2 levels are associated with gray matter volume increases and reduced diffusivity in early Alzheimer's disease. Alzheimer's Dement. 12, 1259–1272. https://doi.org/10.1016/j.jalz.2016.06.005

Goldman, J.S., Farmer, J.M., Wood, E.M., Johnson, J.K., Boxer, A., Neuhaus, J., Lomen-Hoerth, C., Wilhelmsen, K.C., Lee, V.M.Y., Grossman, M., Miller, B.L., 2005. Comparison of family histories in FTLD subtypes and related tauopathies. Neurology 65, 1817–1819. https://doi.org/10.1212/01.wnl.0000187068.92184.63

Gorno-Tempini, M.L., Hillis, A.E., Weintraub, S., Kertesz, A., Mendez, M., Cappa, S.F., Ogar, J.M., Rohrer, J.D., Black, S., Boeve, B.F., Manes, F., Dronkers, N.F., Vandenberghe, R., Rascovsky, K., Patterson, K., Miller, B.L., Knopman, D.S., Hodges, J.R., Mesulam, M.M., Grossman, M., 2011. Classification of primary progressive aphasia and its variants. Neurology 76, 1006–1014. https://doi.org/10.1212/WNL.0b013e31821103e6

Gossye, H., Van Broeckhoven, C., Engelborghs, S., 2019. The use of biomarkers and genetic screening to diagnose frontotemporal dementia: Evidence and clinical implications. Front. Genet. 10, 1–18. https://doi.org/10.3389/fnins.2019.00757

Götzl, J.K., Brendel, M., Werner, G., Parhizkar, S., Sebastian Monasor, L., Kleinberger,

G., Colombo, A., Deussing, M., Wagner, M., Winkelmann, J., Diehl-Schmid, J., Levin, J., Fellerer, K., Reifschneider, A., Bultmann, S., Bartenstein, P., Rominger, A., Tahirovic, S., Smith, S.T., Madore, C., Butovsky, O., Capell, A., Haass, C., 2019. Opposite microglial activation stages upon loss of PGRN or TREM2 result in reduced cerebral glucose metabolism. EMBO Mol. Med. 11, e9711. https://doi.org/10.15252/emmm.201809711

Götzl, J.K., Colombo, A.V., Fellerer, K., Reifschneider, A., Werner, G., Tahirovic, S., Haass, C., Capell, A., 2018. Early lysosomal maturation deficits in microglia triggers enhanced lysosomal activity in other brain cells of progranulin knockout mice. Mol. Neurodegener. 13, 1–16. https://doi.org/10.1186/s13024-018-0281-5

Götzl, J.K., Mori, K., Damme, M., Fellerer, K., Tahirovic, S., Kleinberger, G., Janssens, J., Van Der Zee, J., Lang, C.M., Kremmer, E., Martin, J.J., Engelborghs, S., Kretzschmar, H.A., Arzberger, T., Van Broeckhoven, C., Haass, C., Capell, A., 2014. Common pathobiochemical hallmarks of progranulin-associated frontotemporal lobar degeneration and neuronal ceroid lipofuscinosis. Acta Neuropathol. 127, 845–860. https://doi.org/10.1007/s00401-014-1262-6

Grabert, K., Michoel, T., Karavolos, M.H., Clohisey, S., Kenneth Baillie, J., Stevens, M.P., Freeman, T.C., Summers, K.M., McColl, B.W., 2016. Microglial brain region-dependent diversity and selective regional sensitivities to aging. Nat. Neurosci. 19, 504–516. https://doi.org/10.1038/nn.4222

Graeber, M.B., Bise, K., Mehraein, P., 1994. Letter to the Editor CR3143 , a marker for activated human microglia : application to diagnostic neuropathology. Neuropathol. Appl. Neurobiol. 20, 406–408.

Guerreiro, R.J., Lohmann, E., Brás, J.M., Gibbs, J.R., Rohrer, J.D., Gurunlian, N., Dursun, B., Bilgic, B., Hanagasi, H., Gurvit, H., Emre, M., Singleton, A., Hardy, J., 2013. Using exome sequencing to reveal mutations in TREM2 presenting as a frontotemporal dementia-like syndrome without bone involvement. Arch. Neurol. 70,

78–84. https://doi.org/10.1001/jamaneurol.2013.579

Haller, S., Kövari, E., Herrmann, F.R., Cuvinciuc, V., Tomm, A.-M., Zulian, G.B., Lovblad, K.-O., Giannakopoulos, P., Bouras, C., 2013. Do brain T2/FLAIR white matter hyperintensities correspond to myelin loss in normal aging? A radiologic-neuropathologic correlation study. Acta Neuropathol. Commun. 1, 14. https://doi.org/10.1186/2051-5960-1-14

Heller, C., Foiani, M.S., Moore, K., Convery, R., Bocchetta, M., Neason, M., Cash, D.M., Thomas, D., Greaves, C. V., Woollacott, I.O.C., Shafei, R., Bessi, V., et al., 2020. Plasma glial fibrillary acidic protein is raised in progranulin-associated frontotemporal dementia. J. Neurol. Neurosurg. Psychiatry 91, 1–8. https://doi.org/10.1136/jnnp-2019-321954

Hendrickx, D.A.E., van Eden, C.G., Schuurman, K.G., Hamann, J., Huitinga, I., 2017. Staining of HLA-DR, Iba1 and CD68 in human microglia reveals partially overlapping expression depending on cellular morphology and pathology. J. Neuroimmunol. 309, 12–22. https://doi.org/10.1016/j.jneuroim.2017.04.007

Henjum, K., Almdahl, I.S., Årskog, V., Minthon, L., Hansson, O., Fladby, T., Nilsson, L.N.G., 2016. Cerebrospinal fluid soluble TREM2 in aging and Alzheimer's disease. Alzheimers. Res. Ther. 8, 17. https://doi.org/10.1186/s13195-016-0182-1

Heslegrave, A., Heywood, W., Paterson, R., Magdalinou, N., Svensson, J., Johansson, P., Öhrfelt, A., Blennow, K., Hardy, J., Schott, J., Mills, K., Zetterberg, H., 2016. Increased cerebrospinal fluid soluble TREM2 concentration in Alzheimer's disease. Mol. Neurodegener. 11, 3. https://doi.org/10.1186/s13024-016-0071-x

Höglinger, G.U., Respondek, G., Stamelou, M., Kurz, C., Josephs, K.A., Lang, A.E., Mollenhauer, B., Müller, U., Nilsson, C., Whitwell, J.L., Arzberger, T., Movement Disorder Society-endorsed PSP Study Group, et al., 2017. Clinical diagnosis of progressive supranuclear palsy: The movement disorder society criteria. Mov. Disord. 32, 853–864. https://doi.org/10.1002/mds.26987

Hollak, C.E.M., Van Weely, S., van Oers, M.H., Aerts, J.M.F.G., 1994. Marked Elevation of Plasma Chitotriosidase Activity. J. Clin. Invest. 93, 1288–1292.

Holler, C.J., Taylor, G., Deng, Q., Kukar, T., 2017. Intracellular Proteolysis of Progranulin Generates Stable, Lysosomal Granulins That Are Haploinsufficient in Patients with Frontotemporal Dementia Caused by GRN Mutations. eneuro 18, ENEURO.0100-17.2017. https://doi.org/10.1523/eneuro.0100-17.2017

Hollister, R.D., Xia, M., McNamara, M.J., Hyman, B.T., 1997. Neuronal Expression of Class II Major Histocompatibility Complex (HLA-DR) in 2 Cases of Pick Disease. Arch. Neurol. 54, 243–248. https://doi.org/10.1001/archneur.1997.00550150011008

Hopperton, K.E., Mohammad, D., Trépanier, M.O., Giuliano, V., Bazinet, R.P., 2018. Markers of microglia in post-mortem brain samples from patients with Alzheimer's disease: A systematic review. Mol. Psychiatry 23, 177–198. https://doi.org/10.1038/mp.2017.246

Hu, F., Padukkavidana, T., Vaegter, C., Brady, O.A., Zheng, Y., Mackenzie, I.R., Feldman, H.H., Nykjaer, A., Strittmatter, S.M., 2010. Sortilin-Mediated Endocytosis Determines Levels of the Fronto- Temporal Dementia Protein, Progranulin. Neuron 68, 654–667. https://doi.org/10.1016/j.ajo.2008.07.023.Agreement

Hu, W.T., Chen-Plotkin, A., Grossman, M., Arnold, S.E., Clark, C.M., Shaw, L.M., McCluskey, L., Elman, L., Hurtig, H.I., Siderowf, A., Lee, V.M.Y., Soares, H., Trojanowski, J.Q., 2010. Novel CSF biomarkers for frontotemporal lobar degenerations. Neurology 75, 2079–2086. https://doi.org/10.1212/WNL.0b013e318200d78d

Hu, X., Leak, R.K., Shi, Y., Suenaga, J., Gao, Y., Zheng, P., Chen, J., 2015. Microglial and macrophage polarization—new prospects for brain repair. Nat. Rev. Neurol. 11, 56–64. https://doi.org/10.1038/nrneurol.2014.207

Hutton, M., Lendon, C.L., Rizzu, P., Baker, M., Froelich, S., Houlden, H.H., Pickering-

Brown, S., Chakraverty, S., Isaacs, A., Grover, A., Hackett, J., Heutink, P., et al., 1998. Association of missense and 5'-splice-site mutations in tau with the inherited dementia FTDP-17. Nature 393, 705. https://doi.org/10.1038/31508

Hyman, B.T., Phelps, C.H., Beach, T.G., Bigio, E.H., Cairns, N.J., Carrillo, M.C., Dickson, D.W., Duyckaerts, C., Frosch, M.P., Masliah, E., Mirra, S.S., Nelson, P.T., Schneider, J.A., Thal, D.R., Thies, B., Trojanowski, J.Q., Vinters, H. V., Montine, T.J., 2012. National Institute on Aging-Alzheimer's Association guidelines for the neuropathologic assessment of Alzheimer's disease. Alzheimer's Dement. 8, 1–13. https://doi.org/10.1016/j.jalz.2011.10.007

Illán-Gala, I., Alcolea, D., Montal, V., Dols-Icardo, O., Muñoz, L., de Luna, N., Turón-Sans, J., Cortés-Vicente, E., Sánchez-Saudinós, M.B., Subirana, A., Sala, I., Blesa, R., Clarimón, J., Fortea, J., Rojas-García, R., Lleó, A., 2018. CSF sAPPβ, YKL-40, and NfL along the ALS-FTD spectrum. Neurology 91, e1619–e1628. https://doi.org/10.1212/WNL.0000000000006383

Illán-Gala, I., Pegueroles, J., Montal, V., Alcolea, D., Vilaplana, E., Bejanin, A., Borrego-Écija, S., Sampedro, F., Subirana, A., Sánchez-Saudinós, M.B., Rojas-García, R., Vanderstichele, H., Blesa, R., Clarimón, J., Antonell, A., Lladó, A., Sánchez-Valle, R., Fortea, J., Lleó, A., 2019. APP-derived peptides reflect neurodegeneration in frontotemporal dementia. Ann. Clin. Transl. Neurol. 6, 2518–2530. https://doi.org/10.1002/acn3.50948

Irwin, D.J., Brettschneider, J., McMillan, C.T., Cooper, F., Olm, C., Arnold, S.E., Van Deerlin, V.M., Seeley, W.W., Miller, B.L., Lee, E.B., Lee, V.M.-Y., Grossman, M., Trojanowski, J.Q., 2016. Deep clinical and neuropathological phenotyping of Pick disease. Ann. Neurol. 79, 272–287. https://doi.org/10.1002/ana.24559

Irwin, D.J., McMillan, C.T., Xie, S.X., Rascovsky, K., Van Deerlin, V.M., Coslett, H.B., Hamilton, R., Aguirre, G.K., Lee, E.B., Lee, V.M.Y., Trojanowski, J.Q., Grossman, M., 2018. Asymmetry of post-mortem neuropathology in behavioural-variant

frontotemporal dementia. Brain 141, 288–301. https://doi.org/10.1093/brain/awx319

Ishiki, A., Kamada, M., Kawamura, Y., Terao, C., Shimoda, F., Tomita, N., Arai, H., Furukawa, K., 2016. Glial fibrillar acidic protein in the cerebrospinal fluid of Alzheimer's disease, dementia with Lewy bodies, and frontotemporal lobar degeneration. J. Neurochem. 136, 258–261. https://doi.org/10.1111/jnc.13399

Ishizawa, K., Dickson, D.W., 2001. Microglial activation parallels system degeneration in progressive supranuclear palsy and corticobasal degeneration. J. Neuropathol. Exp. Neurol. 60, 647–57. https://doi.org/10.1093/jnen/60.6.647

Ito, D., Imai, Y., Ohsawa, K., Nakajima, K., Fukuuchi, Y., Kohsaka, S., 1998. Microglia-specific localisation of a novel calcium binding protein, Iba1. Mol. Brain Res. 57, 1–9. https://doi.org/10.1016/S0169-328X(98)00040-0

Janelidze, S., Hertze, J., Zetterberg, H., Landqvist Waldö, M., Santillo, A., Blennow, K., Hansson, O., 2016. Cerebrospinal fluid neurogranin and YKL-40 as biomarkers of Alzheimer's disease. Ann. Clin. Transl. Neurol. 3, 12–20. https://doi.org/10.1002/acn3.266

Jian, J., Chen, Yuehong, Liberti, R., Fu, W., Hu, W., Saunders-Pullman, R., Pastores, G.M., Chen, Ying, Sun, Y., Grabowski, G.A., Liu, C. ju, 2018. Chitinase-3-like Protein 1: A Progranulin Downstream Molecule and Potential Biomarker for Gaucher Disease. EBioMedicine 28, 251–260. https://doi.org/10.1016/j.ebiom.2018.01.022

Jian, J., Zhao, S., Tian, Q., Gonzalez-Gugel, E., Mundra, J.J., Uddin, S.M., Liu, B., Richbourgh, B., Brunetti, R., Liu, C.J., 2013. Progranulin directly binds to the CRD2 and CRD3 of TNFR extracellular domains. FEBS Lett. 587, 3428–3436. https://doi.org/10.1016/j.febslet.2013.09.024

Jiskoot, L.C., Bocchetta, M., Nicholas, J.M., Cash, D.M., Thomas, D., Modat, M., Ourselin, S., Rombouts, S.A.R.B., Dopper, E.G.P., Meeter, L.H., Panman, J.L., van

Minkelen, R., van der Ende, E.L., Donker Kaat, L., Pijnenburg, Y.A.L., Borroni, B., Galimberti, D., Masellis, M., Tartaglia, M.C., Rowe, J., Graff, C., Tagliavini, F., Frisoni, G.B., Laforce, R., Finger, E., de Mendonça, A., Sorbi, S., Papma, J.M., van Swieten, J.C., Rohrer, J.D., 2018. Presymptomatic white matter integrity loss in familial frontotemporal dementia in the GENFI cohort: A cross-sectional diffusion tensor imaging study. Ann. Clin. Transl. Neurol. 5, 1025–1036. https://doi.org/10.1002/acn3.601

Johanson, C.E., Duncan, J.A., Klinge, P.M., Brinker, T., Stopa, E.G., Silverberg, G.D., 2008. Multiplicity of cerebrospinal fluid functions: New challenges in health and disease. Cerebrospinal Fluid Res. 5, 1–32. https://doi.org/10.1186/1743-8454-5-10

Johnson, E., Chase, K., McGowan, S., Mondo, E., Pfister, E., Mick, E., Friedline, R.H., Kim, J.K., Sapp, E., DiFiglia, M., Aronin, N., 2015. Safety of Striatal Infusion of siRNA in a Transgenic Huntington's Disease Mouse Model. J. Huntingtons. Dis. 4, 219–229. https://doi.org/10.3233/JHD-150163

Kahlson, M.A., Colodner, K.J., 2015. Glial tau pathology in tauopathies: functional consequences. J. Exp. Neurosci. 9, 43–50. https://doi.org/10.4137/JEn.s25515

Katisko, K., Solje, E., Koivisto, A.M., Krüger, J., Kinnunen, T., Hartikainen, P., Helisalmi, S., Korhonen, V., Herukka, S.K., Haapasalo, A., Remes, A.M., 2018. Prevalence of immunological diseases in a Finnish frontotemporal lobar degeneration cohort with the C9orf72 repeat expansion carriers and non-carriers. J. Neuroimmunol. 321, 29–35. https://doi.org/10.1016/j.jneuroim.2018.05.011

Kelley, B.J., Haidar, W., Boeve, B.F., Baker, M., Graff-Radford, N.R., Krefft, T., Frank, A.R., Jack, C.R., Shiung, M., Knopman, D.S., Josephs, K.A., Parashos, S.A., Rademakers, R., Hutton, M., Pickering-Brown, S., Adamson, J., Kuntz, K.M., Dickson, D.W., Parisi, J.E., Smith, G.E., Ivnik, R.J., Petersen, R.C., 2009. Prominent phenotypic variability associated with mutations in Progranulin. Neurobiol. Aging 30, 739–751.

https://doi.org/10.1016/j.neurobiolaging.2007.08.022

Keren-Shaul, H., Spinrad, A., Weiner, A., Matcovitch-Natan, O., Dvir-Szternfeld, R., Ulland, T.K., David, E., Baruch, K., Lara-Astaiso, D., Toth, B., Itzkovitz, S., Colonna, M., Schwartz, M., Amit, I., 2017. A Unique Microglia Type Associated with Restricting Development of Alzheimer's Disease. Cell 169, 1276-1290.e17. https://doi.org/10.1016/j.cell.2017.05.018

Kersaitis, C., Halliday, G.M., Kril, J.J., 2004. Regional and cellular pathology in frontotemporal dementia: relationship to stage of disease in cases with and without Pick bodies. Acta Neuropathol. 108, 515–523. https://doi.org/10.1007/s00401-004-0917-0

Kester, M.I., Teunissen, C.E., Sutphen, C., Herries, E.M., Ladenson, J.H., Xiong, C., Scheltens, P., Van Der Flier, W.M., Morris, J.C., Holtzman, D.M., Fagan, A.M., 2015. Cerebrospinal fluid VILIP-1 and YKL-40, candidate biomarkers to diagnose, predict and monitor Alzheimer's disease in a memory clinic cohort. Alzheimer's Res. Ther. 7, 1–9. https://doi.org/10.1186/s13195-015-0142-1

Kim, G., Ahmadian, S.S., Peterson, M., Parton, Z., Memon, R., Weintraub, S., Rademaker, A., Bigio, E., Mesulam, M.M., Geula, C., 2016. Asymmetric pathology in primary progressive aphasia with progranulin mutations and TDP inclusions. Neurology 86, 627–636. https://doi.org/10.1212/WNL.0000000000002375

Kim, G., Bolbolan, K., Gefen, T., Weintraub, S., Bigio, E.H., Rogalski, E., Mesulam, M.M., Geula, C., 2018a. Atrophy and microglial distribution in primary progressive aphasia with transactive response DNA-binding protein-43 kDa. Ann. Neurol. 83, 1096–1104. https://doi.org/10.1002/ana.25240

Kim, G., Vahedi, S., Gefen, T., Weintraub, S., Bigio, E.H., Mesulam, M.M., Geula, C., 2018b. Asymmetric TDP pathology in primary progressive aphasia with right hemisphere language dominance. Neurology 90, e396–e403. https://doi.org/10.1212/WNL.0000000000004891

Kim, M.J., McGwier, M., Jenko, K.J., Snow, J., Morse, C., Zoghbi, S.S., Pike, V.W., Innis, R.B., Kreisl, W.C., 2019. Neuroinflammation in frontotemporal lobar degeneration revealed by 11C-PBR28 PET. Ann. Clin. Transl. Neurol. 6, 1327–1331. https://doi.org/10.1002/acn3.50802

Klein, Z.A., Takahashi, H., Ma, M., Stagi, M., Zhou, M., Lam, T.K.T., Strittmatter, S.M., 2017. Loss of TMEM106B Ameliorates Lysosomal and Frontotemporal Dementia-Related Phenotypes in Progranulin-Deficient Mice. Neuron 95, 281-296.e6. https://doi.org/10.1016/j.neuron.2017.06.026

Kleinberger, G., Brendel, M., Mracsko, E., Wefers, B., Groeneweg, L., Xiang, X., Focke, C., Deußing, M., Suárez-Calvet, M., Mazaheri, F., Parhizkar, S., Pettkus, N., Wurst, W., Feederle, R., Bartenstein, P., Mueggler, T., Arzberger, T., Knuesel, I., Rominger, A., Haass, C., 2017. The FTD-like syndrome causing TREM2 T66M mutation impairs microglia function, brain perfusion, and glucose metabolism. EMBO J. 36, 1837–1853. https://doi.org/10.15252/embj.201796516

Kleinberger, G., Yamanishi, Y., Suarez-Calvet, M., Czirr, E., Lohmann, E., Cuyvers, E., Struyfs, H., Pettkus, N., Wenninger-Weinzierl, A., Mazaheri, F., Tahirovic, S., Lleo, A., Alcolea, D., Fortea, J., Willem, M., Lammich, S., Molinuevo, J.L., Sanchez-Valle, R., Antonell, A., Ramirez, A., Heneka, M.T., Sleegers, K., van der Zee, J., Martin, J.-J., Engelborghs, S., Demirtas-Tatlidede, A., Zetterberg, H., Van Broeckhoven, C., Gurvit, H., Wyss-Coray, T., Hardy, J., Colonna, M., Haass, C., 2014. TREM2 mutations implicated in neurodegeneration impair cell surface transport and phagocytosis. Sci. Transl. Med. 6, 243ra86-243ra86. https://doi.org/10.1126/scitranslmed.3009093

Kneynsberg, A., Combs, B., Christensen, K., Morfini, G., Kanaan, N.M., 2017. Axonal Degeneration in Tauopathies: Disease Relevance and Underlying Mechanisms. Front. Neurosci. 11, 572. https://doi.org/10.3389/fnins.2017.00572

Komori, T., 1999. Tau-positive glial inclusions in progressive supranuclear palsy,

corticobasal degeneration and Pick's disease. Brain Pathol. 9, 663–79.

Koriath, C.A.M., Bocchetta, M., Brotherhood, E., Woollacott, I.O.C., Norsworthy, P., Simón-Sánchez, J., Blauwendraat, C., Dick, K.M., Gordon, E., Harding, S.R., Fox, N.C., Crutch, S., Warren, J.D., Revesz, T., Lashley, T., Mead, S., Rohrer, J.D., 2017. The clinical, neuroanatomical, and neuropathologic phenotype of TBK1-associated frontotemporal dementia: A longitudinal case report. Alzheimer's Dement. Diagnosis, Assess. Dis. Monit. 6, 75–81. https://doi.org/10.1016/j.dadm.2016.10.003

Kuiperij, H.B., Versleijen, A.A.M., Beenes, M., Verwey, N.A., Benussi, L., Paterlini, A., Binetti, G., Teunissen, C.E., Raaphorst, J., Schelhaas, H.J., Küsters, B., Pijnenburg, Y.A.L., Ghidoni, R., Verbeek, M.M., 2017. Tau Rather than TDP-43 Proteins are Potential Cerebrospinal Fluid Biomarkers for Frontotemporal Lobar Degeneration Subtypes: A Pilot Study. J. Alzheimer's Dis. 55, 585–595. https://doi.org/10.3233/JAD-160386

Lam, B.Y.K., Halliday, G.M., Irish, M., Hodges, J.R., Piguet, O., 2014. Longitudinal white matter changes in frontotemporal dementia subtypes. Hum. Brain Mapp. 35, 3547–57.

Landin-Romero, R., Tan, R., Hodges, J.R., Kumfor, F., 2016. An update on semantic dementia: Genetics, imaging, and pathology. Alzheimer's Res. Ther. 8, 1–9. https://doi.org/10.1186/s13195-016-0219-5

Landqvist Waldö, M., Frizell Santillo, A., Passant, U., Zetterberg, H., Rosengren, L., Nilsson, C., Englund, E., 2013. Cerebrospinal fluid neurofilament light chain protein levels in subtypes of frontotemporal dementia. BMC Neurol. 13, 54. https://doi.org/10.1186/1471-2377-13-54

Lant, S.B., Robinson, A.C., Thompson, J.C., Rollinson, S., Pickering-Brown, S., Snowden, J.S., Davidson, Y.S., Gerhard, A., Mann, D.M.A., 2014. Patterns of microglial cell activation in frontotemporal lobar degeneration. Neuropathol. Appl.

Neurobiol. 40, 686–696. https://doi.org/10.1111/nan.12092

Lashley, T., Rohrer, J.D., Mahoney, C., Gordon, E., Beck, J., Mead, S., Warren, J., Rossor, M., Revesz, T., 2014. A pathogenic progranulin mutation and C9orf72 repeat expansion in a family with frontotemporal dementia. Neuropathol. Appl. Neurobiol. 40, 502–513. https://doi.org/10.1111/nan.12100

Lashley, T., Rohrer, J.D., Mead, S., Revesz, T., 2015. Review: An update on clinical, genetic and pathological aspects of frontotemporal lobar degenerations. Neuropathol. Appl. Neurobiol. 41, 858–881. https://doi.org/10.1111/nan.12250

Le Ber, I., Camuzat, A., Hannequin, D., Pasquier, F., Guedj, E., Rovelet-Lecrux, A., Hahn-Barma, V., Van Der Zee, J., Clot, F., Bakchine, S., Puel, M., Ghanim, M., Lacomblez, L., Mikol, J., Deramecourt, V., Lejeune, P., De La Sayette, V., Belliard, S., Vercelletto, M., Meyrignac, C., Van Broeckhoven, C., Lambert, J.C., Verpillat, P., Campion, D., Habert, M.O., Dubois, B., Brice, A., Clerget-Darpoux, F., Didic, M., Desnuelle, C., Duyckaerts, C., Golfier, V., Michel, B.F., Thomas-Anterion, C., Salachas, F., Sellal, F., Camu, W., 2008. Phenotype variability in progranulin mutation carriers: A clinical, neuropsychological, imaging and genetic study. Brain 131, 732–746. https://doi.org/10.1093/brain/awn012

Le Ber, I., De Septenville, A., Millecamps, S., Camuzat, A., Caroppo, P., Couratier, P., Blanc, F., Lacomblez, L., Sellal, F., Fleury, M.C., Meininger, V., Cazeneuve, C., Clot, F., Flabeau, O., LeGuern, E., Brice, A., Didic, M., Dubois, B., Golfier, V., Hannequin, D., Levy, R., Michel, B.F., Pasquier, F., Thomas-Anterion, C., Puel, M., Salachas, F., Vercelletto, M., 2015. TBK1 mutation frequencies in French frontotemporal dementia and amyotrophic lateral sclerosis cohorts. Neurobiol. Aging 36, 3116.e5-3116.e8. https://doi.org/10.1016/j.neurobiolaging.2015.08.009

Lee, E.B., Porta, S., Michael Baer, G., Xu, Y., Suh, E.R., Kwong, L.K., Elman, L., Grossman, M., Lee, V.M.Y., Irwin, D.J., Van Deerlin, V.M., Trojanowski, J.Q., 2017. Expansion of the classification of FTLD-TDP: distinct pathology associated with

rapidly progressive frontotemporal degeneration. Acta Neuropathol. 134, 65–78. https://doi.org/10.1007/s00401-017-1679-9

Lee, S., Viqar, F., Zimmerman, M.E., Narkhede, A., Tosto, G., Benzinger, T.L.S., Marcus, D.S., Fagan, A.M., Goate, A., Fox, N.C., Cairns, N.J., Holtzman, D.M., Buckles, V., Ghetti, B., McDade, E., Martins, R.N., Saykin, A.J., Masters, C.L., Ringman, J.M., Ryan, N.S., F??rster, S., Laske, C., Schofield, P.R., Sperling, R.A., Salloway, S., Correia, S., Jack, C., Weiner, M., Bateman, R.J., Morris, J.C., Mayeux, R., Brickman, A.M., 2016. White matter hyperintensities are a core feature of Alzheimer's disease: Evidence from the dominantly inherited Alzheimer network. Ann. Neurol. 79, 929–939. https://doi.org/10.1002/ana.24647

Lehmer, C., Oeckl, P., Weishaupt, J.H., Volk, A.E., Diehl-Schmid, J., Schroeter, M.L., Lauer, M., Kornhuber, J., Levin, J., Fassbender, K., Landwehrmeyer, B., Schludi, M.H., Arzberger, T., Kremmer, E., Flatley, A., Feederle, R., Steinacker, P., Weydt, P., Ludolph, A.C., Edbauer, D., Otto, M., Danek, A., Feneberg, E., Anderl-Straub, S., Arnim, C., Jahn, H., Schneider, A., Maler, M., Polyakova, M., Riedl, L., Wiltfang, J., Ziegler, G., 2017. Poly-GP in cerebrospinal fluid links C9orf72 -associated dipeptide repeat expression to the asymptomatic phase of ALS / FTD. EMBO Mol. Med. 9, 859–868. https://doi.org/10.15252/emmm.201607486

Leyns, C.E.G., Holtzman, D.M., 2017. Glial contributions to neurodegeneration in tauopathies. Mol. Neurodegener. 12, 50. https://doi.org/10.1186/s13024-017-0192-x

Ling, H., Macerollo, A., 2018. Is it Useful to Classify PSP and CBD as Different Disorders? Yes. Mov. Disord. Clin. Pract. 5, 145–148. https://doi.org/10.1002/mdc3.12581

Litvan, I., Agid, Y., Calne, D., Campbell, G., Dubois, B., Duvoisin, R.C., Goetz, C.G., Golbe, L.I., Grafman, J., Growdon, J.H., Hallett, M., Jankovic, J., Quinn, N.P., Tolosa, E., Zee, D.S., 1996. Clinical Research Criteria for the Diagnosis of

Progressive Supranuclear Gaze Palsy (Steele-Richardson-Olszewski syndrome): Report of the NINDS-PSP International Workshop. Neurology 47, 1–9.

Liu, D., Cao, B., Zhao, Y., Huang, H., McIntyre, R.S., Rosenblat, J.D., Zhou, H., 2018. Soluble TREM2 changes during the clinical course of Alzheimer's disease: A meta-analysis. Neurosci. Lett. 686, 10–16. https://doi.org/10.1016/j.neulet.2018.08.038

Ljubenkov, P.A., Staffaroni, A.M., Rojas, J.C., Allen, I.E., Wang, P., Heuer, H., Karydas, A., Kornak, J., Cobigo, Y., Seeley, W.W., Grinberg, L.T., Spina, S., Fagan, A.M., Jerome, G., Knopman, D., Boeve, B.F., Dickerson, B.C., Kramer, J., Miller, B., Boxer, A.L., Rosen, H.J., 2018. Cerebrospinal fluid biomarkers predict frontotemporal dementia trajectory. Ann. Clin. Transl. Neurol. 5, 1250–1263. https://doi.org/10.1002/acn3.643

Llorens, F., Thüne, K., Tahir, W., Kanata, E., Diaz-Lucena, D., Xanthopoulos, K., Kovatsi, E., Pleschka, C., Garcia-Esparcia, P., Schmitz, M., Ozbay, D., Correia, S., Correia, Â., Milosevic, I., Andréoletti, O., Fernández-Borges, N., Vorberg, I.M., Glatzel, M., Sklaviadis, T., Torres, J.M., Krasemann, S., Sánchez-Valle, R., Ferrer, I., Zerr, I., 2017. YKL-40 in the brain and cerebrospinal fluid of neurodegenerative dementias. Mol. Neurodegener. 12, 83. https://doi.org/10.1186/s13024-017-0226-4

Lopes, K.O., Sparks, D.L., Streit, W.J., 2008. Microglial dystrophy in the aged and Alzheimer's disease brain is associated with ferritin immunoreactivity. Glia 56, 1048–1060. https://doi.org/10.1002/glia.20678

Lui, H., Zhang, J., Makinson, S.R., Cahill, M.K., Kelley, K.W., Huang, H.-Y., Shang, Y., Oldham, M.C., Martens, L.H., Gao, F., Coppola, G., Sloan, S.A., Hsieh, C.L., Kim, C.C., Bigio, E.H., Weintraub, S., Mesulam, M.-M., Rademakers, R., Mackenzie, I.R., Seeley, W.W., Karydas, A., Miller, B.L., Borroni, B., Ghidoni, R., Farese, R. V., Paz, J.T., Barres, B.A., Huang, E.J., 2016. Progranulin Deficiency Promotes Circuit-Specific Synaptic Pruning by Microglia via Complement Activation. Cell 165, 921–935. https://doi.org/10.1016/j.cell.2016.04.001

Ma, L., Morton, A.J., Nicholson, L.F.B., 2003. Microglia density decreases with age in a mouse model of Huntington's disease. Glia 43, 274–280. https://doi.org/10.1002/glia.10261

Mackenzie, I.R., Nicholson, A.M., Sarkar, M., Messing, J., Purice, M.D., Pottier, C., Annu, K., Baker, M., Perkerson, R.B., Kurti, A., Matchett, B.J., Mittag, T., Temirov, J., Hsiung, G.Y.R., Krieger, C., Murray, M.E., Kato, M., Fryer, J.D., Petrucelli, L., Zinman, L., Weintraub, S., Mesulam, M., Keith, J., Zivkovic, S.A., Hirsch-Reinshagen, V., Roos, R.P., Züchner, S., Graff-Radford, N.R., Petersen, R.C., Caselli, R.J., Wszolek, Z.K., Finger, E., Lippa, C., Lacomis, D., Stewart, H., Dickson, D.W., Kim, H.J., Rogaeva, E., Bigio, E., Boylan, K.B., Taylor, J.P., Rademakers, R., 2017. TIA1 Mutations in Amyotrophic Lateral Sclerosis and Frontotemporal Dementia Promote Phase Separation and Alter Stress Granule Dynamics. Neuron 95, 808-816.e9. https://doi.org/10.1016/j.neuron.2017.07.025

Mackenzie, I.R.A., 2007. The neuropathology and clinical phenotype of FTD with progranulin mutations. Acta Neuropathol. 114, 49–54. https://doi.org/10.1007/s00401-007-0223-8

Mackenzie, I.R.A., Neumann, M., 2016. Molecular neuropathology of frontotemporal dementia: insights into disease mechanisms from postmortem studies. J. Neurochem. 138, 54–70. https://doi.org/10.1111/jnc.13588

Mackenzie, I.R.A., Neumann, M., Baborie, A., Sampathu, D.M., Du Plessis, D., Jaros, E., Perry, R.H., Trojanowski, J.Q., Mann, D.M.A., Lee, V.M.Y., 2011. A harmonized classification system for FTLD-TDP pathology. Acta Neuropathol. 122, 111–113. https://doi.org/10.1007/s00401-011-0845-8

Mahoney, C.J., Beck, J., Rohrer, J.D., Lashley, T., Mok, K., Shakespeare, T., Yeatman, T., Warrington, E.K., Schott, J.M., Fox, N.C., Rossor, M.N., Hardy, J., Collinge, J., Revesz, T., Mead, S., Warren, J.D., 2012. Frontotemporal dementia with the C9ORF72 hexanucleotide repeat expansion: Clinical, neuroanatomical and

neuropathological features. Brain 135, 736–750. https://doi.org/10.1093/brain/awr361

Mahoney, C.J., Ridgway, G.R., Malone, I.B., Downey, L.E., Beck, J., Kinnunen, K.M., Schmitz, N., Golden, H.L., Rohrer, J.D., Schott, J.M., Rossor, M.N., Ourselin, S., Mead, S., Fox, N.C., Warren, J.D., 2014. Profiles of white matter tract pathology in frontotemporal dementia. Hum. Brain Mapp. 35, 4163–4179. https://doi.org/10.1002/hbm.22468

Majounie, E., Renton, A.E., Mok, K., Dopper, E.G., Waite, A., Rollinson, S., Chiò, A., Restagno, G., Nicolaou, N., Simon-Sanchez, J., van Swieten, J.C., Traynor, B.J., et al., 2012. Frequency of the C9orf72 hexanucleotide repeat expansion in patients with amyotrophic lateral sclerosis and frontotemporal dementia: a cross-sectional study. Lancet Neurol. 11, 323–330. https://doi.org/10.1016/S1474-4422(12)70043-1

Mann, D.M.A., 1998. Dementia of frontal type and dementias with subcortical gliosis. Brain Pathol. 8, 325–338. https://doi.org/10.1111/j.1750-3639.1998.tb00157.x

Mann, D.M.A., South, P.W., Snowden, J.S., Neary, D., 1993. Dementia of frontal lobe type: Neuropathology and immunohistochemistry. J. Neurol. Neurosurg. Psychiatry 56, 605–614. https://doi.org/10.1136/jnnp.56.6.605

Mao, Q., Zheng, X., Gefen, T., Rogalski, E., Spencer, C.L., Rademakers, R., Fought, A.J., Kohler, M., Weintraub, S., Xia, H., Mesulam, M.M., Bigio, E.H., 2019. FTLD-TDP With and Without GRN Mutations Cause Different Patterns of CA1 Pathology. J. Neuropathol. Exp. Neurol. 78, 844–853. https://doi.org/10.1093/jnen/nlz059

Marchlik, E., Thakker, P., Carlson, T., Jiang, Z., Ryan, M., Marusic, S., Goutagny, N., Kuang, W., Askew, G.R., Roberts, V., Benoit, S., Zhou, T., Ling, V., Pfeifer, R., Stedman, N., Fitzgerald, K.A., Lin, L.-L., Hall, J.P., 2010. Mice lacking Tbk1 activity exhibit immune cell infiltrates in multiple tissues and increased susceptibility to LPS-induced lethality. J. Leukoc. Biol. 88, 1171–80. https://doi.org/10.1189/jlb.0210071

Marelli, C., Hourregue, C., Gutierrez, L.A., Paquet, C., Menjot De Champfleur, N., De Verbizier, D., Jacob, M., Dubois, J., Maleska, A.M.E., Hirtz, C., Navucet, S., Bennys, K., Dumurgier, J., Cognat, E., Berr, C., Magnin, E., Lehmann, S., Gabelle, A., 2020. Cerebrospinal Fluid and Plasma Biomarkers do not Differ in the Presenile and Late-Onset Behavioral Variants of Frontotemporal Dementia. J. Alzheimer's Dis. 74, 903–911. https://doi.org/10.3233/JAD-190378

Marschallinger, J., Iram, T., Zardeneta, M., Lee, S.E., Lehallier, B., Haney, M.S., Pluvinage, J. V., Mathur, V., Hahn, O., Morgens, D.W., Kim, J., Tevini, J., Felder, T.K., Wolinski, H., Bertozzi, C.R., Bassik, M.C., Aigner, L., Wyss-Coray, T., 2020. Lipid-droplet-accumulating microglia represent a dysfunctional and proinflammatory state in the aging brain. Nat. Neurosci. 23, 194–208. https://doi.org/10.1038/s41593-019-0566-1

Martens, L.H., Zhang, J., Barmada, S.J., Zhou, P., Kamiya, S., Sun, B., Min, S.-W., Gan, L., Finkbeiner, S., Huang, E.J., Farese, R. V., 2012. Progranulin deficiency promotes neuroinflammation and neuron loss following toxin-induced injury. J. Clin. Invest. 122, 3955–3959. https://doi.org/10.1172/JCI63113

Martinac, J.A., Craft, D.K., Su, J.H., Kim, R.C., Cotman, C.W., 2001. Astrocytes degenerate in frontotemporal dementia: Possible relation to hypoperfusion. Neurobiol. Aging 22, 195–207. https://doi.org/10.1016/S0197-4580(00)00231-1

Mattsson, N., Tabatabaei, S., Johansson, P., Hansson, O., Andreasson, U., Månsson, J.-E., Johansson, J.-O., Olsson, B., Wallin, A., Svensson, J., Blennow, K., Zetterberg, H., 2011. Cerebrospinal Fluid Microglial Markers in Alzheimer's Disease: Elevated Chitotriosidase Activity but Lack of Diagnostic Utility. NeuroMolecular Med. 13, 151–159. https://doi.org/10.1007/s12017-011-8147-9

Mazaheri, F., Snaidero, N., Kleinberger, G., Madore, C., Daria, A., Werner, G., Krasemann, S., Capell, A., Trümbach, D., Wurst, W., Brunner, B., Bultmann, S., Tahirovic, S., Kerschensteiner, M., Misgeld, T., Butovsky, O., Haass, C., 2017.

TREM2 deficiency impairs chemotaxis and microglial responses to neuronal injury. EMBO Rep. 18, 1186–1198. https://doi.org/10.15252/embr.201743922

McAleese, K.E., Firbank, M., Dey, M., Colloby, S.J., Walker, L., Johnson, M., Beverley, J.R., Taylor, J.P., Thomas, A.J., O'Brien, J.T., Attems, J., 2015. Cortical tau load is associated with white matter hyperintensities. Acta Neuropathol. Commun. 3, 60. https://doi.org/10.1186/s40478-015-0240-0

McAleese, K.E., Walker, L., Graham, S., Moya, E.L.J., Johnson, M., Erskine, D., Colloby, S.J., Dey, M., Martin-Ruiz, C., Taylor, J.P., Thomas, A.J., McKeith, I.G., De Carli, C., Attems, J., 2017. Parietal white matter lesions in Alzheimer's disease are associated with cortical neurodegenerative pathology, but not with small vessel disease. Acta Neuropathol. 134, 459–473. https://doi.org/10.1007/s00401-017-1738-2

McMillan, C.T., Irwin, D.J., Avants, B.B., Powers, J., Cook, P.A., Toledo, J.B., Wood, E.M.C., Van Deerlin, V.M., Lee, V.M.-Y., Trojanowski, J.Q., Grossman, M., 2013. White matter imaging helps dissociate tau from TDP-43 in frontotemporal lobar degeneration. J. Neurol. Neurosurg. Psychiatry 84, 949–955. https://doi.org/10.1136/jnnp-2012-304418

Meeter, L.H., Dopper, E.G., Jiskoot, L.C., Sanchez-Valle, R., Graff, C., Benussi, L., Ghidoni, R., Pijnenburg, Y.A., Borroni, B., Galimberti, D., Laforce, R.J., Masellis, M., Vandenberghe, R., Ber, I. Le, Otto, M., van Minkelen, R., Papma, J.M., Rombouts, S.A., Balasa, M., Öijerstedt, L., Jelic, V., Dick, K.M., Cash, D.M., Harding, S.R., Jorge Cardoso, M., Ourselin, S., Rossor, M.N., Padovani, A., Scarpini, E., Fenoglio, C., Tartaglia, M.C., Lamari, F., Barro, C., Kuhle, J., Rohrer, J.D., Teunissen, C.E., van Swieten, J.C., 2016a. Neurofilament light chain: a biomarker for genetic frontotemporal dementia. Ann. Clin. Transl. Neurol. 3, 623–636. https://doi.org/10.1002/acn3.325

Meeter, L.H., Gendron, T.F., Sias, A.C., Jiskoot, L.C., Russo, S.P., Donker Kaat, L.,

Papma, J.M., Panman, J.L., van der Ende, E.L., Dopper, E.G., Franzen, S., Graff, C., Boxer, A.L., Rosen, H.J., Sanchez-Valle, R., Galimberti, D., Pijnenburg, Y.A.L., Benussi, L., Ghidoni, R., Borroni, B., Laforce, R., del Campo, M., Teunissen, C.E., van Minkelen, R., Rojas, J.C., Coppola, G., Geschwind, D.H., Rademakers, R., Karydas, A.M., Öijerstedt, L., Scarpini, E., Binetti, G., Padovani, A., Cash, D.M., Dick, K.M., Bocchetta, M., Miller, B.L., Rohrer, J.D., Petrucelli, L., van Swieten, J.C., Lee, S.E., 2018. Poly(GP), neurofilament and grey matter deficits in C9orf72 expansion carriers. Ann. Clin. Transl. Neurol. 5, 583–597. https://doi.org/10.1002/acn3.559

Meeter, L.H., Patzke, H., Loewen, G., Dopper, E.G.P., Pijnenburg, Y.A.L., van Minkelen, R., van Swieten, J.C., 2016b. Progranulin Levels in Plasma and Cerebrospinal Fluid in Granulin Mutation Carriers. Dement. Geriatr. Cogn. Dis. Extra 6, 330–340. https://doi.org/10.1159/000447738

Meeter, L.H.H., Steketee, R.M.E., Salkovic, D., Vos, M.E., Grossman, M., McMillan, C.T., Irwin, D.J., Boxer, A.L., Rojas, J.C., Olney, N.T., Karydas, A., Miller, B.L., Pijnenburg, Y.A.L., Barkhof, F., Sánchez-Valle, R., Lladó, A., Borrego-Ecija, S., Diehl-Schmid, J., Grimmer, T., Goldhardt, O., Santillo, A.F., Hansson, O., Vestberg, S., Borroni, B., Padovani, A., Galimberti, D., Scarpini, E., Rohrer, J.D., Woollacott, I.O.C., Synofzik, M., Wilke, C., De Mendonca, A., Vandenberghe, R., Benussi, L., Ghidoni, R., Binetti, G., Niessen, W.J., Papma, J.M., Seelaar, H., Jiskoot, L.C., De Jong, F.J., Donker Kaat, L., Del Campo, M., Teunissen, C.E., Bron, E.E., Van Den Berg, E., Van Swieten, J.C., 2019. Clinical value of cerebrospinal fluid neurofilament light chain in semantic dementia. J. Neurol. Neurosurg. Psychiatry 90, 997–1004. https://doi.org/10.1136/jnnp-2018-319784

Meeter, L.H.H., Vijverberg, E.G., Del Campo, M., Rozemuller, A.J.M., Donker Kaat, L., de Jong, F.J., van der Flier, W.M., Teunissen, C.E., van Swieten, J.C., Pijnenburg, Y.A.L., 2018. Clinical value of neurofilament and phospho-tau/tau ratio in the

frontotemporal dementia spectrum. Neurology 90, e1231–e1239. https://doi.org/10.1212/WNL.0000000000005261

Miller, Z.A., Rankin, K.P., Graff-Radford, N.R., Takada, L.T., Sturm, V.E., Cleveland, C.M., Criswell, L.A., Jaeger, P.A., Stan, T., Heggeli, K.A., Hsu, S.C., Karydas, A., Khan, B.K., Grinberg, L.T., Gorno-Tempini, M.L., Boxer, A.L., Rosen, H.J., Kramer, J.H., Coppola, G., Geschwind, D.H., Rademakers, R., Seeley, W.W., Wyss-Coray, T., Miller, B.L., 2013. TDP-43 frontotemporal lobar degeneration and autoimmune disease. J Neurol Neurosurg Psychiatry 84, 956–962. https://doi.org/10.1136/jnnp-2012-304644

Miller, Z.A., Sturm, V.E., Camsari, G.B., Karydas, A., Yokoyama, J.S., Grinberg, L.T., Boxer, A.L., Rosen, H.J., Rankin, K.P., Gorno-Tempini, M.L., Coppola, G., Geschwind, D.H., Rademakers, R., Seeley, W.W., Graff-Radford, N.R., Miller, B.L., 2016. Increased prevalence of autoimmune disease within C9 and FTD/MND cohorts. Neurol. - Neuroimmunol. Neuroinflammation 3, e301. https://doi.org/10.1212/NXI.0000000000000301

Mimuro, M., Yoshida, M., Miyao, S., Harada, T., Ishiguro, K., Hashizume, Y., 2010. Neuronal and glial tau pathology in early frontotemporal lobar degeneration-tau, Pick's disease subtype. J. Neurol. Sci. 290, 177–182. https://doi.org/10.1016/j.jns.2009.11.002

Minami, S.S., Shen, V., Le, D., Krabbe, G., Asgarov, R., Perez-Celajes, L., Lee, C.H., Li, J., Donnelly-Roberts, D., Gan, L., 2015. Reducing inflammation and rescuing FTD-related behavioral deficits in progranulin-deficient mice with α7 nicotinic acetylcholine receptor agonists. Biochem. Pharmacol. 97, 454–462. https://doi.org/10.1016/j.bcp.2015.07.016

Minett, T., Classey, J., Matthews, F.E., Fahrenhold, M., Taga, M., Brayne, C., Ince, P.G., Nicoll, J.A.R., Boche, D., MRC CFAS, 2016. Microglial immunophenotype in dementia with Alzheimer's pathology. J. Neuroinflammation 13, 135.

https://doi.org/10.1186/s12974-016-0601-z

Mishra, P.S., Vijayalakshmi, K., Nalini, A., Sathyaprabha, T.N., Kramer, B.W., Alladi, P.A., Raju, T.R., 2017. Etiogenic factors present in the cerebrospinal fluid from amyotrophic lateral sclerosis patients induce predominantly pro-inflammatory responses in microglia. J. Neuroinflammation 14, 1–18. https://doi.org/10.1186/s12974-017-1028-x

Mittelbronn, M., Dietz, K., Schluesener, H.J., Meyermann, R., 2001. Local distribution of microglia in the normal adult human central nervous system differs by up to one order of magnitude. Acta Neuropathol. 101, 249–255. https://doi.org/10.1007/s004010000284

Miyoshi, M., Shinotoh, H., Wszolek, Z.K., Strongosky, A.J., Shimada, H., Arakawa, R., Higuchi, M., Ikoma, Y., Yasuno, F., Fukushi, K., Irie, T., Ito, H., Suhara, T., 2010. In vivo detection of neuropathologic changes in presymptomatic MAPT mutation carriers: A PET and MRI study. Park. Relat. Disord. 16, 404–408. https://doi.org/10.1016/j.parkreldis.2010.04.004

Moore, K.M., Nicholas, J., Grossman, M., McMillan, C.T., Irwin, D.J., Massimo, L., Van Deerlin, V.M., Warren, J.D., Fox, N.C., Rossor, M.N., Mead, S., Geschwind, D., et al., 2020. Age at symptom onset and death and disease duration in genetic frontotemporal dementia: an international retrospective cohort study. Lancet Neurol. 19, 145–156. https://doi.org/10.1016/S1474-4422(19)30394-1

Morenas-Rodríguez, E., Alcolea, D., Suárez-Calvet, M., Muñoz-Llahuna, L., Vilaplana, E., Sala, I., Subirana, A., Querol-Vilaseca, M., Carmona-Iragui, M., Illán-Gala, I., Ribosa-Nogué, R., Blesa, R., Haass, C., Fortea, J., Lleó, A., 2019. Different pattern of CSF glial markers between dementia with Lewy bodies and Alzheimer's disease. Sci. Rep. 9, 7803. https://doi.org/10.1038/s41598-019-44173-8

Münch, C., Rosenbohm, A., Sperfeld, A.D., Uttner, I., Reske, S., Krause, B.J., Sedlmeier, R., Meyer, T., Hanemann, C.O., Stumm, G., Ludolph, A.C., 2005. Heterozygous

R1101K mutation of the DCTN1 gene in a family with ALS and FTD. Ann. Neurol. 58, 777–780. https://doi.org/10.1002/ana.20631

Murray, M.E., Vemuri, P., Preboske, G.M., Murphy, M.C., Schweitzer, K.J., Parisi, J.E., Jack, C.R., Dickson, D.W., 2012. A Quantitative Postmortem MRI Design Sensitive to White Matter Hyperintensity Differences and Their Relationship With Underlying Pathology. J. Neuropathol. Exp. Neurol. 71, 1113–1122. https://doi.org/10.1097/NEN.0b013e318277387e

Musi, N., Valentine, J.M., Sickora, K.R., Baeuerle, E., Thompson, C.S., Shen, Q., Orr, M.E., 2018. Tau protein aggregation is associated with cellular senescence in the brain. Aging Cell 17, e12840. https://doi.org/10.1111/acel.12840

Navarro, V., Sanchez-Mejias, E., Jimenez, S., Muñoz-Castro, C., Sanchez-Varo, R., Davila, J.C., Vizuete, M., Gutierrez, A., Vitorica, J., 2018. Microglia in Alzheimer's disease: Activated, dysfunctional or degenerative. Front. Aging Neurosci. 10, 1–8. https://doi.org/10.3389/fnagi.2018.00140

Neary, D., Snowden, J.S., Gustafson, L., Passant, U., Stuss, D., Black, S., Freedman, M., Kertesz, A., Robert, P.H., Albert, M., Boone, K., Miller, B.L., Cummings, J., Benson, D.F., 1998. Frontotemporal lobar degeneration: A consensus on clinical diagnostic criteria. Neurology 51, 1546–1554. https://doi.org/10.1212/WNL.51.6.1546

Neumann, M., Mackenzie, I.R.A., 2019. Review: Neuropathology of non-tau frontotemporal lobar degeneration. Neuropathol. Appl. Neurobiol. 45, 19–40. https://doi.org/10.1111/nan.12526

Nguyen, A.D., Nguyen, T.A., Zhang, J., Devireddy, S., Zhou, P., Karydas, A.M., Xu, X., Miller, B.L., Rigo, F., Ferguson, S.M., Huang, E.J., Walther, T.C., Farese, R. V., 2018. Murine knockin model for progranulin-deficient frontotemporal dementia with nonsense-mediated mRNA decay. Proc. Natl. Acad. Sci. 115, E2849–E2858. https://doi.org/10.1073/pnas.1722344115

Nicholson, A.M., Finch, N.A., Almeida, M., Perkerson, R.B., van Blitterswijk, M., Wojtas, A., Cenik, B., Rotondo, S., Inskeep, V., Almasy, L., Dyer, T., Peralta, J., Jun, G., Wood, A.R., Frayling, T.M., Fuchsberger, C., Fowler, S., Teslovich, T.M., Manning, A.K., Kumar, S., Curran, J., Lehman, D., Abecasis, G., Duggirala, R., Pottier, C., Zahir, H.A., Crook, J.E., Karydas, A., Mitic, L., Sun, Y., Dickson, D.W., Bu, G., Herz, J., Yu, G., Miller, B.L., Ferguson, S., Petersen, R.C., Graff-Radford, N., Blangero, J., Rademakers, R., 2016. Prosaposin is a regulator of progranulin levels and oligomerization. Nat. Commun. 7, 11992. https://doi.org/10.1038/ncomms11992

Nilson, A.N., English, K.C., Gerson, J.E., Barton Whittle, T., Nicolas Crain, C., Xue, J., Sengupta, U., Castillo-Carranza, D.L., Zhang, W., Gupta, P., Kayed, R., 2017. Tau oligomers associate with inflammation in the brain and retina of tauopathy mice and in neurodegenerative diseases. J. Alzheimer's Dis. 55, 1083–1099. https://doi.org/10.3233/JAD-160912

Nordengen, K., Kirsebom, B.E., Henjum, K., Selnes, P., Gísladóttir, B., Wettergreen, M., Torsetnes, S.B., Grøntvedt, G.R., Waterloo, K.K., Aarsland, D., Nilsson, L.N.G., Fladby, T., 2019. Glial activation and inflammation along the Alzheimer's disease continuum. J. Neuroinflammation 16. https://doi.org/10.1186/s12974-019-1399-2

Nugent, A.A., Lin, K., van Lengerich, B., Lianoglou, S., Przybyla, L., Davis, S.S., Llapashtica, C., Wang, J., Kim, D.J., Xia, D., Lucas, A., Baskaran, S., Haddick, P.C.G., Lenser, M., Earr, T.K., Shi, J., Dugas, J.C., Andreone, B.J., Logan, T., Solanoy, H.O., Chen, H., Srivastava, A., Poda, S.B., Sanchez, P.E., Watts, R.J., Sandmann, T., Astarita, G., Lewcock, J.W., Monroe, K.M., Di Paolo, G., 2020. TREM2 Regulates Microglial Cholesterol Metabolism upon Chronic Phagocytic Challenge. Neuron 105, 837-854.e9. https://doi.org/10.1016/j.neuron.2019.12.007

O'Rourke, J.G., Bogdanik, L., Yanez, A., Lall, D., Wolf, A.J., Muhammad, A.K.M.G., Ho, R., Carmona, S., Vit, J.P., Zarrow, J., Kim, K.J., Bell, S., Harms, M.B., Miller, T.M., Dangler, C.A., Underhill, D.M., Goodridge, H.S., Lutz, C.M., Baloh, R.H., 2016.

C9orf72 is required for proper macrophage and microglial function in mice. Science (80-.). 351, 1324–1329. https://doi.org/10.1126/science.aaf1064

Oeckl, P., Weydt, P., Steinacker, P., Anderl-Straub, S., Nordin, F., Volk, A.E., Diehl-Schmid, J., Andersen, P.M., Kornhuber, J., Danek, A., Fassbender, K., Fliessbach, K., Jahn, H., Lauer, M., Müller, K., Knehr, A., Prudlo, J., Schneider, A., Thal, D.R., Yilmazer-Hanke, D., Weishaupt, J.H., Ludolph, A.C., Otto, M., 2019. Different neuroinflammatory profile in amyotrophic lateral sclerosis and frontotemporal dementia is linked to the clinical phase. J. Neurol. Neurosurg. Psychiatry 90, 4–10. https://doi.org/10.1136/jnnp-2018-318868

Ohm, D.T., Kim, G., Gefen, T., Rademaker, A., Weintraub, S., Bigio, E.H., Mesulam, M.M., Rogalski, E., Geula, C., 2018. Prominent microglial activation in cortical white matter is selectively associated with cortical atrophy in primary progressive aphasia. Neuropathol. Appl. Neurobiol. 1–14. https://doi.org/doi: 10.1111/nan.12494

Öhrfelt, A., Axelsson, M., Malmeström, C., Novakova, L., Heslegrave, A., Blennow, K., Lycke, J., Zetterberg, H., 2016. Soluble TREM-2 in cerebrospinal fluid from patients with multiple sclerosis treated with natalizumab or mitoxantrone. Mult. Scler. J. 22, 1587–1595. https://doi.org/10.1177/1352458515624558

Ohsawa, K., Imai, Y., Kanazawa, H., Sasaki, Y., Kohsaka, S., 2000. Involvement of Iba1 in membrane ruffling and phagocytosis of macrophages/microglia. J. Cell Sci. 113, 3073–3084.

Olsson, B., Hertze, J., Lautner, R., Zetterberg, H., Nägga, K., Höglund, K., Basun, H., Annas, P., Lannfelt, L., Andreasen, N., Minthon, L., Blennow, K., Hansson, O., 2013. Microglial markers are elevated in the prodromal phase of Alzheimer's disease and vascular dementia. J. Alzheimer's Dis. 33, 45–53. https://doi.org/10.3233/JAD-2012-120787

Olsson, B., Lautner, R., Andreasson, U., Öhrfelt, A., Portelius, E., Bjerke, M., Hölttä, M., Rosén, C., Olsson, C., Strobel, G., Wu, E., Dakin, K., Petzold, M., Blennow, K.,

Zetterberg, H., 2016. CSF and blood biomarkers for the diagnosis of Alzheimer's disease: A systematic review and meta-analysis. Lancet Neurol. 4422, 1–12. https://doi.org/10.1016/S1474-4422(16)00070-3

Onari, K., Spatz, H., 1926. Anatomische Beiträge zur Lehre von der Pickschen umschriebenen Grosshirnrinden-Atrophie (Picksche Krankheit). Z. Neurol. 101, 470–511.

Onyike, C.U., Diehl-Schmid, J., 2013. The epidemiology of frontotemporal dementia. Int. Rev. Psychiatry 25, 130–137. https://doi.org/10.3109/09540261.2013.776523

Paloneva, J., Kestilä, M., Wu, J., Salminen, A., Böhling, T., Ruotsalainen, V., Hakola, P., Bakker, A.B.H., Phillips, J.H., Pekkarinen, P., Lanier, L.L., Timonen, T., Peltonen, L., 2000. Loss-of-function mutations in TYROBP (DAP12) result in a presenile dementia with bone cysts. Nat. Genet. 25, 357–361. https://doi.org/10.1038/77153

Panman, J.L., Jiskoot, L.C., Bouts, M.J.R.J., Meeter, L.H.H., van der Ende, E.L., Poos, J.M., Feis, R.A., Kievit, A.J.A., van Minkelen, R., Dopper, E.G.P., Rombouts, S.A.R.B., van Swieten, J.C., Papma, J.M., 2019. Gray and white matter changes in presymptomatic genetic frontotemporal dementia: a longitudinal MRI study. Neurobiol. Aging 76, 115–124. https://doi.org/10.1016/j.neurobiolaging.2018.12.017

Papma, J.M., Jiskoot, L.C., Panman, J.L., Dopper, E.G., Den Heijer, T., Donker Kaat, L., Pijnenburg, Y.A.L., Meeter, L.H., Van Minkelen, R., Rombouts, S.A.R.B., Van Swieten, J.C., 2017. Cognition and gray and white matter characteristics of presymptomatic C9orf72 repeat expansion. Neurology 89, 1256–1264. https://doi.org/10.1212/WNL.0000000000004393

Park, H.K., Chung, S.J., 2013. New perspective on parkinsonism in frontotemporal lobar degeneration. J. Mov. Disord. 6, 1–8. https://doi.org/10.14802/jmd.13001

Passamonti, L., Vázquez Rodríguez, P., Hong, Y.T., Allinson, K.S., Richard Bevan-Jones, W., Williamson, D., Simon Jones, P., Arnold, R., Borchert, R.J.,

Surendranathan, A., Mak, E., Su, L., Fryer, T.D., Aigbirhio, F.I., O, J.T., Rowe, J.B., 2018. [11 C]PK11195 binding in Alzheimer disease and progressive supranuclear palsy. Neurology 90, e1989–e1996. https://doi.org/10.1212/WNL.0000000000005610

Paternicò, D., Premi, E., Gazzina, S., Cosseddu, M., Alberici, A., Archetti, S., Cotelli, M.S., Micheli, A., Turla, M., Gasparotti, R., Padovani, A., Borroni, B., 2016. White matter hyperintensities characterize monogenic frontotemporal dementia with granulin mutations. Neurobiol. Aging 38, 176–180. https://doi.org/10.1016/j.neurobiolaging.2015.11.011

Paterson, R.W., Heywood, W.E., Heslegrave, A.J., Magdalinou, N.K., Andreasson, U., Sirka, E., Bliss, E., Slattery, C.F., Toombs, J., Svensson, J., Johansson, P., Fox, N.C., Zetterberg, H., Mills, K., Schott, J.M., 2016. A targeted proteomic multiplex CSF assay identifies increased malate dehydrogenase and other neurodegenerative biomarkers in individuals with Alzheimer's disease pathology. Transl. Psychiatry 6, e952. https://doi.org/10.1038/tp.2016.194

Paulus, W., Bancher, C., Jellinger, K., 1993. Microglial reaction in Pick's disease. Neurosci. Lett. 161, 89–92. https://doi.org/10.1016/0304-3940(93)90147-D

Piccio, L., Buonsanti, C., Cella, M., Tassi, I., Schmidt, R.E., Fenoglio, C., Rinker, J., Naismith, R.T., Panina-Bordignon, P., Passini, N., Galimberti, D., Scarpini, E., Colonna, M., Cross, A.H., 2008. Identification of soluble TREM-2 in the cerebrospinal fluid and its association with multiple sclerosis and CNS inflammation. Brain 131, 3081–3091. https://doi.org/10.1093/brain/awn217

Piccio, L., Deming, Y., Del-Aguila, J.L., Ghezzi, L., Holtzman, D.M., Fagan, A.M., Fenoglio, C., Galimberti, D., Borroni, B., Cruchaga, C., 2016. Cerebrospinal fluid soluble TREM2 is higher in Alzheimer disease and associated with mutation status. Acta Neuropathol. 131, 925–933. https://doi.org/10.1007/s00401-016-1533-5

Pick, A., 1892. Uber die Beziehungen der senilen Hirnatrophie zur Aphasie. Prager Med

Wochenschr 17, 165–167.

Pickering-Brown, S.M., Richardson, A.M.T., Snowden, J.S., Mcdonagh, A.M., Burns, A., Braude, W., Baker, M., Liu, W.-K., Yen, S.-H., Hardy, J., Hutton, M., Davies, Y., Allsop, D., Craufurd, D., Neary, D., Mann, D.M.A., 2002. Inherited frontotemporal dementia in nine British families associated with intronic mutations in the tau gene. Brain 125, 732–751.

Pickering-Brown, S.M., Rollinson, S., Du Plessis, D., Morrison, K.E., Varma, A., Richardson, A.M.T., Neary, D., Snowden, J.S., Mann, D.M.A., 2008. Frequency and clinical characteristics of progranulin mutation carriers in the Manchester frontotemporal lobar degeneration cohort: Comparison with patients with MAPT and no known mutations. Brain 131, 721–731. https://doi.org/10.1093/brain/awm331

Pickford, F., Marcus, J., Camargo, L.M., Xiao, Q., Graham, D., Mo, J.R., Burkhardt, M., Kulkarni, V., Crispino, J., Hering, H., Hutton, M., 2011. Progranulin is a chemoattractant for microglia and stimulates their endocytic activity. Am. J. Pathol. 178, 284–295. https://doi.org/10.1016/j.ajpath.2010.11.002

Pietroboni, A.M., Fumagalli, G.G., Ghezzi, L., Fenoglio, C., Cortini, F., Serpente, M., Cantoni, C., Rotondo, E., Corti, P., Carecchio, M., Bassi, M., Bresolin, N., Galbiati, D., Galimberti, D., Scarpini, E., 2011. Phenotypic heterogeneity of the GRN Asp22fs mutation in a large italian kindred. J. Alzheimer's Dis. 24, 253–259. https://doi.org/10.3233/JAD-2011-101704

Pijnenburg, Y.A.L.L., Janssen, J.C., Schoonenboom, N.S.M.M., Petzold, A., Mulder, C., Stigbrand, T., Norgren, N., Heijst, H., Hack, C.E., Scheltens, P., Teunissen, C.E., 2007. CSF neurofilaments in frontotemporal dementia compared with early onset Alzheimer's disease and controls. Dement. Geriatr. Cogn. Disord. 23, 225–230. https://doi.org/10.1159/000099473

Pottier, C., Bieniek, K.F., Finch, N.C., van de Vorst, M., Baker, M., Perkersen, R., Brown, P., Ravenscroft, T., van Blitterswijk, M., Nicholson, A.M., DeTure, M., Knopman,

D.S., Josephs, K.A., Parisi, J.E., Petersen, R.C., Boylan, K.B., Boeve, B.F., Graff-Radford, N.R., Veltman, J.A., Gilissen, C., Murray, M.E., Dickson, D.W., Rademakers, R., 2015. Whole-genome sequencing reveals important role for TBK1 and OPTN mutations in frontotemporal lobar degeneration without motor neuron disease. Acta Neuropathol. 130, 77–92. https://doi.org/10.1007/s00401-015-1436-x

Pottier, C., Ravenscroft, T.A., Sanchez-Contreras, M., Rademakers, R., 2016. Genetics of FTLD: overview and what else we can expect from genetic studies. J. Neurochem. https://doi.org/10.1111/jnc.13622

Pottier, C., Ren, Y., Perkerson, R.B., Baker, M., Jenkins, G.D., van Blitterswijk, M., DeJesus-Hernandez, M., van Rooij, J.G.J., Murray, M.E., Christopher, E., McDonnell, S.K., Rademakers, R., et al., 2019. Genome-wide analyses as part of the international FTLD-TDP whole-genome sequencing consortium reveals novel disease risk factors and increases support for immune dysfunction in FTLD. Acta Neuropathol. 137, 879–899. https://doi.org/10.1007/s00401-019-01962-9

Pottier, C., Zhou, X., Perkerson, R.B., Baker, M., Jenkins, G.D., Serie, D.J., Ghidoni, R., Benussi, L., Binetti, G., López de Munain, A., Zulaica, M., Rademakers, R., et al., 2018. Potential genetic modifiers of disease risk and age at onset in patients with frontotemporal lobar degeneration and GRN mutations: a genome-wide association study. Lancet Neurol. 17, 548–558. https://doi.org/10.1016/S1474-4422(18)30126-1

Premi, E., Formenti, A., Gazzina, S., Archetti, S., Gasparotti, R., Padovani, A., Borroni, B., 2014. Effect of TMEM106B polymorphism on functional network connectivity in asymptomatic GRN mutation carriers. JAMA Neurol. 71, 216–221. https://doi.org/10.1001/jamaneurol.2013.4835

Premi, E., Grassi, M., Van Swieten, J., Galimberti, D., Graff, C., Masellis, M., Tartaglia, C., Tagliavini, F., Rowe, J.B., Laforce, R., Finger, E., Frisoni, G.B., De Mendonça,

A., Sorbi, S., Gazzina, S., Cosseddu, M., Archetti, S., Gasparotti, R., Manes, M., Alberici, A., Cardoso, M.J., Bocchetta, M., Cash, D.M., Ourselin, S., Padovani, A., Rohrer, J.D., Borroni, B., 2017. Cognitive reserve and TMEM106B genotype modulate brain damage in presymptomatic frontotemporal dementia: A GENFI study. Brain 140, 1784–1791. https://doi.org/10.1093/brain/awx103

Rademakers, R., Eriksen, J.L., Baker, M., Robinson, T., Ahmed, Z., Lincoln, S.J., Finch, N., Rutherford, N.J., Crook, R.J., Josephs, K.A., Boeve, B.F., Knopman, D.S., Petersen, R.C., Parisi, J.E., Caselli, R.J., Wszolek, Z.K., Uitti, R.J., Feldman, H., Hutton, M.L., Mackenzie, I.R., Graff-Radford, N.R., Dickson, D.W., 2008. Common variation in the miR-659 binding-site of GRN is a major risk factor for TDP43-positive frontotemporal dementia. Hum. Mol. Genet. 17, 3631–3642. https://doi.org/10.1093/hmg/ddn257

Rascovsky, K., Hodges, J.R., Knopman, D., Mendez, M.F., Kramer, J.H., Neuhaus, J., van Swieten, J.C., Seelaar, H., Dopper, E.G.P., Onyike, C.U., Hillis, A.E., Josephs, K.A., Boeve, B.F., Kertesz, A., Seeley, W.W., Rankin, K.P., Johnson, J.K., Gorno-Tempini, M.-L., Rosen, H., Prioleau-Latham, C.E., Lee, A., Kipps, C.M., Lillo, P., Piguet, O., Rohrer, J.D., Rossor, M.N., Warren, J.D., Fox, N.C., Galasko, D., Salmon, D.P., Black, S.E., Mesulam, M., Weintraub, S., Dickerson, B.C., Diehl-Schmid, J., Pasquier, F., Deramecourt, V., Lebert, F., Pijnenburg, Y., Chow, T.W., Manes, F., Grafman, J., Cappa, S.F., Freedman, M., Grossman, M., Miller, B.L., 2011. Sensitivity of revised diagnostic criteria for the behavioural variant of frontotemporal dementia. Brain 134, 2456–2477. https://doi.org/10.1093/brain/awr179

Renton, A.E., Majounie, E., Waite, A., Simón-Sánchez, J., Rollinson, S., Gibbs, J.R., Schymick, J.C., Laaksovirta, H., van Swieten, J.C., Myllykangas, L., Kalimo, H., Traynor, B.J., et al., 2011. A hexanucleotide repeat expansion in C9ORF72 is the cause of chromosome 9p21-linked ALS-FTD. Neuron 72, 257–268.

https://doi.org/10.1016/j.neuron.2011.09.010

Rentzos, M., Paraskevas, G.P., Kapaki, E., Nikolaou, C., Zoga, M., Rombos, A., Tsoutsou, A., Vassilopoulos D, D., 2006a. Interleukin-12 is reduced in cerebrospinal fluid of patients with Alzheimer's disease and frontotemporal dementia. J. Neurol. Sci. 249, 110–114. https://doi.org/10.1016/j.jns.2006.05.063

Rentzos, M., Zoga, M., Paraskevas, G.P., Kapaki, E., Rombos, A., Nikolaou, C., Tsoutsou, A., Vassilopoulos, D., 2006b. IL-15 is elevated in cerebrospinal fluid of patients with Alzheimer's disease and frontotemporal dementia. J. Geriatr. Psychiatry Neurol. 19, 114–117. https://doi.org/10.1177/0891988706286226

Rodrigues, F.B., Byrne, L.M., McColgan, P., Robertson, N., Tabrizi, S.J., Zetterberg, H., Wild, E.J., 2016. Cerebrospinal fluid inflammatory biomarkers reflect clinical severity in huntington's disease. PLoS One 11, 1–10. https://doi.org/10.1371/journal.pone.0163479

Rohrer, J.D., Caso, F., Mahoney, C., Henry, M., Rosen, H.J., Rabinovici, G., Rossor, M.N., Miller, B., Warren, J.D., Fox, N.C., Ridgway, G.R., Gorno-Tempini, M.L., 2013. Patterns of longitudinal brain atrophy in the logopenic variant of primary progressive aphasia. Brain Lang. 127, 121–126. https://doi.org/10.1016/j.bandl.2012.12.008

Rohrer, J.D., Crutch, S.J., Warrington, E.K., Warren, J.D., 2010a. Progranulin-associated primary progressive aphasia: A distinct phenotype? Neuropsychologia 48, 288–297. https://doi.org/10.1016/j.neuropsychologia.2009.09.017

Rohrer, J.D., Guerreiro, R., Vandrovcova, J., Uphill, J., Reiman, D., Beck, J., Isaacs, A.M., Authier, A., Ferrari, R., Fox, N.C., MacKenzie, I.R.A., Warren, J.D., De Silva, R., Holton, J., Revesz, T., Hardy, J., Mead, S., Rossor, M.N., 2009a. The heritability and genetics of frontotemporal lobar degeneration. Neurology 73, 1451–1456. https://doi.org/10.1212/WNL.0b013e3181bf997a

Rohrer, J.D., Knight, W.D., Warren, J.E., Fox, N.C., Rossor, M.N., Warren, J.D., 2008.

Word-finding difficulty: a clinical analysis of the progressive aphasias. Brain 131, 8–38. https://doi.org/10.1093/brain/awm251

Rohrer, J.D., Lashley, T., Schott, J.M., Warren, J.E., Mead, S., Isaacs, A.M., Beck, J., Hardy, J., De Silva, R., Warrington, E., Troakes, C., Al-Sarraj, S., King, A., Borroni, B., Clarkson, M.J., Ourselin, S., Holton, J.L., Fox, N.C., Revesz, T., Rossor, M.N., Warren, J.D., 2011. Clinical and neuroanatomical signatures of tissue pathology in frontotemporal lobar degeneration. Brain 134, 2565–2581. https://doi.org/10.1093/brain/awr198

Rohrer, J.D., Nicholas, J.M., Cash, D.M., van Swieten, J., Dopper, E., Jiskoot, L., van Minkelen, R., Rombouts, S.A., Cardoso, M.J., Clegg, S., Espak, M., Rossor, M.N., et al., 2015. Presymptomatic cognitive and neuroanatomical changes in genetic frontotemporal dementia in the Genetic Frontotemporal dementia Initiative (GENFI) study: A cross-sectional analysis. Lancet Neurol. 14, 253–262. https://doi.org/10.1016/S1474-4422(14)70324-2

Rohrer, J.D., Rossor, M.N., Warren, J.D., 2010b. Syndromes of nonfluent primary progressive aphasia: A clinical and neurolinguistic analysis. Neurology 75, 603–610. https://doi.org/10.1212/WNL.0b013e3181ed9c6b

Rohrer, J.D., Warren, J.D., Modat, M., Ridgway, G.R., Douiri, A., Rossor, M.N., Ourselin, S., Fox, N.C., 2009b. Patterns of cortical thinning in the language variants of frontotemporal lobar degeneration. Neurology 72, 1562–1569. https://doi.org/10.1212/WNL.0b013e3181a4124e

Rohrer, J.D., Woollacott, I.O.C., Dick, K.M., Brotherhood, E., Gordon, E., Fellows, A., Toombs, J., Druyeh, R., Cardoso, M.J., Ourselin, S., Nicholas, J.M., Norgren, N., Mead, S., Andreasson, U., Blennow, K., Schott, J.M., Fox, N.C., Warren, J.D., Zetterberg, H., 2016. Serum neurofilament light chain protein is a measure of disease intensity in frontotemporal dementia. Neurology 87, 1329–1336. https://doi.org/10.1212/WNL.0000000000003154

Rosén, C., Andersson, C.-H., Andreasson, U., Molinuevo, J.L., Bjerke, M., Rami, L., Lladó, A., Blennow, K., Zetterberg, H., 2014. Increased Levels of Chitotriosidase and YKL-40 in Cerebrospinal Fluid from Patients with Alzheimer's Disease. Dement. Geriatr. Cogn. Dis. Extra 4, 297–304. https://doi.org/10.1159/000362164

Rosso, S. M., Landweer, E.J., Houterman, M., Donker Kaat, L., Van Duijn, C.M., Van Swieten, J.C., 2003. Medical and environmental risk factors for sporadic frontotemporal dementia: A retrospective case-control study. J. Neurol. Neurosurg. Psychiatry 74, 1574–1576. https://doi.org/10.1136/jnnp.74.11.1574

Rosso, Sonia M., Van Herpen, E., Pijnenburg, Y.A.L., Schoonenboom, N.S.M., Scheltens, P., Heutink, P., Van Swieten, J.C., 2003. Total tau and phosphorylated tau 181 levels in the cerebrospinal fluid of patients with frontotemporal dementia due to P301L and G272V tau mutations. Arch. Neurol. 60, 1209–1213. https://doi.org/10.1001/archneur.60.9.1209

Rostalski, H., Leskelä, S., Huber, N., Katisko, K., Cajanus, A., Solje, E., Marttinen, M., Natunen, T., Remes, A.M., Hiltunen, M., Haapasalo, A., 2019. Astrocytes and microglia as potential contributors to the pathogenesis of C9orf72 repeat expansion-associated FTLD and ALS. Front. Neurosci. 13, 1–11. https://doi.org/10.3389/fnins.2019.00486

Rostgaard, N., Roos, P., Portelius, E., Blennow, K., Zetterberg, H., Simonsen, A.H., Nielsen, J.E., 2018. CSF neurofilament light concentration is increased in presymptomatic CHMP2B mutation carriers. Neurology 90, e157–e163. https://doi.org/10.1212/WNL.0000000000004799

Rubino, E., Rainero, I., Chio, A., Rogaeva, E., Galimberti, D., Fenoglio, P., Grinberg, Y., Isaia, G., Calvo, A., Gentile, S., Bruni, A.C., St. George-Hyslop, P.H., Scarpini, E., Gallone, S., Pinessi, L., 2012. SQSTM1 mutations in frontotemporal lobar degeneration and amyotrophic lateral sclerosis. Neurology 79, 1556–1562. https://doi.org/10.1212/WNL.0b013e31826e25df

Ryan, N.S., Biessels, G.-J., Kim, L., Nicholas, J.M., Barber, P.A., Walsh, P., Gami, P., Morris, H.R., Bastos-Leite, A.J., Schott, J.M., Beck, J., Mead, S., Chavez-Gutierrez, L., de Strooper, B., Rossor, M.N., Revesz, T., Lashley, T., Fox, N.C., 2015. Genetic determinants of white matter hyperintensities and amyloid angiopathy in familial Alzheimer's disease. Neurobiol. Aging 36, 3140–3151. https://doi.org/10.1016/j.neurobiolaging.2015.08.026

Sajjadi, S.A., Patterson, K., Arnold, R.J., Watson, P.C., Nestor, P.J., 2012. Primary progressive aphasia: A tale of two syndromes and the rest. Neurology 78, 1670–1677. https://doi.org/10.1212/WNL.0b013e3182574f79

Sakae, N., Josephs, K.A., Litvan, I., Murray, M.E., Duara, R., Uitti, R.J., Wszolek, Z.K., Graff-Radford, N.R., Dickson, D.W., 2019a. Neuropathologic basis of frontotemporal dementia in progressive supranuclear palsy. Mov. Disord. https://doi.org/10.1002/mds.27816

Sakae, N., Roemer, S.F., Bieniek, K.F., Murray, M.E., Baker, M.C., Kasanuki, K., Graff-Radford, N.R., Petrucelli, L., Van Blitterswijk, M., Rademakers, R., Dickson, D.W., 2019b. Microglia in frontotemporal lobar degeneration with progranulin or C9ORF72 mutations. Ann. Clin. Transl. Neurol. 6, 1782–1796. https://doi.org/10.1002/acn3.50875

Sanchez-Mejias, E., Navarro, V., Jimenez, S., Sanchez-Mico, M., Sanchez-Varo, R., Nuñez-Diaz, C., Trujillo-Estrada, L., Davila, J.C., Vizuete, M., Gutierrez, A., Vitorica, J., 2016. Soluble phospho-tau from Alzheimer's disease hippocampus drives microglial degeneration. Acta Neuropathol. 132, 897–916. https://doi.org/10.1007/s00401-016-1630-5

Sanfilippo, C., Longo, A., Lazzara, F., Cambria, D., Distefano, G., Palumbo, M., Cantarella, A., Malaguarnera, L., Di Rosa, M., 2017. CHI3L1 and CHI3L2 overexpression in motor cortex and spinal cord of sALS patients. Mol. Cell. Neurosci. 85, 162–169. https://doi.org/10.1016/j.mcn.2017.10.001

Sarbu, N., Shih, R.Y., Jones, R. V, Horkayne-Szakaly, I., Oleaga, L., Smirniotopoulos, J.G., 2016. White Matter Diseases with Radiologic-Pathologic Correlation. RadioGraphics 36, 1426–1447. https://doi.org/10.1148/rg.2016160031

Sarlus, H., Heneka, M.T., 2017. Microglia in Alzheimer's disease. J. Clin. Invest. 127, 3240–3249. https://doi.org/10.1172/JCI90606

Sasaki, Y., Ohsawa, K., Kanazawa, H., Kohsaka, S., Imai, Y., 2001. Iba1 Is an Actin-Cross-Linking Protein in Macrophages/Microglia. Biochem. Biophys. Res. Commun. 286, 292–297. https://doi.org/10.1006/bbrc.2001.5388

Scahill, R.I., Zeun, P., Osborne-Crowley, K., Johnson, E.B., Gregory, S., Parker, C., Lowe, J., Nair, A., O'Callaghan, C., Langley, C., Papoutsi, M., McColgan, P., Estevez-Fraga, C., Fayer, K., Wellington, H., Rodrigues, F.B., Byrne, L.M., Heselgrave, A., Hyare, H., Sampaio, C., Zetterberg, H., Zhang, H., Wild, E.J., Rees, G., Robbins, T.W., Sahakian, B.J., Langbehn, D., Tabrizi, S.J., 2020. Biological and clinical characteristics of gene carriers far from predicted onset in the Huntington's disease Young Adult Study (HD-YAS): a cross-sectional analysis. Lancet Neurol. 19, 502–512. https://doi.org/10.1016/S1474-4422(20)30143-5

Schludi, M.H., Becker, L., Garrett, L., Gendron, T.F., Zhou, Q., Schreiber, F., Popper, B., Dimou, L., Strom, T.M., Winkelmann, J., von Thaden, A., Rentzsch, K., May, S., Michaelsen, M., Schwenk, B.M., Tan, J., Schoser, B., Dieterich, M., Petrucelli, L., Hölter, S.M., Wurst, W., Fuchs, H., Gailus-Durner, V., de Angelis, M.H., Klopstock, T., Arzberger, T., Edbauer, D., 2017. Spinal poly-GA inclusions in a C9orf72 mouse model trigger motor deficits and inflammation without neuron loss. Acta Neuropathol. 134, 241–254. https://doi.org/10.1007/s00401-017-1711-0

Schmid, C.D., Sautkulis, L.N., Danielson, P.E., Cooper, J., Hasel, K.W., Hilbush, B.S., Sutcliffe, J.G., Carson, M.J., 2002. Heterogeneous expression of the triggering receptor expressed on myeloid cells-2 on adult murine microglia. J. Neurochem. 83, 1309–1320.

Schofield, E., Kersaitis, C., Shepherd, C.E., Kril, J.J., Halliday, G.M., 2003. Severity of gliosis in Pick's disease and frontotemporal lobar degeneration: Tau-positive glia differentiate these disorders. Brain 126, 827–840. https://doi.org/10.1093/brain/awg085

Seelaar, H., Rohrer, J.D., Pijnenburg, Y.A.L., Fox, N.C., Van Swieten, J.C., 2011. Clinical, genetic and pathological heterogeneity of frontotemporal dementia: a review. J. Neurol. Neurosurg. Psychiatry 82, 476–486. https://doi.org/10.1136/jnnp.2010.212225

Shim, Y.S., Yang, D.-W., Roe, C.M., Coats, M.A., Benzinger, T.L., Xiong, C., Galvin, J.E., Cairns, N.J., Morris, J.C., 2015. Pathological correlates of white matter hyperintensities on magnetic resonance imaging. Dement. Geriatr. Cogn. Disord. 39, 92–104. https://doi.org/10.1159/000366411

Simmons, D.A., Casale, M., Alcon, B., Pham, N., Narayan, N., Lynch, G., 2007. Ferritin accumulation in dystrophic microglia is an early event in the development of Huntington's Disease. Glia 55, 1074–1084. https://doi.org/10.1002/glia.20526

Sjögren, M., Folkesson, S., Blennow, K., Tarkowski, E., 2004. Increased intrathecal inflammatory activity in frontotemporal dementia: pathophysiological implications. J. Neurol. Neurosurg. Psychiatry 75, 1107–1111. https://doi.org/10.1136/jnnp.2003.019422

Skibinski, G., Parkinson, N.J., Brown, J.M., Chakrabarti, L., Lloyd, S.L., Hummerich, H., Nielsen, J.E., Hodges, J.R., Spillantini, M.G., Thusgaard, T., Brandner, S., Brun, A., Rossor, M.N., Gade, A., Johannsen, P., Sørensen, S.A., Gydesen, S., Fisher, E.M.C., Collinge, J., 2005. Mutations in the endosomal ESCRTIII-complex subunit CHMP2B in frontotemporal dementia. Nat. Genet. 37, 806–808. https://doi.org/10.1038/ng1609

Skillbäck, T., Farahmand, B., Bartlett, J.W., Rosén, C., Mattsson, N., Nägga, K., Kilander, L., Religa, D., Wimo, A., Winblad, B., Rosengren, L., Schott, J.M.,

Blennow, K., Eriksdotter, M., Zetterberg, H., 2014. CSF neurofilament light differs in neurodegenerative diseases and predicts severity and survival. Neurology 83, 1945–1953. https://doi.org/10.1212/WNL.0000000000001015

Skrobot, O.A., Attems, J., Esiri, M., Hortobagyi, T., Ironside, J.W., Kalaria, R.N., King, A., Lammie, G.A., Mann, D., Neal, J., Ben-Shlomo, Y., Kehoe, P.G., Love, S., 2016. Vascular cognitive impairment neuropathology guidelines (VCING): the contribution of cerebrovascular pathology to cognitive impairment. Brain 139, 2957–2969. https://doi.org/10.1093/brain/aww214

Smith, K.R., Damiano, J., Franceschetti, S., Carpenter, S., Canafoglia, L., Morbin, M., Rossi, G., Pareyson, D., Mole, S.E., Staropoli, J.F., Sims, K.B., Lewis, J., Lin, W.L., Dickson, D.W., Dahl, H.H., Bahlo, M., Berkovic, S.F., 2012. Strikingly different clinicopathological phenotypes determined by progranulin-mutation dosage. Am. J. Hum. Genet. 90, 1102–1107. https://doi.org/10.1016/j.ajhg.2012.04.021

Snowden, J.S., Rollinson, S., Thompson, J.C., Harris, J.M., Stopford, C.L., Richardson, A.M.T., Jones, M., Gerhard, A., Davidson, Y.S., Robinson, A., Gibbons, L., Hu, Q., DuPlessis, D., Neary, D., Mann, D.M.A., Pickering-Brown, S.M., 2012. Distinct clinical and pathological characteristics of frontotemporal dementia associated with C9ORF72 mutations. Brain 135, 693–708. https://doi.org/10.1093/brain/awr355

Snyder, H.M., Corriveau, R.A., Craft, S., Faber, J.E., Greenberg, S.M., Knopman, D., Lamb, B.T., Montine, T.J., Nedergaard, M., Schaffer, C.B., Schneider, J.A., Wellington, C., Wilcock, D.M., Zipfel, G.J., Zlokovic, B., Bain, L.J., Bosetti, F., Galis, Z.S., Koroshetz, W., Carrillo, M.C., 2015. Vascular contributions to cognitive impairment and dementia including Alzheimer's disease. Alzheimer's Dement. 11, 710–717. https://doi.org/10.1016/j.jalz.2014.10.008

Song, Z., Zhang, X., Zhang, L., Xu, F., Tao, X., Zhang, H., Lin, X., Kang, L., Xiang, Y., Lai, X., Zhang, Q., Huang, K., Dai, Y., Yin, Y., Cao, J., 2016. Progranulin plays a central role in host defense during sepsis by promoting macrophage recruitment.

Am. J. Respir. Crit. Care Med. 194, 1219–1232. https://doi.org/10.1164/rccm.201601-0056OC

Spillantini, M.G., Murrell, J.R., Goedert, M., Farlow, M.R., Klug, A., Ghetti, B., 1998. Mutation in the tau gene in familial multiple system tauopathy with presenile dementia. Proc. Natl. Acad. Sci. U. S. A. 95, 7737–7741. https://doi.org/10.1073/pnas.95.13.7737

Spiller, K.J., Restrepo, C.R., Khan, T., Dominique, M.A., Fang, T.C., Canter, R.G., Roberts, C.J., Miller, K.R., Ransohoff, R.M., Trojanowski, J.Q., Lee, V.M.Y., 2018. Microglia-mediated recovery from ALS-relevant motor neuron degeneration in a mouse model of TDP-43 proteinopathy. Nat. Neurosci. 21, 329–340. https://doi.org/10.1038/s41593-018-0083-7

Spittau, B., 2017. Aging microglia-phenotypes, functions and implications for age-related neurodegenerative diseases. Front. Aging Neurosci. 9, 1–9. https://doi.org/10.3389/fnagi.2017.00194

Srinivasan, K., Friedman, B.A., Etxeberria, A., Huntley, M.A., van der Brug, M.P., Foreman, O., Paw, J.S., Modrusan, Z., Beach, T.G., Serrano, G.E., Hansen, D. V., 2020. Alzheimer's Patient Microglia Exhibit Enhanced Aging and Unique Transcriptional Activation. Cell Rep. 31, 107843. https://doi.org/10.1016/j.celrep.2020.107843

Steinacker, P., Hendrich, C., Sperfeld, A.D., Jesse, S., Von Arnim, C.A.F., Lehnert, S., Pabst, A., Uttner, I., Tumani, H., Lee, V.M.Y., Trojanowski, J.Q., Kretzschmar, H.A., Ludolph, A., Neumann, M., Otto, M., 2008. TDP-43 in cerebrospinal fluid of patients with frontotemporal lobar degeneration and amyotrophic lateral sclerosis. Arch. Neurol. 65, 1481–1487. https://doi.org/10.1001/archneur.65.11.1481

Steinacker, P., Verde, F., Fang, L., Feneberg, E., Oeckl, P., Roeber, S., Anderl-Straub, S., Danek, A., Diehl-Schmid, J., Fassbender, K., Fliessbach, K., Foerstl, H., Giese, A., Jahn, H., Kassubek, J., Kornhuber, J., Landwehrmeyer, G.B., Lauer, M.,

Pinkhardt, E.H., Prudlo, J., Rosenbohm, A., Schneider, A., Schroeter, M.L., Tumani, H., Von Arnim, C.A.F., Weishaupt, J., Weydt, P., Ludolph, A.C., Yilmazer Hanke, D., Otto, M., 2018. Chitotriosidase (CHIT1) is increased in microglia and macrophages in spinal cord of amyotrophic lateral sclerosis and cerebrospinal fluid levels correlate with disease severity and progression. J. Neurol. Neurosurg. Psychiatry 89, 239–247. https://doi.org/10.1136/jnnp-2017-317138

Streit, W.J., Braak, H., Del Tredici, K., Leyh, J., Lier, J., Khoshbouei, H., Eisenlöffel, C., Müller, W., Bechmann, I., 2018. Microglial activation occurs late during preclinical Alzheimer's disease. Glia 66, 2550–2562. https://doi.org/10.1002/glia.23510

Streit, W.J., Braak, H., Xue, Q.-S., Bechmann, I., 2009. Dystrophic (senescent) rather than activated microglial cells are associated with tau pathology and likely precede neurodegeneration in Alzheimer's disease. Acta Neuropathol. 118, 475–485. https://doi.org/10.1007/s00401-009-0556-6

Streit, W.J., Sammons, N.W., Kuhns, A.J., Sparks, D.L., 2004. Dystrophic Microglia in the Aging Human Brain. Glia 45, 208–212. https://doi.org/10.1002/glia.10319

Streit, W.J., Xue, Q.-S., Tischer, J., Bechmann, I., 2014. Microglial pathology. Acta Neuropathol. Commun. 2, 142. https://doi.org/10.1186/s40478-014-0142-6

Strong, M.J., Grace, G.M., Freedman, M., Lomen-Hoerth, C., Woolley, S., Goldstein, L., Murphy, J., Shoesmith, C., Rosenfeld, J., Leigh, P.N., Bruijn, L., Ince, P., Figlewicz, D., 2009. Consensus criteria for the diagnosis of frontotemporal cognitive and behavioural syndromes in amyotrophic lateral sclerosis. Amyotroph. Lateral Scler. 10, 131–146. https://doi.org/10.1080/17482960802654364

Suárez-Calvet, M., Caballero, M.Á.A., Kleinberger, G., Bateman, R.J., Fagan, A.M., Morris, J.C., Levin, J., Danek, A., Ewers, M., Haass, C., 2016a. Early changes in CSF sTREM2 in dominantly inherited Alzheimer's disease occur after amyloid deposition and neuronal injury. Sci. Transl. Med. 8. https://doi.org/10.1126/scitranslmed.aag1767

Suárez-Calvet, M., Kleinberger, G., Araque Caballero, M.Á., Brendel, M., Rominger, A., Alcolea, D., Fortea, J., Lleó, A., Blesa, R., Gispert, J.D., Sánchez-Valle, R., Haass, C., et al., 2016b. sTREM2 cerebrospinal fluid levels are a potential biomarker for microglia activity in early-stage Alzheimer's disease and associate with neuronal injury markers. EMBO Mol. Med. 8, e201506123. https://doi.org/10.15252/emmm.201506123

Suárez-Calvet, M., Morenas-Rodríguez, E., Kleinberger, G., Schlepckow, K., Caballero, M.Á.A., Franzmeier, N., Capell, A., Fellerer, K., Nuscher, B., Eren, E., Levin, J., Deming, Y., Piccio, L., Karch, C.M., Cruchaga, C., Shaw, L.M., Trojanowski, J.Q., Weiner, M., Ewers, M., Haass, C., 2019. Early increase of CSF sTREM2 in Alzheimer's disease is associated with tau related-neurodegeneration but not with amyloid-β pathology. Mol. Neurodegener. 14, 1–14. https://doi.org/10.1186/s13024-018-0301-5

Suárez-Calvet, M., Capell, A., Araque Caballero, M.Á., Morenas-Rodríguez, E., Fellerer, K., Franzmeier, N., Kleinberger, G., Eren, E., Deming, Y., Piccio, L., Karch, C.M., Cruchaga, C., Paumier, K., Bateman, R.J., Fagan, A.M., Morris, J.C., Levin, J., Danek, A., Jucker, M., Masters, C.L., Rossor, M.N., Ringman, J.M., Shaw, L.M., Trojanowski, J.Q., Weiner, M., Ewers, M., Haass, C., 2018. CSF progranulin increases in the course of Alzheimer's disease and is associated with sTREM 2, neurodegeneration and cognitive decline . EMBO Mol. Med. 10, 1–21. https://doi.org/10.15252/emmm.201809712

Sudre, C.H., Bocchetta, M., Cash, D., Thomas, D.L., Woollacott, I., Dick, K.M., van Swieten, J., Borroni, B., Galimberti, D., Masellis, M., Tartaglia, M.C., Rowe, J.B., Graff, C., Tagliavini, F., Frisoni, G., Laforce, R., Finger, E., de Mendonça, A., Sorbi, S., Ourselin, S., Cardoso, M.J., Rohrer, J.D., 2017a. White matter hyperintensities are seen only in GRN mutation carriers in the GENFI cohort. NeuroImage Clin. 15, 171–180. https://doi.org/10.1016/j.nicl.2017.04.015

Sudre, C.H., Bocchetta, M., Heller, C., Convery, R., Neason, M., Moore, K.M., Cash, D.M., Thomas, D.L., Woollacott, I.O.C., Foiani, M., Heslegrave, A., Shafei, R., Greaves, C., van Swieten, J., Moreno, F., Sanchez-Valle, R., Borroni, B., Laforce, R., Masellis, M., Tartaglia, M.C., Graff, C., Galimberti, D., Rowe, J.B., Finger, E., Synofzik, M., Vandenberghe, R., de Mendonça, A., Tagliavini, F., Santana, I., Ducharme, S., Butler, C., Gerhard, A., Levin, J., Danek, A., Frisoni, G.B., Sorbi, S., Otto, M., Zetterberg, H., Ourselin, S., Cardoso, M.J., Rohrer, J.D., 2019. White matter hyperintensities in progranulin-associated frontotemporal dementia – a longitudinal GENFI study. NeuroImage Clin. 24, 102077. https://doi.org/10.1016/j.nicl.2019.102077

Sudre, C.H., Cardoso, M.J., Bouvy, W.H., Biessels, G.J., Barnes, J., Ourselin, S., 2015. Bayesian Model Selection for Pathological Neuroimaging Data Applied to White Matter Lesion Segmentation. IEEE Trans. Med. Imaging 34, 2079–2102. https://doi.org/10.1109/TMI.2015.2419072

Sudre, C.H., Cardoso, M.J., Ourselin, S., Alzheimer's Disease Neuroimaging Initiative, 2017b. Longitudinal segmentation of age-related white matter hyperintensities. Med. Image Anal. 38, 50–64. https://doi.org/10.1016/j.media.2017.02.007

Sudre, C.H., Gomez Anson, B., Davagnanam, I., Schmitt, A., Mendelson, A.F., Prados, F., Smith, L., Atkinson, D., Hughes, A.D., Chaturvedi, N., Cardoso, M.J., Barkhof, F., Jaeger, H.R., Ourselin, S., 2018. Bullseye's representation of cerebral white matter hyperintensities. J. Neuroradiol. 45, 114–122. https://doi.org/10.1016/j.neurad.2017.10.001

Sudria-Lopez, E., Koppers, M., de Wit, M., van der Meer, C., Westeneng, H.J., Zundel, C.A.C., Youssef, S.A., Harkema, L., de Bruin, A., Veldink, J.H., van den Berg, L.H., Pasterkamp, R.J., 2016. Full ablation of C9orf72 in mice causes immune system-related pathology and neoplastic events but no motor neuron defects. Acta Neuropathol. https://doi.org/10.1007/s00401-016-1581-x

Sullivan, P.M., Zhou, X., Robins, A.M., Paushter, D.H., Kim, D., Smolka, M.B., Hu, F., 2016. The ALS/FTLD associated protein C9orf72 associates with SMCR8 and WDR41 to regulate the autophagy-lysosome pathway. Acta Neuropathol. Commun. 4, 51. https://doi.org/10.1186/s40478-016-0324-5

Sutphen, C.L., McCue, L., Herries, E.M., Xiong, C., Ladenson, J.H., Holtzman, D.M., Fagan, A.M., 2018. Longitudinal decreases in multiple cerebrospinal fluid biomarkers of neuronal injury in symptomatic late onset Alzheimer's disease. Alzheimer's Dement. 14, 869–879. https://doi.org/10.1016/j.jalz.2018.01.012

Synofzik, M., Born, C., Rominger, A., Lummel, N., Schöls, L., Biskup, S., Schüle, C., Grasshoff, U., Klopstock, T., Adamczyk, C., 2014. Targeted high-throughput sequencing identifies a TARDBP mutation as a cause of early-onset FTD without motor neuron disease. Neurobiol. Aging 35, 1212.e1-1212.e5. https://doi.org/10.1016/j.neurobiolaging.2013.10.092

Taipa, R., Brochado, P., Robinson, A., Reis, I., Costa, P., Mann, D.M., Melo Pires, M., Sousa, N., 2017. Patterns of Microglial Cell Activation in Alzheimer Disease and Frontotemporal Lobar Degeneration. Neurodegener. Dis. 17, 145–154. https://doi.org/10.1159/000457127

Tanaka, Y., Chambers, J.K., Matsuwaki, T., Yamanouchi, K., Nishihara, M., 2014. Possible involvement of lysosomal dysfunction in pathological changes of the brain in aged progranulin-deficient mice. Acta Neuropathol. 2, 1–15. https://doi.org/10.1186/s40478-014-0078-x

Tanaka, Y., Matsuwaki, T., Yamanouchi, K., Nishihara, M., 2013a. Increased lysosomal biogenesis in activated microglia and exacerbated neuronal damage after traumatic brain injury in progranulin-deficient mice. Neuroscience 250, 8–19. https://doi.org/10.1016/j.neuroscience.2013.06.049

Tanaka, Y., Matsuwaki, T., Yamanouchi, K., Nishihara, M., 2013b. Exacerbated inflammatory responses related to activated microglia after traumatic brain injury in

progranulin-deficient mice. Neuroscience 231, 49–60. https://doi.org/10.1016/j.neuroscience.2012.11.032

Tang, W., Lu, Y., Tian, Q.Y., Zhang, Y., Guo, F.J., Liu, G.Y., Muzaffar Syed, N., Lai, Y., Alan Lin, E., Kong, L., Su, J., Yin, F., Ding, A.H., Zanin-Zhorov, A., Dustin, M.L., Tao, J., Craft, J., Yin, Z., Feng, J.Q., Abramson, S.B., Yu, X.P., Liu, C.J., 2011. The growth factor progranulin binds to TNF receptors and is therapeutic against inflammatory arthritis in mice. Science (80-.). 332, 478–484. https://doi.org/10.1126/science.1199214

Teunissen, C.E., Dijkstra, P.C., Polman, C., 2005. Biological markers in CSF and blood for axonal degeneration in multiple sclerosis. Lancet Neurol. 4, 32–41. https://doi.org/10.1016/S1474-4422(04)00964-0

Teunissen, C.E., Elias, N., Koel-Simmelink, M.J.A., Durieux-Lu, S., Malekzadeh, A., Pham, T. V., Piersma, S.R., Beccari, T., Meeter, L.H.H., Dopper, E.G.P., van Swieten, J.C., Jimenez, C.R., Pijnenburg, Y.A.L., 2016. Novel diagnostic cerebrospinal fluid biomarkers for pathologic subtypes of frontotemporal dementia identified by proteomics. Alzheimer's Dement. Diagnosis, Assess. Dis. Monit. 2, 86–94. https://doi.org/10.1016/j.dadm.2015.12.004

Thompson, A.G., Gray, E., Thézénas, M.L., Charles, P.D., Evetts, S., Hu, M.T., Talbot, K., Fischer, R., Kessler, B.M., Turner, M.R., 2018. Cerebrospinal fluid macrophage biomarkers in amyotrophic lateral sclerosis. Ann. Neurol. 83, 258–268. https://doi.org/10.1002/ana.25143

Thurner, L., Preuss, K.D., Fadle, N., Regitz, E., Klemm, P., Zaks, M., Kemele, M., Hasenfus, A., Csernok, E., Gross, W.L., Pasquali, J.L., Martin, T., Bohle, R.M., Pfreundschuh, M., 2013. Progranulin antibodies in autoimmune diseases. J. Autoimmun. 42, 29–38. https://doi.org/10.1016/j.jaut.2012.10.003

Tischer, J., Krueger, M., Mueller, W., Staszewski, O., Prinz, M., Streit, W.J., Bechmann, I., 2016. Inhomogeneous distribution of Iba-1 characterizes microglial pathology in

Alzheimer's disease. Glia 64, 1562–1572. https://doi.org/10.1002/glia.23024

Tofts, P.S., Jackson, J.S., Tozer, D.J., Cercignani, M., Keir, G., MacManus, D.G., Ridgway, G.R., Ridha, B.H., Schmierer, K., Siddique, D., Thornton, J.S., Wroe, S.J., Fox, N.C., 2008. Imaging cadavers: Cold FLAIR and noninvasive brain thermometry using CSF diffusion. Magn. Reson. Med. 59, 190–195. https://doi.org/10.1002/mrm.21456

Tolboom, N., Koedam, E.L.G.E., Schott, J.M., Yaqub, M., Blankenstein, M.A., Barkhof, F., Pijnenburg, Y.A.L., Lammertsma, A.A., Scheltens, P., van Berckel, B.N.M., 2010. Dementia Mimicking Alzheimer's Disease Owing to a Tau Mutation: CSF and PET Findings. Alzheimer Dis. Assoc. Disord. 24, 303–307. https://doi.org/10.1097/WAD.0b013e3181cf35ec

Torres-Platas, S.G., Comeau, S., Rachalski, A., Bo, G.D., Cruceanu, C., Turecki, G., Giros, B., Mechawar, N., 2014. Morphometric characterization of microglial phenotypes in human cerebral cortex. J. Neuroinflammation 11, 1–13. https://doi.org/10.1186/1742-2094-11-12

Tortelli, R., Ruggieri, M., Cortese, R., D'Errico, E., Capozzo, R., Leo, A., Mastrapasqua, M., Zoccolella, S., Leante, R., Livrea, P., Logroscino, G., Simone, I.L., 2012. Elevated cerebrospinal fluid neurofilament light levels in patients with amyotrophic lateral sclerosis: A possible marker of disease severity and progression. Eur. J. Neurol. 19, 1561–1567. https://doi.org/10.1111/j.1468-1331.2012.03777.x

Townley, R.A., Boeve, B.F., Benarroch, E.E., 2018. Progranulin: Functions and neurologic correlations. Neurology 90, 118–125. https://doi.org/10.1212/WNL.0000000000004840

Umoh, M.E., Dammer, E.B., Dai, J., Duong, D.M., Lah, J.J., Levey, A.I., Gearing, M., Glass, J.D., Seyfried, N.T., 2017. A proteomic network approach across the ALS-FTD disease spectrum resolves clinical phenotypes and genetic vulnerability in human brain. EMBO Mol. Med. 10, 48–62.

https://doi.org/10.15252/emmm.201708202

Van Blitterswijk, M., Mullen, B., Nicholson, A.M., Bieniek, K.F., Heckman, M.G., Baker, M.C., Dejesus-Hernandez, M., Finch, N.A., Brown, P.H., Murray, M.E., Hsiung, G.Y.R., Stewart, H., Karydas, A.M., Finger, E., Kertesz, A., Bigio, E.H., Weintraub, S., Mesulam, M., Hatanpaa, K.J., White, C.L., Strong, M.J., Beach, T.G., Wszolek, Z.K., Lippa, C., Caselli, R., Petrucelli, L., Josephs, K.A., Parisi, J.E., Knopman, D.S., Petersen, R.C., Mackenzie, I.R., Seeley, W.W., Grinberg, L.T., Miller, B.L., Boylan, K.B., Graff-Radford, N.R., Boeve, B.F., Dickson, D.W., Rademakers, R., 2014. TMEM106B protects C9ORF72 expansion carriers against frontotemporal dementia. Acta Neuropathol. 127, 397–406. https://doi.org/10.1007/s00401-013-1240-4

van der Ende, E.L., Meeter, L.H., Poos, J.M., Panman, J.L., Jiskoot, L.C., Dopper, E.G.P., Papma, J.M., de Jong, F.J., Verberk, I.M.W., Teunissen, C., Rizopoulos, D., Heller, C., Convery, R.S., Moore, K.M., Bocchetta, M., Neason, M., Cash, D.M., Borroni, B., Galimberti, D., Sanchez-Valle, R., Laforce, R., Moreno, F., Synofzik, M., Graff, C., Masellis, M., Carmela Tartaglia, M., Rowe, J.B., Vandenberghe, R., Finger, E., Tagliavini, F., de Mendonça, A., Santana, I., Butler, C., Ducharme, S., Gerhard, A., Danek, A., Levin, J., Otto, M., Frisoni, G.B., Cappa, S., Pijnenburg, Y.A.L., Rohrer, J.D., van Swieten, J.C., 2019. Serum neurofilament light chain in genetic frontotemporal dementia: a longitudinal, multicentre cohort study. Lancet Neurol. 18, 1103–1111. https://doi.org/10.1016/S1474-4422(19)30354-0

van der Ende, E.L., Xiao, M., Xu, D., Poos, J.M., Panman, J.L., Panman, J.L., Jiskoot, L.C., Jiskoot, L.C., Meeter, L.H., Dopper, E.G.P., Papma, J.M., Van Swieten, J.C., et al., 2020. Neuronal pentraxin 2: A synapse-derived CSF biomarker in genetic frontotemporal dementia. J. Neurol. Neurosurg. Psychiatry 91, 612–621. https://doi.org/10.1136/jnnp-2019-322493

van Olst, L., Verhaege, D., Franssen, M., Kamermans, A., Roucourt, B., Carmans, S.,

Ytebrouck, E., van der Pol, S.M.A., Wever, D., Popovic, M., Vandenbroucke, R.E., Sobrino, T., Schouten, M., de Vries, H.E., 2020. Microglial activation arises after aggregation of phosphorylated-tau in a neuron-specific P301S tauopathy mouse model. Neurobiol. Aging 89, 89–98. https://doi.org/10.1016/j.neurobiolaging.2020.01.003

Vance, C., Rogelj, B., Hortobágyi, T., De Vos, K.J., Nishimura, A.L., Sreedharan, J., Hu, X., Smith, B., Ruddy, D., Wright, P., Ganesalingam, J., Williams, K.L., Tripathi, V., Al-Saraj, S., Al-Chalabi, A., Leigh, P.N., Blair, I.P., Nicholson, G., De Belleroche, J., Gallo, J.M., Miller, C.C., Shaw, C.E., 2009. Mutations in FUS, an RNA processing protein, cause familial amyotrophic lateral sclerosis type 6. Science (80-.). 323, 1208–1211. https://doi.org/10.1126/science.1165942

Varghese, A.M., Sharma, A., Mishra, P., Vijayalakshmi, K., Harsha, H.C., Sathyaprabha, T.N., Bharath, S.M.M., Nalini, A., Alladi, P.A., Raju, T.R., 2013. Chitotriosidase - A putative biomarker for sporadic amyotrophic lateral sclerosis. Clin. Proteomics 10, 1–9. https://doi.org/10.1186/1559-0275-10-19

Vijverberg, E.G.B., Dols, A., Krudop, W.A., Del Campo Milan, M., Kerssens, C.J., Gossink, F., Prins, N.D., Stek, M.L., Scheltens, P., Teunissen, C.E., Pijnenburg, Y.A.L., 2017. Cerebrospinal fluid biomarker examination as a tool to discriminate behavioral variant frontotemporal dementia from primary psychiatric disorders. Alzheimer's Dement. Diagnosis, Assess. Dis. Monit. 7, 99–106. https://doi.org/10.1016/j.dadm.2017.01.009

Vogels, T., Murgoci, A.-N., Hromádka, T., 2019. Intersection of pathological tau and microglia at the synapse. Acta Neuropathol. Commun. 7, 109. https://doi.org/10.1186/s40478-019-0754-y

Walker, D.G., Lue, L., 2015. Immune phenotypes of microglia in human neurodegenerative disease : challenges to detecting microglial polarization in human brains. Alzheimers. Res. Ther. 7, 56. https://doi.org/10.1186/s13195-015-

0139-9

Wang, S., Mustafa, M., Yuede, C.M., Salazar, S.V., Kong, P., Long, H., Ward, M., Siddiqui, O., Paul, R., Gilfillan, S., Ibrahim, A., Rhinn, H., Tassi, I., Rosenthal, A., Schwabe, T., Colonna, M., 2020. Anti-human TREM2 induces microglia proliferation and reduces pathology in an Alzheimer's disease model. J. Exp. Med. 217, e20200785. https://doi.org/10.1084/jem.20200785

Ward, M.E., Chen, R., Huang, H.-Y., Ludwig, C., Telpoukhovskaia, M., Taubes, A., Boudin, H., Minami, S.S., Reichert, M., Albrecht, P., Gelfand, J.M., Cruz-Herranz, A., Cordano, C., Alavi, M. V., Leslie, S., Seeley, W.W., Miller, B.L., Bigio, E., Mesulam, M.-M., Bogyo, M.S., Mackenzie, I.R., Staropoli, J.F., Cotman, S.L., Huang, E.J., Gan, L., Green, A.J., 2017. Individuals with progranulin haploinsufficiency exhibit features of neuronal ceroid lipofuscinosis. Sci. Transl. Med. 9, eaah5642. https://doi.org/10.1126/scitranslmed.aah5642

Wardlaw, J.M., Valdés Hernández, M.C., Muñoz-Maniega, S., 2015. What are white matter hyperintensities made of? Relevance to vascular cognitive impairment. J. Am. Heart Assoc. 4, 001140. https://doi.org/10.1161/JAHA.114.001140

Warren, J.D., Rohrer, J.D., Rossor, M.N., 2013. Frontotemporal dementia. BMJ 347, f4827–f4827. https://doi.org/10.1136/bmj.f4827

Watabe-Rudolph, M., Song, Z., Lausser, L., Schnack, C., Begus-Nahrmann, Y., Scheithauer, M.O., Rettinger, G., Otto, M., Tumani, H., Thal, D.R., Attems, J., Jellinger, K.A., Kestler, H.A., Von Arnim, C.A.F., Rudolph, K.L., 2012. Chitinase enzyme activity in CSF is a powerful biomarker of Alzheimer disease. Neurology 78, 569–577. https://doi.org/10.1212/WNL.0b013e318247caa1

Watts, G.D.J., Wymer, J., Kovach, M.J., Mehta, S.G., Mumm, S., Darvish, D., Pestronk, A., Whyte, M.P., Kimonis, V.E., 2004. Inclusion body myopathy associated with Paget disease of bone and frontotemporal dementia is caused by mutant valosin-containing protein. Nat. Genet. 36, 377–381. https://doi.org/10.1038/ng1332

Wennström, M., Surova, Y., Hall, S., Nilsson, C., Minthon, L., Hansson, O., Nielsen, H.M., 2015. The inflammatory marker YKL-40 is elevated in cerebrospinal fluid from patients with Alzheimer's but not Parkinson's disease or dementia with Lewy bodies. PLoS One 10, 1–13. https://doi.org/10.1371/journal.pone.0135458

Williams, K.L., Topp, S., Yang, S., Smith, B., Fifita, J.A., Warraich, S.T., Zhang, K.Y., Farrawell, N., Vance, C., Hu, X., Chesi, A., Blair, I.P., et al., 2016. CCNF mutations in amyotrophic lateral sclerosis and frontotemporal dementia. Nat. Commun. 7, 11253. https://doi.org/10.1038/ncomms11253

Wils, H., Kleinberger, G., Pereson, S., Janssens, J., Capell, A., Van Dam, D., Cuijt, I., Joris, G., De Deyn, P.P., Haass, C., Van Broeckhoven, C., Kumar-Singh, S., 2012. Cellular ageing, increased mortality and FTLD-TDP-associated neuropathology in progranulin knockout mice. J. Pathol. 228, 67–76. https://doi.org/10.1002/path.4043

Wood, E.M., Falcone, D., Suh, E.R., Irwin, D.J., Chen-Plotkin, A.S., Lee, E.B., Xie, S.X., Van Deerlin, V.M., Grossman, M., 2013. Development and validation of pedigree classification criteria for frontotemporal lobar degeneration. JAMA Neurol. 70, 1411–1417. https://doi.org/10.1001/jamaneurol.2013.3956

Woollacott, I.O.C., Bocchetta, M., Sudre, C.H., Ridha, B.H., Strand, C., Courtney, R., Ourselin, S., Cardoso, M.J., Warren, J.D., Rossor, M.N., Revesz, T., Fox, N.C., Holton, J.L., Lashley, T., Rohrer, J.D., 2018. Pathological correlates of white matter hyperintensities in a case of progranulin mutation associated frontotemporal dementia. Neurocase 24, 166–174. https://doi.org/10.1080/13554794.2018.1506039

Woollacott, I.O.C., Mead, S., 2014. The C9ORF72 expansion mutation: Gene structure, phenotypic and diagnostic issues. Acta Neuropathol. 127, 319–332. https://doi.org/10.1007/s00401-014-1253-7

Woollacott, I.O.C., Rohrer, J.D., 2016. The clinical spectrum of sporadic and familial forms of frontotemporal dementia. J. Neurochem. 138, 6–31.

https://doi.org/10.1111/jnc.13654

Woollacott, I.O.C., Toomey, C.E., Strand, C., Courtney, R., Benson, B.C., Rohrer, J.D., Lashley, T., 2020. Microglial burden, activation and dystrophy patterns in frontotemporal lobar degeneration. J. Neuroinflammation 17, 234. https://doi.org/10.1186/s12974-020-01907-0

Yin, F., Banerjee, R., Thomas, B., Zhou, P., Qian, L., Jia, T., Ma, X., Ma, Y., Iadecola, C., Beal, M.F., Nathan, C., Ding, A., 2009. Exaggerated inflammation, impaired host defense, and neuropathology in progranulin-deficient mice. J. Exp. Med. 207, 117–128. https://doi.org/10.1084/jem.20091568

Yin, F., Dumont, M., Banerjee, R., Ma, Y., Li, H., Lin, M.T., Beal, M.F., Nathan, C., Thomas, B., Ding, A., 2010. Behavioral deficits and progressive neuropathology in progranulin-deficient mice: a mouse model of frontotemporal dementia. FASEB J. 24, 4639–4647. https://doi.org/10.1096/fj.10-161471

Yoshiyama, Y., Higuchi, M., Zhang, B., Huang, S.-M., Iwata, N., Saido, T.C., Maeda, J., Suhara, T., Trojanowski, J.Q., Lee, V.M.-Y., 2007. Synapse loss and microglial activation precede tangles in a P301S tauopathy mouse model. Neuron 53, 337–51. https://doi.org/10.1016/j.neuron.2007.01.010

Zetterberg, H., Skillbäck, T., Mattsson, N., Trojanowski, J.Q., Portelius, E., Shaw, L.M., Weiner, M.W., Blennow, K., 2016. Association of cerebrospinal fluid neurofilament light concentration with Alzheimer disease progression. JAMA Neurol. 73, 60–67. https://doi.org/10.1001/jamaneurol.2015.3037

Zhang, H., Ng, K.P., Therriault, J., Kang, M.S., Pascoal, T.A., Rosa-Neto, P., Gauthier, S., 2018. Cerebrospinal fluid phosphorylated tau, visinin-like protein-1, and chitinase-3-like protein 1 in mild cognitive impairment and Alzheimer's disease. Transl. Neurodegener. 7, 1–12. https://doi.org/10.1186/s40035-018-0127-7

Zhao, W., Beers, D.R., Bell, S., Wang, J., Wen, S., Baloh, R.H., Appel, S.H., 2015. TDP-43 activates microglia through NF-κB and NLRP3 inflammasome. Exp. Neurol. 273,

24–35. https://doi.org/10.1016/j.expneurol.2015.07.019

Zhong, L., Chen, X.-F., Wang, T., Wang, Zhe, Liao, C., Wang, Zongqi, Huang, R., Wang, D., Li, X., Wu, L., Jia, L., Zheng, H., Painter, M., Atagi, Y., Liu, C.-C., Zhang, Y.-W., Fryer, J.D., Xu, H., Bu, G., 2017. Soluble TREM2 induces inflammatory responses and enhances microglial survival. J. Exp. Med. 214, 597–607. https://doi.org/10.1084/jem.20160844

Zhong, L., Xu, Y., Zhuo, R., Wang, T., Wang, K., Huang, R., Wang, D., Gao, Y., Zhu, Y., Sheng, X., Chen, K., Wang, N., Zhu, L., Can, D., Marten, Y., Shinohara, M., Liu, C.C., Du, D., Sun, H., Wen, L., Xu, H., Bu, G., Chen, X.F., 2019. Soluble TREM2 ameliorates pathological phenotypes by modulating microglial functions in an Alzheimer's disease model. Nat. Commun. 10, 1–16. https://doi.org/10.1038/s41467-019-09118-9

Zhou, X., Sun, L., de Oliveira, F.B., Qi, X., Brown, W.J., Smolka, M.B., Sun, Y., Hu, F., 2015. Prosaposin facilitates sortilin-independent lysosomal trafficking of progranulin. J. Cell Biol. 210, 991–1002. https://doi.org/10.1083/jcb.201502029

Zhukareva, V., Mann, D., Pickering-Brown, S., Uryu, K., Shuck, T., Shah, K., Grossman, M., Miller, B.L., Hulette, C.M., Feinstein, S.C., Trojanowski, J.Q., Lee, V.M.Y., 2002. Sporadic Pick's disease: A tauopathy characterized by a spectrum of pathological τ isoforms in gray and white matter. Ann. Neurol. 51, 730–739. https://doi.org/10.1002/ana.10222

Zigdon, H., Savidor, A., Levin, Y., Meshcheriakova, A., Schiffmann, R., Futerman, A.H., 2015. Identification of a biomarker in cerebrospinal fluid for neuronopathic forms of Gaucher disease. PLoS One 10, 1–11. https://doi.org/10.1371/journal.pone.0120194

11 Appendices

Appendix 1 – All cases used in histological studies in Chapters 5 and 6. na = not available

Case code	Pathological diagnosis	Clinical diagnosis	Genetic mutation	Sex	Age at onset (years)	Age at death (years)	Disease duration (years)	Post-mortem delay (hours)	Brain weight (grams)
Controls									
1	Normal / pathological aging	Control	-	F	-	80	-	49.2	1242
2	Normal	Control	-	F	-	68	-	45.1	1330
3	Normal	Control	-	M	-	38	-	80.6	1581
4	Normal / pathological aging	Control	-	F	-	73	-	24.0	1214
5	Normal / pathological aging	Control	-	F	-	78	-	29.5	1225
AD									
6	AD	AD	-	F	65	70	5	46.9	1233
7	AD	AD	-	M	65	72	7	38.9	1325
8	AD	AD	-	M	52	69	17	35.1	891
9	AD	AD	-	M	63	73	10	31.2	1269
10	AD	AD	-	F	49	62	13	76.7	996
FTLD-tau									
11	FTLD-CBD	nfvPPA	-	F	65	73.8	8.8	37.3	996
12	FTLD-CBD	PSPS	-	F	64	69.5	5.5	80.8	1100
13	FTLD-CBD	nfvPPA	-	M	57	68.0	11.0	81.6	980
14	FTLD-CBD	CBS	-	F	58	69.1	11.1	103.3	917
15	FTLD-CBD	nfvPPA	-	M	57	64.8	7.8	41.4	1137
16	FTLD-*MAPT*	bvFTD	*MAPT 10+16*	M	58	66.4	8.4	58.2	1399
17	FTLD-*MAPT*	bvFTD	*MAPT 10+16*	M	37	52.8	15.8	52.6	1046
18	FTLD-*MAPT*	bvFTD	*MAPT 10+16*	F	52	68.4	16.4	24.0	na
19	FTLD-*MAPT*	bvFTD	*MAPT 10+16*	F	43	52.4	9.4	64.0	na
20	FTLD-*MAPT*	bvFTD	*MAPT 10+16*	F	50	58.1	8.1	31.0	na
21	FTLD-Picks	bvFTD	-	M	64	75.6	11.6	46.5	933
22	FTLD-Picks	bvFTD	-	M	58	63.5	5.5	24.0	1166
23	FTLD-Picks	bvFTD	-	M	55	65.6	10.6	43.5	1040
24	FTLD-Picks	bvFTD	-	M	52	67.6	15.6	30.5	982
25	FTLD-Picks	bvFTD	-	M	59	68.1	9.1	94.8	1209
26	FTLD-PSP	PSPS	-	F	65	74.0	9.0	72.5	1182
27	FTLD-PSP	PSPS	-	M	62	68.0	6.0	25.6	na
28	FTLD-PSP	PSPS	-	M	70	78.3	8.3	86.4	1249

Case code	Pathological diagnosis	Clinical diagnosis	Genetic mutation	Sex	Age at onset (years)	Age at death (years)	Disease duration (years)	Post-mortem delay (hours)	Brain weight (grams)
29	FTLD-PSP	PSPS	-	M	67	73.7	6.7	69.3	1303
30	FTLD-PSP	nfvPPA	-	M	71	84.0	13.0	32.6	1137
FTLD-TDP									
31	FTLD-TDPA	FTD-MND	-	F	76	78.6	2.6	36.3	1119
32	FTLD-TDPA	bvFTD	-	M	63	75.2	10.2	41.0	na
33	FTLD-TDPA	nfvPPA	-	F	65	64.4	2.4	na	na
34	FTLD-TDPA	FTD-MND	-	M	62	53.1	2.1	54.0	na
35	FTLD-TDPA	bvFTD	-	M	51	62.0	4.0	92.9	na
36	FTLD-TDPA	bvFTD	*TBK1 A705fs*	M	58	72.2	9.2	97.4	1320
37	FTLD-TDPA	bvFTD	*GRN Q130fs*	F	62	68.1	6.1	99.8	na
38	FTLD-TDPA	bvFTD	*GRN C31fs*	M	53	61.4	8.4	72.6	994
39	FTLD-TDPA	nfvPPA	*GRN C31fs*	F	67	74.2	7.2	157.6	1025
40	FTLD-TDPA	bvFTD	*GRN C31fs*	F	58	63.8	5.8	85.4	851
41	FTLD-TDPA	bvFTD	*GRN C31fs*	M	50	55.3	5.3	29.4	974
42	FTLD-TDPA	FTD-MND	*C9orf72*	F	68	75.1	7.1	85.8	782
43	FTLD-TDPA	nfvPPA	*C9orf72*	F	57	67.3	10.3	85.6	789
44	FTLD-TDPA	nfvPPA	*C9orf72*	F	55	62.7	7.7	63.1	981
45	FTLD-TDPA	FTD-MND	*C9orf72*	M	66	71.7	5.7	51.9	1431
46	FTLD-TDPA	FTD-MND	*C9orf72*	F	58	66.3	8.3	107.1	850
47	FTLD-TDPB	bvFTD	*C9orf72*	F	60	66.0	6.0	94.1	1186
48	FTLD-TDPB	bvFTD	*C9orf72*	M	54	62.1	8.1	na	na
49	FTLD-TDPB	FTD-MND	*C9orf72*	F	54	59.0	5.0	na	na
50	FTLD-TDPB	FTD-MND	-	F	63	67.2	4.2	45.5	1232
51	FTLD-TDPB	FTD-MND	-	M	50	56.2	6.2	10.8	na
52	FTLD-TDPC	svPPA	-	F	59	73.0	14.0	37.9	976
53	FTLD-TDPC	svPPA	-	F	55	73.7	18.7	83.7	936
54	FTLD-TDPC	svPPA	-	M	64	78.6	14.6	26.8	1110
55	FTLD-TDPC	svPPA	-	M	64	74.3	10.3	19.0	1230
56	FTLD-TDPC	svPPA	-	M	52	65.4	13.4	51.8	1057
FTLD-FUS									
57	FTLD-FUS (aFTLD-U)	bvFTD	-	M	44	51.4	7.4	24.0	na
58	FTLD-FUS (aFTLD-U)	bvFTD	-	M	51	60.4	9.4	48.0	na
59	FTLD-FUS (aFTLD-U)	bvFTD	-	M	47	52.5	5.5	72.0	na
60	FTLD-FUS (aFTLD-U)	bvFTD	-	M	40	51.3	11.3	12.0	na

Appendix 2 – Bland-Altman analysis to determine the number of random squares required for microglial analysis in Chapter 5

a

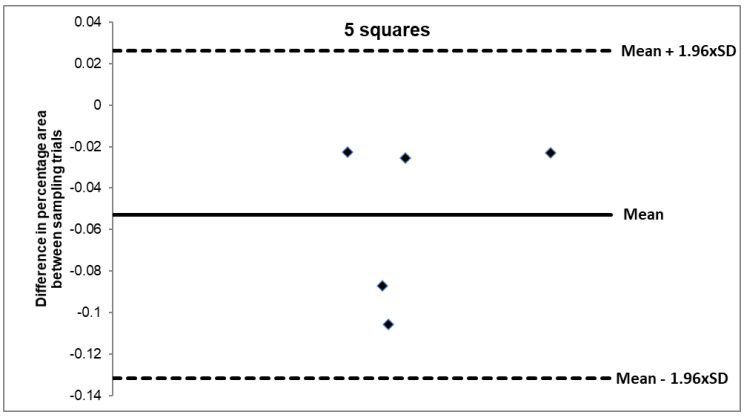

b

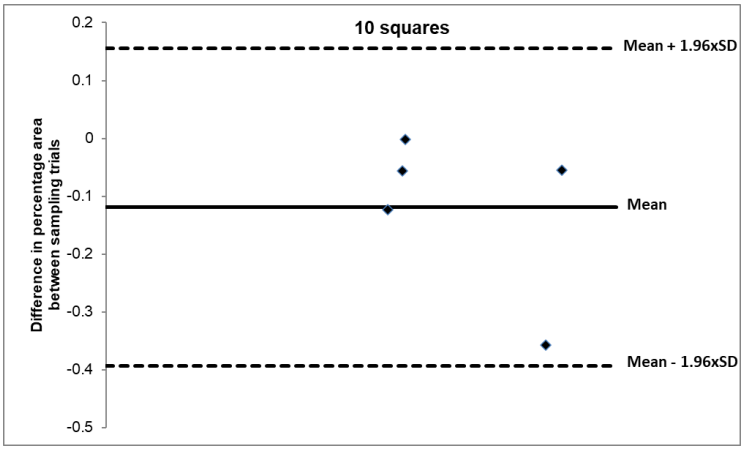

c

	5 squares	10 squares
R square	0.114	0.242
Regression significance (*P* value)	0.578	0.399

Bland-Altman plots for microglial percentage area calculated twice for five cases, first using (**a**) 5 random squares and then using (**b**) 10 random squares each time. These plots show how mean percentage area values varied between the two sampling trials for the five cases (y axes = difference in means), with more consistent results (less variability, data points overall closer to the mean) when using 10 squares compared with when using 5 squares. (**c**) Statistics from linear regressions of both analyses (using the difference between percentage area measurements as the dependent variable and the mean of the measurements as the independent variable). The R square and *P* values for 10 squares indicate a more reliable method, so 10 squares were chosen for analysis in all cases within the cohort.

Appendix 3 – Heat maps of *P* values for all comparisons of microglial burden, circularity and perimeter in Chapter 5

Within each heat map, *P* values are presented in each box and represent results of comparisons between groups listed on corresponding vertical versus horizontal axes. *P* values are shown for comparisons between groups for each region and between grey and white matter for each group. The colour of each box represents the degree of statistical significance in the difference between groups, with red indicating a highly significant difference, blue a non-significant difference and white borderline (trend) or moderately significant difference, with gradations in between. FG = frontal grey matter; FW = frontal white matter; TG = temporal grey matter; TW = temporal white matter.

Microglial burden: CD68-positive microglia in the frontal lobe

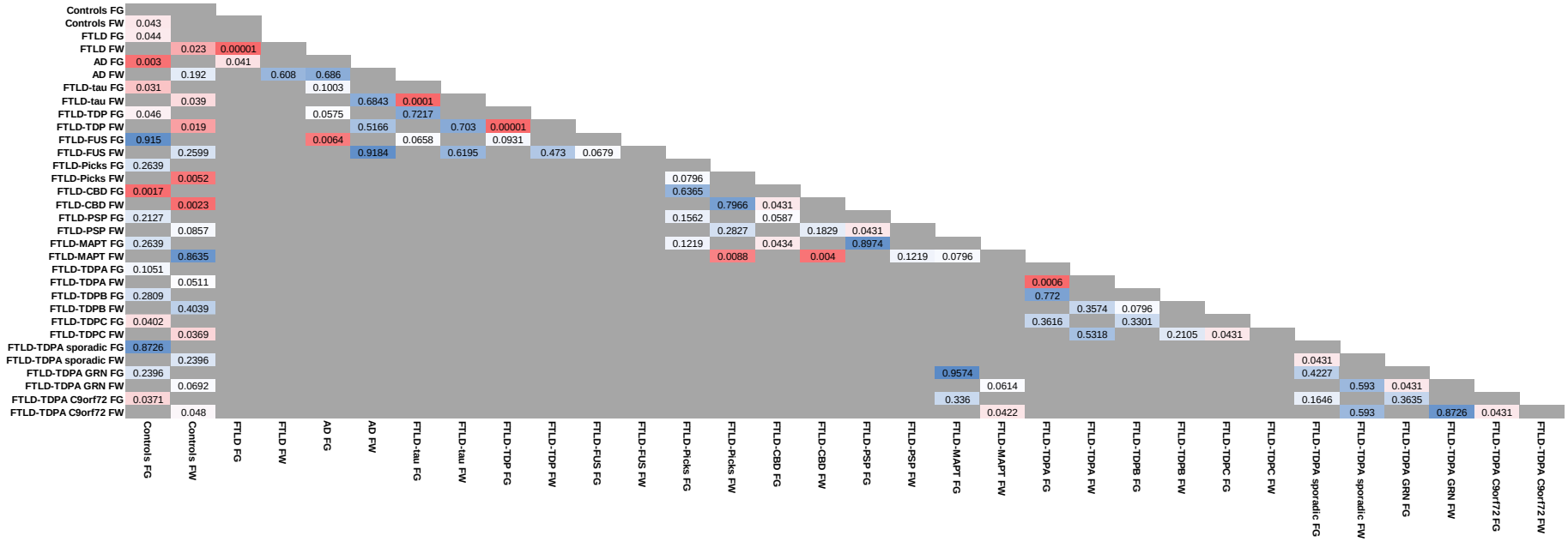

Microglial burden: CD68-positive microglia in the temporal lobe

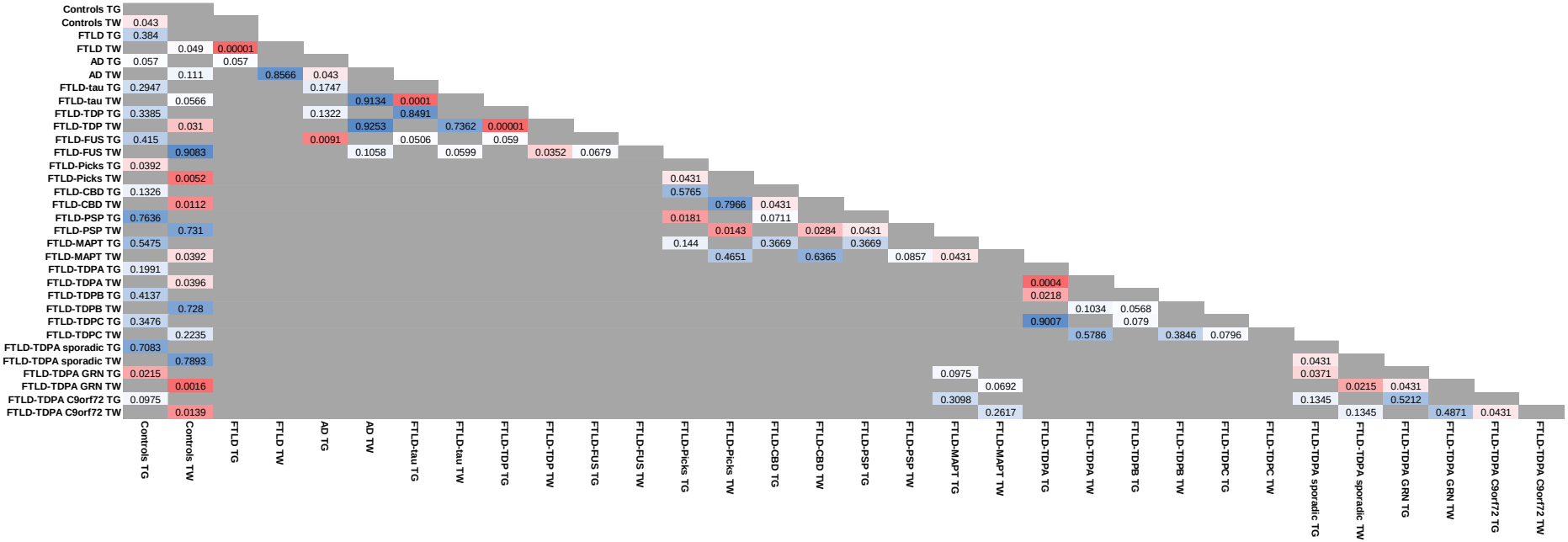

Microglial burden: CR3/43-positive microglia in the frontal lobe

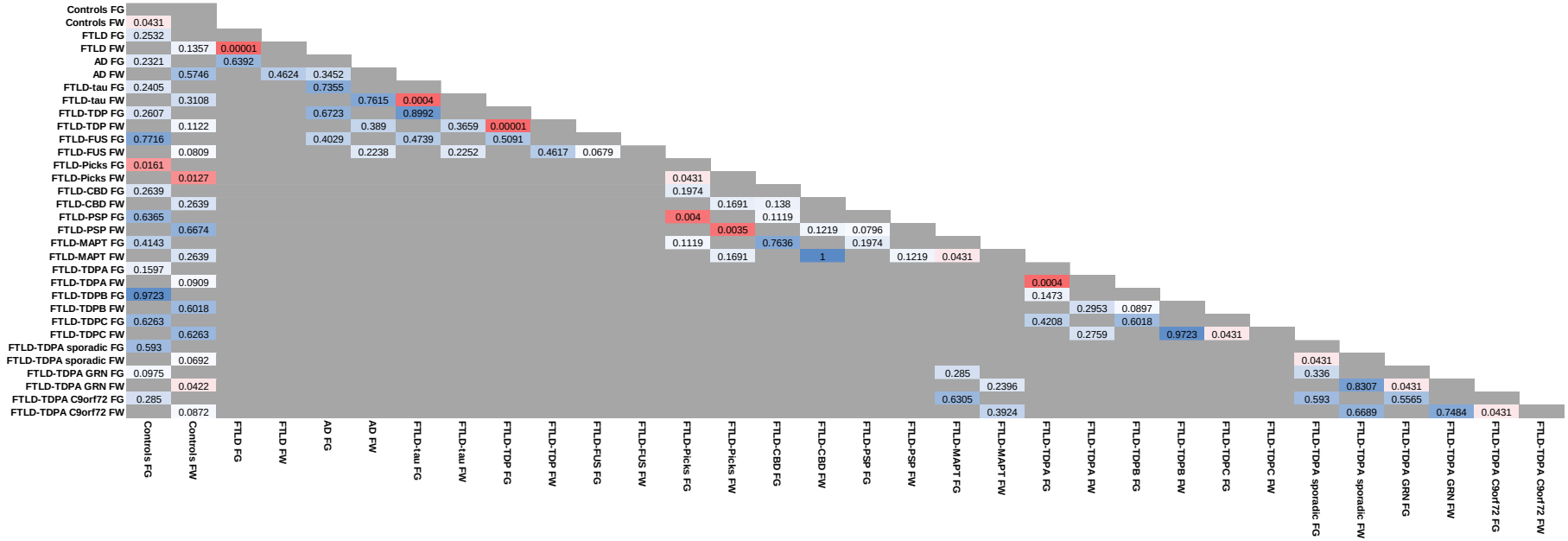

Microglial burden: CR3/43-positive microglia in the temporal lobe

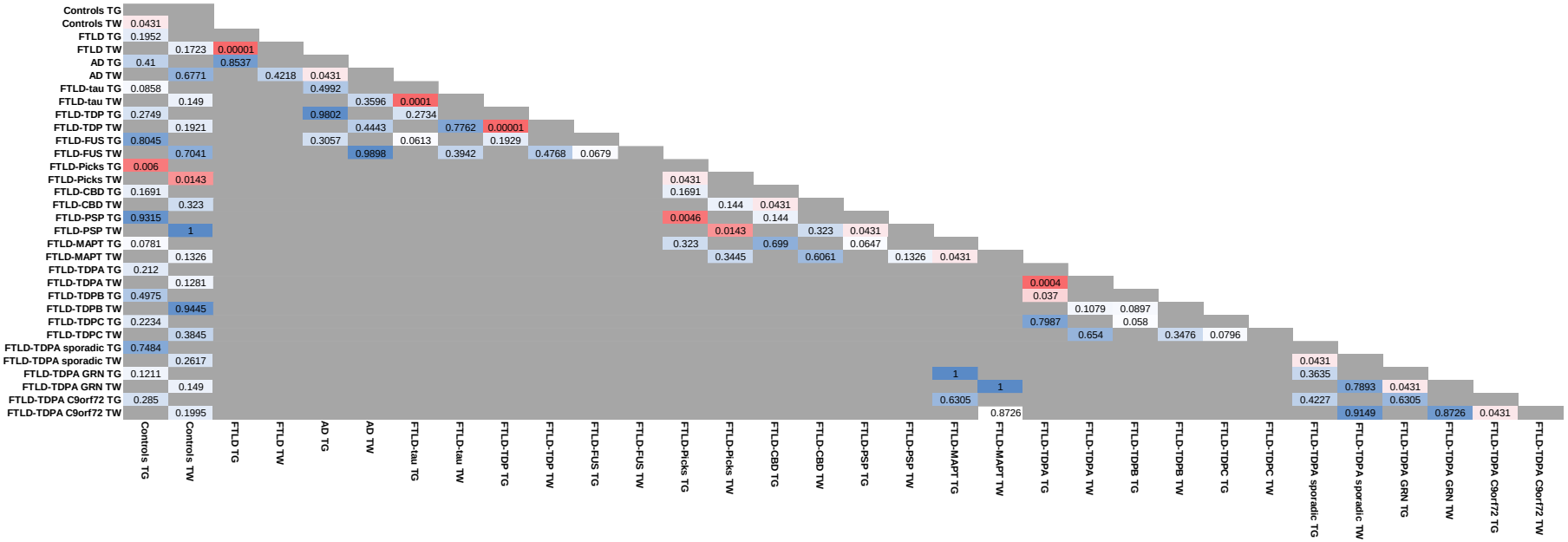

Microglial burden: Iba1-positive microglia in the frontal lobe

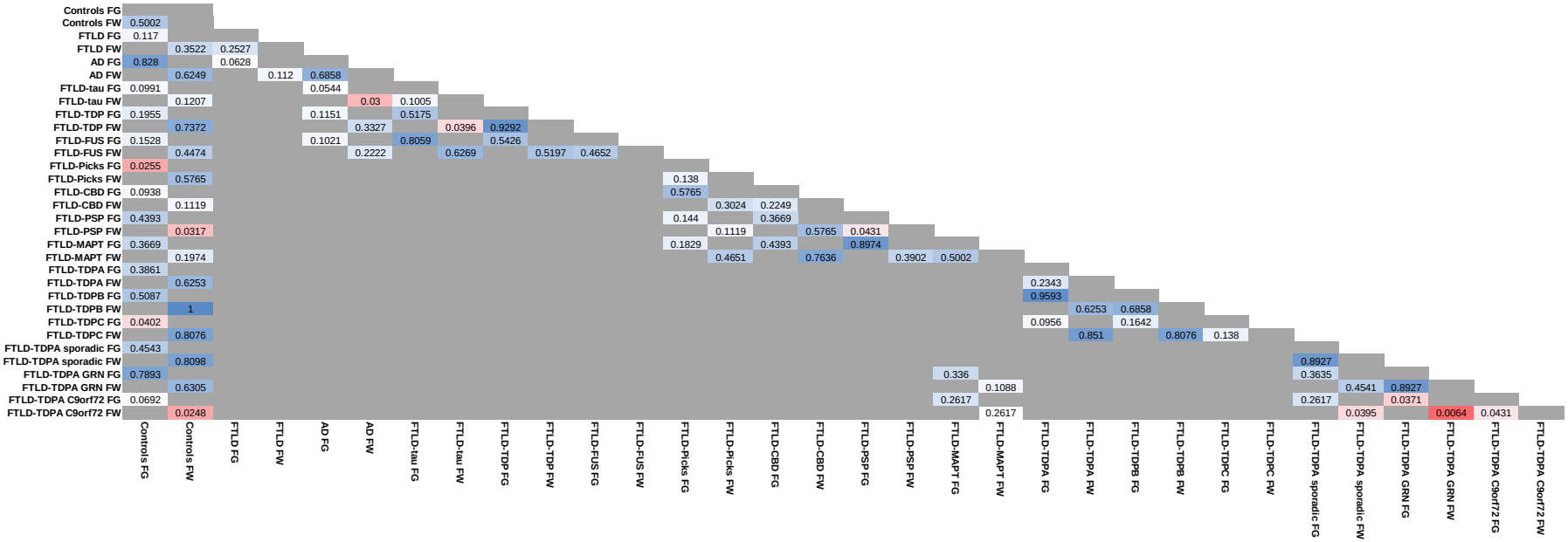

Microglial burden: Iba1-positive microglia in the temporal lobe

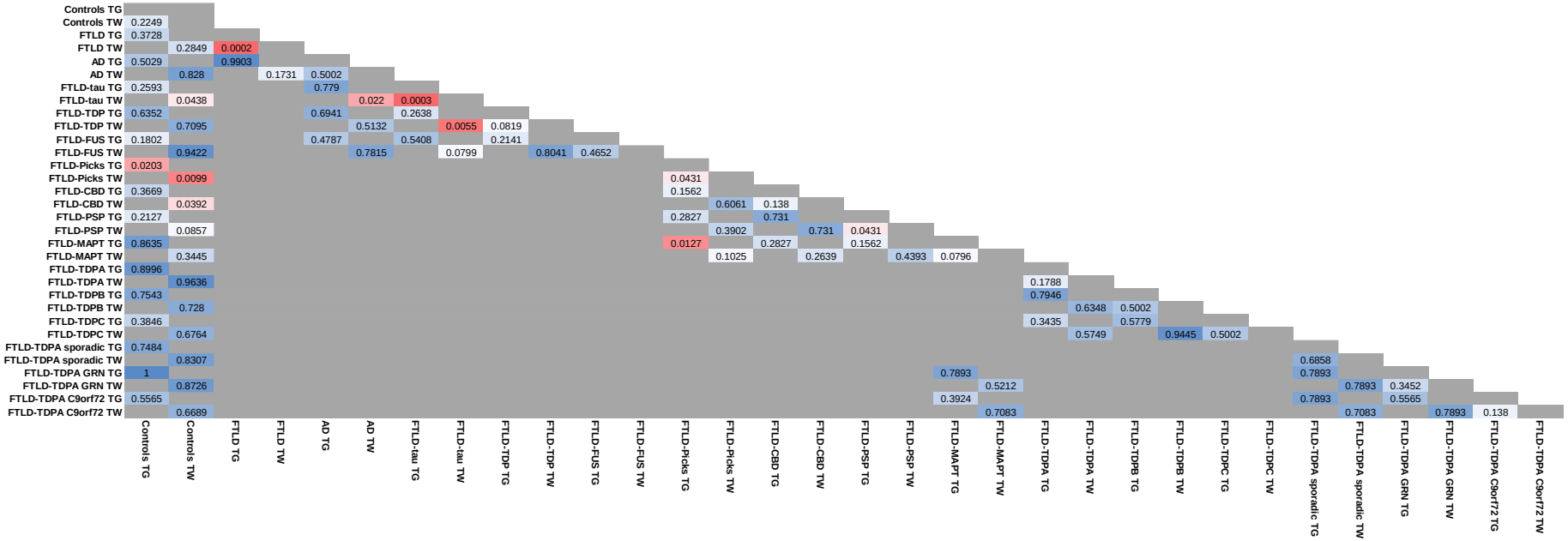

Microglial circularity: CD68-positive microglia in the frontal lobe

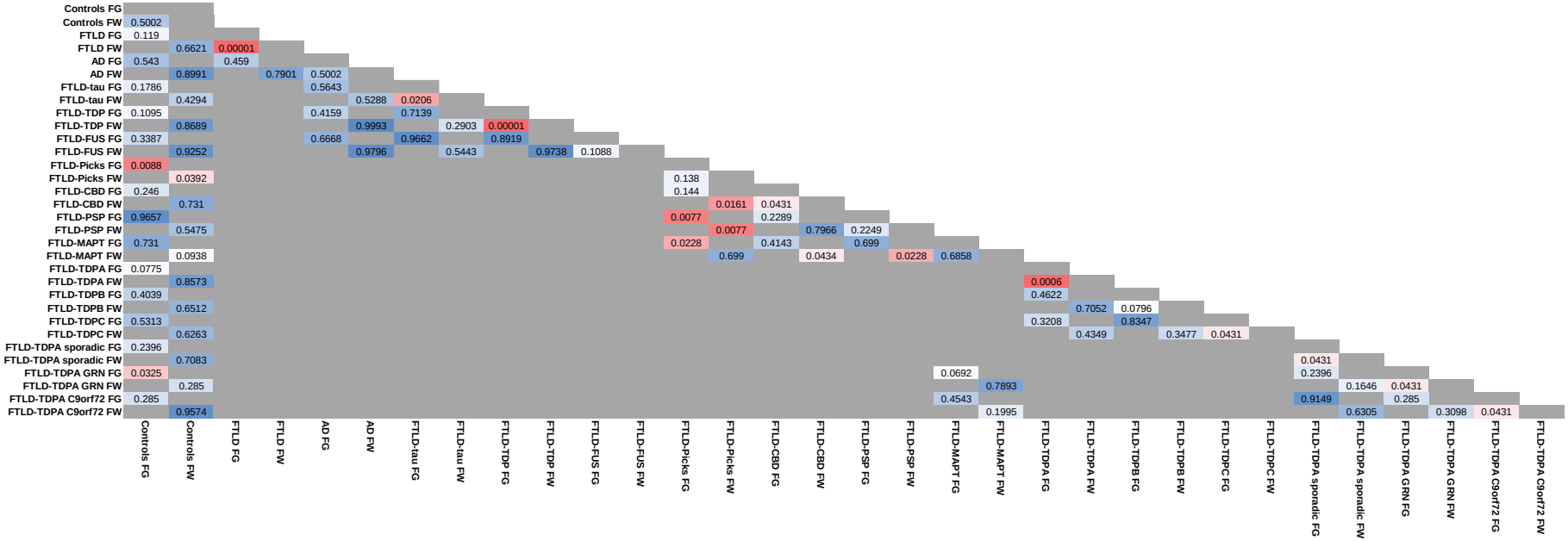

Microglial circularity: CD68-positive microglia in the temporal lobe

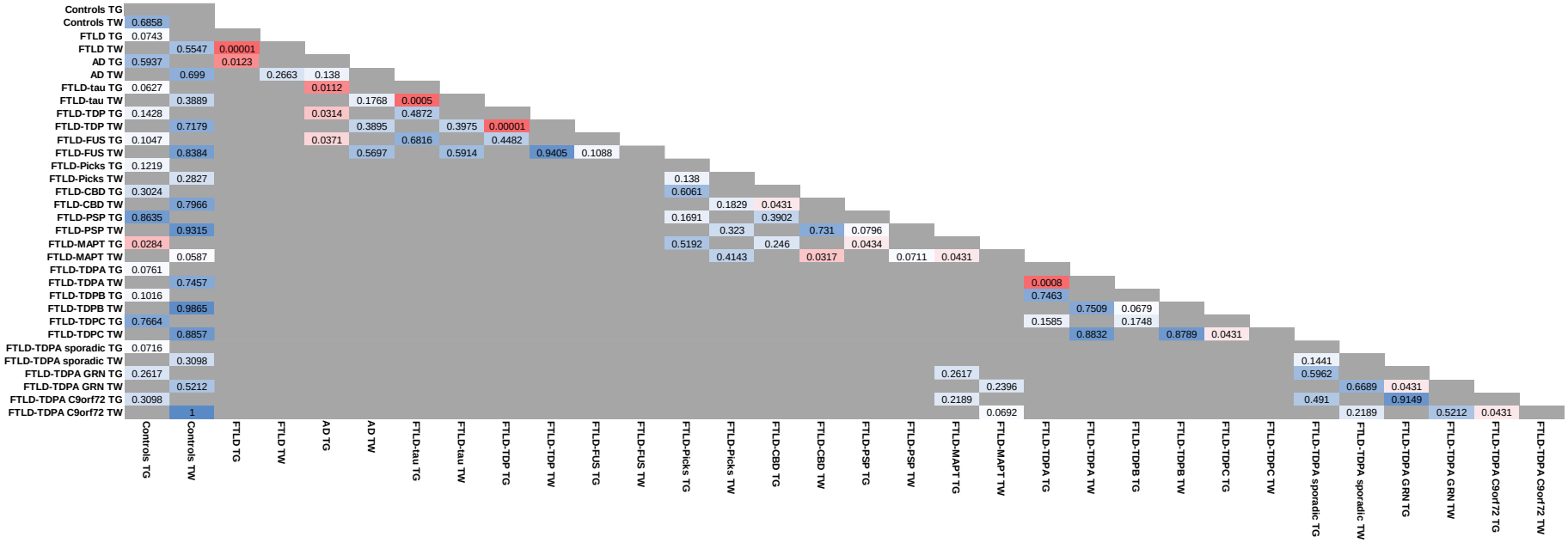

Microglial circularity: CR3/43-positive microglia in the frontal lobe

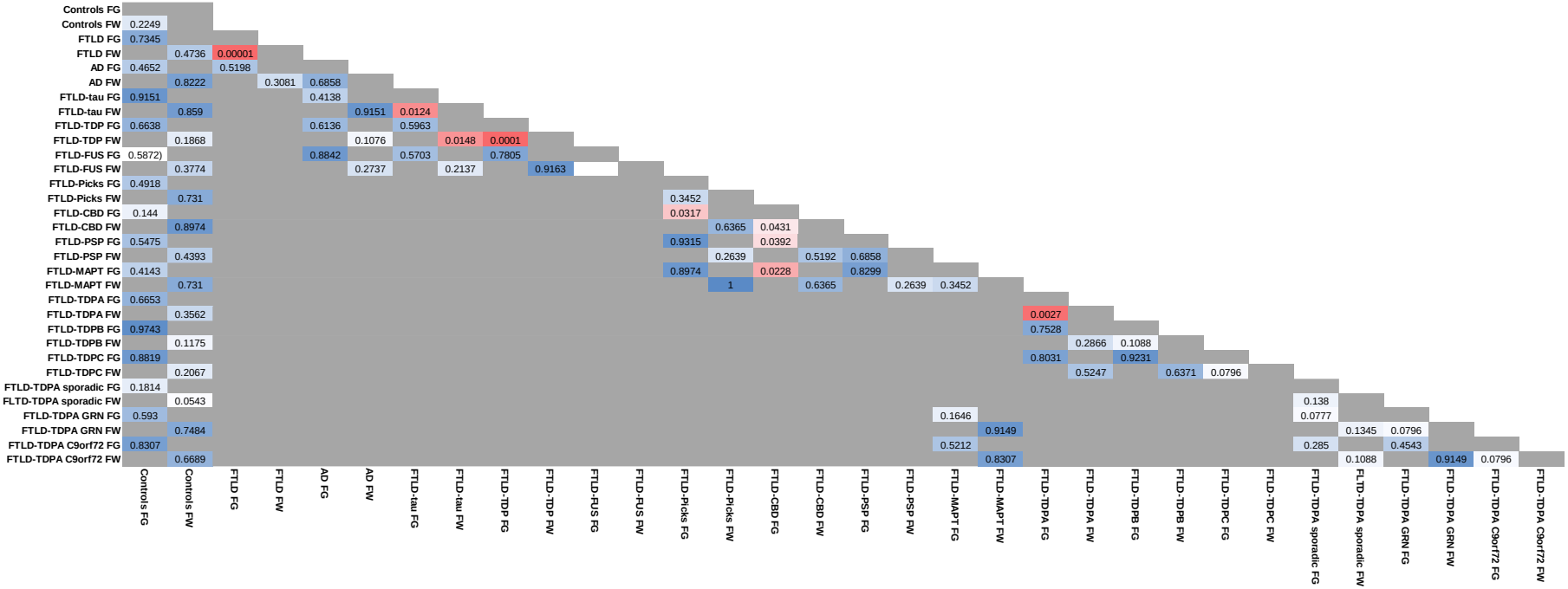

Microglial circularity: CR3/43-positive microglia in the temporal lobe

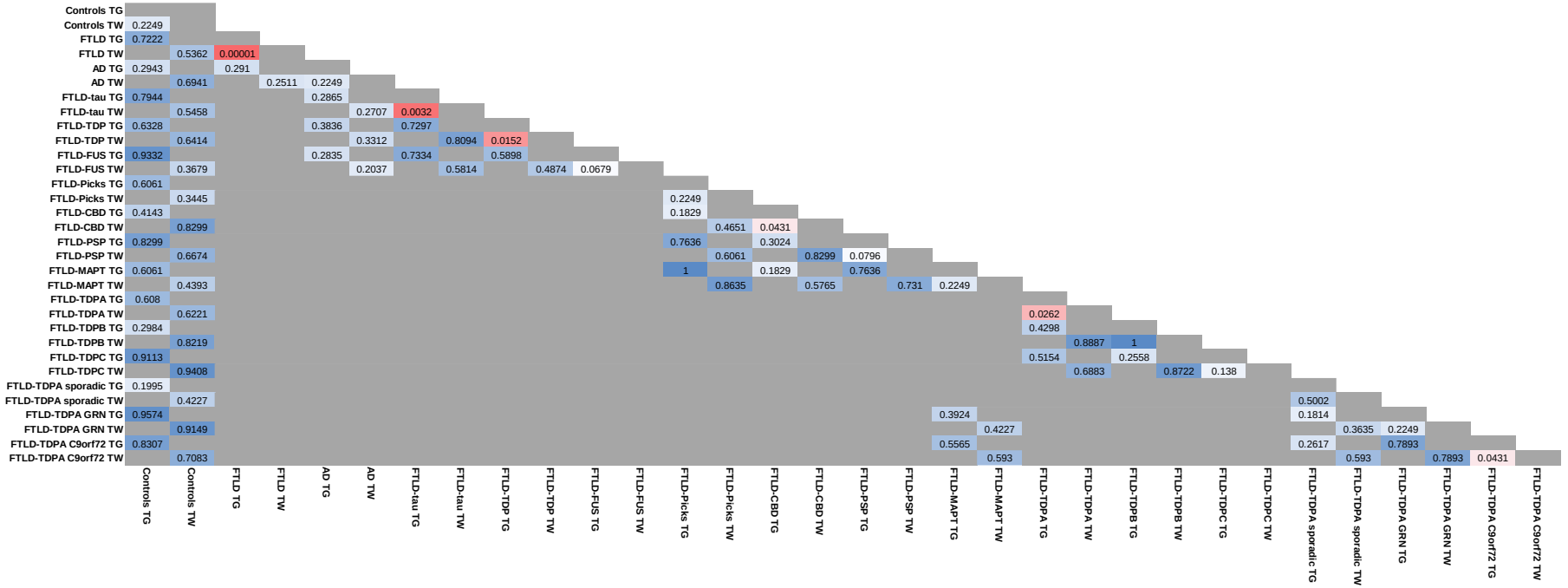

Microglial circularity: Iba1-positive microglia in the frontal lobe

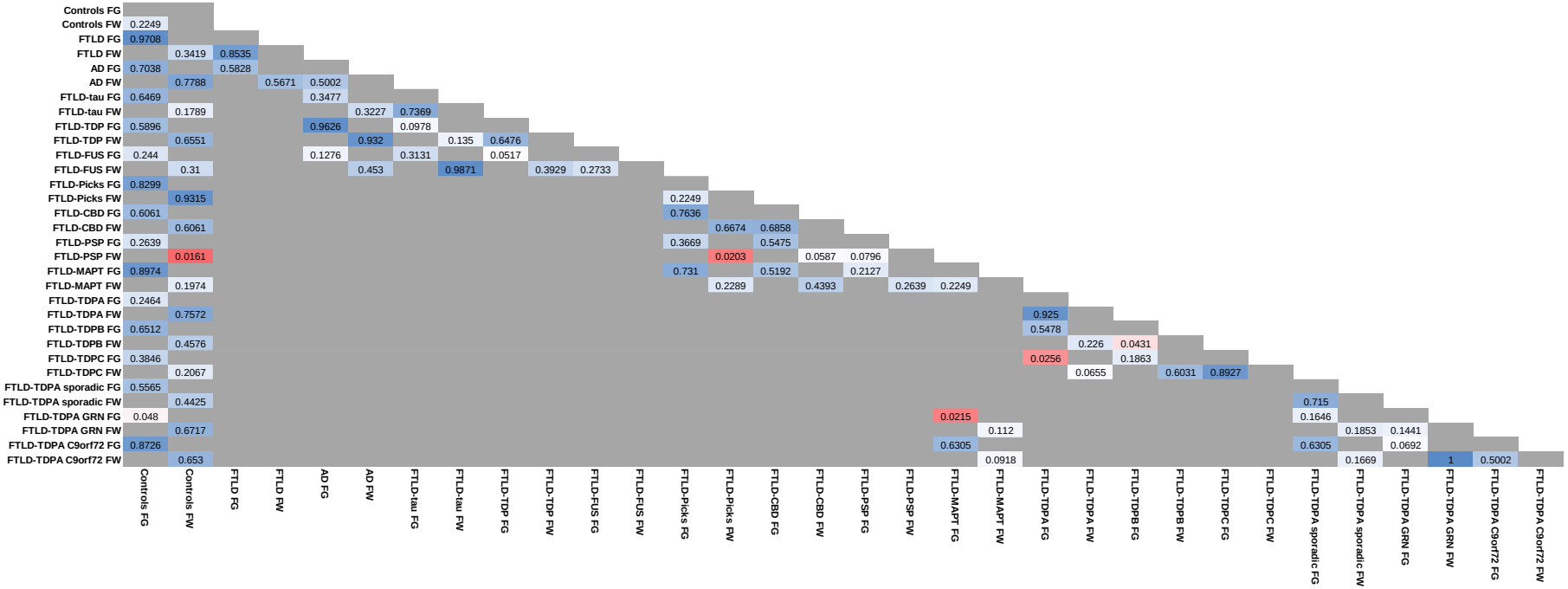

Microglial circularity: Iba1-positive microglia in the temporal lobe

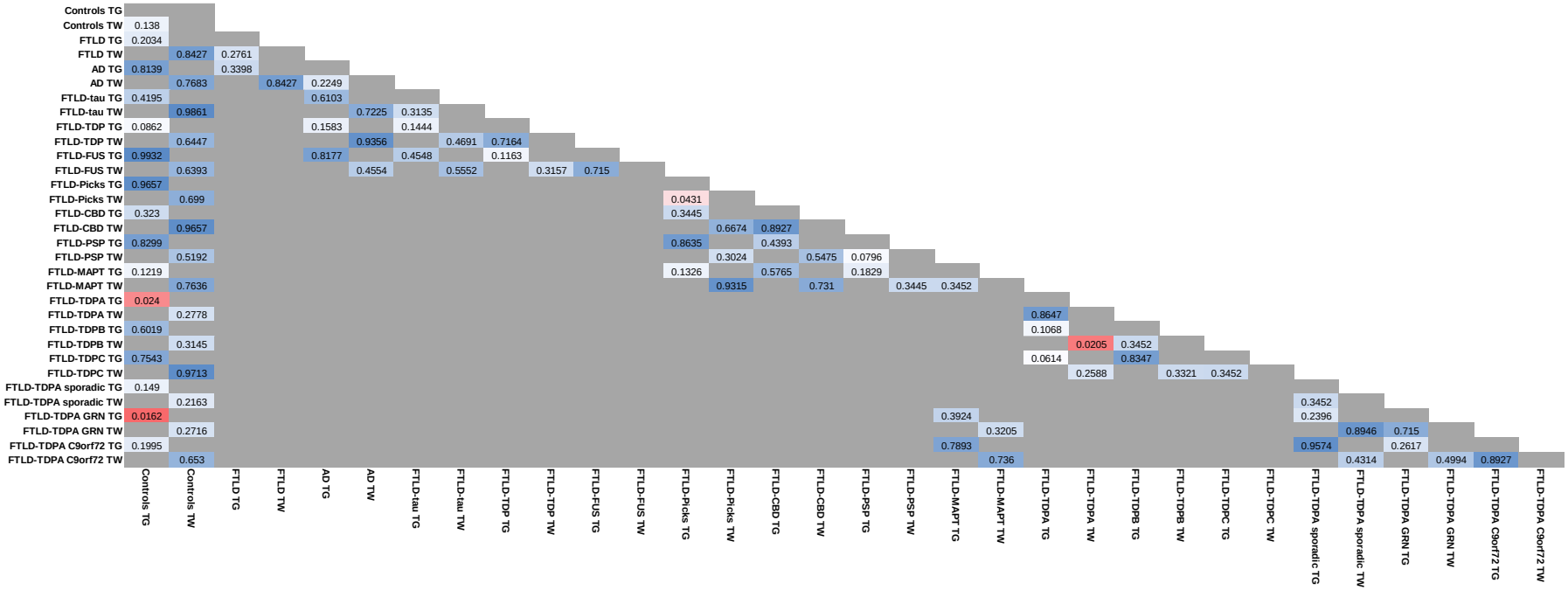

Microglial perimeter: CD68-positive microglia in the frontal lobe

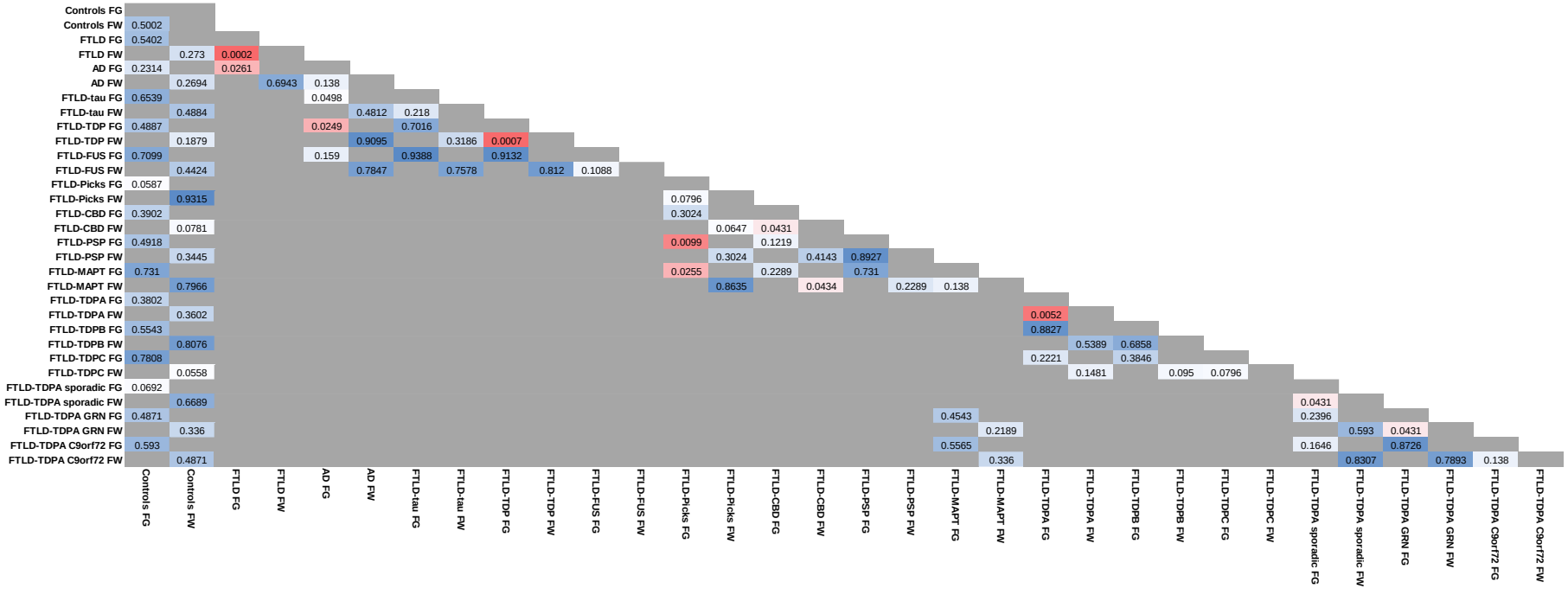

Microglial perimeter: CD68-positive microglia in the temporal lobe

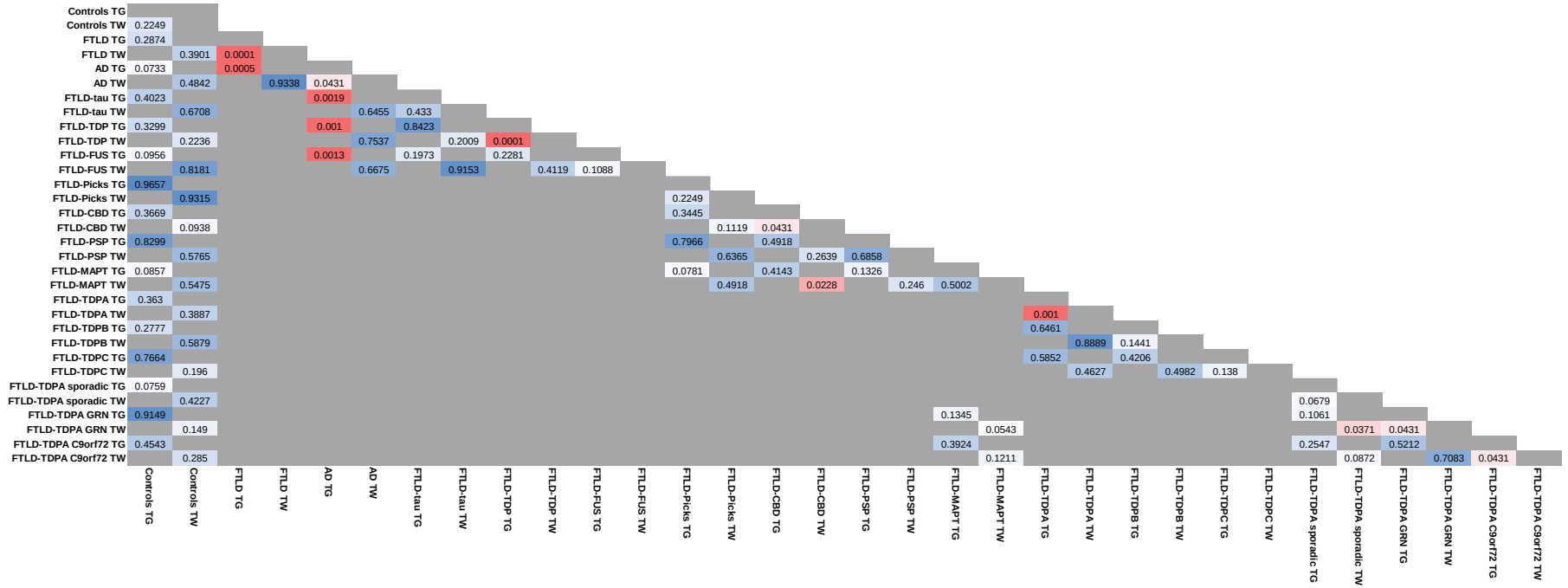

Microglial perimeter: CR3/43-positive microglia in the frontal lobe

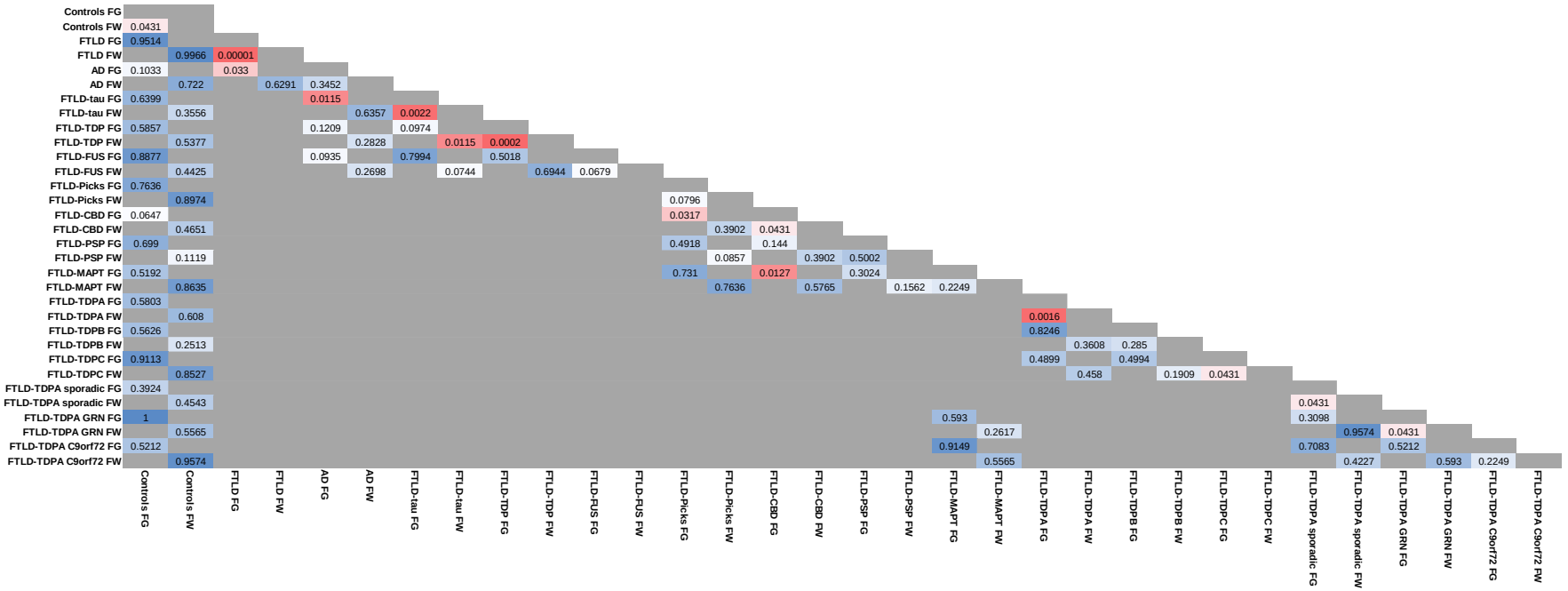

Microglial perimeter: CR3/43-positive microglia in the temporal lobe

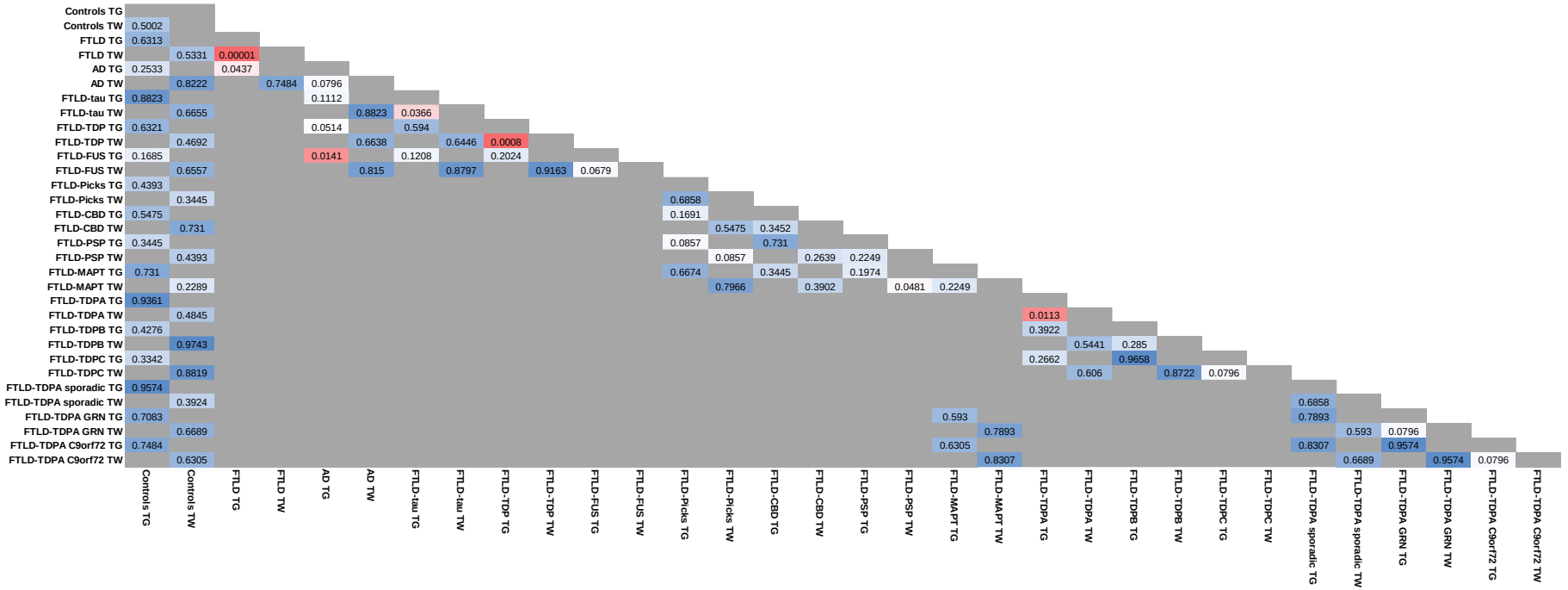

Microglial perimeter: Iba1-positive microglia in the frontal lobe

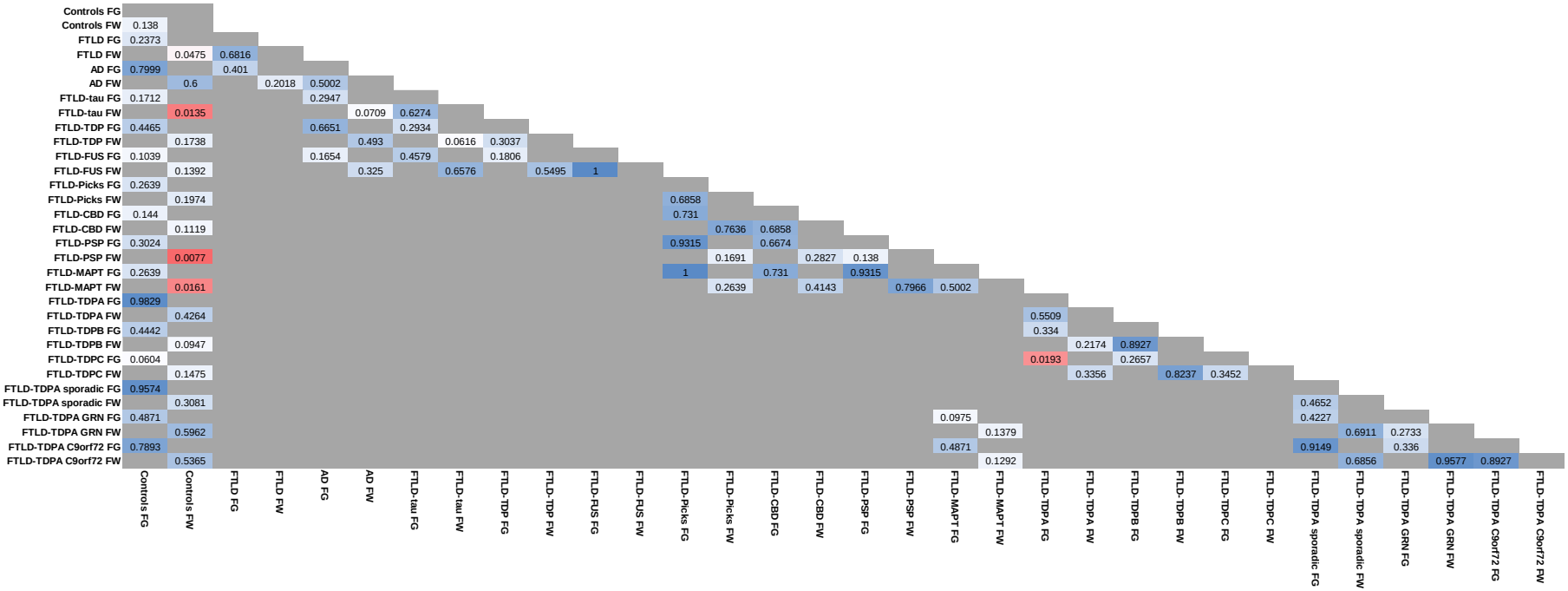

Microglial perimeter: Iba1-positive microglia in the temporal lobe